BULLETIN OF THE MINERAL RESEARCH AND EXPLORATION

Foreign Edition 2014 149

CONTENTS

Facies Characteristics And Control Mechanisms of Quaternary Deposits In The Lake Tuz Basin
.....Alper GÜRBÜZ and Nizamettin KAZANCI 1

Neotectonic-Period Characteristics, Seismicity, Geometry And Segmentation of The Tuz Gölü Fault Zone
.....Akın KÜRÇER and Y. Ergun GÖKTEN 19

Neogene Stratigraphy And Paleogeographic Evolution of The Karaburun Area, İzmir, Western Turkey
.....Fikret GÖKTAŞ 69

Benthic Foraminiferal Fauna of Malatya Oligo-Miocene Basin (Eastern Taurids, Eastern Turkey)
.....Fatma GEDİK 93

Protolith Nature And Tectonomagmatic Features of Amphibolites From The Qushchi Area, West Azerbaijan, NW Iran
.....Mohssen MOAZZEN 139

Glauberite-Halite Association In Bozkır Formation (Pliocene Çankırı-Çorum Basin, Central Anatolia, Turkey)
.....İlhan SÖNMEZ 153

Estimation of Swelling Pressure Using Simple Soil Indices
.....Kamil KAYABALI and Özgür YALDIZ 177

Two Examples For Imaging Buried Geological Boundaries: Sinkhole Structure And Seyit Hacı Fault, Karapınar, Konya
.....Ertan TOKER, Yahya ÇİFTÇİ, Aytekin AYVA and Akın KÜRÇER 189

The Assessment of Geothermal Potential of Turkey By Means Of Heat Flow Estimation
.....Uğur AKIN, Emin Uğur ULUGERGERLİ and Semih KUTLU 201

A Brief Note On Mineral Evolution And Biochemistry
.....José Mario AMİGO 211

Critisism on the paper "Possible Incision of The Large Valleys In Southern Marmara Region, Turkey (Nizamettin KAZANCI, Ömer EMRE, Korhan ERTURAÇ, Suzanne A.G. LEROY, Salim ÖNCEL, Özden İLERİ and Özlem TOPRAK)
.....Nizamettin KAZANCI 219

Acknowledgement 221

Notes to the authors 223

Bull. Min. Res. Exp. (2014) 149: 1-18

Bulletin of the
Mineral Research and Exploration

http://bulletin.mta.gov.tr

FACIES CHARACTERISTICS AND CONTROL MECHANISMS OF QUATERNARY DEPOSITS IN THE LAKE TUZ BASIN

Alper Gürbüz[a,b*] and Nizamettin Kazancı[a]

[a] *Ankara Üniversitesi, Mühendislik Fakültesi, Jeoloji Mühendisliği Bölümü, 06100, Tandoğan, Ankara*
[b] *Niğde Üniversitesi, Mühendislik Fakültesi, Jeoloji Mühendisliği Bölümü, 51240, Niğde*

Keywords:
Central Anatolia, Quaternary, lake level changes, sedimentology, climate, tectonism.

ABSTRACT

Although there are several studies discussing the pre-Neogene development of the Lake Tuz basin, which is the largest terrestrial basin in Turkey, investigations delineating the characteristics of the Neogene and particularly Quaternary period of this basin are quite limited. Whereas studies regarding such periods of the basin are quite informative for both active tectonics and climate change issues that are of significant public concern. In this study, results of field observations on temporal and spatial characteristics of Quaternary deposits in the Lake Tuz Basin and processes controlling these features are presented. For this, as a result of sequence studies conducted in 17 different areas, Quaternary units were described and examined under 12 lithofacies and 5 facies associations. Facies properties imply that tectonism is spatially determinant factor whilst climate is the dominant controlling mechanism in the Quaternary evolution.

1. Introduction

The Lake Tuz Basin in Central Anatolia is the largest terrestrial basin in Turkey (Figure 1). The basin with an area of about 15000 km^2 has been thought to be a deposition site since the upper Cretaceous (Görür and Derman, 1978; Turgut, 1978). Due to the plain morphology, which indicates that basin has a thick basin fill and has not been significantly affected by young tectonic activity, for many years the basin has been the subject of studies on economic resources such as oil and natural gas (Arıkan, 1975; Uğurtaş, 1975; Uygun, 1981; Aydemir and Ateş, 2008; Huvaz, 2009). In addition to these studies on Paleogene units, there are also other surveys regarding evaporitic characteristics of younger units and determination of mineral resources of economic value (Irion and Müller, 1968; Erol, 1969; Uygun and Şen, 1978; Çamur and Mutlu, 1996; Derman, 2003; Tekin et al., 2007). In all these studies, the younger-stage evolution of the basin, which has been hitherto neglected, is of great importance as regards to both active tectonism and climate investigations. Within this scope, except for the half-century old pioneering and valuable efforts of Oğuz Erol (1969), limited number of studies and publications are available (Ulu et al., 1994*a, b*; Kashima, 2002; Kürçer and Gökten, 2012; Özsayın et al., 2013). On the other hand, there are exceptionally detailed studies on the Konya basin (just south of the Lake Tuz Basin) and the ancient Lake Konya (Roberts et al., 1979, 1999; Roberts, 1983; Karabıyıkoğlu et al., 1999; Kuzucuoğlu et al., 1999; Leng et al., 1999; Reed et al., 1999). Since the study of Erol (1969), which was carried out beyond the means of today's conditions, the number of exposures in the region has been increased and the advancements in research techniques necessitated the elaboration of recent stage characteristics of the Lake Tuz Basin.

* *Corresponding author: Alper GÜRBÜZ, agurbuz@nigde.edu.tr*

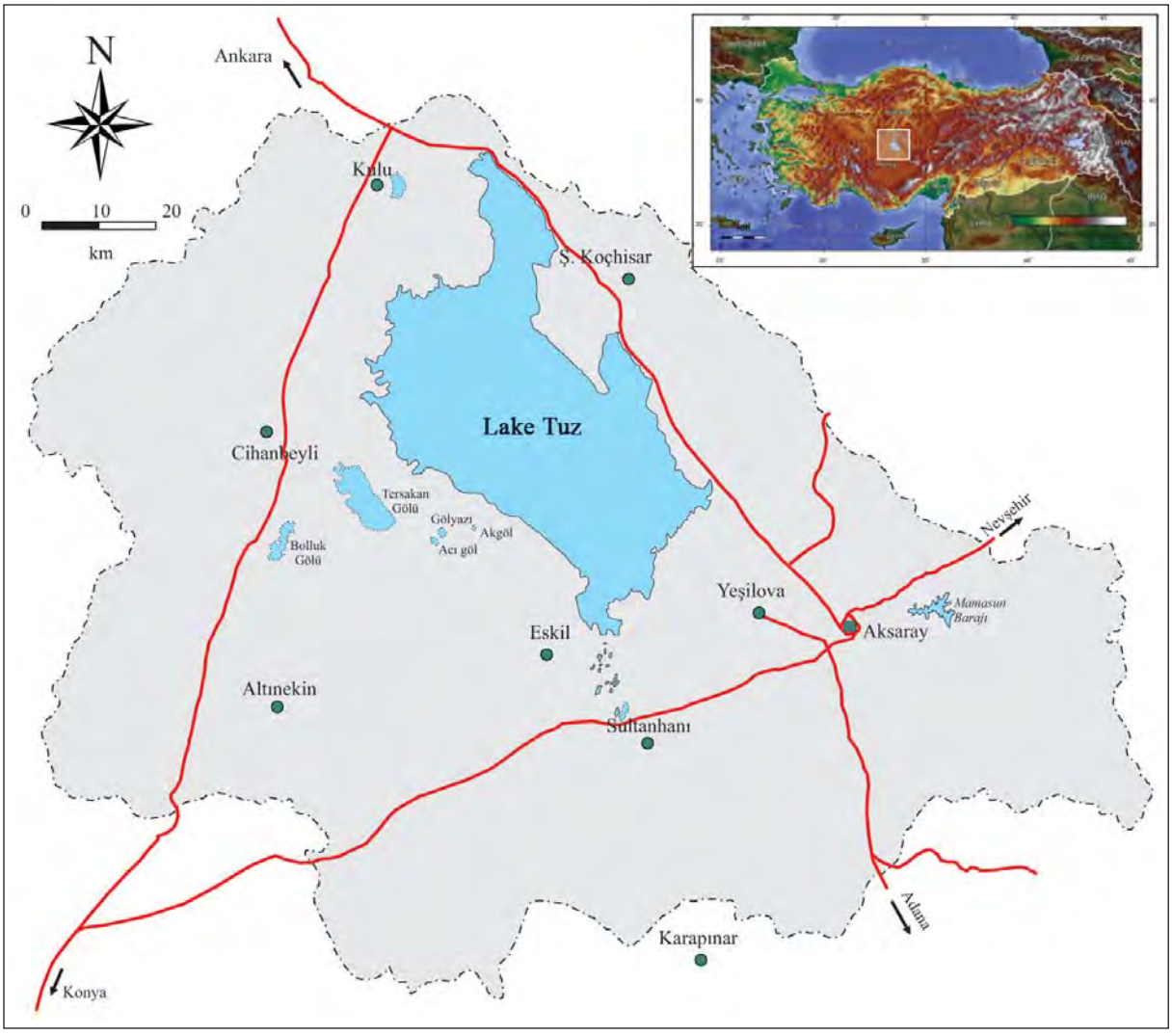

Figure 1- Location map of the Lake Tuz draigane basin.

Lacustrine deposition systems are the best places to study their origin and evolution in conjunction with tectonism and climate factors which directly affect these parameters (Karabıyıkoğlu, 2003). These areas, which can be thought as natural archive systems with direct records of paleo/recent climate changes and tectonic controls, still have maintained their importance in the earth science since the pioneering works of Gilbert (1885, 1890). The interrelations between alluvial and lacustrine environments, particularly of Quaternary closed lake basins, record Pleistocene and Holocene tectonic- and climate-induced environmental changes and long-term sedimentologic and geomorphologic lake level oscillations as well (Karabıyıkoğlu, 2003). The facies of Quaternary deposits in Lake Tuz Basin and processes that control these facies are the materials of present study.

2. Pre-Quaternary Basement Units

The Lake Tuz Basin in western part of the central Anatolia is a tectonic deposition site filled with late Cretaceous-Quaternary sediments with a measurable thickness of 5000 m (Figure 2). The basement under this thick fill is represented mostly by the Central Anatolian Crystalline Complex and the Kütahya-Bolkardağı Metamorphics (Erler et al., 1991; Göncüoğlu et al., 1991, 1992, 1993, 1996; Akıman et al., 1993; Türeli et al., 1993; Yalınız et al., 1996, 2000; Yalınız and Göncüoğlu, 1998; Dirik and Erol, 2003; Kadıoğlu et al., 2003; Göncüoğlu, 2011).

The basin fill starts with a terrestrial unit consisting of red colored clastics which unconformably set above the basement unit at east and west parts of the study area (Figure 3). It is

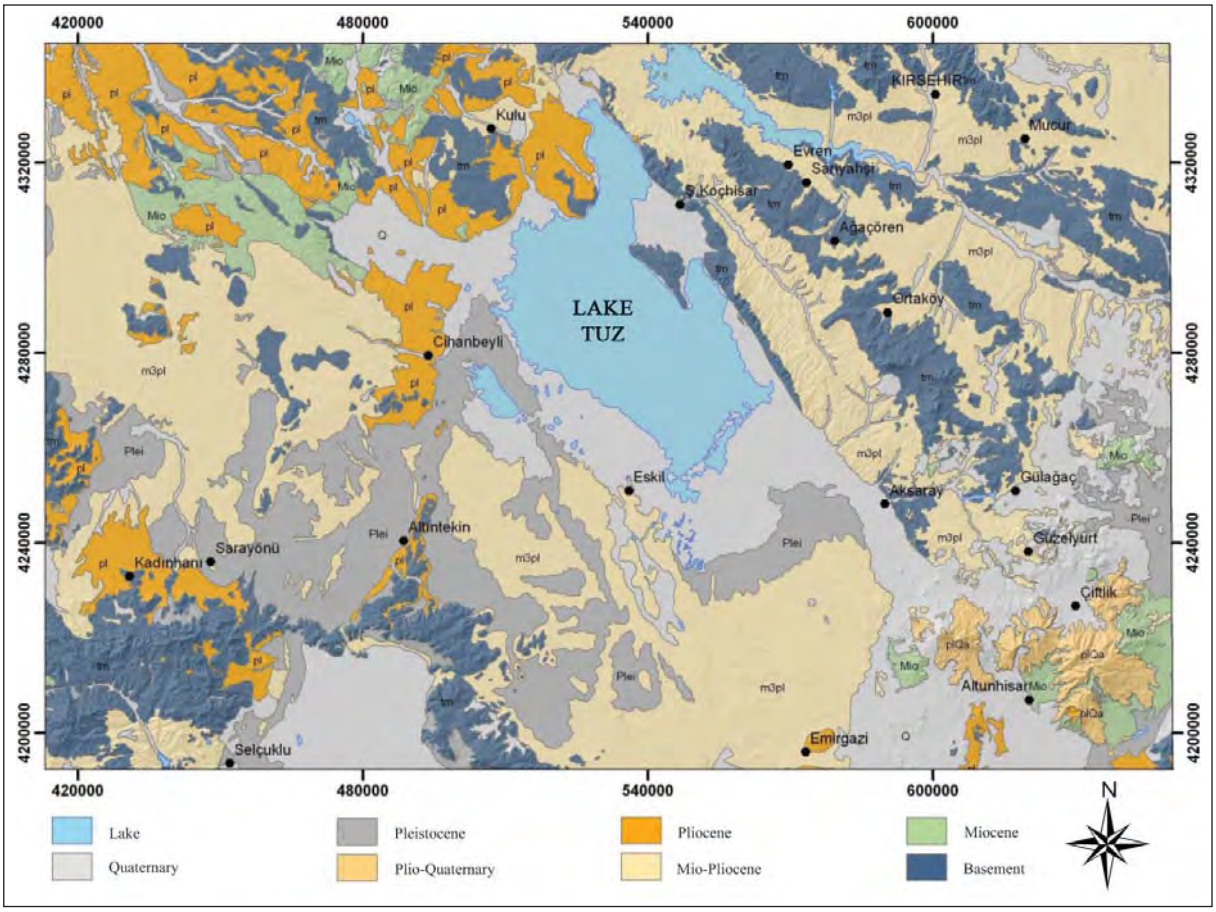

Figure 2- 1:500.000 scaled geology map of Lake Tuz Basin and its surrounding (compiled from MTA, 2002).

believed that this unit composing of alluvial fan deposits was developed under the control of border faults in the basin which opened in the late Cretaceous (Çemen et al., 1999). Above this red clastic unit is a thick sequence which was deposited in shallow-deep-shallow marine environments (Figure 3; Sirel, 1975; Ünalan et al., 1976; Görür and Derman, 1978; Görür, 1981; Dellaloğlu and Aksu, 1984; Görür et al., 1984; Atabey et al., 1987; Oktay and Dellaloğlu, 1987; Özer, 1988; Sonel et al., 1995; Göncüoğlu et al., 1996; Dellaloğlu, 1997; Çemen et al., 1999; Varol et al., 2000; Derman, 2003; Derman et al., 2003; Dirik and Erol, 2003; Ayyıldız, 2006; Uçar, 2008; Huvaz, 2009; Nairn, 2010). Mio-Pliocene deposits represented by terrestrial clastics and carbonates which unconformably overlie the underlying units are the second most widespread unit in the study area after the Quaternary deposits (Figure 2). Because Quaternary deposits are interfingered with the Mio-Pliocene unit, it is important to describe characteristic features of both units.

The Mio-Pliocene deposits start at the bottom with coarse clastics and light brown, loosely-compacted conglomerate-sandstone alternation. They continue to the middle parts with yellowish mudstone-sandstone alternation and end up with greenish, yellowish gray marl and limestone (Figure 4; Ulu et al., 1994*a, b*; Uçar, 2008). Cross-bedding and lensoidal geometry are very common in clastic levels. The unit also contains tuff and gypsum levels. It discordantly overlies underlying lithologies and according to ostracoda species collected from limestone levels the age of unit is suggested to be Pliocene by Tunoğlu et al. (1995) and Beker (2002) and based on spore and pollen data a Mio-Pliocene age is given by Dellaloğlu (1997).

3. Quaternary Units

Quaternary studies have become a separate discipline since active tectonic studies have gained more importance as the mankind could predict his future with the ascertaining of paleo-climate data (Kazancı and Gürbüz, 2012). Young units, so called alluvium in previous works, were not subjected to detailed investigation and therefore they have come

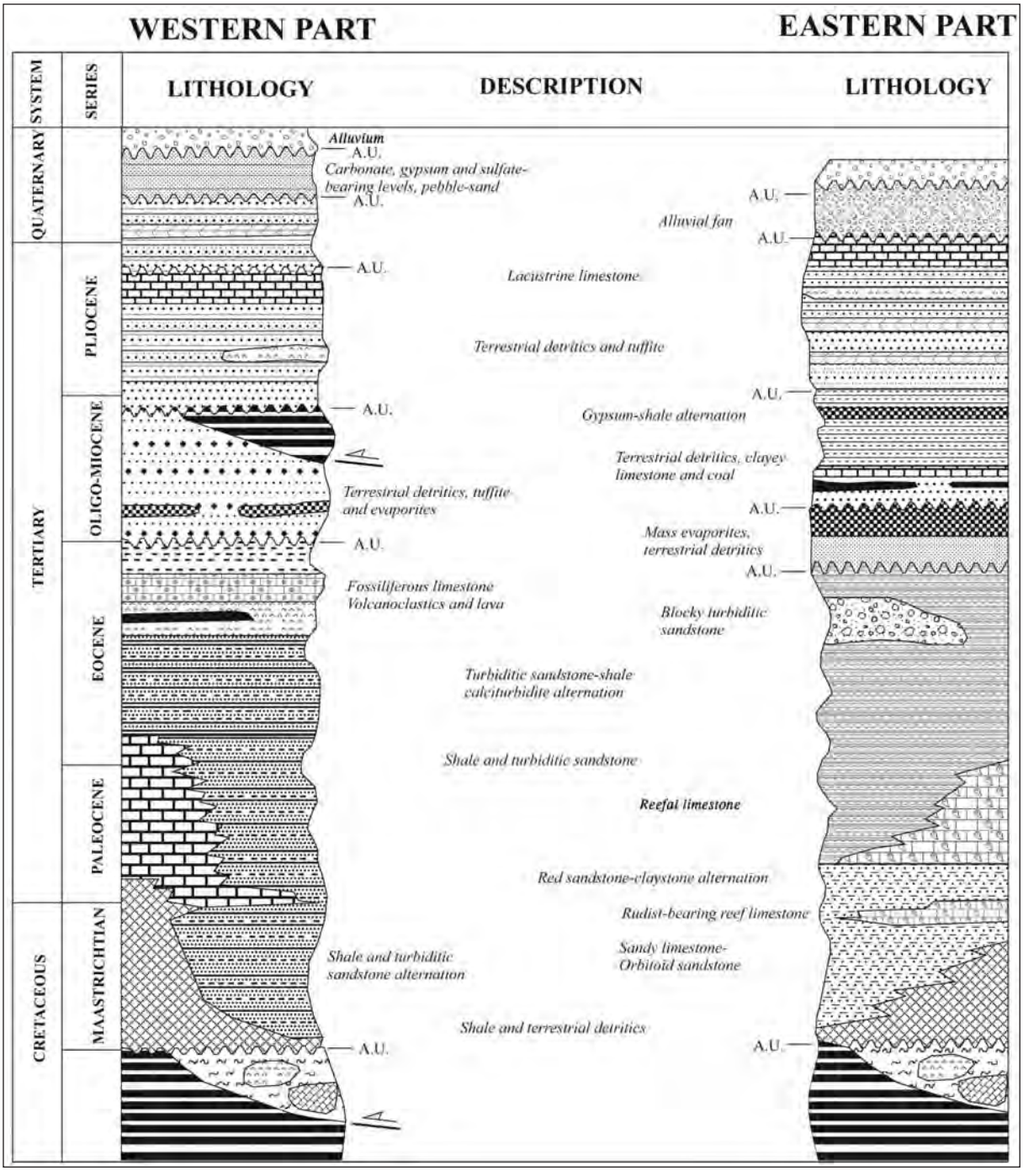

Figure 3- The generalized stratigraphic sections of eastern and western parts of the Lake Tuz Basin (compiled from Dirik and Erol, 2003)

into prominence. Recently this approach has been getting more popular giving rise to investigation in the formation scale of units, which are mapped previously as "young deposits", "recent units" and "alluvium". Likewise, in previous studies on the Lake Tuz Basin, Quaternary deposits that are mapped as alluvium were first mentioned by Erol (1969) and named by Ulu et al. (1994*a, b*) as the Tuzgölü formation of Pleistocene-Quaternary age (Figure 4). Although their bottom-top relations may be different, in recent studies this nomenclature has been frequently adopted (Dirik and Erol, 2003; Özsayın, 2007; Özsayın and Dirik, 2007). In the present study sedimentary facies properties described belong to

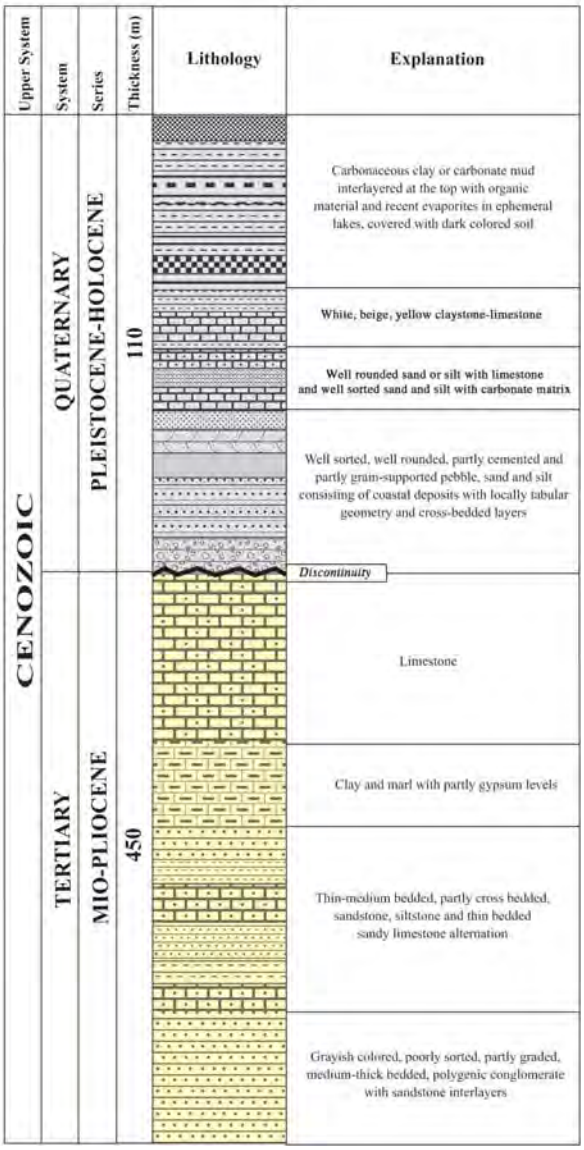

Figure 4- The generalized stratigraphic section for young deposits of the Lake Tuz Basin (from Ulu et al., 1994).

aforementioned adopted unit. This unit is quite important to propound characteristics of old shore lines of Lake Tuz which covered a larger area in the Pleistocene.

In previous works units that are mapped as Plio-Quaternary together with late Pliocene levels have been studied as the Quaternary units considering that the time range of Quaternary era was expanded from 1.8 Ma to 2.6 Ma with an update of International Stratigraphic Guide in 2009 (Mascarelli, 2009; Kazancı, 2009).

Today's Lake Tuz Basin comprising the study area is the Quaternary equivalent of a large and long-lived deposition system. The Miocene units are ended with firm carbonate unit which facilitates separation of these units from younger ones. Drilling works and measured stratigraphic sections in the same region indicate that Pliocene and Quaternary deposits resemble each other in many aspects and stratigraphic borders cannot be often distinguished (Gürbüz, 2012). It was noticed during the surface investigations that red colored Pliocene sediments which are overlain by the Quaternary deposits are loosely compacted and in some sites easily distinguished with their firm character.

As indicated above, lowermost parts of the unit can be only determined with samples from relatively deep boreholes and seismic sections. DSI well logs indicate that lithology of unexposed parts is almost similar to that of exposed rocks. As revealed from drilling data, Quaternary deposits in the basin attain a maximum thickness of 190 m and dominant lithofacies at depths are represented by lacustrine clays (Gürbüz, 2012). It is concluded that facies observed in the upper and lower parts of Quaternary deposits are quite similar.

4. Sedimentology

In order to determine spatial and temporal environmental properties and sedimentary evolution of Quaternary units in the Lake Tuz Basin, areas operated by the private sector as aggregate quarry and the trenches opened by the General Directorate of Highways for extraction of material to be used for road construction and maintenance were utilized and detailed surveys were conducted in 17 different areas and sections with thickness exceeding 10 m were evaluated. Along these sections, 12 lithofacies and 5 facies unit were described (Table 1; Figure 5). Sequences for which facies analysis are completed are from the uppermost part of Tuzgölü formation. They are mostly old lake shore terraces and their equivalent lacustrine deposits differentiated by Erol (1969) are at between 912-980 m. In facies descriptions, definitions of Miall (1978, 1996) and facies described for the Konya Basin (Karabıyıkoğlu, 2003) were considered, which has similar geologic history and geographic features with the study area.

4.1. Lithofacies characteristics of Quaternary deposits

F1- Massive, matrix supported pebble facies: It is red or light/dark brown colored, mostly matrix supported and has slight amount of sand and fine pebble

Table 1- Facies and facies associations of Quaternary deposits based on surface data. Some lithofacies and their explanations are from Miall (1996) and Karabıyıkoğlu (2003).

Facies	Explanations	Facies Association	
Massive, matrix-supported pebble facies	Debris flow deposits, red, dark brown colored, matrix supported. Angular, sub-angular grains. Maximum grain size is 60 cm	Alluvial fan	Basin margin deposits
Massive, red mud facies	Flood plain deposits; red silt and sand lenses, interlayered with matrix supported pebble facies		
Lateral bedded pebble and sand facies	Debris flow deposits, light brown colored poorly sorted moderate to well rounded	Fluvial	Deposits within the basin
Cross bedded, brown pebble and sand facies	River bar deposits; reddish brown colored, moderate to well sorted, well rounded, matrix supported		
Lateral and parallel bedded fine sand, silt and clay facies	Flood plain deposits; red to brown colored		
Ripple-planar sand facies	Wave-current ripples, symmetrical, well sorted lensoidal	Fan delta	
Cross bedded, gray pebble and sand facies	Lateral transition deposits; asymmetrical, moderate to well sorted		
Laminated sand and silt facies	Parallel laminated, well rounded, well sorted, grain components are dark heavy minerals and light colored quartz	Beach	
Clayey carbonate facies	White, grizzly colored	Lake flat	
Massive, beige mud facies	Lake floor sediments, beige, grizzly colored		
Evaporites	Gypsums interlayered with clayey carbonate and marls		
Travertines	Cones or patches with diameter up to a few hundred m		

bounding (Figure 6). Pebbles in the facies are scattered within mud cement. Angular-subangular pebbles are varied depending on the lithology of source rock. Grains are of mostly coarse size and blocks of 60 cm are also found. Massive character and chaotic structure of the unit indicate deposition of debris flow as a result of mass movements.

F2- Massive red mud facies: This facies is composed of red, light/dark brown colored massive mud deposits and silt-clay levels and lenses with lesser amount of pebble (Figure 6). As reflected by textural and color tone differences, bedding is peculiar. Clastic material packing within the facies is indicative of wind-blown process whilst mud deposits indicate that suspended materials are deposited in stagnant water conditions and therefore the unit can be described as flood plain sediment which is observed to alternate with the matrix supported pebble facies.

F3- Lateral bedded pebble and sand facies: This facies is represented by light brown colored, poorly sorted and moderate to well rounded, lateral or low-angle parallel layered mud and grain-supported pebble and sand deposits (Figure 6). Deposits that are found as lenses or mantling within or on the debris flow type sediments with grain size up to block range reveal that they occur not only as debris flows but also over-saturated flood flows as a result of intense rainfall and subsequent ceasing (Karabıyıkoğlu, 2003).

F4- Cross bedded, brown pebble and sand facies: This facies is composed of reddish brown, moderate to well sorted, well rounded, grain-supported pebble and sand deposits (Figure 6). Internally graded cross beddings show that bed load is transported in lateral direction (Rust, 1978). The facies which is deposited on an erosional surface has a limited lateral extent. The unit consisting of river bar deposits changes laterally and vertically to flood plain deposits.

F5- Lateral and parallel bedded fine sand, silt and clay facies: The unit consists of lateral- and parallel-bedded, red and brown fine detrital materials and shows tens of meter lateral extent. It is generally observed below and/or above the lateral- and cross-bedded pebbles (Figure 6). Contacts between the layers are sharp and transitional. In this fine-material facies plant root relicts and desiccation cracks are noticeable. The unit as a whole is a flood plain deposit but fine sand and silt levels within it are crevasse deposits.

F6- Ripple-planar sand facies: This facies is composed of well sorted, tabular-shaped pebble, sand and silt deposits displaying lateral extent and lensoidal geometry with a limited distribution (Figure 6). The unit is in symmetrical form and represented by sigmoidal and wedge-shaped geometry and comprises wave flow and wave deposits of a few to 10-15 cm thickness.

F7- Cross bedded, gray pebble and sand facies: The unit with an asymmetric form and combined sets is

Figure 5- Measured sections and location map of Quaternary deposits on which detailed sequence observations are available.

composed of medium-poorly sorted, medium-well rounded, cross bedded, grain supported pebble and sand deposits (Figure 6). Grain components are varied with respect to spatial distribution of deposits and are mostly of limestone and volcanic rock origin. Erosional forms on the lower surfaces are in planar or trough geometry. Fine mud laminations noticed between the sets are indicative of stagnant water conditions. This facies is generally associated with ripple-planar sand facies. The unit is simply a lateral transition deposit.

F8- Laminated sand and silt facies: This facies is composed of parallel-laminated, well rounded and well sorted slightly pebble and dominantly sand and silt deposits (Figure 6). It has a thickness of 3-8 cm and grains are composed of dark colored heavy minerals and light colored quartz. Deposits that correspond to lower sections of F6 and F7 facies show lateral continuity as long as overlying units are not significantly eroded.

F9- Clayey carbonate facies: The unit which consists of white, grizzly and pinkish colored clayey carbonate and marl deposits is interlayered with F10 and F11 facies or occurs as a thick massive level below and above these facies (Figure 6). Depending on deepening and shallowness of the environment color tone of unit changes occasionally and the pebble-size material of debris flow is also noticeable.

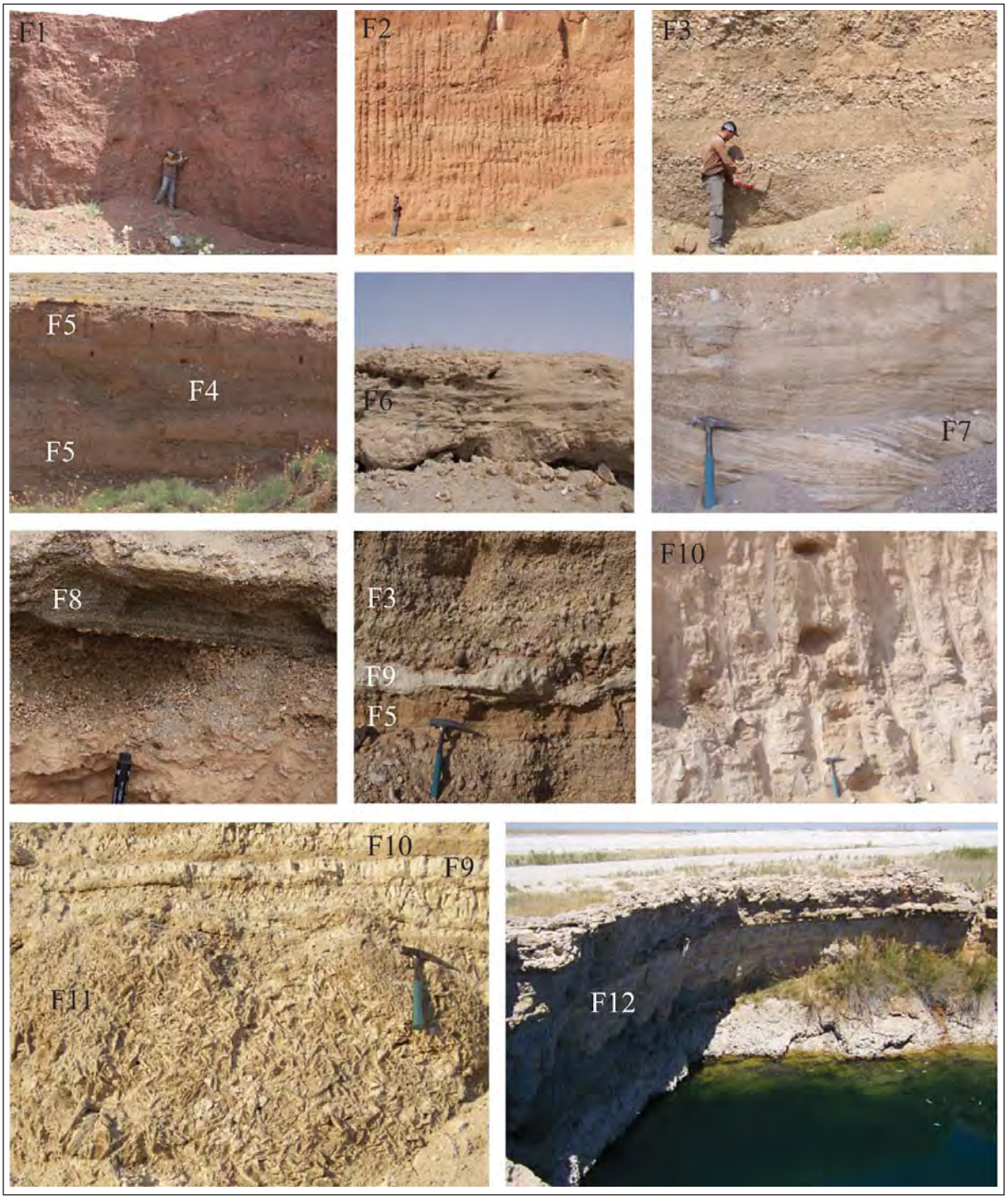

Figure 6- Typical exposures for lithofacies characteristics of Quaternary deposits in the study area. Compare with descriptions given in table 1.

F10- Massive, beige mud facies: The unit is generally in beige, light brown colors but shows dark gray/blackish levels depending on organic material input (Figure 6). Like F9 facies, it rarely contains pebbly flood sediments. In deposits dominated by organic matter herbaceous plant relicts are observed.

F11- Evaporite facies: The unit which is alternated with clayey carbonate and marls is represented by beige, yellow gypsums. It is found as 3-20 cm thickened layers and longitudinal and transverse massive masses within Quaternary units at western part of the basin (Figure 6).

F12- Travertine facies: This facies is determined on old lake flats rather than measured stratigraphic sections (Figure 6). Therefore, stratigraphically it is the youngest unit and can be considered as an independent occurrence with respect to other basin deposits. In areas particularly close to western border of the basin the facies has a conical morphology and is represented by a number of about 60 white travertine cones with diameter ranging from a few to a few hundred m (Figure 7a; Erol, 1967, 1968). At this area aforementioned lithofacies contains abundant plant relicts and relevant pore texture (Figure 7b) and therefore can be named tufa, as will be explained under facies association in the forthcoming section, we name the unit "travertine" since it is more common than the term "tufa" as also described by Erol (1967, 1968). Travertine deposits are also found around thermal water springs in the Aksaray region.

4.2. Depositional environments of Quaternary deposits

As mentioned in previous sections, Quaternary deposits were formed during the closure of the basin. Facies and their spatial distributions indicate that the present sequence with a larger water mass surrounding the recent Lake Tuz covers shore and backshore facies. In this section, facies associations corresponding to depositional environments of each studied facies are introduced. The facies associations are grouped based on their genetic relations (Miall, 1978; Rust, 1978).

FB1- Alluvial fan deposits: This association is composed chiefly of red, light/dark brown, massive, matrix supported pebble facies (F1) and massive red mud facies (F2) (Table 1). In addition, lateral or low-angle layered pebble and sand facies (F3) is also slightly observed. This association that is mainly represented by debris flow and flood plain deposits is particularly traced along the eastern border of the basin. At this area, alluvial fan deposits occur in a narrow belt between the recent shore line of Lake Tuz and the Tuzgölü fault, in front of fault scarps at west part of basin, in areas excavated for material extraction and along the valleys opening to the Lake Tuz. Following the lake deposits, alluvial fan deposits represent the second widespread facies association in the basin. During the field studies, 10-m thickened sequences of these units were examined and it was noticed that alluvial fan facies has lateral and/or low-angle planar surfaces. Particularly most of late Quaternary fans preserve their ideal geometries. The early Quaternary fans overlain by these fans are laterally coalescence.

FB2- Fluvial deposits: The fluvial deposits are found at margins and within the basin and are composed of red and light/dark lateral layered pebble and sand facies (F3), cross bedded, brown pebble and sand facies (F4) and lateral and parallel bedded fine sand, silt and clay facies (F5) (Table 1). Regarding the features of facies association, the deposits are composed of debris flow mostly reflecting braided and meandering river systems, flood flow, river bar, flood plain and crevasse deposits. Deposits which are laterally and vertically transitional to alluvial fan association at margins are very common particularly at east and southeast parts of the basin. At southeast part of the basin, they are in lateral transitional to fan delta deposits (FB3) and in vertical transitional to lake flat deposits (FB5).

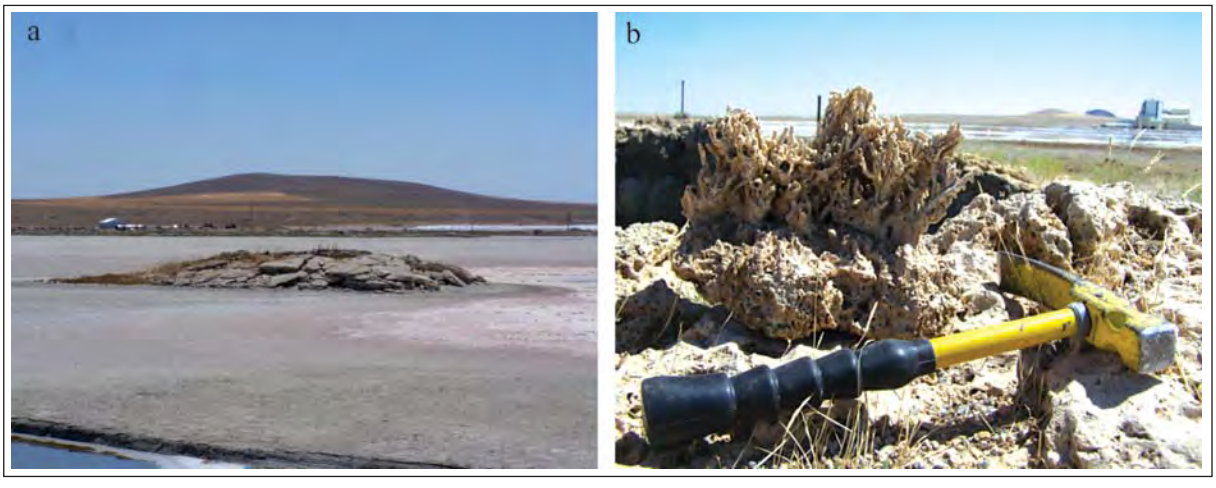

Figure 7- (a) Travertine cones around the Lake Bolluk; (b) Close view of structures with abundant plant relicts.

FB3- Fan delta deposits: This facies association is composed of gray, grizzle and beige ripple-planar sand (F6) and cross bedded, gray pebble and sand (F7) facies. This association is crucially important to reflect the deep character of paleo Lake Tuz (Table 1). Field observations indicated that they are exposed in wide areas just above and in front of the Obruk Plateau in southern part of the basin. The facies is occasionally laterally transitional to fluvial deposits and mostly in vertical transitional to lacustrine muds. This association shows a sequence character with grain size getting coarser to the top and then getting finer. These deposits are well observed along shorelines and correspond to 955 and 930 m of Erol (1969). They are generally composed of volcanic rock fragments and deposits transported by rivers are derived from volcanites at south and southeastern parts of the area. The sequence at the upper level is coarse grained whilst deposits in the lower part (~930 m) are made up of relatively finer grains. Sequences investigated within their own borders display 1.5-2 m thickness indicating relatively deep and high-energy water environment.

FB4- Beach deposits: These deposits that are composed of laminated sand and silt facies (F8) just below the delta sediments represented by the least areal and volumetric distributions (Table 1). However, they are critically important to reveal a larger beach environment which might have an old paleogeographic meaning since sandbank develops in only wave-dominant shores. This means that water depth is relatively higher. From this point of view, it can be said that water level in the old Lake Tuz might occasionally attain depths sufficient enough to generate large waves.

FB5- Mud flat deposits: This association with the widest distribution in the basin is composed of clayey carbonate (F9), massive, beige mud (F10), evaporite (F11) and travertine (F12) facies (Table 1). Lake deposits which have the least thickness but wider exposure area are found to be quite thickened in boreholes opened in the basin (Gürbüz, 2012). The unit was mostly deposited in shallow and calm lacustrine conditions, however considering bluish/greenish colored lower levels, it might also indicate a setting where deep lacustrine environment changes to fluctuating or relatively shallow conditions. Evaporites in western part of basin may be evident for this shoaling process. As stated by Ford and Pedley (1996), travertines at west of basin are mostly laterally and vertically in transition with lacustrine facies indicating that alkaline spring waters flow into a lacustrine area and intense algae production in shallow conditions are accompanied by aquatic plants (Alçiçek et al., 2004). In systems where lake margins are directly leaned on basement rocks such carbonate formations might be indicative of concurrent tectonism and groundwater recharge to the lake. Erol (1967-68, 1969) described these occurrences along the shore as travertine cones (Atabey, 2003). These formations with detailed lithofacies descriptions can be termed as tufa because they have abundant plant relicts and pore structures. In lacustrine environments tufas develop at depths less than 1 m (Atabey, 2003). If the lake water is salty they can be generated by bacteria and blue-green algae accumulations around the freshwater manifestations (Pedley, 1990; Atabey, 2003). Pentecost (1993), Pentecost and Viles (1994) and Ford and Pedley (1996) combined all tufa descriptions under the travertine term and classified travertines with respect to temperature condition (Atabey, 2003). In the literature, America, Europe and all Spanish-speaking countries (21 countries), tufa description is considered within the context of travertine and not used as a different term (Atabey, 2003).

5. Discussion: Control Mechanisms

Sequence examinations in the field indicate that Lake Tuz, which is recently receded to the northeast of the basin, covered large areas in the Pleistocene towards the south and west (Figures 5, 8). Fan delta sequences and very thick, widespread lake basement deposits imply that depth of paleo Lake Tuz was much more than that of present-day. Taking into account the surface area and water depth of this high-energy lake, the Lake Tuz is classified as large lake (500-5000 km^2) and very shallow lake (1-5 m) by Kazancı (2012), however in Pleistocene it was a very large lake (~7500 km^2) with respect to area and shallow or moderate-depth lake (20-100 m) with respect to depth. Similar approaches for the Lake Tuz were first put forward by Salomon-Calvi and Kleinsorge (1939) and their study was improved nearly half-century ago by Oğuz Erol who first used the geomorphologic data. In addition, based on his studies in southeast part of the basin, Kashima (2002) suggested that in late Pleistocene (about 20 ka before present) the Lake Tuz floor was 15 m higher than today. In the Konya basin which is the equivalent of Lake Tuz basin, a lacustrine environment covering an area of about 4500 km^2 with depth of 25-30 m was reported in late Pleistocene (see Karabıyıkoğlu and Kuzucuoğlu, 1998). Since these two large Pleistocene lakes are within the same recharge area and are interconnected regarding

groundwater dynamics, conjugate results from these lakes are not too much surprised.

The closed basin lakes are very sensitive to changes at the bottom of basin. In general, tectonism controls the surface area of basin and, in case of contemporaneous with the deposition, it defines the characteristics of deposition systems. The climate is primarily responsible for the amount of water that enters to the basin via precipitation and drainage and removed from the basin through evaporation. Other factors such as the effect of climate on vegetation and the amount of sediment transported also play important role in this process (Ilgar, 2004).

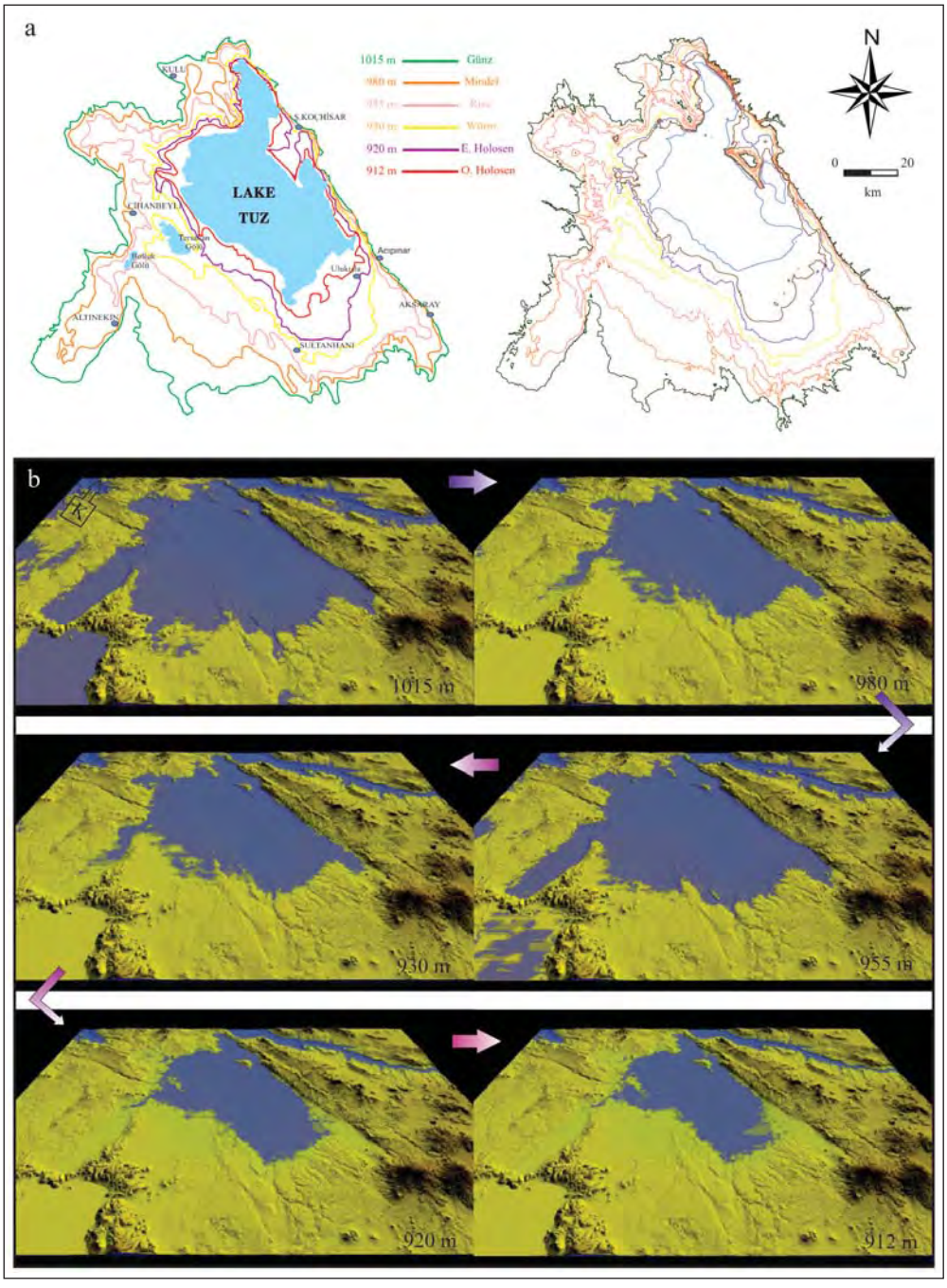

Figure 8- (a) On 1:100.000 scaled map distributions of variations and stages of shore line of Lake Tuz (Erol, 1969) in the Quaternary (left) and reconstructed shore lines of Erol (1969) on 1:25.000 scaled map (right); (b) spatial distribution of Quaternary shore lines of Erol (1969) reconstructed with respect to recent topography and their relation with surrounding areas based on this topography.

As stated by Erol (1969; Figure 8), in the Lake Tuz basin there is a lacustrine sediment distribution which gradually covered and/or leaved both Lake Tuz sub-basin and other sub-basins such as Kulu, Yeniceoba, Altınekin and Tersakan (Figures 8, 9 and 10). Spatial distribution of these deposits can only be controlled by tectonic events. Although, like in other regions in Turkey, an apparent steepness showing the effect of tectonic disturbance is not noticed in morphology, these sub-basins, in regional scale, are ultimately separated from each other by structural factors and thus, most are active even though the region is seismologically inactive (Figures 9, 10). The main ones of these structures are Eskişehir fault zone (Şaroğlu et al., 1987; Altunel and Barka, 1998; Ocakoğlu, 2007), Yeniceoba, Cihanbeyli and Altınekin fault zones (Çemen et al., 1999; Dirik and Erol, 2003; Özsayın, 2007; Özsayın and Dirik, 2007, 2011; Akıl, 2008; Gürbüz, 2012; Özsayın et al., 2013), Tersakan-Sultanhanı fault zone (Gürbüz, 2012) and Tuzgölü fault zone (Beekman, 1966; Şaroğlu et al., 1987; Leventoğlu, 1994; Çemen et al., 1999; Koçyiğit, 2003; Toprak, 2003; Kürçer and Gökten, 2012). Alluvial fan deposits, which are well developed particularly at east of the basin, are deposited under the control of NW-SE extending Tuzgölü fault. The results of dating studies of Kashima (2002) and Kürçer and Gökten (2012) indicate that fan deposits are formed at the beginning of Holocene. This implies that the high lake level in late Pleistocene was lowered because of climate-induced effects. In addition, the Quaternary volcanism at south of basin is another agent controlling the amount and diversity of material transported to the basin. This is supported by the

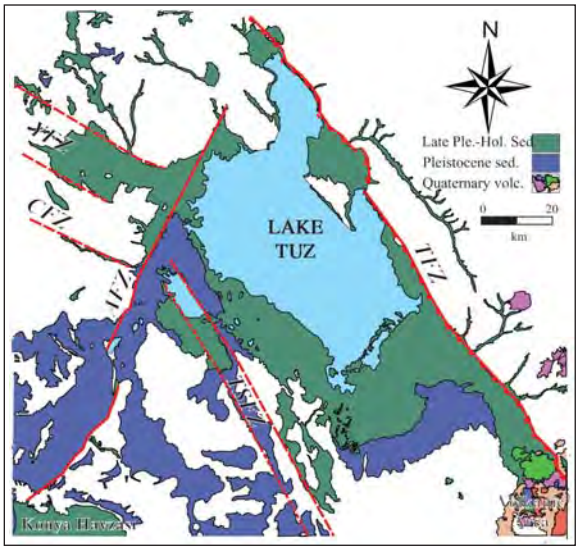

Figure 9- Simplified map of Quaternary units in the study area and major structural elements controlling them (distribution and ages of units are compiled from MTA, 2002). Compare the spatial distribution of faults with shore lines in figure 8. TFZ – Tuzgölü Fault Zone; TSFZ – Tersakan-Sultanhanı Fault Zone; AFZ – Altınekin Fault Zone; YFZ – Yeniceoba Fault Zone; CFZ – Cihanbeyli Fault Zone.

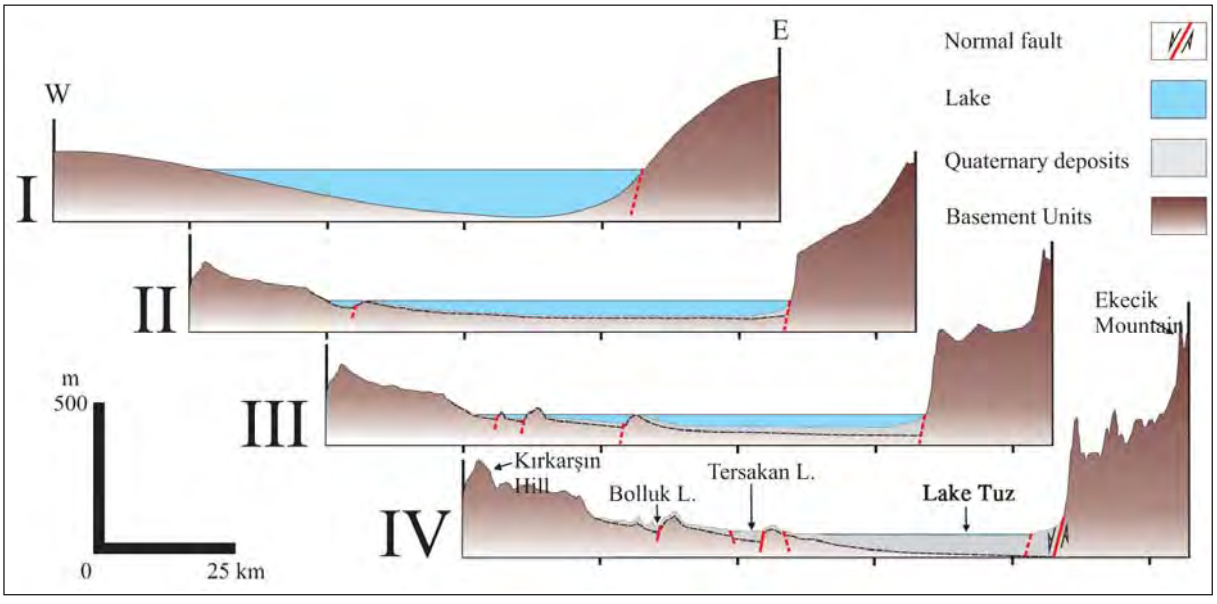

Figure 10- Evolution of Lake Tuz basin in E-W direction in time-independent 4 different stages. Sketch showing the fragmentation of paleo lake area and Quaternary deposition sites while basin has been gradually collapsing to gain its recent shape since the early Pleistocene.

volcanic origin of components in clastics comprising the beach deposits and Pleistocene fan delta which is exposed along the southern part.

Special structures of conical-shaped travertine deposits at west have a unique meaning to the basin regarding tectonic and climate events. In the area where cones widely occur, their linear-like appearance, as stated previously by Erol (1967-68), is indicative of a structural control. This is also supported by the presence of an active fault along this line, which is named Zıvarık fault by Erol (1969), Konya fault zone by Eren (2003), Konya-Bulok fault zone by Koçyiğit (2003) and Altınekin fault in several studies (Çemen et al., 1999; Dirik and Erol, 2003; Özsayın and Dirik, 2007, 2011; Gürbüz, 2012). On the other hand, climate was also shown to be powerful agent in development of travertine deposits. Although these cones seem to be developed along a structurally-controlled line in that part of basin, individual structures with their conical geometry may indicate that each cone is associated with water manifestation. As mentioned in the previous section, development of these deposits is related with freshwater flux. Moreover, individual structure of travertines requires different geochemical conditions for the fluids by means of chemistry and temperature (Pedley, 1990). Cold freshwaters that precipitate such cones might have been released into a saline and relatively hot lacustrine environment. This indicates that chemistry and temperature of Bolluk lake water during the deposition of travertines are very similar to those of present time.

Considering the width and relatively deeper water level of lake that occupied the basin during the Pleistocene, water-evaporation balance that could recharge this lake must have been much greater than current difference (50 x10^3 m^3/y) which is in favor of recharge waters. It is revealed from the morphology of the Lake Tuz drainage basin is that, for such a region, where river network is not beyond the borders of Lake Tuz and Konya basins, the expected direct recharge from the rainfall and groundwater is more than the current value. Since the basin under investigation is a closed one, evaporation process will be very limited and takes place under wet/rainy conditions. These conditions are also suggested for the Konya basin which is the equivalent of Lake Tuz basin (Karabıyıkoğlu, 2003). Although there are findings implying intermittent short-term wet and cold climate conditions in last period of Pleistocene, pollen analysis yielded strong data to suggest this period was arid and cold (van Zeist and Bottema, 1982, 1991; Bottema, 1987). This contradiction is explained by Roberts (1983) as the facilitation of low evaporation by cold and cloudy climate conditions (Karabıyıkoğlu, 2003).

On the other hand, it should be taken into account that during the Pleistocene lake basin was connected to the Konya basin to the south and therefore it must have had a wider recharge area. This, in turn, means that Lake Tuz is recharged from a wide area through the Taurus Mountains at south. Moreover, the river network must have been established by strong-flow streams rather than today's ephemeral low-current streams. This is strongly supported by the presence of fan delta sediments on old shorelines extending along the southern part of the basin. It is thought that the "Konya Plain Main Discharge Canal" is connected to Lake Tuz via a natural channel between the two basins and as a result, the region, in a large scale, has been regarded as the "Konya Closed Basin" (Figure 11). Although groundwater is interconnected under these basins, there has been no surface water connection with the exception of discharge canal. In the frame of Konya Wastewater Treatment Facility project which was taken into operation in 2009, discharge canal was disconnected. Therefore, Lake Tuz closed basin and Konya closed basin should be investigated separately. As mentioned previously, in Pleistocene these basins were connected to each other, however, by Holocene the basins were disconnected as a result of different climatic and tectonic controls.

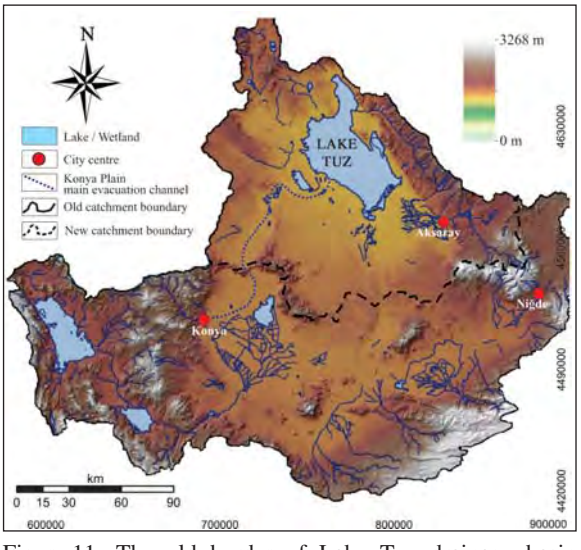

Figure 11- The old border of Lake Tuz drainage basin within the Konya Closed Basin and the border of new surface drainage basin that has been narrowed by the termination of the Konya Plain Main Discharge Canal.

Lake level fluctuations presented by Erol (1969) spatially coincide with our results. Therefore, it is possible to say that studies of Erol (1969) are far beyond the expectations of that period and the boundaries he suggested for lake shore oscillations are confirmed by our observation of proposed deposits. However, such consistency by means of morphosedimentary could not be noticed temporally because all fluctuations have been previously linked to fluvial stages.

6. Results

In this study detailed sequence examinations were carried out particularly in south and east parts of the Lake Tuz basin and as a result the Quaternary deposits were differentiated under 12 lithofacies and 5 facies units. As shown from the these facies distributions, the Lake Tuz, which corresponds to large and very shallow lake category, in Pleistocene covered an area nearly 5 times larger than its present area which classifies the Lake Tuz into a very large, shallow/moderate depth lake. Considering spatial characteristics of lithofacies, material was transported to the lake chiefly from east and southeastern parts where morphology is controlled by tectonism and volcanism. Tectonism played an important role in recession of lake area gradually into recent position. Sub-basins which are the relicts of Lake Tuz such as Bolluk, Tersakan, Eşmekaya lakes and several waterlands have been situated as separate benches within depressions formed by several faults. In the basin lake flat deposits are the most widespread deposits which are followed by alluvial fan sediments. During the Pleistocene which was prevailed by tectonism and climate dynamics, the amount of water recharging the basin is believed to be greater than recent time, however, a slight change in water level due to low relief of basin floor resulted in the expansion of lake. Therefore, in the basin there is no well-developed fluvial system reaching to the lake. Climate-induced lake level drop at the beginning of Holocene gave rise to deposition of thick alluvial fan sequences at eastern part of basin which is controlled by the Tuzgölü fault.

Acknowledgements

This study was supported by the Ankara University under grand no. 09B4343017. The study covers a part of Alper Gürbüz's Ph.D. thesis which was completed at the Ankara University by the supervision of Dr. Nizamettin Kazancı. Uğur Erdem Dokuz (AU), Sonay Boyraz Aslan and Esra Gürbüz (ASU) helped during the field studies, Zeynep Ataselim, Mustafa Eruzun, Ezgi Güllü (AU), Koray Koç (AKDU) and Tuğba Sezen (FSU) helped in the laboratory works and Sinan Akıska, Özgür Yedek (AU) and Azad Sağlam Selçuk (YYU) are greatly acknowledged for their help in the office works. We are grateful for helpful comments and constructive reviews by Drs. Baki Varol, Gürol Seyitoğlu, Yusuf Kağan Kadıoğlu, Abdullah Ateş (AU), İsmail Ömer Yılmaz (METU), Ömer Feyzi Gürer (KOU), Fuat Şaroğlu (JEMIRKO), Attila Çiner (ITU) and an anonymous reviewer.

Received: 20.11.2013
Accepted: 21.04.2014
Published: December 2014

References

Akıl, B. 2008. İnönü-Eskişehir Fay Sistemi'nin Günyüzü (Eskişehir) - Yeniceoba (Konya - Türkiye) arasındaki bölümünün yapısal evrimi. Ph.D. Thesis, Hacettepe University, 126 s, Ankara (in Turkish; unpublished).

Akıman, O., Erler, A., Göncüoğlu, M.C., Güleç, N., Geven, A., Türeli, K., Kadıoğlu, Y.K. 1993. Geochemical characteristics of granitoids along the western margin of the Central Anatolian Crystalline Complex and their tectonic implications. *Geological Journal*, 28, 371-382.

Alçiçek M.C., Kazancı, N., Özkul, M., Şen, Ş. 2004. Çameli (Denizli) Neojen Havzası'nın tortul dolgusu ve jeolojik evrimi. *Bulletin of the Mineral Research and Exploration*, 128, 99-123 (in Turkish).

Altunel, E., Barka, A. 1998. Eskişehir fay zonunun İnönü-Sultandere arasında neotektonik aktivitesi. *Türkiye Jeoloji Bülteni*, 41, 41-52 (in Turkish).

Arıkan, Y. 1975. Tuzgölü havzasının jeolojisi ve petrol imkanları. *Bulletin of the Mineral Research and Exploration*, 85, 17-38 (in Turkish).

Atabey, E., 2003. Tufa ve traverten. TMMOB Jeoloji Mühendisleri Odası Yayınları No:75, 106 s (in Turkish).

Atabey, E., Tarhan, N., Akarsu, B., Taşkıran, A. 1987. Şereflikoçhisar, Panlı (Ankara) Acıpınar (Niğde) Yöresinin Jeolojisi. *Maden Tetkik ve Arama Genel Müdürlüğü Raporu*, Derleme no; 8155, Ankara (unpublished).

Aydemir, A., Ateş, A. 2008. Determination of hydrocarbon prospective areas in the Tuzgölü (Saltlake) Basin, central Anatolia, by using geophysical data, *Journal of Petroleum Science and Engineering*, 62, 36-44.

Ayyıldız, T. 2006. Hydrocarbon potential of Karapınar-yaylası formation (Paleocene to Eocene) source

rock in the Tuz Gölü Basin, Central Anatolia, Turkey", *Petroleum Geoscience*, 12, 41-48.

Beekman, P. H. 1966. The Pliocene and Quaternary volcanism in the Hasan Dağ- Melendiz Dağ region. *Bulletin of the Mineral Research and Exploration*, 66, 90-105.

Beker, K. 2002. İnsuyu Kireçtaşları (Karapınar/Konya) Ostrakod Topluluğunun Biyostratigrafik ve Kronostratigrafik İncelenmesi. Hacettepe University Fen Bilimleri Enstitüsü, Ankara, M.Sc. Thesis, 93 s. (in Turkish; unpublished).

Bottema, S. 1987. Chronology and climatic phases in the Near East: From 16000 to 10000 BP, In: Chronologies in the Near East, Eds: O. Aurenche, J. Evin, P. Hours, BAR International Series, 295-310. Oxford.

Çamur, M. Z., Mutlu, H. 1996. Major-ion geochemistry and mineralogy of the Salt-Lake (Tuz Gölü) basin, Turkey. *Chemical Geology*, vol.127, pp.313-329.

Çemen, İ., Göncüoğlu, M.C., Dirik, K. 1999. Structural evolution of the Tuzgölü basin in Central Anatolia. Turkey, *Journal of Geology*, 107 (6), 693-706.

Dellaloğlu, A. 1997. Ankara ili-Tuzgölü arasındaki Neotetis'in kuzey kolunun evrimi (Haymana-Tuzgölü Basenlerinin stratigrafileri ve jeoteknik evrimleri), Ph.D. Thesis, Çukurova University, Adana 332 s. (in Turkish; unpublished).

Dellaloğlu, A., Aksu, R., 1984. Kulu-Şereflikoçhisar-Aksaray dolayının jeolojisi ve petrol olanakları. *TPAO Rapor* no: 2020 (in Turkish; unpublished).

Derman, A. S. 2003. Tuzgölü baseni evaporit problemi ve yeni veriler. TPJD Özel sayı, 5, 99-112 (in Turkish).

Derman, A. S., Rojay, B., Güney, H., Yıldız, M. 2003. Koçhisar-Aksaray fay zonu'nun evrimi hakkında yeni veriler. Haymana-Tuzgölü-Ulukışla basenlerinin uygulamalı çalışması, Aksaray. Bildiri Özleri Kitabı, 1 (in Turkish).

Dirik, K., Erol, O. 2003. Tuzgölü ve çevresinin tektonomorfolojik evrimi, Orta Anadolu-Türkiye, *TPJD Özel sayı*, 5, 27-46 (in Turkish).

Eren, Y., 2003. Konya bölgesinin depremselliği. TPJD Özel Sayı, 5, 85-98 (in Turkish).

Erler, A., Akıman, O., Unan, C., Dalkılıç, B., Geven, A., Önen, P. 1991. Kaman (Kırşehir) ve Yozgat yörelerinde Kırşehir Masifi magmatik kayaçlarının petrolojisi ve jeokimyası. *Doğa*, 15, 76-100 (in Turkish).

Erol, O. 1967-68. Cihanbeyli güneyinde, Boluk Gölü çevresindeki traverten konileri, *Türk Coğrafya Dergisi*, 24-25, 65-98 (in Turkish).

Erol, O. 1969. Tuzgölü Havzasının jeolojisi ve jeomorfolojisi. TÜBİTAK Raporu (in Turkish; unpublished).

Ford, T.D., Pedley, H.M. 1996. A review of tufa and travertine deposits of the world. *Earth Science Reviews*, 41, 117-175.

Gilbert, K.G. 1885. The topographic features of lake shore. USGS 5th annual report, 69-123.

Gilbert, K.G. 1890. Lake Bonneville, USGS Monograph 1, 438 p.

Göncüoğlu, M. C. 2011. Kütahya-Bolkardağı kuşağının jeolojisi. *Bulletin of the Mineral Research and Exploration*, 142, 227-282 (in Turkish).

Göncüoğlu, M.C., Toprak, G.M.V., Kuşçu, İ., Erler, A., Olgun, E. 1991. Geology of the western part of the Central Anatolian Massif, Part 1: Southernpart, Ankara, Turkey. *METU-TPAO Proje Raporu*, 140 s. (in Turkish; unpublished).

Göncüoğlu, M. C., Erler, A., Toprak, V., Yalınız, K., Olgun, E., Rojay, B. 1992. Orta Anadolu Masifi'nin batı bölümünün jeolojisi, Bölüm 2: Orta Kesim. *TPAO Rapor* No: 3535 (in Turkish; unpublished).

Göncüoğlu, M.C., Erler, A., Toprak, V., Olgun, E., Yalınız, K., Kuşçu, İ., Köksal, S., Dirik, K. 1993, Orta Anadolu Masifinin Orta Bölümünün Jeolojisi, Bölüm 3: Orta Kızılırmak Tersiyer Baseninin Jeolojik Evrimi. *TPAO Rapor* No: 3313, 104 s (in Turkish).

Göncüoğlu, M. C., Dirik, K., Erler, A., Yalınız, K., Özgül, L., Çemen, İ. 1996. Tuzgölü havzası batı kısmının temel jeolojik sorunları. TPAO Rapor No: 3753 (in Turkish; unpublished).

Görür, N. 1981. Tuzgölü-Haymana havzasının stratigrafik analizi. İç Anadolu'nun Jeolojisi Sempozyumu, TJK 35. Bilimsel ve Teknik Kurultayı Bildiriler Kitabı, 60-65 (in Turkish).

Görür, N., Derman, A.S. 1978. Tuzgölü-Haymana havzasının stratigrafik ve tektonik analizi. TPAO Raporu no: 1514, 60 s. (in Turkish; unpublished).

Görür, N., Oktay, F.Y., Seymen, İ., Şengör, A.M.C. 1984. Paleotectonic evolution of the Tuzgölü basin complex, Central Turkey Sedimentary Record of a Neo- Tethyan closure, The Geological Evolution of the Eastern Mediterranean. Geology Society Special Publication, 17, In J.E. Dixon and A.H.F. Robertson (eds.) Oxford, 467-482.

Gürbüz, A. 2012. Tuz Gölü Havzası'nın Pliyo-Kuvaterner'deki Tektono-sedimanter evrimi, Ph.D. Thesis, Ankara University, 130 s (in Turkish; unpublished).

Huvaz, Ö. 2009. Comparative petroleum systems analysis of the interior basins of Turkey: Implications for petroleum potential. *Marine and Petroleum Geology*, 26, 1656–1676.

Ilgar, A. 2004. Zorunlu regresyon, transgresyon ve sediman getiriminin, havza kenarı çökelme sistemlerinin sedimantolojik ve istif stratigrafik gelişimi üzerindeki kontrolü, Ermenek Havzası (Orta Toroslar). *Bulletin of the Mineral Research and Exploration*, 128, 49-78 (in Turkish).

Irion, G., Müller, G. 1968, Huntite, magnesite, and polyhalite of recent age from Tuz Gölü, Turkey: *Nature*, 220, 1309-1310.

Kadıoğlu, Y.K., Dilek, Y., Güleç, N., Foland, K.A. 2003. Tectonomagmatic Evolution of Bimodal Plutons in the Central Anatolian Crystalline Complex, Turkey. *The Journal of Geology* 111, 671-690.

Karabıyıkoğlu, M. 2003. Konya Havzasının Geç Kuvaterner Evrimi. Ph.D. Thesis, Istanbul University, 239 s., Istanbul (in Turkish; unpublished).

Karabıyıkoğlu, M., Kuzucuoğlu, C. 1998. Late Quaternary chronology, environmental evolution and climatic change of the Konya basin. Mineral Research and Exploration Report No: 10168, 189, (unpublished).

Karabıyıkoğlu, M., Kuzucuoğlu, C., Fontugne, M., Kaiser, B., Mouralis, D. 1999. Facies and depositional sequences of the Late Pleistocene Göçü shoreline system, Konya basin, Central Anatolia: Implications for reconstructing lake level changes, In: N. Roberts, C. Kuzucuoğlu and M. Karabıyıkoğlu (Eds.) The Late Quaternary in the Eastern Mediterranean Region, *Quaternary Science Reviews*, 18, 593–609.

Kashima, K. 2002. Environmental and climatic changes during the last 20000 years at Lake Tuz, central Turkey. *Catena*, 48, 3-20.

Kazancı, N. 2009. Neojen-Kuvaterner sınırının değişmesi ve beklenen gelişmeler. *Türkiye Jeoloji Bülteni*, 52(3), 367-374 (in Turkish).

Kazancı, N. 2012. Göller ve gölsel süreçler. İç: Kuvaterner Bilimi, Ed: Kazancı, N. ve Gürbüz, A., Ankara Üniversitesi Yayınları No:350. s. 389-410. ISBN:978-605-136-056-0 (in Turkish).

Kazancı, N., Gürbüz, A. (Ed.) 2012. Kuvaterner Bilimi. Ankara Üniversitesi Yayınları No:350, 570 s. ISBN: 978-605-136-056-0 (in Turkish).

Koçyiğit, A. 2003. Orta Anadolu'nun genel neotektonik özellikleri ve depremselliği, TPJD Özel Sayı, 5, 1-26 (in Turkish).

Kuzucuoğlu, C., Bertaux, J., Black, S., Denefle, M., Fontugne, M., Karabıyıkoğlu, M., Kashima, K., Limondin-Lozouet, N., Mouralis, D., Orth, P. 1999. Reconstruction of climatic changes during the late Pleistocene, based on sediment records from the Konya basin (Central Anatolia, Turkey), *Geological Journal*, Special Issue on Turkish Geology, 34, 175-198.

Kürçer, A., Gökten, E. 2012, Paleoseismological three dimensional virtual photography method; a case study: Bağlarkayası-2010 trench, Tuz Gölü Fault Zone, Central Anatolia, Turkey. InTech (Tectonics-Recent Advances), p. 201–228, doi: 10.5772/48194.

Leng, M. J., Roberts, N., Reed, J. M., Sloane, H. J. 1999. Late Quaternary palaeohydrology of the Konya basin, Turkey based on isotope studies of modern hydrology and lacustrine carbonates. *Journal of Paleolimnology*, 22, 187-204.

Leventoğlu, H. 1994. Neotectonic Characteristics of the Central Part of the Tuzgölü Fault Zone Around Mezgit (Aksaray). M.Sc. Thesis, ODTÜ, Ankara, 86 s (in Turkish).

Mascarelli, A.L. 2009. Quaternary geologists win time scale vote. *Nature* 459/4 (June), p. 624.

Miall, A.D. 1978. Lithofacies types and vertical profile models in bradied river deposits: A summary. Miall, A.D. (ed). Fluvial Sedimentology. *Canadian Society of Petroleum Geologists Memoir* 5, 597-604.

Miall, A.D. 1996. The Geology of Fluvial Deposits. Springer-Verlag, Heidelberg. 582 s.

MTA, 2002. 1/500 000 ölçekli Türkiye Jeoloji Haritası, 18 pafta. Ankara.

Nairn, S. 2010. Testing alternative models of continental collision in Central Turkey by a study of the sedimentology, provenance and tectonic setting of Late Cretaceous–Early Cenozoic syn-tectonic sedimentary basins. The University of Edinburgh, PhD Thesis. 395 p (in Turkish).

Ocakoğlu, F. 2007. A re-evaluation of the Eskişehir fault zone as a recent extensional structure in NW Turkey. *Journal of Asian Earth Sciences*, 31, 91-103.

Oktay, F. Y. Dellaloğlu, A. A. 1987. Tuzgölü Havzası (Orta Anadolu) stratigrafisi üzerine yeni görüşler. Türkiye 7. Petrol Kongresi bildiriler kitabı, 312-321 (in Turkish).

Özer, S. 1988. Orta-Doğu-Güneydoğu Anadolu ve Kocaeli Yarımadasında bulunan Pironaea (Rudist) türlerinin paleontolojisi ve Biyocoğrafyası, *Türkiye Jeoloji Kurumu Bülteni*, 31, 47-58 (in Turkish).

Özsayın, E. 2007. İnönü-Eskişehir Fay Sisteminin Yeniceoba-Cihanbeyli (Konya – Türkiye) Arasındaki Bölümünün Neojen-Kuvaterner Yapısal Evrimi. Ph.D. Thesis, Hacettepe University, Ankara, 120 (in Turkish; unpublished).

Özsayın, E., Dirik, K. 2007. Quaternary activity of the Cihanbeyli and Yeniceoba Fault Zones: İnönü-Eskişehir Fault System, Central Anatolia. *Turkish Journal of Earth Sciences*, 16, 471-492.

Özsayın, E., Dirik, K. 2011. The role of oroclinal bending in the structural evolution of the Central Anatolian Plateau: evidence of a regional change over from shortening to extension. *Geologica Carpathica*, 62 (4), 345-359.

Özsayın, E., Çiner, A., Rojay, B., Dirik, K., Melnick, D., Fernandez-Blanco, D., Bertotti, G., Schildgen, T.F., Garcin, Y., Strecker, M.R., Sudo, M. 2013, Plio-Quaternary Extensional Tectonics of the Central Anatolian Plateau: A case study from the Tuz Gölü Basin, Turkey. *Turkish Journal of Earth Sciences*, , doi:10.3906/yer-1210-5.

Pedley, H. M. 1990. Classification and environmental models of cool freshwater tufas. *Sedimentary Geology*, 68, 143-154.

Pentecost, A. 1993. British travertine: a review. *Proc. Geol. Assoc*. 104, 23-39.

Pentecost, A., Viles, H. 1994. A review and reassesment of travertine classification. *Geogr. Phys. Quaternaire* 48, 305-314.

Reed, J. M., Roberts, N., Leng, M. J. 1999. An evaluation of the diatom response to Late Quaternary environmental change in two lakes in the Konya Basin, Turkey, by comparison with stable isotope data. *Quaternary Science Reviews* 18, 631-646.

Roberts, N. 1983, Age, palaeoenvironments, and climatic significance of Late Pleistocene Konya Lake, Turkey. *Quaternary Research*, v. 19, p. 154-171.

Roberts, N., Erol, O., de Meester, T., Uerpmann, H. P. 1979. Radiocarbon chronology of Late Pleistocene Konya Lake, Turkey. *Nature*, 281, 662-664.

Roberts, N., Black, S., Boyer, P., Eastwood, W. J., Leng, M., Parish, R., Reed, J.,Twigg, D., Yiğitbaşoğlu, H. 1999. Chronology and stratigraphy of Late Quaternary sediments in the Konya Basin, Turkey: results from the KOPAL project. *Quaternary Science Reviews*, 18, 611-630.

Rust, B.R. 1978. Depositional models for braided alluvium. Miall, A.D. (ed). Fluvial sedimentology, *Canadian Society of Petroleum Geologists Memoir* 5, 605-625.

Salomon-Calvi, W., Kleinsorge, H. 1939. Merkezi Anadolu'nun birkaç tuz gölünde yapılmış olan tetkikata ait rapor. MTA Rapor No: 972, Ankara (in Turkish; unpublished).

Sirel, E., 1975. Polatlı (GB Ankara) güneyinin stratigrafisi. *Türkiye Jeoloji Bülteni*, 18, 181-192 (in Turkish).

Sonel, N., Kulke, H., Sarı, A., Acar, A., Ayyıldız, T., Kadıoğlu, Y., Özkul, M., Yıldız, A., Doğan, U., Habo, M., Paeghe, W., Doğan, M. 1995. Tuzgölü havzasının jeolojisi ve hidrokarbon potansiyelinin değerlendirilmesi projesi. TPAO 1. Faaliyet Raporu, 27 s (in Turkish) (unpublished).

Şaroğlu, F., Emre Ö., Boray, A. 1987. Türkiye'nin Diri Faylari ve Depremsellikleri: Maden Tetk. Arama Genel Müdürlüğü Jeol. Etüd. Dairesi Başkanlığı, Ankara, III+394 s.+11 harita (in Turkish).

Tekin, E., Ayyıldız, T., Gündoğan, İ., Orti, F. 2007. Modern halolites (halite oolites) in the Tuz Gölü, Turkey, *Sedimentary Geology*, 195, 101-112.

Toprak, V. 2003. Tuzgölü Fay kuşağı Hasandağ kesiminin özellikleri. TPJD Özel Sayı, 5, 71–84 (in Turkish).

Tunoğlu, C., Temel, A., Gençoğlu, H. 1995. Pliocene ostracoda association and environmental characteristics of Sivrihisar (Eskişehir)-Central Anatolia; 12nd. Inter. Ostracoda Symp., Ostracoda and Biostratigraphy (Ed. Riha, J.) Belkama/Rotterdam, 265-275.

Turgut, S. 1978. Tuz Gölü havzasının stratigrafik ve çökelsel gelişimi. Türkiye IV. Petrol Kongresi Bildirileri, p. 115-126 (in Turkish).

Türeli, T.K., Göncüoğlu, M. C., Akıman, O. 1993. Origin and petrology of Ekecikdağ granitoid in western Central Anatolian Crystalline Complex. *Bulletin of the Mineral Research and Exploration* 115, 15-28.

Uçar, L. 2008. Hanobası-Karapınar (KB Aksaray) alanının stratigrafik incelenmesi. *Geosound*, 52, 1.

Uğurtaş, G. 1975. Tuzgölü havzasının bir bölümünün jeofizik yorumu. *Bulletin of the Mineral Research and Exploration*, 85, 38-45 (in Turkish).

Ulu, Ü., Bulduk, A.K., Ekmekçi, E., Karakaş, M., Öcal, H., Arbas, A., Saçlı, L, Taşkıran, A., Adır, M., Sözeri, Ş., Karabıyıkoğlu, M. 1994*a*. İnlice-Akkise ve Cihanbeyli-Karapınar Alanının Jeolojisi. *Maden Tetkik ve Arama Genel Müdürlüğü Rapor* no: 9720, 219 s (in Turkish; unpublished).

Ulu, Ü., Ocal, H., Bulduk, A.K., Karakaş, M., Arbas, A., Saçlı, L, Taşkıran, A., Ekmekçi, E., Adır, M., Sözeri, Ş., Karabıyıkoğlu, M. 1994*b*. Cihanbeyli-Karapınar yöresi geç Senozoyik çökelme sistemi: Tektonik ve iklimsel önemi. *TJK Bülteni*, 9, 149-163 (in Turkish).

Uygun, A. 1981. Tuzgölü havzasının jeolojisi, evaporit oluşumları ve hidrokarbon olanakları. TJK İç Anadolu'nun Jeolojisi Simpozyumu, Ankara, 66-71 (in Turkish).

Uygun, A, Şen, E. 1978, Tuz Gölü havzası ve doğal kaynakları: I. Tuz Gölü suyunun jeokimyası: *Türkiye Jeoloji Kurumu Bülteni*, 21, 113-120 (in Turkish).

Ünalan, G., Yüksel, V., Tekeli, T., Gönenç, O., Seyirt, Z., Hüseyin, S. 1976. Haymana Polatlı yöresinin (GB Ankara) Üst Kretase-Alt Tersiyer stratigrafisi ve paleocoğrafik evrimi. *TJK Bülteni*, 19, 159-176 (in Turkish).

Varol, B., Kazancı, N., Gültekin, F. 2000. Tuzgölü ve yakın civarı Eosen-Oligosen jipslerinin sedimantolojik ve izotopik özellikleri. *Haymana-Tuzgölü-Ulukışla Basenleri Uygulamalı Çalıştayı Bildiri Özleri Kitabı*, Aksaray, s.19 (in Turkish).

van Zeist, W., Bottema, S. 1982. Vegetational history of the Eastern Mediterranean and the Near East during the last 20000 years. In: Paleoclimates, paleoenvironments and human communities in the eastern Mediterranean region in later prehistory, Eds.: J. L. Blintliff, W. van Zeist, BAR International Series, 133, 277-321. Oxford.

van Zeist, W., Bottema, S. 1991. Late Quaternary vegetation of the Near East, Behiefte zum Tubinger Atlas der Vorderen Orients. Rehie A18, 156 s.

Yalınız, K., Göncüoğlu, M.C., Floyd, P.A. 1996. Supra-subduction zone ophiolites of Central Anatolia: Geochemical evidence from the Sarikaraman ophiolite, Aksaray, Turkey. *Mineralogical Magazine*, 60, 697-710.

Yalınız, K., Göncüoğlu, M.C., Özkan-Altıner, S. 2000. Formation and emplacement ages of the SSZ-type Neotethyan ophiolites in Central Anatolia, Turkey: paleotectonic implications. *Geological Journal*, 35, 53-68.

Yalınız, M.K., Göncüoğlu, M.C. 1998. General geological characteristics and distribution of the Central Anatolian Ophiolites. *Yerbilimleri*, 20, 19-30.

BULLETIN OF THE MINERAL RESEARCH AND EXPLORATION

Foreign Edition 2014 149

CONTENTS

Facies Characteristics And Control Mechanisms of Quaternary Deposits In The Lake Tuz Basin
.....Alper GÜRBÜZ and Nizamettin KAZANCI 1

Neotectonic-Period Characteristics, Seismicity, Geometry And Segmentation of The Tuz Gölü Fault Zone
.....Akın KÜRÇER and Y. Ergun GÖKTEN 19

Neogene Stratigraphy And Paleogeographic Evolution of The Karaburun Area, İzmir, Western Turkey
.....Fikret GÖKTAŞ 69

Benthic Foraminiferal Fauna of Malatya Oligo-Miocene Basin (Eastern Taurids, Eastern Turkey)
.....Fatma GEDİK 93

Protolith Nature And Tectonomagmatic Features of Amphibolites From The Qushchi Area, West Azerbaijan, NW Iran
.....Mohssen MOAZZEN 139

Glauberite-Halite Association In Bozkır Formation (Pliocene Çankırı-Çorum Basin, Central Anatolia, Turkey)
.....İlhan SÖNMEZ 153

Estimation of Swelling Pressure Using Simple Soil Indices
.....Kamil KAYABALI and Özgür YALDIZ 177

Two Examples For Imaging Buried Geological Boundaries: Sinkhole Structure And Seyit Hacı Fault, Karapınar, Konya
.....Ertan TOKER, Yahya ÇİFTÇİ, Aytekin AYVA and Akın KÜRÇER 189

The Assessment of Geothermal Potential of Turkey By Means Of Heat Flow Estimation
.....Uğur AKIN, Emin Uğur ULUGERGERLİ and Semih KUTLU 201

A Brief Note On Mineral Evolution And Biochemistry
.....José Mario AMİGO 211

Critisism on the paper "Possible Incision of The Large Valleys In Southern Marmara Region, Turkey (Nizamettin KAZANCI, Ömer EMRE, Korhan ERTURAÇ, Suzanne A.G. LEROY, Salim ÖNCEL, Özden İLERİ and Özlem TOPRAK)
.....Nizamettin KAZANCI 219

Acknowledgement 221

Notes to the authors 223

Bull. Min. Res. Exp. (2014) 149: 19-68

Bulletin of the
Mineral Research and Exploration

http://bulletin.mta.gov.tr

NEOTECTONIC-PERIOD CHARACTERISTICS, SEISMICITY, GEOMETRY AND SEGMENTATION OF THE TUZ GÖLÜ FAULT ZONE

Akın KÜRÇER[a*] and Yaşar Ergun GÖKTEN[b]

[a] *Maden Tetkik ve Arama Genel Müdürlüğü, Jeoloji Etütleri Dairesi Başkanlığı, Yer Dinamikleri Araştırma ve Değerlendirme Koordinatörlüğü, Aktif Tektonik Araştırmalar Birimi, ANKARA*

[b] *Turgut Özal Mahallesi, 2204. Sokak, Erce Sitesi, C.1, Batıkent, ANKARA*

Keywords:
Tuz Gölü Fault Zone, Anatolia, Neotectonic, segment, seismicity

ABSTRACT

The Tuz Gölü Fault Zone (TGFZ) is one of the most important active intra-continental fault zones in central Anatolia. The TGFZ with nearly 200 km in length and 2-25 km in width is a NW trending, active normal fault zone with minor right-lateral strike-slip component. It extends between the north of Lake Tuz at NW and at Kemerhisar (Niğde) SE. This zone is a transition zone that separates the Central Anatolian Neotectonic Region into two-sub neotectonic regions, namely Kayseri-Sivas and Konya-Eskişehir neotectonic regions. In this study, Neotectonic-period characteristics, seismicity, geometry and segmentation of TGFZ are investigated. TGFZ is composed of a total of eleven parallel or sub-parallel geometric fault segments with length ranging from 9 to 30 km. In calculations based on empirical equations proposed for normal faults, TGFZ segments are found to generate earthquakes with maximum magnitudes of M=6.11-6.80 and during these earthquakes vertical displacements will be 0.34-1.41 m at maximum with average of 0.25-0.68 m. Fault kinematic analysis studies conducted on TGFZ showed that a NE-SW trending extensional tectonic regime is effective in the region. According to structural observations, stratigraphic relations and age data, neotectonic period for TGFZ started early Pliocene. TGFZ is a structure of NE-SW trending extensional tectonic regime that was activated by the early Pliocene. This structure borders the recent Tuz Gölü Plio-Quaternary basin to the east. By the early Pliocene, total normal slip is found 200-268 m. Based on geologic age and slip amount, average annual slip-rate on TGFZ is 0.046 mm.

1. Introduction

Owing to its special geotectonic setting, Turkey is one of the most active deformation regions in the eastern Mediterranean region. Neotectonic development of Turkey and its surroundings is closely associated with continental convergence resulting from collision between African-Arabian and Eurasian plates and subsequent geologic events. Neotectonic of are Turkey and nearby regions are controlled mainly by the right-lateral North Anatolian Fault System (NAFS), left-lateral East Anatolian Fault System (EAFS), Dead Sea Fault System (DSFS) and the active Aegean-Cyprus subduction zone.

As a result of progressing deformation, which is represented by a continental convergence between African-Arabian and Eurasian plates, four main neotectonic regions were developed that are separated from each other by aforementioned main structural elements. They are; East Anatolian compressional region, North Anatolian region, Western Anatolian extensional region and the Central Anatolia "Ova" province (Şengör et al., 1985). The East Anatolian compressional region has been deformed under an N-S trending compressional tectonics (Dewey et al., 1986). This region consistent with the compression direction is represented by E-W trending folds and reverse faults, NW-SE trending right-lateral, NE-SW

* *Corresponding author: Akın KÜRÇER, akin.kurcer@mta.gov.tr*

trending leftt-lateral strike-slip faults, N-S trending extensional fissures and young interplate volcanism. The Anatolian region stands for the area at north of NAFS and is represented by a series of strike-slip faults of significant reverse component. Western Anatolian extensional region which is represented by NNW-SSE trending continental extension has typical structures of E-W trending normal faults that shape horst and grabens (Şengör, 1980; Bozkurt, 2001). In central Anatolia, unparallel extensional basins (e.g. Tuz Gölü and Konya basins) bordered by oblique-slip faults are defined as "Ova" and this region is named "Central Anatolian Ova Province" (Şengör, 1980). This region is prolongation of Western Anatolian extensional region which weakens towards the east (Şengör, 1980). The Central Anatolian Ova Province also comprises the transition zone among three neotectonic regions (Dirik and Göncüoğlu 1996; Koçyiğit and Beyhan 1998; Dirik 2001; Koçyiğit and Erol 2001; Dirik and Erol 2003; Koçyiğit and Özacar 2003; Koçyiğit, 2005).

In addition to these main structures, there are secondary fault systems and fault zones that separate Anatolia into smaller blocks contributing to neotectonic development of Anatolia. Among them, left-lateral Central Anatolia Fault System, Tuz Gölü Fault Zone of oblique-slip character, İnönü-Eskişehir Fault System and Akşehir Fault Zone (Figure 1) (Dirik and Göncüoğlu, 1996; Koçyiğit and Beyhan, 1998; Dirik, 2001; Dirik and Erol, 2003; Koçyiğit, 2003; Koçyiğit and Özacar, 2003; Koçyiğit, 2005; Kürçer, 2012).

Due to its morphotectonic properties and recent micro-seismic activity, the Tuz Gölü Fault Zone (TGFZ) is one of the most important active fault zones in central Anatolia (Şaroğlu et al., 1987; Emre, 1991; Şaroğlu et al., 1992; Leventoğlu, 1994; Dirik and Göncüoğlu, 1996; Koçyiğit and Beyhan, 1998; Çemen et al., 1999; Dirik and Erol 2000; Koçyiğit, 2000; Toprak, 2000; Koçyiğit and Özacar, 2003; Özsayın and Dirik, 2007; Özmen, 2008; Kürçer, 2012; Kürçer and Gökten, 2012). TGFZ also separates the Kayseri-Sivas Neotectonic Region, which is represented by a transtensional neotectonic regime, from the Konya-Eskişehir Neotectonic Region which is represented by an extensional regime (Koçyiğit, 2000). TGFZ has been studied by several researchers regarding its potential to form a trap for oil accumulation and its effect on facies formation in the basin (Rigo de Righi and Contesini 1960; Arıkan 1975; Capraru 1977, 1991; Görür and Derman 1978; Derman 1980; Uygun 1981; Görür 1981; Uygun et al., 1982; Görür et al., 1984, 1998; Dellaloğlu and Aksu 1984; Çemen and Dirik 1992; Göncüoğlu et al., 1992, 1996; Çemen et al., 1999; Derman et al., 2000). In addition, neotectonic works were also carried out in certain parts of TGFZ (Leventoğlu 1994; Dirik and Göncüoğlu 1996; Toprak 2000). The age, geometry and nature of TGFZ are investigated by various researchers using different methods on different parts of the fault; however, results of these studies reach no agreement. Assessment of results from such works on certain parts of TGFZ considering the whole fault zone resulted in a literature chaos. In literature, issues on the age, geometry, segment structure, extent and nature of TGFZ are controversial and/or deficient.

Different ages have been proposed for TGFZ. According to some researchers, the age of TGFZ is as old as late Cretaceous (Görür and Derman 1978; Uygun et al., 1982; Görür et al., 1984; Çemen et al., 1999; Dirik and Erol 2000). Arıkan (1975) states that TGFZ is of Eocene age whilst Dellaloğlu and Aksu (1984) assert that it is Miocene in age. On the other hand, considering the recent character of TGFZ, Koçyiğit (2000) suggested that first activation of TGFZ might have postdated early Pliocene.

The character of TGFZ is also contradictive. For instance, according to Şengör et al. (1985) and Şaroğlu et al. (1987), TGFZ is a high-angle right-lateral strike slip fault with reverse component dipping to the NE which is also shown in the Active Fault Map of Turkey by Şaroğlu et al. (1992). Derman et al. (2000) asserted that TGFZ was initiated as a normal fault and then gained a left-lateral strike slip character in Eocene and changed to a normal faulting. A group of researchers (Emre, 1991; Toprak and Göncüoğlu, 1993; Dirik and Göncüoğlu, 1996; Koçyiğit and Beyhan, 1998; Toprak, 2000; Dirik and Erol, 2000; Koçyiğit, 2000), based on morphotectonic data and Çemen et al. (1999) based on seismic reflection profile, described the TGFZ in neotectonic period as a right-lateral strike-slip fault with a normal component dipping to SW which is high-angle at the surface but shows a listric character to the depth. On the other hand, Leventoğlu (1994), who studied 14-km long part of TGFZ in the Hanındağ region at SE of Şereflikoçhisar, states that fault zone is a normal fault with right-lateral strike-slip component.

It is widely accepted that TGFZ is a fault zone extending between Paşadağ at NW (north of Lake Tuz) and Bor (Niğde) at SE (Şaroğlu et al., 1987, 1992; Dirik and Göncüoğlu, 1996; Dirik and Erol,

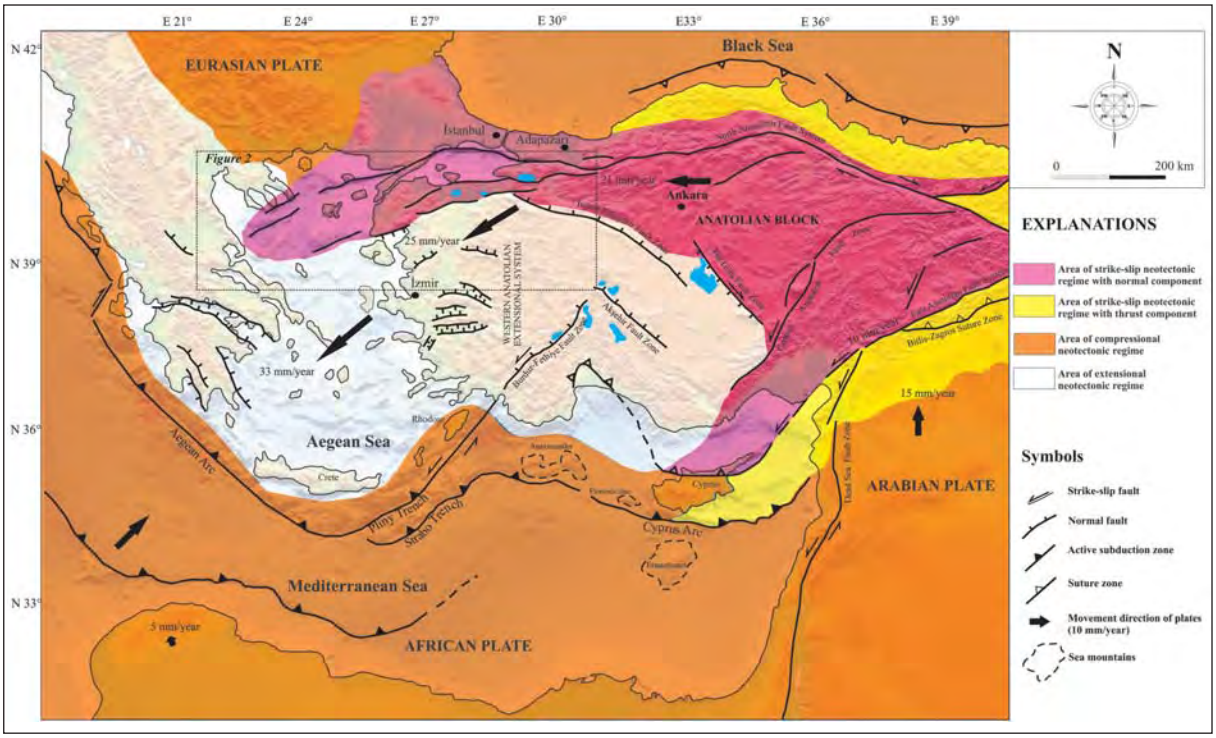

Figure 1- The main neotectonic elements and neotectonic regions in Turkey and neighboring areas (compiled by Kürçer, 2012 from Okay et al., 2000; Woodside et al., 2002; Koçyiğit and Özacar, 2003; Zitter et al., 2005; Çiftçi, 2007; Özsayın, 2007; Yolsal-Çevikbilen and Taymaz, 2012). Black arrows are GPS vectors, related numbers are GPS velocities (mm/y) (Reilinger et al., 2006). Shuttle Radar Topography Mission (SRTM) data were used for digital elevation model.

2000; Koçyiğit, 2000). On the contrary, Koçyiğit and Beyhan (1998) suggested that TGFZ extends to Çamardı (Niğde) at SE and in the area between Bor and Çamardı it gains a significant reverse character. These workers regarded the TGFZ as a strike-slip fault conjugating with left-lateral Central Anatolian Fault Zone.

In spite of studies conducted with various methods in different parts of TGFZ, a neotectonic work comprising the entire fault zone has not been performed as yet.

In this study, the age, extention, character and kinematic properties, geometry and segment structure of TGFZ and its relation to the Tuz Gölü Basin and its setting and importance in the regional neotectonic frame are discussed.

In this respect, field geology studies were conducted in an area of 250 km in length and 20 km in width. For the field study, a geological map of fault zone was constructed based on 1/5000.000 scaled Kayseri and Adana quadrangles. In addition, in two sub-areas which can elucidate the beginning of neotectonic period 1/25.000 scaled geology mapping was done. In order to manifest kinematic properties of the fault zone, detailed structural observations were made and fault plane slip data were collected. Segmentation model of TGFZ has been first described in this study and using empirical equations the largest earthquake to be generated by these segments and the largest and average displacements were calculated.

2. Regional Geology

In TGFZ region various rocks units with ages ranging from Paleozoic to recent time are exposed (Figure 2). Northern (east of Lake Tuz), central (around Aksaray and Hasan Dağı) and southern parts (between Niğde and Çamardı) display different tectono-stratigraphic characteristics (Figure 3a, b, c).

At north of the study area, the basement is comprised by Central Anatolian Crystalline Complex (CACC) (Göncüoğlu, 2010) which is continuation of the Anatolides in Anatolia. In the study area CACC is represented by Kaman Group Metamorphites of the Kırşehir Massif (Seymen, 1982). Above these units is the Central Anatolian Ophiolite Complex (CAOC)

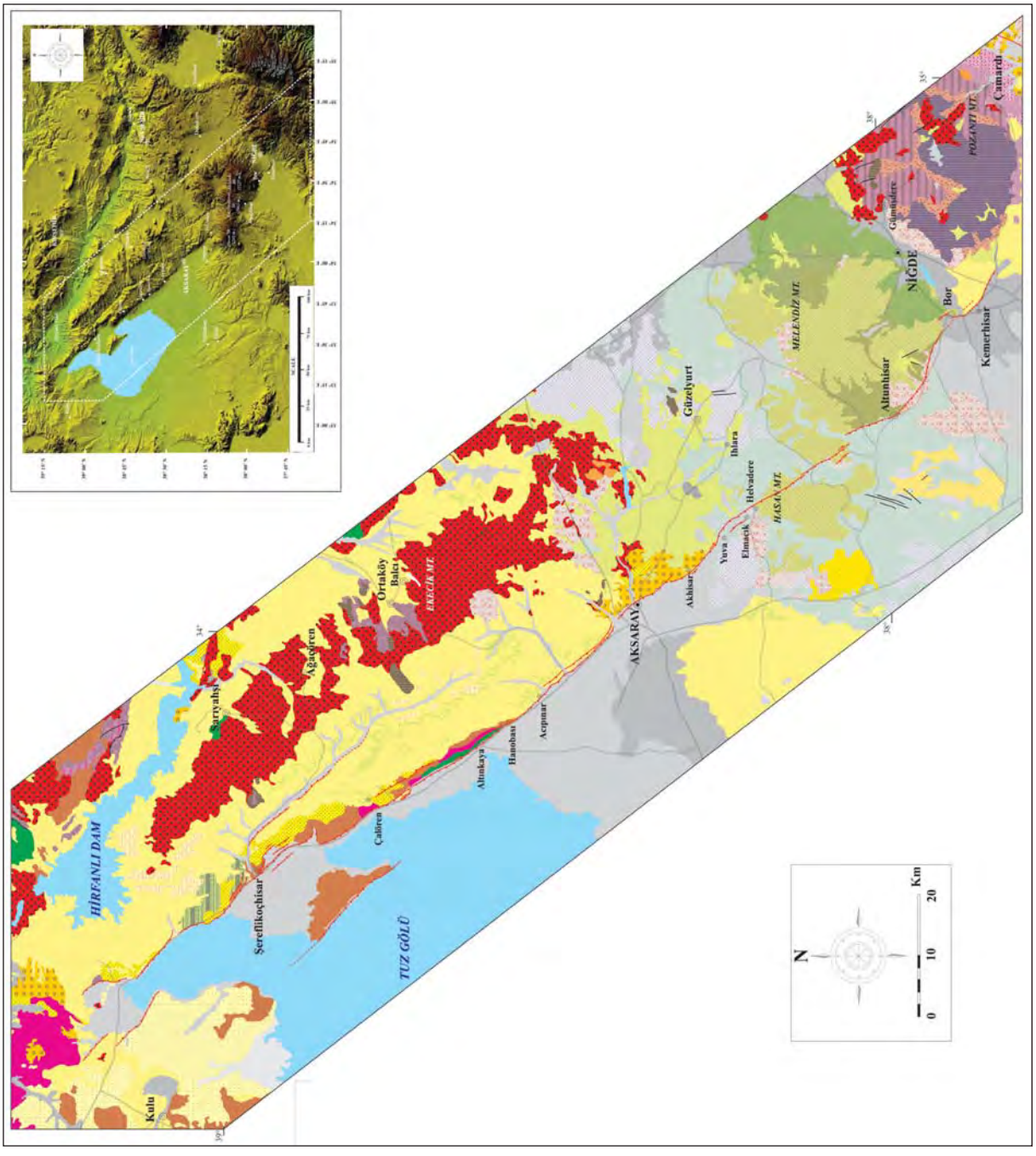

Figure 2- Geology map of the Tuz Gölü Fault Zone (compiled by Kürçer, 2012 from MTA, 2002).

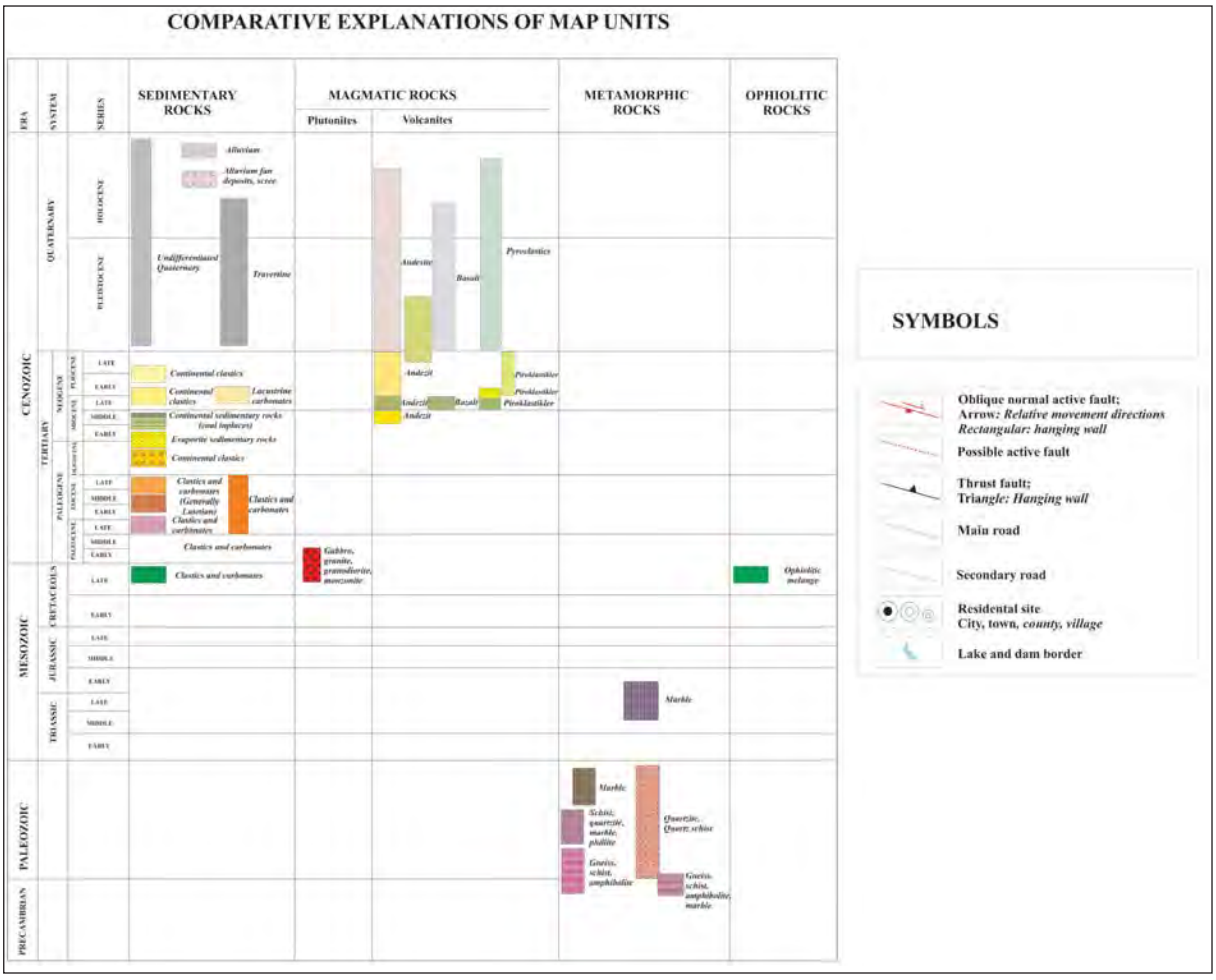

Figure 2- (continued)

(Göncüoğlu et al., 1991, 1992, 1993, 1994). CAOC is represented by accretionary prism material which is formed by the closure of İzmir - Ankara - Erzincan Ocean and obducted southwards onto the units of the Kütahya - Bolkardağ Belt (Dirik and Erol, 2000). The Kaman Group Metamorphites and Central Anatolian Ophiolite Complex are cut by late Cretaceous Ağaçören Granitoid (Kadıoğlu, 1991) which represents the Central Anatolian Granitoids consisting of collision-type granitoids and post-collisional alkalen magmatics (Göncüoğlu et al., 1991, 1992, 1993, 1994, 1996, 1997; Erler et al., 1991; Akiman et al., 1993; Türeli et al., 1993; Yalınız and Göncüoğlu, 1998; Yalınız et al., 1996, 2000; Dirik and Erol, 2000; Işık, 2009; Boztuğ et al., 2009).

The Tuz Gölü Basin was developed on CACC as a result of extensional tectonic activity in the upper Cretaceous (Dirik and Erol, 2000). In the Tuz Gölü Basin there is a sequence with thickness up to 10 km (Arıkan, 1975) deposited from late Cretaceous to recent. Sedimentation in the Tuz Gölü Basin was started with extensional tectonic activity during the upper Cretaceous and this tectonic regime was ended in the middle Eocene (Dirik and Erol, 2000). The basement of the Tuz Gölü Basin is composed of vertically and laterally transmissive Kartal formation of late Cretaceous – early Paleocene age and the Asmaboğazı formation. These formations are conformably overlain by Paleocene aged Çaldağ formation and have transitional contact with Karapınaryaylası formation of late Paleocene – early Eocene age (Dirik and Erol, 2000). The Karapınaryaylası formation concordantly passes to Eocene (Lutetian) Boyalı formation (Atabey et al., 1987). The basin which was subjected to compressional tectonism by the upper Eocene became shallow and it was disconnected to the open sea (Dirik and Erol, 2000). As a result, late Eocene – Oligocene aged Yassıpur formation consisting of clastics and thick evaporites were deposited on the

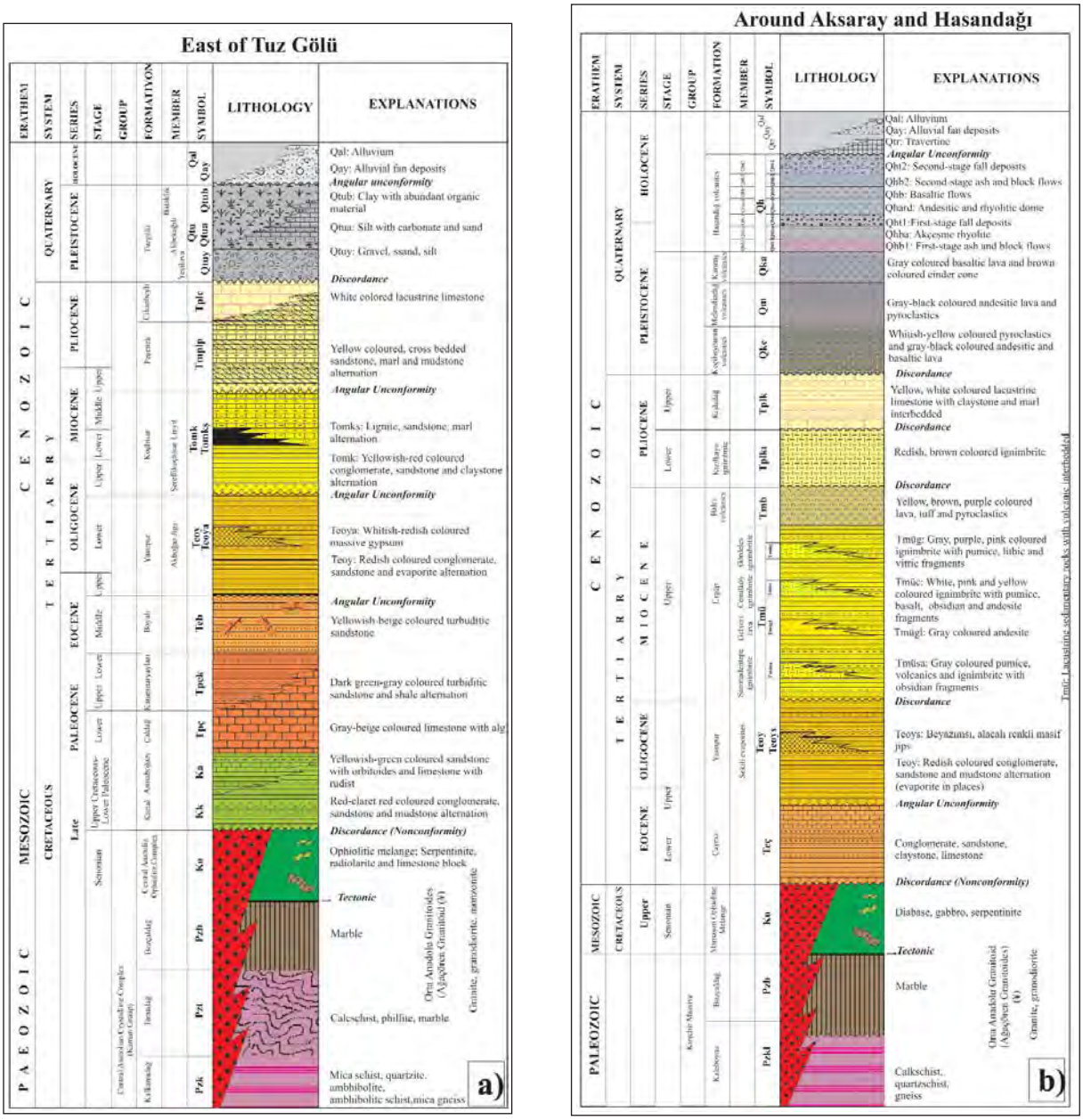

Figure 3- Generalized comparative tectonostratigraphic sections for northern, central and eastern parts of the Tuz Gölü Fault Zone region (not to scale); a) East of Lake Tuz (compiled by Kürçer, 2012 from Atabey et al., 1987; Göncüoğlu et al., 1996; Çemen et al., 1999; Dirik and Erol, 2000), b) Around Aksaray and Hasandağ (complied by Kürçer, 2012 from Dönmez et al., 2005).

Boyalı formation with an angular unconformity (Göncüoğlu et al., 1996; Çemen et al., 1999; Varol et al., 2000; Dirik and Erol, 2000). The Yassıpur formation is overlain with an angular unconformity by late Oligocene – middle Miocene Koçhisar formation of terrestrial origin that includes Şereflikoçhisar lignites (Dellaloğlu and Aksu, 1984). Following the uplift and subsequent erosion in upper Eocene-Oligocene, during lower-middle Miocene a plateau was formed in central Anatolia that covered a large area (Anatolian peneplain) (Dirik and Erol, 2000). During this period, horizontal-bedded Peçenek formation with an angular unconformity and Cihanbeyli formation that laterally and vertically interlayered with Peçenek formation were deposited on the Koçhisar formation. During the Quaternary, depending on climatic and seasonal changes and lacustrine, marsh, evaporation and arid conditions,

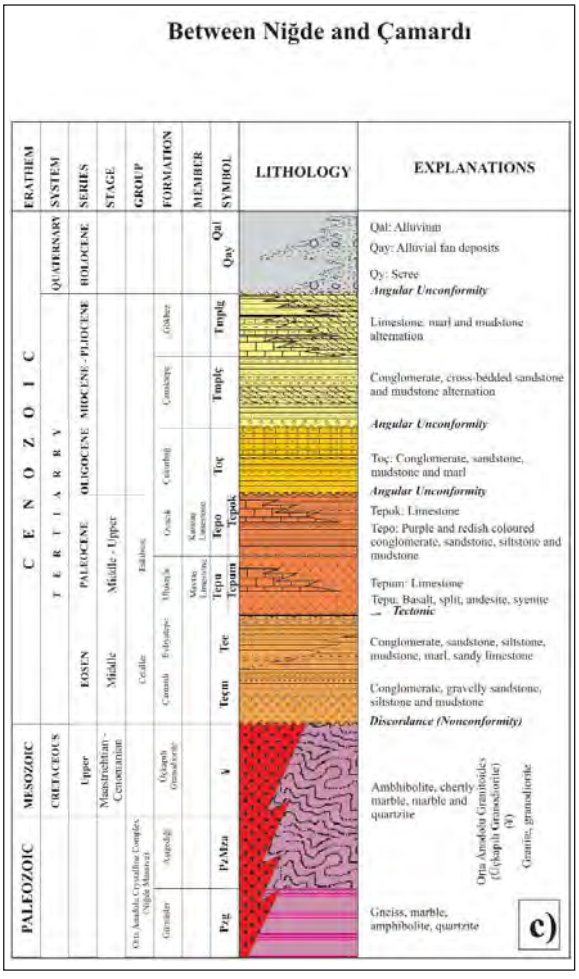

Figure 3c- Between Niğde and Çamardı (compiled by Kürçer, 2012 from Yetiş, 1978; Göncüoğlu et al., 1991; Demircioğlu and Eren, 2000; Parlar et al., 2006).

the Tuz Gölü formation was deposited in the Lake Tuz and around the surrounding areas. The most important structural elements in northern part of the study area are SW dipping fault segments of NW-SE trending TGFZ. Along these fault segments, several alluvial fan deposits are developed on downthrown blocks of the faults by the accumulation of sediments transported from ascending NE block. Alluvium formation is still continued along the margins of modern rivers and flood plains (Figure 3a).

In central part of the study area (around Aksaray and Hasan Dağı), metamorphites of the Paleozoic Kırşehir massif comprise the basement. These units are overlain by a tectonic contact by Mamasun Ophiolite Complex (Dönmez et al., 2005) which is an extension of Central Anatolian Ophiolite Complex in this region. Kırşehir massif metamorphites and Mamasun Ophiolite Complex are cut by the late Cretaceous Ağaçören Granitoid (Dönmez et al., 2005). These units are unconformably covered by Çayraz formation (Schmidt, 1960) of Eocene (Ypresian) age (Dönmez et al., 2005). The region which was subjected to compressional tectonism by the upper Eocene has become shallow and disconnected to the open sea (Dirik and Erol, 2000). During this period, late Eocene-Oligocene Yassıpur formation consisting of clastics and thick evaporites (Göncüoğlu et al., 1996; Çemen et al., 1999; Varol et al., 2000; Dirik and Erol, 2000) was unconformably deposited onto the Çayraz formation. The central part of study area comprising Aksaray and Hasan Dağ is located within the Central Anatolian Volcanic Province (CAVP). By the Miocene CAVP was formed as a result of convergence between the African-Arabian and Eurasian plates and subsequent subduction that resulted in extension of crust on the subducting lithospheric slab (Innocenti et al., 1975; Batum, 1978; Tokel et al., 1988; Toprak and Göncüoğlu, 1993). In this region various volcanic rocks are exposed with ages ranging from late Miocene to Holocene (including Holocene). Volcanites which are composed of lava, tuff and ignimbrites of the Keçikalesi, Keçiboyduran, Erciyes, Acıgöl, Göllüdağ, Melendiz and Hasan Dağı volcanism are accompanied laterally and vertically by lacustrine and terrestrial deposits. The initial deposits of this volcano-sedimentary sequence is the Ürgüp formation that is composed of terrestrial clastics, limestone, ignimbrite interlayers and andesitic lava (Pasquare, 1968). Various ignimbritic and andesitic lava levels in the Ürgüp formation are divided into four members as Sarımadentepe ignimbrite member, Gelveri lava member, Cemilköy ignimbrite member and Gördeles ignimbrite member (Dönmez et al., 2005).

The Ürgüp formation is conformably overlain by Balcı Volcanite of late Miocene age (Türkecan et al., 2003) which consists of lava, tuff and various pyroclastics. The Kızılkaya Ignimbrite which is widely exposed in central part of the study area (Beekman, 1966) is in early Pliocene age, based on radiometric age data (Innocenti et al., 1975; Schumacher and Schumacher, 1996; Le Pennec et al., 2005 Aydar et al., 2012), and unconformably overlies the older units. The Kızılkaya Ignimbrite is unconformably covered by the Kışladağ formation which is composed of lake carbonates and accepted to be late in Pliocene age because of its stratigraphic position (Dönmez et al., 2005). Quaternary volcanism was quite effective in central part of the study area. The Keçiboyduran Volcanites consisting of andesite

and basaltic andesite are the first products of Quaternary volcanism (Dönmez et al., 2005). Based on radiometric age data, Keçiboyduran Volcanites are of Pleistocene age (Dönmez et al., 2005). Above the Keçiboyduran Volcanites is the Melendiz Volcanites with radiometric age of early-middle Pleistocene Miocene (Türkecan et al., 2003). All these units are overlain by late Pleistocene aged Karataş Volcanites consisting of basaltic lava and scoria cones (Ercan et al., 1990). The Hasandağ Volcanites of Holocene age are the youngest volcanic products in the study area (e.g. Ercan et al., 1990). The Hasandağ Volcanites are made of ash and block flows, fall deposits and pyroclastic flows and andesitic-basaltic lavas (Dönmez et al., 2005). In Holocene in some areas travertines and alluvial fans were formed along TGFZ and alluvium deposition still continues (Figure 3b).

In farthermost southeast part of the study area possible extents of TGFZ are investigated. In southern part of the area basement is comprised by metamorphic rocks of the Niğde Massif which represents the CACC in this region (Yetiş, 1978, Göncüoğlu et al., 1991; Demircioğlu and Eren, 2000; Parlar et al., 2006). Metamorphic rocks are cut by Cenomanian-Maastrichtian aged Üçkapılı Granodiorite (Göncüoğlu, 1977, 1982, 1985; Kuşçu et al., 1993). These basement units unconformably are overlain by Celaller Group (Göncüoğlu et al., 1991) of middle Eocene age (Parlar et al., 2006). The Celaller Group is represented from bottom to the top by Çamardı and Evliyatepe formations. The Celaller Group is tectonically (Demircioğlu and Eren, 2000) overlain by Eskiburç Group Göncüoğlu et al., 1991) of middle-late Paleocene age (Parlar et al., 2006). The Eskiburç Group is represented at the bottom by Ulukışla formation and Ovacık formation that is alternated with the Ulukışla formation (Dellaloğlu ve Aksu, 1986). These units are overlain with an angular unconformity by terrestrial Çukurbağ formation of Oligocene age (Yetiş, 1978). The late Miocene-Pliocene Çanaktepe formation which consists of conglomerate, cross-bedded sandstone and mudstone alternation (Atabey and Ayhan, 1986) and the alternating Gökbez formation cover all the older units with an angular unconformity (Demircioğlu and Eren, 2000). Quaternary alluvial fan deposits and alluvium unconformably set above all the units (Figure 3c).

3. Segmentation of the Tuz Gölü Fault Zone and fault kinematic analysis studies on these segments

TGFZ with nearly 200 km in length and 2-25 km in width is a NW-SE trending, SW-dipping, active normal fault with right-lateral strike-slip component. It extends between the north of Lake Tuz at NW and Kemerhisar (Niğde) at SE (Figure 4). Sub-parts of a fault which can be separated from each other based on certain criteria are called segment.

Fault segments are categorized into five groups as (dePolo vd., 1989, 1991; McCalpin, 2009 compiled from Knuepfer, 1989);

– Earthquake segment
– Behavioral segment
– Structural segment
– Geologic segment
– Geometric segment

The earthquake segment represents fault sections which are limited by historical earthquake ruptures. The behavioral segment is a segmentation model that can be propounded as a result of paleoseismic studies. For this, earthquake information is needed that is well dated with multi-trench works. In order to apply behavioral segmentation, slip rate changes in segment borders should be well described and recurrence interval of earthquakes on different segments must be defined as much as possible. The structural segment explains fault sections that are interrupted by other faults, folds or structures perpendicular or transverse to the segment direction. The geologic segment may localize Quaternary basins, or volcanic terrains, only one metamorphic basement or unit. The geologic segments may also be localized some geophysical anomalies. In some cases, considering the geomorphologic characteristics geologic segment may be defined. The geometric segment may be described by changes in fault direction, jumps in fault branches, splits and gaps.

In this study, geometric segment model was applied to TGFZ. In this model, TGFZ is composed of parallel or sub-parallel 11 geometric fault segments with length ranging from 9 to 30 km (Figure 4 and Table 1). These segments are separated from each other by changes in fault direction, gradual jumps, step-overs and other geologic structures. According to surface geology data, lithology is the main factor controlling the start and end points of segments.

Although slip data on fault plane for certain parts of TGFZ are presented in previous studies (Leventoğlu, 1994; Toprak, 2000), such data are not sufficient to delineate kinematic properties of the

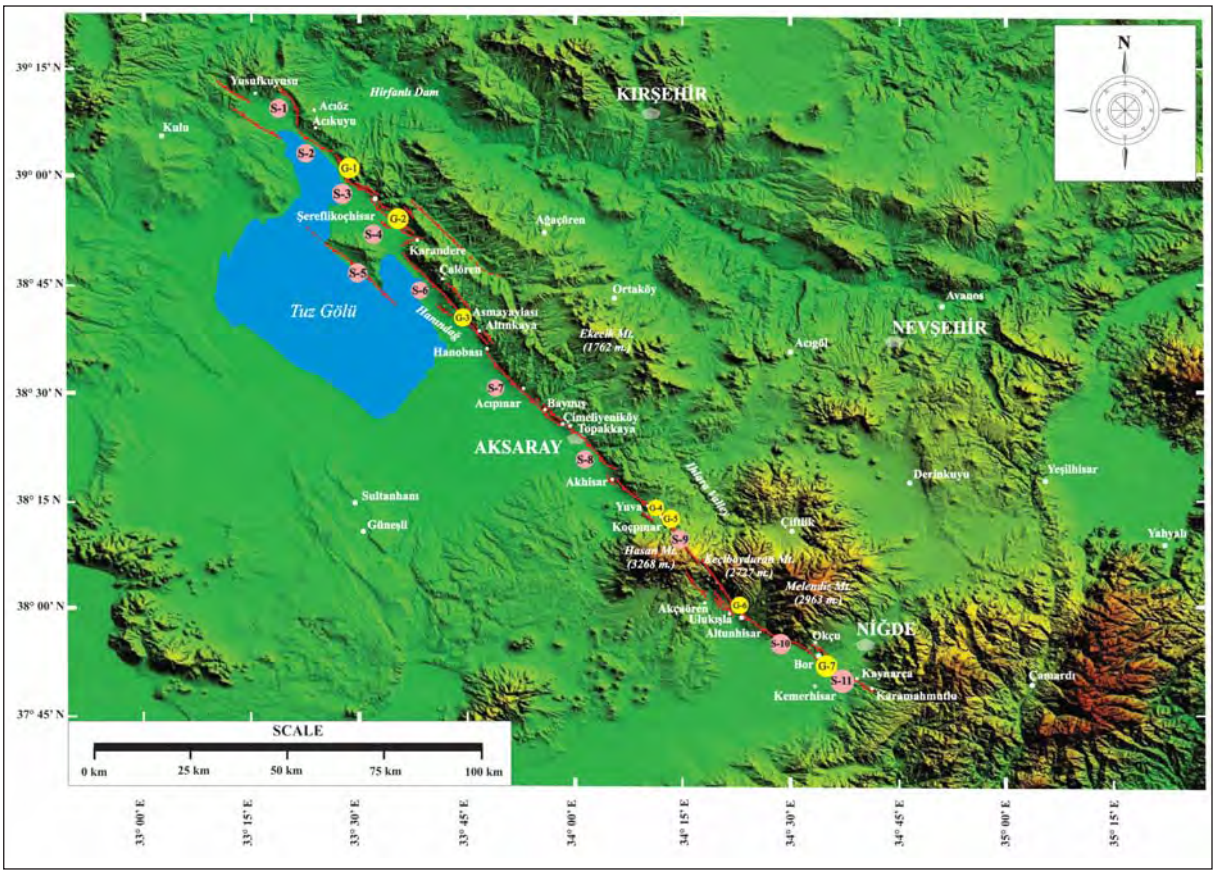

Figure 4- Positions of segments of the Tuz Gölü Fault Zone on the digital elevation model for the region (Kürçer, 2012). S-1/11 are segment numbers, G-1/7 are the structural observation points (see table 1 for coordinate information).

Table 1- Segments of the Tuz Gölü Fault Zone and their general characteristics.

Segment number	Segment name	Segment length (km)	Segment direction
S - 1	Yusufkuyusu	9	N 40° W / N-S
S - 2	Acıkuyu	10	N 50° W
S - 3	Akboğaz	13	N 30° W / N 40° W
S - 4	Şereflikoçhisar	14	N 45° W
S - 5	İnceburun	23	N 40° W
S - 6	Tuz Gölü	30	N 35° W
S - 7	Acıpınar	26	N 45° W
S - 8	Aksaray	13	N 32° W
S - 9	Akhisar-Kılıç	27	N 25° W / N 30° W
S - 10	Altunhisar	30	N 30° W / N 70° W
S - 11	Bor	17	N-G / N 55° W

fault zone as whole. In order to fill this deficiency fault plane slip data were collected on 7 structural observation points on various segments of TGFZ (Tables 2 and 3). At these stations, a total of 32 fault planes, slickenlines and rake were measured. Data collected from each measurement point are evaluated separately and principal stress axes for each point are shown on six different hemispheric equal area projection nets.

Table 2- Information on observation sites along the Tuz Gölü Fault Zone where kinematic analysis were made.

Station code and name	**Quadrangle no and coordinates (UTM)**	**Formation**	**Age**
G-1 Şereflikoçhisar	K 30 b2 542303 E - 4315245 N	Boyalı formation (Teb)	Middle Eocene
G-2 Deldah Düzü	K 31 a1 551800 E - 4308650 N	Yassıpur formation Akboğaz Gypsum Member (Teoya)	Upper Eocene – Lower Oligocene
G-3 Amayaylası	K31 c1 566270 E - 4278286 N	Asmaboğazı formation (Ka)	Upper Cretaceous – Lower Paleocene
G-4 Yuva	L 32 d2 601450 E – 4234000 N 601984 E – 4233726 N	Hasan Dağı volcanics First-stage ash and block flows (Qhb1)	Quaternary
G-5 Koçpınar	L32 d2 604694 E- 4231266 N 606111 E - 4228966 N	Hasan Dağı volcanics First-stage ash and block flows (Qhb1)	Quaternary
G-6 Altunhisar	L32 c4 619831 E - 4208270 N	Hasan Dağı volcanics First-stage fall deposits (Qht1)	Quaternary
G-7 Bor	M33 a1 637592 E - 4193282 N	Gökbez formation	Upper Miocene - Pliocene

Table 3- Fault plane slip data collected from stations.

Station name and no	**Strike**	**Dip angle (°)**	**Dip direction**	**Rake (°)**	**Fault type**
Station A (Şereflikoçhisar)	K 70 B	71	SW	78	Normal fault with right-lateral strike-slip component
	K75 B	78	SW	80	Normal fault with right-lateral strike-slip component
	K 74 B	75	SW	77	Normal fault with right-lateral strike-slip component
	K 65 B	67	SW	70	Normal fault with right-lateral strike-slip component
	K 55 B	73	SW	76	Normal fault with right-lateral strike-slip component
Station B (Deldah Düzü)	K 40 B	70	SW	88	Normal fault with right-lateral strike-slip component
	K42 B	74	SW	84	Normal fault with right-lateral strike-slip component
	K 38 B	79	SW	75	Normal fault with right-lateral strike-slip component
	K 42 B	81	SW	78	Normal fault with right-lateral strike-slip component
	K 39 B	78	SW	90	Pure normal fault
Station C (Asmayaylası)	K 44 B	54	SW	38	Right-lateral strike-slip fault with normal component
	K36 B	47	SW	23	Right-lateral strike-slip fault with normal component
	K 40 B	56	SW	37	Right-lateral strike-slip fault with normal component
	K 42 B	55	SW	32	Right-lateral strike-slip fault with normal component
Station D (Yuva)	N 37 W	71	SW	78	Normal fault with right-lateral strike-slip component
	N 52 W	68	SW	68	Normal fault with right-lateral strike-slip component
	N 50 W	71	SW	85	Normal fault with right-lateral strike-slip component
	N 46 W	70	SW	79	Normal fault with right-lateral strike-slip component
Station E (Koçpınar)	N 35 W	61	SW	84	Normal fault with right-lateral strike-slip component
	N 35 W	65	SW	81	Normal fault with right-lateral strike-slip component
	N 38 W	67	SW	85	Normal fault with right-lateral strike-slip component
	N 35 W	68	SW	83	Normal fault with right-lateral strike-slip component
	N 30 W	74	SW	78	Normal fault with right-lateral strike-slip component
	N 26 W	79	SW	75	Normal fault with right-lateral strike-slip component

Table 3- (continued)

Station name and no	Strike	Dip angle (°)	Dip direction	Rake (°)	Fault type
Station F (Altunhisar)	N 40 W	65	SW	90	Pure Normal fault
	N50 W	84	SW	85	Normal fault with right-lateral strike-slip component
	N 70 W	75	SW	88	Normal fault with right-lateral strike-slip component
	N 60 W	70	SW	90	Pure Normal fault
	N 15 W	61	NE	86	Normal fault with right-lateral strike-slip component
	N 14 W	69	NE	84	Normal fault with right-lateral strike-slip component
Station G (Bor)	N 10 W	SW	SW	80	Normal fault with left-lateral strike-slip component
	N12 W	82	SW	87	Normal fault with right-lateral strike-slip component
	N 10 W	81	SW	90	Pure Normal fault
	N 16 W	78	SW	87	Normal fault with right-lateral strike-slip component

For kinematic analysis of fault assemblages, single-plane solution (Marshak and Mitra, 1988) was used. For this, from fault planes measured at each station the measurement that is thought to represent station of interest was chosen and that plane was evaluated with the single-plane solution model of Marshak and Mitra (1988) to determine the principal stress axes (Table 4).

3.1. Yusufkuyusu segment (S-1)

The Yusufkuyusu segment with length of 9 km is the farther northwesternmost segment of TGFZ. It extends between the Yusufkuyusu village and NE corner of TGFZ (Figure 4). The Yusufkuyusu segment makes the contact between late Miocene-Pliocene Peçenek formation (Tmplp) and Quaternary alluvial deposits at east of Yusufkuyusu village. In this area fault strike is N40°W. In a narrow area at west of Acıöz village, the fault comprising the boundary between the alluvium and metamorphites of the Tamadağ formation (Pzt) that are a part of CACC bends towards the south. It extends nearly N-S between the northwest of Acıöz and northeastern corner of Lake Tuz where the Akboğaz Gypsum Member of the late Eocene-early Oligocene Yassıpur formation (Teoya) and the alluvium are in contact (Figure 2).

3.2. Acıkuyu segment (S-2)

The Acıkuyu segment starts from the NE corner of Lake Tuz and extends towards the Kocadere creek at SE. The segment with length of 10 km is mostly exposed parallel to the Ankara-Adana state highway (Figure 4). The fault in N50°W direction comprises the border at NW between the Akboğaz Gypsum Member of the late Eocene-early Oligocene Yassıpur formation (Teoya) and the alluvium and also the border at SE between late Miocene-Pliocene Peçenek formation (Tmplp) and the Quaternary alluvium (Figure 2).

3.3. Akboğaz segment (S-3)

The Akboğaz segment with length of 13 km extending between the south of Kocadere creek and the north of Şereflikoçhisar is composed of two parts (Figure 4). The northern part of Akboğaz segment that extends in N30°W direction comprises the area between Kocadere creek and Gökhöyük hill where it makes the boundary between late Oligocene – middle Miocene Koçhisar formation (Tomk) and the Quaternary alluvium (Figures 2 and 5a). Around the Gökhöyük hill the fault bends to the right and continues 10 km in SE direction with strike of N45°W and reaches at north of Şereflikoçhisar. In this area, it forms the contact between late Eocene-early Oligocene Yassıpur formation (Teoya) and the alluvium and then the contact between middle Eocene Boyalı formation (Teb) and Quaternary alluvium (Figure 6a).

The roadcut at 7 km NW of Şereflikoçhisar is the first observation site where the fault plane on TGFZ is exposed from NW (station 1 in Figure 5a). At this site, middle Eocene Boyalı formation (Teb) and Quaternary scree come across along the Akboğaz segment (Figures. 5a and 6a). Although we have no direct evidence on that if the Quaternary scree have been affected by the fault, regarding formation mechanics, it is expected that scree at the beginning might have smeared to the slope with angle of 15 to 17°. However, at station 1 scree rests against the fault

Table 4- Fault planes and slickenlines measured at all stations and principal stress axes acquired from selected measurements. Measurements with bold character are those used for single-plane solution.

Station	Unit	Age	Measurement no	Strike (°N)	Dip angle / direction (°)	Rake (°)	Fault type	Principle stress axes
A	Boyalı fm	Middle Eocene	**1**	**290**	**71 S**	**78 W**	**Normal**	α1= 343° / 75° α2= 110° / 10° α3= 205° / 10°
			2	285	78 S	80 W	Normal	
			3	284	75 S	77 W	Normal	
			4	295	67 S	70 W	Normal	
			5	305	73 S	76 W	Normal	
B	Yassıpur fm Akboğaz Gypsum Member	Oligo-Miocene	1	320	70 S	88 W	Normal	α1= 026° / 74° α2= 140° / 06° α3= 232° / 14°
			2	**318**	**74 S**	**84 W**	**Normal**	
			3	322	79 S	75 W	Normal	
			4	318	81 S	78 W	Normal	
			5	321	78 S	89 W	Normal	
C	Asmaboğazı fm	Upper Cretaceous-Lower Paleocene	1	316	54 S	38 W	Right Latoral	α1=170°/ 07° α2= 254° / 49° α3= 070° /43°
			2	324	47 S	23 W	Right Latoral	
			3	320	56 S	37 W	Right Latoral	
			4	**318**	**55 S**	**32 W**	**Right Latoral**	
D	Hasandağ Volkanics	Quaternary	1	323	71 S	78 W	Normal	α1= N-S° / 75° α2= 137° / 10° α3= 230° / 10°
			2	308	68 S	68 W	Normal	
			3	310	71 S	85 W	Normal	
			4	**314**	**70 S**	**79 W**	**Normal**	
E	Hasandağ Volkanics	Quaternary	1	325	61 S	84 W	Normal	α1= 020° / 80° α2= 147°/ 08° α3= 240°/ 08°
			2	325	65 S	81 W	Normal	
			3	322	67 S	85 W	Normal	
			4	**325**	**68 S**	**83 W**	**Normal**	
F	Hasandağ Volkanics	Quaternary	1	350	80 W	80 N	Normal	α1= 075° / 67° α2= 167° / 03° α3= 260° / 23°
			2	**348**	**82 W**	**87 N**	**Normal**	
			3	350	81 W	89 N	Normal	
			4	346	78 W	87 N	Normal	
			5	345	61 E	86 S	Normal	
			6	46	69 E	84 S	Normal	
G	Gökbez fm	Upper Miocene-Pliocene	1	350	80 W	80 S	Normal	α1= 059° / 66° α2= 168 / 08° α3=260 / 22°
			2	**348**	**82 W**	**82 N**	**Normal**	
			3	350	81 W	81 N	Normal	
			4	344	78 W	78 N	Normal	

in horizontal position (Figure 6b). In this case, it can be thought that the scree has gained its present state depending on the movement of Akboğaz segment later than its formation. The Akboğaz segment of TGFZ that controls the recent morphology is thought to be active.

Fault plane solutions at station 1 on the Akboğaz segment (Şereflikoçhisar station – G-1) showed that the Akboğaz segment is a normal fault with a minor right-lateral strike-slip component (Figure 6c; Table 3).

At station 1 (Şereflikoçhisar station) a total of 5 fault planes and slickenlines were measured. Among these measurements, measurement no.1 which is thought to best represent the station 1 was solved in accordance with Marshak and Mitra (1988) and then principal stress axes were found (Table 4; Figure 5b).

3.4. Şereflikoçhisar segment (S-4)

The 14-km part of TGFZ in the area between Şereflikoçhisar and Karandere village is called Şereflikoçhisar segment (Figure 4). The Şereflikoçhisar segment is composed of a main branch and a few fault sections parallel to this main branch (Figures 4 and 7a). The main branch extends in N45°W between the north of Şereflikoçhisar and Karandere village. From the north of Şereflikoçhisar,

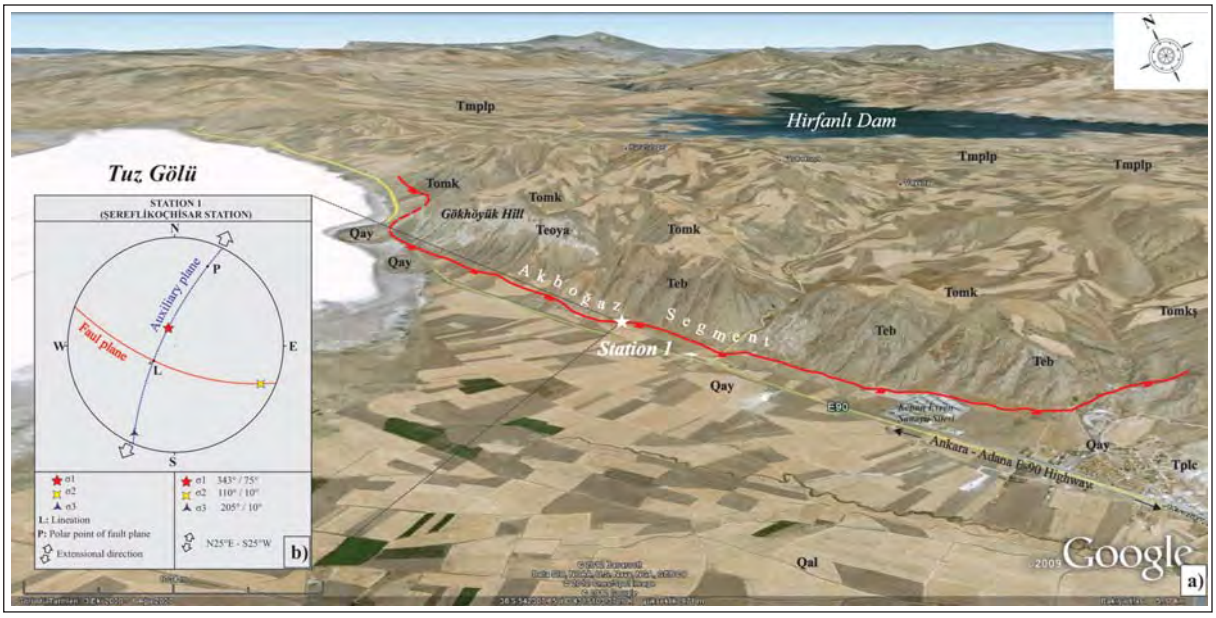

Figure 5- Google Earth view of the Akboğaz segment (vertical scale three times exaggerated, view to NE with oblique angle). Teb: Boyalı for., Tomk: Koçhisar for., Tomkş: Şeferlikoçhisar lignite member, Tmplp: Peçenek for., Tpcl: Cihanbeyli for., Qal: Alluvium, Qay: Alluvial fan, Station 1: Structural observation point on the Akboğaz segment (Şeferlikoçhisar station); b) Presentation on the lower hemisphere of Schmidt net projection of single-plane solution of fault plane no 1 measured at Station 1 (Şereflikoçhisar station) in accordance with Marshak and Mitra (1988). The arrow on the fault plane shows the relative movement direction of hanging wall.

it comprises the boundary between late Pliocene Cihanbeyli formation (Tplc) and Quaternary alluvial deposits and around Şereflikoçhisar and its near south it makes the contact between the middle Eocene Boyalı formation (Teb) and Quaternary alluvium. From the south of Şereflikoçhisar, fault enters to the alluvium Deldah Düzü site and the fault reappears from the NW of Karandere where it follows the contact between Akboğaz Gypsum Member (Teoya) of the late Eocene-early Oligocene Yassıpur formation and the alluvium. Around the Karandere village, Şereflikoçhisar segment is transferred to the Tuz Gölü segment via E-W trending Karandere normal fault of nearly 4 km in length (Figure 7a).

In the area between Şereflikoçhisar and Karandere village, another fault that extends parallel to the main branch of TGFZ surrounds to the east the Deldah Düzü site at SE of Şereflikoçhisar (Figure 7a). The fault in this area is called as eastern branch of Şereflikoçhisar segment. In this section, fault is observed in N45°W direction along a length of 4 km and it makes the contact between Akboğaz Gypsum Member (Teoya) of the late Eocene-early Oligocene Yassıpur formation and the alluvium.

Station 2 is the only measurement site where structural properties of TGFZ on the eastern branch of Şereflikoçhisar segment can be observed (Figure 7a). At this site, all structural properties of TGFZ were examined in an operated gypsum quarry in the Akboğaz Gypsum Member (Teoya) of Yassıpur formation (Figure 8).

Fault plane measurements at station 2 on the eastern branch of Şereflikoçhisar segment indicated that this segment is a normal fault with a minor right-lateral strike-slip component (Figure 8b, c, d; Table 3). Brecciated zone of about 1 m thickness and, in front of that, 30 cm-thickened fault gouge are observed on the fault plane (Figure 8e).

In previous studies on segment structure of Şereflikoçhisar part of TGFZ different arguments were propounded. For example, in Active Fault Map of Turkey by Şaroğlu et al. (1992), the area between NW Şereflikoçhisar (Kocadere) of Tuz Gölü Fault Zone and Karamandere village is taken as a single segment of 38 km in length extending in NW-SE direction (Şaroğlu et al., 1992). In Kayseri quadrangle of the 1/500.000 scaled Turkey Geology Map (MTA, 2002), interested part of Tuz Gölü Fault is shown as a 74-km long continuous segment extending from the north of Şereflikoçhisar to the Baymış village around Aksaray at SE. However, Koçyiğit (2000) states that TGFZ from south of Şereflikoçhisar first jumps to left

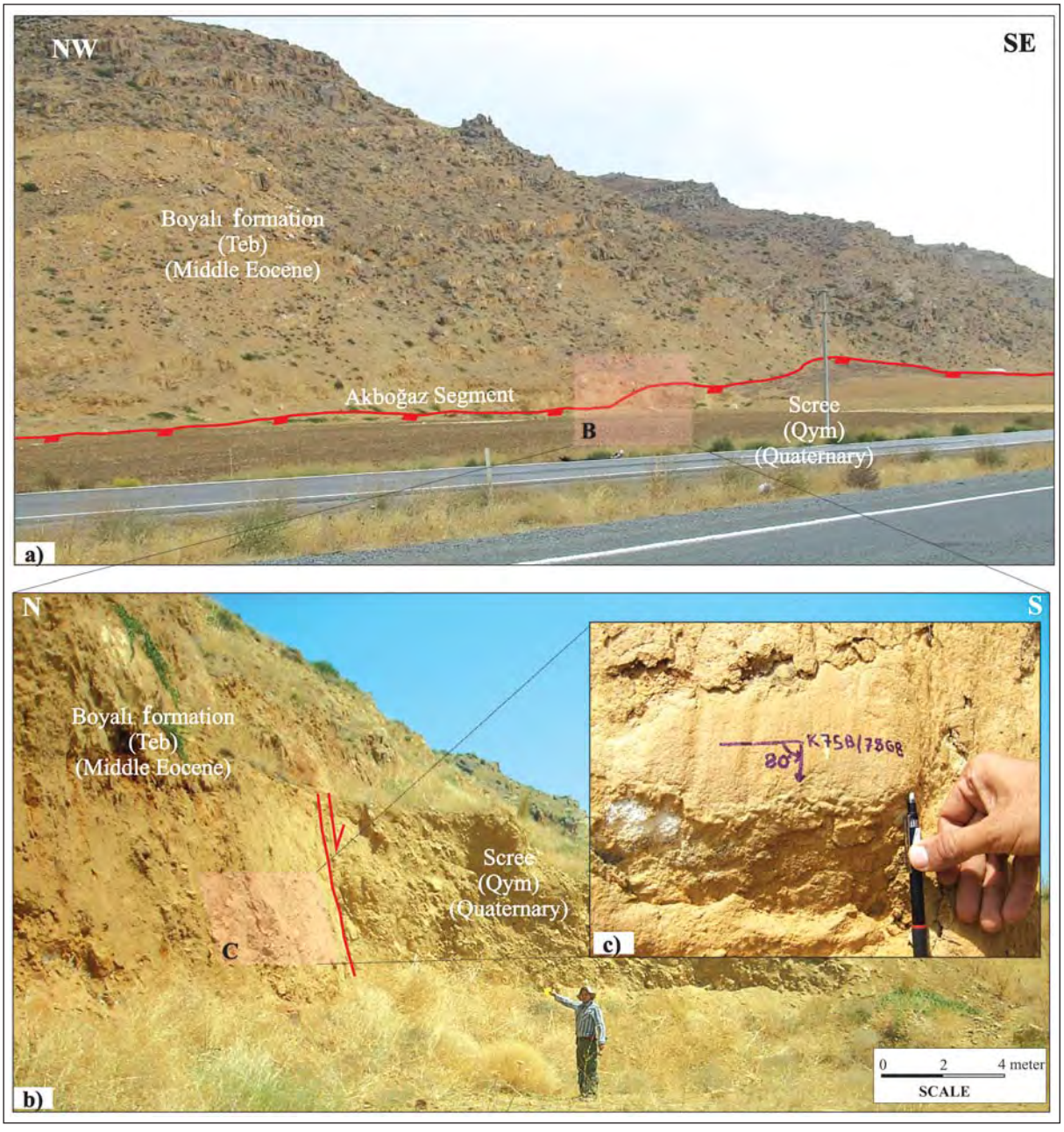

Figure 6- a) General view, b) close view of the Akboğaz segment that brings the middle Eocene Boyalı formation (Teb) and Quaternary talus deposit side-by-side at station 1 (K 30 b2 quadrangle; 542303 E – 4315245 N) and c) close view of fault plane.

Figure 7- Google Earth view of the Şeferlikoçhisar segment (vertical scale three times exaggerated, view to NE with oblique angle). Teb: Boyalı for., Teoya: Akboğaz Gypsum Member of the Yassıpur Formation, Tomkş: Şeferlikoçhisar lignite member, Tmplp: Peçenek for., Tpcl: Cihanbeyli for., Qtub: Bataklık Member of the Tuz Gölü formation, Qal: Alluvium, Station 1: Structural observation site on eastern branch of the Şeferlikoçhisar segment (Deldah düzü station), A-B: High Resolution Seismic Reflection Profile Line, TG-1: TPAO (1975) borehole location; b) Presentation on the lower hemisphere of Schmidt net projection of single-plane solution of fault plane no 2 measured at Station 2 (Deldah düzü station) in accordance with Marshak and Mitra (1988). The arrow on the fault plane shows the relative movement direction of hanging wall.

and then to right thus forming compressional and extensional structures specific to strike-slip faults.

In order to resolve literature chaos regarding Şereflikoçhisar part of TGFZ, two-dimensional high resolution seismic reflection profile work was conducted along a line of 7-km long (Kürçer, 2012; Kürçer et al., 2012) (for location of profile line see Figure 7a). The Şereflikoçhisar Two-Dimensional High Resolution Seismic Reflection Profile Section was integrated with well log of Turkish Petroleum Corporation (TPAO) (1975) and regional geology information and then evaluated (Kürçer, 2012; Kürçer et al., 2012) (Figures 9 and 10).

The Şereflikoçhisar segment was mapped based on surface geology information and geophysical data obtained from high resolution seismic reflection profile shown in figure 10 as well.

At station 2 (Deldah düzü station) a total of 5 fault planes and slickenlines were measured. Among them, measurement no 2 which is thought to best represent the station 2 was solved in accordance with Marshak and Mitra (1988) and then principal stress axes were found (Table 4; Figure 7b).

3.5. İnceburun segment (S-5)

N40°W trending 23-km long fault that morphologically surrounds the Şereflikoçhisar peninsula from SW is called as İnceburun segment (Figures 4 and 11). The İnceburun segment comprises the border between middle Eocene Boyalı formation (Teb) and alluvium deposits and causes morphologically uplift of Boyalı formation within the Tuz Gölü depression area (Figure 11).

The Tuz Gölü is divided into two sub-regions as shallow main lake region and deep region that are represented by different hydrochemical properties (Uygun and Şen, 1978) (Figure 11). The shallow main lake region has a depth of about 60-80 cm whilst deep region is a depth of 1.5-2 m (Uygun and Şen, 1978). The İnceburun segment is a barrier separating these two sub-regions. The deep region on rising foot wall of the İnceburun segment is at the same time on the hanging wall of the Tuz Gölü segment. Jointly operation of Tuz Gölü and İnceburun segments has given rise to deep region to deepen towards northeast (back tilting) and gain its recent morphology (Figure 11).

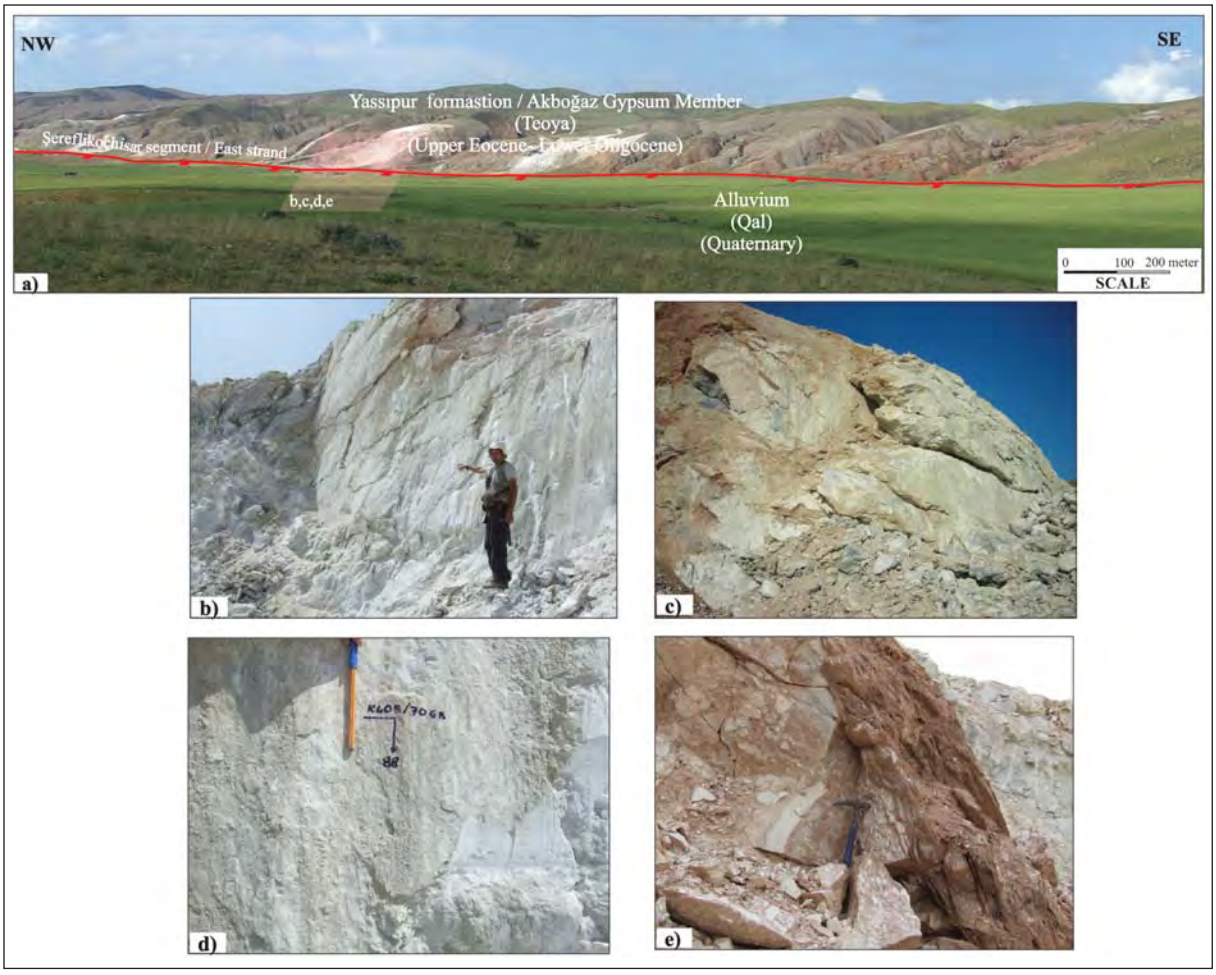

Figure 8- a) General view of the eastern branch of Şeferlikoçhisar segment that brings the Akboğaz Gypsum Member (Teoya) of the late Eocene-early Oligocene Yassıpur formation and alluvium side-by-side at station 2 (K 31 a1 quadrangle; 551800 E – 4308650 N), b) and c) general views of fault plane, d) close view of fault plane, e) fault breccia and fault gouge.

3.6. Tuz Gölü segment (S-6)

The Şereflikoçhisar segment which is transferred to the west from the Karandere village via an E-W extending normal fault of about 4 km-long (Karandere fault, see Figure 7a) extends 30 km from this point to the north of Hanobası in SE direction with strike of N35°W (Figure 12a). This part of TGFZ is called as Tuz Gölü segment (Figure 12a). In the part from NW starting point to the NW of Çalören village (Mezgit), the Tuz Gölü segment comprises the contact between middle Eocene Boyalı formation (Teb) and alluvial deposits and partly cuts alluvial fan deposits. The fault which cuts limestones of the early Paleocene Çaldağ formation (Tpç) from NW of Çalören village follows the contact between limestones and alluvium and cuts alluvial fan deposits to some extent. In the part from SW of Çalören to the north of Hanındağ, it comprises the contact between middle Eocene Boyalı formation and alluvial fan deposits and partly cuts alluvial fan deposits. At station 3 shown in figure 12a, the Tuz Gölü segment cuts an alluvial fan and this fan uplifted by fault (Figure 12c).

At east of Hanındağ, the Tuz Gölü segment brings the Boyalı formation (Teb) and Pliocene Peçenek formation side by side. Southwestern margin of Hanındağ Uplift where sandstones of the Boyalı formation are exposed is surrounded by a SW-dipping, N55ºW trending fault of about 5-km in length. The Hanındağ Fault which is sub-parallel to the Tuz Gölü segment has been appraised within the scope of Tuz Gölü segment.

In the part from SE of Hanındağ to the Asmayaylası village, the Tuz Gölü segment mostly

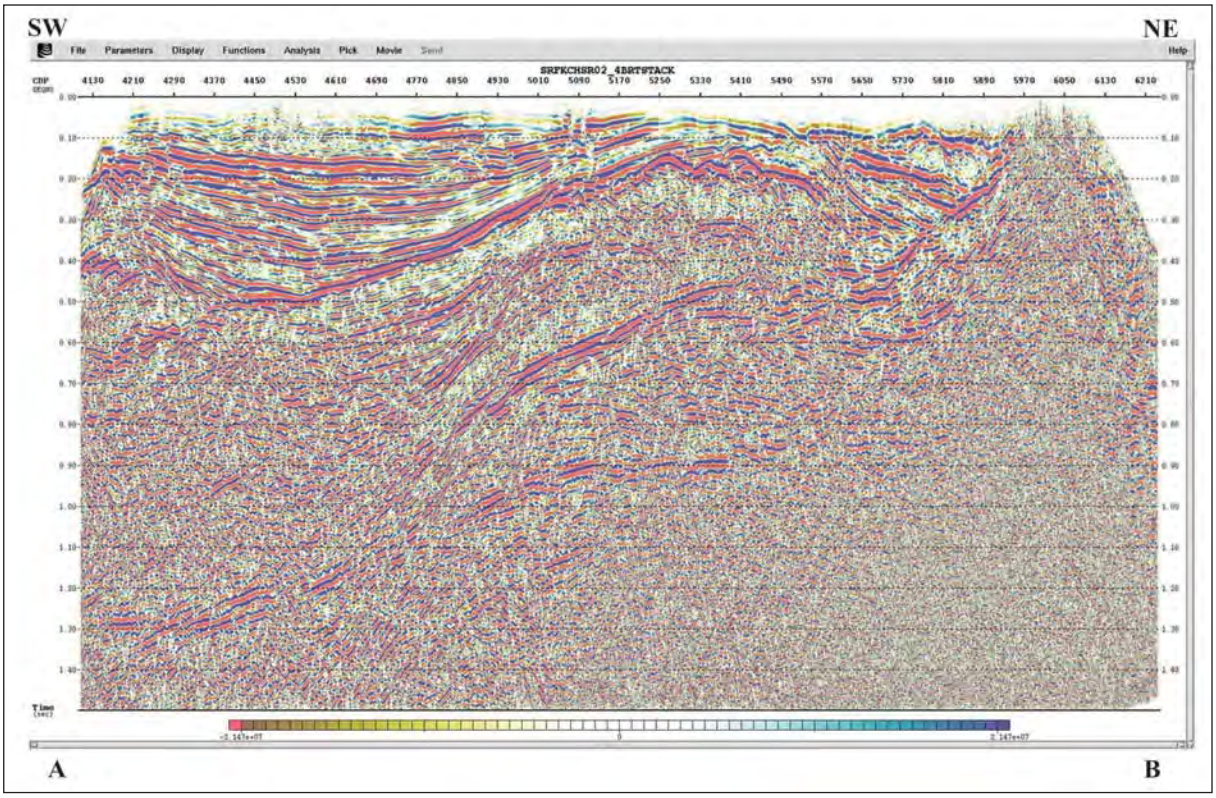

Figure 9- Migrated Two-Dimensional High Resolution Shallow Seismic Reflection Profile final section (with no geologic interpretation) taken in SW-NE direction at south of Şeferlikoçhisar (see figure 7a for profile location).

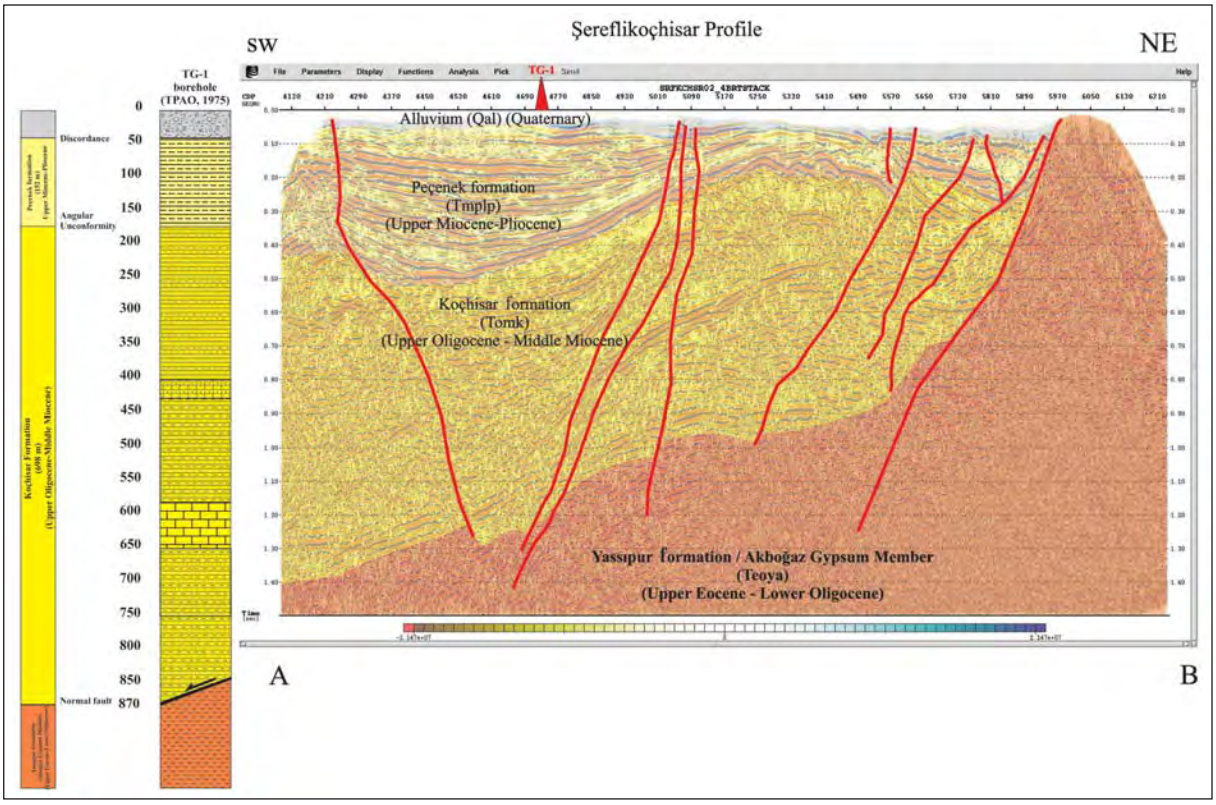

Figure 10- Migrated Two-Dimensional High Resolution Shallow Seismic Reflection Profile final section (interpreted) taken in SW-NE direction at south of Şeferlikoçhisar (see figure 7a for profile location).

Figure 11- Google Earth view of the İnceburun segment (vertical scale three times exaggerated, view to NE with oblique angle). Teb: Boyalı Fm, Qtub: Bataklık Member of the Tuz Gölü formation, Qal: Alluvium, Qay: Alluvial fan.

Figure 12- a) Google Earth view of the Tuz Gölü segment (vertical scale three times exaggerated, view to NE with oblique angle). Kk: Kartal fm., Ka: Asmaboğazı fm, Tç; Çaldağ fm, Teb: Boyalı fm, Teoya: Akboğaz Gypsum Member of the Yassıpur fm, Teomk: Koçhisar fm, Tmplp: Peçenek fm, Tpcl: Cihanbeyli fm, Qtuy: Yeşilova Member of the Tuz Gölü formation, Qtub: Bataklık Member of the Tuz Gölü formation, Qal: Alluvium, Qay: Alluvial fan, Stations 3 and 4: structural observation sites on the Tuz Gölü segment; b) Presentation on the lower hemisphere of Schmidt net projection of single-plane solution of fault plane no 4 measured at Station 4 (Asmayaylası station) in accordance with Marshak and Mitra (1988). The arrows on the fault plane show the relative movement direction of hanging wall; c) An alluvial fan (Qay) cut by the Tuz Gölü segment at station 3 (K 31 a3 quadrangle; 558393 E – 4289644

cuts the alluvial fan deposits whilst in the Asmayaylası village it cuts units of the late Cretaceous-early Paleocene Asmaboğazı formation. At station 4 shown in Figure 12a (Asmaboğazı station), fault plane of Tuz Gölü segment is clearly observed in limestone level of the Asmaboğazı formation (Figure 13).

Fault plane solutions at station 4 (Asmayaylası station) showed that the Tuz Gölü segment is dominated by a right-lateral strike-slip component (Figure 13b and c; table 3).

At station 4 (Asmayaylası station) a total of 4 fault planes and slickenlines were measured. Among them, measurement no 4 which is thought to best represent the station 4 was solved in accordance with Marshak and Mitra (1988) and then principal stress axes were found (Table 4; figure 12b).

3.7. Acıpınar segment (S-7)

The Acıpınar segment is separated from the Tuz Gölü segment with a 500 m right step-over at north of Hanobası (Figure 12a). The Acıpınar segment with length of 26 km extends in N45°W direction between Hanobası and Çimeliyeniköy (north of Aksaray) (Figures 4 and 14). The segment which mostly forms the boundary between late Oligocene – middle Miocene Koçhisar formation (Tomk) and alluvial sediments, in a limited area between Baymış and Çimeliyeniköy, cuts the late Miocene-Pliocene Peçenek formation of terrestrial character with a secondary fault section that is parallel to the main fault (Figure 14a). Structural observations on Acıpınar segment of TGFZ are limited to station no 5 (Figure 14a). In an area within the Baymış village late Miocene-Pliocene Peçenek formation (Tmplp) is cut by the Acıpınar segment (Figures 14b and c).

3.8. Aksaray segment (S-8)

TGFZ which jumps 600 m to the left from the south of Çimeliyeniköy, crosses the city center of Aksaray in NW-SE direction and extends to the north of Akhisar village. Nearly N32°W extending 13-km long part of the fault is called Aksaray segment (Figures 4 and 15). In this area, the Aksaray segment forms the contact between terrestrial clastics of the

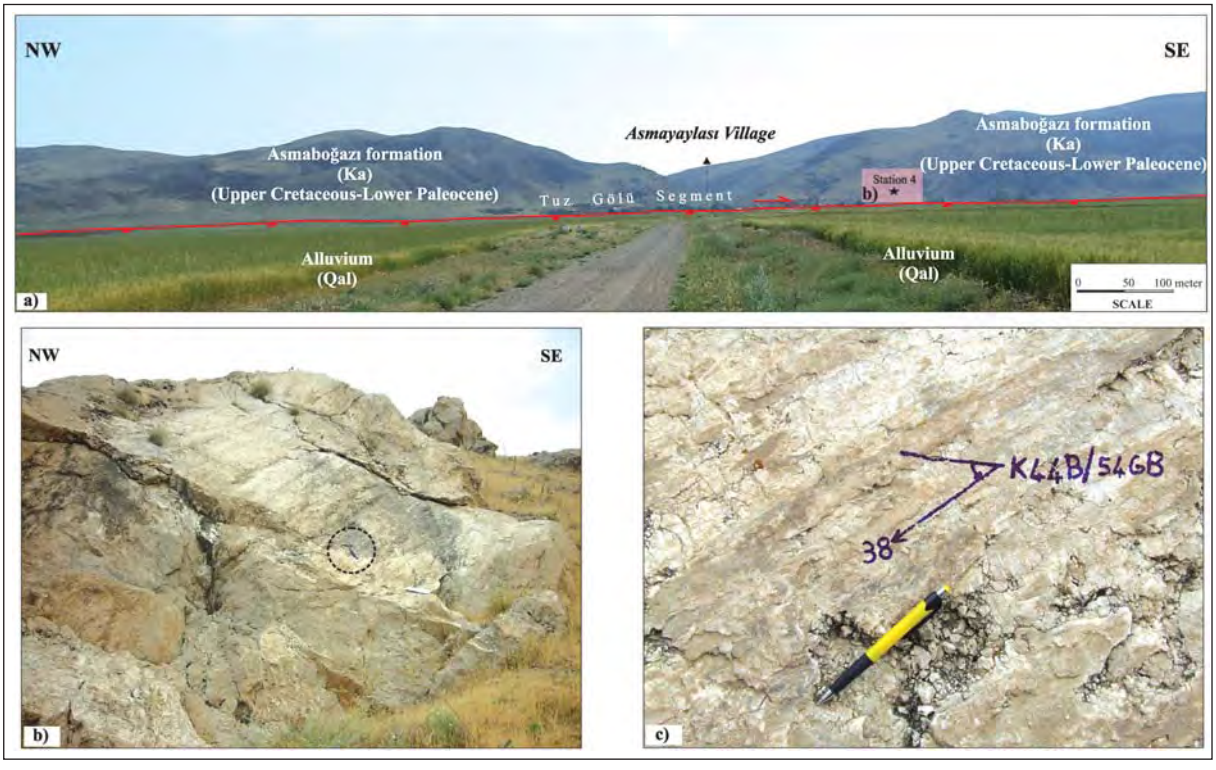

Figure 13- a) Panoramic view of Tuz Gölü segment that cuts a limestone level of the late Cretaceous-early Paleocene Asmaboğazı formation (Ka) and brings the Asmaboğazı formation and alluvium deposits (Qal) side-by-side at station 4 (Asmayaylası station) (K 31 c1 quadrangle; 566270 E – 4278286 N) (view to NE), b) General view of fault plane (view to NE, scale hummer is 33 cm), c) Close view of fault plane (view to NE, scale pen is 13 cm).

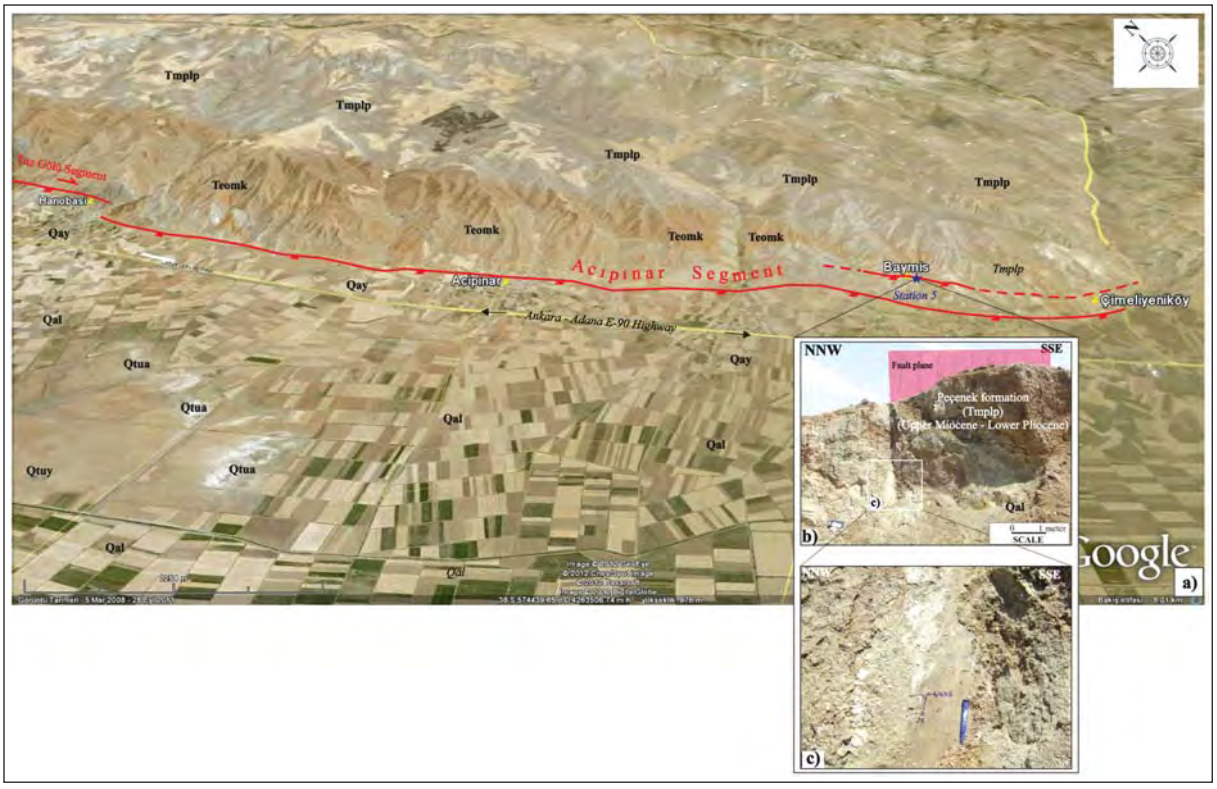

Figure 14- a) Google Earth view of the Acıpınar segment (vertical scale three times exaggerated, view to NE with oblique angle). Teomk: Koçhisar fm, Tmplp: Peçenek fm, Qtuy: Yeşilova Member of the Tuz Gölü formation, Qtua: Alibekağılı Member of the Tuz Gölü formation, Qal: Alluvium, Qay: Alluvial fan, Station 5: Structural observation point on the Acıpınar segment; b) Panoramic view of the Acıpınar segment that cuts terrestrial deposits of late Miocene-early Pliocene Peçenek formation (Tmplp) at station 5 (K 31 c3 quadrangle; 578097 E – 4262063 N) (view to NE), c) Close view of fault plane (view to NNE, scale pen is 13 cm).

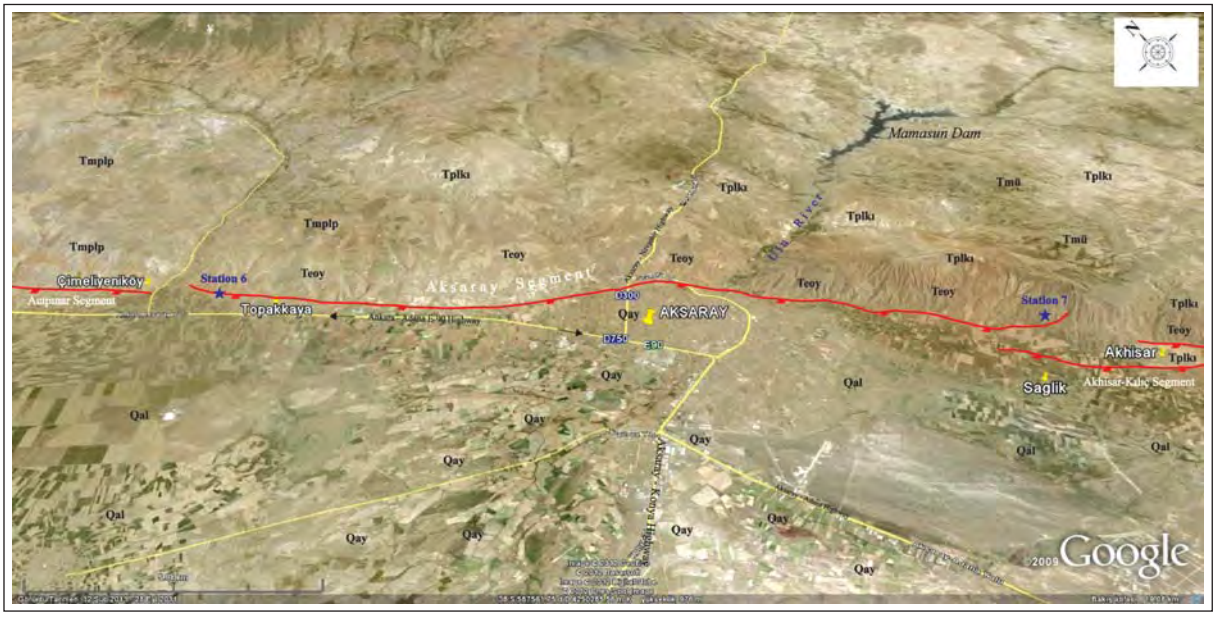

Figure 15- Google Earth view of the Aksaray segment (vertical scale three times exaggerated, view to NE with oblique angle). ¥: Ağaçören granitoid, Teoy: Yassıpur fm, Tmplp: Peçenek fm, Tplkı: Kızılkaya Ignimbrite, Qal: Alluvium, Qay: Alluvial fan (mostly Aksaray Alluvial fan), stations 6 and 7: structural observation sites on the Aksaray segment.

late Eocene – Oligocene aged Yassıpur formation (Teoy) and alluvial fan deposits. In the city center of Aksaray it cuts the Aksaray alluvial fan.

On the Aksaray segment structural observations were made at stations 6 and 7 as shown in figure 15. In a sand quarry opened on the flank of Çatak Hill 3 km NW of Topakkaya village (station 6 in Figure 15) the Aksaray segment cuts the terrestrial clastics of the late Eocene–Oligocene aged Yassıpur formation and caused them to dip nearly 40° towards the fault (to NE) (Figure 16).

The second observation site on the Aksaray segment is located at SE corner of the segment (station 7 in Figure 15). At this site, an antithetic fault that dips NE at foot wall of the Aksaray segment cuts terrestrial clastics of the late Eocene–Oligocene aged Yassıpur formation (Fig. 17). The main of Aksaray segment extends about 100 m SW of this point.

3.9. Akhisar-Kılıç segment (S-9)

TGFZ that jumps 750 m right at north of the Akhisar village continues 27 km in SE direction reaches at Kılıç ridge on east of the Hasan Mountain. This part of fault that extends in N25-30°W is called as Akhisar-Kılıç segment (Figures. 4 and 18). Around the Akhisar village the Akhisar-Kılıç segment cuts the early Pliocene Kızılkaya Ignimbrite which sets with an angular unconformity above the terrestrial clastics of the late Eocene–Oligocene aged Yassıpur

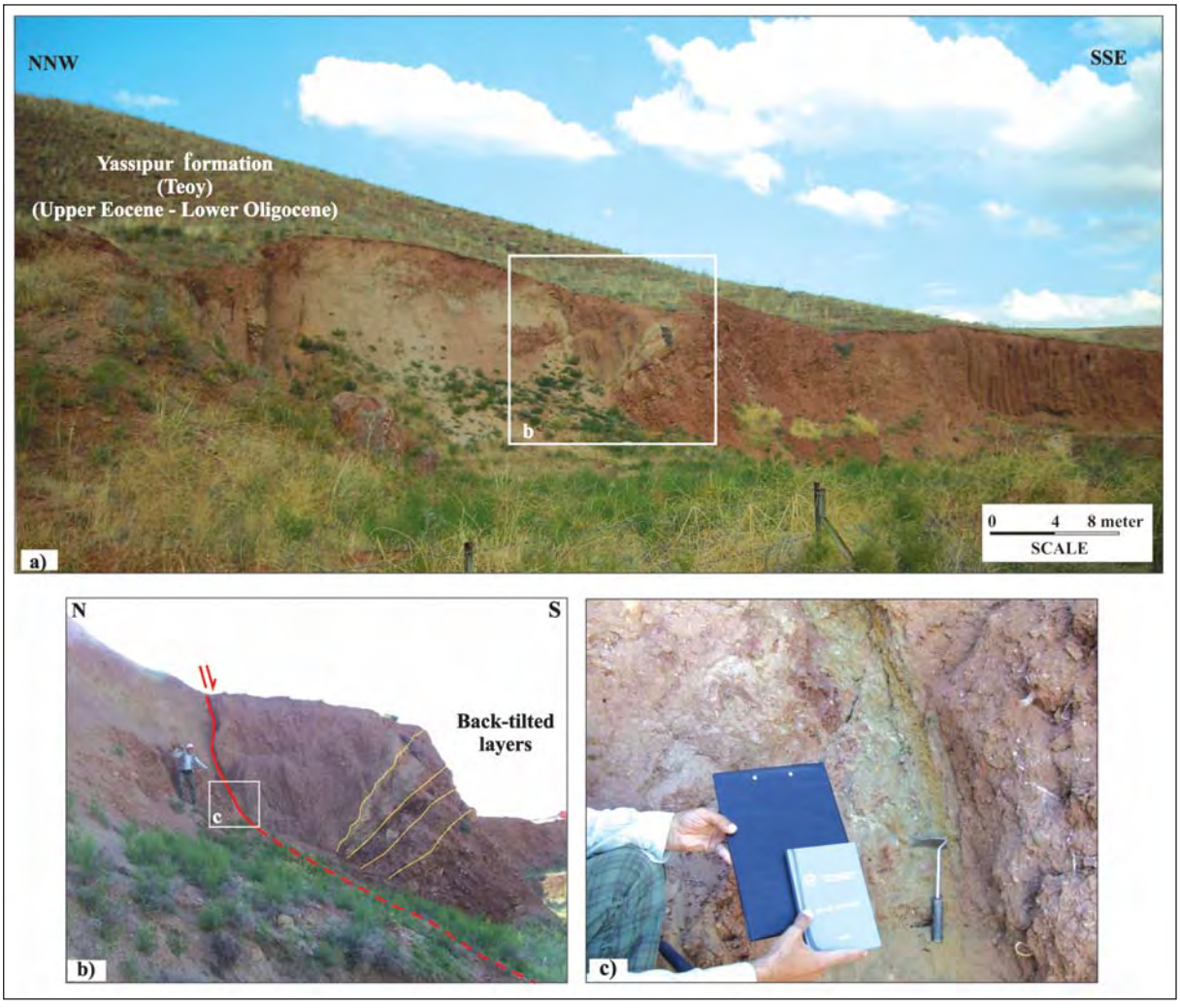

Figure 16- a) Panoramic view of Aksaray segment that cuts terrestrial deposits of late Eocene-early Oligocene Yassıpur formation (Teoy) at station 6 (L 31 b2 quadrangle; 579796 E – 4259575 N) (view to NNE), b) General view of layers dipping towards the fault (back-tilting) (view to t N, scale hummer is 1.8 m), c) Crushed zone along the fault plane (scale shovel is 22 cm).

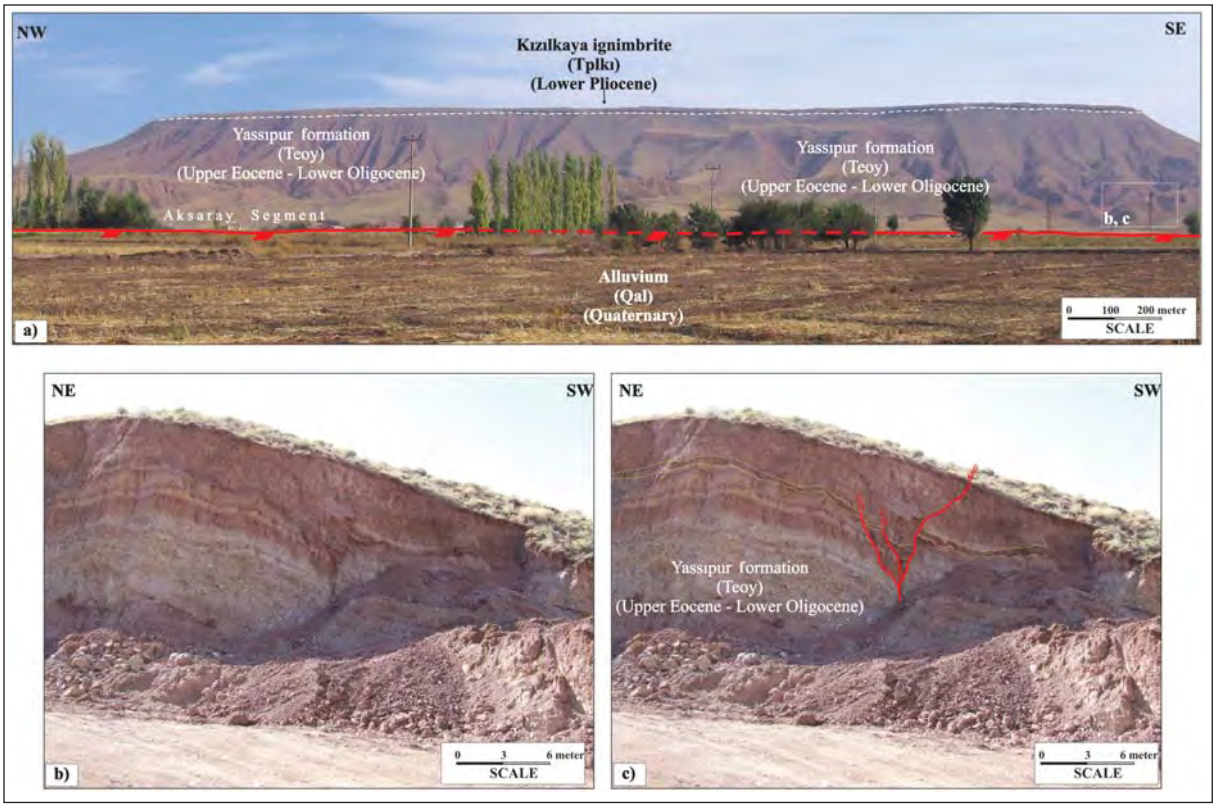

Figure 17- a) Panoramic view of Aksaray segment that cuts terrestrial deposits of late Eocene-early Oligocene Yassıpur formation (Teoy) at SE of Aksaray (view to NNE), b) Unprocessed view of an antithetic normal fault on foot wall of the Aksaray segment at station 7 (L 32 a4 quadrangle; 594475 E – 4243125 N), c) Processed view of normal fault at station 7 (view to SE).

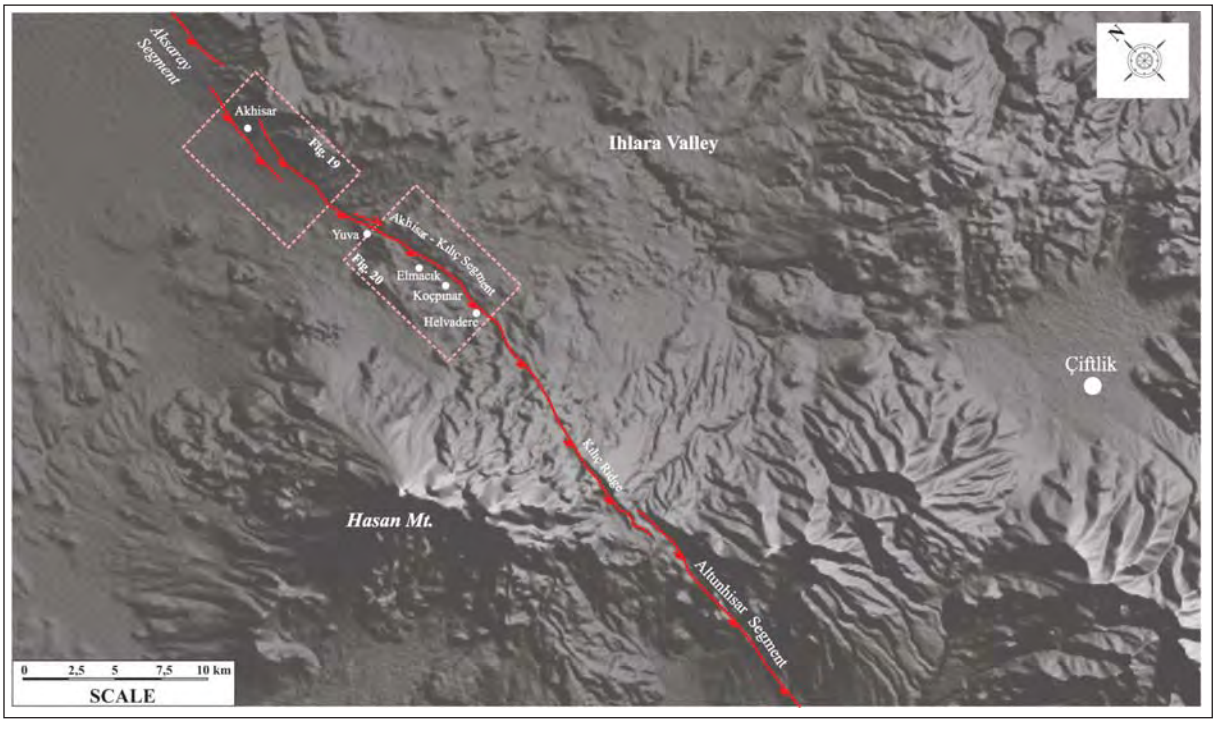

Figure 18- Digital Elevation Model (DEM) for the Akhisar-Kılıç segment. For DEM Shuttle Radar Topography Mission (SRTM) data were used (vertical scale three times exaggerated, view to NE).

formation lowering them to the plain altitude (Figure 19). The fault comprising the contact of terrestrial clastics of the Yassıpur formation and alluvium between the Akhisar and Yuva villages locally cuts the alluvial fan deposits. The fault that cuts first-stage ash and block flows of the Hasandağ Volcanites around NW of Yuva village surrounds the NW-SE extending depression area of an ellipsoidal geometry between Yuva and Helvadere villages at NE (Figure 20a). In this area the fault locally cuts the late Pleistocene-Holocene deposits and in the part from SE of Helvadere to the Kılıç ridge again cuts various units of Quaternary Hasandağ Volcanites (Qh) and ends up at the Kılıç ridge.

The Akhisar-Kılıç segment is characteristic with alluvial fans and linear fault scasrps that are aligned in parallel between Akhisar and Yuva villages. Starting from SE of the Yuva village, several structural observations were made on the fault (stations 8, 9, 10, 11 and 12 in figure 20a).

Station 8 is located on eastern flank of narrow and deep valley at east of the Yuva village (Figure 20a). At this site, the Akhisar-Kılıç segment cuts the first-stage ash and block flows of the Hasandağ Volcanites (Qhb1) and this relation is clearly shown on the exposure (Figure 21a and b).

Station 9 is located 600 m SE of the Yuva village (Figure 20a). At this point, the Akhisar-Kılıç segment cuts the first-stage ash and block flows of the Hasandağ Volcanites (Qhb1) and this relation is clearly shown on the exposure (Figure 21c and d).

Fault plane measurements on observation points 8 and 9 (Yuva station) at the Akhisar-Kılıç segment showed that this segment is an oblique-slip normal fault with right-lateral strike-slip component (Table 3).

On two different exposures 500 m in distance at E and SE of the Yuva village (stations 8 and 9 in figure 20a), the first-stage ash and block flows of the Quaternary Hasandağ Volcanites (Qhb1) is cut by the Akhisar-Kılıç segment. These two outcropes are evaluated jointly and named as the Yuva station. At the Yuva station a total of 5 fault planes and slickenlines scratches were measured. Among these measurements, measurement no. 4 which is thought to best represent the Yuva station was solved in accordance with Marshak and Mitra (1988) and then principal stress axes were found (Table 4; Figure 20b).

Another observation site where fault planes of the Akhisar-Kılıç segment are examined is found at east of Koçpınar village (Koçpınar station) (station 10 in Figure 20a). Similar to previous observation sites, at station 10, Akhisar-Kılıç segment cuts the first-stage ash and block flows of the Quaternary Hasandağ

Figure 19- Google Earth view of northern part of the Akhisar-Kılıç segment (see Figure 18 for location) (vertical scale three times exaggerated, view to NE). Teoy: Yassıpur fm, Tmü: Ürgüp fm, Tplkı: Kızılkaya Ignimbrite, Qka: Karataş volcanites, Qhb1: first-stage ash and block flows of the Hasandağ volcanites, Qal: Alluvium, Qay: Alluvial fan.

Figure 20- a) Google Earth view of central part of the Akhisar-Kılıç segment (see Figure 18 for location) (vertical scale three times exaggerated, view to NE). Tmü: Ürgüp fm, Tplkı: Kızılkaya Ignimbrite, Qka: Karataş Volcanites, Qht1: First-stage air fall and flow tuffs of the Hasandağ Volcanites, Qal: Alluvium, Stations 8, 9, 10, 11 and 12: structural observation site on the Akhisar-Kılıç segment, b) Presentation on the lower hemisphere of Schmidt net projection of single-plane solution of fault plane no 4 measured at Station 4 (Yuva station) in accordance with Marshak and Mitra (1988). The arrow on the fault plane shows the relative movement direction of hanging wall; c) Presentation on the lower hemisphere of Schmidt net projection of single-plane solution of fault plane no 4 measured at Stations 10-11 (Koçpınar station) in accordance with Marshak and Mitra (1988). The arrow on the fault plane shows the relative movement direction of hanging wall.

Volcanites (Qhb1) and this relation is clearly shown on the exposure (Figure 22a).

In the part of Akhisar-Kılıç segment between the Elmacık and Yuva villages, several gaseous and brackish water springs are issued. These springs are aligned along a zone of 50 m width parallel to the fault. Among them, the most important one is the Ayazma point within the Koçpınar village (station 11 in Figures 20 and 23). Assessment of water chemistry of Koçpınar springs is done by Afşin and Baş (1996). The results indicate that fractured and fissured marbles of the Paleozoic Bozçaldağ formation (Pzb) are the aquifer of Koçpınar springs. According to Afşin and Baş (1996), as a result of density decrease by endogenic CO_2, meteoric waters penetrating downward along discontinuities might have mixed with waters from the aquifer and moved upward into ignimbrite (Kızılkaya Ignimbrite), andesite and tuffs (Hasandağ Volcanites). During rise to the surface, waters are interacted with rocks which changed their chemical composition (Afşin and Baş, 1996). Chemical composition of spring waters is strongly affected by CO_2 dissolution. Temperature of waters rising from the aquifer should have been decreased due to mixing with shallow groundwater and atmospheric effects.

The last observation site where structural data on faults are examined on the Akhisar-Kılıç segment is located at east of artificial pond in the Helvadere town (station 12 in figure 20). At station 12, the Akhisar-Kılıç segment cuts the first-stage ash and block flows of the Quaternary Hasandağ Volcanites (Qhb1) (Figure 22c and d).

Fault plane measurements conducted on Koçpınar station at the Akhisar-Kılıç segment showed that this segment is an oblique-slip normal fault with right-lateral strike-slip component (Table 3).

At Koçpınar station a total of 4 fault planes and slickenlines were measured. Among them, measurement no 4 which is thought to best represent the Koçpınar station was solved in accordance with Marshak and Mitra (1988) and then principal stress axes were found (Table 4; Figure 20c).

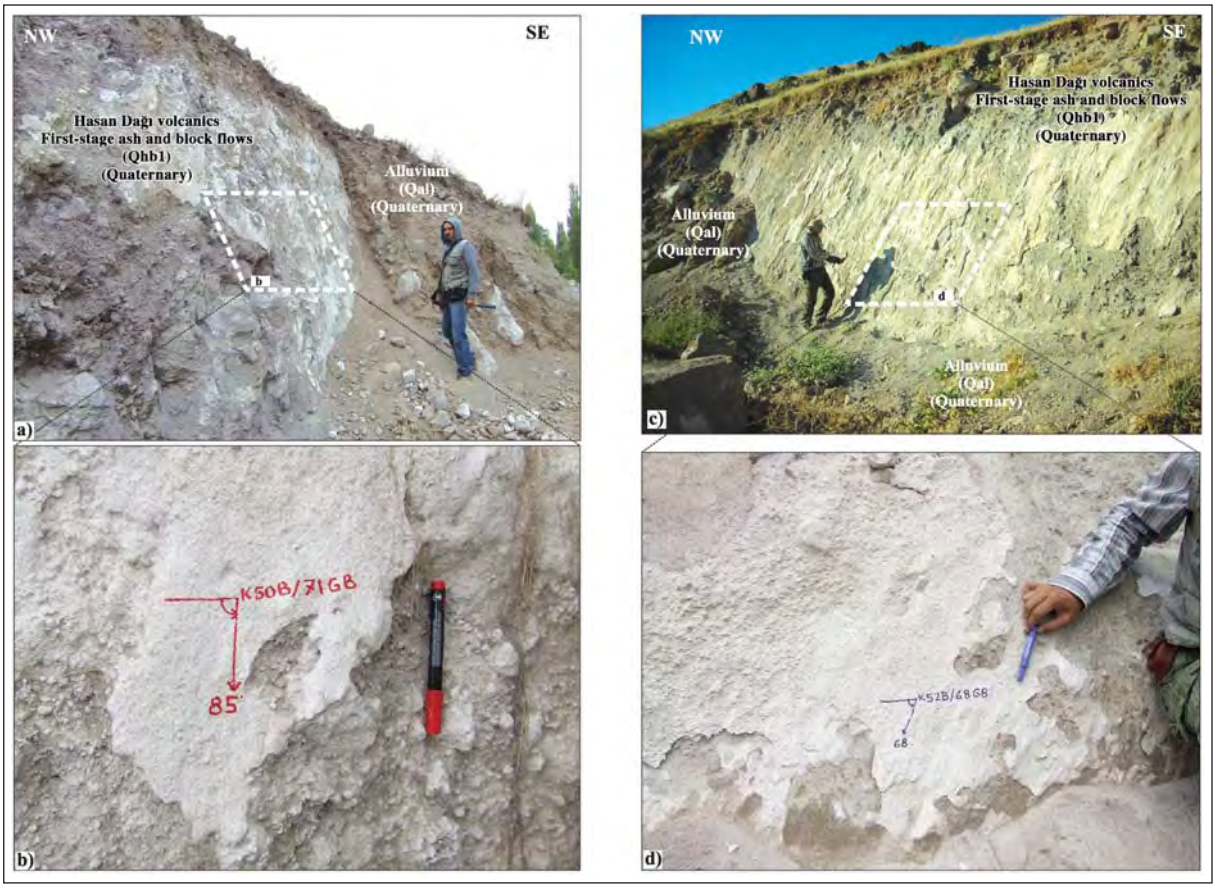

Figure 21- a) General view of fault plane of the Akhisar-Kılıç segment that cuts first-stage ash and block flow s of the Hasandağ Volcanites (Qhb1) at east of Yuva village (L 32 d2 quadrangle; 601450 E – 4234000 N) (view to NE scale geologist is 1.80 m), b) Close view of fault plane (view to NE scale pen is 12 cm), c) General view of fault plane of the Akhisar-Kılıç segment that cuts first-stage ash and block flow s of the Hasandağ Volcanites (Qhb1) at SE of Yuva village (L 32 d2 quadrangle; 601984 E – 4233726 N) (view to NE scale geologist is 1.80 m), d) close view of fault plane (view to NE scale pen is 12 cm).

3.10. Altunhisar segment (S-10)

TGFZ that jumps 500 m left from SE of Kılıç ridge extends in N20°W direction to Altunhisar via a few parallel fault sections. It bends to 30°SE around Altunhisar and continues in N50°W direction to the south of Tepeköy. From this location fault bends again to 20°SE and is ended at NW of Bor town. The 30-km part of the fault outlined above is called as Altunhisar segment (Figures 4 and 24a).

The Altunhisar segment cuts the first-stage ash and block flows of the Quaternary Hasandağ Volcanites (Qhb1) in the area between east of Kılıç ridge and Altunhisar and it cuts the Balcı Volcanite of late Miocene age (Tmb) at NW of Altunhisar. The fault cuts Quaternary alluvial fan deposits (Qay) and talus deposits and from this point to SE edge of segment if follows the border of Balcı Volcanite (Tmb) and alluvial deposits (Qal).

Structural observations were made on two points at the Altunhisar segment (stations 13 and 14 in figure 24). At station 13, the Altunhisar segment cuts the first-stage air-fall flow tuffs of the Quaternary Hasandağ Volcanites (Qht1). This relation is shown in a pumice quarry opened on the road from Altunhisar to Kirteli village (Figure 25).

Another measurement point at the Altunhisar segment is located about 1.5 km NW of Altunhisar. On a road cut between Altunhisar and Çiftlik, the Altunhisar segment is observed as a normal fault in a 30-m area (Figure 26). At this site, fault cuts the first-stage fall deposits and flow tuffs of the Quaternary Hasandağ Volcanites (Qht1).

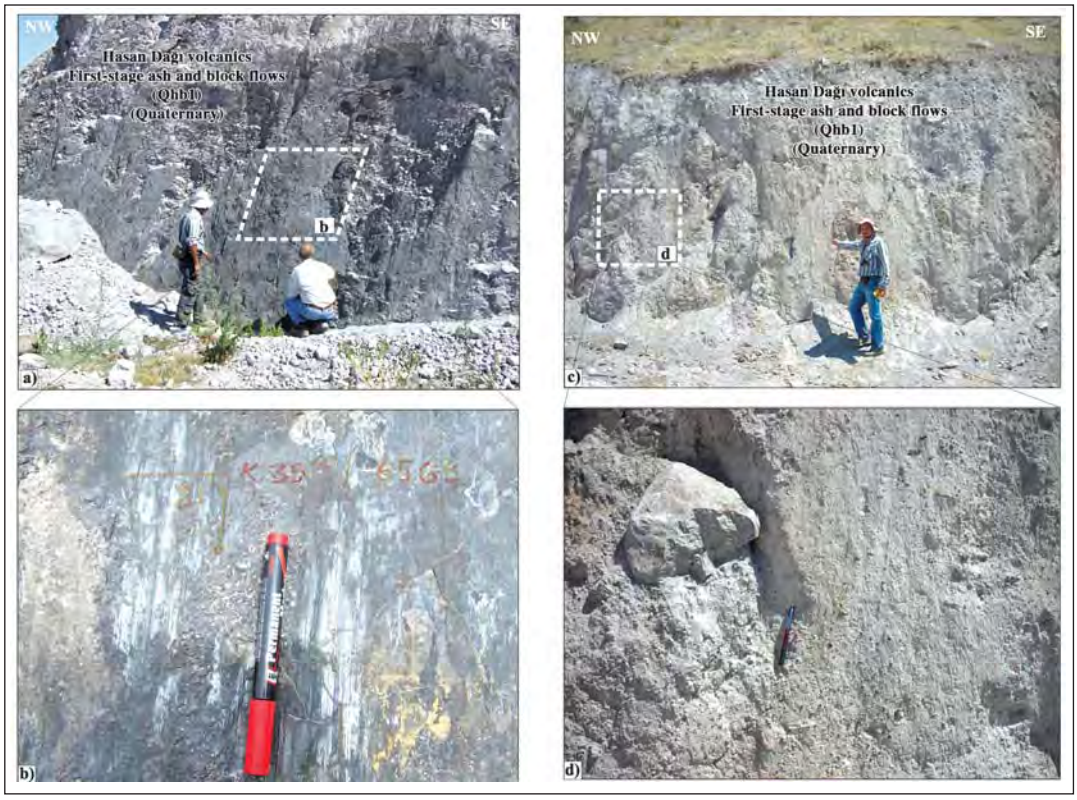

Figure 22- a) General view of fault plane of the Akhisar-Kılıç segment that cuts first-stage ash and block flow s of the Hasandağ Volcanites (Qhb1) at east of Koçpınar village (L 32 d2 quadrangle; 604694 E – 4231266 N) (view to NE scale geologist is 1.80 m), b) Close view of fault plane (view to NE scale pen is 12 cm), c) General view of fault plane of the Akhisar-Kılıç segment that cuts first-stage ash and block flow s of the Hasandağ Volcanites (Qhb1) at east of Helvadere pond (L 32 d2 quadrangle; 606111 E – 4228966 N) (view to NE scale geologist is 1.80 m), d) Close view of fault plane (view to NE scale pen is 12 cm).

Figure 23- Gaseous and brackish water manifestation point at Ayazma site in the Koçpınar village (L 32 d2 quadrangle; 604661 E – 4231053 N) (view to N scale geologist is 1.80 m).

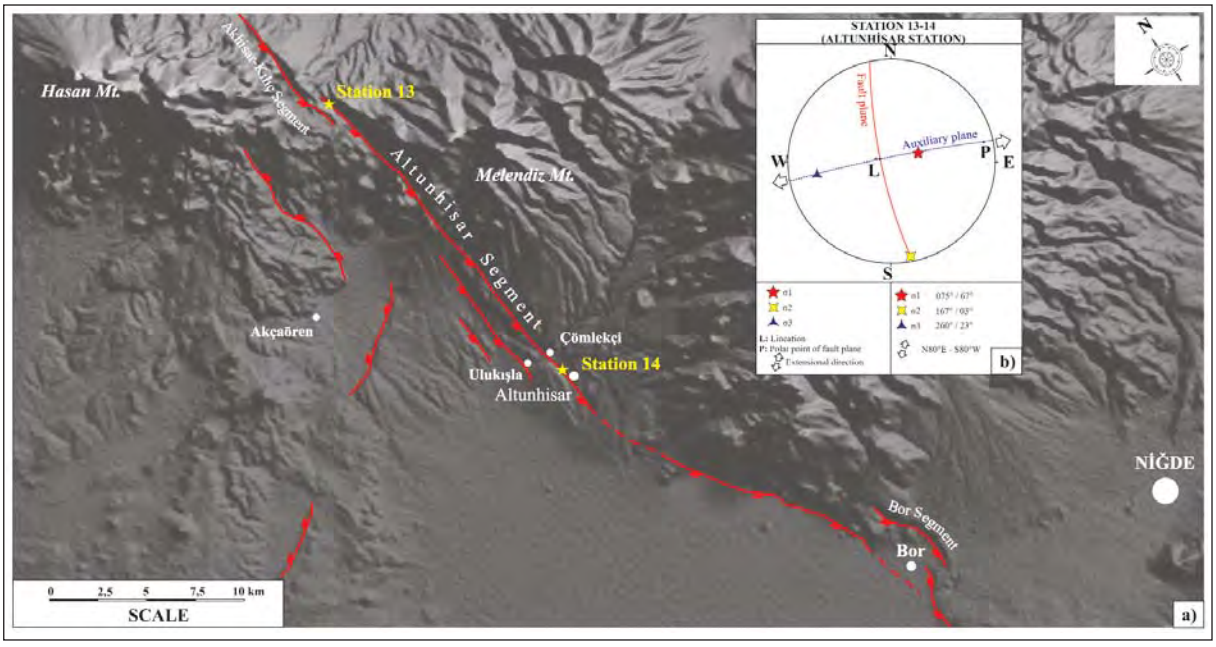

Figure 24- a) Digital Elevation Model (DEM) for the Altunhisar segment. For DEM Shuttle Radar Topography Mission (SRTM) data were used (vertical scale three times exaggerated, view to NE). Stations 13 and 14: structural observation points on the Altunhisar segment, b) Presentation on the lower hemisphere of Schmidt net projection of single-plane solution of fault plane no 2 measured at Stations 13-14 (Altunhisar) in accordance with Marshak and Mitra (1988). The arrow on the fault plane shows the relative movement direction of hanging wall.

Fault plane measurements conducted on Altunhisar segment (stations 13 and 14) showed that this segment is a normal fault with minor right-lateral strike-slip component (Table 3).

At Altunhisar station a total of 6 fault planes and slickenlines were measured. Among them, measurement no 2 which is thought to best represent the Altunhisar station was solved in accordance with Marshak and Mitra (1988) and then principal stress axes were found (Table 4; Figure 24b).

3.11. Bor segment (S-11)

The Bor segment represents the most SE part of TGFZ. The Bor segment with nearly 17 km in length is composed of two sub-parts (Figures 4 and 27a). The 4 km long northern part starts from SSW of Okçu village (Bor, Niğde) and extends to the Bor Çarşı Neighborhood. In this area, fault forms the boundary between pyroclastic rocks of Quaternary Melendiz Dağ Volcanites (Qm) and alluvial deposits (Qal). The Bor segment that jumps about 400 m right in the Çarşı Neighborhood continues to the south and then bends to SE around the Acıgöl graveyard (Bor) and reaches at Karamahmutlu village along N50ºW direction. In this area, the Bor segment cuts the lacustrine limestones of late Miocene-Pliocene Gökbez formation (Tmplg) and pyroclastic rocks of Quaternary Melendiz Dağ Volcanites (Qm) and brings the alluvium deposits and the Gökbez formation side by side. At NE of Kemerhisar, the Bor segment is represented by Holocene fault scarps.

The last observation point where structural features of TGFZ can be seen is located in central part of the Bor segment (station 15 in figure 27a). At station 15, fault plane of the Bor segment is observed on an outcrop 500 m east of Acıgöl graveyard in Bor town center. At this exposure, fault cuts late Miocene-Pliocene Gökbez formation (Tmplg) and unconformably overlying pyroclastic of Quaternary Melendiz Dağ Volcanites (Qm) (Figure 28).

Fault plane measurements conducted on the Bor segment (stations 15) showed that this segment is a normal fault with minor strike-slip component (Table 3).

At Bor station a total of 4 fault planes and slickenlines were measured. Among them, measurement no 2 which is thought to best represent the Bor station was solved in accordance with Marshak and Mitra (1988) and then principal stress axes were found (Table 4; Figure 27b). As a result of kinematic analysis conducted on TGFZ, an NE-SW

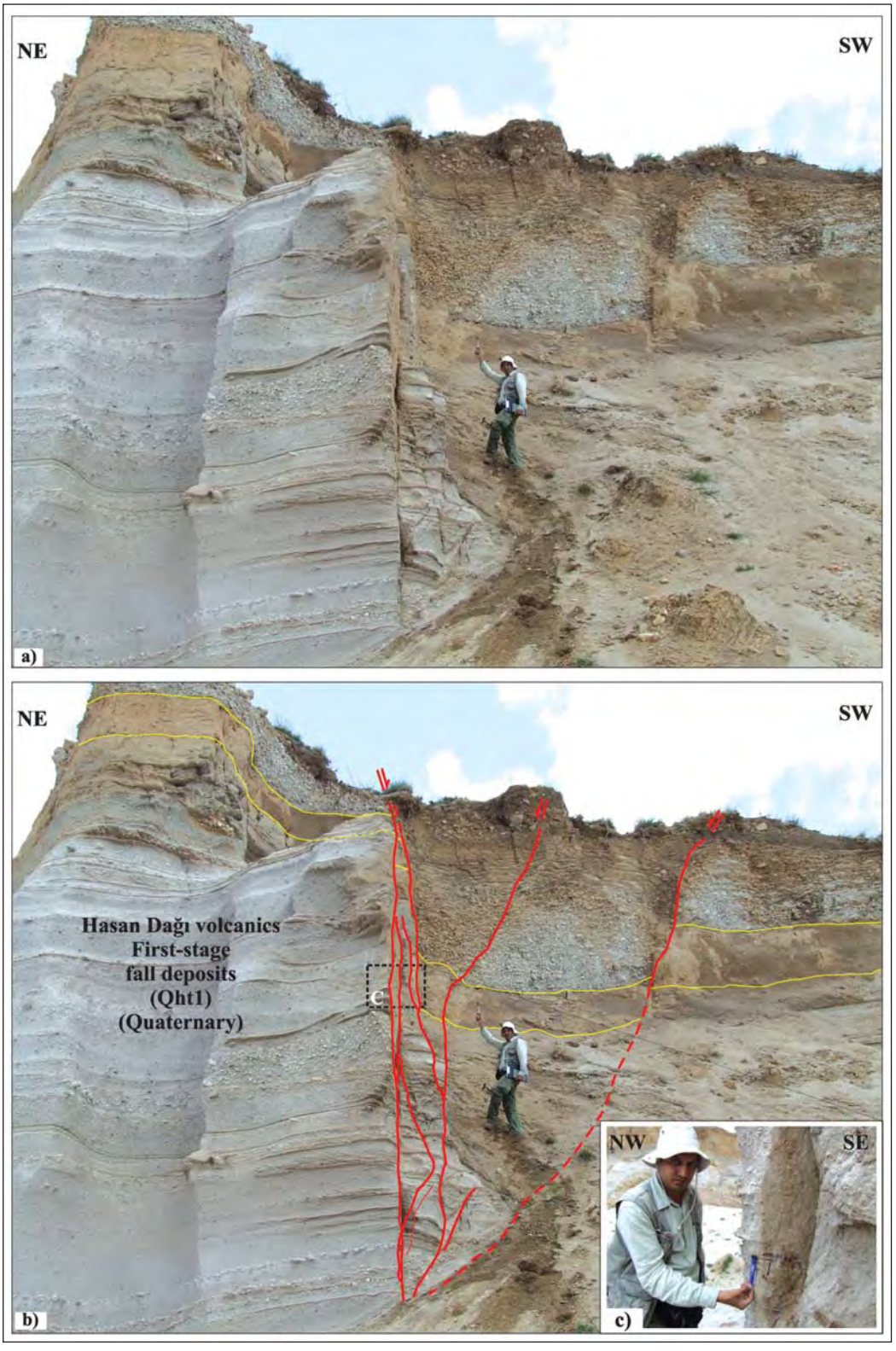

Figure 25- a) Uncommented section view of the Altunhisar segment (L 32 c4 quadrangle; 611968 E – 4220234 N) that cuts the first-stage air fall and flow tuffs of the Quaternary Hasandağ Volcanites (Qht1) in pumice quarry at east of the Kılıç ridge (Figure 24, station 13), b) Interprated section view, c) Close view of fault plane (view to SE for a and b, scale geologist is 1.80 m; view to NE for c, scale pen is 12 cm).

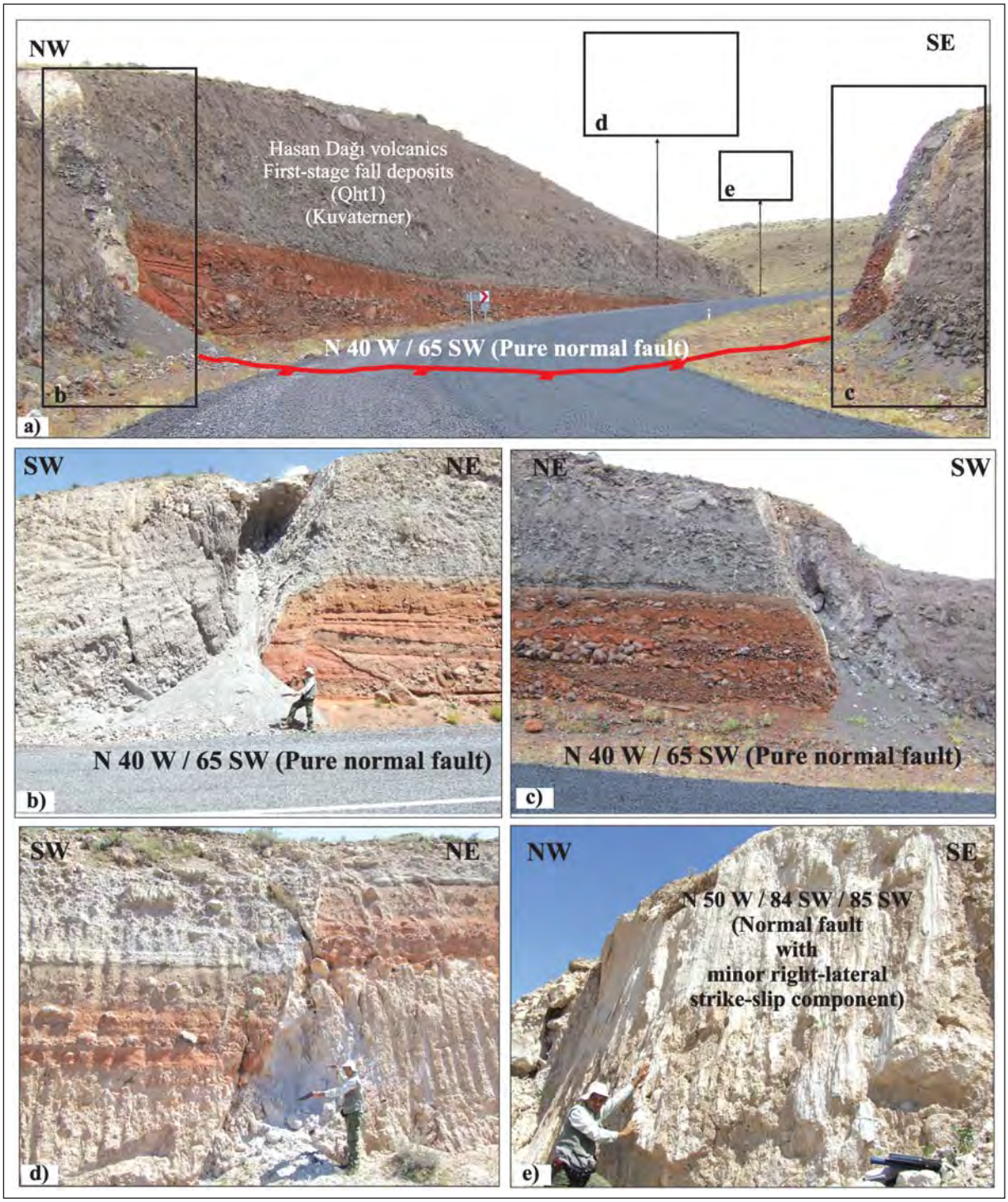

Figure 26- a) Panoramic view of Altunhisar segment (L 32 c4 quadrangle; 619831 E – 4208270 N) that cuts the first-stage air fall and flow tuffs of the Quaternary Hasandağ Volcanites (Qht1) on Altunhisar-Çiftlik road cut (Figure 24, station 14) (view to NE), b) General view of fault plane on NW side of road cut (view to NW), c) General view of fault plane on SE side of road cut (view to SE), d) A small-scale graben structure on NW side of the road, nearly 25 m NE of front fault (view to NW), e) A normal fault plane on NW side of road nearly 15 m NE of front fault (view to NE).

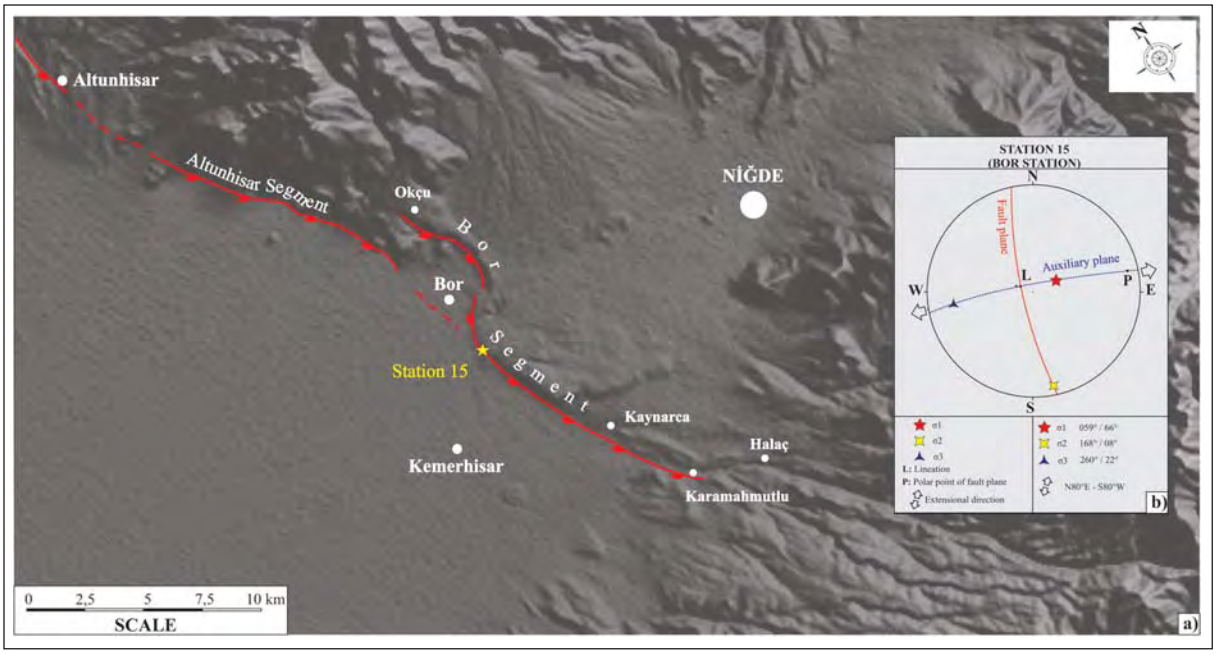

Figure 27- a) Digital Elevation Model (DEM) for the Bor segment. For DEM Shuttle Radar Topography Mission (SRTM) data were used (vertical scale three times exaggerated, view to NE). Stations 15: structural observation site on the Bor segment, b) Presentation on the lower hemisphere of Schmidt net projection of single-plane solution of fault plane no 2 measured at station 15 (Bor) in accordance with Marshak and Mitra (1988). The arrow on the fault plane shows the relative movement direction of hanging wall.

trending extensional regime was found to be effective in the region (Figure 29).

This result is consistent with NNE-SSW trending extensional regime deduced from studies on the Cihanbeyli and Yeniceoba Fault Zones at west of Lake Tuz (Özsayın, 2007; Özsayın and Dirik, 2007). In addition, moment tensor solution (Figure 30) of the 13 June 2011 Ataköy (Aksaray) earthquake (M=3.9) indicates (Kandilli Observatory and Earthquake Research Institute) that the Ataköy earthquake is produced by a N34ºW trending 80ºSW dipping oblique-slip normal fault with right-lateral strike-slip component. This finding is quite compatible with fault plane slip data on TGFZ.

4. Seismicity of the Tuz Gölü Fault Zone

4.1. Historical (before 1900) and Instrumental (after 1900) Seismicity of the Tuz Gölü Fault Zone

Morphotectonic properties, epicenter distributions of small and moderate-size earthquakes and structural data from this study indicate that TGFZ is seismically active.

In order to investigate historical (before 1900) earthquakes associated with TGFZ, a number of earthquake catalogs were examined (e.g. Ergin et al., 1967; Soysal et al., 1981, Ambraseys and Jackson, 1998; Tan et al., 2008). Among them, in Soysal et al. (1981) only one historical earthquake was found to be associated with TFGZ. In this catalog, based on study of Ambraseys (1970), a very strong earthquake was occurred (I_0=IX) in 1104 around Niğde and Adana which that killed 40.000 people. In the catalog coordinate of earthquake is not given and it is stated that literature on this earthquake is not sufficient.

Data on instrumental (after 1900) earthquakes occurred around TGFZ are compiled from the Kandilli Observatory and Earthquake Research Institute (Figure 31).

As shown in figure 31, a number of earthquakes were occurred around TGFZ. Among 4151 earthquakes shown in Figure 31, 203 earthquakes are selected that are possibly associated with TGFZ (Table 5; Figure 32). In addition to these earthquakes, Dirik and Erol (2000) suggest two other earthquakes associated with TGFZ. The first is the one that occurred in 1940 (M=5.2). This earthquake with

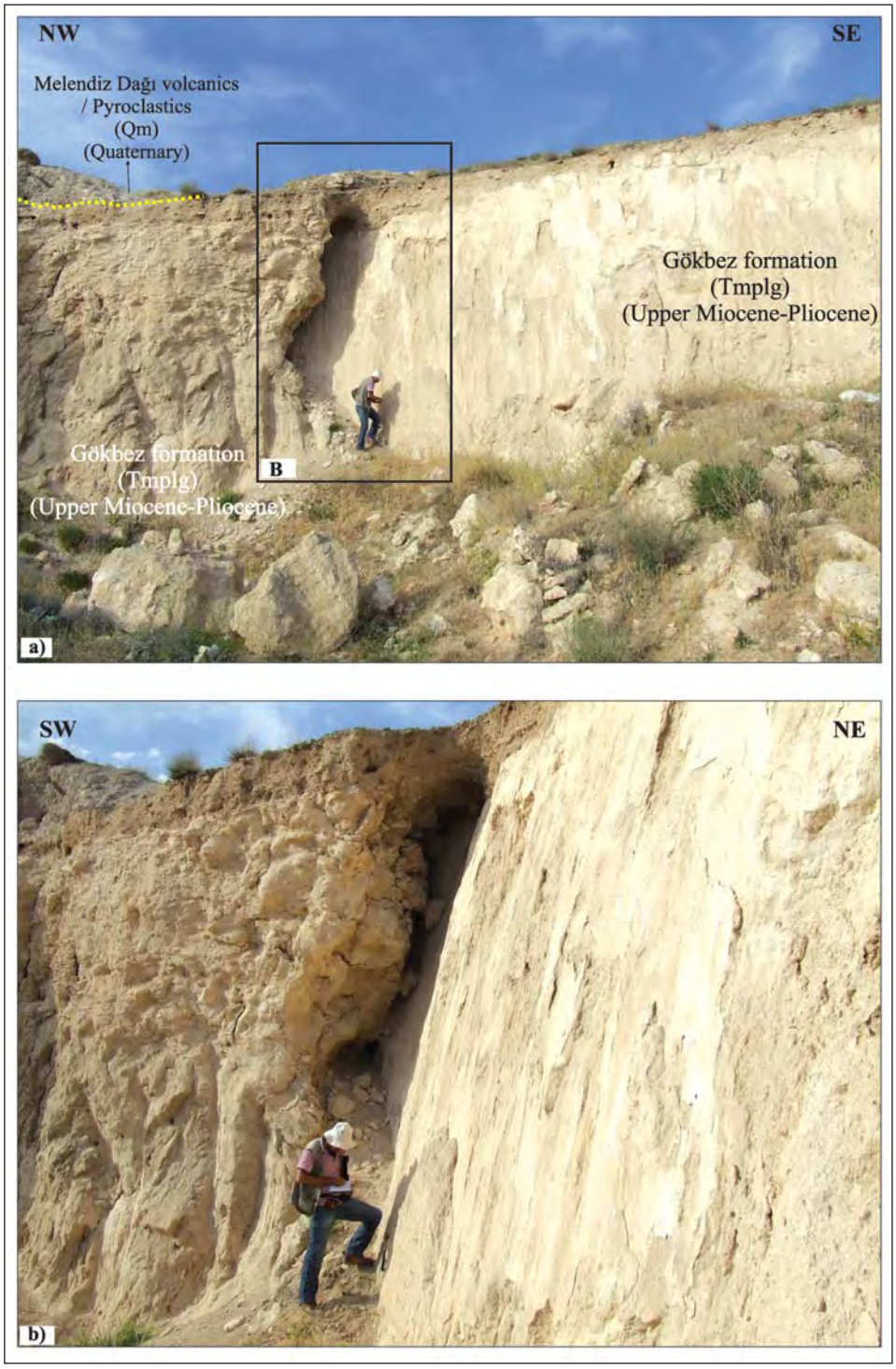

Figure 28- a) Panoramic view of Bor segment that cuts late Miocene-Pliocene Gökbez formation (Tmplg) and Quaternary Melendiz Dağı Volcanites (Qm) at east of Acıgöl graveyard in the Bor town center (Figure 27, station 15) (M 33 a1 quadrangle; 637592 E – 4193282 N) (view to NE), b) Section view of fault plane (view to NW; for both photos scale geologist is 1.80 m).

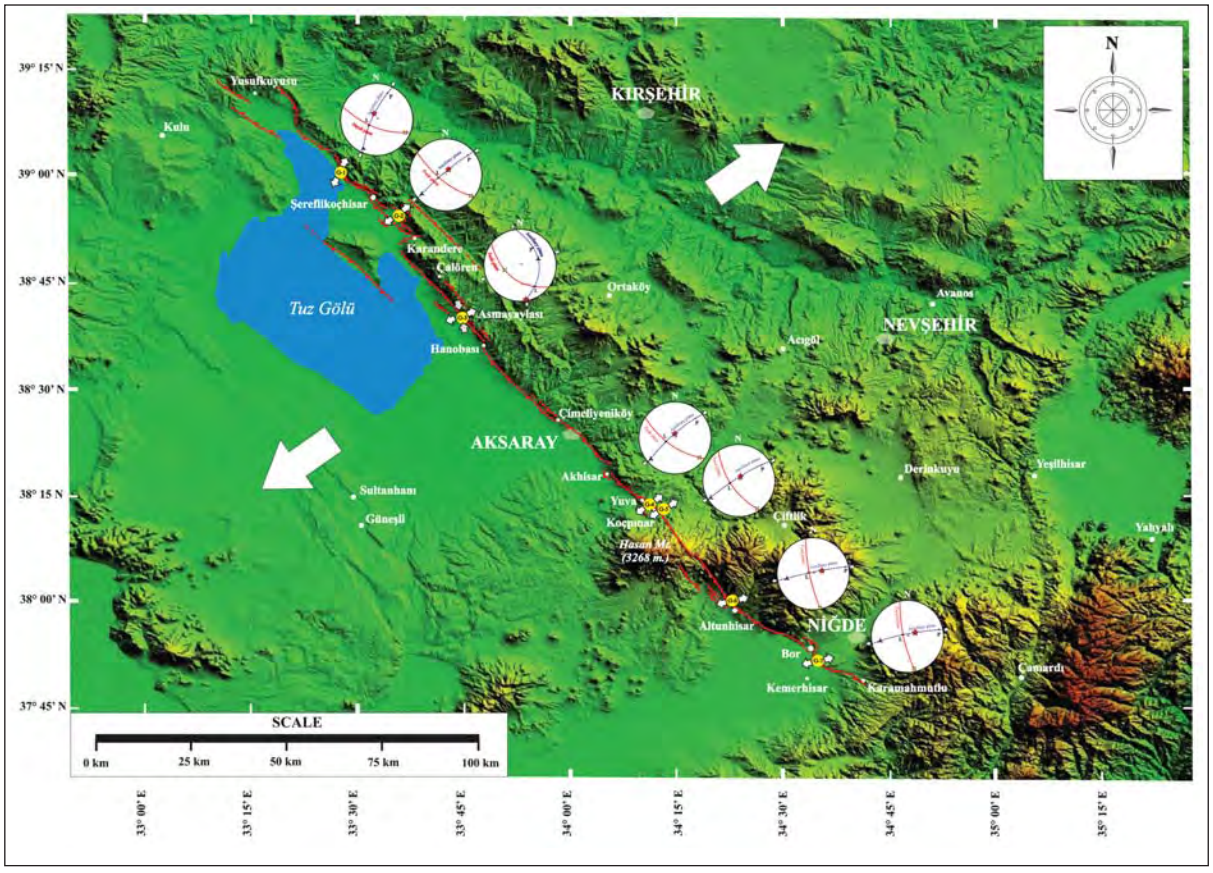

Figure 29- Collective presentation of kinematic analysis on the Tuz Gölü Fault Zone (Big arrows on the map represent for regional extension direction)

epicenter coordinates of 34.2 East – 38.0 North is located in Uluören village (west of Altunhisar) which is governed by the Altunhisar segment of TGFZ. The second one with magnitude of 4.0 was occurred on 22 October 1971. The epicenter coordinates of this earthquake is 33.9 East – 38.6 North which locates around Bostanlık village at east of Hanobası.

Statistical assessment of earthquake focal depths showed that earthquakes on TGFZ were occurred at an average depth of 10 km. It was shown that earthquakes around Hasandağ and Altunhisar have focal depths deeper than the average. This might indicate that some of earthquakes in the region are volcanogenic earthquakes.

Considering the statistical assessment of earthquake magnitudes, among 205 earthquakes (two earthquakes by Dirik and Erol (2000) are also taken into consideration), 136 are of M=1.3-2.9, 60 are of M=3.0-3.9, 7 are of M=4.0-4.9 and 1 is of M=5.2. The largest earthquake recorded during the instrumental period is the Uluören (Altunhisar) earthquake with magnitude of M=5.2 (Dirik and Erol, 2000). Additionally, 1924 Başaran (Eskil) (M=4.9), 1985 Şekerköy (Şereflikoçhisar) (M=4.3), 1998 Altunhisar (Niğde) (M=4.0), 2001 Ulukışla (Aksaray) (M=4.1), 2002 Taşpınar (Aksaray) and 2007 Acıkuyu (Kulu) (M=4.9) earthquakes are other important earthquakes recorded on TGFZ.

4.2. Earthquake potential of the Tuz Gölü Fault Zone segments

In paleoseismology works to be conducted active fault zones consisting of several fault segments such as TGFZ, geometric and structural characteristics of fault segments within the fault zone should be determined and deformed young deposits (Quaternary) should be mapped in detail. In Part 3 segmentation of TGFZ is presented with all details. In paleoseismology works, the length of fault segment and the largest earthquake to be occurred and the maximum and average displacements in each earthquake can be estimated with empirical equations. In this study, using the equations for

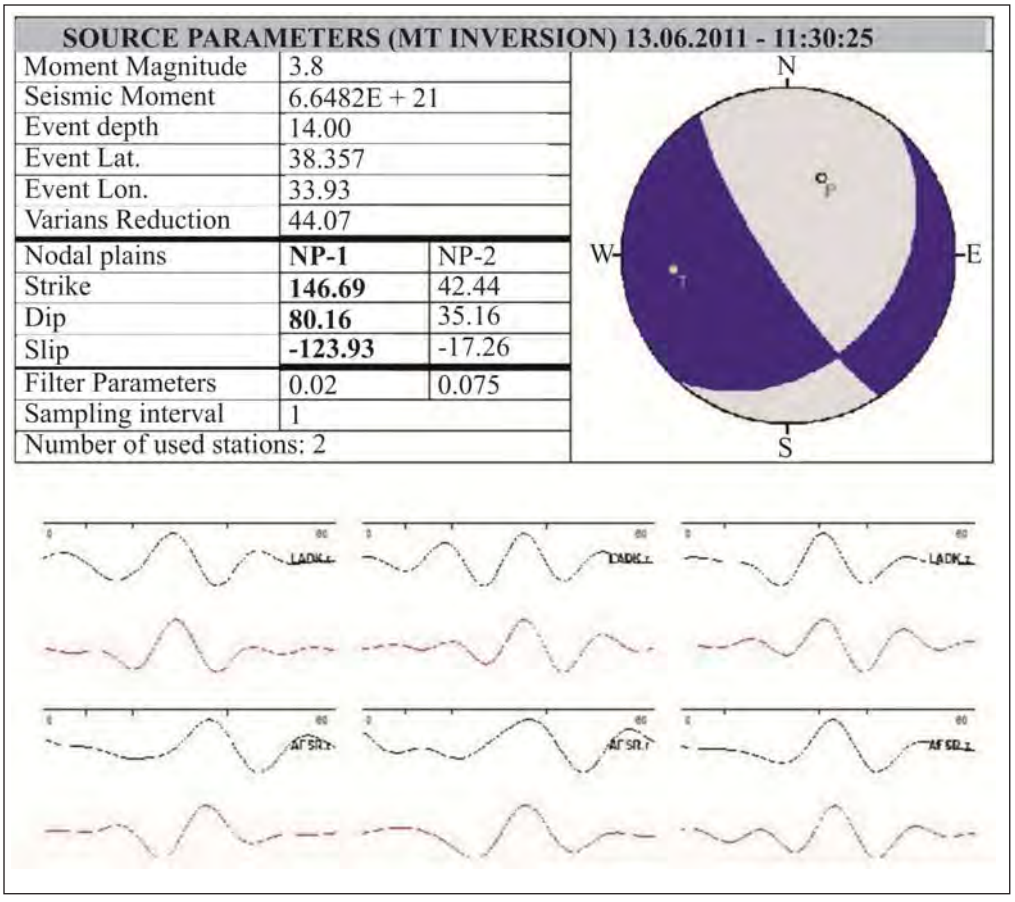

Figure 30- Moment tensor solution for 13 June 2011 Ataköy (Aksaray) earthquake (M=3.9).

normal faults suggested by Wells and Coppersmith (1994), the largest earthquake produced by each segment of TGFZ and the maximum and average displacements were calculated (Table 6). In the calculations following equations were used:

The empirical equation used for the largest earthquake magnitude (M):

M= a+b x log (SRL)

a= 4,86

b= 1,32

SRL= Surface rupture length, a and b are the standard error and coefficients.

The empirical equation used for the maximum displacement (MD) for each earthquake:

Log (MD) = a+b x M

a = -5,90

b = 0,89

MD= the maximum displacement, M= earthquake magnitude, a and b are the standard error and coefficients.

The empirical equation used for average displacement for any earthquake (AD):

Log (AD) = a+b x M

a= -4,45

b= 0,63

AD= average displacement, M= earthquake magnitude, a and b are the standard error and coefficients.

As shown in table 6, the Tuz Gölü, Altunhisar and Akhisar-Kılıç segments are the most important segments of TGFZ. In an assessment considering the length, morphotectonic properties of fault segments, deformed young geologic units, density of residential sites in the impact area and the presence of areas suitable for paleoseismic trench excavations on the segment, Tuz Gölü and Akhisar-Kılıç segments come into prominence.

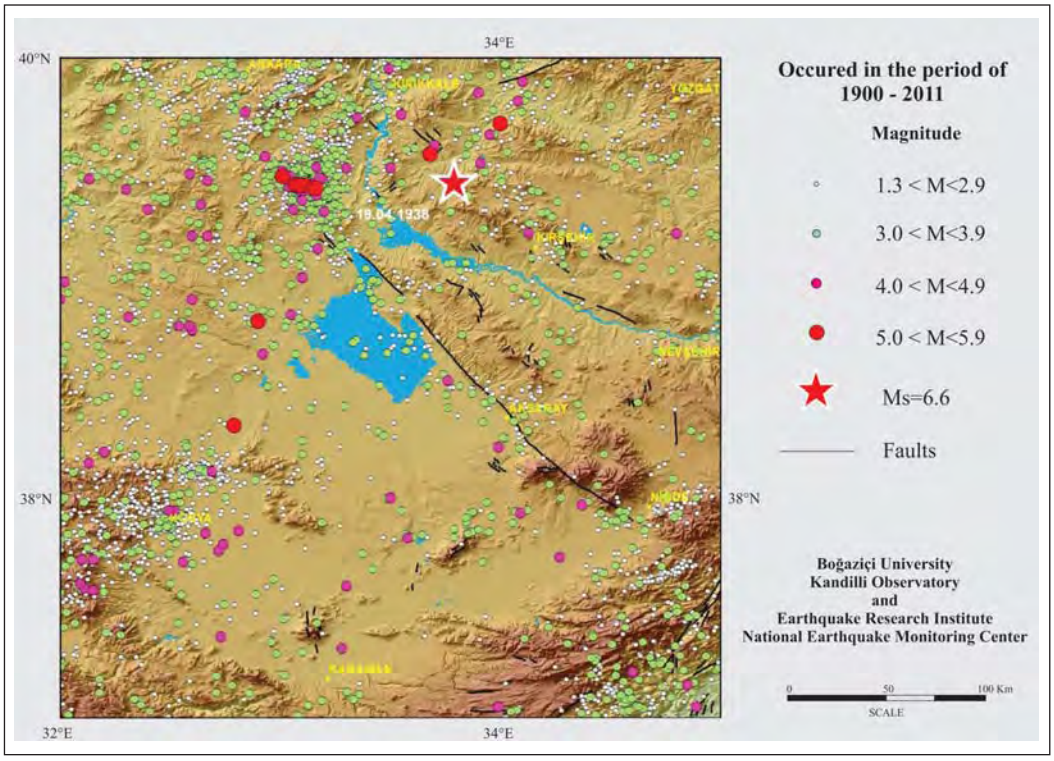

Figure 31- Epicenter distribution map for earthquakes (M ?1,3) occurred in the 1900-2011 period the Tuz Gölü Fault Zone and surrounding (data from the Kandilli Observatory and Earthquake Research Institute National Earthquake Monitoring Center).

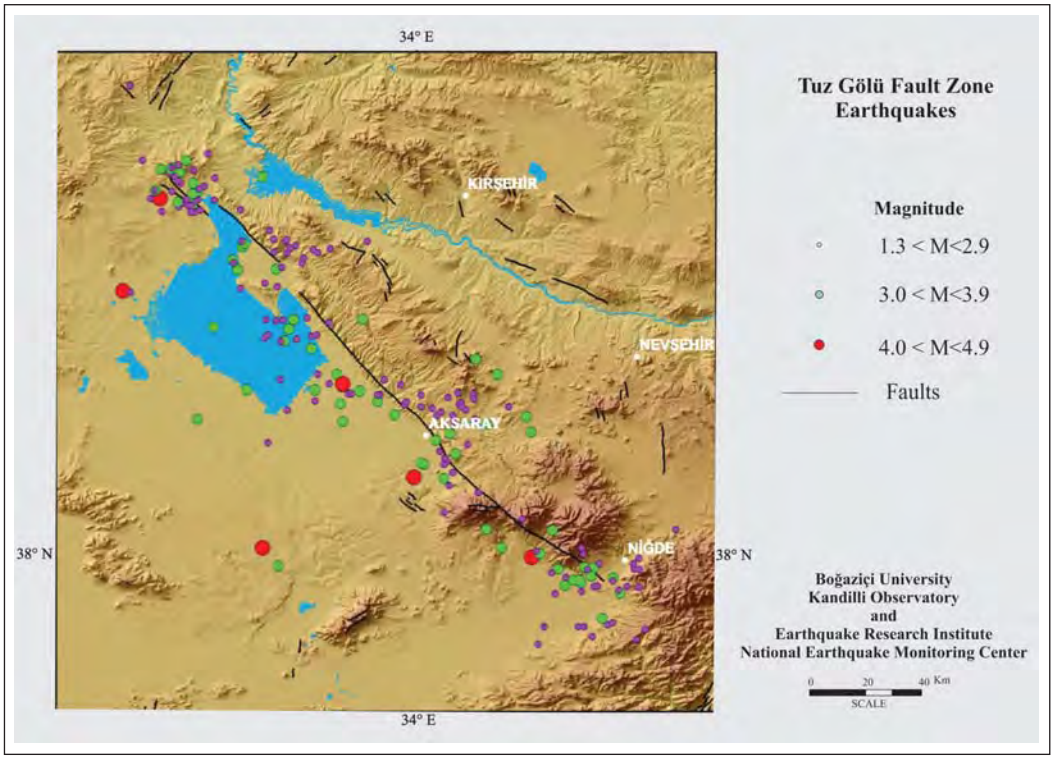

Figure 32- Epicenter distribution map for earthquakes (M ?1,3) occurred in the 1900-2011 period around the Tuz Gölü Fault Zone (data from the Kandilli Observatory and Earthquake Research Institute National Earthquake Monitoring Center).

Table 5- Earthquake parameters of earthquakes occurred along the Tuz Gölü Fault Zone during the 1900-2011 period (data from the Kandilli Observatory and Earthquake Research Institute National Earthquake Monitoring Center).

No	Date	Time	Lat.	Lon.	M	MD	ML	MS	Mw	Mb	Depth (km)	Location
1	13.12.1924	18:53:30.00	38	33,5	**4,9**	**4,9**	**4,9**	**4,9**	**5,2**	**4,9**	30	BAŞARAN-ESKİL (AKSARAY) [SW 3.8 km]
2	24.04.1977	20:49:06.00	39,2	33,5	**3,1**						5	ŞANLIKIŞLA-ŞEREFLİKOÇHİSAR (ANKARA) [NE 6.1 km]
3	14.05.1981	04:37:13.40	39,23	33,21	**3,9**						10	DOĞANKAYA-ŞEREFLİKOÇHİSAR (ANKARA) [NE 2.8 km]
4	03.03.1985	13:02:12.90	39,13	33,17	**4,3**	**4,3**	**4,2**	**4,0**	**4,4**	**4,3**	10	ŞEKERKÖY-ŞEREFLİKOÇHİSAR (ANKARA) [SW 3.6 km]
5	17.07.1988	23:40:05.70	38,99	33,84	**2,7**						10	SARIYAHŞİ (AKSARAY) [NW 0.7 km]
6	18.11.1991	19:48:50.70	38,9	33,42	**3,9**						10	HAMZALI-ŞEREFLİKOÇHİSAR (ANKARA) [NW 4.2 km]
7	11.12.1993	05:21:21.40	38,51	33,45	**3,3**						8	ESKİL (AKSARAY) [NE 12.5 km]
8	11.03.1994	08:15:26.00	38,51	33,67	**3,8**						5	ULUKIŞLA- (AKSARAY) [W 8.1 km]
9	02.03.1997	21:07:52.10	38,61	34,19	**3,4**						8	SARIAĞIL- (AKSARAY) [N 1.0 km]
10	01.10.1998	17:02:41.90	37,97	34,37	**4,0**	**4,0**	**4,0**	**3,6**	**4,1**	**4,0**	34	ALTUNHİSAR (NİĞDE) [S 3.1 km]
11	18.07.1999	10:51:44.80	38,56	33,74	**3,6**						5	ULUKIŞLA- (AKSARAY) [NW 6.8 km]
12	18.05.2000	03:08:24.30	38,41	33,76	**3,9**						33	YEŞİLTEPE- (AKSARAY) [S 5.9 km]
13	11.03.2001	19:21:45.60	38,53	33,76	**4,1**	**4,1**	**4,0**	**3,6**	**4,1**	**4,0**	4	ULUKIŞLA- (AKSARAY) [N 3.2 km]
14	07.03.2002	06:12:39.00	38,23	33,99	**4,1**	**4,1**	**4,0**	**3,6**	**4,1**	**4,0**	10	TAŞPINAR- (AKSARAY) [NW 6.9 km]
15	17.04.2002	06:52:01.00	38,418	33,289	**3,0**	**3,0**					6,9	ESKİL (AKSARAY) [W 10.9 km]
16	11.06.2002	09:30:05.00	37,932	34,456	**3,4**	**3,4**					5	BALCI-BOR (NİĞDE) [S 4.5 km]
17	18.07.2002	13:37:21.00	38,74	33,825	**3,4**	**3,4**					31,6	GÖYNÜK-AĞAÇÖREN (AKSARAY) [SE 1.5 km]
18	01.11.2003	19:40:05.00	38,426	34,354	**3,8**	**3,8**	**3,6**				5	GÜLPINAR-GÜLAĞAÇ (AKSARAY) [NW 1.2 km]
19	02.11.2003	03:36:15.00	38,3757	34,368	**3,3**	**3,3**					5	GÜLAĞAÇ (AKSARAY) [SE 2.8 km]
20	18.02.2004	15:56:43.00	38,9743	33,436	**3,5**	**3,5**					5	ŞEREFLİKOÇHİSAR (ANKARA) [NW 9.8 km]
21	09.07.2004	11:23:46.00	38,0612	34,223	**3,3**	**3,3**					5	ULUÖREN-ALTUNHİSAR (NİĞDE) [SE 3.2 km]
22	11.07.2004	17:25:26.00	38,4008	34,226	**3,0**	**3,0**					8,1	ÇATALSU-GÜLAĞAÇ (AKSARAY) [E 1.3 km]
23	08.08.2004	18:58:30.00	37,9427	33,551	**3,1**	**3,1**					9,8	BAŞARAN-ESKİL (AKSARAY) [S 8.3 km]
24	02.09.2004	09:17:46.00	37,9382	34,542	**3,1**	**3,1**					5	OKCU-BOR (NİĞDE) [S 0.2 km]
25	11.11.2004	12:06:31.00	37,9352	34,57	**3,1**	**3,1**					2,4	OKCU-BOR (NİĞDE) [SE 2.5 km]
26	20.01.2005	00:51:11.79	38,5597	34,261	**3,0**	**3,0**					57,4	TATLICA- (AKSARAY) [E 2.4 km]
27	17.02.2005	10:33:51.56	37,888	34,528	**3,3**	**3,3**					8	BOR (NİĞDE) [SW 3.0 km]
28	29.06.2005	17:23:04.98	38,9633	33,665	**2,7**	**2,7**					0,1	SEYMENLI- ŞEREFLİKOÇHİSAR (ANKARA) [E 2.1 km]
29	18.07.2005	09:26:08.95	38,0577	34,44	**3,0**	**3,0**					18,3	YEŞİLYURT-ALTUNHİSAR (NİĞDE) [NE 7.0 km]
30	01.08.2005	05:34:11.01	39,178	33,236	**2,7**	**2,7**					8,9	AKARCA- ŞEREFLİKOÇHİSAR (ANKARA) [NE 1.3 km]
31	17.08.2005	12:30:27.98	39,094	33,431	**2,8**	**2,8**					32	ACIKUYU- ŞEREFLİKOÇHİSAR (ANKARA) [SW 5.0 km]
32	19.08.2005	10:18:36.24	39,211	33,202	**2,6**	**2,6**					26,7	DOĞANKAYA- ŞEREFLİKOÇHİSAR (ANKARA) [NE 0.8 km]
33	24.08.2005	15:55:22.54	38,9905	33,574	**2,5**	**2,5**					17,5	SADIKLI- ŞEREFLİKOÇHİSAR (ANKARA) [S 2.5 km]
34	31.08.2005	13:02:15.26	37,8782	34,476	**3,1**	**3,1**					9,8	KAYI-BOR (NİĞDE) [SE 6.8 km]
35	13.11.2005	22:14:36.33	39,088	33,176	**2,9**	**2,9**					5,3	ŞEKERKÖY- ŞEREFLİKOÇHİSAR (ANKARA) [SW 7.9 km]
36	20.12.2005	21:58:44.65	39,2538	33,112	**2,7**	**2,7**					20,7	AKTAŞ- ŞEREFLİKOÇHİSAR (ANKARA) [NW 3.7 km]
37	03.01.2006	13:55:33.73	38,4457	33,581	**2,9**	**2,9**					5,6	ESKİL (AKSARAY) [NE 15.4 km]
38	05.01.2006	07:18:38.60	38,9013	33,545	**3,0**	**3,0**					18,6	ŞEREFLİKOÇHİSAR (ANKARA) [S 4.1 km]
39	07.01.2006	05:49:44.08	39,0258	33,524	**2,6**	**2,6**					22,7	HACIBEKTAŞLI- ŞEREFLİKOÇHİSAR (ANKARA) [SE 4.1 km]
40	05.02.2006	17:33:28.12	39,1798	33,275	**3,3**	**3,3**					5,9	BÜYÜKKIŞLA- ŞEREFLİKOÇHİSAR (ANKARA) [SE 2.4 km]
41	01.05.2006	06:45:30.21	37,91	34,562	**3,2**	**3,2**					1,6	BOR (NİĞDE) [N 1.8 km]
42	08.05.2006	20:45:46.01	39,1523	33,294	**3,0**	**3,0**					5,3	AKIN- ŞEREFLİKOÇHİSAR (ANKARA) [NE 4.5 km]
43	03.06.2006	01:43:08.93	39,2145	33,232	**3,2**	**3,2**					5,5	BÜYÜKKIŞLA- ŞEREFLİKOÇHİSAR (ANKARA) [NW 3.1 km]
44	30.08.2006	02:59:40.24	38,2712	34,022	**3,4**	**3,4**					0,4	BAĞLI- (AKSARAY) [NW 5.1 km]
45	03.09.2006	14:25:00.84	38,9957	33,578	**2,6**	**2,6**					7,8	SADIKLI- ŞEREFLİKOÇHİSAR (ANKARA) [SE 2.0 km]
46	27.09.2006	11:23:53.61	39,0863	33,282	**2,9**	**2,9**					17,6	AKIN- ŞEREFLİKOÇHİSAR (ANKARA) [SE 4.5 km]
47	08.10.2006	15:54:18.49	38,9067	33,564	**2,6**	**2,6**					15,8	ŞEREFLİKOÇHİSAR (ANKARA) [SE 4.1 km]
48	06.01.2007	10:34:53.71	38,3498	34,061	**3,0**	**3,0**					16,9	AKSARAY [SE 3.2 km]
49	22.02.2007	14:06:42.56	37,9328	34,702	**2,9**	**2,9**					5,4	NİĞDE [SE 4.1 km]
50	17.03.2007	21:41:35.68	38,0003	34,274	**3,1**	**3,1**					8,6	AKÇAÖREN-ALTUNHİSAR (NİĞDE) [S 2.0 km]
51	08.05.2007	00:21:11.61	38,668	33,57	**3,2**	**3,2**					5,3	ÇALÖREN- ŞEREFLİKOÇHİSAR (ANKARA) [SW 16.3 km]
52	17.05.2007	06:31:10.23	37,9048	34,48	**2,9**	**2,9**					12	OKCU-BOR (NİĞDE) [SW 6.7 km]
53	26.07.2007	13:17:12.20	37,8955	34,506	**3,0**	**3,0**					5,4	BOR (NİĞDE) [W 4.9 km]
54	19.08.2007	09:26:24.08	38,9568	33,539	**2,8**	**2,8**					4,9	ŞEREFLİKOÇHİSAR (ANKARA) [N 2.1 km]

Table 5- (continued)

No	Date	Time	Lat.	Lon.	M	MD	ML	MS	Mw	Mb	Depth (km)	Location
55	19.08.2007	23:07:28.52	38,275	34,012	**3,6**	**3,6**					0,3	SAĞLIK- (AKSARAY) [SW 5.9 km]
56	07.09.2007	13:39:30.21	38,0008	34,532	**2,9**	**2,9**					2,2	FESLEĞEN- (NİĞDE) [NW 2.6 km]
57	28.09.2007	13:01:25.07	38,667	33,561	**2,8**	**2,8**					5,3	ÇALÖREN- ŞEREFLİKOÇHİSAR (ANKARA) [SW 17.0 km]
58	03.10.2007	11:28:31.43	37,9047	34,633	**3,0**	**3,0**					0,2	SAZLICA- (NİĞDE) [NW 0.7 km]
59	13.12.2007	18:06:18.70	38,83	33,05	**4,9**	**4,5**	**4,8**	**4,9**	**4,9**	**4,8**	5	ACIKUYU-KULU (KONYA) [E 5.2 km]
60	13.12.2007	21:40:00.42	38,8257	33,075	**2,9**	**2,9**					10,6	ACIKUYU-KULU (KONYA) [E 7.4 km]
61	17.12.2007	06:50:18.06	37,8962	34,525	**3,1**	**3,1**					5,4	BOR (NİĞDE) [W 3.2 km]
62	23.12.2007	15:21:32.53	38,9827	33,442	**3,0**	**3,0**					3,3	ŞEREFLİKOÇHİSAR (ANKARA) [NW 9.8 km]
63	28.12.2007	09:28:52.26	39,1025	33,231	**2,9**	**2,9**					14,3	AKIN- ŞEREFLİKOÇHİSAR (ANKARA) [SW 3.3 km]
64	29.12.2007	06:33:15.52	39,1995	33,218	**2,7**	**2,7**					9,2	DOĞANKAYA- ŞEREFLİKOÇHİSAR (ANKARA) [SE 2.3 km]
65	30.12.2007	00:04:21.47	39,2522	33,254	**3,3**	**3,3**					8,5	ODUNBOĞAZI- ŞEREFLİKOÇHİSAR (ANKARA) [W 3.7 km]
66	04.01.2008	10:24:28.91	39,2238	33,176	**2,8**	**2,8**					9,9	DOĞANKAYA- ŞEREFLİKOÇHİSAR (ANKARA) [NW 2.3 km]
67	24.01.2008	08:41:31.13	38,7142	33,343	**3,0**	**3,0**					4,2	ÇAVUŞKÖY- ŞEREFLİKOÇHİSAR (ANKARA) [SW 19.6 km]
68	28.01.2008	12:35:46.66	37,8733	34,716	**2,9**	**2,9**					6,3	HALAÇ-BOR (NİĞDE) [NE 5.3 km]
69	06.02.2008	11:55:52.06	38,3797	34,108	**2,7**	**2,7**					0,3	SEVİNÇLİ- (AKSARAY) [NW 2.0 km]
70	10.02.2008	01:52:08.44	37,9812	34,398	**3,0**	**3,0**					5,5	ALTUNHİSAR (NİĞDE) [SE 3.0 km]
71	10.04.2008	13:08:29.34	38,4583	34,014	**2,7**	**2,7**					0,5	AKIN- (AKSARAY) [NW 2.9 km]
72	22.04.2008	13:25:04.91	37,9297	34,718	**2,9**	**2,9**					5,2	NİĞDE [SE 5.3 km]
73	18.09.2008	09:18:44.51	39,1865	33,228	**2,7**	**2,7**					14,8	AKARCA- ŞEREFLİKOÇHİSAR (ANKARA) [NE 1.4 km]
74	18.09.2008	12:29:43.42	37,9503	34,699	**2,7**	**2,7**					1,1	NİĞDE [SE 2.6 km]
75	05.12.2008	12:44:04.68	38,735	33,567	**2,9**	**2,9**					17,8	KARAMOLLAUŞAĞI- ŞEREFLİKOÇHİSAR (ANKARA) [SE 12.4 km]
76	15.01.2009	15:36:37.45	38,728	33,716	**2,7**	**2,7**					7,3	ÇALÖREN- ŞEREFLİKOÇHİSAR (ANKARA) [SE 4.8 km]
77	23.01.2009	10:47:14.74	37,7453	34,411	**2,6**	**2,6**					37,8	BADAK-BOR (NİĞDE) [North West 1.9 km]
78	31.01.2009	07:14:49.25	38,7345	33,544	**2,9**	**2,9**					5,4	KARAMOLLAUŞAĞI-ŞEREFLİKOÇHİSAR (ANKARA) [S 12.0 km]
79	03.02.2009	14:07:23.14	37,9668	34,717	**2,9**	**2,9**					8,1	NİĞDE (NİĞDE) [E 3.6 km]
80	18.02.2009	10:52:52.41	37,7135	34,566	**2,6**	**2,6**					5,6	BEREKET-BOR (NİĞDE) [SE 2.4 km]
81	03.03.2009	18:20:29.76	38,5598	33,681	**2,7**	**2,7**					12,4	ULUKIŞLA- (AKSARAY) [NW 9.7 km]
82	03.03.2009	19:08:59.09	38,4972	33,88	**2,7**	**2,7**					16,5	BAYMIŞ- (AKSARAY) [SW 0.9 km]
83	11.03.2009	16:27:37.38	37,7728	34,599	**3,0**	**3,0**					5,8	HAVUZLU-BOR (NİĞDE) [SW 3.5 km]
84	31.03.2009	10:00:27.50	37,7513	34,616	**2,8**	**2,8**					8,5	GÖNWEZ-BOR (NİĞDE) [W 3.7 km]
85	02.05.2009	13:41:12.50	38,179	34,198	**2,9**	**2,9**					9,5	HELVADERE- (AKSARAY) [SW 1.8 km]
86	30.05.2009	23:28:53.79	38,6432	33,658	**3,4**	**3,4**					5,2	ALTINKAYA- (AKSARAY) [NW 11.3 km]
87	10.06.2009	10:30:15.18	37,8533	34,447	**2,8**	**2,8**					2,2	EMEN-BOR (NİĞDE) [N 4.0 km]
88	20.06.2009	22:12:03.42	39,109	33,275	**3,0**	**3,0**					6,2	AKIN- ŞEREFLİKOÇHİSAR (ANKARA) [SE 2.1 km]
89	23.06.2009	15:03:33.53	37,7575	34,631	**2,8**	**2,8**					7,5	GÖNWEZ-BOR (NİĞDE) [NW 2.5 km]
90	09.07.2009	15:39:59.05	37,6893	34,392	**2,4**	**2,4**					2,7	BADAK-BOR (NİĞDE) [SW 5.8 km]
91	01.08.2009	04:15:20.84	39,1448	33,276	**2,9**	**2,9**					7,3	AKIN- ŞEREFLİKOÇHİSAR (ANKARA) [NE 2.9 km]
92	25.08.2009	12:18:19.09	38,7438	33,645	**2,8**	**2,8**					0	ÇALÖREN- ŞEREFLİKOÇHİSAR (ANKARA) [SW 6.0 km]
93	29.09.2009	13:50:58.54	37,7457	34,521	**2,5**	**2,5**					4,5	BEREKET-BOR (NİĞDE) [NW 3.0 km]
94	02.11.2009	12:24:49.40	39,2237	33,204	**3,3**	**3,3**					7,1	DOĞANKAYA- ŞEREFLİKOÇHİSAR (ANKARA) [NE 2.0 km]
95	06.11.2009	11:45:35.00	37,7455	34,54	**2,7**	**2,7**					15,1	BEREKET-BOR (NİĞDE) [NW 1.8 km]
96	25.11.2009	10:42:32.36	37,9492	34,589	**2,8**	**2,8**					0,1	KOYUNLU- (NİĞDE) [S 3.7 km]
97	17.12.2009	16:13:10.43	37,8748	34,573	**2,7**	**2,7**					12,6	BOR (NİĞDE) [SE 2.3 km]
98	25.12.2009	13:53:12.24	38,28	34,097	**2,9**	**2,9**					10	AKHİSAR- (AKSARAY) [S 1.4 km]
99	17.01.2010	19:37:24.85	38,7063	33,587	**3,1**	**3,1**					7,6	ÇALÖREN- ŞEREFLİKOÇHİSAR (ANKARA) [SW 12.4 km]
100	22.01.2010	17:48:15.50	39,1552	33,154	**3,0**	**3,0**					10,6	ŞEKERKÖY- ŞEREFLİKOÇHİSAR (ANKARA) [W 3.3 km]
101	26.01.2010	13:45:27.99	38,115	34,088	**2,6**	**2,6**					24	KARACAÖREN- (AKSARAY) [SE 2.6 km]
102	08.02.2010	23:34:10.41	38,6778	33,508	**2,9**	**2,9**					10,9	KARAMOLLAUŞAĞI- ŞEREFLİKOÇHİSAR (ANKARA) [S 18.2 km]
103	10.02.2010	12:04:58.67	38,6883	33,517	**2,4**	**2,4**					4,7	KARAMOLLAUŞAĞI- ŞEREFLİKOÇHİSAR (ANKARA) [S 17.0 km]
104	04.03.2010	21:10:44.67	39,1285	33,139	**2,9**	**2,9**					16,7	ŞEKERKÖY- ŞEREFLİKOÇHİSAR (ANKARA) [SW 5.6 km]
105	14.03.2010	23:07:12.38	39,157	33,153	**2,8**	**2,8**					19,4	ŞEKERKÖY- ŞEREFLİKOÇHİSAR (ANKARA) [W 3.4 km]
106	28.04.2010	10:56:15.74	38,4873	34,1	**2,8**	**2,8**					3,9	EKECİKTOLU- (AKSARAY) [S 2.1 km]
107	04.05.2010	12:34:13.21	38,225	34,087	**3,2**	**3,2**					8	KARATAŞ- (AKSARAY) [SW 3.0 km]
108	11.05.2010	11:27:16.39	37,8762	34,585	**2,6**	**2,6**					17,7	BOR (NİĞDE) [SE 2.8 km]
109	25.05.2010	09:10:24.73	37,8535	34,655	**3,0**	**3,0**					3,6	KAYNARCA-BOR (NİĞDE) [E 1.6 km]
110	29.05.2010	13:11:36.38	38,8548	33,508	**2,8**	**2,8**					4	KARAMOLLAUŞAĞI- ŞEREFLİKOÇHİSAR (ANKARA) [NW 2.1 km]

Table 5- (continued)

No	Date	Time	Lat.	Lon.	M	MD	ML	MS	Mw	Mb	Depth (km)	Location
111	27.06.2010	03:22:30.52	39,1247	33,292	**2,4**	**2,4**					5,8	AKIN- ŞEREFLİKOÇHİSAR (ANKARA) [E 2.9 km]
112	29.06.2010	15:33:08.09	39,1133	33,248	**2,8**	**2,8**					6,6	AKIN- ŞEREFLİKOÇHİSAR (ANKARA) [SW 1.4 km]
113	01.07.2010	17:21:06.25	38,9207	33,629	**2,2**	**2,2**					5	FADILLI- ŞEREFLİKOÇHİSAR (ANKARA) [W 2.6 km]
114	01.07.2010	20:48:11.79	39,095	33,271	**2,7**	**2,7**					15,1	AKIN- ŞEREFLİKOÇHİSAR (ANKARA) [SE 3.3 km]
115	02.07.2010	00:41:30.45	39,1252	33,262	**3,0**	**3,0**					8,7	AKIN- ŞEREFLİKOÇHİSAR (ANKARA) [NE 0.4 km]
116	02.07.2010	02:25:46.67	39,1087	33,26	**2,3**	**2,3**					5	AKIN- ŞEREFLİKOÇHİSAR (ANKARA) [S 1.6 km]
117	04.07.2010	02:01:52.08	39,1058	33,271	**2,5**	**2,5**					8,5	AKIN- ŞEREFLİKOÇHİSAR (ANKARA) [SE 2.2 km]
118	10.07.2010	15:46:00.25	38,9767	33,606	**2,6**	**2,6**					18,6	KARABÜK- ŞEREFLİKOÇHİSAR (ANKARA) [SW 2.1 km]
119	16.07.2010	00:17:41.51	38,6837	33,658	**2,2**	**2,2**					24,5	ÇALÖREN- ŞEREFLİKOÇHİSAR (ANKARA) [SW 10.5 km]
120	17.07.2010	07:41:10.23	39,1207	33,284	**2,6**	**2,6**					2,6	AKIN- ŞEREFLİKOÇHİSAR (ANKARA) [E 2.2 km]
121	19.07.2010	18:06:37.00	39,0858	33,269	**2,7**	**2,7**					9,9	AKIN- ŞEREFLİKOÇHİSAR (ANKARA) [SE 4.2 km]
122	20.07.2010	04:22:10.29	39,1275	33,255	**2,7**	**2,7**					5,2	AKIN- ŞEREFLİKOÇHİSAR (ANKARA) [NW 0.6 km]
123	20.07.2010	22:55:56.28	39,0922	33,298	**2,8**	**2,8**					5,3	AKIN- ŞEREFLİKOÇHİSAR (ANKARA) [SE 4.8 km]
124	22.07.2010	09:12:05.22	37,8758	34,678	**2,4**	**2,4**					17,2	KAYNARCA-BOR (NİĞDE) [NE 4.5 km]
125	27.07.2010	19:58:17.28	39,1172	33,227	**3,3**		**3,3**				2,3	AKIN- ŞEREFLİKOÇHİSAR (ANKARA) [SW 2.8 km]
126	27.07.2010	20:56:30.50	39,1597	33,295	**2,8**	**2,8**					8,5	YUSUFKUYUSU- ŞEREFLİKOÇHİSAR (ANKARA) [S 4.1 km]
127	28.07.2010	12:52:43.14	39,1448	33,274	**3,2**	**3,2**					1,5	AKIN- ŞEREFLİKOÇHİSAR (ANKARA) [NE 2.8 km]
128	05.08.2010	04:18:16.78	38,7368	33,512	**2,2**	**2,2**					11,7	KARAMOLLAUŞAĞI- ŞEREFLİKOÇHİSAR (ANKARA) [S 11.7 km]
129	06.08.2010	13:22:33.35	38,244	34,115	**2,7**	**2,7**					14,2	KARAÖREN- (AKSARAY) [W 1.5 km]
130	08.08.2010	07:25:16.77	38,5023	34,132	**2,2**	**2,2**					3,5	EKECİKYENİ- (AKSARAY) [SE 2.9 km]
131	08.08.2010	11:14:13.73	38,9367	33,634	**2,8**	**2,8**					3,3	FADILLI- ŞEREFLİKOÇHİSAR (ANKARA) [NW 2.6 km]
132	09.08.2010	16:24:36.87	38,4098	34,119	**2,4**	**2,4**					11,5	GÜCÜNKAYA- (AKSARAY) [NW 1.9 km]
133	17.08.2010	08:16:10.78	38,5252	33,948	**2,5**	**2,5**					4,7	BAĞLIKAYA- (AKSARAY) [N 2.5 km]
134	17.08.2010	11:45:51.84	38,4637	33,96	**2,4**	**2,4**					7,9	TOPAKKAYA- (AKSARAY) [NE 3.0 km]
135	21.08.2010	23:55:21.17	39,2292	33,208	**2,5**	**2,5**					6,9	DOĞANKAYA- ŞEREFLİKOÇHİSAR (ANKARA) [NE 2.7 km]
136	29.08.2010	05:33:14.09	38,4298	34,065	**2,6**	**2,6**					7,5	GENÇOSMAN- (AKSARAY) [N 1.7 km]
137	03.09.2010	20:51:49.08	38,0948	34,339	**2,6**	**2,6**					6,8	ÇÖMLEKÇİ-ALTUNHİSAR (NİĞDE) [N 4.4 km]
138	15.09.2010	12:01:55.34	38,9672	33,72	**2,4**	**2,4**					9,9	İBRAHİMBEYLİ-EVREN (ANKARA) [E 1.6 km]
139	18.09.2010	13:22:21.57	38,3408	33,517	**2,3**	**2,3**					0,7	YEŞİLTÖMEK- (AKSARAY) [N 5.4 km]
140	29.09.2010	00:59:44.74	39,2185	33,18	**2,9**	**2,9**					5,4	DOĞANKAYA- ŞEREFLİKOÇHİSAR (ANKARA) [NW 1.7 km]
141	29.09.2010	03:04:21.83	39,2387	33,228	**2,7**	**2,7**					5,2	DOĞANKAYA- ŞEREFLİKOÇHİSAR (ANKARA) [NE 4.5 km]
142	01.10.2010	17:35:01.48	39,225	33,172	**3,3**	**3,3**					6	DOĞANKAYA- ŞEREFLİKOÇHİSAR (ANKARA) [NW 2.7 km]
143	05.10.2010	17:02:40.80	38,844	33,549	**2,3**	**2,3**					13,7	KARAMOLLAUŞAĞI- ŞEREFLİKOÇHİSAR (ANKARA) [E 2.0 km]
144	07.10.2010	01:52:10.48	39,1527	33,209	**2,5**	**2,5**					7,9	ŞEKERKÖY- ŞEREFLİKOÇHİSAR (ANKARA) [SE 1.5 km]
145	12.10.2010	04:57:43.63	38,4397	34,078	**2,0**	**2,0**					2,2	GENÇOSMAN- (AKSARAY) [NE 2.9 km]
146	12.10.2010	14:55:22.01	38,3133	34,074	**2,9**	**2,9**					4,3	SAĞLIK- (AKSARAY) [NE 1.3 km]
147	15.10.2010	11:02:03.87	38,9547	33,68	**2,3**	**2,3**					11,1	İBRAHİMBEYLİ-EVREN (ANKARA) [SW 2.4 km]
148	16.10.2010	09:26:52.11	37,8605	34,533	**2,6**	**2,6**					24,7	BOR (NİĞDE) [SW 4.5 km]
149	11.11.2010	11:13:10.16	37,7368	34,738	**2,9**	**2,9**					8,4	POSTALLI-BOR (NİĞDE) [NW 1.3 km]
150	27.11.2010	04:41:15.64	37,99	34,386	**2,6**	**2,6**					5,4	ALTUNHİSAR (NİĞDE) [SE 1.5 km]
151	02.12.2010	00:20:09.63	39,1235	33,345	**2,1**	**2,1**					8,8	ACIÖZ- ŞEREFLİKOÇHİSAR (ANKARA) [SW 6.9 km]
152	07.12.2010	14:35:15.13	38,2708	34,086	**2,8**	**2,8**					6,5	BAĞLI- (AKSARAY) [NE 1.4 km]
153	11.12.2010	10:39:40.14	38,5	34,182	**2,8**	**2,8**					7,3	YALNIZCEVİZ- (AKSARAY) [NE 1.9 km]
154	15.12.2010	08:51:29.72	38,417	34,188	**2,7**	**2,7**					0,1	GÖKÇE- (AKSARAY) [E 1.3 km]
155	27.12.2010	14:22:31.41	38,9703	33,588	**2,0**	**2,0**					5,2	KARABÜK- ŞEREFLİKOÇHİSAR (ANKARA) [SW 3.7 km]
156	28.12.2010	09:23:48.06	39,275	33,324	**2,4**	**2,4**					19,8	ODUNBOĞAZI- ŞEREFLİKOÇHİSAR (ANKARA) [NE 3.3 km]
157	31.12.2010	09:55:04.88	38,4732	33,966	**2,8**	**2,8**					7,2	BAĞLIKAYA- (AKSARAY) [SE 3.9 km]
158	31.12.2010	10:24:27.85	38,4312	33,928	**3,0**	**3,0**					0	TOPAKKAYA- (AKSARAY) [S 2.5 km]
159	04.01.2011	12:48:29.13	38,2907	34,088	**2,5**	**2,5**					13,3	AKHİSAR- (AKSARAY) [SW 0.9 km]
160	24.01.2011	09:17:07.07	38,6887	33,675	**2,5**	**2,5**					5,3	ÇALÖREN- ŞEREFLİKOÇHİSAR (ANKARA) [SW 9.5 km]
161	28.01.2011	11:00:52.23	38,6753	33,612	**2,4**	**2,4**					14,5	ÇALÖREN- ŞEREFLİKOÇHİSAR (ANKARA) [SW 13.3 km]
162	01.02.2011	02:06:27.13	38,5428	33,895	**2,7**	**2,7**					11	SAPMAZ- (AKSARAY) [NE 2.0 km]
163	01.02.2011	11:48:07.29	37,7032	34,71	**2,5**	**2,5**					4,1	KÜRKÇÜ-BOR (NİĞDE) [SW 1.4 km]
164	03.02.2011	09:17:11.30	37,9803	34,538	**2,6**	**2,6**					12,7	FESLEĞEN- (NİĞDE) [SW 1.7 km]
165	16.02.2011	14:33:54.15	38,06	34,836	**2,8**	**2,8**					5,7	YEŞİLOVA- (NİĞDE) [SW 0.6 km]
166	24.02.2011	08:22:03.75	37,9208	34,436	**2,9**	**2,9**					0,4	KAYI-BOR (NİĞDE) [NE 3.6 km]

Table 5- (continued)

No	Date	Time	Lat.	Lon.	M	MD	ML	MS	Mw	Mb	Depth (km)	Location
167	26.02.2011	09:14:59.44	37,9302	34,552	**2,8**	**2,8**					11,6	OKCU-BOR (NİĞDE) [SE 1.4 km]
168	07.04.2011	11:15:27.14	38,4512	34,049	**2,6**	**2,6**					5,4	AKIN- (AKSARAY) [NE 1.6 km]
169	08.04.2011	13:24:27.60	38,202	34,103	**2,8**	**2,8**					20,1	GÖZLÜKUYU- (AKSARAY) [N 2.4 km]
170	23.04.2011	21:39:36.18	38,8387	33,431	**2,7**	**2,7**					5,4	HAMZALI- ŞEREFLİKOÇHİSAR (ANKARA) [SW 4.2 km]
171	05.05.2011	16:00:18.74	39,1687	33,311	**2,9**	**2,9**					12,8	YUSUFKUYUSU- ŞEREFLİKOÇHİSAR (ANKARA) [SE 3.3 km]
172	13.05.2011	10:57:57.05	38,9985	33,537	**2,1**	**2,1**					3,2	SADIKLI- ŞEREFLİKOÇHİSAR (ANKARA) [SW 3.4 km]
173	24.05.2011	13:46:29.75	38,3353	34,164	**2,7**	**2,7**					18,3	ÇELTEK- (AKSARAY) [NE 2.1 km]
174	28.05.2011	15:23:52.38	38,4825	34,183	**2,4**	**2,4**					3,3	YALNIZCEVİZ- (AKSARAY) [SE 1.3 km]
175	29.05.2011	02:12:14.86	38,5	33,778	**2,9**	**2,9**					8,1	ULUKIŞLA- (AKSARAY) [E 1.3 km]
176	29.05.2011	02:13:38.93	38,4925	33,879	**2,8**	**2,8**					5,4	BAYMIŞ- (AKSARAY) [SW 1.3 km]
177	29.05.2011	02:17:53.29	38,5	33,789	**2,9**	**2,9**					7,9	ULUKIŞLA- (AKSARAY) [E 2.2 km]
178	29.05.2011	02:19:39.89	38,5307	33,716	**2,8**	**2,8**					6,1	ULUKIŞLA- (AKSARAY) [NW 5.3 km]
179	29.05.2011	02:25:55.50	38,507	33,814	**3,3**	**3,3**					0,1	ACIPINAR- (AKSARAY) [SW 4.1 km]
180	29.05.2011	02:28:05.80	38,4747	33,872	**3,0**	**3,0**					5,3	ÇİMELİYENİKÖY- (AKSARAY) [SW 3.3 km]
181	29.05.2011	02:57:22.34	38,4757	33,671	**2,9**	**2,9**					12,6	YEŞİLTEPE- (AKSARAY) [W 8.4 km]
182	29.05.2011	05:08:25.52	38,468	33,752	**3,2**	**3,2**					8	YEŞİLTEPE- (AKSARAY) [NW 1.3 km]
183	29.05.2011	16:14:31.61	38,9318	33,406	**3,4**	**3,4**					5,4	HAMZALI- ŞEREFLİKOÇHİSAR (ANKARA) [NW 7.8 km]
184	05.06.2011	01:54:59.90	38,7372	33,602	**3,2**	**3,2**					0,1	ÇALÖREN- ŞEREFLİKOÇHİSAR (ANKARA) [SW 9.6 km]
185	13.06.2011	11:30:25.89	38,3463	33,9202	**3,9**		**3,9**				0,1	ATAKÖY – AKSARAY [SE 1,0 km]
186	05.07.2011	08:09:44.20	38,465	34,136	**2,5**	**2,5**					5,2	AĞZIKARAHAN- (AKSARAY) [N 2.3 km]
187	05.07.2011	13:28:57.84	38,4955	33,871	**2,5**	**2,5**					24,8	BAYMIŞ- (AKSARAY) [SW 1.7 km]
188	09.07.2011	10:01:37.95	38,4485	34,157	**2,6**	**2,6**					0,2	AĞZIKARAHAN- (AKSARAY) [NE 1.6 km]
189	19.07.2011	11:21:03.20	38,4712	34,142	**2,9**	**2,9**					1,9	YALNIZCEVİZ- (AKSARAY) [SW 2.9 km]
190	21.07.2011	09:51:49.45	38,9907	33,434	**2,5**	**2,5**					19,9	HACIBEKTAŞLI- ŞEREFLİKOÇHİSAR (ANKARA) [SW 9.9 km]
191	30.07.2011	10:24:30.80	38,9525	33,581	**2,0**	**2,0**					14	ŞEREFLİKOÇHİSAR (ANKARA) [NE 3.9 km]
192	01.08.2011	12:40:13.00	38,5423	33,557	**1,9**		**1,9**				0,1	ULUKIŞLA- (AKSARAY) [NW 18.5 km]
193	05.08.2011	13:54:23.04	38,305	34,125	**3,0**	**3,0**					9,3	AKHİSAR- (AKSARAY) [NE 2.7 km]
194	16.08.2011	09:05:55.20	38,458	34,297	**2,6**	**2,6**					4,6	AKMEZAR-GÜLAĞAÇ (AKSARAY) [SW 1.5 km]
195	23.08.2011	11:35:51.46	38,4573	34,144	**2,5**	**2,5**					11,6	AĞZIKARAHAN- (AKSARAY) [NE 1.5 km]
196	09.09.2011	01:05:14.19	39,22	33,276	**2,7**	**2,7**					17,5	BÜYÜKKIŞLA- ŞEREFLİKOÇHİSAR (ANKARA) [NE 2.6 km]
197	14.09.2011	07:40:11.06	37,8948	34,634	**1,9**		**1,9**				10,9	SAZLICA- (NİĞDE) [SW 0.5 km]
198	15.09.2011	14:20:06.26	38,4282	34,115	**2,6**	**2,6**					2,3	AĞZIKARAHAN- (AKSARAY) [SW 2.8 km]
199	21.09.2011	12:25:40.13	37,8635	34,652	**2,7**	**2,7**					0,6	KAYNARCA-BOR (NİĞDE) [NE 1.9 km]
200	26.09.2011	20:17:42.07	38,9227	33,408	**2,8**	**2,8**					5,5	HAMZALI- ŞEREFLİKOÇHİSAR (ANKARA) [NW 6.8 km]
201	29.10.2011	04:16:32.84	39,1968	33,347	**2,8**	**2,8**					8	BÜYÜNEAMLACIK- ŞEREFLİKOÇHİSAR (ANKARA) [SE 2.1 km]
202	06.12.2011	13:05:29.95	38,3718	34,106	**3,0**	**3,0**					9,7	SEVİNÇLİ- (AKSARAY) NW 1.3 km]
203	21.12.2011	13:14:46.90	38,4958	34,013	**2,1**		**2,1**					GÜLTEPE- (AKSARAY) [NW 4.7 km]

Kürçer (2012) conducted 4 paleoseismic trench works (two for each segment) on the Tuz Gölü and Akhisar-Kılıç segments. Paleoseismic results of these studies are published in several journal (Kürçer and Gökten, 2012; Kürçer et al. (2012); Kürçer and Gökten, 2014).

5. Comments on the Age of Neotectonic Period in the Tuz Gölü Fault Zone Region

In this study, 1/25.000 scaled geology maps of two different areas have been renewed to clarify the age of Neotectonic period in the TGFZ region (Figure 33). After rectification, produced geology maps were spread out in the Google Earth program and relief geology maps were acquired for the sub-regions (Figures 34 and 35).

For the renewal of geology maps, 1/25.000 scaled geology maps in the archives of Geology Department of the General Directorate of the Mineral Research and Exploration of Turkey (MTA) were referenced and renewed in detail in accordance with the aim of study.

In renewal of geology maps for Şereflikoçhisar and surrounding areas studies of Uygun et al. (1982), Atabey (1986), Atabey et al. (1987) and Atabey

Table 6- The maximum earthquake magnitudes, the maximum and average displacements generated by the segments of the Tuz Gölü Fault Zone (in calculations equations by Wells and Coppersmith (1994) suggested for normal faults are used).

Segment name	Segment length (km)	The largest eartquake expected from the segment (M)	The largest displacement expected from each eartquake (m)	The average displacement expected from each eartquake (m)
Yusufkuyusu	9	6,11	0,34	0,25
Acıkuyu	10	6,18	0,39	0,27
Akboğaz	13	6,33	0,54	0,34
Şereflikoçhisar	14	6,37	0,58	0,36
İnceburun	23	6,65	1,04	0,54
Tuz Gölü	30	6,80	1,41	0,68
Acıpınar	26	6,72	1,20	0,60
Aksaray	13	6,33	0,54	0,34
Akhisar-Kılıç	27	6,74	1,25	0,62
Altunhisar	30	6,80	1,41	0,68
Bor	17	6,48	0,73	0,42

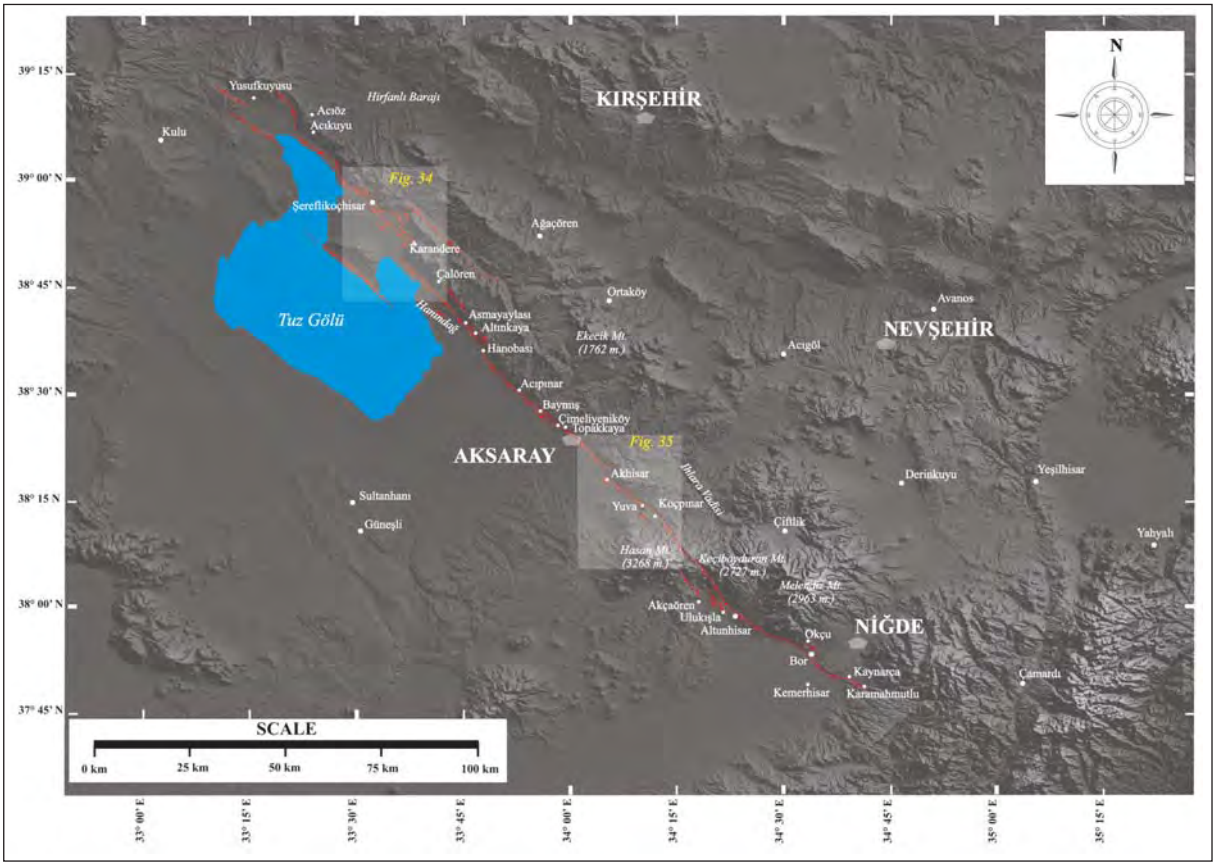

Figure 33- Map showing sub-areas where 1/25.000 scaled geological map renewal was done in the Tuz Gölü Fault Zone region

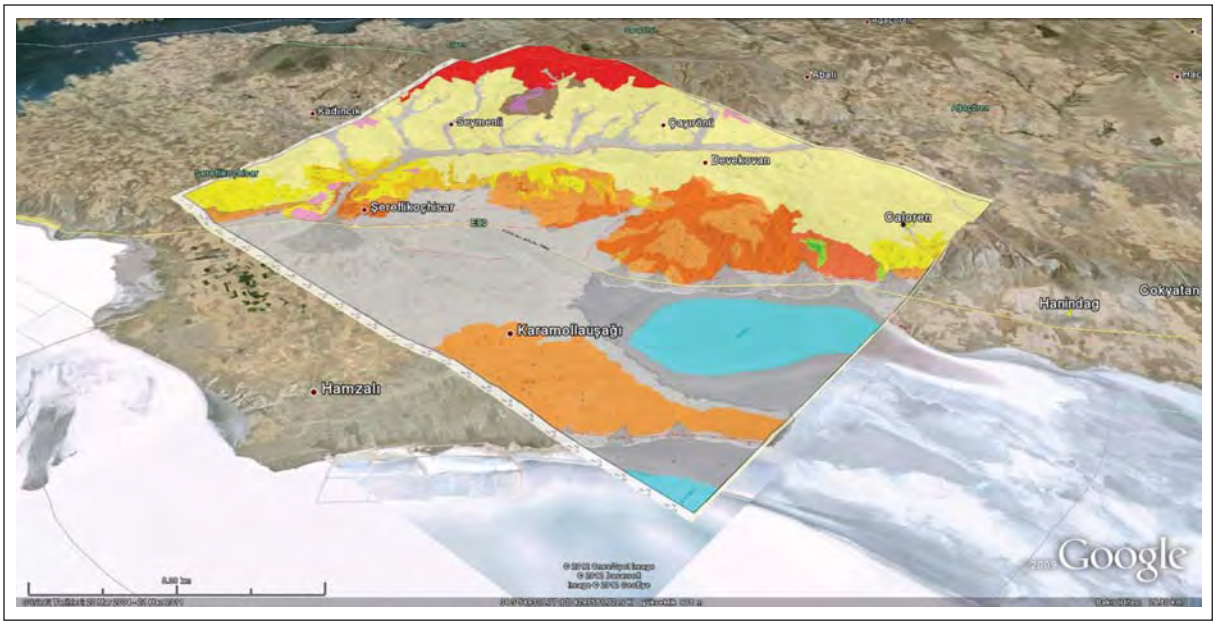

Figure 34- Relief geology map of Şereflikoçhisar and surrounding (K31 a1,a2,a3,a4) (in the Google Earth image vertical scale three times exaggerated, view to NE with oblique angle)

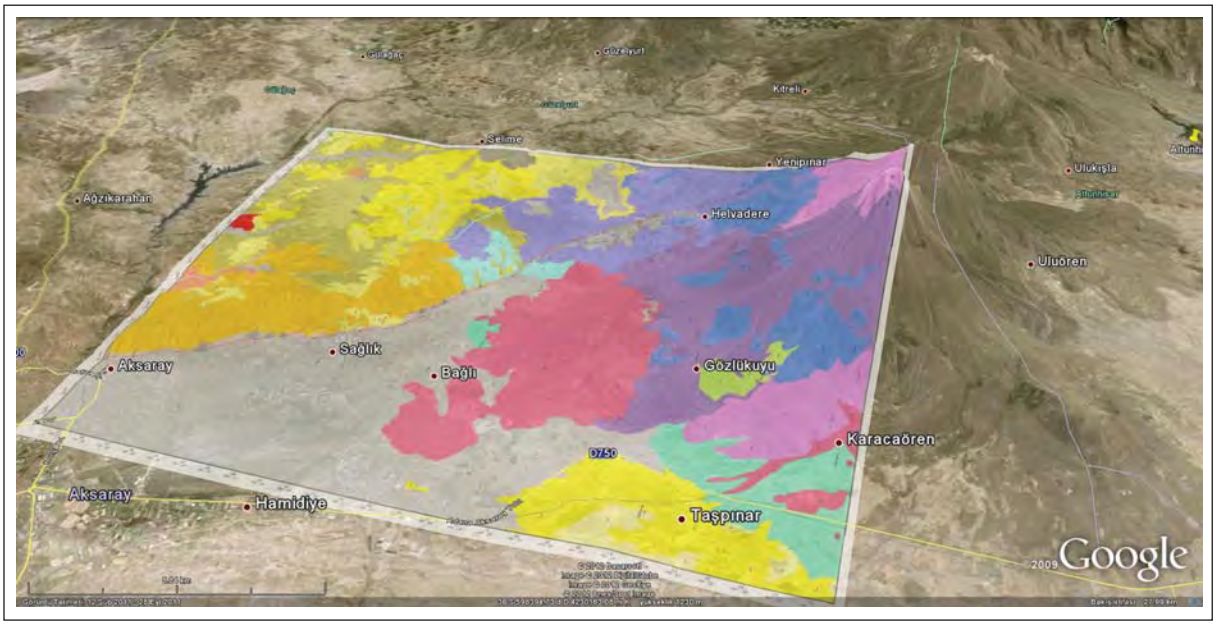

Figure 35- Relief geology map of the area between Aksaray and Hasandağı (L32 a3,a4,d1,d2) (in the Google Earth image vertical scale three times exaggerated, view to NE with oblique angle)

(1989) were utilized. In renewal of geology maps for the area between Aksaray and Hasandağı, geology maps of Beekman (1965), Erdem (1985), Papak (1985) and Dönmez et al. (2005) were used.

The first area of map renewal comprises Şereflikoçhisar and surrounding (K31 a1,a2, a3 and a4 quadrangles) (Figure 34). Structural elements in the map area indicate that more than one tectonic regime are effective. In units below the late Miocene-Pliocene Peçenek formation (Tmplp) and Pliocene Cihanbeyli formation (Tplc) fold axes in three different directions are noticeable. Among them, E-W trending fold axis is the relatively oldest one that is

observed in the Paleozoic Tamadağ formation (Pzt) and Bozçaldağ formation (Pzb). In Mesozoic and Cenozoic sedimentary rocks between the Paleozoic metamorphic basement and late Miocene-Pliocene neotectonic units (Peçenek and Cihanbeyli formations) fold axis in two different directions (N15°E and N50°W) are observed. N15°E-trending folding was effective in relatively older units (Kartal, Asmaboğazı, Çaldağ, Karapınaryaylası and Boyalı formations). N50ºW-trending folding axis is dominated in relatively younger units (Karapınaryaylası, Boyalı, Yassıpur and Koçhisar formations).

The Peçenek formation and laterally and vertically interlayered Cihanbeyli formation cover the older units with an angular unconformity. This stratigraphic relation is well seen around the Ağasivri Hill NE of Şereflikoçhisar (Figure 36). At the Ağasivri Hill (1180 m) Pliocene aged Cihanbeyli formation is exposed. The unit is cut and lowered to the 950-m elevation by a series of SW-dipping normal faults that belong to TGFZ that is generated during the neotectonic period (Figure 37). In an assessment considering the basement of Cihanbeyli formation, total oblique slip rate on TGFZ following the deposition of Cihanbeyli formation (Paleocene to recent) is found 200 m (1078 m – 878 m).

In this study, due to aforementioned stratigraphic relation, the Peçenek and Cihanbeyli formations are regarded as neotectonic units. Although there has been no absolute age on the Cihanbeyli formation, Tunoğlu et al. (1995) and Beker (2002) determined the following ostracode species in samples collected from limestone levels of the Cihanbeyli formation: *Cyprideis torosa* Jones, 1850; *Candona (Candona) neglecta* Sars, 1888; *Candona (Candona) paralella pannonica* Zalanyi; *Candona (Candona) altoides Petkovski,* 1961; *Candona (Pseudocandona) compressa* Koch 1837; *Heterocypris ponticus* Krstic, 1973. Based on this fossil assemblage, the Cihanbeyli formation is of Pliocene age (Tunoğlu et al., 1995; Beker 2002).

Another area where geology map renewal has been made is the region between Aksaray and Hasandağı (L32 a3, a4, d1 and d2 quadrangles) (Figure 35). Stratigraphic relations in the map area indicate that at least two different tectonic regimes are effective in the region. Horizontally bedded early Pliocene Kızılkaya Ignimbrites around Akhisar village SE of Aksaray set above the late Eocene – Oligocene aged, 45-60º NE-dipping Yassıpur formation with an angular unconformity. At east of Akhisar village, the base of Kızılkaya Ignimbrite is exposed at an elevation of 1293 m. The unit is cut and lowered to the plain altitude (1025 m) around the Akhisar village by TGFZ which is generated during the neotectonic period (Figure 38). In an assessment considering the base of Kızılkaya Ignimbrite, total slip rate on TGFZ following the deposition of unit (early Pliocene to recent) is found 268 m (1293 m - 1025 m).

As a result of geology map renewal studies, beginning of neotectonic period for TGFZ region is found as early Pliocene (around 5 million years). The total slip rate on TGFZ which is a structure of neotectonic period is 200 m at north (around

Figure 36- A panoramic view showing stratigraphic relations of units on the Ağasivri Hill at northeast of Şereflikoçhisar (view to NW)

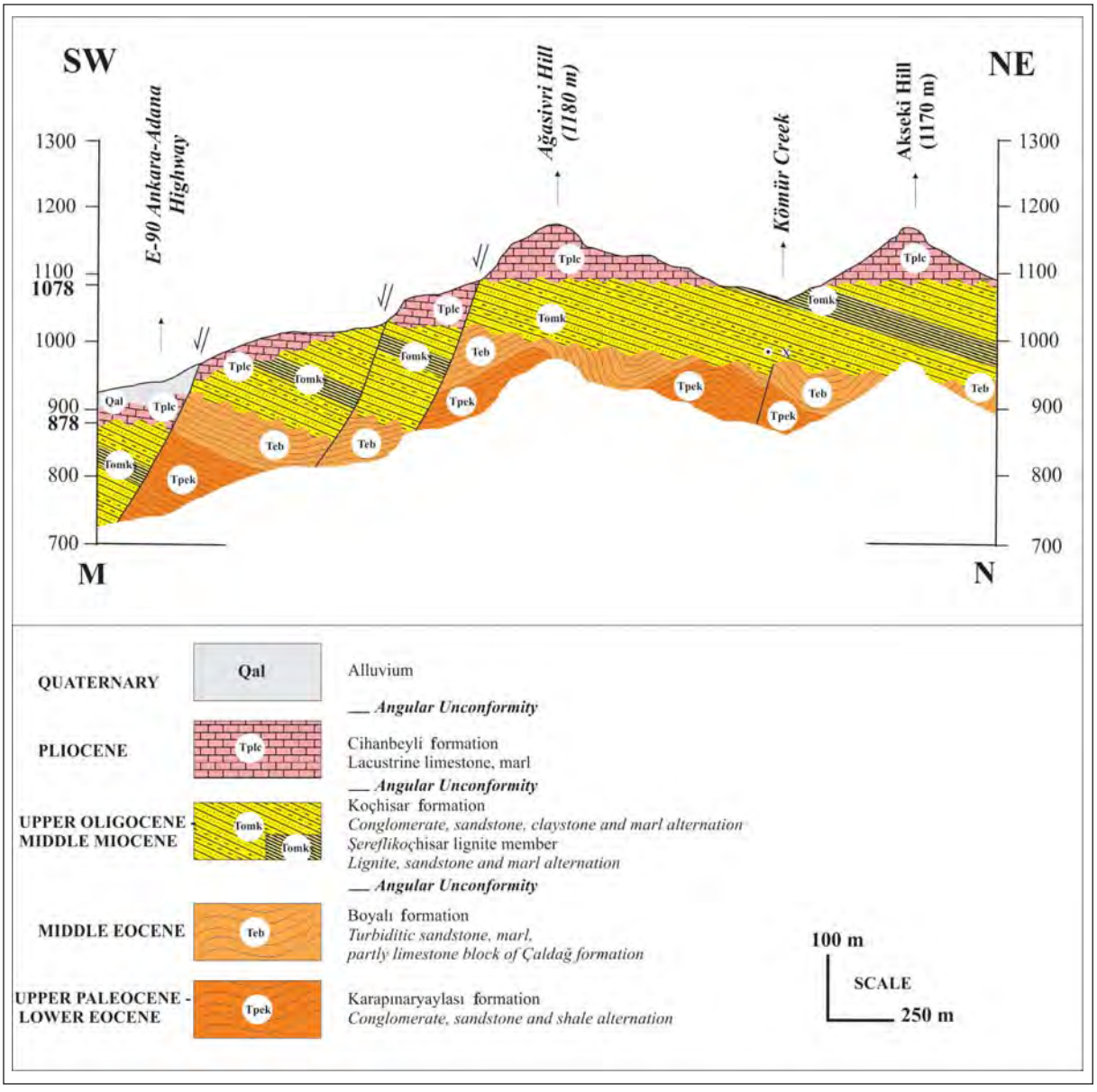

Figure 37- Geological cross section taken from the Ağasivri Hill at northeast of Şereflikoçhisar

Şereflikoçhisar) and 268 m at south (around Akhisar village). Evaluation of paleontological and radiometric age data of previous studies together with total slip rates deduced from this work reveals that the annual slip on TGFZ in the last 5 years has been found as 0,040 – 0,053 mm (average 0,046 mm).

6. Results and Discussion

1- In mapping studies conducted around Şereflikoçhisar to examine the age of TGFZ and beginning age of neotectonic period in the region, it was found that the Pliocene Cihanbeyli formation and laterally and vertically interlayered Peçenek formation cover the older units with an angular unconformity (Figures 36 and 37). The base of Pliocene Cihanbeyli formation is exposed at an elevation of 1078 m on the Ağasivri hill NE of Şereflikoçhisar. The unit is cut and lowered to the 878-m elevation by a series of SW-dipping normal faults that belong to TGFZ that is generated during the neotectonic period (Figure 37). In an assessment considering the basement of Cihanbeyli formation, total oblique slip rate on TGFZ following the deposition of Cihanbeyli formation (Paleocene to recent) is found 200 m (1078 m – 878 m).

Stratigraphic relations of the units between Aksaray and Hasandağı, which is another area where geology map renewal has been made, indicate that at least two different tectonic regimes are effective in the region. Horizontally bedded early Pliocene Kızılkaya Ignimbrites around Akhisar village SE of Aksaray set above the late Eocene – Oligocene aged, 45-60° NE-dipping Yassıpur formation with an angular unconformity. At east of Akhisar village, the base of Kızılkaya Ignimbrite is exposed at an elevation of 1293 m. The unit is cut and lowered to the plain altitude (1025 m) around the Akhisar village by TGFZ (Figure 38). In an assessment considering the base of Kızılkaya Ignimbrite, total slip rate on TGFZ following the deposition of unit (early Pliocene to recent) is found 268 m (1293 m - 1025 m).

Considering these stratigraphic relations and structural data, the initiation age of neotectonic period for TGFZ region is early Pliocene (around 5 million years). The total slip rate on TGFZ is 200 m at north (around Şereflikoçhisar) and 268 m at south (around Akhisar village). Evaluation of paleontological and radiometric age data of previous studies together with total slip rates deduced from this work yields that the annual slip on TGFZ in the last 5 years has been found as 0,040 – 0,053 mm (average 0,046 mm).

In literature different ages are suggested for TGFZ. According to Görür and Derman (1978), Uygun et al. (1982), Görür et al. (1984), Çemen et al. (1999), Dirik and Erol (2000), the age of TGFZ is as old as late Cretaceous. Arıkan (1975) states that TGFZ is of Eocene age whilst Dellaloğlu and Aksu (1984) assert that it is Miocene in age. On the other hand, considering the recent character of TGFZ, Koçyiğit (2000) suggested that first activation of TGFZ might have postdated early Pliocene. Data from this work for the initiation age of neotectonic period for TGFZ are in support of post early Pliocene age suggested by Koçyiğit (2000).

In various paleoseismic studies conducted on TGFZ, recent period (late Pleistocene/Holocene – recent) annual slip rate of TGFZ is found to range from 0.034 mm (Kürçer and Gökten, 2014) to 0.0536 mm (Kürçer and Gökten, 2012) and the average earthquake recurrence interval is determined as 10,930 years (Kürçer and Gökten, 2014). Average long-period (Pliocene to recent) slip rate deduced from this work are consistent with recent period slip rate acquired from paleoseismological studies.

2- Dirik and Erol (2000) pointed out that the Tuz Gölü Basin was developed on the Central Anatolian Crystalline Complex in association with extensional tectonic movements in the upper Cretaceous time and the basin floor is represented by late Cretaceous-early Paleocene Kartal formation and laterally-vertically interbedded Asmaboğazı formation. In addition, in

Figure 38- Processed Google Earth image showing stratigraphic relations of units around the Akhisar village (vertical scale three times exaggerated, view to NE with oblique angle)

studies on the Tuz Gölü Basin, TGFZ is indicated to be a structural element bordering the basin from the east (Arıkan 1975, Görür et al., 1984; Şaroğlu et al., 1987; Emre 1991; Çemen et al., 1999; Koçyiğit 2000; Genç and Yürür 2010).

According to geological map for prepared along the TGFZ, Kartal and Asmaboğazı formations are exposed on foot wall of SW-dipping TGFZ (Figure 2). Therefore, TGFZ which is a neotectonic period structure, cannot border the Tuz Gölü Basin from the east. Kartal and Asmaboğazı formations, which are the first deposits of the Tuz Gölü Basin, are thought to be deposited during the first stage of basin formation in front of a normal fault (probably a detachment fault) that borders the basin from the east and facilitated the uplift of Kırşehir Massif. During the period from upper Cretaceous to recent time, the Tuz Gölü Basin has continued its development and the today's TGFZ gained its recent character far after the basin development (post early Pliocene) and broke down the basin. In other words, the Tuz Gölü Fault Zone is a structural element bordering not the Tuz Gölü Basin but the recent Tuz Gölü Quaternary depression area from the east.

3- In general, it is commonly accepted that TGFZ is a fault zone extending in between Paşadağ at NW (north of Lake Tuz) and Bor (Niğde) at SE (Şaroğlu et al., 1987, 1992; Dirik and Göncüoğlu 1996; Dirik and Erol 2000; Koçyiğit 2000). Moreover, Koçyiğit and Beyhan (1998) suggested that TGFZ extends to Çamardı (Niğde) at SE and in the area between Bor and Çamardı it gains a significant reverse component. These authors regarded TGFZ and the left-lateral Central Anatolian Fault Zone as a conjugate strike-slip fault.

In this study, field studies carried out along TGFZ yielded that TGFZ starts from Lake Tuz at NW and ends around Kemerihisar (Niğde) at SE. In the part from Kemerihisar to Çamardı no field data were found for the prolongation of TGFZ.

4- The character of TGFZ is still debated. For example, Şengör et al. (1985) and Şaroğlu et al. (1987) regarded TGFZ a NE-dipping, right-lateral strike-slip fault with a high-angle reverse component and this was shown in the Active Fault Map of Turkey by Şaroğlu et al. (1992). Derman et al. (2000) suggested that TGFZ was first started as a normal fault and then in Eocene gained a left-lateral strike-slip character and later achieved again a normal faulting character. A group of researchers (Emre 1991; Toprak and Göncüoğlu 1993; Dirik and Göncüoğlu 1996; Koçyiğit and Beyhan 1998; Toprak 2000; Dirik and Erol 2000; Koçyiğit 2000), based on morphotectonic data, and Çemen et al. (1999) based on seismic reflection profile, pointed out that TGFZ operated in the neotectonic period as a right-lateral strike-slip fault with a high-angle normal component. On the other hand, Leventoğlu et al. (1994) who studied 14-km part of TGFZ in Hanındağ area at SE of Şereflikoçhisar concludes that TGFZ is a normal fault with a right-lateral strike-slip component.

In this study, based on direct fault plane measurements, a total of 32 fault plane slip data were taken at 7 stations along TGFZ. As a result of kinematic analysis of these data, it was shown that an NE-SW trending extensional regime is active in the TGFZ region (Figure 29). This finding is consistent with NNE-SSW trending extensional regime deduced from studies on the Cihanbeyli and Yeniceoba Fault Zones at west of Lake Tuz (Özsayın, 2007; Özsayın and Dirik, 2007). In addition, moment tensor solution of the 13 June 2011 Ataköy (Aksaray) earthquake (M=3.9) indicates the presence of a N34ºW trending 80ºSW dipping oblique-slip normal fault with right-lateral strike-slip component. This result is quite compatible with fault plane slip data on TGFZ.

According to structural observations conducted to determine the character of TGFZ, TGFZ was regarded as a NW-SE trending, SW-dipping, active, 200-km long, 2-25 km width normal fault zone with a minor right-lateral strike-slip component.

5- Geometry and segmentation of TGFZ is debated. There are different suggestions particularly for segmentation of Şereflikoçhisar part. For example, in Active Fault Map of Turkey by Şaroğlu et al. (1992), the area between NW Şereflikoçhisar (Kocadere) of Tuz Gölü Fault and Karamandere village is shown as a single segment of 38 km in length (Şaroğlu et al., 1992). In Kayseri quadrangle of the 1/500.000 scaled Turkey Geology Map (MTA, 2002), that part of Tuz Gölü Fault is mapped as a 74-km long continuous segment extending from the north of Şereflikoçhisar to the Baymış village around Aksaray at SE. However, Koçyiğit (2000) states that TGFZ from south of Şereflikoçhisar first jumps to left and then to right thus forming compressional and extensional structures specific to strike-slip faults.

In order to resolve literature chaos regarding Şereflikoçhisar part of TGFZ, two-dimensional high resolution seismic reflection profile work was conducted along a 7-km long line (Kürçer, 2012; Kürçer et al., 2012) (for location of profile line Figure 7). The Şereflikoçhisar Two-Dimensional High Resolution Seismic Reflection Profile Section was integrated with well log of Turkish Petroleum Corporation (TPAO) (1975) and regional geology information and then evaluated (Figure 10). The Şereflikoçhisar segment was mapped based on surface geology information and geophysical data obtained from high resolution seismic reflection profile shown in figure 10 and then geometry of this segment was propounded in detail.

In addition, field and laboratory (air photo and remote sensing) studies conducted on TGFZ yield that TGFZ is composed of parallel or sub-parallel 11 geometric fault segments. The length of segments is between 9 and 30 km.

6- According to Koçyiğit and Beyhan (1998), TZFZ is a conjugate fault of left-lateral Central Anatolian Fault Zone. In the present study, we have no data to indicate that TGFZ is a pure right-lateral strike-slip fault. Most of fault plane slip data measured on TGFZ show signs of normal faulting. Along the fault planes, chronologic faulting tracks as one on top of another are also absent. Considering the TGFZ is a structure formed in the neotectonic period, it is clear that this zone have no connection with the Central Anatolian Fault Zone since the beginning of neotectonic period. Today TGFZ is a normal fault zone with a minor right-lateral strike-slip shaping the Tuz Gölü Quaternary Basin

7- On the other hand, in all neotectonic works regarding Central Anatolia, TGFZ is accepted as an active structure but seismicity of TGFZ and earthquake potential of segments have not been examined.

In the present study, instrumental-period earthquakes (1900-2011) for a large area comprising the TGFZ region were compiled from the Kandilli Observatory and Earthquake Research Institute and they were evaluated. Statistical assessment of earthquake focal depths showed that earthquakes on TGFZ were occurred at an average depth of 10 km. It was shown that earthquakes around Hasandağ and Altunhisar have focal depths deeper than the average. This might indicate that some of earthquakes in the region are volcanogenic earthquakes.

Considering the statistical assessment of earthquake magnitudes, among 205 earthquakes, 136 are of M=1.3-2.9, 60 are of M=3.0-3.9, 7 are of M=4.0-4.9 and 1 is of M=5.2. The largest earthquake recorded during the instrumental period is the Uluören (Altunhisar) earthquake with magnitude of M=5.2. Additionally, 1924 Başaran (Eskil) (M=4.9), 1985 Şekerköy (Şereflikoçhisar) (M=4.3), 1998 Altunhisar (Niğde) (M=4.0), 2001 Ulukışla (Aksaray) (M=4.1), 2002 Taşpınar (Aksaray) and 2007 Acıkuyu (Kulu) (M=4.9) earthquakes are other important earthquakes recorded on TGFZ.

In this study, using the equations for normal faults suggested by Wells and Coppersmith (1994), the largest earthquake produced by each segment of TGFZ and the maximum and average displacements were calculated. The largest earthquakes generated by TGFZ segments are in the range of M = 6.11-6.80 and the maximum displacement is between 0.34 – 1.41 m and average displacements are between 0.25- 0.68 m.

8- According to stratigraphic and structural data from areas where geology map renewal studies are conducted, the beginning of neotectonic period for TGFZ region is found as early Pliocene (around 5 million years). The total slip rate on TGFZ is 200 m at north (around Şereflikoçhisar) and 268 m at south (around Akhisar village). Evaluation of paleontological and radiometric age data of previous studies together with total slip rates deduced from this work reveals that the annual slip on TGFZ in the last 5 years (early Pliocene) has been found as 0,040 – 0,053 mm (average 0,046 mm).

9- TGFZ is a fault zone with a quite low annual slip rate (average 0,046 mm/y) and consistently a relatively wide earthquake recurrence interval (10,390 years; Kürçer and Gökten, 2014).

There is a relation among the average earthquake recurrence interval, earthquake magnitude and annual slip rate of active faults (Slemmons, 1982). These relations for TGFZ were examined on a chart developed by (Slemmons, 1982) (Figure 39). In this respect, for an earthquake of M=6.11-6.80 with recurrence interval of 10,000 years, the annual slip rate on the source fault is 0.05 mm. This value is quite consistent with the value of 0.046 mm/y from the present study.

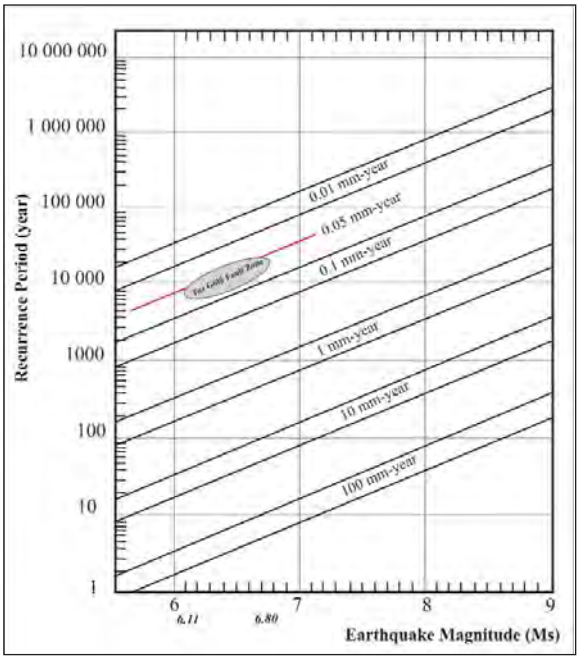

Figure 39- Average earthquake recurrence interval vs. magnitude and slip rate graphic (Slemmons, 1982). Ellipse shows the area of overlap that was acquired by adapting the Slemmons (1982) graphic to the TGFZ.

Yıldırım (2014) made a great contribution to tectonic activity of TGFZ. Using some morphologic indices such as the mountain front sinuosity and the valley-width to valley-height ratio, he investigated tectonic activity of TGFZ. Based on classification by Bull and McFadden (1977), TGFZ segments are "moderately active fault zone" with vertical uplift rate between 0.05 – 0.5 mm/y corresponding to class 2.

Acknowledgement

This study was implemented in the frame of "Neotectonic-Period Characteristics and Paleoseismology of the Tuz Gölü Fault Zone, Central Anatolia, Turkey" project (2010-30-14-02-3) carried out by the Geology Department of the General Directorate of the Mineral Research and Exploration of Turkey (MTA). The Şereflikoçhisar Two-Dimensional High Resolution Shallow Seismic Reflection Profile study was conducted by the Geophysics Department of the General Directorate of MTA. The instrumental earthquakes occurred in the study area were evaluated by Dr. Doğan Kalafat of the Kandilli Observatory and Earthquake Research Institute. Authors thank to these organizations and persons. Prof. Erdin Bozkurt (METU) and Prof. Nureddin Kaymakçı (METU) are greatly acknowledged for their helpful comments which improved the manuscript.

Received: 20.11.2013
Accepted: 01.08.2014
Published: December 2014

References

Afşin, M., Baş, H. 1996. Koçpınar (Aksaray) kaynaklarının su kimyası açısından değerlendirilmesi. *Türkiye Jeoloji Kurumu Bülteni*, 39(1), 75-86.

Akıman, O., Erler, A., Göncüoğlu, M.C., Güleç, N., Güven, A., Türeli, T.K., Kadıoğlu, Y. 1993. Geochemical characteristics of granitoides along the western margin of the Central Anatolian Crystalline Complex and their tectonic implications. *Geological Journal*, 28, 371-382.

Ambraseys, N. N., Jackson, J.A. 1998. Historical recent earthquakes Eastern Mediterranean. *Geophy. J. Int.* (1998), 133, 390-406.

Andreasyan, H. 1970. Ermeni kaynaklarından derlenmiş deprem listesi. Prof. Dr. H. Soysal's personal archive, (unpublished), İstanbul.

Arıkan, Y. 1975. Tuzgölü havzasının jeolojisi ve petrol imkanları. *Maden Tetkik ve Arama Dergisi*, 85, 17-38.

Atabey, E. 1986. Maden Tetkik ve Arama 1/25 000 ölçekli arşiv haritaları Aksaray K 31 a1, a2, a3 ve a4 paftaları, Ankara, (unpublished).

Atabey, E. 1989. Maden Tetkik ve Arama 1/100 000 Ölçekli açınsama nitelikli Türkiye Jeoloji Haritaları Serisi, Aksaray-H 17 (K 31) paftası, Ankara.

Atabey, E., Ayhan, A. 1986. Niğde, Ulukışla, Çamardı, Çiftehan yöresinin jeolojisi, *Maden Tetkik ve Arama Genel Müdürlüğü Report* No: 8064, 60 s. Ankara, (unpublished).

Atabey, E., Tarhan, N., Akarsu, B., Taşkıran, M.A. 1987. Şereflikoçhisar, Panlı (Ankara) – Acıpınar (Niğde) yöresinin jeolojisi. *Maden Tetkik ve Arama Genel Müdürlüğü Report* No: 8155. 69 s. Ankara, (unpublished).

Aydar, E, Schmitt, A.K.., Çubukçu, H.E., Akın, L., Ersoy, O., Şen, E., Duncan, R.A., Atici, G. 2012. Correlation of ignimbrites in the central Anatolian volcanic province using zircon and plagioclase ages and zircon compositions. *Journal of Volcanology and Geothermal Research* 213-214, 83–97.

Batum, İ. 1978. Nevşehir güneybatısındaki Göllüdağ ve Acıgöl volkanitlerinin jeokimyası ve petrolojisi. *Yerbilimleri*, 4/1-2, 70-88.

Beker, K. 2002. İnsuyu Kireçtaşları (Karapınar/Konya) Ostrakod Topluluğunun Biyostratigrafik ve

Kronostratigrafik İncelenmesi. Hacettepe Üniversitesi Fen Bilimleri Enstitüsü, Ankara, Yüksek Mühendislik Tezi, 93s. (unpublished).

Beekman, P.H. 1965. Maden Tetkik ve Arama Genel Müdürlüğü, 1/25.000 ölçekli arşiv haritaları Aksaray L 32 d1 ve d2 paftaları, Ankara, (unpublished).

Beekman, P.H. 1966. Hasandağı-Melendiz dağı bölgesinde Pliyosen ve Kuvaterner volkanizma faaliyetleri. *Maden Tetkik ve Arama Dergisi* 66, 88-103.

Bozkurt, E. 2001. Neotectonics of Turkey–a synthesis. *Geodinamica Acta* 14, 3–30.

Boztuğ, D., Joncheere, R.C., Heizler, M., Ratschbacher, L., Harlavan, Y., Tichomirova, M. 2009. Timing of post-obduction granitoids from intrusion through cooling to exumation in central Anatolia, Turkey. *Tectonophysics* 473, 223-233.

Bull, W.B., McFadden, L.D. 1977. Tectonic geomorphology north and south of the Garlock fault, California. In: Doehering, D.O. (Ed.), Geomorphology in arid regions. *Proceedings at the Eighth Annual Geomorphology Symposium*. State University of New York, Binghamton, NY, pp. 115–138.

Capraru, C. 1977. Considerations regarding the oil possibilities of Tuz Gölü Basin. *TPAO Report*, Ankara, (unpublished).

Capraru, C. 1991. Hydrocarbon trap types in the structural units of the Tuz Gölü Basin. *Ozan Sungurlu Sempozyumu*, Proceedings, 156-173.

Çemen, İ., Dirik, K. 1992. Tuzgölü havzasının kuzeydoğu kısmının stratigrafisi, yapısal jeolojisi ve jeoloji tarihi. *TPAO Report No*: 3115 (unpublished).

Çemen, İ., Göncüoğlu, M.C., Dirik, K. 1999. Structural evolution of the Tuzgölü basin in Central Anatolia, Turkey. *Journal of Geologys*, 107, 693-706.

Çiftçi, B. 2007. Geological Evolution of the Gediz Graben, SW Turkey: Temporal and Spatial Variation of the Graben. *ODTÜ Fen Bilimleri Enstitüsü, Ankara*, Doktora Tezi, 290 s.

Dellaloğlu, A., Aksu, R. 1984. Kulu-Şereflikoçhisar-Aksaray dolayının jeolojisi ve petrol olanakları. *TPAO Report No:* 2020, Ankara, (unpublished).

Dellaloğlu, A.A., Aksu, R. 1986, Ereğli (Konya)- Ulukışla-Çiftehan-Çamardı (Niğde) Dolayının Jeolojisi ve Petrol Olanakları, *TPAO Report No*. 2205, Ankara, (unpublished).

Demircioğlu, R., Eren, Y. 2000, Çamardı (Niğde) civarında Niğde Masifi örtü birimlerinin yapısal özellikleri, *N.Ü. Aksaray Mühendislik Fakültesi, Haymana-Tuzgölü-Ulukışla basenleri uygulamalı çalışma (Workshop), Bildiri özleri*, s. 6.

dePolo, C. M., Clark, D. G., Slemmons, D. B., Aymand, W. H. 1989. Historical Basin and Range Province surface faulting and fault segmentation. In Fault Segmentation and Controls of Rupture Initiation and Termination (D. P. Schwartz, and R. H. Sibson, Eds.), *U.S. Geol. Surv. Open File Rep*. 89–315, pp. 131–162.

DePolo, C.M., Claek, D.C., Slemmons, D.B., Ramelli, A.R. 1991. Historical surface faulting in the basin and range province, Western North America: İmplications for fault segmentation, *J. Struct. Geol*. 13. 123-136.

Derman, A.S. 1980. Tuz Gölü ve kuzeyinin jeolojisi, *TPAO Report No*: 1512, Ankara, (unpublished).

Derman, A.S., Rojay, B., Güney, H., Yıldız, M. 2000. Koçhisar-Aksaray fay zonu'nun evrimi hakkında yeni veriler. *Haymana-Tuzgölü-Ulukışla basenlerinin uygulamalı çalışması. Bildiri Özleri*, 1, Aksaray.

Dewey J.F., Hempton M.R., Kidd W.S.F., Şaroğlu F., Şengör A.M.C. 1986. Shortening of continental lithosphere: the neotectonics of eastern Anatolia – a young collision zone, in: Coward M.O., Ries A.C. (Eds.), Collisional Tectonics, *Geological Society Special Publication no*: 19, pp. 3–36.

Dirik, K. 2001. Neotectonic evolution of the northwestward arched segment of the Central Anatolian fault zone, Central Anatolia, Turkey. *Geodinamica Acta* 14, 147-158.

Dirik, K., Göncüoğlu, M.C. 1996. Neotectonic characteristics of Central Anatolia, *Int. Geology Review* 38, 807-817.

Dirik, K., Erol, O. 2000. Tuzgölü ve civarının tektonomorfolojik evrimi Orta Anadolu, Türkiye. *Haymana-Tuzgölü-Ulukışla Basenleri Uygulamalı Çalışma (Workshop), TPJD Bülteni*, Özel sayı 5.

Dirik, K., Erol, O. 2003. Tectonomorphologic evolution of Tuzgölü and surrounding area, central Anatolia-Turkey. *Turkish Association of Petroleum Goelogists Special Publication* 5, 27-46.

Dönmez, M., Akçay, A.E., Kara, H., Türkecan, A., Yergök, A.F., Esentürk, K., 2005. MTA 1/100.000 Ölçekli açınsama nitelikli Türkiye Jeoloji Haritaları Serisi. Aksaray-L 32 paftası, Ankara

Emre, Ö. 1991. Hasandağı-Keçiboyduran dağı yöresi volkanizmasının jeomorfolojisi, *İstanbul Üniversitesi, Deniz bilimleri ve Coğrafya Enstitüsü Doktora tezi*, 198 s., İstanbul.

Erdem, E. 1985. Maden Tetkik ve Arama Genel Müdürlüğü, 1/25.000 ölçekli arşiv haritaları Aksaray L 32 a4 ve d1 paftaları, Ankara, (unpublished).

Ercan ,T., Ercan, T., Fujitani, T., Matsuda, J.I., Tokel, S., Notsu, K., Ul, T., Can, B., Selvi, Y., Yıldırım, T., Fişekçi, A., Ölmez, M., Akbaşlı, A. 1990. Hasandağı-Karacadağı bölgesi (Orta Anadolu) Senozoyik volkanizmasının başlangıcı ve evrimi, *Jeomorfoloji Dergisi* 18, 39-54.

Ergin, K., Güçlü, Ü., Aksay, G. 1967. A Cataloques of Earthquakes of Turkey and Surrounding Area, 1965-1970. *Arz. Fiziği Enst. Yayın., No:*28, Maden Fakültesi, İstanbul Teknik Üniversitesi, İstanbul.

Erler, A., Akıman, O., Unan, C., Dalkılıç, B., Geven, A., Önen, P. 1991. Petrology and geochemistry of the magmatic rokcs of the Kırşehir Massive in the Kaman (Kırşehir) and Yozgat regions. *TUBİTAK, Doğa-Tr. Journal of Engineering and Environmental Science*, 15, 76-100 (Türkçe).

Genç, Y., Yürür, T. 2010. Coeval extension and compression in Late Mesozoice Recent thin–skinned extensional tectonics in central Anatolia, Turkey. *Journal of Structural Geology* 32, 623-640.

Göncüoğlu, M.C. 1977. Geologie des Westlichen Niğde - Massivs: *Bonn Univ., Doktora tezi,* (unpublished).

Göncüoğlu, M.C. 1982. Niğde Masifi peragnayslarında U/Pb yaşları. *Türkiye Jeoloji Kurumu Bülteni* 25, 61-66.

Göncüoğlu, M.C. 1985. Niğde Masifi batı yarısının jeolojisi, *Maden Tetkik ve Arama Genel Müdürlüğü, Report* No: 5883 (unpublished), Ankara.

Göncüoğlu, M.C., 2010. Türkiye Jeolojisine Giriş: Alpin ve Alpin öncesi tektonik birliklerin jeodinamik evrimi. *Maden Tetkik ve Arama Genel Müdürlüğü, Monografi serisi No*: 5, 69 s., (Ankara).

Göncüoğlu, M.C., Toprak, G.M.V., Kuşçu, I., Erler, A., Olgun, E. 1991. Orta Anadolu Masifinin Batı Bölümünün Jeolojisi, Bölüm 1: Güney Kesim. *TPAO Report No*. 2909 (unpublished).

Göncüoğlu, M.C., Erler, A., Toprak, V., Yalınız, K., Olgun, E., Rojay, B. 1992. Orta Anadolu Masifi'nin batı bölümünün jeolojisi, Bölüm 2: Orta Kesim. *TPAO Report No*. 3535, Ankara, (unpublished).

Göncüoğlu, M.C., Erler, A., Toprak, V., Olgun, E., Yalınız, K., Kuşçu, İ., Köksal, S., Dirik, K. 1993. Orta Anadolu Masifinin Orta Bölümünün Jeolojisi,Bölüm 3: Orta Kızılırmak Tersiyer Baseninin Jeolojik Evrimi. *TPAO Report No*: 3313, 104 s., Ankara, (unpublished).

Göncüoğlu, M.C., Dirik, K., Erler, A.,Yalınız, K. 1994. Orta Anadolu Masifi doğu bölümünün jeolojisi Bölüm 4: Orta Anadolu masifinin Sivas baseni ile ilişkisi, *TPAO Report No*: 3535, 135p.

Göncüoğlu, M.C., Dirik, K., Erler, A., Yalınız, K., Özgül, L., Çemen, İ. 1996. Tuzgölü havzası batı kısmının temel jeolojik sorunları: *TPAO Report No*: 3753, Ankara, (unpublished).

Göncüoğlu, M.C., Kozlu, H., Dirik, K. 1997. Pre-Alpine and Alpine terranes in Turkey: explanotary notes to the terane map of Turkey. *Ann. Geol. Pays Helleniques*, 37, 515-536.

Görür, N. 1981, Tuzgölü Haymana havzasının stratigrafik analizi, İç Anadolu"nun Jeolojisi Sempozyumu, *TJK 35. Bilimsel ve Teknik Kurultayı Bildiriler Kitabı*, 60-65.

Görür, N., Derman, A. S. 1978. Tuz Gölü-Haymana havzasının stratigrafik ve tektonik analizi. *TPAO Report* No: 1514, Ankara, (unpublished).

Görür, N., Oktay, F.Y., Seymen, İ., Şengör, A.M.C. 1984. Paleotectonic evolution of the Tuzgölü basin complex, Central Turkey: Sedimentary record of a Neo-Tethyan closure, in Dixon, J.E. and Robertson, A.H.F. eds., The Geological evolution of the Eastern Mediterranean: *Geol.Soc.London. Spec. Publ. no:* 17, 467-482.

Görür, N., Tüysüz, O., Şengör, A.M.C. 1998. Tectonic evolution of the Central Anatolian Basins. *International Geology Review* 40, 831-850.

Innocenti, F., Mazzuoli, G., Pasquare, F., Radicati di Brozola, F., Villari, L. 1975. Neogene calk-alcaline volcanism of Central Anatolia: Geo-chronological data on Kayseri-Niğde area. *Geol. Mag*. 112, 349-360.

Işık, V. 2009. The ductile shear zone in granitoid of the Central Anatolian Crystalline Complex, Turkey: Implications for the origins of the Tuzgolu basin during the Late Cretaceous extensional deformation. *Journal of Asian Earth Sciences* 34, 507-521.

Kadıoğlu, Y. K. 1991. Geology, petrography and geochemistry of Ağaçören (Aksaray) magmatic rocks. Msc. *Thesis Middle East Technical University*. Ankara, 144 p.

Knuepfer, P. L. K. 1989. Implications of the characteristics of end-points of historical surface fault ruptures for the nature of fault segmentation. *U.S. Geol. Surv. Open File Rep*. 89–315, pp. 193–228.

Koçyiğit, A. 2000. Orta Anadolu'nun Genel Neotektonik Özellikleri ve Depremselliği. *Haymana-Tuzgölü-Ulukışla basenlerinin uygulamalı çalışması. Bildiri Özleri, TPJD Bülteni*, Özel sayı 5, 1-26, Aksaray.

Koçyiğit, A. 2003. General neotectonic characteristics and seismicity of central Anatolia. *Turkish Association of Petroleum Geologist Special Publication* 5, 1-26.

Koçyiğit, A. 2005. The Denizli graben-horst system and the eastern limit of western Anatolian continental extension: basin fill, structure, deformational mode, throw amount and episodic evolutionary history, SW Turkey. *Geodinamica Acta* 18 (3-4), 167-208.

Koçyiğit, A. Beyhan, A. 1998. A new intracontinental transcurrent structure: the Central Anatolian fault zone, Turkey. *Tectonophysics* 284, 317?336.

Koçyiğit, A., Erol, O. 2001. A tectonic escape structure: Erciyes pull-apart basin, Kayseri, Central Anatolia, Turkey. *Geodinamica Acta*, 14, 1-13.

Koçyiğit, A., Özacar, A. 2003. Extensional neotectonic regime through the NE edge of the Outer Isparta Angle, SW Turkey: New Field an Seismic Data. *Turkish Journal of Earth Sciences* 12, 67-90.

Kuşcu, İ., Erler, A., Göncüoğlu, M.C. 1993. Geology Of The Çamardı (Niğde) *Region. Geosound*, 23, 1-16.

Kürçer, A., 2012. Tuz Gölü Fay Zonu'nun Neotektonik Özellikleri ve Paleosismolojisi, Orta Anadolu,

Türkiye. Doktora Tezi, Tez no: 318203, Ankara Üniversitesi, Fen Bilimleri Enstitüsü, 318 sayfa, Ankara. (unpublished).

Kürçer, A., Gökten, Y.E. 2012. A New Photography Method for Paleoseismological Trenching: "Paleoseismological Three Dimensional Virtual Photography Method", A Case Study: Tuzgölü Fault Zone, Central Anatolia, Turkey, Tectonics - Recent Advances, Evgenii Sharkov (Ed.), ISBN: 978-953-51-0675-3, InTech, Available from: http://www.intechopen.com/books/tectonics-recent-advances/paleoseismological-three-dimensional-virtual-photography-method-a-case-study-ba-larkayas-2010-trench

Kürçer, A., Yeleser, L., Karzaoğlu, H., Izladı, E., Aykaç, S., Kutlu, S., Köse, K., Bostan, S., Kurdal, S. 2012. Tuz Gölü Fay Zonu'nun Neotektonik Dönem Özellikleri ve Paleosismolojisi, Orta Anadolu, Türkiye. *Maden Tetkik ve Arama Genel Müdürlüğü Report No*: 11573, Ankara, (unpublished).

Kürçer, A., Gökten, Y.E. 2014. Paleosismolojik Üç Boyutlu Sanal Fotoğraflama Yöntemi, Örnek Çalışma: Duru-2011 Hendeği, Tuz Gölü Fay Zonu, Orta Anadolu, Türkiye. *Türkiye Jeoloji Bülteni*, 57-1, s:45-71.

Le Pennec, J.-L., Temel, A., Froger, J.-L., Sen, S., Gourgaud, A., Bourdier, J.-L. 2005. Stratigraphy and age of the Cappadocia ignimbrites, Turkey : reconciling field constraints with paleontologic, radiochronologic, geochemical and paleomagnetic data. *Journal of Volcanology and Geothermal Research* 141, 45–64.s

Leventoğlu, H. 1994. Neotectonic characteristics of the central part of the Tuzgölü fault zone around Mezgit (Aksaray), *METÜ M.Sc. thesis*, 86 p.

Marshak, S., Mitra, G. 1988. Basic methods of Structural Geology. *Prentice Hall, New Jersey*, 446 p.

McCalpin, J.P., Nelson, A.R. 2009. Introduction to Paleoseismology. *In Paleoseismology, International Geophysics Series vol*. 95. James P. McCalpin (ed). Academic Pres is an imprint of Elsevier, pp. 1-25., California, USA.

MTA, 2002. 1/500 000 Ölçekli Türkiye Diri Fay Haritası Serisi, Kayseri ve Adana Paftaları.

Okay, A.İ., Kaşlılar-Özcan, A., İmren, C., Boztepe-Güney, A., Demirbağ, E., Kuşçu, İ. 2000. Active faults and evolving strike-slip basins in the Marmara Sea, NW Turkey: a multichannel seismic re£lectives study. *Tectonophysics* 321, 189-218.

Özmen, B. 2008, Ankara için deprem senaryosu, Ankara'nın Deprem Tehlikesi ve Riski çalıştayı Bildiriler kitabı. (Editörler: Prof. Dr. Süleyman Pampal, Bülent Özmen) *Gazi Üniversitesi Mimar Kemaleddin Salonu*, 19 Mart, s. 87-103, Ankara.

Özsayın, E. 2007. İnönü-Eskişehir fay sisteminin Yeniceoba - Cihanbeyli (Konya - Türkiye) arasındaki bölümünün Neojen-Kuvaterner yapısal evrimi, Doktora Tezi, Hacettepe Üniversitesi, Fen Bilimleri Enstitüsü Jeoloji Mühendisliği Anabilim Dalı, 120 s., Ankara, (unpublished).

Özsayın, E., Dirik, K. 2007. Quaternary activity of the Cihanbeyli and Yeniceoba Fault Zones: İnönü-Eskişehir Fault System, Central Anatolia. *Turkish Journal of Earth Sciences* 16, 471-492.

Papak, İ. 1985. Maden Tetkik ve Arama 1/25 000 ölçekli arşiv haritaları Aksaray L 32 a3 ve d2 paftaları Ankara, (unpublished).

Parlar, Ş., Görmüş, M., Eren, Y. 2006. Çamardı (Niğde) çevresinde Paleosen-Eosen yaşlı kayaların stratigrafisi, iri bentik foraminifer sayısal verileri ve biyofabriği, *İstanbul Üniversitesi, Mühendislik Fakültesi Yerbilimleri Dergisi* 19-1, 1-25.

Pasquare, G. 1968. Geology of the Cenozoic volcanic area of Central Anatolia. *Atti Accad. Naz. Lincei*, 9, 53-204.

Reilinger, R., McClusky, S., Vernant, P., Lawrence, S., Ergintav, S., Çakmak, R., Özener, H., Kadırov, F., Guliev, I., Stepanyan, R., Nadarıya, M., Hahubia, G., Mahmoud, S., Sakr, K., ArRajehı, A., Paradissis, D., Al-Aydrus, A., Prilepin, M., Guseva, T., Evren, E., Dmitrotsa, A., Filikov, S.V., Gomez, F., Al-Ghazzi, R., Karam, G. 2006. GPS constraints on continental deformation in the Africa-Arabia-Eurasia continental collision zone and implications for the dynamics of plate interactions. *Journal of Geophysical Research* 111, B05411.

Rigo de Righi, M., Cortesini, A. 1960. Regional studies of the Central Anatolian basins progress report. *PDR Turkish Gulf Oil Co. Report No*. II / 11-12 (unpublished).

Schmidt, C. C. 1960. AR/MEM/365-366-367 sahalarının nihai terk raporu, Pet. İş. Gn. Müd., Ankara, (unpublished).

Schumacher, R., Mues-Schumacher, U. 1996. The Kizilkaya ignimbrite—an unusual low-aspect-ratio ignimbrite from Cappadocia, Central Turkey. *Journal of Volcanology and Geothermal Research* 70, 107–121.

Seymen, İ. 1982. Kaman dolayında Kırşehir masifinin jeolojisi, *İTÜ Maden Fak. Doç. Tezi* s. 164, İstanbul, (unpublished).

Slemmons, D. B. 1982. Determination of design earthquakes magnitudes for microzonation. In *Proceedings of the 3rd International Earthquake Microzonation Conference, Seattle, WA*, vol. 1, pp. 110–130.

Soysal, H., Sipahioğlu, S., Kolçak, D., Altınok, Y. 1981. Türkiye ve çevresinin tarihsel deprem kataloğu. *TUBİTAK Report no*: TBAG 341. 86 s.

Şaroğlu, F., Boray, A., Emre, Ö. 1987. Türkiye'nin aktif fayları. *Maden Tetkik ve Arama Genel Müdürlüğü Report No*. 8643. 394 s., Ankara, (unpublished).

Şaroğlu, F., Emre, Ö., Kuşçu, İ. 1992. Türkiye Diri Fay Haritası, *Maden Tetkik ve Arama Genel Müdürlüğü*, Ankara.

Şengör A.M.C. 1980. Türkiye'nin Neotektoniği'nin Esasları, *Türkiye Jeoloji Kurumu Konferans Serisi* 2.

Şengör, A.M.C., Yılmaz, Y., Sungurlu, O. 1985. Tectonics of the Mediterranean Cimmerides: nature and evolution of the western termination of Palaeotethys. In: Robertson, A.H.F. and Dixon, J.E. (eds) The Geological Evolution of the Eastern Mediterranean, *Geological Society, London, Special Publications*, 17, 77-112.

Tan, O., Tpırdamaz, C., Yörük, A. 2008. The Earthquakes cataloques for Turkey. *Turkish Journal of Earth Sciences* 17, 405-418.

Tokel, S., Ercan, T., Akbaşlı, A., Yıldırım, T., Fişekçi, A., Selvi, Y., Ölmez, M., Can, B. 1988. Neogene Tholeitic province of central Anatolia: Implication for magma genesis and post-collision lithosferic Dynamics, METU *Journal of Pure and Applied Sciences. Series A "Geosciences"* I, 21, 1-3, 461-477.

Toprak, V. 2000. Tuzgölü Fay Kuşağı Hasandağ Kesiminin Özellikleri, Haymana-Tuzgölü-Ulukışla Basenleri Uygulamalı Çalışma 9-11 Ekim, 2000, *Türkiye Petrol Jeologları Derneği* Özel sayı: 5, 71-84.

Toprak, V., Göncüoğlu, C. 1993. Keçiboyduran-Melendiz fayı ve bölgesel anlamı (Orta Anadolu). *Yerbilimleri,* 16, 55-65.

Tunoğlu, C., Temel, A., Gençoğlu, H. 1995. Pliocene ostracoda association and environmental characteristics of Sivrihisar (Eskişehir)-Central Anatolia; 12nd. Inter. Ostracoda Symp., ostracoda and Biostratigraphy (Ed. Riha, J.) Belkama/Rotterdam, 265-275.

Türeli, T.K, Göncüoğlu, M.C. ve Akıman, O. 1993. Origin and petrology of Ekecikdag granitoid in western Central Anatolian Crystalline Complex. *Maden Tetkik ve Arama Genel Müdürlüğü Dergisi* 115, 15-28.

Türkecan, A., Akçay, A. E., Satır, M., Dönmez, M., Ercan, T. 2003. Melendiz dağları (Niğde) volkanizması, 56. Türkiye *Jeoloji Kurultayı Bildiri Özleri Kitabı* 16.

Uygun, A. 1981. Tuz Gölü havzasının jeolojisi, evaporit oluşumları ve hidrokarbon olanakları. *İç Anadolu'nun Jeolojisi Sempozyumu*. 66-71.

Uygun, A., Yaşar M., Erkan, M.C., Baş, H., Çelik, E., Aygün, M., Bilgiç, T., Kayakıran, S., Ayok, F. 1982. Tuzgölü Havzası projesi, Cilt 2. *Maden Tetkik ve Arama Genel Müdürlüğü Report No*: 6859, Ankara, (unpublished).

Uygun, A., Şen, E. 1978. Tuz Gölü Havzası ve Doğal Kaynakları I: Tuz Gölü Suyunun Jeokimyası. *Türkiye Jeoloji Kurumu Bülteni* 21, 113-130.

Varol, B. Kazancı, N., Gültekin, F., 2000. Tuzgölü ve yakın civarı Eosen-Oligosen jipslerinin sedimantolojik ve izotopik özellikleri. *Haymana-Tuzgölü-Ulukışla basenlerinin uygulamalı çalışması. Bildiri Özleri*, 19, Aksaray.

Yalınız, K. Göncüoğlu, M.C., Floyd, P.A. 1996. Supra-subduction zone ophiolites of Central Anatolia: Geochemical evidence from the Sarıkaraman ophiolite, Aksaray, Turkey. *Mineral Mag*. 60, 697-710.

Yalınız, K. Göncüoğlu, M.C. 1998. General geological characteristics and distribution of the Central Anatolian Ophiolites. *Yerbilimleri* 20, 19-30.

Yalınız, K. Göncüoğlu, M.C., Özkan-Altıner, S., Parlak, O., 2000. Formation and emplacement ages of the SSZ-type Neotethyan Ophiolites in Central Anatolia, Turkey: Paleotectonic implications. *Geological Journal*, 35, 53-68.

Yetiş, C. 1978, Çamardı (Niğde) Yakın ve Uzak Dolayının Jeoloji İncelemesi ve Ecemiş Yarılım Kuşağı'nın Maden Boğazı-Kamışlı Arasındaki Özellikleri, *Doktora Tezi: İstanbul Üniversitesi*, 164 s. (unpublished).

Yıldırım, C. 2014. Relative tectonic activity assessment of the Tuz Gölü Fault Zone; Central Anatolia, Turkey. *Tectonophysics*, http://dx.doi.org/10.1016/j.tecto.2014.05.023

Yolsal, Ç., Taymaz, T. 2012. Earthquake source parameters along the Hellenic subduction zone and numerical simulations of historical tsunamis in the Eastern Mediterranean. *Tectonophysics*, 536-537, 61-100.

Wells, D.L., Coppersmith, K.J. 1994. New Empirical Relationships among Magnitude, Rupture Length, Rupture Width, Rupture Area, and Surface Displacement. *Bulletin of the Seismological Society of America*, 84-4, 974-1002.

Woodside, J.M., Mascle, J., Zitter, T.A.C., Limonov, A.F., Ergün, M., Volkonskaia, A. 2002. Shipboard Scientists of the PRISMED II Expedition, The Florence Rise, the western bend of the Cyprus arc. *Marine Geology*, 185, 177-194.

Zitter, T.A.C., Huguen, C., Woodside, J.M. 2005, Geology of mud volcanoes in the eastern Mediterranean from combined sidescan sonar and submersible surveys. *Deep-Sea Research* I 52, 457–475.

BULLETIN OF THE MINERAL RESEARCH AND EXPLORATION

Foreign Edition 2014 149

CONTENTS

Facies Characteristics And Control Mechanisms of Quaternary Deposits In The Lake Tuz Basin
.....Alper GÜRBÜZ and Nizamettin KAZANCI 1

Neotectonic-Period Characteristics, Seismicity, Geometry And Segmentation of The Tuz Gölü Fault Zone
.....Akın KÜRÇER and Y. Ergun GÖKTEN 19

Neogene Stratigraphy And Paleogeographic Evolution of The Karaburun Area, İzmir, Western Turkey
.....Fikret GÖKTAŞ 69

Benthic Foraminiferal Fauna of Malatya Oligo-Miocene Basin (Eastern Taurids, Eastern Turkey)
.....Fatma GEDİK 93

Protolith Nature And Tectonomagmatic Features of Amphibolites From The Qushchi Area, West Azerbaijan, NW Iran
.....Mohssen MOAZZEN 139

Glauberite-Halite Association In Bozkır Formation (Pliocene Çankırı-Çorum Basin, Central Anatolia, Turkey)
.....İlhan SÖNMEZ 153

Estimation of Swelling Pressure Using Simple Soil Indices
.....Kamil KAYABALI and Özgür YALDIZ 177

Two Examples For Imaging Buried Geological Boundaries: Sinkhole Structure And Seyit Hacı Fault, Karapınar, Konya
.....Ertan TOKER, Yahya ÇİFTÇİ, Aytekin AYVA and Akın KÜRÇER 189

The Assessment of Geothermal Potential of Turkey By Means Of Heat Flow Estimation
.....Uğur AKIN, Emin Uğur ULUGERGERLİ and Semih KUTLU 201

A Brief Note On Mineral Evolution And Biochemistry
.....José Mario AMİGO 211

Critisism on the paper "Possible Incision of The Large Valleys In Southern Marmara Region, Turkey (Nizamettin KAZANCI, Ömer EMRE, Korhan ERTURAÇ, Suzanne A.G. LEROY, Salim ÖNCEL, Özden İLERİ and Özlem TOPRAK)
.....Nizamettin KAZANCI 219

Acknowledgement 221

Notes to the authors 223

Bull. Min. Res. Exp. (2014) 149: 69-92

Bulletin of the
Mineral Research and Exploration

http://bulletin.mta.gov.tr

NEOGENE STRATIGRAPHY AND PALEOGEOGRAPHIC EVOLUTION OF THE KARABURUN AREA, İZMİR, WESTERN TURKEY

Fikret GÖKTAŞ[a*]

[a] *Maden Tetkik ve Arama Genel Müdürlüğü, Ege Bölge Müdürlüğü, İZMİR*

Keywords:
Karaburun Peninsula,
Neogene stratigraphy,
Neogene volcanism,
paleogeography,
K/Ar geochronology.

ABSTRACT

The western margin of the Foça Depression (FD) is located in the NE of the Karaburun Peninsula. Terrestrial Neogene sediments in the study area which partly representing the western margin of the FD and the mafic volcanics have NW-SE directions towards İzmir bay and are separated from the basement rocks by synthetic normal faults. During the Miocene deposition the basin's boundaries became structurally narrower and two main sedimentary successions have been defined namely the Karaburun group and the Eşendere group which have been separated with angular unconformity in regional scale. The Karaburun group is represented with dominantly lacustrine deposition in Early-Middle Miocene period that includes Haseki and Hisarcık formations and Karaburun volcanics. The Lower Miocene Haseki formation is represented by the Salman member developed in the alluvial fan environment and lacustrine deposits of algal-biostromal Yeniliman limestone and micritic limestone dominated Aktepe member. NW trending basin margin faults which formed a boundary between Karaburun high and the FD and caused the effective second stages of mafic volcanism did not interrupt the lacustrine deposition at the beggining of the Early Miocene. But it caused relative deepening of the basin, changed depositional conditions and lacustrine sedimentation continued with the Hisarcık formation. The activity shaping the FD from the western part and partly coinciding with the Early Miocene basin margin faults has been documented with the unconformity showing no time gap between Haseki and Hisarcık formations. Hacıhüseyintepe member has unconformity with the lavas that represent the second stage of Karaburun volcanics and laterally passes into the Karabağları member. The Karabağları member consists of green coloured lacustrine shoreface sediments which lie on the Aktepe succession with sublacustrine paraconformity. Değirmentepe limestone transitionally lies on the top and it is the last member of the Karaburun group. Eşendere group lies on the Hisarcık formation with regional scale angular uncoformity and presents the Late Miocene-early Early Pliocene(?) sedimentation grading from alluvial fan deposits of the Saip formation to lacustrine Çukurcak limestone. Calc-alkaline Karaburun volcanism which is represented with potassium rich andesitic products has three stages that laterally connected with the Early Miocene-early Middle Miocene deposition The first two stages have dual facies namely, pyroclastics at the base and lavas on the top. The first stage products are laterally discontinuous reference level that is separating Yeniliman limestone and Aktepe member. Second stage products are in/on the Aktepe member. The third stage lava flows are dated as K/Ar 16.0±1.3 Ma age which is thought to be located at the bottom of the Değirmentepe limestone that is the last member of the Karaburun group.

* *Corresponding author: F. GÖKTAŞ, fikretgoktas50@gmail.com*

1. Introduction

The purpose of this study was to prepare 1/25000 scale geological map and study the stratigraphic and paleogeographic evolution of the terrestrial Neogene sediments and volcanics along the NE margin of the Karaburun Peninsula (Figure 1). In the study area there has not been any previous work dealing with the same topic but there have been numbers of previous work. Some important of these previous geological work as it has been listed in Çakmakoğlu and Bilgin (2006) are mainly related to the Pre-Neogene rock units. Previous work for Neogene units are, for magmatism (Innocenti and Mazzuoli, 1972;

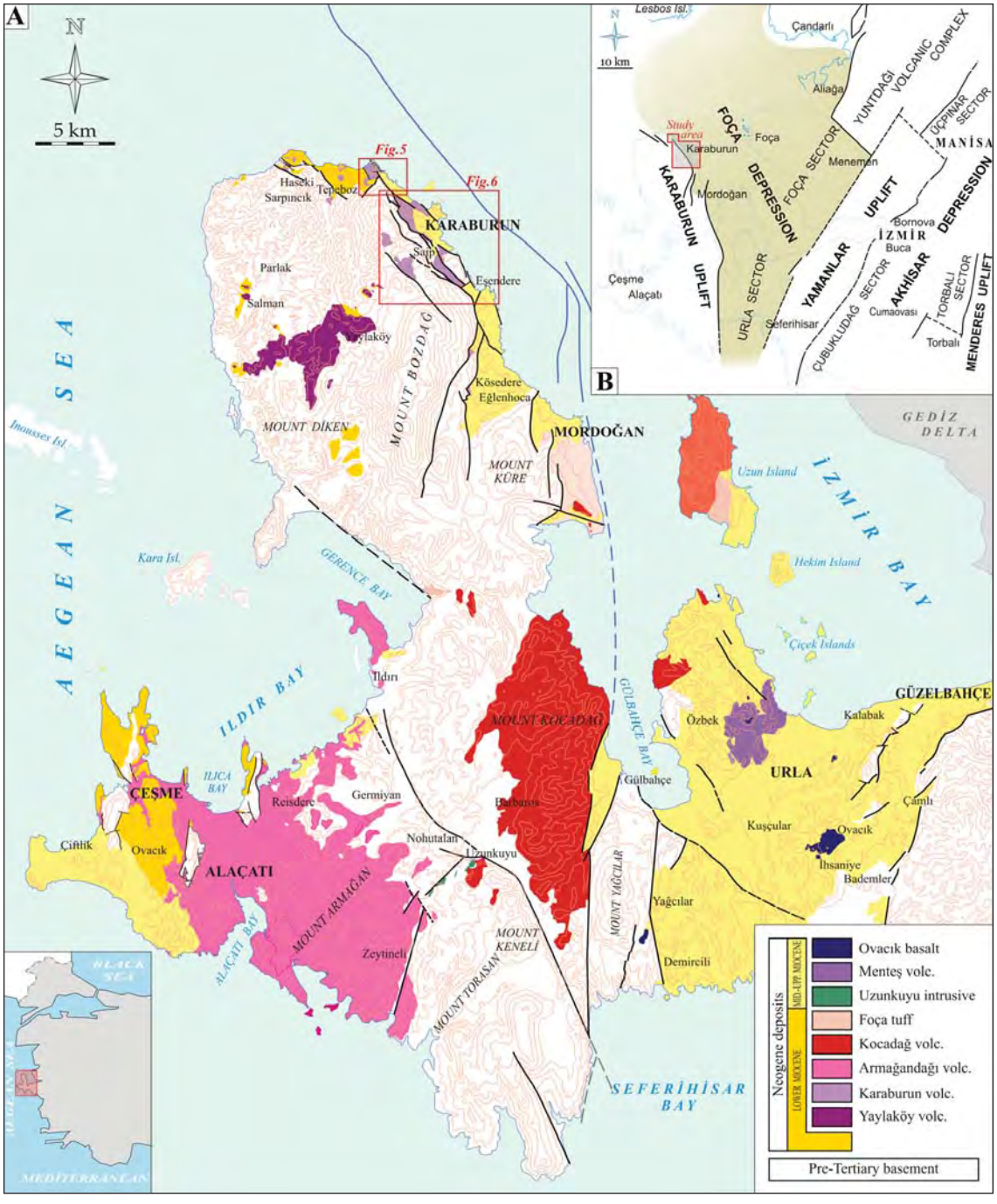

Figure 1- The location of study area (A) and its position in the Foça depression (B; modified from Kaya, 1979). The submarine faults at the east of Karaburun Peninsula are taken from Aksu et al. (1987).

Borsi et al., 1972; Türkecan et al., 1998; Helvacı et al., 2009; Agostini et al., 2010), for tectono-stratigraphy (Kaya, 1978; 1979; 1981) and for Cenozoic structural evolution of the region (Uzel et al., 2013) (Figure 2). Aras et al. (1999) and Çakmakoğlu et al. (2013) studied economic potential of the Early Miocene clays in the northern part of the peninsula around Salman village. They studied and mapped preliminary products of Early Miocene sedimentations, Yaylaköy volcanics and their lithostratigraphical connections. Türkecan et al. (1998) and Helvacı et al. (2009) proposed a generalized stratigraphic column. In this succession it was indicated that Neogene sedimentations and the volcanics in the Karaburun Peninsula show lateral connected developments from base to the top. In these studies, lithostratigraphy was not studied in detail and sedimentary rock units and their lateral-vertical relations with the multi stage volcanics were also not studied enough, the relative stratigraphic connections have been re-constructed with the radiometric age data.

2. General Geology

Terrestrial Tertiary sedimentation and volcanism in the Karaburun Peninsula are represented with Neogene rock units. It is considered that the area has been subjected to deformations and erosions during the time interval between tectonic emplacement of the İzmir flysch (Öngür, 1972; Eşder, 1988; Çakmakoğlu ve Bilgin, 2006) and the development of the Early Miocene basin. In the study area Çakmakoğlu and Bilgin (2006) defined the Carboniferous-Silurian Dikendağı formation, Ladinian Camiboğazı formation, Rhaetian-Carnian, Güvercinlik Formation and Late Cretaceous-Early Tertiary İzmir flysch basement rocks (Figure 3). They all have angular unconformity contact relations with the Miocene sediments. In general the faults which developed or became active after sedimentation have marked the present day lithological boundaries. In the NE part of the peninsula Miocene sediments and volcanics have extended in a step faulting zone with NW-SE, 50º-80º NE trend. Ersoy et al. (2006) and

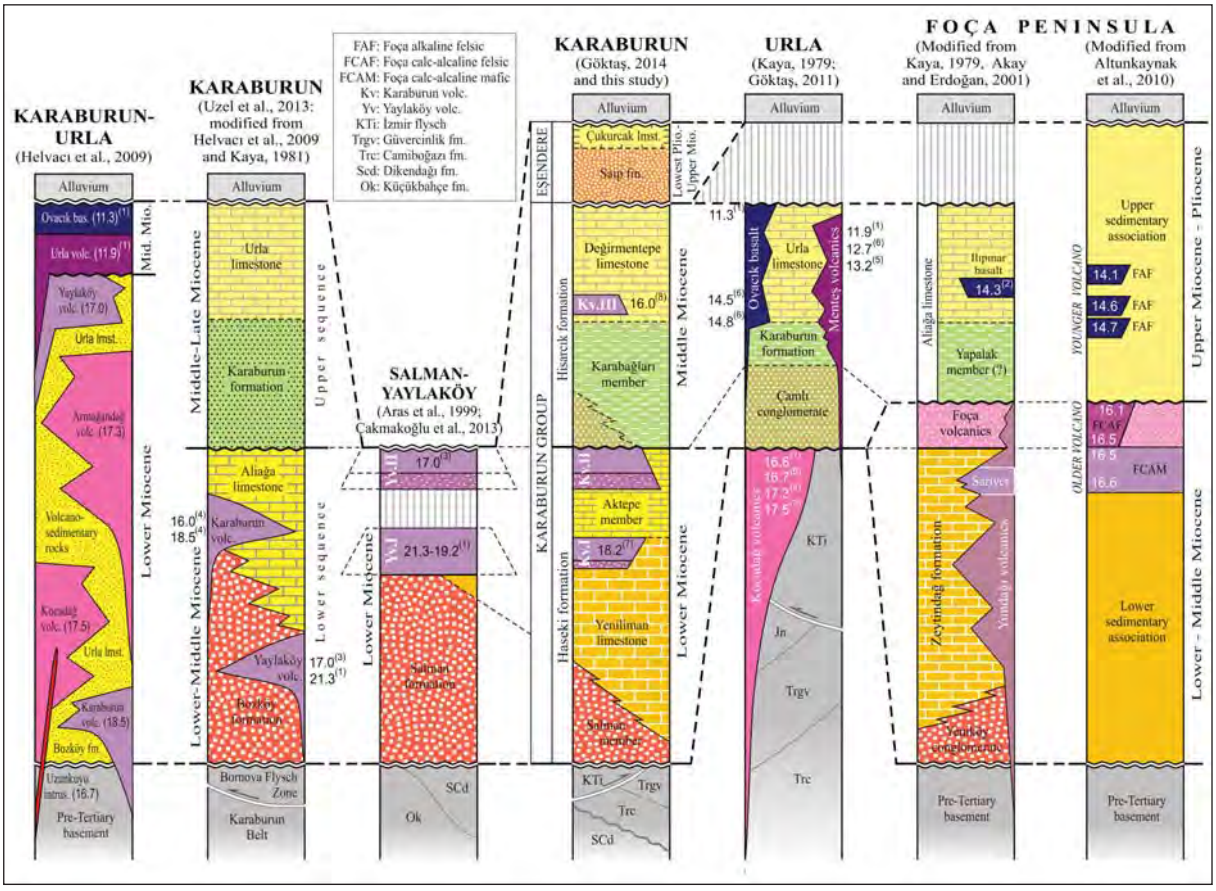

Figure 2- Correlation of generalized Neogene stratigraphies proposed for Foça Depression and Karaburun Uplift. (1)Borsi et al. (1972), (2)Ercan et al. (1997), (3)Helvacı et al. (2009), (4)Türkecan et al. (1998), (5)Karacık et al. (2013), (6)Göktaş (2011), (7)Göktaş (2014), (8)This study.

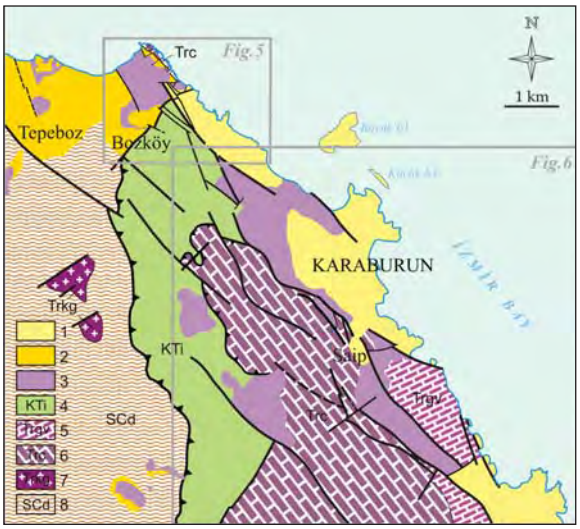

Figure 3- Geological map of the pre-Tertiary rock units in the study area (modified after Çakmakoğlu and Bilgin, 2006). 1) Middle-Upper Miocene deposits, 2) Lower Miocene deposits, 3) Karaburun volcanics, 4) İzmir flysch, 5) Güvercinlik fm., 6) Camiboğazı fm., 7) Karaburun granodiorite, 8) Dikendağı fm.

Uzel et al. (2013) defined this zone as 'Karaburun fault zone'. They are normal faults with oblique displacements and have over 75° dip angles (Mean rake is 60° W).

The calk-alkaline ~16-18 Ma volcanism in the Karaburun Peninsula is represented with "Karaburun" (olivine bearing andesites and shoshonites), "Yaylaköy", "Armağandağı", "Kocadağ" (high potassium bearing andesites, dacites and latites) volcanics.

3. Neogene Stratigraphy

In the study area wide spread Early-Middle Miocene lacustrine deposits and laterally associated mafic volcanics have been defined as the Karaburun group. Eşendere group from base to top consists of alluvial fan and lacustrine deposits and overlies the Karaburun group with angular unconformity. Eşendere group represents Late Miocene-early Early Pliocene(?) sedimentations (Figure 4).

3.1. Karaburun Group

Karaburun group is the chronostratigraphic equivalent of the Çeşme group (Göktaş 2010) in Çeşme Peninsula. Karaburun group consist of Haseki and Hisarcık formations and Karaburun volcanics (KV). The Lower Miocene Haseki formation and Middle Miocene Hisarcık formation have been separated by an uncoformity which has not caused sedimentation interruption. As they deposited in the same basin in a superimposed manner so they were included into the Karaburun group. As Haseki formation have been explained in detail in the Göktaş (2014), here details of the Hisarcık formation and Eşendere group will be given.

3.1.1. Haseki Formation

Haseki formation starts with alluvial fan/delta deposits *(Salman member)* and predominantly consists of lacustrine deposits of Yeniliman limestone and Aktepe member (Göktaş 2014). First two stages of the Karburun volcanisms (KV1 and KV2) are within the lacustrine sediments. KV1 lavas separating Yeniliman limestone and Aktepe member is considered to be a reference level. KV2 products are placed on to the top of the Aktepe successions. In the Karaburun Peninsula that during the sedimentation of the Salman member and Yeniliman limestones and it's equivalents, Neogene volcanisms had not yet started. Although related geochronological (Borsi et al., 1972; Helvacı et al., 2009; Göktaş 2014) and biochronological (Saraç, 2003) data strongly indicates late Early Miocene, but it has been accepted that in a general sense sedimentation of the Haseki Formation developed in Early Miocene (Figure 4).

Salman member: Salman member is the base of the terrestrial Neogene sedimentations, representing Early Miocene basin margin sedimentations. In the study area overlying Yeniliman limestone from bottom to the top has laterally interfingering of red-claret coloured alluvial fan depositions. It is reported that it was marked as fan delta sedimentation around Salman village (Çakmakoğlu et al., 2013). The succession sedimented on to the basement rocks with an angular unconformity and consists mainly of gravelstone, sandstone and with limited amounts of mudstone. Around Bozköy in the main part most of the proximal sediments have been eroded. So in the study area the unit is mainly represented with braided stream deposits, characterizing medial parts of the alluvial fans (Figure 5).

Yeniliman Limestone: Yeniliman limestone consists of algal-biostromal limestones deposited nearshore the Early Miocene lake. Biogenic limestones shaped by locally groving stratiform stromatolites and generally have 100-30 cm thick beddings, locally 30-

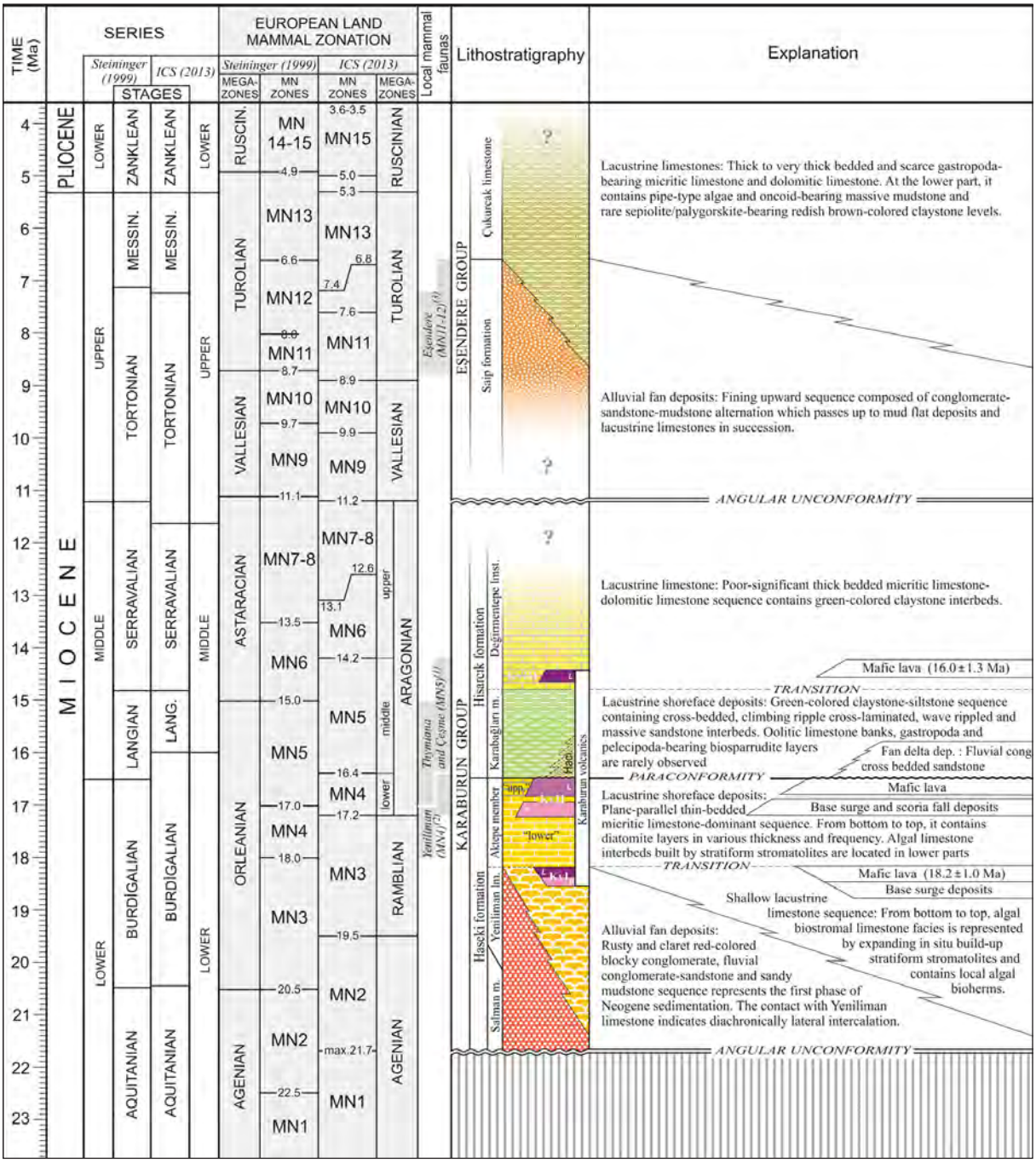

Figure 4- Generalized stratigraphic section of the study area. (1)Besenecker (1973), (2)Saraç (2003), (3)Kaya et al. (2005). Kv: Karaburun volcanics. L: Lava, P: Pyroclastic.

10 cm or very thick (>100 cm) algal laminated and plane-parallel beddings. Outcrops are mainly in the northern part of Bozköy (Figure 5). The subunit could be correlated with the Şifne formation, defined by Göktaş (2010) in the Çeşme Peninsula.

Aktepe Member: Aktepe member reflects continuation of lacustrine sedimentation outside the KV1 products spread area. It has been marked by micritic limestones with parallel thin-medium thick beddings. Main outcrops are near the NE of Bozköy. With the emplacement of the KV1 products, the basin gradually became deeper and Aktepe succession with diatomite interbeds has been deposited (Göktaş 2014). KV2 and Aktepe sedimentations are coeval and KV2 products relatively divide the Aktepe

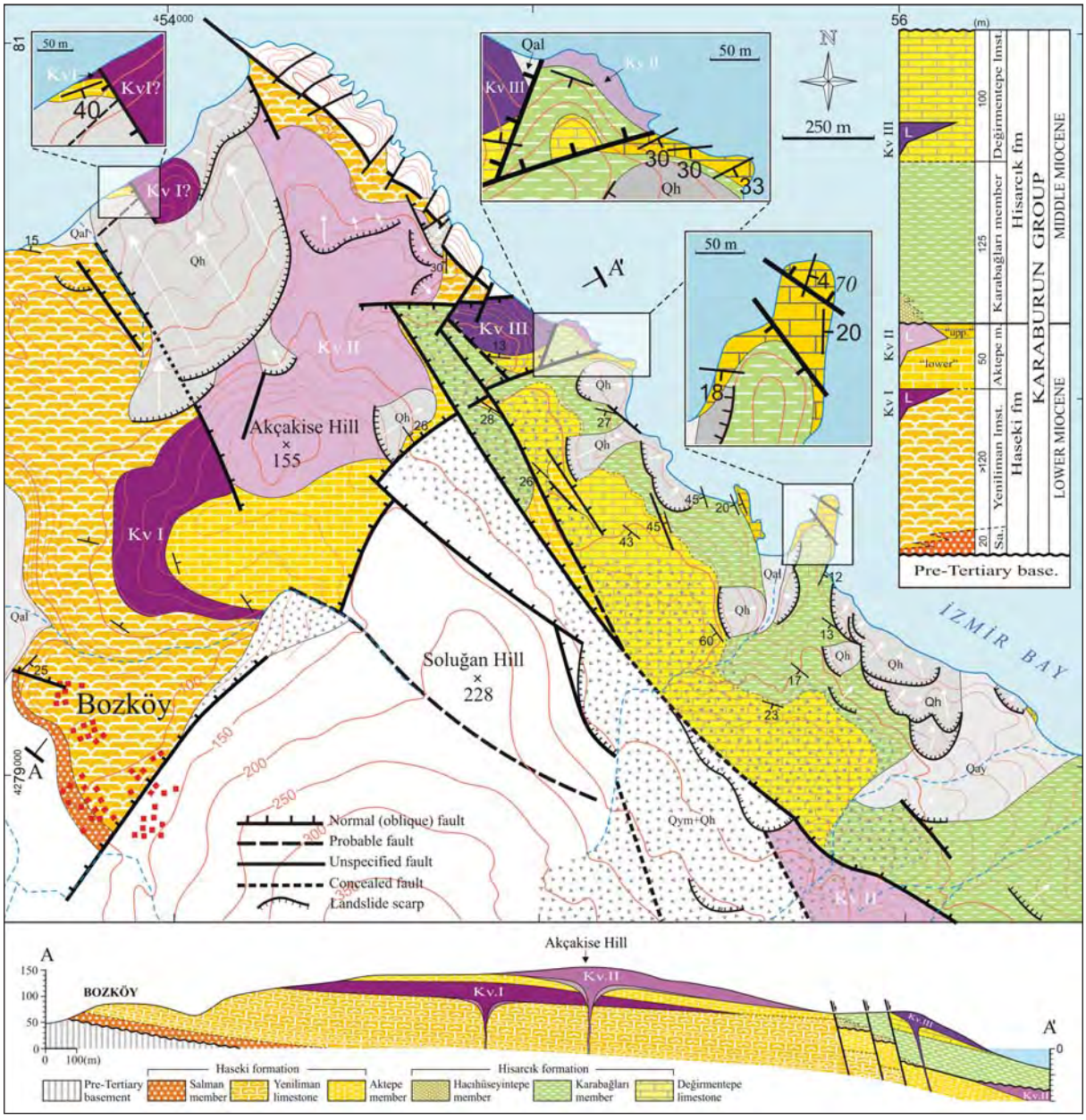

Figure 5- Geological map of Bozköy area. Qal: Alluvium, Qay: Alluvial fan deposits, Qh: Landslide debris, Qym: Scree deposits, Ky: Karaburun volcanics, L: Lava.

succession into 'lower' and 'upper' parts (Figure 4). The subunit, lithostratigraphically equivalent of the Ovacık formation (Göktaş, 2010) defined in the Çeşme Peninsula. Saraç (2003) defined some small mammal fossils belong to the MN4 biozone in the fine grained parts in the unit cropping out in the north of Tepeboz village (Göktaş, 2014). According to ICS 2013, MN4 biozone corresponding Aragonian is limited by 16.4 Ma-17.2 Ma (Figure 4).

3.1.2. Hisarcık Formation

In a general sense the succession reflects Middle Miocene lacustrine sedimentations and starts with basin margin type pebblestone-sandstone assemblage of the Hacıhüseyintepe member. With lateral-vertical transitions on the top it has lacustrine shoreface succession mainly consisting of green claystone-siltstone assemblage with sandstone interbeds which have been defined as the Karabağları member. The

sedimentary succession ends with the Değirmentepe limestone reflecting the final stage of lacustrine deposition. The Hisarcık formation name was first used by Göktaş (2014). Hisarcık is a quarter about 2 km NW of the Karaburun town centre (Figure 6). The sediments crop out in the area between Eşendere and to the NE of Bozköy (Figures 5, 6).

Lacustrine sediments of the Hisarcık formation are the equivalent of the Çiftlik formation in the Çeşme Peninsula (Göktaş 2010). The lower part of the Çiftlik formation has fine grained shoreface sediments of the Azmakdere member. In the Chios Island the equivalent of the Azmakdere member is the 'Keramaria unit' defined by Besenecker (1973). In the Keramaria unit defined 'Thymiana mammal fauna' have been indicating MN5 biozone. According to Bonis et al. (1998) and Koufos (2006) it gives 15.5 Ma age for the Thymiana fauna (Figure 4). From the points of stratigraphic position and lithological similarity the Karabağları member is considered to be the equivalent of the Keramaria and Azmakdere successions which have Early Middle Miocene mammal fossils. There has not been any data available indicating upper time limit of the sedimentation in the Middle Miocene.

Haseki formation and KV2 in the Karaburun Peninsula, Foça tuffs in Foça Peninsula and in Uzun Island, Kocadağ volcanics, Güvercinlik formation and İzmir flysch in the Urla depression, overlaid by Hisarcık formation and the equivalents (present the Middle Miocene sedimentation around FD) with unconformity (Göktaş, 2010, 2011, 2014 and the references therein). The contact with the overlying Eşendere sediments is marked with the Late Miocene angular unconformity.

In the Foça Peninsula the 'Aliağa limestone' (Kaya, 1979, 1981; Dönmez et al., 1998) and it's equivalent 'the Çamdağ limestone' (Eşder et al 1991) may be correlated with the lacustrine deposits of the Hisarcık formation. 'Çamlı conglomerate + Karaburun unit + Urla limestone' (Kaya, 1979, 1981), 'Çamlı formation + Bozavlu formation + Urla limestone' (Sümer 2007) which described in the Urla depression are total equivalents of the Hisarcık Formation.

Hacıhüseyintepe Member: The subunit consists of basin margin gravelstone-sandstones assemblage. The name has being used first time in this study. Hacıhüseyintepe is a hill to the NW part of the Karaburun town centre (Figure 6).

Mapable outcrops are in the western part of the town centre. Visible thickness is about 75 m.

The faults have limited the spread of the Hisarcık formation and have caused post-sedimentary vertical displacements so proximal sediments on the footwall blocks have been totally eroded and sediments on the hangingwall blocks have been covered by younger sediments. Thereof, in the study area subunits have limited outcrops. The outcrops of the member in the west of Hacıhüseyin Hill have laterally limited spread on the hangingwall block of the N10°W trending reactivated(?) boundary fault zone. Around the NE of the Hisarcık quarter the alluvial fan and possible beach sediments cropping out under the scree debris have not been mapped.

At the type locality they have assemblage of fluvial pebblestone-pebbly sandstones consist of well rounded pebbles and coarse sands. They display cross bedded or massive channel fills have greenish gray colours and are weakly compacted. The coarse grained sandstones are cropping out in the NE of the Hisarcık quarter are light gray coloured, grain supported, well sorted and weakly compacted. The sandstones have very low-angle large-scale cross beds also consist of granule series which are suitable for cross-bedding.

Alluvial deposits in front of the baundary faults are overlying KV2 with unconformity. The observed structural contact between the KV2 which is on the footwall block and the rock units of the Hisarcık formation are on the hangingwall block of the fault which is considered to be primarily limiting the basin which has developed as a result of vertical displacements following Middle Miocene deposition (Figure 5, 6). The relationship with the overlying Karabağları member is laterally interfingering and has vertical transitions.

In the generalized stratigraphy fluvial succession at the base of the Hisarcık formation makes one think of alluvial fan/delta(?) deposition at the basin margin limited by the boundary fault. Overlying shoreface succession (Karabağları member) has lateral interfingerings with the medial fan fluvial sediments, with their colours indicating paleoreduction conditions may support underwater deposition. Cross beddings with very low-angles and with advanced textural maturity may indicate beach depositions.

The Karabağları member along the northern shore of the Karaburun Peninsula described by Göktaş

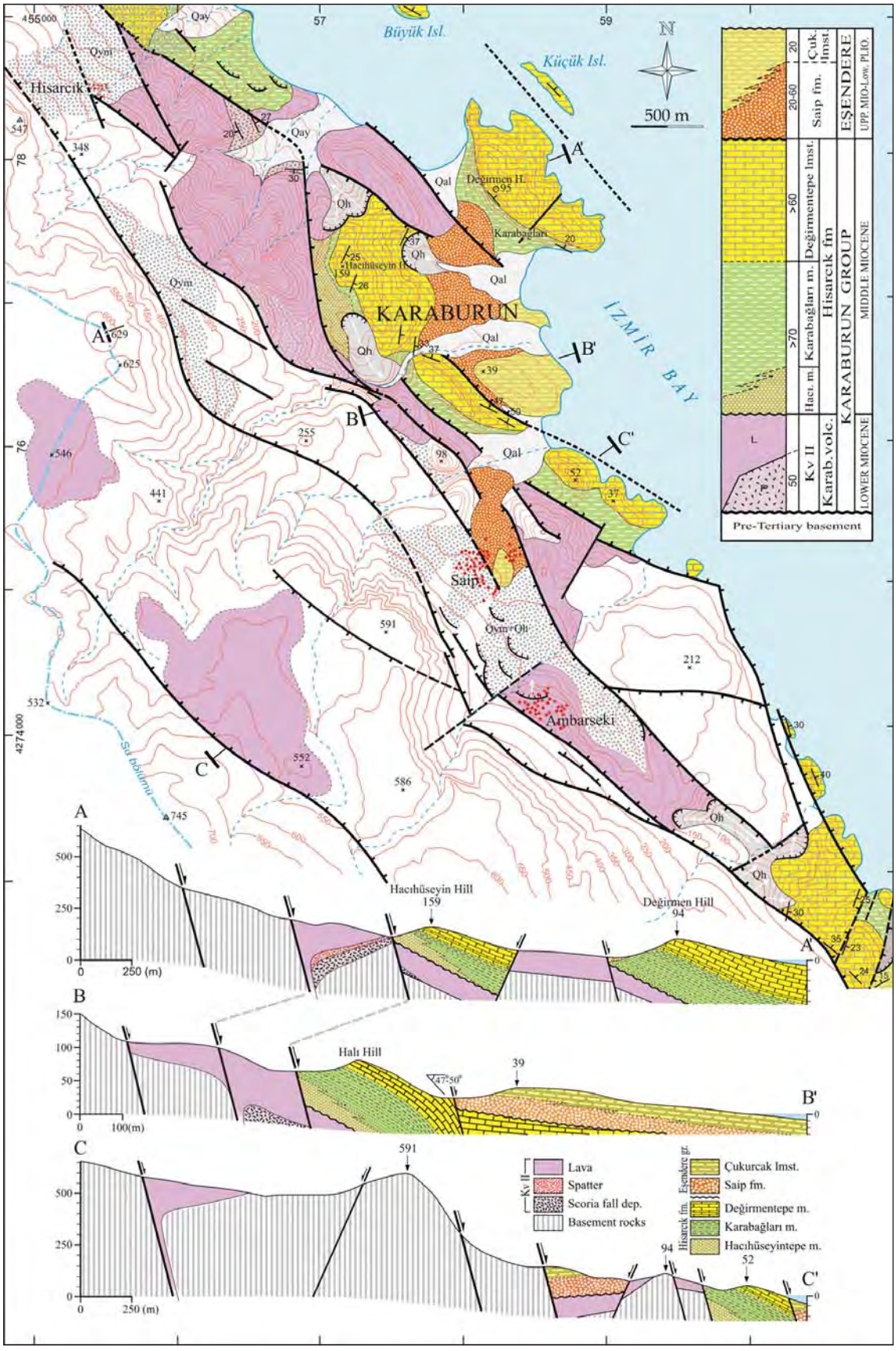

Figure 6- Geological map of the area between Hisarcık village and Eşendere.

(2014) contain of fan delta deposits may be correlated with the Hacıhüseyintepe member. The equivalent of subunit in the Urla depression may be the 'Çamlı conglomerate' (Kaya, 1979; 1981) and 'Çamlı formation' (Sümer, 2007; Göktaş, 2011) reflecting alluvial fan depositions. Equivalent sediments have not been reported in the Foça peninsula (Kaya, 1978, 1979, 1981; Eşder et al., 1991; Dönmez et al., 1998; Genç and Yılmaz, 2000; Altunkaynak and Yılmaz, 2000).

Karabağları Member: The subunit mainly with green coloured succession with plane-parallel claystone-siltstone beds described as the 'Karaburun formation' for the first time by Kaya (1979). In Göktaş (2014) and in this study as the Karaburun name has been used as at the group level so the subunit needed to be renamed. The new member name 'Karabağları' is a location about 1 km to the NE of Karaburun town centre and was first used by Göktaş (2014).

Type locality of the Karabağları member is in the NE of Bozköy along the shore clif. Visible thickness of the succession varies from 80 m to 175 m.

The succession of the Karabağları member consist of carbonaceous claystone, siltstone and sandstone lithofacieses. Claystone-siltstone assemblages are the main rock type present. They are green coloured with thin-medium thick plane-parallel beddings. Thickness and the amounts of the sandstone interbeds show an increase at the lower levels of the succession. Sandstones are some decimetres thick, mostly coarse grained, grain supported, well shorted and in general well compacted. It is observed disorganized sandstone with some level of climbing ripple cross laminated (Figure 7A) and upper flow regime lineaments bearing sandstone beds. Rarely observed sandstones with hummocky and swaley cross beddings reflecting storm sedimentation conditions (Figures 7B,C). Wave ripple cross laminated sandstone interbeds are quite common (Figure 7D). Wave ripples have caused laterally connected lenticular beddings or isolated wave ripples of 1.5-3.0 cm ripple heights (Figures 7E, F). Within the green coloured massive claystones in some places there are euhedral compozite nodules like calcified colemanite(?) pseudomorphs, possible borate concentration (Figures 7G, H). Within the same zones there are some networks of calcified voids representing the remains of the dissolved-removed evaporates.

Within the two different levels of the succession there are some oolitic limestone beds made of autochthonous ooids (Flügel 2010). At the lower oosparit bed is 40 cm thick. Its beige coloured, rather strong, generally grain supported with spar calcite cement and according to the compositional definition of carbonate rocks of Folk (1962) represents 'well shorted oosparit' microfacies. Ooids in generally ovoidal with 0.10-0.20 mm size, are single laminated belong to 'superficial ooid' class (Flügel 2010). Same size uncoated grains and 0.30-0.80 mm size subangular extraclasts with cryptalgal micrite coatings can rarely be found. Laminas coatings the nucleus, tangential-concentric microfabrics represent more agitated hydrodynamic conditions (Flügel, 2010). Ooid nucleuses are made of quartz, plagioclase, mica, epidote, chert and calcite extraclasts (Figure 8A). About 80 cm thick oolitic limestone bed (ooidal grainstone) located at the upper part of the succession has been consist of spherical and multi laminated 'normal ooids' (Flügel 2010). Normal graded thickly coated ooids with 0.1 mm-2.5 mm dimensions have been divided into several decimetre thick zones with mm size undulated stromatolitic crusts (Figure 8 B). Ooids are grain supported and have been cemented by spar calcite and the primary pores have been in most cases kept open (Figure 8 C). Extraclasts seen in the spar calcite cement are mostly quartz, feldspat, biotite, muscovite, epidote, chert and calcite fragments. Among the primary voids in the medium-well sized ooids, extra clast fragments of carbonates from the basement units can be seen as rare disseminations. Their angular-subangular shapes and centimetric sizes reflect textural reversing (Figure 8B). Some of the extraclasts have been coated in thin stromatolitic crusts. In places bioclasts have been represented by ostracode piles (Figure 8D). At the bottom of the oolitic limestone there is a 20 cm thick bed with densely bioturbation features. Below this, there is a 120 cm thick clayey limestone bed. It has medium-thick layers with plant icnofossils which are marked by empty plant tubes.

KV2 lavas have been transgresively overlain by the succession. At the bottom of this succession there is a 1 m thick calsirudite layer. According to textural classifications of Dunham (1962); gray or faded pink coloured limestone is 'rudestone', according to Folk (1962) classification it belongs to 'gastropod-bivalve bearing biosparite' facieses (Figure 8E). Texture wise, it is grain supported and has spar calcite cement. Allochems larger than 2 mm include gastropods, bivalvias and bioclasts. Coarse-very coarse (between 1-2 mm) sand sizes extraclasts and intraclasts are not widespread. Dominant macro fossil

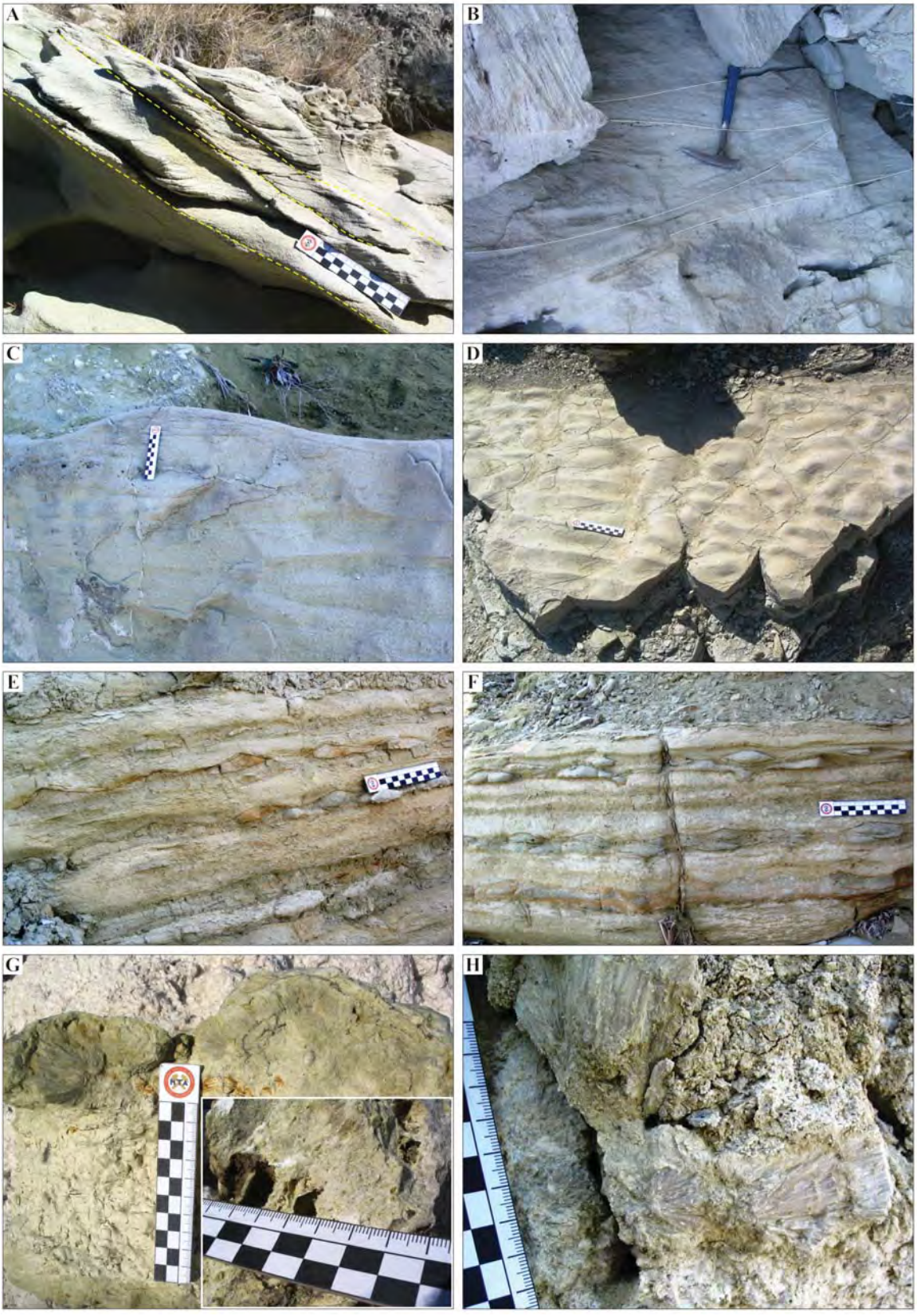

Figure 7- Specific sedimentary structures observed in the Karabağları sedimentary sequence. A) Climbing-rippled sandstone, B,C) Sandstone with HCS and SCS(?), D) Wave rippled sandstone, E,F) Lenticular-bedded wave-rippled sandstone, G,H) Probably boron salt (collemanite?) pseudomorphs.

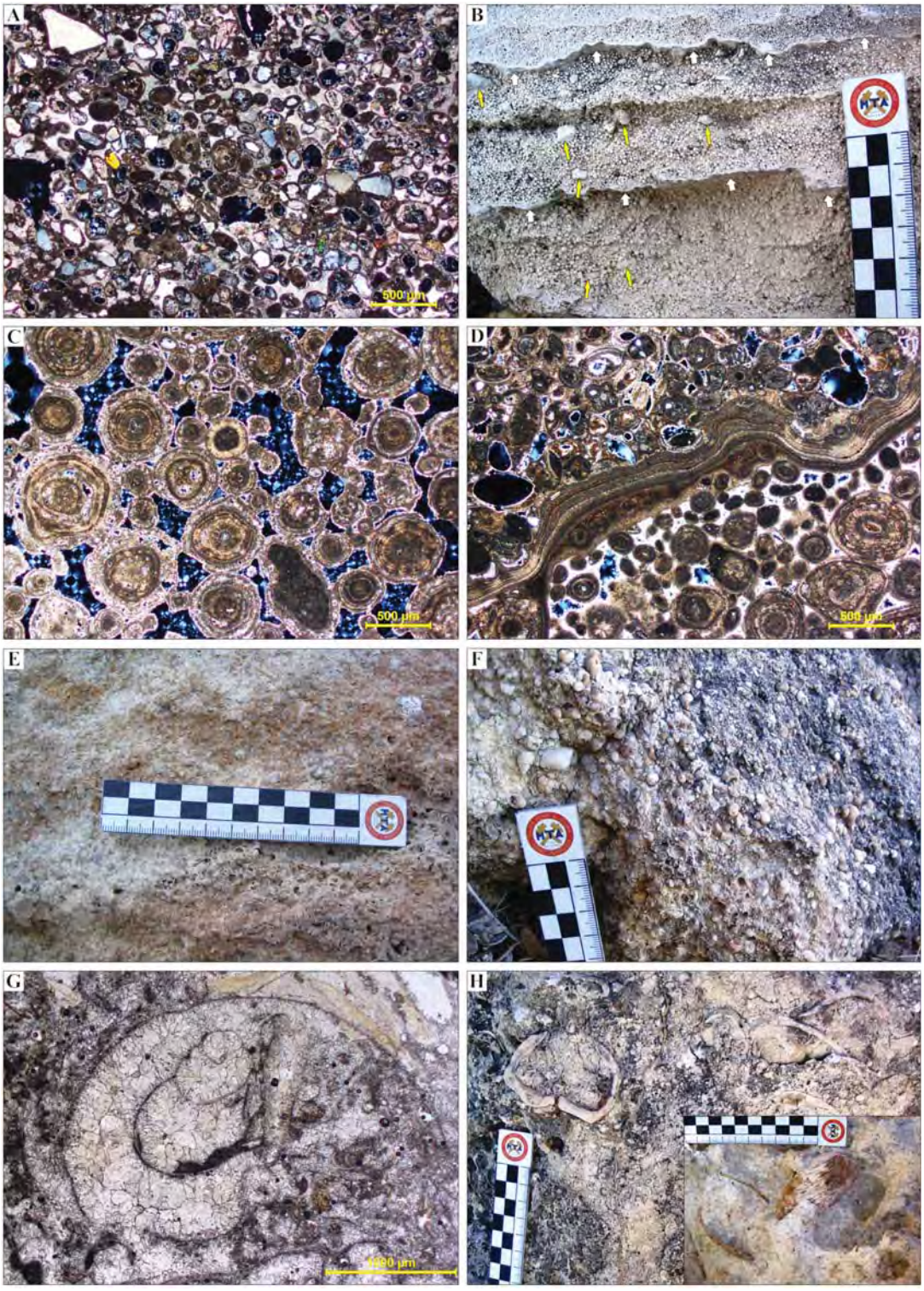

Figure 8- The specific textures of carbonate rocks in the Karabağları sedimentary succession. A) Microphotograph of relatively well-sorted superficial ooids (2,5 x); B) Macroscopic view of a normally graded oolitic limestone level. White arrows show stomatolitic crusts while the yellow ones point the extraclasts belonging to basement rocks; C) Microphotograph of oosparite (ooidal grainstone) facies (2,5x); D) Ooid-ostracoda clustering in the upper part of same facies, seperated by an stromatolitic crust; E) Macroscopic view of gastopoda-bivalvia bearing biosparrudite (rudstone) facies; F, G) A macroscopic view and a microphotograph of a part of the same facies with abundant gastropoda (2,5x); H) Another macroscopic view of gastropoda-bivalvia bearing biosparrudite facies.

contents are uniform gastropods (Figure 8F). Gastropods are in mm size and have thin white shells (Figure 8 G). On the other hand bivalvia shells are not as common as gastropods but they have thick shells and have been well preserved. They may be up to 10 cm in size (Figure 8H).

KV2 has been transgresively overlaid by the Karabağları member. Outside the KV2 lavas emplacement areas underlying Aktepe member has sharp concordant contact. This indicates sublacustrine paraconfomity, indicating continuity of lacustrine sedimentations. The contact with the overlying Değirmentepe limestone is concordant and in a limited area it is consecutively transitional.

Sedimentary facieses defined in the sedimentary successions indicate lacustrine shoreface sedimentations developed on the storm wave base. At the bottom of the successions there are sandstones with the features indicating sedimentations developed under high energy conditions and in the upper levels the amount of suspension sediments present increases, indicating that from lower levels towards the top sedimentation energy has decreased. Aktepe and Karabağları successions have sedimented at the shoreface of the same basin. But paraconformity between these successions was caused by the basin margin faults. These faults sharply changed the sedimentation conditions, sediments transported from the land areas increased and mainly green coloured detritics with fine grain developed on the carbonate rock dominant Aktepe succession.

The 'Azmakdere member' (Göktaş, 2010) in the Çeşme Peninsula, 'Karaburun shale-litharenite unit' (Kaya, 1979) and the 'Bozavulu formation' (Sümer, 2007) in the Urla depression are the lithostratigraphic equivalents of the Karabağları member. The 'Yapalak member' has been described in Aliağa limestone by Kaya (1979) is the possible equivalent of the subunit in the Foça Peninsula.

Değirmentepe Limestone: The subunit is marked with the carbonate rocks present in the upper parts of the Hisarcık formation. The name for the first time is used in this study. Değirmentepe is the name of a hill located about 1.25 km to the NE of the Karaburun town centre (Figure 6).

Type locality is around the Karaburun town centre, thickness of the succession varies from 75-150 m.

The succession is composed of limestone-dolomitic limestone and has centimetric claystone interbeds in the lower levels. The limestone are thick layered but not well marked, has micritic texture, in places have some gastropods, fresh water algae and have fenestrates. They are concretionary aspect in the NW-SE outcrop area to the NE of the Soluğan Tepe (Figure 5). They have sands and granules derived from the KV2 and from the Pre-Neogene carbonate rocks.

In the generalized stratigraphy they are overlaid with an angular unconformity by Upper Miocene alluvial fan deposits (Saip formation). The fault zone running N45ºW direction from the Karaburun town centre towards Bozköy is considered to be primarily bordering the Middle Mioce basin. This reactivated fault separates the KV2 in the footwall block and the limestone which has become tilted towards the fault plane in the hangingwall block (Figure 5). The lavas here are considered to represent 3rd stage of the Karaburun volcanisms and are at the low part of the succession.

'Beyazıt member' (Göktaş, 2010) in the Çeşme peninsula, 'Urla limestone' (Kaya, 1979; Sümer, 2007; Göktaş, 2011) in the Urla depression and the carbonate rocks of the Aliağa limestone in the upper part are the regional equivalents of the lower unit.

3.1.3. Karaburun Volcanics

Late Early Miocene calc-alkaline mafic volcanics (Mg#=54–72: Helvacı et al., 2009), are located in the NE coastal part of the Karaburun Peninsula. First time Türkecan et al. (1998) named then as 'Karaburun volcanics' and considered that they were emplaced at least in three stages. Lava flows and limited pyroclastics emplacement and outcrops are controlled by the oblique fault system extending NW-SE direction (Karaburun Fault Zone: Uzel et al., 2013) (Figure 9).

Karburun volcanism has lateral connection with the Lower-Middle Miocene lacustrine sedimentation in the study area (Figure 10). Previous to the first two stage eruptions, related pyroclastics of the base surge and scoria air fall deposits were emplaced.

In the previous studies (Türkecan et al., 1998; Helvacı et al., 2009; Göktaş, 2014) and in this study, major element analyses (Table 1) of the samples are shown in the TAS diagram of Le Bas et al. (1986). The majority of the analysed 29 samples indicated andesite (9) and basaltic trachyandesite (10) and less numbers of samples indicate basaltic andesite (6) and

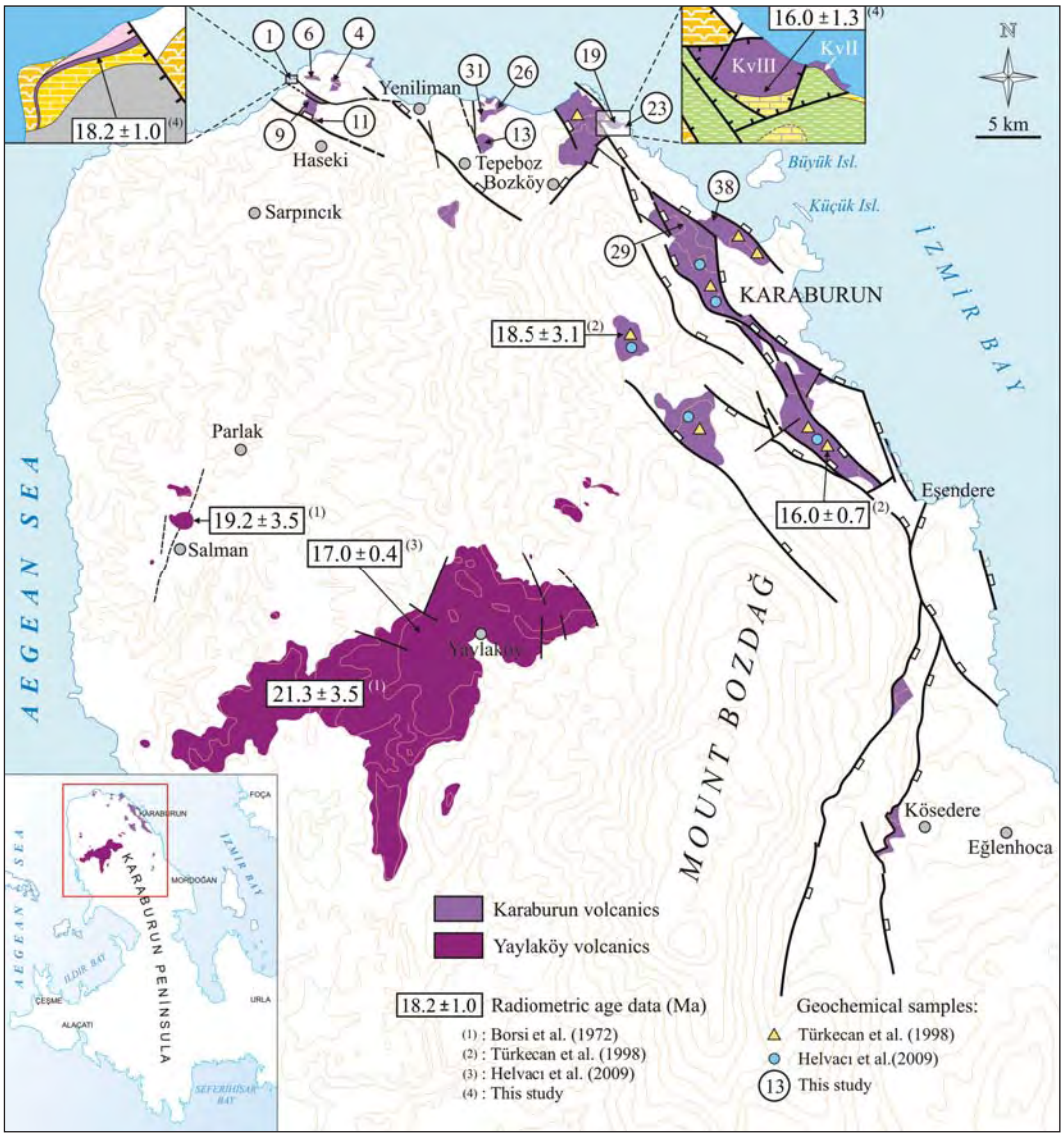

Figure 9- The mafic volcanics from the northern part of Karaburun Peninsula.

trachyandesite (4) compositions (Figure 11A). Göktaş (2014) and in this study 7 out of 12 samples have given andesite and 3 samples indicated basaltic andesite and 2 samples trachyandesite compositions. Analyses of the samples collected by Helvacı et al. (2009) have been concentrated in the basaltic andesite (shoshonite) field in the diagram. All of the analyses of the samples of Le Maitre et al. (2002) SiO_2 vs K_2O in the diagram fall into the high potassium bearing basaltic andesite (Figure 11B). All of the samples are in subalkali and calc-alkaline characters. Within the general extension of the KV all of the samples studied in the northern part in this study show a change in total alkali-silica contents towards the volcanics in the southern part which were the subject of the previous study. In the northern volcanics (in this study) SiO_2 contend shows variation between 53.4-56.9%. In the northern volcanics (Türkecan et al., 1998; Helvacı et al., 2009) it varies between 46.3-57.8%.

Textures of the lavas are quite similar. Studied samples have hypocrystalline porphyritic texture. Olivine is the main phenocryst. In general they have pilotaxitic and less interstitial matrix material, irregular distribution or in parts vague flow structure marked by the orientation of plagioclases, pyroxene, olivine microliths/micrcrytstals and rare volcanic glass. Quarts xenocrysts by magmatically corroded and encircled pyroxene microliths/microcrystals indicates magma mixing.

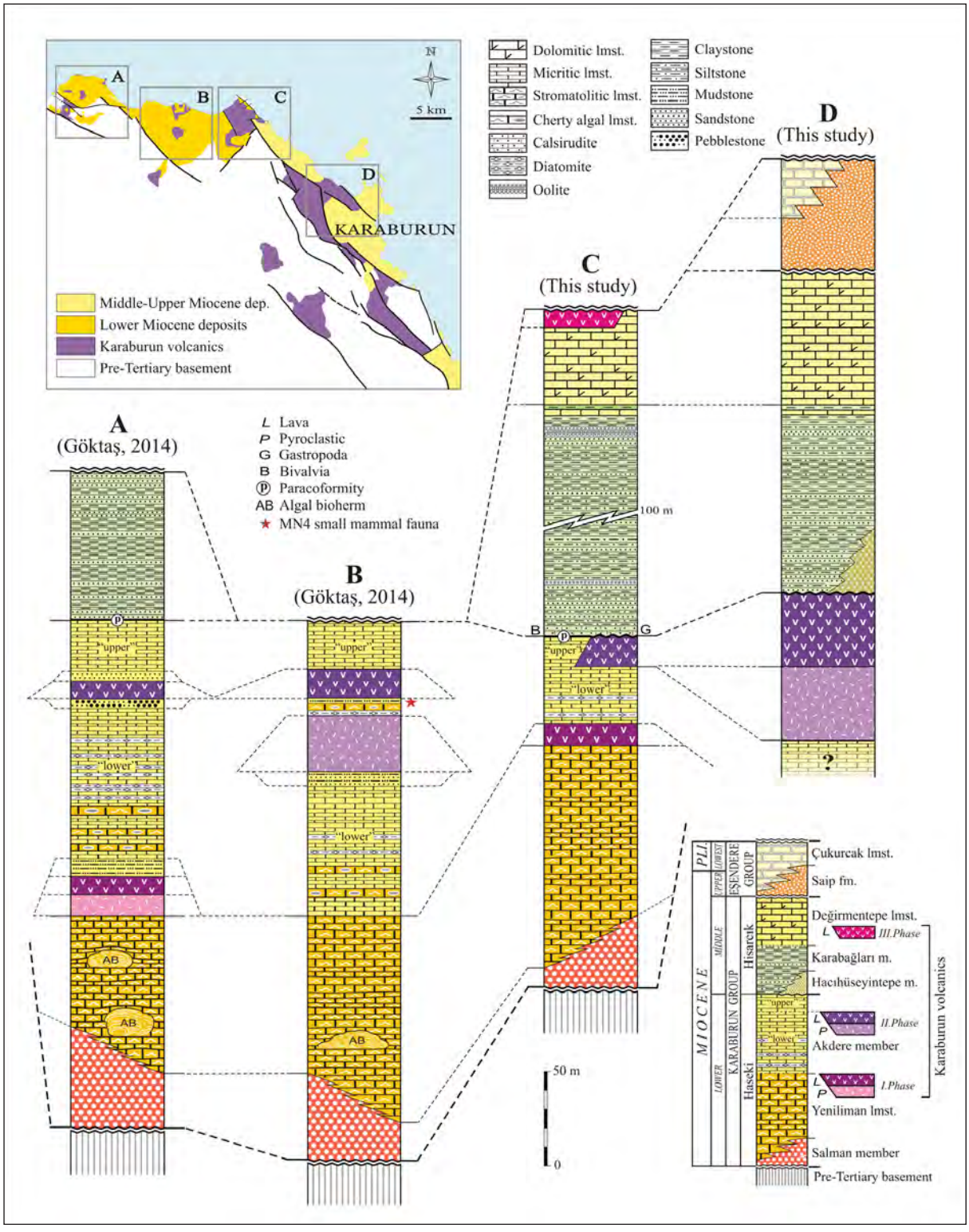

Figure 10- The stratigraphic position and correlation of Karaburun volcanics.

Table 1- Results of major element analyses of samples collected for this study from Karaburun volcanics (gray coloured ones) and samples given in Göktaş (2014).

Sample	*UTM Coordinate*	SiO_2	Al_2O_3	Fe_2O_3	MgO	CaO	Na_2O	K_2O	TiO_2	P_2O_5	MnO	SrO	BaO	LOI
1K	*0448690E-4281115N*	53.6	14.4	6.8	3.4	9.4	3.0	2.1	0.7	0.2	0.2	0.08	0.08	5.85
4K	*0449415E-4281065N*	56.4	16.4	7.1	5.2	6.5	3.4	2.1	0.7	0.3	0.2	0.08	0.08	1.45
6K	*0449072E-4281155N*	54.9	15.8	7.6	6.0	7.2	3.3	1.8	0.7	0.3	0.1	0.07	0.08	1.60
9K	*0449088E-4280757N*	53.5	14.9	6.9	2.8	9.3	3.0	2.2	0.7	0.3	0.1	0.08	0.08	5.80
11K	*0449140E-4280285N*	53.4	14.7	6.9	3.3	9.3	2.9	2.2	0.7	0.2	0.1	0.08	0.08	5.80
13K	*0452355E-4279932N*	55.4	16.4	7.2	4.2	8.1	3.2	2.1	0.6	0.2	0.1	0.07	0.07	2.05
19K	*0454935E-4280165N*	56.9	16.4	6.9	3.7	6.4	3.7	2.3	0.6	0.3	0.1	0.09	0.11	2.25
23K	*0455140E-4280170N*	53.8	15.4	7.3	4.4	9.3	3.2	2.3	0.8	<0.1	0.1	0.10	0.10	2.75
26K	*0452715E-4280655N*	54.8	16.4	7.5	5.3	7.6	3.2	2.0	0.7	0.2	0.2	0.07	<0.01	1.85
29K	*0456360E-4278135N*	54.8	15.5	7.1	3.8	8.0	3.2	2.6	0.7	0.5	0.2	0.10	0.10	3.05
31K	*0452320E-4280265N*	56.4	16.2	6.9	3.2	7.2	3.6	2.3	0.6	0.3	0.1	0.09	0.11	2.60
38K	*0456850E-4278315N*	55.3	16.3	7.3	3.3	8.3	3.5	2.6	0.8	0.4	0.2	0.09	0.11	1.60

KV1 and KV2 lavas have been aged by K/Ar method. As a result of the radiometric dating the KV1 located between Yeniliman limestone and Aktepe member gave 18.2±1.0 Ma (Göktaş, 2014) and lava located at the lower level Değirmentepe limestone which is the last member of the Karaburun group gave 16.0±1.3 Ma (Table 2).

First stage volcanics: Göktaş (2014) for the first time reported lithostratigraphic position, petrographical characters and age of these volcanics. These volcanics represent beginning of calc-alkaline mafic volcanisms in the NE of Karaburun Peninsula. KV1 lavas has outcrops in the north of Bozköy and here they separate Yeniliman limestone from the Aktepe member (Figures 5, 10A, C).

Second stage volcanics: They have extensive lava flows and are the most volumetrically important volcanics of the Karaburun volcanics. KV2 volcanism started while Aktepe member was continuing sedimentation, so these volcanics relatively separated the lacustrine succession into 'upper' and 'lower' sections (Figures 10A, B). The lavas at the bottom of the Karabağlar succession have been considered in the framework of KV2 (Figures 5, 6 and 10C, D). Base surge sediments emplaced at the initial stage of the volcanism in the north of Tepeboz (Göktaş, 2014). In the study area pyroclastics are represented with scoria air falls.

There is a NW trending normal fault with oblique displacement extending from the east of Hisarcık quarter towards Eşendere separating Neogene rock units from the basement rocks. KV2 products have

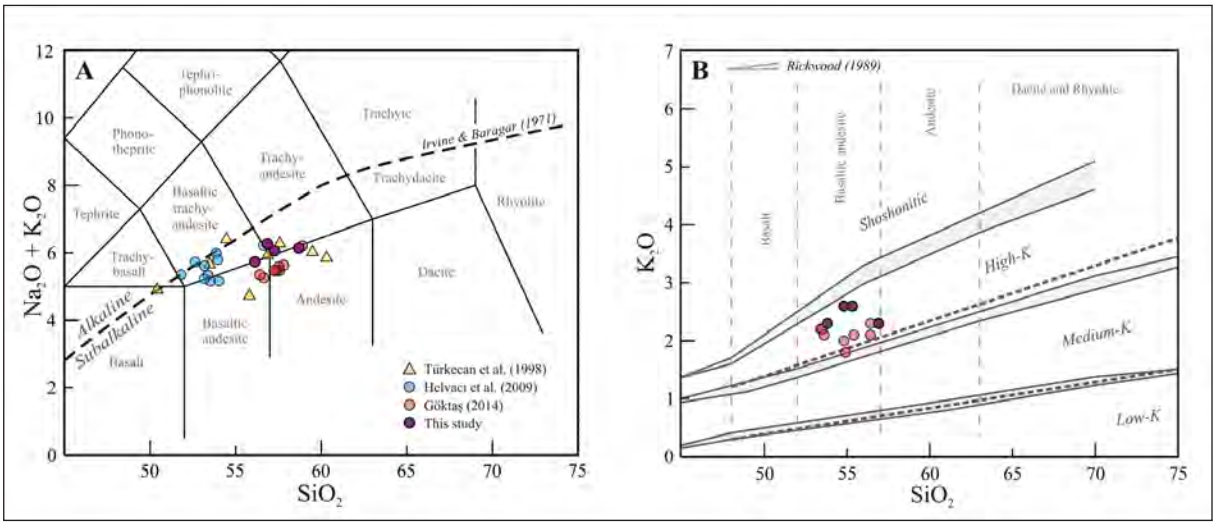

Figure 11- The evaluation of Karaburun volcanics using the diagrams of total alkali-silica(A) of Le Bas et al. (1986) and K_2O vs SiO_2 (B) of Le Maitre et al. (2002).

Table 2- K/Ar ages from the first stage (1K: Göktaş, 2014) and third stage (19K: this study) of Karaburun volcanics.

Sample	Material	K (%)	$^{40}Ar^{rad}$ (ccSTP/gr)	$^{40}Ar^{rad}$ (%)	Age (Ma)
1K	Whole rock	2.234	1.591×10^{-6}	28.9	18.2±1.0
19K	Whole rock	1.354	8.462×10^{-7}	17.3	16.0±1.3

maximum extension on the footwall block of this fault and it underlies of the Hisarcık formation (Figure 6). There are spatter lavas and scoria air falls under the lavas between Hisarcık quarter and Karaburun town centre. Because of thermal oxidation typically red coloured spatter lavas have been weakly agglutinated. General alteration colour of mafic pyroclastics is yellowish gray. Thickness of the plane-parallel scoria fall layers is in the range of decimetres. 60-80 cm thick welded tuff beds consist of coarse ash (1/16-2 mm: Fisher, 1966) containing 2-4 mm size subangular lava clasts are dark gray coloured. Scoria lapilli (2-64 mm: Fisher, 1966) sediments increase upwards in the succession (Figure 12 A). Average grain size of the lava fragments (fine vesiculated or non-vesiculated) is about 10 mm. The framework is clast supported and mainly it does not have any matrix material. Coarse ash tuffs have lapilli size scoria fragments, in some places they may also have armoured/cored lapillies ("core-type lapilli": Schumacher ve Schmincke, 1991) (Figure 12B). In the upper part of the succession there may be ballistic blocks containing coarse lava fragments with less vesicles. Approaching to the lavas on the top, sizes (maximum 60 cm), numbers and gas vesicles of blocks.

Third stage volcanites: Small volume of lava eruptions on the Değirmentepe limestone defined the third stage lavas. Their presence has been established from the relative stratigraphy and from the radiometric data. Type locality is 1.25 km to the NE of Bozköy (Figure 5). Türkecan et al. (1998) collected samples from the area between Hisarcık quarter the Eşendere harbour and had them analysed. The samples were weakly alkaline (SiO_2: 46.3%; K_2O+Na_2O: 4.50%) contemporary lavas (16.0 ± 0.7 Ma) may belong to the third stage (Figure 9).

3.2. Eşendere Group

Late Miocene-early Early Pliocene terrestrial succession has been limited by regional scale angular unconformities both on the top and at the bottom which consists of alluvial fan deposits (Saip formation) at the lower part and lacustrine limestones (Çukurcak limestones) with lateral-vertical transitions on the top. The groups name Eşendere is related to the Eşendere fishing port in the Ambarseki village.

In the near SE part of the study area around Eşendere port, mudstone is the dominant rock type in the succession. 'Eşendere large mammal fauna' (Kaya et al., 2005) in the mudstone has been correlated with the MN11+12 biozones indicating Turolian (Figure 4). Biostratigraphic data showed

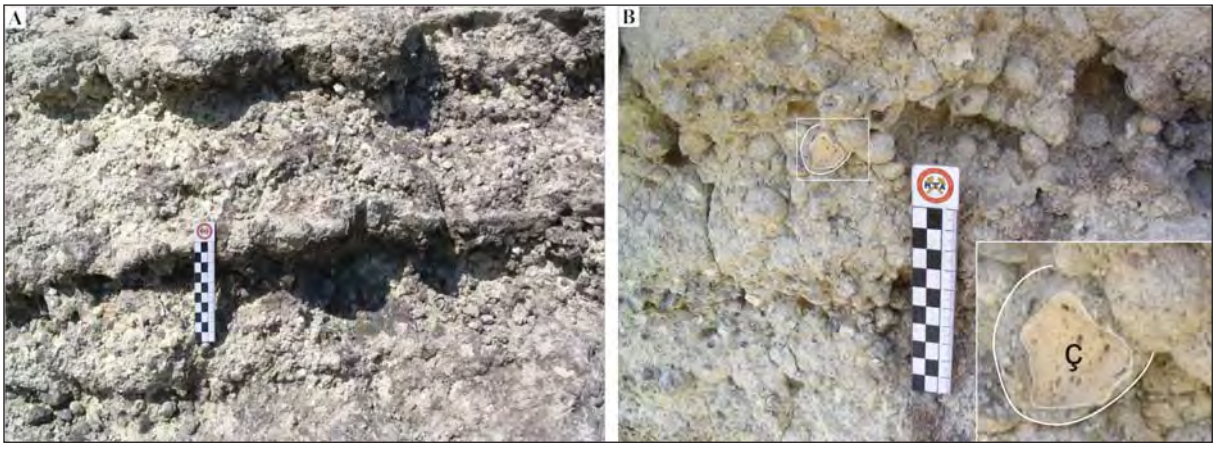

Figure 12- The second stage pyroclastics are exposed at the ~1,5 km southeast of Hisarcık village. A) Scoria fall deposits, B) Armoured/cored lapillies are observed in scoria falls (c: core).

that in the Akhisar depression Late Miocene regional sedimentation continued until the end of early Early Pliocene (~5 my) (Kaya et al 2004). In a general sense this data indicates that Eşendere group sedimentation developed during Late Miocene-early Early Pliocene(?).

Eşendere group is the stratigraphic equivalent of the 'Kaştepe group' described by Göktaş (2010) in the Çeşme Peninsula. The presence of equivalent sediments in the Foça Peninsula and in the Urla depression has not been reported in the previous work.

3.2.1. Saip Formation

The succession consisting of faded reddish brown coloured pebblestones and sandstones has for the first time has been defined under the 'Saip formation' name. Name of the unit comes from the Saip village near by.

The unit with lateral discontinuity has outcrops in the area between Değirmen Hill and Saip village (Figure 6). Thickness of the sedimentary succession is 30-50 m.

The fining-upward succession represents low profiled alluvial fan deposition. Alluvial succession consist of pebblestones-pebbly sandstones, representing braided stream sedimentation. In the upper parts it has sandy mudstone beds. Channel fills consist of rounded-subrounded pebbles.

The unit represents Late Miocene basin margin sedimentation. During late Middle Miocene compression phase (Yılmaz, 2000; Yılmaz et al., 2000) the unit was deformed and covered the Hisarcık formation with angular unconformity. The contacts with the basement rocks and with KV2 have been controlled by the faults either developed during sedimentation or reactivated at a later stage. Çukurcak limestone, with lateral-vertical transitions overlay the unit.

Saip formation could be correlated with the Karagöz formation defined by Göktaş (2010) in the Çeşme Peninsula.

3.2.2. Çukurcak limestone

It is marked with lacustrine carbonate rocks. The unit is the first time defined and named in this study. Çukurcak is the name of the area near SE of the study area where the unit has typical outcrops.

The thickness of the succession around Karaburun town centre is about 25 m.

The lacustrine succession consists of limestones and dolomitic limestones. Altered surfaces of the limestone are whitish light gray coloured, fresh rocks are beige coloured. In general they have micritic texture and are very compact. They have mainly thick-very thick, in places thin-medium layered and in some places rarely with gastropods. Towards the base the unit is light red brown colour, has massive mudstone with fresh water alga's and sepiolite/palygorskite bearing scarlet red brown coloured massive claystone interbeds.

The limestone succession is the last representatives of the Neogene sedimentations in the Karaburun Peninsula. In the generalized stratigraphy it is covered by Holocene alluviums.

The unit is the equivalent of the 'İnlice formation? defined by Göktaş (2010) in the Çeşme Peninsula.

4. Structural-Stratigraphic and Paleogeographic Evolution

Early Miocene paleogeography of the coastal part of Aegean region has been marked by a big perennial lake with low energy sedimentation conditions. The lacustrine sedimentation in the NE of Karaburun Peninsula started with the stromatolitic-algal limestones and continued with micritic limestones. In a wide neighbourhood in the Foça Peninsula, thinly plane parallel bedded limestones and bituminous shales sedimented (Zeytindağı formation: Kaya, 1979). In the area of Foça Peninsula is, freatomagmatic eruptions produced felsic ignimbrites (Foça tuff: Kaya, 1979) during end of the Early Miocene. Although emplacement of ignimbrites interrupted the sedimentation of the Zeytindağı formation it continued with the Aliağa limestone (Kaya, 1979) all through early Middle Miocene. Within the distribution area in FD, rhyolitic ignimbrites are a reference stratigraphic level separating Early Miocene and Middle Miocene lacustrine sedimentations. Late Middle Miocene (Yılmaz, 1989; 1990, 2000; Yılmaz et al., 2000, 2001) is considered to be magmaticaly quite period in Western Anatolia but there are no reported sediments in FD. Under the compressions in Foça and Urla areas early Middle Miocene sediments are deformed and became subjected to erosion. Following compressions the area was subjected to extensional forces in Late Miocene (Yılmaz, 2000; Yılmaz et al.,

2000). It is accepted that in the newly developed basins fillings continued until end of early Early Pliocene (Kaya et al., 2004).

In the NE part of the Karaburun Peninsula dominant lacustrine sedimentation is considered to have started in Early Miocene and have continued until the end of early Early Pliocene(?). At the end of Early Miocene and at the beginning of Late Miocene boundaries of the sedimentation basin became narrower and sedimentation continued in this newly shaped basin. At about in the Early-Middle Miocene border defined discordance between Haseki and Hisarcık lacustrine sedimentations indicated the presence of the fault there. The faults shaped the western margin of the FD and vertical movements of the faults changed sedimentation conditions in the basin but did not cause sedimentation discontinuity. In the eastern part of FD, rhyolitic ignimbrites are present between Zeytindağı formation and Aliağa limestone successions. The explosive magmatism producing these rhyolitic ignimbrites became active at about the same time.

Around the Karaburun Peninsula there have not been any reliable data indicating beginning of Neogene sedimentation and so, opening time of the Miocene basin in this part. In the study area the Salman member starting with alluvial fan/delta deposition of Early Miocene lacustrine sedimentation is marked by the Yeniliman limestone and on its continuation the Aktepe member. The KV1 products have been locally emplaced on to the Yeniliman limestone platform, so lake depositions have not been disrupted and micritic limestone of the Aktepe member as the dominant succession transitionally and concordantly overlaid the algal limestone within a rather wide time interval. Chrono-lithostratigraphic equivalence of KV1 in the Çeşme Peninsula could be the latite andesites of 18.2 Ma of age (Borsi et al., 1972). Geochronological and lithostratigraphic data suggest that in different parts of the Karaburun Peninsula (Armağandağı, Kocadağ, Yaylaköy and Karaburun) effective calc-alkaline volcanism started following the initial products of Miocene terrestrial sedimentation (Salman member and Yeniliman limestone and its equivalent the Şifne formation in the Çeşme Peninsula) developed (Figure 13).

In the northern part of the Karaburun Peninsula the distribution of Lower Miocene alluvial and lacustrine deposits, Bozdağ in present position was a peninsula placed in the widely spread Early Miocene lake. With this position it is considered to be the ancestor of the Karaburun peninsula. It is known that in the western and eastern part of the ?Bozdağ High? Lower Miocene successions have been represented with different sedimentary facieses, to that Middle Miocene successions are rather simple and uniform (Besenecker, 1973; Kaya, 1979; Göktaş, 2010, 2011, 2014; Çakmakoğlu et al., 2013). In the Foça Peninsula all along Early Miocene volcanites developed along with the lacustrine simple sedimentations and caused frequent interruption of the sedimentation in vertical and lateral directions causing change of order of the sedimentation. From the beginning of Middle Miocene onwards sedimentation developed in a rather monotonous way. The reasons for these may be explained; i) Calc

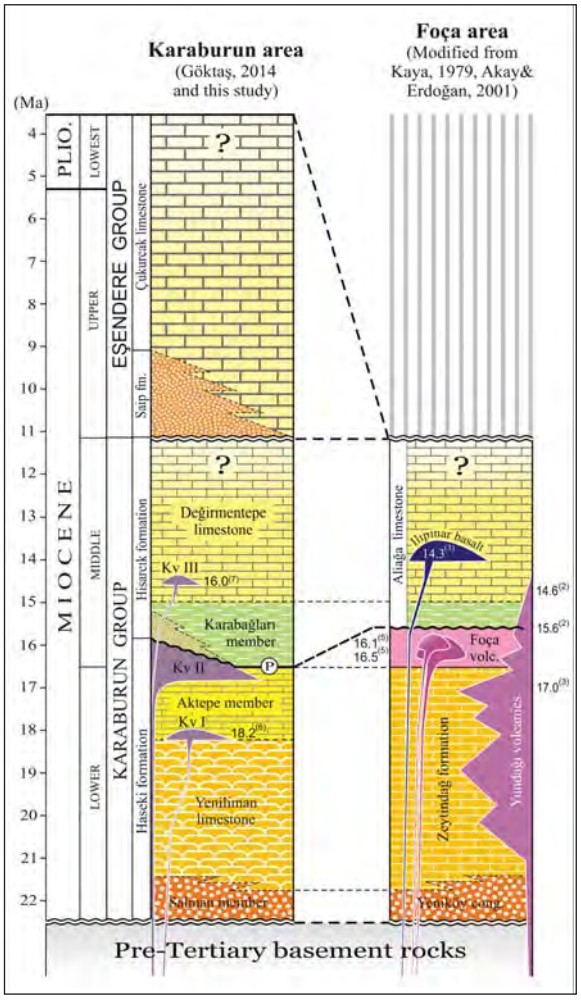

Figure 13- The stratigraphical correlation of volcanism and sedimentation from Karaburun and Foça areas. (1)Borsi et al. (1972), (2)Ejima et al. (1987), (3)Ercan et al. (1996), (4)Helvacı et al. (2009), (5)Altunkaynak et al. (2010), (6)Göktaş (2014), (7)This study. P: Paraconformity, Kv: Karaburun volcanics.

alkali felsic-mafic volcanism which caused local changes in the Early Miocene lacustrine sedimentation became extinct at the beginning of Middle Miocene [According to Altunkaynak et al. (2010) youngest ages are between 16.1-16.6 Ma], ii) ~2 Ma stagnation changing from calc-alkaline to alkaline volcanism (Altunkaynak et al., 2010), iii) Alkaline volcanism mainly became active in early Middle Miocene (between 14.7-14.1 Ma; Altunkaynak et al., 2010) and it was mostly represented with the extrusions in the parts outside sedimentation basins or they were small enough extrusives not to cause any changes in the sedimentation order [14.3 Ma age (Ercan et al., 1997) like Ilıpınar basalt (Kaya, 1979)]. As is the case in the study area lacustrine sedimentations kept their continuity outside the felsic ignimbrite (Foça tuff) extension areas. Haseki and Hisarcık depositions are evidence of this. Ignimbrite flows extend from Uzun Ada to the area around Mordoğan. These areas were subjected to lake transgression and Hisarcık formation and the equivalents at least continued sedimentation all through early Middle Miocene (Figure 13). Altunkaynak et al. (2010) had 16.5-16.1 Ma age by $^{40}Ar/^{39}Ar$ method for the underwater rhyolite domes. Lateral connections of ignimbrites with these rhyolite domes have been proven. Akay and Erdoğan (2001) by using age data of Altunkaynak et al. (2010) for the rhyolite domes, conclude that calc-alkaline asidic volcanism in the Foça Peninsula continued becoming effective during between latest Early Miocene and earliest Middle Miocene.

The NW trending normal fault zone between Karaburun high and the FD became distinct in Middle Miocene. With the emplacement of KV2 products following limited disruption of sedimentation this fault zone controlled the Hisarcık lacustrine deposition (Figure 14). At the basin margin alluvial sediments of Hacıhüseyintepe member overlie KV2 lavas with erosive unconformity. These alluvial sediments in a lateral direction pass into fine grained shoreface sediments which sediments on the Aktepe platform limestones with paraconformity. Deposition of Hisarcık formation transitionally overlies shoreface sediments and ends with the Değirmentepe limestone where it is leaning at the basin?s coastal margin.

Late Miocene succession overlies Hisarcık formation with angular unconformity, from base towards the top it consist of alluvium fan deposits grading into lacustrine limestones of the Eşendere group. Angular unconformity at the base of the Late Miocene is related to the compressional deformation in late Middle Miocene. There are no sedimentary deposits in the areas representing internal parts of the Foça depression basin (Urla area, Uzun Island, Hekim Island, Çiçek Islands) on the Aliağa limestone

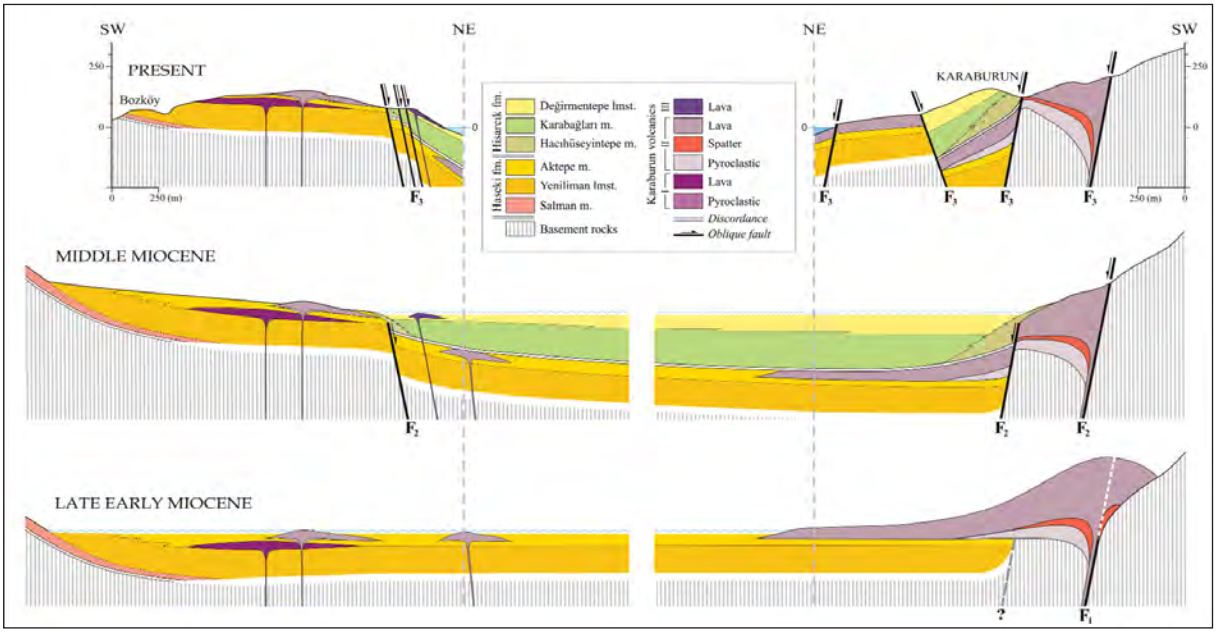

Figure 14- The stratigraphical-structural evolution of early-middle Miocene sedimentation and volcanism of Karaburun group. F_1: late early Miocene fault, F_2: early middle Miocene faults, F_3: Post-middle Miocene to pre-Holocene faulting.

to be correlated with the Eşendere sedimentary succession (Göktaş, 2011). Compressional movements in late Middle Miocene caused westward tilting of the Foça basin and the probability of the sedimentation axis slipping towards Karaburun Peninsula may explain the reason. As mentioned before that lacustrine sediments equivalent to the Çukurcak limestone which developed in the Late Miocene basins beyond FD are known to have continued developing in early Early Pliocene. In Western Anatolia late Early Pliocene compression phase (Koçyiğit et al., 1999; Yılmaz, 2000; Bozkurt, 2000; Bozkurt and Sözbilir, 2004; Kaya et al., 2004) is considered to have separated the consecutive two phase extensional process. It may be suggested that during the Pliocene compression phase Çukurcak limestone rose above the water level and became subjected to erosion.

5. Discussion

In the generalized stratigraphy of Helvacı et al. (2009) terrestrial Neogene sediments altogether were considered to be Lower Miocene age and these Middle and Upper Miocene sedimentary successions explained in this study have been considered non exist. It was also claimed that in the volcanostratigraphy of the Karaburun Peninsula the Karaburun volcanics represent the oldest (18.5 Ma), Yaylaköy volcanics represent the youngest (17.0 Ma) calc-alkaline volcanisms. As it is known Yaylaköy volcanism is two phases (Aras et al., 1999; Çakmakoğlu et al., 2013). Borsi et al. (1972) suggested 19.2-21.3 Ma age for the first phase volcanism. Accuracy of these age interval is questionable but even so, it is obvious that 17.0 Ma of age for the second phase volcanism can not by itself represent Yaylaköy volcanism. In this study it has been suggested that Yaylaköy and Karaburun volcanics are at about in the same lithostratigraphic position and no other volcanism developed before these two (Figure 2).

Uzel et al (2013) presented simple Neogene map of the Karaburun peninsula. According to this map and to the general stratigraphic order, lacustrine sediments of the Haseki and Hisarcık formations explained in this study are considered to be the equivalents of the 'Aliağa limestones' (Akay and Erdoğan, 2001) in the Foça Peninsula and have been considered to be the 'Lower sequence? (Lower-Middle Miocene) (Figure 2). Proposed succession order for the 'Upper sequence' (Middle-Upper Miocene) makes one think of lithostratigraphic correlation with Middle Miocene Hisarcık formation. In this study Hisarcık formation is said to lie on the Haseki formation with uncoformity, is the equivalent of the Aliağa limestone (Kaya, 1979) in Foça Peninsula and the Urla limestone (Kaya, 1979) in the Urla depression. This conclusion is based on the age of the alkali volcanics with which they have transitional relations with (Figure 2).

Altunkaynak and Yılmaz (2000), Altunkaynak et al. (2006) have divided the Neogene succession in Foça Peninsula mainly into two sediment groups such as 'lower' and 'upper' groups. Calc-alkaline volcanics at 16.1-16.6 Ma age and the alkaline volcanics at 14.1-14.7 Ma age, have lateral connection with the lower group and have been considered to be Lower-Middle Miocene, and the overlying with unconformity the marl-limestone succession to be Upper Miocene-Pliocene. In the referred studies proposed ages for the sedimentary successions have been based on relative chronostratigraphy. There is no primary evidences available proving the presence or age of the upper sedimentary succession. Altunkaynak et al. (2010) mapped the early Middle Miocene volcanics and all of these volcanics have been placed on the calc-alkaline volcanics but their contact relations with the lower group can not be observed (In the Foça Peninsula the only alkaline volcanic rock outcrop which has clear cut contact relations with the sedimentary successions is the Ilıpınar basalts within the Aliağa limestone). In the same map proposed relative Upper Miocene-Pliocene age for the limestone outcrops were descripted to be the Aliağa limestone (Kaya 1978; Eşder et al., 1991; Dönmez et al., 1998). As chrono stratigraphic position of the Ilıpınar basalts has been proven, Altunkaynak et al (2010) reported that early Middle Miocene alkali volcanism crops out in the form of mafic-felsic doms/dykes which indicates the volcanism is in the same age with deposition of the Aliağa limestones (Figure 2). In this study it was shown that Aliağa limestone represents early Middle Miocene sedimentation and transgressively overlay Foça tuffs and Late Miocene-early Early Pliocene(?) sedimentation did not develop in the Foça Peninsula.

The suggestion of there is no deposition at Upper Miocene-lowest Pliocene period in Miocene successions of Foça Peninsula and Urla depression, based on the lithostratigraphic data in the previous work and are also based on the unpublished field observations of the author. This evaluation is also based on the information that in Western Anatolia in

the Late Miocene basins, sedimentation on unconformity planes starts with alluvial fan sediments, but in the said area these fan sediments are not present. To investigate the reason for this gap in the Neogene stratigraphy is considered to be beyond the scope of this work. But on the other hand presence of these sediments only in the eastern coastal region of Karaburun Peninsula may be explained; i) with the reactivation of the faults determining the eastern border of the Bozdağ High, there is one sided tilting of the FD base westwards and as a result migration of the sedimentation axis to the same direction and ii) rising of the Miocene platform limestones in other parts of the basin (Foça and Urla areas) above lake water and changing into non-depositional areas.

In FD, there has not been any reliable time data indicating upper and lower boundaries of Middle Miocene and Late Miocene-early Early Pliocene(?) sedimentation processes. i) Direct or indirect time data obtained from Hisarcık formation and the regional equivalents all indicate early Middle Miocene sedimentations (Besenecker, 1973; Ercan et al., 1997; Kaya et al., 2003; Koufos, 2006; Altunkaynak et al., 2010; Göktaş, 2011; Karacık et al., 2013). Main radiometric age data indicating late Middle Miocene sedimentation have been obtained from the alkali volcanics which have lateral connections with the Urla limestone, indicating 11.3-11.9 Ma K/Ar age (Borsi et al., 1972). But these referred radiometric ages have quite high error range (± 3.5 Ma), so they are not very reliable. But, still latest studies indicate early Middle Miocene for synsedimentar age (Göktaş, 2011: 14.8, 14.5, 12.5 Ma; Karacık et al., 2013: 13.2 Ma). There is no data available to indicate volcanic activity during late Middle Miocene. This may be related to the compression phase previous to the Late Miocene extension. ii) The only proof of Late Miocene sedimentation in the FD is the large mammal fossil found by Kaya et al. (2005) in the Eşdere group sediments. The MN 11+12 biozones indicated by the fauna suggest early Turolian (Figure 4). iii) In the generalized stratigraphy of FD, lack of sufficient data prevents evaluation of 4 million years of time gap between late Middle Miocene-early Late Miocene. This period is needed to be studied.

6. Results

In this study in the NE coastal region of the Karaburun Peninsula, lateral and vertical distribution of KV with terrestrial Neogene sediments and their stratigraphical relations have been established. In the generalized stratigrapic order, rock units have been classified and have been mapped at 1:25.000 scale, rock units in the Çeşme and Foça peninsulas and in the Urla depression have been correlated with each other, and suggestions have been made towards structural-stratigraphic and paleogeographic evolutions.

In the generalized stratigraphy, Neogene sequence sedimented on the Upper Cretaceous-Lower Tertiary İzmir flysch with angular unconformity. Within the Neogene sequence on a regional scale mainly two sedimentary successions separated from each other with angular unconformity have been defined in the Karaburun group (Lower-Middle Miocene) and Eşendere group (Upper Miocene-Lowermost Pliocene(?)). Haseki (Lower Miocene) and Hisarcık (Middle Miocene) formations belonging Karaburun group, an unconformity with no sedimentation disruption has been identified between these formations.

Lower Miocene sedimentary successions cropping out in the Karaburun Peninsula have been considerably eroded vertically and laterally since then. Early Miocene basin has been represented by isolated sediment remains. As initial records of the boundaries have been wiped out so explanation details of structural-paleogeographic characters of the period have been insufficient. It has been concluded that the faults observable now separating the Lower Miocene sediments from the basement rocks developed after the sedimentation. NW-SE trending oblique/normal faults controlling Middle Miocene lacustrine sedimentations have developed with an unconformity on the Lower Miocene basin fillings without any time gap. Upper Miocene sediments have been deposited with an angular unconformity on the Middle Miocene rock units which rise above water as a result of regional compression.

Early-Middle Miocene sedimentation of the Karaburun group has been studied by dividing them into two formations. It has been concluded that they were mainly developed in the lacustrine environments. Early Miocene sedimentation of the Haseki formation starts with the alluvial/fan delta sediments of Salman member, continues with lateral intricate time overlapping algal-biostromal Yeniliman limestone and ends with dominantly micritic limestone of the Aktepe member following emplacement of the 1st stage KV. Hisarcık formation lies with unconformity on the Aktepe member and 2nd stage KV. Hisarcık formation from base to the

top has been divided into fan delta sediments of Hacıhüseyintepe member, fine grained shoreface sediments of Karabağlar member and Değirmentepe limestone and studied. Unconformity at the base of Hisarcık formation has been correlated with the vertical movements of the fault which shaped the eastern edge of the Bozdağ rise while FD were developing (Figure 14). It was suggested that boundaries of the structural highs between FD and Karaburun and Yamanlar were shaped at the beginning of Middle Miocene and Hisarcık and equivalents sedimented in the basin which acquired basin character in FD in general. It has been shown that basin margin sediments of the Hacıhüseyintepe member lean at the KV lavas with erosional unconformity, lateral equivalence, the shoreface sediments of the Karabağları member overlay the Aktepe platform carbonate with well defined concordant contact. This contact may reflect paraconformity developed under water. Based on the biochronological and geochronological data obtained from the regional equivalents of the Hisarcık formation it has been accepted that Hisarcık formation developed mainly in early Middle Miocene and sedimentation processes ended with Late Middle Miocene regional compression.

In the generalized stratigraphy the Eşendere group lies on the Hisarcık formation with angular unconformity. Rock units from bottom to the top consisting Upper Miocene-Lowermost Pliocene(?) alluvial fan deposits grading to lacustrine deposits have been defined within the Eşendere group. Presence of Upper Miocene sediments only on the western margin of FD may be explained by possible reactivation of the remains of the Middle Miocene old boundary faults at the beginning of Late Miocene, causing westward tilting of the sedimentation axis and so sedimentation continued in a narrower basin.

Depending on the relative lithostratigraphical relations; calc-alkaline mafic volcanics which have lateral relationship with the Karaburun group lacustrine sediments have been concluded to have developed in three stages; the lava flows of the last stage have been determined by the K/Ar method to be 16.0±1.3 Ma. Pyroclastic facieses emplaced prior to the lava flows have been for the first time identified as a map unit. The data on the lavas have been evaluated together with the previous work data and it has been concluded that they have calc-alkaline-neutral composition; in the study area from north towards south they show compositional change; from andesite (-trachyandesite) field to (basaltic andesite-) basaltic trachyandesite. In the same direction they display high potassium calc-alkaline series to shoshonite series. The KV sample analyses conducted within the frame of this work and the analyses of the geochemical data of the Yaylaköy volcanics in Helvacı et al. (2009) have been correlated and it has been concluded that both groups have accumulations in the high potassium andesite field. Chrono-lithostratigraphic data of the volcanics in this study and Salman-Yaylaköy area fit well with the previous work data, both volcanic groups mainly have positioned in about the same level. First products of calc-alkaline volcanism in the northern part of Karaburun Peninsula were emplaced following the start of alluvial fan/delta and laterally connected lacustrine deposition in the Early Miocene basin.

Acknowledgements

During the process of studying geology of the study area under the coordination of the Geology Department of the MTA General Directorate for the preparation of the 1/500.000 scale geological map of the İzmir sheet has mostly been completed. The work on the "Startigraphy and paleogeographic evolution of Neogene-Quaternary basins in the Çeşme, Urla, Cumaovası, Kemalpaşa-Torbalı depressions" was completed in 2008 and has been revised within the concept of the project. The lava samples collected from the Karaburun volcanites have been analysed for the major elements in the laboratories of the Mineral Analyses and Technology Department of the MTA General Directorate. K/Ar age dating analyses were carried out at Tubingen University in Germany. Geological engineer Murat Yükünç M.Sc, contributed to the field studies. Asst.Prof. İsmail Işıktek's critics on the carbonate rock facieses is greatly appreciated. Ph.D H.Yavuz Hakyemez, geological engineers Aytekin Çolak M.Sc, Ferliz Menlikli M.Sc, Berk Çakmakoğlu M.Sc have contributed in various ways.

Received: 19.07.2013
Accepted: 21.05.2014
Published: December 2014

References

Agostini, S., Tokçaer, M., Savaşçın, M.Y. 2010. Volcanic rocks from Foça-Karaburun and Ayvalık-Lesvos Grabens (Western Anatolia) and their petrogenic-geodynamic significance. *Turkish Journal of Earth Sciences* 19, 157-184.

Akay, E., Erdoğan, B. 2001. Formation of subaqueus felsic domes and accompanying pyroclastic deposits on the Foça Peninsula (İzmir, Turkey). *International Geology Review* 43, 661-674.

Aksu, A.E., Piper, D.J.W., Konuk, T. 1987. Late Quarternary tectonic and Sedimentation history of outer İzmir and Çandark Bay, Western Turkey. *Marine Geology* 76, 89-104.

Altunkaynak, Ş., Yılmaz, Y. 2000. Foca yöresinin jeolojisi ve aktif tektoniği, Batı Anadolu. *Batı Anadolu?nun Depremselliği Sempozyumu (BADSEM 2000),* 24-27 Mayıs 2000, İzmir, Bildiriler, 160?165.

Altunkaynak, Ş., Yılmaz, Y., Rogers, N., Kelley, S. 2006. Batı Anadolu?daki Çarpışma Sonrası Magmatizmanın Petrojenetik Evrimi; Foça Volkanikleri. *59. Türkiye Jeoloji Kurultayı,* 20-24 Mart 2006, Ankara, Bildiriler, 37-38.

Altunkaynak, Ş., Rogers, N.W., Kelley S.P. 2010. Causes and effects of geochemical variations in late Cenozoic volcanism of the Foça volcanic centre, NW Anatolia, Turkey. *International Geology Review* 52, 579-607.

Aras, A., Göktaş, F., Demirhan, M., Demirhan, H., İçöz, S. 1999. Karaburun kilinin stratigrafisi, mineralojisi ve pişme özellikleri. *1. Batı Anadolu Hammadde Kaynakları Sempozyumu (BAKSEM?99),* 8-14 Mart 1999, İzmir, 238-247. Besenecker, H. 1973. Neogen und Qartär der Insel Chios (Ägäis): PhD Thesis. Freien Universität Berlin, 195 s.

Bonis, L.De, Koufos, G.D., Şen, Ş. 1998. Ruminants (Bovidae and Tragulidae) from the Middle Miocene (MN5) of the Island of Chios, Aegean Sea (Greece). *Neues Jahrbuch für Geologie und Paläontologie-Abhandlungen* 210, 339-420.

Borsi, J., Ferrara, G., Innocenti, F., Mazzuoli, R. 1972. Geochronology and petrology of recent volcanics in the eastern Aegean Sea (West Anatolia and Lesbos Island), *Bulletin of Volcanology* 36, 473–496.

Bozkurt E. 2000. Timing of extension on the Büyük Menderes Graben, western Turkey and its tectonic implications. Bozkurt E., Winchester J.A., Piper J.D.A. (eds.). Tectonics and Magmatism in Turkey and the Surrounding Area. *Geological Society of London*. Special Publication 173, 385–403.

Bozkurt, E., Sözbilir, H. 2004. Tectonic evolution of the Gediz Graben: field evidence for an episodic, two stage extension in western Turkey. *Geological Magazine* 141, 63–79.

Çakmakoğlu, A., Bilgin, Z.R. 2006. Karaburun Yarımadası'nın Neojen öncesi stratigrafisi. *Maden Tetkik ve Arama Dergisi* 132, 33-62.

Çakmakoğlu, B., Göktaş, F., Demirhan, M., Helvacı, C. 2013. Karaburun Yarımadası'nın kuzey kesimindeki killerin stratigrafisi, sedimantolojisi ve ekonomik kullanım olanaklarının araştırılması. *Türkiye Jeoloji Bülteni* 56/1, 39-58.

Dönmez, M., Türkecan, A., Akçay, A.E., Hakyemez, Y., Sevin, D. 1998. İzmir ve kuzeyinin jeolojisi, Tersiyer volkanizmasının petrografik ve kimyasal özellikleri. *Maden Tetkik ve Arama Genel Müdürlüğü Rapor No: 10181*, 123 s. Ankara (unpublished).

Dunham, R.J. 1962. Classification of carbonate rocks according to depositional texture. In: W.E. Ham (ed). Classification of carbonate rocks. *American Association Petroleum Geologist-Memoirs* 1, 108-121.

Ejima, Y., Fujina., Togaki, H., Shimada, K., Iwagana, T., Yoneda, Y., Murakami, Y. 1987. The pre-feasibility study on the Dikili-Bergama geothermal development project in the Rebuplic of Turkey, Progress Report II. (unpublished).

Ercan, T., Satır, M., Sevin, D., Türkecan, A. 1997. Batı Anadolu?da Tersiyer ve Kuvaterner yaşlı volkanik kayaçlarda yeni yapılan radyometrik yaş ölçümlerinin yorumu. *Maden Tetkik ve Arama Dergisi* 119, 103-112.

Ersoy, Y., Sözbilir, H., Erkül. F., Helvacı, C., Uzel, B., Aktaş, U., Leblebicioğlu, O. 2006. Karaburun ilçesinin aktif tektoniği. *Aktif Tektonik Araştırma Grubu 10. Toplantısı (ATAG 10),* 02-04 Kasım 2006, İzmir, s.30.

Eşder, T., Yakabağ, A., Sarıkaya, H., Çiçekli, K. 1991. Aliağa (İzmir) yöresinin jeolojisi ve jeotermal enerji olanakları. *Maden Tetkik ve Arama Genel Müdürlüğü Rapor No: 9467*, 213 s. Ankara (unpublished).

Eşder, T. 1988. Gümüldür-Cumaovası (İzmir) alanının jeolojisi ve jeotermal enerji olanaklarının araştırılması. Doktora Tezi, İstanbul Üniversitesi Fen Bilimleri Enstitüsü Jeoloji Mühendisliği Bölümü Anabilim Dalı, 401 s. (unpublished).

Fisher, R.V. 1966. Rock composed of volcanic fragments and their classification. *Earth Science Reviews* 1, 287-298.

Flügel, E. 2010. Microfacies of Carbonate Rocks: Analysis, Interpretation and Application. *Springer-Verlag*, 984 p.

Folk, R.L. 1962. Spectral subdivision of limestone types. W.E. Ham (ed). Classification of carbonate rocks. *American Association Petroleum Geologist-Memoirs* 1, 62-84.

Genç, Ş.C., Yılmaz, Y. 2000. Aliağa dolaylarının jeolojisi ve genç tektoniği. *Batı Anadolu'nun Depremselliği Sempozyumu (BADSEM 2000),* 24-27 Mayıs 2000, İzmir, Bildiriler, 152?159.

Göktaş, F. 2010. Çeşme Yarımadası'ndaki Neojen tortullaşması ve volkanizmasının jeolojik etüdü. *Maden Tetkik ve Arama Genel Müdürlüğü Rapor No: 11389*, 64 s. Ankara (unpublished).

Göktaş, F. 2011. Urla (İzmir) çöküntüsündeki Neojen tortullaşması ve volkanizmasının jeolojik etüdü. *Maden Tetkik ve Arama Genel Müdürlüğü Rapor No: 11568*, 112 s. Ankara (unpublished).

Göktaş, F. 2014. Karaburun Yarımadası kuzey kıyı kesiminin Neojen stratigrafisi. *Maden Tetkik ve Arama Dergisi* 148, 43- 61.

Helvacı, C., Ersoy, Y., Sözbilir, H., Erkül, F., Sümer, Ö., Uzel, B. 2009. Geochemistry and $^{40}Ar/^{39}Ar$ geochronology of Miocene volcanic rocks from the Karaburun Peninsula: Implications for amphibole-bearing lithospheric mantle source, Western Anatolia. *Journal of Volcanology and Geothermal Research* 185, 181-202. ICS, 2013. International Stratigraphic Chart, International Commision on Stratigraphy. http://www.stratigraphy.org/index.php/ics-chart-timescale.

Innocenti, F., Mazzuoli, R. 1972. Petrology of İzmir-Karaburun volcanic area. *Bulletin of Volcanology* 36, 83-104.

Irvine, N., Baragar, W.R.A. 1971. A guide to chemical classification of the common volcanic rocks. *Canadian Journal of Earth Sciences* 8, 523?548.

Karacık, Z., Genç, Ş.C., Gülmez, F. 2013. Petrochemical features of Miocene volcanism around the Çubukludağ graben and Karaburun peninsula, western Turkey: Implications for crustal melting related silicic volcanism. *Journal of Asian Earth Sciences* 73, 199-217.

Kaya, O. 1978. Ege kıyı kuşağı (Dikili-Zeytindağı-Menemen-Yenifoça) Neojen stratigrafisi. *Ege Üniversitesi Fen Fakültesi Monografiler Serisi* 17.

Kaya, O. 1979. Orta Doğu Ege çöküntüsünün (Neojen) stratigrafisi ve tektoniği. *Türkiye Jeoloji Kurumu Bülteni* 22/1, 35-58.

Kaya, O. 1981. Miocene reference section for the coastal parts of West Anatolia. *Newsletters on Stratigraphy* 10, 164-191.

Kaya, O., Ünay, E., Saraç, G., Eichhorn, S., Hassenrück, S., Knappe, A., Pekdeğer, A., Mayda, S. 2004. Halitpaşa Transpressive Zone: Implications for an Early Pliocene compressional phase in Central Western Anatolia, Turkey. *Turkish Journal of Earth Sciences* 13, 1-13.

Kaya, T., Geraads, D., Tuna, V. 2003. A new Middle Miocene fauna from Mordoğan (Western Turkey). *Paläontologische Zeitschrift* 77/2, 293-302.

Kaya, T., Geraads, D., Tuna, V.A. 2005. New late Miocene mammalian fauna in the Karaburun Peninsula (Western Turkey). *Neues Jahrbuch für Geologie und Paläontologie Abhandlungen* 236/3, 321-349.

Koçyiğit, A., Yusufoğlu H., Bozkurt E. 1999. Evidence from the Gediz graben for episodic two-stage extension in western Turkey. *Journal of the Geological Society* 156, 605–616.

Koufos, G.D. 2006. The Neogene mammal localities of Greece: Faunas, chronology and biostratigraphy. *Hellenic Journal of Geosciences* 41, 183-214.

Le Bas, M.J., Le Maitre, R.W., Streckeisen, A., Zanettin, B. 1986. A chemical classification of volcanic rocks based on total alkali-silica diagram. *Journal of Petrology* 27, 745-750.

Le Maitre, R.W. (ed) 2002. Igneous Rocks: A Classification and Glossary of Terms. Recommendations of the International Union of Geological Sciences Subcommission on the Systematics of Igneous Rocks. *Cambridge University Press*. 236 p.

Öngür, T. 1972. İzmir-Urla jeotermal araştırma sahasına ilişkin jeolojik rapor. *Maden Tetkik ve Arama Genel Direktörlüğü Rapor No: 4835,* Ankara (unpublished).

Rickwood, P.C. 1989. Boundary lines within petrologic diagrams which use oxides of major and minor elements. *Lithos* 22, 247-263.

Saraç, G. 2003. Türkiye omurgalı fosil yatakları. *Maden Tetkik ve Arama Genel Müdürlüğü Rapor No: 10609*, Ankara (unpublished).

Steininger, F.F. 1999. Chronostratigraphy, Geochronology and Biochronology of the Miocene ?European Land Mammal Mega-Zones (ELMMZ) and the Miocene Mammal-Zones (MN-Zones)?, Rössner, E.G., Heissig, K. (eds). *The Miocene Land Mammals of Europe*, 9-24, München.

Sümer, Ö. 2007. Güzelbahçe (İzmir) Çevresinin alüvyonel sedimantolojisi ve aktif tektoniği. Yüksek Lisans Tezi, DEÜ Fen Bilimleri Enstitüsü, Jeoloji Mühendisliği Bölümü, Uygulamalı Jeoloji Anabilim Dalı, 103 s. İzmir (unpublished).

Türkecan, A., Ercan, T., Sevin, D. 1998. Karaburun Yarımadası?nın Neojen volkanizması. *Maden Tetkik ve Arama Genel Müdürlüğü Rapor No: 10185*, 35 s. Ankara, (unpublished).

Uzel, B., Sözbilir, H., Özkaymak, Ç., Kaymakçı, N., Cornelis, G.L. 2013. Structural evidence for strike-slip deformation in the İzmir-Balıkesir transfer zone and consequences for Late Cenozoic evolution of western Anatolia (Turkey). *Journal of Geodynamics* 65, 94-116.

Yılmaz, Y. 1989. An approach to the origin of young volcanic rocks of Western Turkey. A.M.C. Şengör (ed). Tectonic evolution of the Tethyan Region. *Kluwer Academic Publishers*. 159-189.

Yılmaz, Y. 1990. Comparison of young volcanic associations of western and eastern Anatolia formed under a compressional regime: a review. *Journal of Volcanology and Geothermal Research* 44, 1-19.

Yılmaz, Y. 2000. Ege bölgesinin aktif tektoniği. *Batı Anadolu'nun Depremselliği Sempozyumu (BADSEM-2000),* 24-27 Mayıs 2000, İzmir, Bildiriler, 3-14.

Yılmaz, Y., Genç, Ş.C., Gürer, O.F., Bozcu, M., Yılmaz, K., Karacık, Z., Altunkaynak, Ş, Elmas, A. 2000. When did the western Anatolian grabens begin to develop?, Bozkurt, E., Winchester, J.A., Piper, J.A.D. (eds), Tectonics and Magmatism in Turkey and the Surrounding Area. *Geological Society of London*, Special Publication 173, 353-384.

Yılmaz, Y., Genç, Ş.C., Karacık, Z., Altunkaynak Ş. 2001. Two contrasting magmatic associations of NW Anatolia and their tectonic significance. *Journal of Geodynamics* 31, 243-271.

BULLETIN OF THE MINERAL RESEARCH AND EXPLORATION

Foreign Edition 2014 149

CONTENTS

Facies Characteristics And Control Mechanisms of Quaternary Deposits In The Lake Tuz Basin
.....Alper GÜRBÜZ and Nizamettin KAZANCI 1

Neotectonic-Period Characteristics, Seismicity, Geometry And Segmentation of The Tuz Gölü Fault Zone
.....Akın KÜRÇER and Y. Ergun GÖKTEN 19

Neogene Stratigraphy And Paleogeographic Evolution of The Karaburun Area, İzmir, Western Turkey
.....Fikret GÖKTAŞ 69

Benthic Foraminiferal Fauna of Malatya Oligo-Miocene Basin (Eastern Taurids, Eastern Turkey)
.....Fatma GEDİK 93

Protolith Nature And Tectonomagmatic Features of Amphibolites From The Qushchi Area, West Azerbaijan, NW Iran
.....Mohssen MOAZZEN 139

Glauberite-Halite Association In Bozkır Formation (Pliocene Çankırı-Çorum Basin, Central Anatolia, Turkey)
.....İlhan SÖNMEZ 153

Estimation of Swelling Pressure Using Simple Soil Indices
.....Kamil KAYABALI and Özgür YALDIZ 177

Two Examples For Imaging Buried Geological Boundaries: Sinkhole Structure And Seyit Hacı Fault, Karapınar, Konya
.....Ertan TOKER, Yahya ÇİFTÇİ, Aytekin AYVA and Akın KÜRÇER 189

The Assessment of Geothermal Potential of Turkey By Means Of Heat Flow Estimation
.....Uğur AKIN, Emin Uğur ULUGERGERLİ and Semih KUTLU 201

A Brief Note On Mineral Evolution And Biochemistry
.....José Mario AMİGO 211

Critisism on the paper "Possible Incision of The Large Valleys In Southern Marmara Region, Turkey (Nizamettin KAZANCI, Ömer EMRE, Korhan ERTURAÇ, Suzanne A.G. LEROY, Salim ÖNCEL, Özden İLERİ and Özlem TOPRAK)
.....Nizamettin KAZANCI 219

Acknowledgement 221

Notes to the authors 223

Bull. Min. Res. Exp. (2014) 149: 93-136

Bulletin of the
Mineral Research and Exploration

http://bulletin.mta.gov.tr

BENTHIC FORAMINIFERAL FAUNA OF MALATYA OLIGO-MIOCENE BASIN, (EASTERN TAURIDS, EASTERN TURKEY)

Fatma GEDİK[a*]

[a] *Maden Tetkik ve Arama Genel Müdürlüğü, Jeoloji Etütleri Dairesi, 06800, Ankara-Turkey.*

Keywords:
Malatya, Oligo-Miocene, Benthic foraminifera, Systematic, Paleontology.

ABSTRACT

In this study, systematic description of 28 benthic foraminiferal taxa were carried out which had been detected in Oligo-Miocene aged Muratlı and Petekkaya formations cropping out over wide areas around Akçadağ town, west of Malatya province in Eastern Taurids. Miogypsina globulina which is a cosmopolite species located in Burdigalian aged shallow marine carbonates is described on wide geographical areas ranging from Central America to Indo-Pacific and Mediterranean Tethys. Miogypsina polymorpha on the other hand was reported only from Indo-Pacific in stratigraphical records until today. Considering the association of these species, the assumption of a probable marine connection mentioned between Indo-Pacific and Mediterranean Tethys in Burdigalian period in the region was strongly supported. Also considering the presence of marker planktonic foraminiferal species Globoquadrina dehiscens and Sphenolithus delphix from nannoplanktons which are described in marls between Chattian and Burdigalian units it was determined that these marls most probably indicated Aquitanian age.

1. Introduction

Malatya Oligo-Miocene basin is located in Eastern Anatolia Region around the town of Akçadağ at the junction point of Tauride-Anatolide platform (W Malatya) and is surrounded by towns of Doğanşehir in south, Hekimhan in north, Darende in northwest, Yazıhan in northeast and by Yeşilyurt in southeast (Figure 1). Marine sediments observed in and around the study area were deposited between Jurassic-Middle Miocene times (Figure 2). In this study, Oligocene and Lower Miocene units were investigated in detail; however Eocene-pre Eocene basement rocks and post Miocene young units were excluded from the scope of study (Figure 3). Middle Triassic-Cretaceous, Jurassic-Cretaceous and Upper Senonian neritic limestones, Mesozoic ophiolites, Late Cretaceous-Paleocene clastic and carbonate rocks, Early-Middle Eocene terrigenous clastic and sedimentary deposits consisting of Middle-Late Eocene neritic limestones, clastic and carbonate rocks form pre Oligo-Miocene basement geological units in the region. As for the younger sediments deposited which outcrop in the vicinity of the study area are composed of Late Miocene-Pliocene terrigenous clastic and pyroclastic rocks, Pliocene and Plio-Quaternary terrigenous sediments, alluvial fan, debris and young alluvial deposits. Detailed information about basement units and young deposits can be obtained from studies of Ayan (1961), Akkuş (1971), Yoldaş (1972), Kurtman (1978), Örçen (1986), Karaman et al. (1993) and Alkan (1997).

Muratlı and Petekkaya formations in which benthic foraminiferal fauna is rich among Oligo-Miocene units in the region were studied in detail and four stratigraphic sections were measured namely the Edilme (SW Akçadağ), Kuzkaya (W Akçadağ), Develi (W Akçadağ) and Karamağara (NE Akçadağ) measured stratigraphical sections (Gedik, 2010). In this study, systematic characteristics of benthic foraminiferal fauna were explained and all

* *Corresponding author: Fatma GEDİK, fatmagedik@yahoo.com*

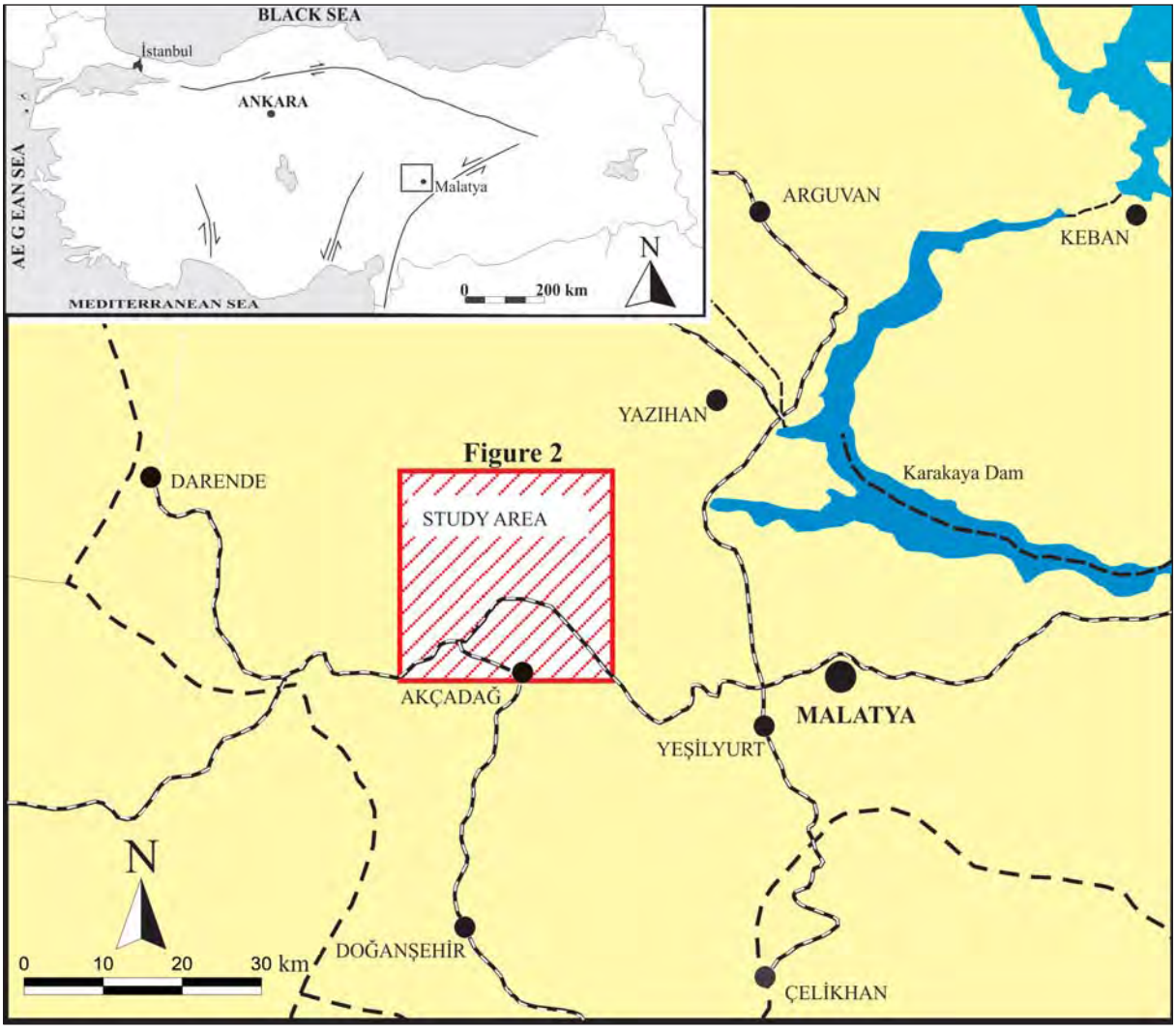

Figure 1- Location map of the study area.

stratigraphic sections were correlated by means of their stratigraphical ranges (Figure 4).

All thin sections of the foraminiferal species described and figured in this paper are deposited in the collection of General Directorate of Mineral Research and Exploration, Ankara, Turkey, under the numbers shown in Plates 1-13.

2. Systematic Paleontology

With this study, 28 taxa obtained from benthic foraminifers of Oligocene Muratlı and Lower Miocene Petekkaya formations were defined and their stratigraphic ranges were given. The author followed the systematic classification of Loeblich and Tappan (1987). Also, the systematic classification of the miogypsinid genera was based upon the taxonomy of Sirel and Gedik (2011).

Group: Protozoa Goldfuss, 1817

Sub Group: Sarcodina Schamarda, 1871

Class: Rhizopodea Von Siebold, 1845

Order: Foraminiferida Eichwald, 1830

Sub Order: Miliolina Delage and Herouard, 1896

Family: Soritidae Ehrenberg, 1839

Sub Family: Archaiasinae Cushman, 1927

Genus: *Archaias* de Montfort, 1808

Type Species: *Nautilus angulatus* Fichtel and Moll, 1798

Archaias kirkukensis Henson, 1950

(Plate 1, Figure 1-15)

1950 *Archaias kirkukensis* Henson, p. 43, plate 7, figures 3, 4, 9; plate 8, figures 1-5.

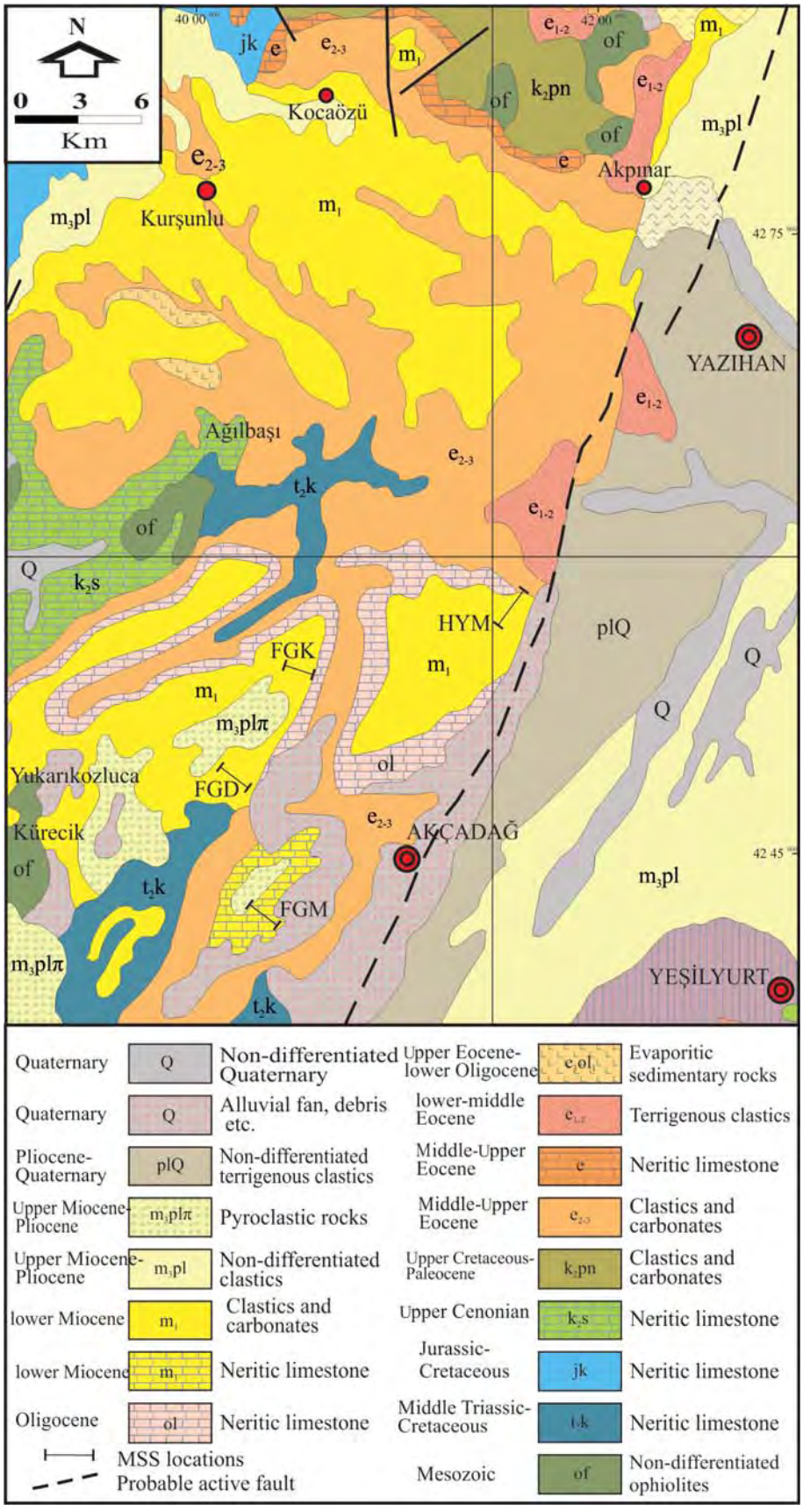

Figure 2- Geological map of the study area (MTA, 2002).

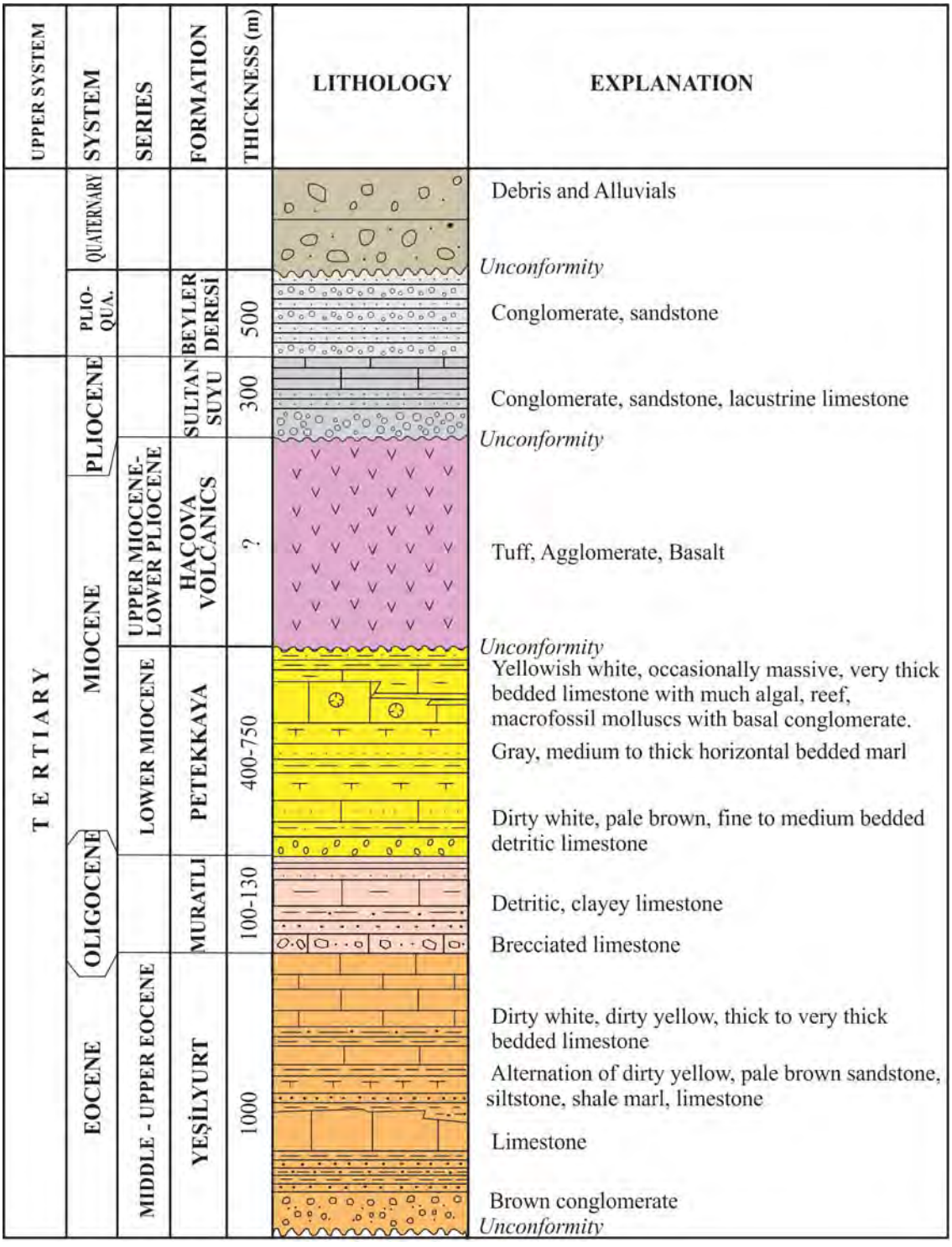

Figure 3- Generalized stratigraphical section of the study area (taken from Karaman et al., 1993).

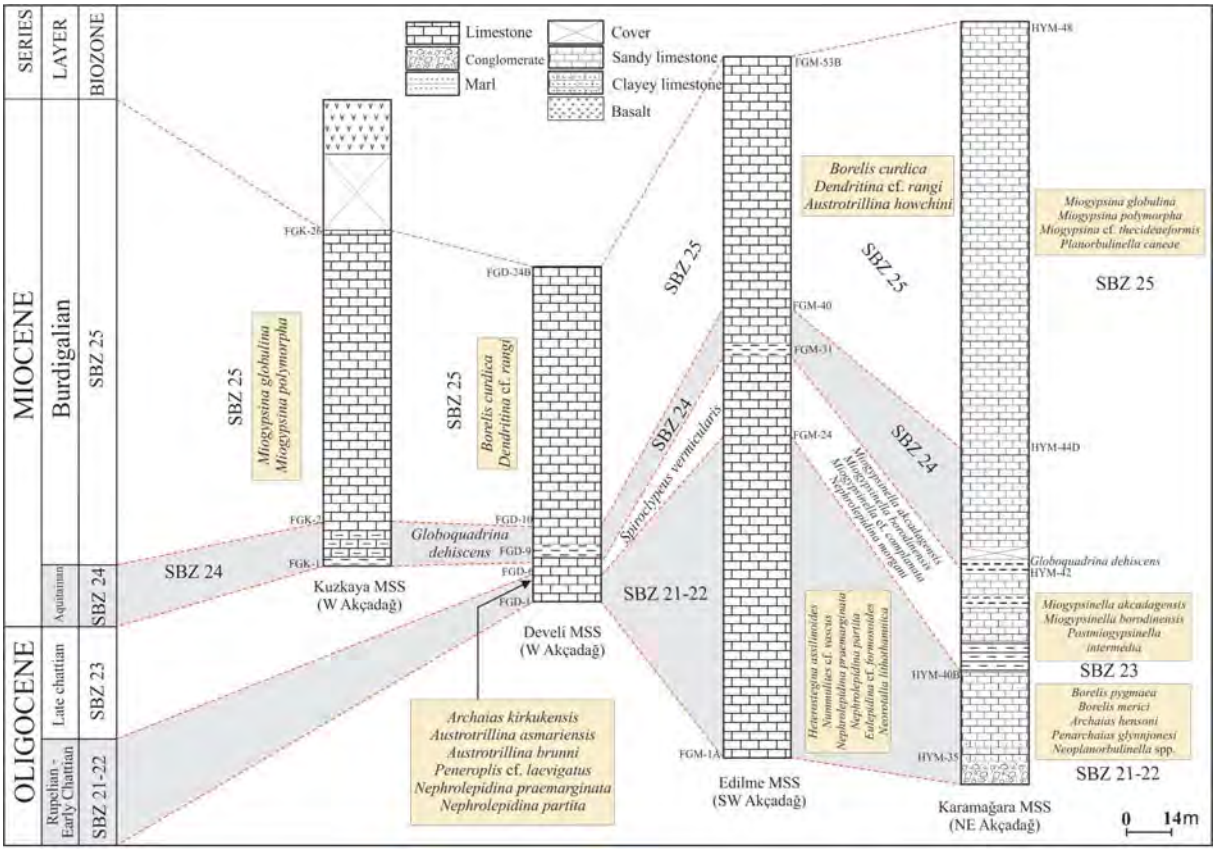

Figure 4-Lithological and biostratigraphical correlation tables of measured stratigraphical sections in the study area.

2013 *Archaias kirkukensis* Henson, Sirel et al., p. 103, plate 9, figures 1-8; plate 10, figures 14; plate 11, figures 1).

Description: The test is discoidal with slightly rounded periphery. The largest shell diameter reaches 3.9 mm in the megalospheric generations. Spheric megalosphere (its diameter 0.13-0.22 mm) followed by undivided planispiral-involute early chambers. The adult chambers are cyclical and evolute dividing by the interseptal pillars. The apertures of the early chambers are areal slits but in the cyclical chambers apertures consist of rows of openings.

Stratigraphic range: Rupelian-Early Chattian in Develi measured section.

Archaias hensoni Smout and Eames, 1958

(Plate 2, Figures 1-6)

1958 *Archaias hensoni* sp. nov., Smout and Eames, p. 219-220, plate 40, figures, 16-20; plate 41, figures 1-5, 21, 26, 28-29.

2007 *Archaias hensoni* Smout and Eames, Bassi et al., plate 2, figures 1-16.

Description: Only megalospheric form is observed. The specimens are characterized by their comparatively small size. The diameter of the test ranges from 1,05 to 3,05 mm and the central thickness 0,36 to 0,52 mm respectively. Spheric megalosphere (its diameter 0,16 - 0,22 mm) followed by undivided planispiral-involute early chambers. The adult chambers are cyclical and evolute dividing by the interseptal pillars. The apertures of the early chambers are areal slits but in the cyclical chambers apertures consist of rows of openings.

Stratigraphic range: Rupelian-Early Chattian in Karamağara measured stratigraphic section.

Genus: *Penarchaias* Hottinger, 2007

Type Species: *Peneroplis glynnjonesi* Henson, 1950

Penarchaias glynnjonesi (Henson, 1950)

(Plate 2, Figures 7-9)

1950 *Peneroplis glynnjonesi* Henson, p. 35, plate 9, figures 8-9.

2004 *Peneroplis* aff. *glynnjonesi* Henson, Sirel, p. 36, plate 35, figures 2, 3, 5, 10.

2007 *Penarchaias glynnjonesi* (Henson), Hottinger, p. 11-12, plate 1, figure 3; plate 6, figures 2, 10; plate 7, figures 7, 8; plate 8, figures 6, 10; plate 9, figures 6; plate 12, figures 2; plate 13, figures 3; plate 14, figures 13; plate 15, figures 1-5, 9.

Description: Only megalospheric form is observed. Test lenticular, its diameter 0,9 mm early stage, the diameter and the thickness of the test ranges from 1,31 to 1,36 mm and 0,47 to 0,52 mm respectively. Spheric megalosphere followed by planispiral early chambers and later chambers becoming uniserial (plate 2, figures 7, 9). Interior skeletal apertures are observed on the septum (Hottinger 2007; plate 7, figures 7, 9). Apertures which are one of the most important characteristics of the genus are observed in plate 2 and figures 7, 9.

Stratigraphic range: Rupelian-Early Chattian in Karamağara measured section.

Family: Peneroplidae Schultze, 1854

Genus: *Dendritina* d'Orbigny, 1826

Type Species *Dendritina arbuscula* d'Orbigny, 1826

Dendritina cf. *rangi* d'Orbigny, 1904 in Fornasini

(Plate 9, Figures 6-8)

1904 *Dendritina* cf. *rangi* d'Orbigny, in Fornasini, plate 1, figures 13, 13a.

1950 *Dendritina* cf. *rangi* d'Orbigny, Henson, p. 31, plate 5, figure 2; plate 6, figures 2-3, plate 10, figure 3.

1963 *Dendritina* cf. *rangi* d'Orbigny, Hottinger, p. 970, plate 4, figures 1, 2.

1976 *Dendritina* cf. *rangi* d'Orbigny, Bignot and Guernet, p. 17, plate 1, figures 2-4.

Description: Test is planispiral and involute, its diameter 1.4 mm and the thickness 0.45 mm in megalospheric form. Chambers are simple and not subdivided. The diameter of the large megalosphere is 0.065 mm. It is characterized by dendritic type aperture.

Stratigraphic range: Burdigalian in Develi measured section.

Genus: *Peneroplis* de Montfort, 1808

Type Species *Nautilus planatus* Fichtel and Moll, 1798

Peneroplis cf. *laevigatus* d'Orbigny in Fornasini, 1904

(Plate 3, Figures 2, 3)

1904 *Peneroplis* cf. *laevigatus* d'Orbigny in Fornasini, plate 1, figures 15, 15a.

1963 *Peneroplis* cf. *laevigatus* d'Orbigny in Fornasini, Hottinger, p. 968, plate 3, figures 9-10.

Description: Test is flabelliform, its diameter 1.4-1.5 mm. The protoconch is followed by $1^{1/2}$ planispiral-involute whorls, later chambers flaring and arranged in peneropline and flabelliform (plate 3, figure 3). The connection between the chambers is provided by numerous foramen (plate 3, figure 2).

Stratigraphic range: Rupelian-Early Chattian in Develi measured section.

Family: Austrotrillinidae Loeblich and Tappan, 1986

Genus *Austrotrillina* Parr, 1942

Type Species: *Trillina howchini* Schlumberger, 1893

Austrotrillina asmariensis Adams, 1968

(Plate 3, Figure 25; Plate 4, Figures 1-13)

1947 *Trillina howchini* Schlumberger, Bursch, p. 12, plate 1, figures 1, 2, 9, 13, 14.

1962 *Austrotrillina howchini* (Schlumberger), Dizer, plate 3, figure 7.

1968 *Austrotrillina asmariensis* Adams, p. 82, plate 1, figures 1-12.

1996 *Austrotrillina howchini* (Schlumberger), Sirel, p. 171, figures 11, 13-15.

2003 *Austrotrillina asmariensis* Adams, Sirel, p. 294, plate 9, figures 1-15.

Description: Megalospheric form: Test is porcelain calcareous. Large test is triangular with bluntly rounded margin in transverse and ovate in the longitudinal sections. The lenght of the test ranges from 1,2 to 1,8 mm and the width from 0,9 to 1,1 mm. Very large, spherical proloculus (its diameter varies between 0,1and 0,2 mm; plate 4, figures 3, 6, 8, 10, 12) is followed by the early chambers arranged in triloculine. Outer wall of the chambers consisting simple, thick subepidermal partitions arranged closely.

Microspheric form: This form has a large elongated ovate test in transverse sections (plate 4,

figure1). The lenght of the test ranges from 1,6 to 2,5 mm and the width from 1,1 to 1,3 mm. Very small (diameter could not be measured), spherical microsphere is followed by the early chambers arranged in quinqueloculine mode, later chambers arranged in triloculine pattern (plate 4, figure 1). Outer wall of the chambers consist of two order of thick subepidermal partitions forming alveolar subepidermal network (plate 4, figures 2, 4, 9, 12).

Stratigraphical range: Rupelian-Early Chattian in Develi measured section, Late Chattian in Edilme measured section.

Austrotrillina brunni Marie, 1955

(Plate 3, Figures 5, 12-16, 18-22)

1955 *Austrotrillina brunni* Marie, p. 203, plate 9, figures 4-8.

1968 *Austrotrillina brunni* Marie, Adams, p. 85, plate 6, figures 6, 8.

2003 *Austrotrillina brunni* Marie, Sirel, p. 294, plate 10, figures 10-16.

Description: Megalospheric form: The test is small and the peripheral margin is rounded in transverse sections (plate 3, figure 21). The lenght of the test ranges from 0,62 to 0,75 mm and the width from 0,39 to 0,49 mm. The spheric megalosphere (0,11-0,19 mm in diameter) is followed by small individed chambers arranged in triloculine mode. Later adult chambers with fine subepidermal partitions are also lined up in triloculine pattern. Two types of subepidermal partitions form small alveolar compartments.

Microspheric form: The small test is triangular with rounded margin in transverse sections. The lenght of this species unknown, the width of the test 0,8 mm. Very small, spherical microsphere is followed by the early chambers arranged in quinqueloculine mode, later chambers arranged in triloculine pattern (plate 3, figure 15).

Stratigraphical range: Rupelian-Early Chattian in Develi and Karamağara measured sections and Late Chattian in Edilme measured section.

Austrotrillina howchini (Schlumberger, 1893)
(Plate 3, Figures 17, 23, 24)

1893 *Trillina howchini* Schlumberger, p. 119-120, plate 3, figure 6.

1968 *Austrotrillina howchini* (Schlumberger), Adams, plate 2, figures 1-7; plate 6, figures 1-5, 7.

Description: Only megalospheric form is observed. Test has a diameter of 0.82 mm and a width of 0.52 mm in longitudinal section; however it has a diameter of 0.65 mm and a width of 0.55 mm in transverse section. The diameter of the spherical microsphere which cannot be well observed could not be measured. Spherical microsphere is followed by the early chambers arranged in triloculine mode. Subepidermal partitions show thick and complex structure.

Stratigraphical range: Burdigalian in Edilme measured section.

Family: Alveolinidae Ehrenberg, 1839

Genus: *Borelis* de Montfort, 1808

Type Species: *Nautilus melo* Fichtel and Moll, 1798

Borelis curdica (Reichel, 1937)

(Plate 5, Figures 1-28)

1937 *Neoalveolina melo curdica* n. ssp., Reichel, p. 108, plate 10, figures 4-7.

1966 *Borelis melo curdica* (Reichel), Reiss and Gvirtzman, plate 1, figure 8; plate 2, figure 1.

1976 *Borelis curdica* (Reichel), Bignot and Guernet, p. 19, plate 2, figures 1-10.

Description: Test is spheric to subspheric and is mainly nautiloid in shape. The diameter and width of test in which megalosphericand microspheric forms cannot be well differentiated vary between 0.29-0.85 mm and 0.32-0.82 mm, respectively. Elongation index (the ratio of axial diameter to equatorial diameter) ranges between 0.79-1.14. Diameter of the proloculus could not be measured in any of the forms. Preseptal canal in equatorial sections (plate 5, figure 1), uniserial aperture in subaxial sections (plate 5, figure 5) and fully ordered spine knob chambers in tangential sections are definite (plate 5, figures 10, 13).

Stratigraphical range: Burdigalian in Develi, Edilme and Kuzkaya measured section.

Borelis pygmaea (Hanzawa, 1930)

(Plate 3, Figure 11)

1930 *Borelis* (*Fasciolites*) *pygmaea* Hanzawa, p. 94, plate 26, figures 14, 15.

1932 *Neoalveolina pygmaea* (Hanzawa), Bakx, p. 237, plate 3, figures 18, 19.

1947 *Neoalveolina pygmaea* (Hanzawa), Bursch, p. 28, plate 1, figures 11, 15, 19.

1965 *Neoalveolina pygmaea* (Hanzawa), Adams, p. 25 a-c.

2003 *Borelis pygmaea* (Hanzawa), Sirel, p. 298, plate 11, figures 1-7.

Description: The specimens of the megalospheric form have a medium size, fusiform with axial diameter of 2.10 mm and equatorial diameter of 0.68mm at the 6^{th} whorls. Index of elongation is 3.05 mm. The small spherical megalosphere (its diameter is 0.65 mm; (plate 3, figure 11) is followed by tightly coiled four or five oval shape and it's both axial and equatorial thickenings are rigorous. However, the chambers in adult stage were arranged in fusiform. Chambers are much rigorous in equatorial region but loose in axial region. Therefore, the axial thickening is abundant in adult stage such that it reaches 4-5 times more than the size of chambers. Nevertheless, this thickening decreases during last two rounds compared to previous whorls. Lobes are closely arranged and mainly spheroidal. Lobes in last three whorls exhibit an oval shaped structure towards upper parts.

Stratigraphic range: Rupelian-Early Chattian in Karamağara measured section.

Borelis merici Sirel and Gündüz, 1981

(Plate 3, Figures 8-10)

1981 *Borelis merici* Sirel and Gündüz, p. 73-74, plate 1, figures 9-13.

2003 *Borelis merici* Sirel and Gündüz, Sirel, p. 299, plate 11, figures 8, 9.

Description: Test is slightly elongated oval with an axial diameter of 1.01-1.41 mm and equatorial diameter of 0.45-0.78 mm. Index of elongation is 1.79-2.71 mm. There is not any axial thickening along 5 whorls after the proloculus. Therefore, the shape of the test at this stage is ovoid. Axial thickening slightly increases in last 4 whorls. Therefore, test is elongated and oval in adult stage. Diamorphism is indefinite.

Stratigraphical range: Rupelian-early Chattian in Karamağara measured section.

Suborder: Rotaliina Delage and Herouard, 1896

Family: Planorbulinidae Schwager, 1877

Genus: *Planorbulina* d'Orbigny, 1826

Type Species: *Planorbulina mediterranensis* d'Orbigny, 1826

Planorbulina brönnimanni Bignot and Decrouez, 1982

(Plate 2, Figures 10-22)

1982 *Planorbulina brönnimanni* Bignot and Decrouez, p. 144, plate 1, figures 1-9; plate 2, figures 1-5; plate 3, figures 1-3; plate 4, figures 1-6, plate 5, figures 1-9; plate 6, figures 1-8.

1993 *Planorbulina brönnimanni* Bignot and Decrouez, Sirel and Acar, p. 181, 183, plate 2, figure 21.

Description: Test discoidal with calcareous wall and its diameter varies in between 0.55-1.89 mm. It is diamorphic and there are chambers in megalospheric forms with trochospiral whorls after the proloculus (plate 2, figures 10, 12, 13, 16, 20). The following chambers are irregularly arranged in different sizes. As it was clearly seen in well oriented sections, the connection between chambers is provided by base stolons (plate 2, figures 10, 12, 13, 14, 15, 21).

Stratigraphical range: Early-Late Chattian in Develi measured section and Rupelian-Early Chattian in Karamağara and Edilme measured section.

Genus: *Neoplanorbulinella* Matsumaru, 1976

Type Species: *Neoplanorbulinella saipanensis* Matsumaru, 1976

Neoplanorbulinella spp.

(Plate 2, Figures 23-30)

Description: The diamorphism is observed in these forms as test size and embryonic chambers are different. Test form ranges from low conical to very high conical; the spiral side is strongly convex however the umbilical side is concave. The base diameter and height of the cone range between 0.5-1.1 mm and 0.4-0.8 mm, respectively. Spiral angle shows variation between 90°-140°. The first and second chambers are located at top of the cone and are spherical. Diameters of the first and second chambers vary between 0.07-0.09 mm and 0.03-0.07 mm, respectively. Equatorial chambers which follow embryonic chambers are regularly arranged on margin of the cone in external skeletal, and their

diameters are in the form of arch gradually growing towards the bottom of cone. The diameter of umbilical pore ranges between 0.2-0.8 mm, and this pore is filled by numerous lateral chambers.

Stratigraphical range: Rupelian-Early Chattian in Karamağara measured section.

Genus: *Planorbulinella* Cushman, 1927

Type Species: *Planorbulina vulgaris* d'Orbigny var. *larvata* Parker and Jones, 1865

Planorbulinella caneae Freudenthal, 1969

(Plate 9, Figure 9)

Description: Description was based into one equatorial section. Test is small discoidal and has a diameter of 1.2 mm. Chambers are trochospirally coiled in early stage. Later chambers developed in the form of circular series, and the connection between chambers is provided by stolons.

Stratigraphical range: Burdigalian in Karamağara measured section.

Family: Lepidocyclinidae Scheffen, 1932

Genus: *Nephrolepidina* Douvillé, 1911

Type Species *Nummulites marginata* Michelotti, 1841

Nephrolepidina praemarginata Douvillé, 1908

(Plate 6, Figures 1-14)

1908 *Lepidocyclina praemarginata* Douvillé**,** p. 91 - 92, figures 1, 2, 4a.

2003 *Nephrolepidina praemarginata* (Douvillé), Sirel, p. 302, plate 4, figures 1 - 13.

Description: The small test is inflated lenticular with central umbo, so that the shell is getting thicker towards the center (plate 6, figures 7, 10, 12). The diameter of the test ranges from 1.6 to 3.2 mm and the thickness from 0.7-1.3 mm. The large, central umbo consists of numerous small pustules. This feature is well observed neither in external side nor in axial-transversal sections (plate 6, figures 5, 7, 9, 11). Lateral chambers are numerous at the surface of test and are rosette shaped, and this feature forms comb view at the surface (plate 6, figures 11, 12). The embryo consists of hemisphere small protoconch (its diameter is 0.06-0.3 mm) and reniform deuteroconch (its diameter is 0.1-0.4 mm). Secondary chambers are very small and their sizes are almost equal to each other. The equatorial chambers are subrectangular or rhombic in outline. There are 6-7 orders of lateral chambers in the center of the test.

Stratigraphical range: Rupelian-Early Chattian in Develi and Edilme measured section.

Nephrolepidina partita Douvillé, 1924

(Plate 7, Figure 1-9)

1924 *Nephrolepidina partita* Douvillé, p. 76, plate 6, figures 1- 4.

2003 *Nephrolepidina partita* Douvillé, Sirel, p. 302, plate 5, figures 1-10.

Description: The description was based on axial sections and on one equatorial section which belong to limited megalospheric forms. The small test is lenticular with central umbo with large pustules, so that the shell of this species is getting thicker toward the center (plate 7, figure 1-4, 5-8). The diameter of the test ranges from 1.1 to 2.4 mm and the thickness from 0.7 to 1.2 mm. The embryo consists of small protoconch (its diameter is 0.1 mm) and large reniform deuteroconch (its diameter is 0.2 mm). The equatorial chambers are rectangular in outline.

Stratigraphic range: Rupelian-Early Chattian in Develi and Edilme measured section.

Nephrolepidina morgani (Lemoine and Douvillé, 1904)

(Plate 7, Figures 12, 13)

1904 *Lepidocyclina morgani* Lemoine and Douvillé**,** p. 5-41, plate 1, figures 12, 15, 17; plate 2, figures 4, 12; plate 3, figure 2.

1924 *Nephrolepidina morgani* (Lemoine and Douvillé), Douvillé**,** p. 80.

1929 *Nephrolepidina morgani* (Lemoine and Douvillé), Gomez Llueca, p. 1-400, plate 33, figures 29, 32.

1991 *Lepidocyclina* (*Nephrolepidina*) *morgani* (Lemoine and Douvillé), Less, p. 445-446, plate 7, figures 1-6; plate 8, figures 1-6; plate 9, figures 1-2.

2003 *Nephrolepidina morgani* (Lemoine and Douvillé), Sirel, p. 303, plate 5, figures 11-16; plate 6, figures 1-7.

Description: The test is inflated lenticular with numerous central pustules, so that the shell of this species is getting thicker towards the center. The diameter of the shell ranges from 1.08 to 2.94 mm and

the thickness from 0.35 to 1.05 mm. The embryo consists of small spherical protoconch (its diameter is 0.2 mm) and large semilunar deuteroconch (its diameter is 0.3 mm; plate 7, figure 13). The equatorial chambers are rhomboidal in shape.

Stratigraphical range: Late Chattian in Edilme measured section.

Eulepidina cf. *formosoides* Douvillé, 1924

(Plate 7, Figures 10, 11)

1924 *Eulepidina formosoides* Douvillé, p. 71, plate 3, figures 2- 4.

1967 *Eulepidina formosoides* Douvillé, Poignant, p. 208, plate 5, figures 9, 11; plate 6, figures 1, 6.

1975 *Eulepidina favosa* Cushman, Sirel et al., p. 179, plate 4, figures 2, 3.

1975 *Eulepidina dilatata* Michelotti, Sirel et al., p. 179, plate 4, figures 1.

2003 *Eulepidina formosoides* Douvillé, Sirel, p. 272, figure 2.

Description: The test is lenticular with large umbo, so that the shell is getting thicker towards the center. The diameter of the test ranges from 4.6 to 5.2 mm. Embryonic apparatus consists of small protoconch (its diameter is 0.4-1.08 mm) and large sub spheric deuteroconch (its diameter is 0.8-1.7 mm). The equatorial chambers are polygonal in shape.

Stratigraphical range: Rupelian-Early Chattian in Develi and Edilme measured section.

Family: Miogypsinidae Vaughan, 1928

Genus: *Miogypsinella* Hanzawa, 1940

Type Species: *Miogypsinella borodinensis* Hanzawa, 1940

Miogypsinella akcadagensis (Gedik and Sirel), 2009

(Plate 8, Figures 1-3)

2009 *Miogypsinoides akcadagensis* n. sp., Gedik and Sirel, p. 35-43, plate 1, figures 1-7.

2011 *Miogypsinella akcadagensis* (Gedik and Sirel), Sirel and Gedik, p. 591-603, plate 2, figures 1-5.

Description: The equatorial (plate 8, figures 1, 2) and axial sections (plate 8, figure 3) clearly show that the general shape of the test is fan-like with rather thickened apical portion. The test of this species is formed in two periods: the early stage is typical rotaliid manner coiled trochospirally, adult period chambers arranged in miogypsinid pattern. The diameter of the test measured along the apical-frontal line (Amato and Drooger, 1969) ranges from 0.5 to 1.3 mm. The diameter and height in rotallid period are 0.6-1.08 mm and 0.5-0.7 mm, respectively. The embryonic apparatus positioned at the apex of the fan, consisting of spheric protoconch (0,1 mm - 0,2 mm in diameter) and hemispherical deutroconch (0,20 mm - 0,28 mm in diameter), that are followed by 8-10 spiral chambers of the early stage (plate 8, figures 1, 2). The miogypsinid chambers in the adult stage are smaller in comparison with the spiral chambers.

Stratigraphical range: Late Chattian in Edilme and Karamağara measured section.

Miogypsinella borodinensis Tan, 1936

(Plate 8, Figures 4, 5)

1936 *Miogypsinoides* (*Miogypsinoides*) *complanata* (Schlumberger) forma *bantamensis* Tan Sin Hok, plate 1, figure 13.

1940 *Miogypsinoides borodinensis* Hanzawa, p.755-802, plate 39, figures1-9; s.767, figures 2.

1940 *Miogypsinoides bantamensis* Tan, Hanzawa, plate 39, figures 15-19.

1951 *Miogypsinoides bermudezi* Drooger, p. 357-365, figures 4-6; p.358, figures 1a-c, 2a-c, 3a-b.

2007 *Miogypsinoides bantamensis* Tan, Bassi et al., plate 2, figures 18, 19.

2011 *Miogypsinella borodinensis* Hanzawa, Sirel and Gedik, p. 591-603, plate 2, figures 6-8.

Description: The equatorial (plate 8, figure 5) and axial sections (plate 8, figure 4) show that the general shape of the test is fan-like with rather thickened apical portion. The early stage is typical rotaliid manner coiled trochospirally, adult period chambers arranged in miogypsinid pattern. The diameter of the test is ranges from 1,06 mm to 1,63 mm. The diameter and height of the rotaliid stage are 0,6 - 0,8 mm and 0,6 - 0,9 mm respectively. The embryonic apparatus positioned at the apex of the fan, consisting of spheric protoconch (0,1 mm-0,2 mm in diameter) and hemispherical deutroconch (0,15 mm-0,18 mm in diameter), that are followed by 12-14

spiral chambers of the early stage (plate 8, figure 5). The miogypsinid chambers in the adult stage are smaller in comparison with the spiral chambers.

Stratigraphical range: Late Chattian in Edilme and Karamağara measured section.

Miogypsinella cf. *complanata* (Schlumberger, 1900)

(Plate 9, Figures 4, 5)

1900 *Miogypsina complanata* Schlumberger, p. 330, plate 2, figures 13-16; plate 3, figures 18-21.

1937 *Miogypsina* (*Miogypsinoides*) *complanata* (Schlumberger), Barker and Grimsdale, p. 161-178, plate 5, figures 6; plate 6, figures 1-6; plate 7, figures 1; plate 8, figures 6.

1957 *Miogypsinoides complanatus* (Schlumberger), Cole, p. 318, 319, plate 25, figures 1, 2.

2003 *Miogypsinoides complanatus* (Schlumberger), Sirel, p. 301, plate15, figures 1-16.

2011 *Miogypsinella* cf. *complanata* (Schlumberger), Sirel and Gedik, p. 591-603, plate 3, figures 1-3.

Description: Though several samples were prepared, no equatorial sections were obtained therefore; the description was made based only on axial sections. Chambers were arranged in typical rotaliid order in early stage and in miogypsinid model in adult stage. The diameter and thickness were measured as between 1.60-2.01 mm and as 0.59 mm, respectively. The diameter and height in rotaliid stage are 0.63-0.83 mm and 0.45-0.61 mm, respectively. The diameter of the spherical shaped first chamber varies between 0.15-0.21 mm. Embryonic chambers in early stage are followed by minimum 16 spiral chambers. However, this feature was not figured out in this study as it did not have any equatorial section. It was seen that miogypsinid chambers in adult stage were bigger and closer to each other when compared with spiral chambers.

Stratigraphical range: Late Chattian in Edilme measured section.

Genus: *Postmiogypsinella* Sirel and Gedik, 2011

Type Species: *Postmiogypsinella intermedia* Sirel and Gedik, 2011

Postmiogypsinella intermedia Sirel and Gedik, 2011

(Plate 8, Figures 6-10)

2011 *Postmiogypsinella intermedia* n.gen., n. sp., Sirel and Gedik, p. 591-603, plate 1, figures 1-12.

Description: Test is fan-like, small sized and hyaline calcareous. The diameter of the test measured along the apical-frontal line (Amato and Drooger, 1969) and ranges from 0.7 to 1.18 mm. Diameter and height in rotaliid stage range between 0.4-0.5 mm and 0.3-0.5 mm, respectively. The first chamber is spherical and surrounded by a thick wall. Its diameter was measured as 0.06-0.1 mm. The second chamber is hemispherical and has a diameter of 0.1 mm. There are around 10-11 spiral chambers of rotaliid period after the first chamber. Later chambers are ordered in the form of miogypsinid model, and are in arch shaped. Approximately, pent serial of chambers arranged in miogypsinid order is observed.

Stratigraphical range: Late Chattian in Karamağara measured section.

Genus: *Miogypsina* Sacco, 1893

Type Species: *Nummulites globulina* Michelotti, 1841

Miogypsina globulina (Michelotti, 1841)

(Plate 10, Figures 1-7)

1841 *Nummulites globulina* Michelotti, p. 297, plate 3, figure 6.

1952 *Miogypsina irregularis* (Michelotti) in Drooger, p. 54, plate 2, figures 25-29.

1959 *Miogypsina globulina* (Michelotti) in Drooger and Socin, plate 1, figure 5.

1974 *Miogypsina* (*Miogypsina*) *globulina* (Michelotti) in Raju, p. 82-83, plate 2, figures 1-4; plate 5, figures 6, 7; plate 6, figure 1.

2009 *Miogypsina globulina* (Michelotti), Özcan and Less, p. 33, plate 1, figures 24-25; plate 2, figure 6.

Description: Test is in the form of enlarging fan and there are radiating pillars on either side. Traces of these pillars are observed as granules at the upper surface. Granules are clearly observed in equatorial and axial sections (plate 10, figures 1, 3, 5, 6, 7). The diameter of the test measured along apical-frontal line and ranges from 0.35 to 2 mm (Amato and Drooger, 1969), and the width is around 0.3-0.6 mm. Chambers were arranged in short spiral order in early stage and as miogypsinid model in adult stage. Embryonic

chambers are located at top of the test, and are made up of spherical first chamber and hemispherical second chamber. Diameters of the first and second chambers were measured as 0.06-0.33 mm and 0.1-0.26 mm, respectively. Chambers in miogypsinid pattern in equatorial sections were observed in spatula shape.

Stratigraphical range: Burdigalian in Karamağara and Kuzkaya measured section.

Miogypsina polymorpha (Rutten, 1912)

(Plate 11, Figures 1-4)

1912 *Miogypsina polymorpha* Rutten, p. 201-217, plate 12, figures 6-9.

Description: Test is typical with its variable shapes. The upper part is generally thick in axial sections and thins out towards frontal region. The test with this structure exhibits an appearance of resembling to frog larva. The diameter of the test measured along apical-frontal line (Amato and Drooger, 1969). Diameter and thickness range between 1.3-4.3 mm and 0.4-1 mm, respectively. The first chamber is spherical and located at a point close to the top part of test. Its diameter is 0.1-0.2 mm. Pre-embryonic chambers which follow the first chamber are variable in size and different shapes, though spherical in general (plate 11, figures 1, 3, 4). Equatorial chambers are typical and polygonal (Rutten 1912, plate 11, figure 4). Granules are observed on both sides of test though not very clear.

Stratigraphical range: Burdigalian in Karamağara and Kuzkaya measured section.

Miogypsina cf. *thecideaeformis* (Rutten, 1912)

(Plate 9, Figures 1, 2)

1912 *Miogypsina thecideaeformis* Rutten, p. 201-217, plate 12, figures 1, 4-5.

Description: The test is inflated lenticular. Embryonic chambers are generally located at top of the symmetrical test, and equatorial chamber divides the test into two equal parts. The first chamber is spherical and has a diameter of 0.16 mm. The second chamber is hemispherical and is almost as big as the first chamber. Equatorial chambers are arranged as decreasing in size starting from one pole of the test to the other pole. Lateral chambers which are observed on both sides of test are in different shapes, though rectangular in general. Lateral chamber series were separated by pillars.

Stratigraphical range: Burdigalian in Karamağara measured section.

Family: Rotaliidae Ehrenberg, 1839

Genus: *Neorotalia* Bermudez, 1952

Type Species: *Rotalia mexicana* Nuttall, 1928

Neorotalia lithothamnica Uhlig, 1886

(Plate 12, Figures 1-8)

1886 *Rotalia lithothamnica* Uhlig, Bd. 36, p. 195.

1991 *Pararotalia lithothamnica* (Uhlig), Cahuzac and Poignant, p. 69-78, plate 2, figures 1-6, 9, 10.

1998 *a, b Neorotalia lithothamnica* (Uhlig), Cahuzac and Poignant, p. 155-169.

2003 *Neorotalia lithothamnica* Uhlig, Sirel, p. 304, plate 8, figures 1-5.

Description: The test is small, plano-convex to biconvex; occasionally the ventral side is more convex than dorsal side. The diameter of the test ranges from 1.16 to 2.06 mm and the thickness from 0.5 to1.3 mm. The edge of test is sharp and last 4-5 chambers have short spines (plate 12, figures 1, 4, 6). The sutures are radiate but depressed on the ventral side. The ornamentation is distinct on the umbilical edge side when compared the spiral side (plate 12, figures 2, 3). The large solid umbilical plug is observed at the center of the ventral side.

Stratigraphical range: Rupelian-Early Chattian in Develi and Edilme measured section.

Family: Nummulitidae de Blainville, 1827

Genus: *Spiroclypeus* Douvillé, 1905

Type Species: *Spiroclypeus orbitoideus* Douvillé, 1905

Spiroclypeus vermicularis Tan, 1937

(Plate 13, Figures 1, 2, 5)

1937 *Spiroclypeus vermicularis* Tan, p. 187, plate 1, figures 7, 8; plate 4, figures 15, 16.

Description: Description was based on megalospheric forms. The central part of the test is inflated lenticular structure which thins out towards sides. Thickness is 1 mm at the center and 0.4 mm on edges. The diameter of the test ranges from 2.4 to 3.06 mm. The first chamber is spherical and has a diameter of 0.33 mm. Semicircular chambers starting

from the first chamber towards last whorl almost fill out spiral interval which gradually thickens. These chambers are divided into several chamberlets in rectangle/rectangle like shapes. There are few pillars which spread out from first chamber.

Stratigraphical range: Late Chattian in Develi measured section.

Spiroclypeus sp.

(Plate 13, Figures 3, 4, 6, 7)

Description: Description was made on equatorial section belonging to only one megalospheric form. The test is lenticular and has a diameter of 1.9 mm. The first chamber is large and spherical (its diameter is 0.2 mm). Semicircular chambers starting from the first chamber towards last whorl almost fill out spir interval which gradually thickens. These chambers were divided into several chamberlets in rectangle/rectangle like shapes. Chamberlets in early stage are small rectangular but in adult stage they become rectangles of which its height is larger than width.

Stratigraphical range: Late Chattian in Develi measured section.

Genus: *Heterostegina* d'Orbigny, 1826

Type Species: *Heterostegina depressa* d'Orbigny, 1826

Heterostegina assilinoides Blanckenhorn, 1890 emend. Henson, 1937

(Plate 13, Figures 8-10, 12-15)

1890 *Heterostegina assilinoides* n. sp., Blanckenhorn, p. 342, plate 17, figure 5.

1937 *Heterostegina assilinoides* Blanckenhorn emend. Henson, p. 48. plate 4, figures 1 - 5; plate 6, figure 2.

1966 *Grzybowskia assilinoides* (Blanckenhorn), Butt, p. 93 - 94, plate 8, figures 24 - 26.

1977 *Heterostegina assilinoides* Blanckenhorn emend. Henson, Hottinger, figure 47 A-B.

1991 *Heterostegina assilinoides* Blanckenhorn emend. Henson, Less, p. 443, plate 4, figures 4 - 5; plate 5, figures 1 - 2.

Description: The description was made based on megalospheric generations. Test is thin and small. The diameter of the test ranges from 2.5 to 3.6 mm. The test surface is shaped with dense granulation (plate 13, figures 10, 14, 15). Mesh network is not observed at the surface. Equatorial section of the megalospheric form possesses first and second chambers which are medium sized, semi isolepidin in shape (plate 13, figure 12). Septa are dense, high and curved. Secondary septa are mainly observed after 2-4 operculine chambers and reaches until chamber wall. Equatorial section belonging to microspherical form was not observed.

Stratigraphical range: Rupelian-Early Chattian in Edilme measured section.

Genus: *Nummulites* Lamarck, 1851

Type Species: *Camerina laevigata* Bruguiere, 1792

Nummulites cf. *vascus* (Joly and Leymerie, 1848)

(Plate 13, Figures 16-19)

1848 *Nummulites vasca* Joly and Leymerie, p. 38, 67; plate 1, figures 15-17; plate 2, figure 7.

1883 *Nummulites boucheri* de la Harpe, p. 137-156; plate 1, figures 2a, 5a, 6a, 8-10.

1937 *Nummulites boucheri* de la Harpe, Silvestri, p. 45- 264, plate 5, figures 1- 6; plate 2, figures 1, 2; plate 12, figures 1, 5; plate 15, figures 5, 6.

1952 *Nummulites vascus* Joly and Leymerie, Grimsdale, p. 224, plate3.

1961 *Nummulites vascus* Joly and Leymerie, Montanari, p. 570- 579, plate 1, figures 1, 2a-2c.

1962 *Nummulites vascus* Joly and Leymerie, Eames et al., plate 1, figures A.

1975 *Nummulites vascus* Joly and Leymerie, Sirel et al., plate 2, figures 1-3, 5-8.

1981 *Nummulites vascus* Joly and Leymerie, Schaub, p. 123, plate 53, figures 1-6.

2003 *Nummulites vascus* Joly and Leymerie, Sirel, p. 292, plate 2, figures 4, 5.

2008 *Nummulites vascus* Joly and Leymerie, Gedik, p. 36, plate 1, figures 17; plate 2, figures 1-5.

Description: Description was made on axial sections of only megalospheric forms. Test is inflated lenticular with a diameter of 1.5-2.2 mm and a thickness of 0.6-0.7 mm. The first chamber is small,

spherical; however its diameters could not be measured. Spir is rather thick and septa are slightly curved and arranged in order (plate 13, figure 17).

Stratigraphical Range: Rupelian-Early Chattian in Edilme measured section.

3. Results

In the study area, measurements of four stratigraphic sections were made which cover Oligo-Miocene successions, and systematically 182 hard rock samples were taken in these sections. As a result of paleontological studies, 28 taxa belonging to families of Soritidae, Planorbulinidae, Peneroplidae, Austrotrillinidae, Alveolinidae, Lepidocyclinidae, Miogypsinidae and Nummulitidae were described.

Oligo-Miocene transition in the region was observed based on biostratigraphical locations of benthic foraminiferal taxa which were described in Develi, Edilme, Kuzkaya and Karamağara measured stratigraphical sections. Marine units ranging from Oligocene to Miocene which were correlated lithostratigraphically and biostratigraphically exhibit a characteristic of continuous succession in these sections. Paleontological findings do also support this observation.

Stratigraphically; the marls between Chattian and Burdigalian units in the region constitute rich planktik foraminifera and nannoplankton assemblages. The indicative planktonic foraminiferal species *G. dehiscens* which were described in Develi and Karamağara measured sections occurs with *S. delphix*. Besides, marls stratigraphically occur in Late Chattian-Burdigalian shallow marine carbonates which were described in the succession. All these facts point out that the age of these marls with different lithology is most probably Aquitanian.

Cosmopolite species *M. globulina* is observed in Burdigalian shallow marine carbonates in Kuzkaya and Karamağara measured sections, and is described over large geographic regions ranging from Central America to Indo-Pacific and West (Mediterranean) Tethys. The co-occurrence of this species with *M. polymorpha* which is seen in stratigraphical records (only from Indo-Pacific) highly support the assumption of a probable marine connection between Indo-Pacific and Mediterranean Tethys in Burdigalian time in the region (Harzhauser et al., 2002; Reuter et al., 2009, Qom formation, Iran).

Acknowledgement

This article covers one part of the study which was prepared as PhD thesis in Geological Engineering Department of the Institute of Sciences in Ankara University, Ankara, Turkey. The author fully thanks to Dr. Ercüment Sirel (Ankara University) for his support, knowledge and contributions in all stages of this study, to Prof. Yavuz Okan (Ankara University) who supervised this thesis, to Dr. Aynur Hakyemez (MTA) who described planktonic foraminifera and to Ayşegül Aydın (MTA) for nannoplankton determinations.

Received: 14.04.2014
Accepted: 26.08.2014
Published: December 2014

References

Adams, C. G.1965. The Foraminifera and stratigraphy of the Melinau Limestone, Sarawak and its importance in Tertiary correlation. Quart. J. *Geol. London*, 121: 283-338.

Adams, C. G.1968. A revision of the foraminiferal genus Austrotrillina Parr. *Bulletin of the British Museum (Natural History), Geology*, 16: 73-97.

Akkuş, M.F. 1971. Darende-Balaban Havzasının (Malatya, ESE Anadolu) jeolojik ve stratigrafik incelenmesi: *Maden Tetkik ve Arama Genel Müdürlüğü Dergisi*, 76: 1-60, Ankara.

Alkan, H. 1997. Malatya Baseninin Jeolojisi ve Petrol Olanakları. *TPAO Raporu*. 3766, Ankara.

Amato, V., Drooger, C. W. 1969. How to measure the angle in the Miogypsinidae. *Revista Espanola de Micropaleontologia*, I (1): 19-24.

Ayan, T. 1961. Malatya Kuzeyindeki Hekimhan-Ebreme köyü bölgesinin (K39-c3) detay jeolojisi ve petrol imkanları. *Maden Tetkik ve Arama Genel Müdürlüğü Raporu*, 4186, Ankara, (unpublished).

Bakx, L. A. J. 1932. De genere Fasciolites en Neoalveolina in het Indo-Pacifische gebied. *Verhandelingen Geologisch Mijnbouwkundig Genootschap voor Naderland en Kolonien, Geol. Ser*. 9: 205-266.

Barker, R. W., Grimsdale, T. F. 1937. Studies of Mexican fosil foraminifera. *Ann. Mag. Nat. Hist., London, ser*. 10, 19 (110): 161-178.

Bassi, D., Hottinger, L., Nebelsick, James H. 2007. Larger Foraminifera from the upper Oligocene of the Venetian area, North-East Italy, *Palaeontology*, 50 (4): 845-868.

Bermudez, P. J. 1952. Estudio sistematico de los foraminiferos rotaliformes, *Boletin de Geologia*, Venezuela, 2 (4): 1-230.

Bignot, G., Guernet, C. 1976. Sur la présence de Borelis curdica (Reichel) dans le Miocène de I'ile de Kos (Grèce). Géologie méditerranéenne Tome III, 1, pp. 15 á 26.

Bignot, G., Decrouez, D. 1982. Un Planorbulinidae (Foraminiferida) Nouveau Du Priabonian et de l'Oligocene de l'Europe Meridionale et Occidentale, *Revue de Paléobiologie, Genève*, 1 (2): 141-163.

Blainville, H. M. 1827. Manuel de malacologie et de conchyliologie (1825). Paris: F. G. Levrault.

Blanckenhorn, H. 1890. Das Eozan in Syrien mit besonderer Berücksichtigung Nord – Syriens. - Zeitschr. *Deutsch. Geol. Ges*. 63: 318-342.

Bruguière, J. G. 1792. Encyclopédie méthodique. Histoire naturelle des Vers. Tome Premier, A-Cone, Paris: Panckoucke.

Bursch, J. G. 1947. Micropaläontologische Untersuchungen des Tertiärs von Gros Key (Molukken). Mem. Suisse. *Paläontology*, Bâle, 65: 1-69.

Butt, A. 1966. Late Oligocene Foraminifera from Escornebéou, SW France. Thesis, Ed. Schotanus et Jens, Utrecht.

Cahuzac, B., Poignant, A. 1991. Morphologie des espèces de Pararotalia et de Miogypsinoides (Foraminiferida) dans I'Oligocène d'Aquitaine Méridionale. Géobios, 13: 69-78.

Cahuzac, B., Poignant, A. 1998. Larger benthic foraminifera (Neogene). In: Graciansky, P. C. de, J. Hardenbol, T. Jacquin & P. R. Vail (Eds.), Mesozoic-Cenozoic sequence stratigraphy of western European Basins. *Soc. Econ. Paleont. Miner., spec. Publ.,* Tulsa: 1-786.

Cole, W. S. 1957. Larger Foraminifera. In: Geology of Saipan, Mariana Islands. Part 3 - Paleontology. U. S. Geol. Survey, Prof. Paper, Washington, D. C. No: 280-I, pp. 321-360, pl. 112, figs. 1-15; pl. 113, figs. 1-17; pl. 114, figs. 1-20.

Cushman, J. A. 1927. An outline of a re-classification of the foraminifera, Contributions from the Cushman Laboratory for Foraminiferal Research, 3: 1-105.

Delage, Y., Hérouard, E. 1896. Traité de Zoologie Concrète, Vol. 1, La Cellule et les Protozoaires. Paris: Schleicher Frères.

Dizer, A. 1962. Foraminifera of the Miocene of the Sivas Basin (Turkey). Revue de la Faculté des Sciences de l'Université d'Istanbul. (B), 27: 49-85.

Douvillé, H. 1905. Les foraminifères dans le Tertiaire de Bornéo, *Bulletin de la Société Géologique de France, sér*. 4, 5: 435-464.

Douvillé, H. 1908. Observations sur les faunes à foraminifères du sommet du nummulitique Italien. *Bulletin de la Société Géologique de France, ser*. 4, 8: 88-95.

Douvillé, H. 1911. Les foraminifères dans le Tertiaire des Philippines, *Philippine Journal of Science,* Manila 6 (D): 53-80.

Douvillé, H. 1924 - 1925. Revision des lépidocyclines. Deuxième et troisième partie, *Mém. Soc. géol. France*, 2: 1-115.

Drooger, C. W. 1951. Notes on some represantatives of Miogypsinella. K. Nederl. Akad. Wetensch., Proc., Amsterdam, Netherlands, ser. B, 54 (4): 357-365.

Drooger, C. W. 1952. Study of American Miogypsinidae: Thesis, University of Utrecht, Utrecht, Netherlands, 80 p.

Drooger, C. W., Socin, C. 1959. Miocene foraminifera from Rosignano, northern Italy: *Micropaleontology*, 5 (3): 415-426.

Eames, F. E., Banner, F. T., Clarke, W. J. 1962. Fundamentals of Mid - Tertiary stratigraphical correlation: Part 1. *University Pres, Cambridge*, England: 1-59.

Ehrenberg, C. G. 1839. Über die Bildung der Kreidefelsen und des Kreidemergels durch unsichtbare Organismen, Physikalische Abhandlungen der Königlichen Akademie der Wissenschaften zu Berlin, 1838 [1840: separate 1839], pp. 59-147.

Eichwald, C. E.,1830. Zoologia specialis, vol. 2, Vilnae: D. E. Eichwaldus, pp. 1-323.

Fichtel, L., Moll, J. P. C. 1798. Testacea microscopia, aliaque minuta ex generibus Argonauta et Nautilus, ad naturam picta et descripta Microscopische und andere klein Schalthiere aus den geschlechtern Argonaute und Schiffer. Vienna: Camesina.

Fornasini, C. R. 1904. Accad. Sci. Ist. Bologna, Mem. Sci. Nat., Bologna, ser. 6, tomo 1, pp., 6-7, pl. 1, fig. 13.

Freudenthal, T. 1969. Stratigraphy of Neogene deposits in the Khania Province, Crete, with special reference to Foraminifera in the family Planorbulinidae and the genus *Heterostegina*. Utrecht Micropal. Bull., 1, 1-208, 53 figs, 10 tabs., 15 pls, Utrecht.

Gedik, F. 2008. Foraminiferal description and biostratigraphy of the Oligocene shallow marine sediments in Denizli region, SW Turkey, *Revue de Paléobiologie*, Genève, 27(1): 25-41.

Gedik, F. 2010. Malatya Havzasındaki Sığ Denizel Sedimanların Oligo-Miyosen Bentik Foraminifer Tanımlaması ve Biyostratigrafisi, PhD Thesis, 184 s., 25 lev., Ankara.

Gedik, F., Sirel, E. 2009. Şattiyen Çökellerinde Saptanan Yeni Bir Miogypsinoides türü: *Miogypsinoides akcadagensis* n. sp., Akçadağ Yöresi (Malatya, Türkiye), Maden Tetkik ve Arama Genel Müdürlüğ Dergisi 138, 35-43.

Goldfuss, G.A. 1817. Uber die Entwicklungsstufen des Thieres. Leonard Schrag, Nuremberg.

Gomez Llueca, F. 1929. Los numulitidos de España. Com. Invest. Pal. Prehist. Mem., Madrid, 36, ser. Pal. 8: 1-400.

Grimsdale, T. F. 1952. Cretaceous and Tertiary foraminifera from the Middle East. *Bull. British Museum. (Nat. Hist.) Geol., London*, 1 (8): 221-248.

Hanzawa, S. 1930. Note on Foraminifera found in the Lepidocyclina limestone from Pabehasan, Java.

Sci. Rep. Tohoku Imp. Univ., Sendai, S. 2, (Geol.), 14 (1): 85-96.

Hanzawa, S. 1940. Micropaleontological studies of drill cores from a deep well in Kita-Daito-zima (North Borodino Island). In: Jubilee Publication in commemoration of Prof. H. Yabe's 60th Birtday. Sendai, Japan: Tôhoku Imp. Univ., vol. 2, 2 pp. 755-802, pl. 39, figs. 1-9; p. 767, tf. 2.

Harpe, P. de La 1883. Etudes des Nummulites de la Suisse et révision des espèces Eocène des genres Nummulites et Assilina; troisième et dernière partie. Soc. Pal. Suisse, Mem., Basel, 10, 4, 141-180.

Harzhauser, M., Piller, W.E., Steininger, F.F. 2002. Circum - Mediterranean Oligo - Miocene biogeographic evolution the gastropods point of view, Palaeogeography, Palaeoclimatology, Palaeoecology, 183: 103-133.

Henson, F. R. S. 1937. Larger foraminifera from Aintab, Turkish Syria. Eclogae Geologicae Helvetiae, Basel, 30: 45 - 57.

Henson, F.R.S. 1950. Middle eastern Tertiary Peneroplidae (Foraminifera) with remarks on the phylogeny and taxonomy of the family. - Ph.D. thesis, Leiden University, West Yorkshire Printing Co., Wakefield, 70 p., 10 pls.

Hottinger, L. 1963. Quelques Foraminifères porcelanés oligocènes dans la série sédimentaire prébétique de Moratalla (Espagne méridionale). - Eclogae Geologicae Helvetiae, Basel, 56 (2): 963-972.

Hottinger, L. 1977. Foraminiféres operculiniformes. - Mém. Mus. Natn. Hist. Nat. C40.

Hottinger, L. 2007. Revision of the foraminiferal genus Globoreticulina RAHAGHI, 1978, and of its associated fauna of larger foraminifera from the late Middle Eocene Iran,Carnets de Géologie / Notebooks on Geology - Article 2007/06, p. 11-12.

Joly, N., Leymerie, A. 1848. Mémoire sur les Nummulites considérées zoologiquement et géologiqoement. Mémoires de l'Académie des Sciences Toulouse (3), 4: 1-70.

Karaman, T., Poyraz, N., Bakırhan, B., Alan, İ., Kadınkız, G., Yılmaz, H., Kılınç, F. 1993. Malatya-Doğanşehir-Çelikhan dolayının jeolojisi. *Maden Tetkik ve Arama Genel Müdürlüğü Raporu*, 9587, Ankara, (unpublished).

Kurtman, F. 1978. Gürün Bölgesinin jeolojisi ve tektonik özellikleri. *Maden Tetkik ve Arama Genel Müdürlüğü Dergisi*, 91: 1-12.

Lemoine, P., Douvillé, R., 1904. Resultats paleontologiques et stratigraphiques de l'étude des Lépidocyclines. Bulletin de la Société Géologique de France, (4), 4: 347-350, Paris.

Less, G. 1991. Upper Oligocene larger Foraminifers of the Bükk Mountains. Földt. Int. Évi Jel. 1989 rõl: 411-465.

Loeblich, A. R., Tappan, H. 1986. Some new and redefined genera and families of Textulariina, Fusulinina, Involutinina and Miliolina (Foraminiferida), Journal of Foraminiferal Research, 16: 334-346.

Loeblich, A. R., Tappan, H. 1987. Foraminiferal genera and their classification. I: 970 p.; II: 212 p., 847 pl., New York (Van Nostrand Reinhold).

Marie, P. 1955. Quelques formes nouvelles de l'Oligocène et du Miocène du N. W. de la Grèce. II. Foraminifères. *Bulletin de la Société Géologique de France*, 6, (5): 193-205.

Matsumaru, K. 1976. Larger foraminifera from the islands of Saipan and Guam, Micronesia, in Y. Takayanagi and T. Saito, eds., Progress in Micropaleontology. Micropaleontology Press Special Publication Newyork: *American Museum of Natural History*, pp. 190-213.

Michelotti, G. 1841. Saggio storico dei Rizopodi caratterictici dei terreni supracretacei. *Mem. Fis. Soc. Ital. Sci.*, Modena, 22: 296.

Montanari, L. 1961. Das Nummulitikum von Sciacca (Sizilien). *Eclogae Geologicae Helvetiae*, Basel, 54 (2): 570-579.

Montfort, P. Denys de. 1808. Conchyliologie Systématique et Classification Méthodique des Coquilles, vol. 1, Paris: F. Schoell.

Nuttall, W. L. F. 1928. Notes on the Tertiary foraminifera of southern Mexico, *Journal of Paleontology*, 2: 372-376.

Orbigny, A. d'. 1826. Tableau méthodique de la classe des Céphalopodes, Annales des Sciences Naturelles, 7: 245-314.

Örçen, S. 1986. Medik-Ebreme (KB Malatya) dolayının biyostratigrafisi ve paleontolojisi: *Maden Tetkik ve Arama Genel Müdürlüğü Dergisi*, 105/106, 39-68, Ankara.

Özcan, E., Less, G. 2009. First record of the co-occurrence of western Tethyan and Indo-Pacific larger foraminifera in the Burdigalian of the Mediterranean province, *Journal of Foraminiferal Research*, 39 (1): 23-39.

Parker, W. K., Jones, T. R. 1865. On some foraminifera from the North Atlantic and Arctic Oceans, including Davis Straits and Baffin's Bay, Philosophical Transactions of the Royal Society, 155: 325-441.

Parr, W. J. 1942. New genera of foraminifera from the Tertiary of Victoria. *Mining and Geological Journal*, 2: 361-363.

Poignant, A. 1967. Aperçu sur les lépidocyclines d' Aquitaine. Commitee Mediterranean Neogene Stratigraphy, Proc. IV Session Bologna 1967. *Giornale di Geologia* (2): 197 - 216.

Raju, D. S. N. 1974. Study of Indian Miogypsinidae. *Utrecht Micropal*. Bull. 9.

Reichel, M. 1937. Etude sur les Alvéolines. Mémoires de la Société Paléontologique Suisse, Basel, vol. 59, p. 95-146.

Reiss, Z., Gvirtzman, G. 1966. Borelis from Israel. *Eclogae Geologicae Helvetiae*, Basel, 59 (1): 438-449.

Reuter, M., Piller, W.E., Harzhauser, M., Mandic, O., Berning, B., Rögl, F., Kroh, A., Aubry, M.P., Wielandt-Schuster, U., Hamedani, A. 2009. The Oligo-Miocene Quom Formation (Iran): evidence for an early Burdigalian restriction of the Tethyan Seaway and closure of its Iranian gateways, *International Journal of Asian Earth Sciences*, 98, 627-650.

Rutten, L. 1912. Studien über Foraminiferen aus Ost-Asien. Leiden, Geol. Reichs-Mus., Samml., Netherlands, ser. 1, vol. 9 (1911-1914), no:2, pp. 201-217, pl.12, figs. 6-9.

Sacco, F. 1893. Sur quelques Tinoporinae du Miocène de Turin, *Bulletin de la Société Belge de Géologie, de Paléontologie, et d'Hydrologie* (1893-1894), 7: 204-207.

Schaub, H. 1981. Nummulites et Assilines de la Téthys Paléogène, Taxonomie, Phylogenèse et Biostratigraphie. Mémories Suisses de Paleontologie, 104-106: 236.

Scheffen, W. 1932. Zur morphologie und morphogenese der 'Lepidocyclinen', Paläontologische Zeitschrift, 14: 233-256.

Schlumberger, C. 1893. Note sur les genres *Trillina* et *Linderina*. *Bulletin de la Société Géologique de France*, (3), 21 (2): 118-123, 5 figs., pl. 3, Paris.

Schlumberger, C. 1900. Note sur le genre Miogypsina. *Bulletin de la Société Géologique de France, Ser*. 3, 28: 327-333.

Schultze, M. S. 1854. Über den Organismus der Polythalamien (Foraminiferen), nebst Bermerkungen über die Rhizopoden im Allgemeinen. Leipzig: Wilhelm Engelmann.

Schwager, C. 1877. Quadro del proposto sistem adi classificazione dei foraminiferi con guscio, Bolletino R. Comitato Geologico d'Italia, 8: 18-27.

Siebold, C.T.E. 1845. Lehrbuch ver vergleichenden Anatomie der Wirbellossen Thiere. *In*: Lehrbuch der Vergleichenden Anataomie (eds: C.T.E. von Siebold and H. Stannius. Von Veit, Berlin.

Silvestri, A. 1937. Paleontologia delle Somalia. V. Fossili dell'Oligocene e dell Miocene. 3. Foraminiferi dell'Oligocene e dell Miocene della Somalia. Paleontogr. Italica, Pisa, 37: 101-143.

Sirel, E. 1996. Praearchaias, a new soritid genus (Foraminiferida) and its Oligocene shallow - water foraminiferal assemblage from the Diyarbakır region (SE Turkey). *Geologica Romana*, 32: 167 - 181.

Sirel, E. 2003. Foraminiferal description and biostratigraphy of the Bartonian, Priabonian and Oligocene shallow-water sediments of the southern and eastern Turkey. *Revue de Paléobiologie*, Genève, 22 (1): 269-339.

Sirel, E. 2004. Türkiye'nin Mesozoyik ve Senozoyik Yeni bentik Foraminiferleri. - *Jeoloji Mühendisleri Odası Yayınları* 84, Ankara, Emeğin Bilimsel Sentezi, special edition 1, p. 219.

Sirel, E., Metin, S., Sözeri, B. 1975. Palu (KD Elazığ) denizel Oligosen'in stratigrafisi ve mikropaleontolojisi. Bulletin of the *Geological Society of Turkey*, 18: 175 - 180.

Sirel, E., Gündüz, H. 1981. Description of new Borelis species from the Hatay (S of Turkey) and Elazıg region (E of Turkey). *Bulletin Of The Mineral Research and Exploration*, Turkey, 92: 70-74.

Sirel, E., Acar, S. 1993. Malatyna, a new foraminiferal genus from the Lutetian of Malatya region (East Turkey). *Geologia Croatica, Zagreb*, 46 (2): 181-188.

Sirel, E., Gedik, F. 2011. *Postmiogypsinella*, a new Miogypsinidae (Foraminifera) from the Late Oligocene in Malatya Basin, Turkey, *Revue de Paléobiologie, Genève*, 30 (2): 591-603.

Sirel, E., Özgen-Erdem, N., Kangal, Ö. 2013. Systematics and biostratigraphy of Oligocene (Rupelian-Early Chattian) foraminifera from lagoonal-very shallow water limestone in the eastern Sivas Basin (central Turkey). *Geologia Croatica, Zagreb*, 66/2, 83-109.

Smout, A., Eames, F. E. 1958. The genus Archaias (Foraminifera) its stratigraphical distribution. *Paleontology*, 1 (3): 207 - 225.

Tan Sin Hok, 1936. Zur Kenntnis der Miogypsiniden. Ingenieur Nederl. Indie, Bandoeng, Java, Jaarg, 3, Afd. 4 (Mijnb. Geol.), pp. 45-61, 84-98, 109-123, pl. 1, fig. 13.

Tan Sin Hok, 1937. On the genus *Spiroclypeus* H. Douvillé with a description of the Eocene *Spiroclypeus vermicularis* nov. sp. from Koetai in East Borneo. De Ingenieur in Nederlandsch-Indiè, (4, Mijnb. en Geol.), De Mijningenieur, 4 (10): 177-193, 1 fig., pls. 1-4.

Uhlig, Y. 1886. Über eine Mikrofauna aus dem Alttertiar des westgalizischen Karpathen. *Jarhb. Geol. Reichsanst.,* 36 (1): 141-214.

Vaughan, T. W. 1928. Yaberinella jamaicensis, a new genus and species of arenaceous foraminiferai, Journal of Paleontology, 2: 7-12.

Yoldaş, R. 1972. Malatya kuzeyinin jeolojisi ve petrol olanakları: Maden Tetkik ve Arama Genel Müdürlüğü Raporu, 4936, Ankara (unpublished).

PLATES

PLATE - 1

Figures 1-15: *Archaias kirkukensis* Henson

Rupelian-Early Chattian, Develi measured stratigraphical section, W Malatya, Eastern Turkey, (figure 1 not included) X20.

1: Views of *Archaias kirkukensis* Henson in different plans and Miliolidae, (FGD-2A/5/1).

2: Subaxial section and Miliolidae, (FGD-2A/9/1).

3: Equatorial section, A form, (FGD-2A/11/1).

4: Axial section, A form, (FGD-2B/12/7).

5: Section crossing margin chord (aperture surface), (FGD-2A/10/4).

6: Equatorial section, A form, (FGD-2A/7/2).

7: Equatorial section, A form, (FGD-2A/11/4).

8: Section passing through margin chord (aperture surface), (FGD-2A/3/10).

9: Axial section, A form, (FGD-2A/11/2).

10: Axial section, A form, subaxial section and Miliolidae (FGD-2A/9/9).

11: Subaxial section, (FGD-2A/3/2).

12: Slightly oblique equatorial section, (FGD-2A/11/3).

13: Equatorial section, A form, (FGD-2B/5/2).

14: Axial section, A form, (FGD-2A/4/5).

15: Axial section (left), subaxial section (right), A form, (FGD-2A/3/3).

PLATE- 1

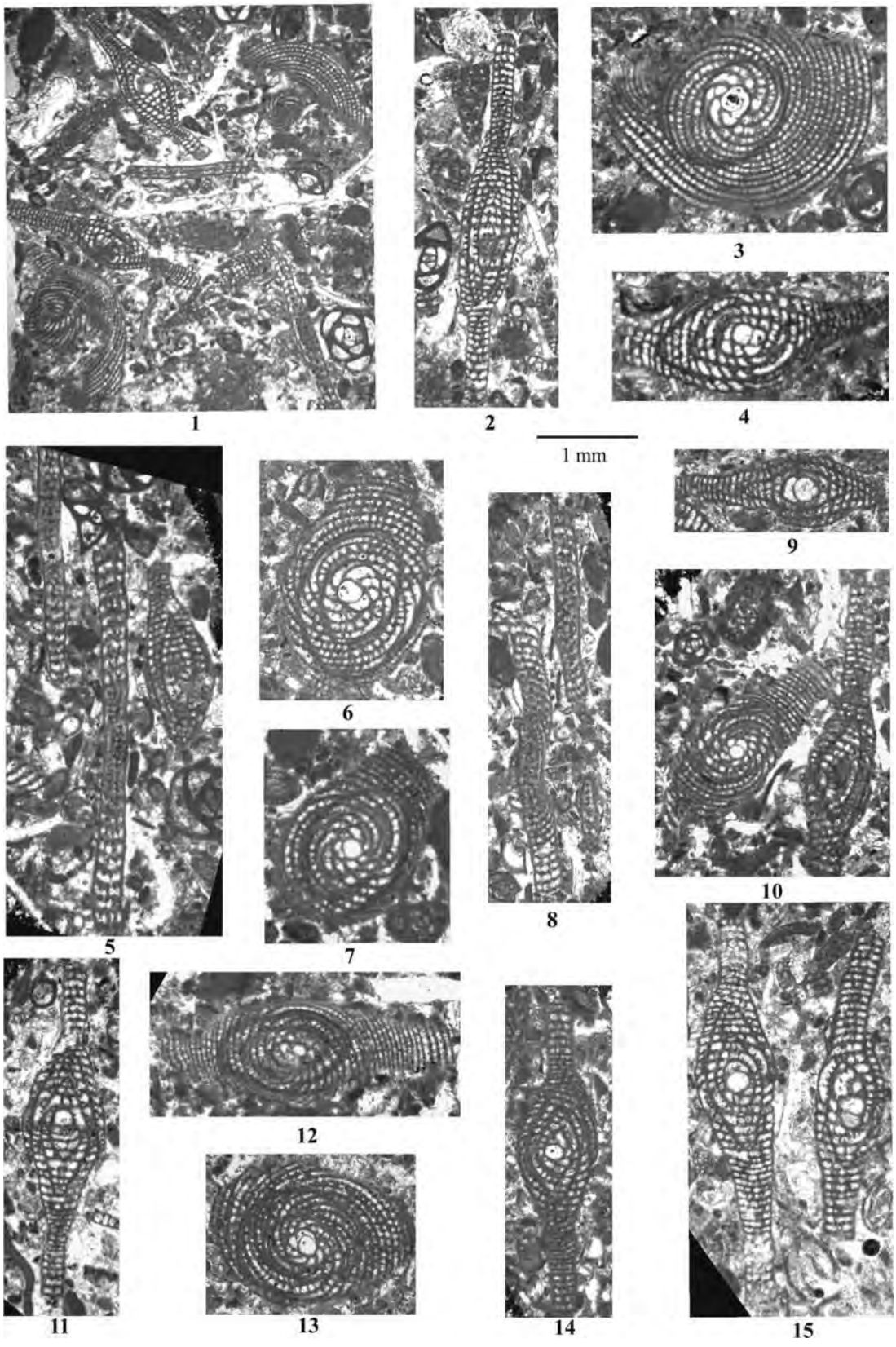

PLATE - 2

Figure 1-6: *Archaias hensoni* Smout and Eames

Rupelian-Early Chattian, Karamağara measured stratigraphical section, NE Akçadağ, W Malatya, Eastern Turkey, X 20.

1, 6: Axial section, A form, (HYM-38/1, HYM-38/2).

2, 3: Subaxial section, (HYM-36A/3/3, HYM-36A/4).

4, 5: Equatorial section, A form, (HYM-36B/8/1, HYM-38/2/1).

Figure 7-9: *Penarchaias glynnjonesi* (Henson)

Rupelian-Early Chattian, Karamağara measured stratigraphical section, NE Akçadağ, W Malatya, Eastern Turkey, X40.

7, 9: Axial section, A form, planispiral chambers following the first chamber and chambers of the uniserial stage are observed, (HYM-36A/3, HYM-36A).

8: Axial section, A form, following the first chamber planispiral chambers are observed, (HYM-36A).

Figures 10-22: *Planorbulina brönnimanni* Bignot and Decrouez.

Oligocene, Develi, Karamağara and Edilme measured stratigraphical sections, W Malatya, Eastern Turkey, X35.

10, 12, 14: Tangential section, (MA-91, MA-89, MA-92, FGM-4A/1).

11: Subaxial section, (MA-90).

13, 15, 19-21: Transverse section, (MA-90, MA-69, FGM-4G/1, FGM-4A/3, FGM-16/2).

16: Equatorial section, only planispiral chambers following the first chamber were observed, (HYM-36A/6/1).

17, 18, 22: Subaxial section, (FGM-2/1, FGM-4G/3, FGM-12D/1).

Figures 23-30: *Neoplanorbulinella* spp.

Rupelian-Early Chattian, Karamağara measured stratigraphical section, NE Akçadağ, W Malatya, Eastern Turkey, X72.

23: Axial section, A form, (HYM-36A/11/1).

24: Axial section, A form, following the first chamber equatorial chambers and lateral chambers in umbilical pores are observed, (HYM-36A/3/2).

25: Axial section, B form, (HYM-36A/4/1).

26: Axial section, A form, equatorial chambers and lateral chambers in umbilical pores following the small, spheroidal first chamber are observed, (HYM-36A/8/1).

27: Axial section, (HYM-36A).

28: Axial section, A form, following the first chamber equatorial chambers and lateral chambers in umbilical pores are observed, (HYM-36A/5/2).

29: Axial section, (HYM-36A/10/4).

30: Axial section, B form, (HYM-36A/2/1).

PLATE - 2

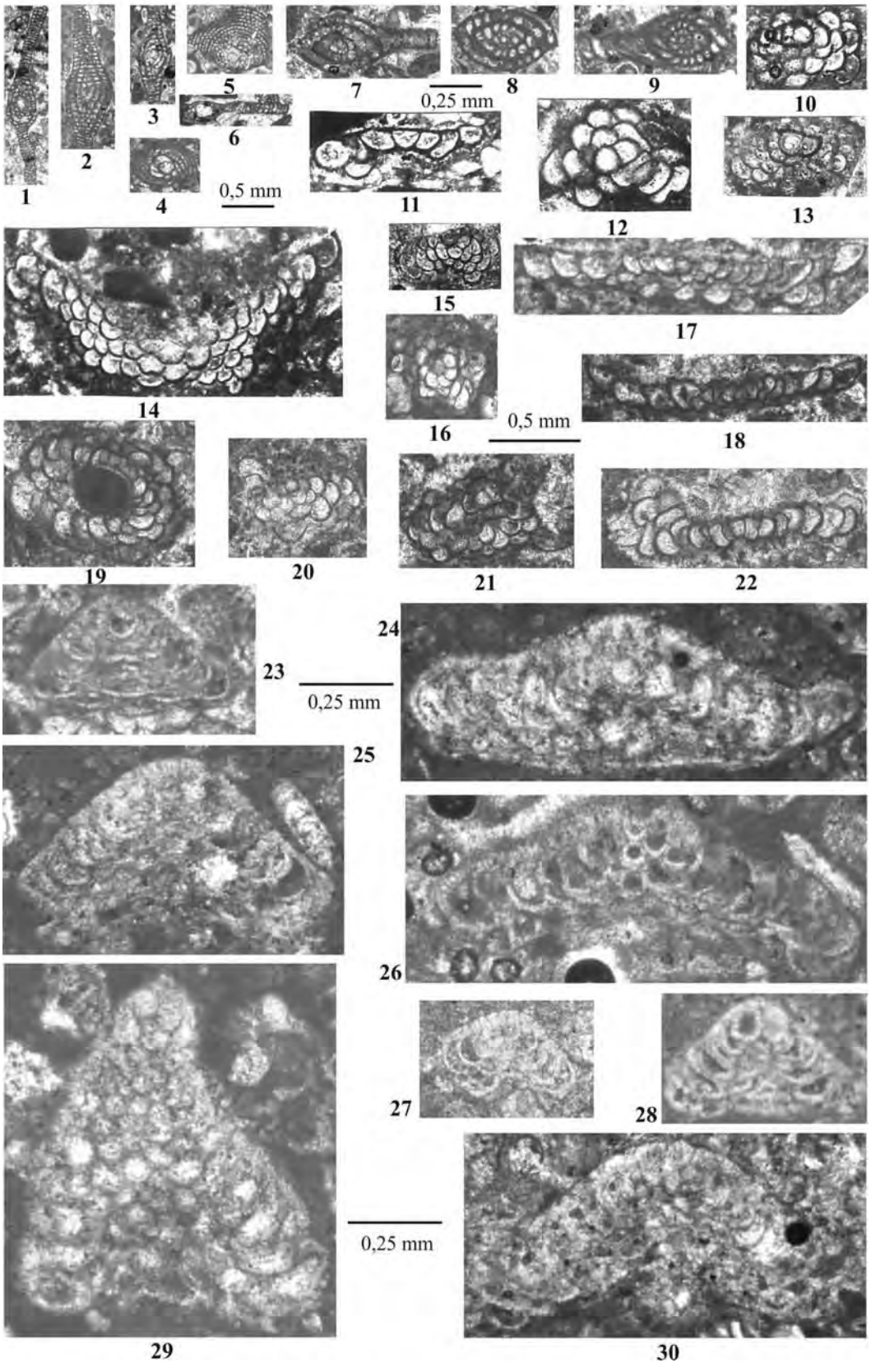
1
2
3
4
5
6
7
8
9
10
11
12
13
14
15
16
17
18
19
20
21
22
23
24
25
26
27
28
29
30
0,5 mm
0,25 mm
0,5 mm
0,25 mm

PLATE - 3

Figures 2, 3: *Peneroplis* cf. *laevigatus* d'Orbigny

Rupelian-Early Chattian, Develi measured stratigraphical section, W Malatya, Eastern Turkey, X20.

Equatorial section, (FGD-2A, FGD-2B).

Figure 1: *Archaias kirkukensis* (A), *Peneroplis* sp. (P), *Nephrolepidina* sp., limestones with (N), X26, (FGD-2A).

Figure 4: *Peneroplis* sp.

Equatorial section, X 20, (FGD-2B).

Figures 5, 12-16, 18-22: *Austrotrillina brunni* Marie

Rupelian-Early Chattian, Develi and Karamağara measured stratigraphical sections, W Malatya, Eastern Turkey, X36.

Figures 5, 22: Late Chattian, Edilme measured stratigraphical section, W Malatya, Eastern Turkey, X36.

5: Equatorial section, (FGM-29/7/2).

22: Off centered equatorial section, (FGM-29/6/1).

12: Tangential section, (FGM-3/2/1).

13, 14, 15,19, 20: Equatorial section, (FGD-2A/9/7, FGD-2B/7/1, FGD-2B/13/3, HYM-35/1/1, FGD-2B/12/1).

16, 18: Sub equatorial section, (HYM-36A/10/1, HYM-36A/3/1).

21: Equatorial section, A form, (HYM-36A/1).

Figures 6, 7: Agglutinated Miliolid forms, X30, (FGD-6, FGD-7).

Figures 8-10: *Borelis merici* Sirel.

Rupelian-Early Chattian, Karamağara measured stratigraphical section, W Malatya, Eastern Turkey, X60.

8: Axial section, young specimen, (HYM-36B/2).

9: Noncentered equatorial section, only the chamber front of the *Borelis* genus indicates the presence of canal system (HYM-36A/2/2).

10: Off centered axial section, (HYM-36A/5/4).

Figure 11: *Borelis pygmaea* Hanzawa

Rupelian- Early Chattian, Karamağara measured stratigraphical section, W Malatya, Eastern Turkey, X60.

Axial section, A form, (HYM-36A/1/1).

Figures 17, 23, 24: *Austrotrillina howchini* (Schlumberger)

Burdigalian, Edilme measured stratigraphical section, W Malatya, Eastern Turkey, X36.

17: Tangential section showing subepidermal thick alveolarine structure, (FGM-52/1).

23: Tangential section, (FGM-52/2).

24: Noncentered equatorial section, (FGM-52/2).

Figure 25: *Austrotrillina asmariensis* Adams

Late Chattian, Edilme measured stratigraphical section, W Malatya, eastern Turkey, X36.

Equatorial section, (FGM-29/1/6).

PLATE - 3

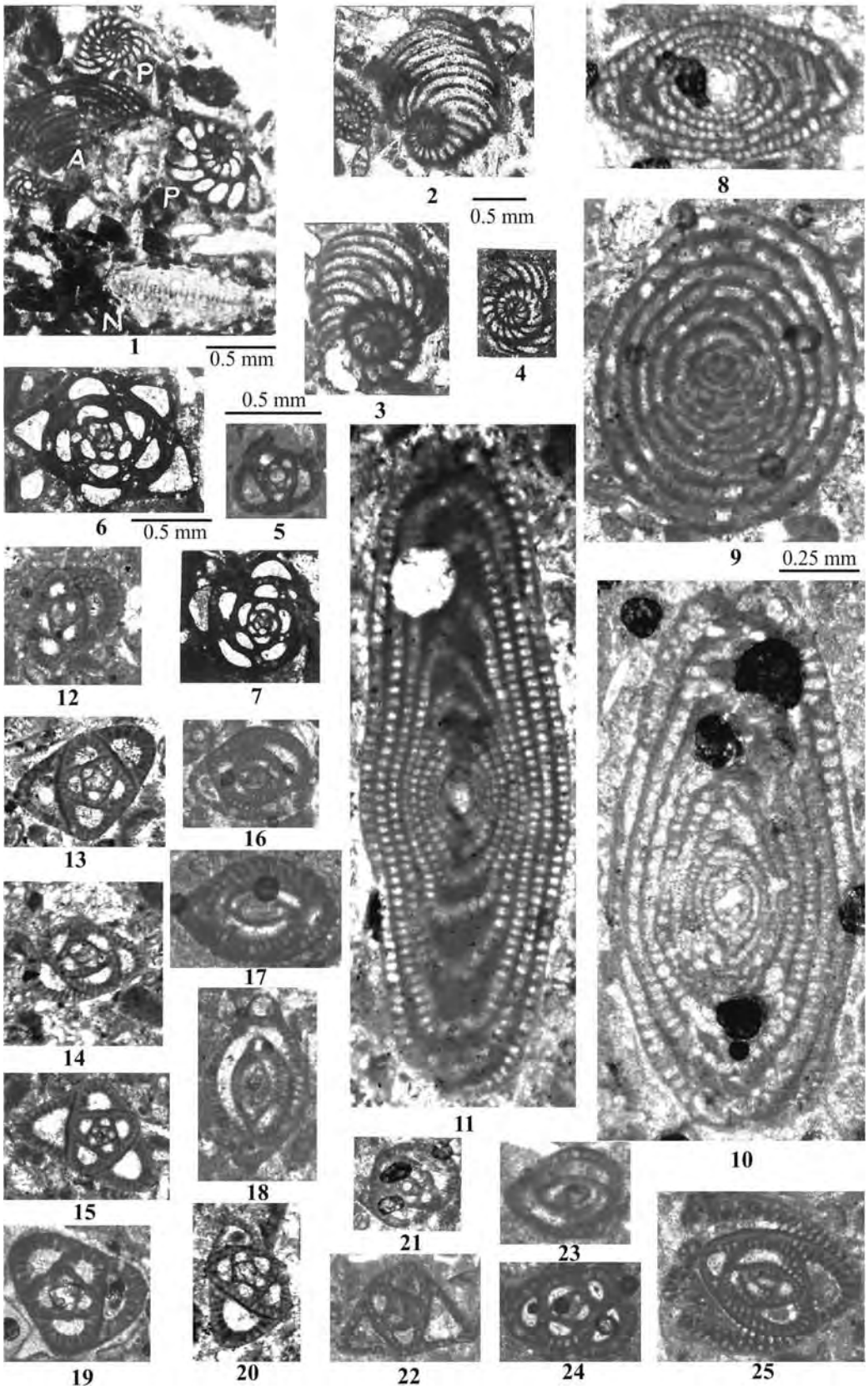
P
A
P
N
1
0.5 mm
2
0.5 mm
8
3
4
0.5 mm
6
0.5 mm
5
9
0.25 mm
12
7
13
16
17
14
18
11
10
15
21
23
19
20
22
24
25

PLATE - 4

Figures 1-13: *Austrotrillina asmariensis* Adams

Rupelian-Early Chattian, Develi measured stratigraphical section, W Malatya, Eastern Turkey, X36.

1: Equatorial section, B form (FGD-2A/7/1).

2: Tangential section, (FGD-2A/10/6).

3: Equatorial section, A form, (FGD-2B/1/1).

4: Slightly transversal equatorial section, A form, (FGD-2A/1/1).

5: Subequatorial section, A form, (FGD-2A/7/6).

6: Equatorial section, A form, (FGD-2A/11/5).

7: Slightly transversal equatorial section, (FGD-2A/3/13).

8: Equatorial section, A form,(FGD-2A/6/6).

9: Tangential sections, (FGD-2B/5/4).

10: Equatorial section, A form, (FGD-2A/3/12).

11: Subequatorial section, (FGD-2A/7/7).

12: Equatorial section, A form, (FGD-2A/3/8).

13: Slightly transversal equatorial section, (FGD-2B/8/2).

PLATE - 4

1

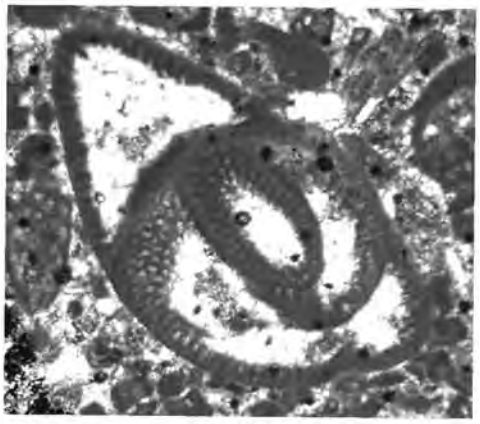

2

0.5 mm

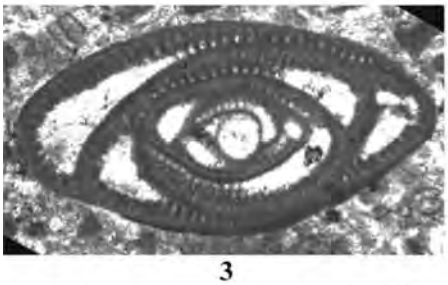

3

4

5

6

7

8

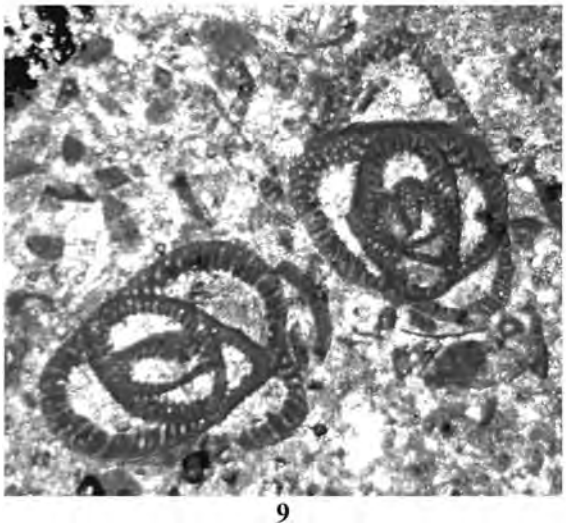

9

10

11

12

13

PLATE - 5

Figures 1-28: *Borelis curdica* (Reichel)

Burdigalian, Develi and Edilme measured stratigraphical sections, W Malatya, Eastern Turkey, X 40.

1: Equatorial section, (FGD-11/7/1).

2: Axial section, young individual, (FGD-11/5/2).

3: Highly transversal axial section, young specimen, (FGD-11/6/4).

4: Axial section, (FGD-11/6/1).

5: Axial section showing especially the mouth opening in the last whorl, adult individual, (FGD-13B/1/1).

6: Transversal axial section, young individual, (FGD-11/4/3).

7: Transversal axial section, young individual, (FGD-11/6/2).

8: Axial section, young individual, (FGD-11/5/8).

9: Transversal axial section, young specimen, (FGD-11/5/5).

10: Tangential section of which chambers are observed in central part, (FGD-11/5/7).

11: Partly tangential, partly equatorial section, (FGD-11/4/1).

12: Axial section, (FGD-11/5/4).

13: Tangential section, (FGD-11/7/2).

14: Equatorial section, (FGD-11/5/3).

15: Badly fossilized equatorial section, (FGD-13B/5/1).

16: Partly tangential partly axial section showing uniserial mouth aperture, (FGD-11/4/2).

17: Tilted axial section, (FGD-11/6/6).

18: Transversal equatorial section, (FGD-11/6/5).

19: Axial section, (FGD-19B/2/1).

20: Partly tangential partly axial section, young individual, (FGD-11/6/3).

21: Axial section, (FGD-13B/3/1).

22: Tangential section, young specimen, (FGD-11/5/6).

23: 26-28. Axial section, (FGM-40/2; FGM-53A/1; FGM-40A/1; FGM-43B/1).

24: Equatorial section, (FGM-40/3).

25: Transversal axial section, (FGM-50/1).

PLATE - 5

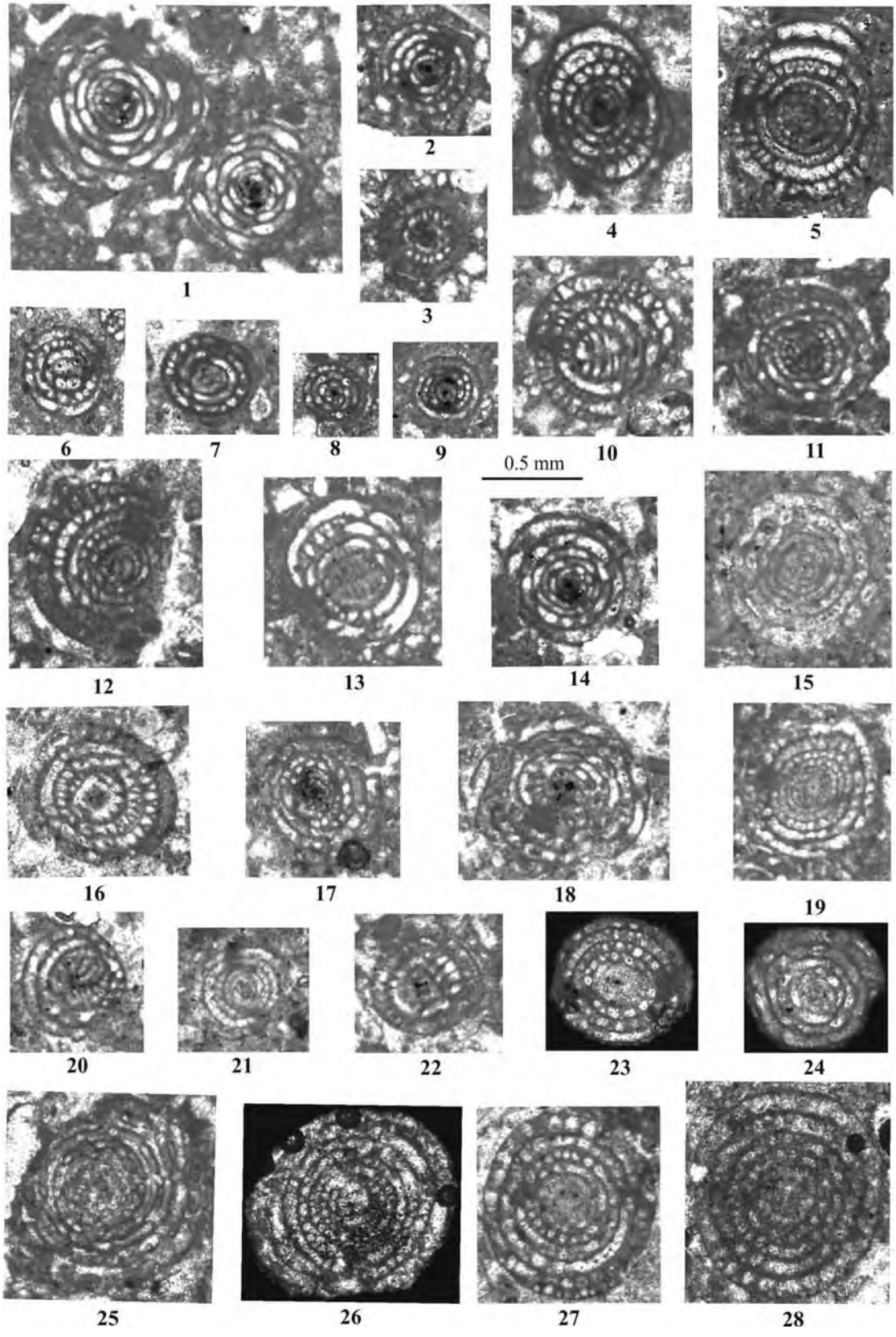
1
2
3
4
5
6
7
8
9
10
11
0.5 mm
12
13
14
15
16
17
18
19
20
21
22
23
24
25
26
27
28

PLATE - 6

Figures 1-7, 9, 10, 12-14: *Nephrolepidina praemarginata* Douvillé

Rupelian-Early Chattian, Edilme and Develi measured stratigraphical section, W Malatya, Eastern Turkey, all figures (figures 4, 10, 14 not included) X30, Figures 4, 10, X15, Figure 14 not scaled.

1: Equatorial section, (FGM-19/3).

2: Transversal equatorial section, (FGM-19/4/1).

3: Transversal equatorial section, (FGM-19/9).

4: Transversal equatorial section, (FGD-2B).

5: Equatorial section, (FGD-2B).

6, 7, 9, 10, 12: Axial section, (FGM-19/3/3, FGM-19/13/1, FGM-19/4/2, MA-88).

13: Transversal axial section, they are also observed from granular surface, (FGM-19/13/1).

14: *N. praemarginata*, *Neorotalia lithothamnica* and much algal limestones, (FGM-19).

Figures 8, 11: *Nephrolepidina* sp.

8: Transversal equatorial section, (FGM-19/13/4), 11. Transversal axial section, (FGM-19/3/2).

PLATE - 6

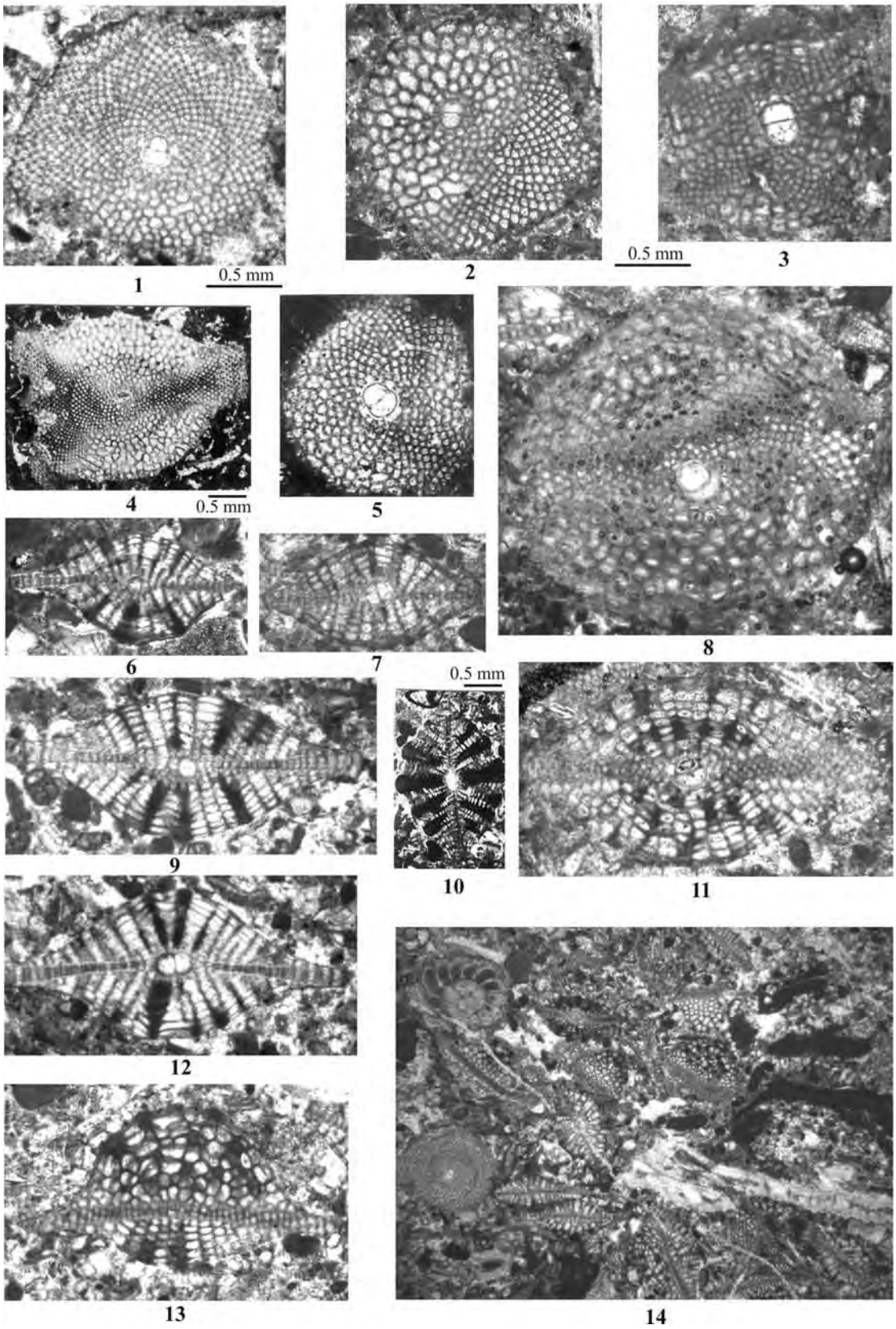

PLATE - 7

Figures 1-9: *Nephrolepidina partita* Douvillé

Rupelian-Early Chattian, Edilme and Develi measured stratigraphical sections, W Malatya, Eastern Turkey, X 30.

1-8: Axial section, large umbo at the center of shell is clearly observed, (FGD-3/1/1, FGM-5E/6/1, FGM-5E/2/2, FGM-19/24/4, FGM-19/15/2, FGM-19/14/2, FGM-13C/1, FGM-4G/2).

9: Equatorial section, small sphericalfirst chamber and semilunar shaped second chamber are observed, (FGM-19/27/4).

Figure 10: *Eulepidina* cf. *formosoides* Douvillé

Equatorial section, (FGM-19/11/1).

Figure 11: *Eulepidina* sp.

Axial section, (FGM-19/11/3).

Figures 12, 13: *Nephrolepidina morgani* (Lemoine and Douvillé)

Late Chattian, Edilme measured stratigraphical section, W Malatya, Eastern Turkey, X 30.

12: Axial section, (FGM-29/1/4).

13: Equatorial section, (FGM-29/7/5).

PLATE - 7

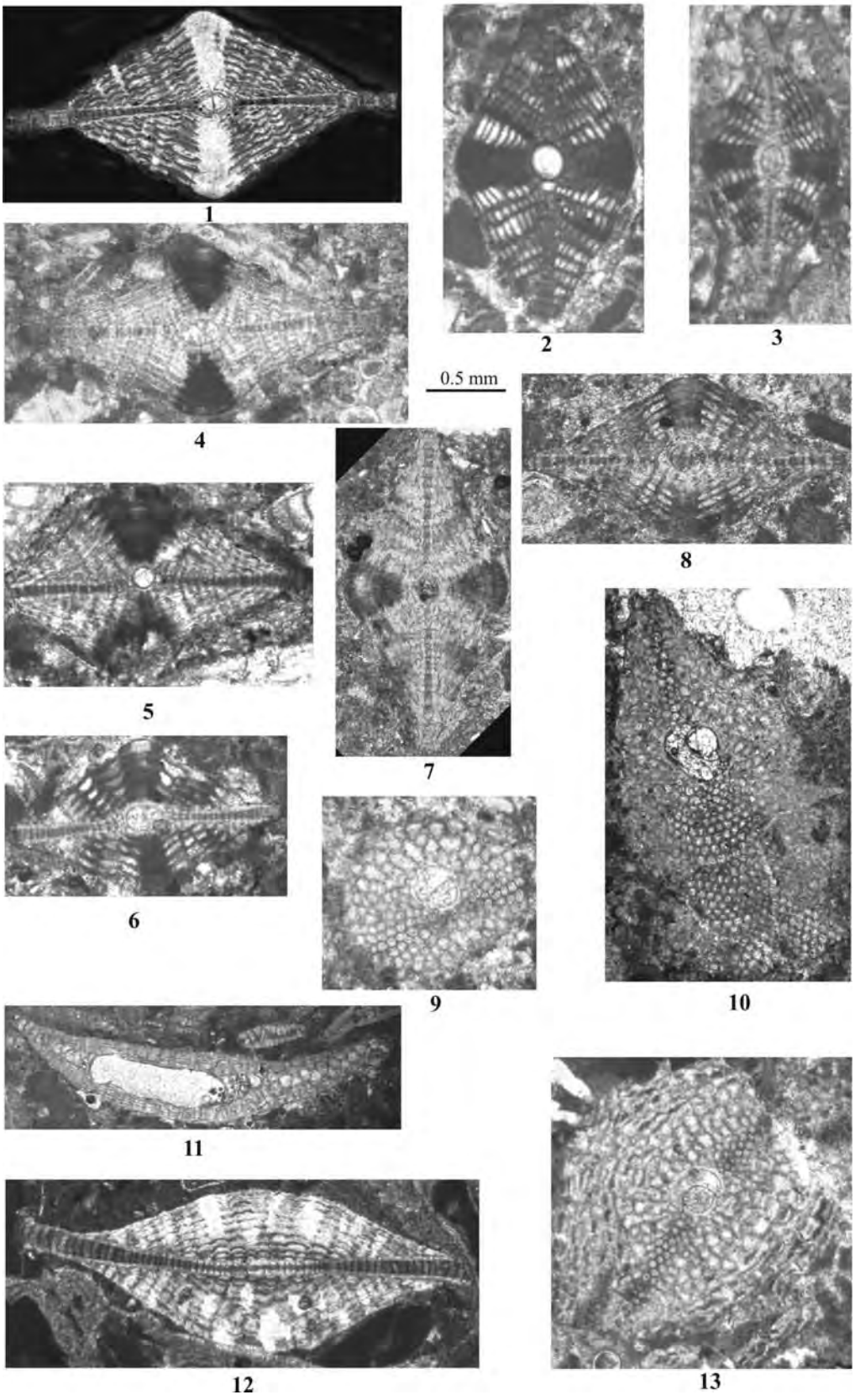

PLATE - 8

Late Chattian, Edilme measured stratigraphical section, W Malatya, Eastern Turkey, X 60.

Figures 1-3. *Miogypsinella akcadagensis* (Gedik and Sirel)

1: Equatorial section, (FGM-30A/12/1), embryonic chambers, spiral chambers in early stage and miogypsinid chambers are observed.

2: Equatorial section, (FGM-30A/3/1), embryonic chambers, spiral chambers in early stage and miogypsinid chambers are observed.

3: Centered axial section, (FGM-30A/5/2), chambers in rotaliid period and miogypsinid order are observed.

Figures 4, 5: *Miogypsinella borodinensis* Hanzawa

4: Axial section, (FGM-30A/11/1), chambers in rotallid order with coarse plug and miogypsinid order are observed.

5: Equatorial section, (FGM-30A/6/3), spherical shaped first chamber and semilunar shaped second chamber, 13 spiral and equatorial chambers are seen.

Figures 6-10: *Postmiogypsinella intermedia* Sirel and Gedik

Late Chattian, Karamağara and Edilme measured stratigraphical sections, W Malatya, Eastern Turkey, X 60.

Figure 6: Axial section, A form, (FGM-30A/9/3).

Figure 7: Subaxial section, A form, (FGM-30A/2/3).

Figure 8: Equatorial section, A form, spiral chambers in rotaliid period and the development of equatorial chamber in miogypsinid order are seen. (HYM-42/2/2).

Figure 9: Equatorial section, A form, (HYM-42/7/4).

Figure 10: Subaxial (right) and axial section (left), A form belonging to young specimens, (HYM-42/7/4).

PLATE - 8

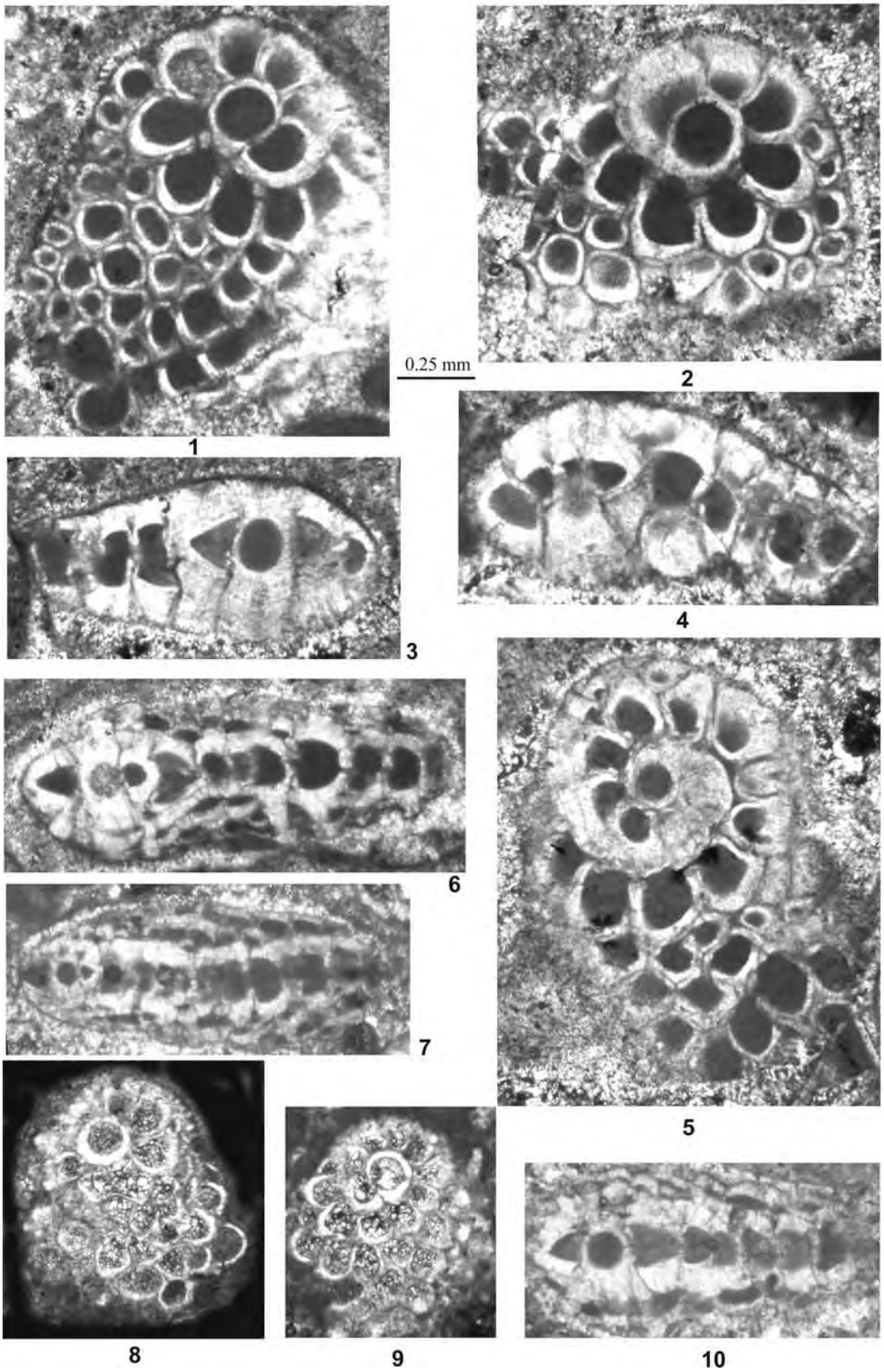

PLATE - 9

Burdigalian, Karamağara and Kuzkaya measured stratigraphical section, W Malatya, Eastern Turkey, X60.

Figures 1, 2: *Miogypsina* cf. *thecideaeformis* (Rutten)

Axial sections, (HYM-45B, HYM-47B), inflated lenticular shell, spherical first chamber located on top of shell and semi spherical second chamber, equatorial chambers following embryonic chambers degrading in size, rectangular lateral chambers on both sides of shell and internal pillars are observed.

Figure 3: Nephrolepidinid form, axial section, (HYM-45A/8/3).

Figures 4-5: *Miogypsinella* cf. *complanata* (Schlumberger)

Late Chattian, Edilme measured stratigraphical section, W Malatya, Eastern Turkey, X 60.

Axial section, (FGM-30A/12/3, FGM-30B/2/2), equatorial chambers in rotaliid order where spherical first chamber takes place and miogypsinid orders are seen.

Figures 6-8: *Dendritina* cf. *rangi* d'Orbigny

Burdigalian, Develi and Edilme measured stratigraphical sections, W Malatya, Eastern Turkey, X 40.

6: Axial section, (FGM-40A).

7, 8: Equatorial section, A form, (FGD-11/6/7, FGD-11/5/1).

Figure 9: *Planorbulinella caneae* Freudenthal

Equatorial section, (HYM-46).

Figure 10: *Nephrolepidina* sp.

Axial section, (HYM-45A/6/2), lenticular shell, nephrolepidin type first and second chambers and following equatorial chambers, lateral chambers on both sides of the shell and granules which are the traces of pillars between lateral chambers.

PLATE - 9

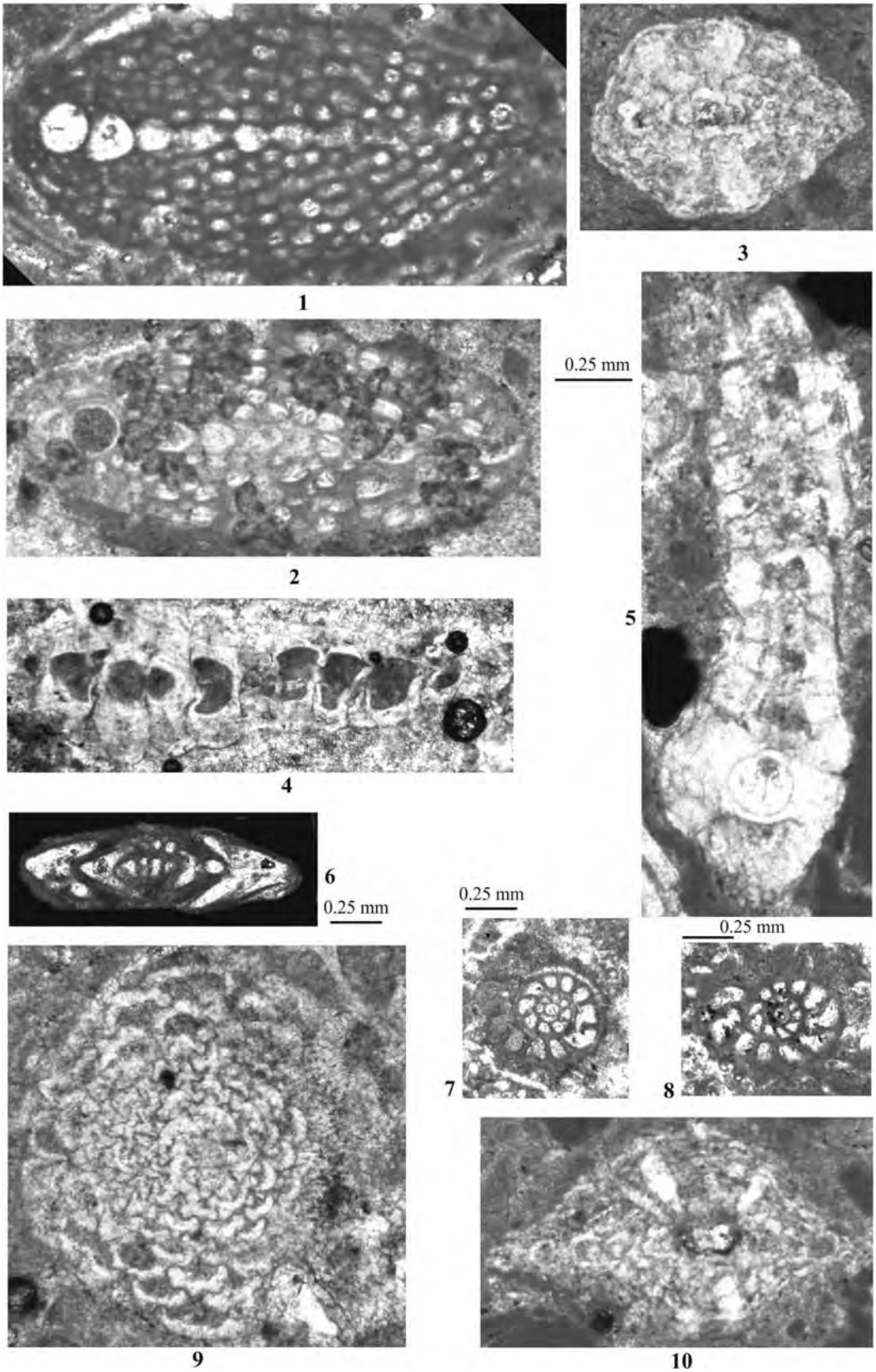

PLATE - 10

Burdigalian, Karamağara measured stratigraphical section, W Malatya, Eastern Turkey, X 60.

Figures 1-7: *Miogypsina globulina* (Michelotti)

1: Equatorial section, (HYM-45A), embryonic chambers formed by first and second chambers and pillars observed in granules on the surface of shell are clearly seen.

2-7: Axial sections, (HYM-45A, HYM-45A, HYM-45A, HYM-45A/3/6, HYM-45A/3/7, HYM-45A, HYM-45A), embryonic chambers and granules are seen.

PLATE - 10

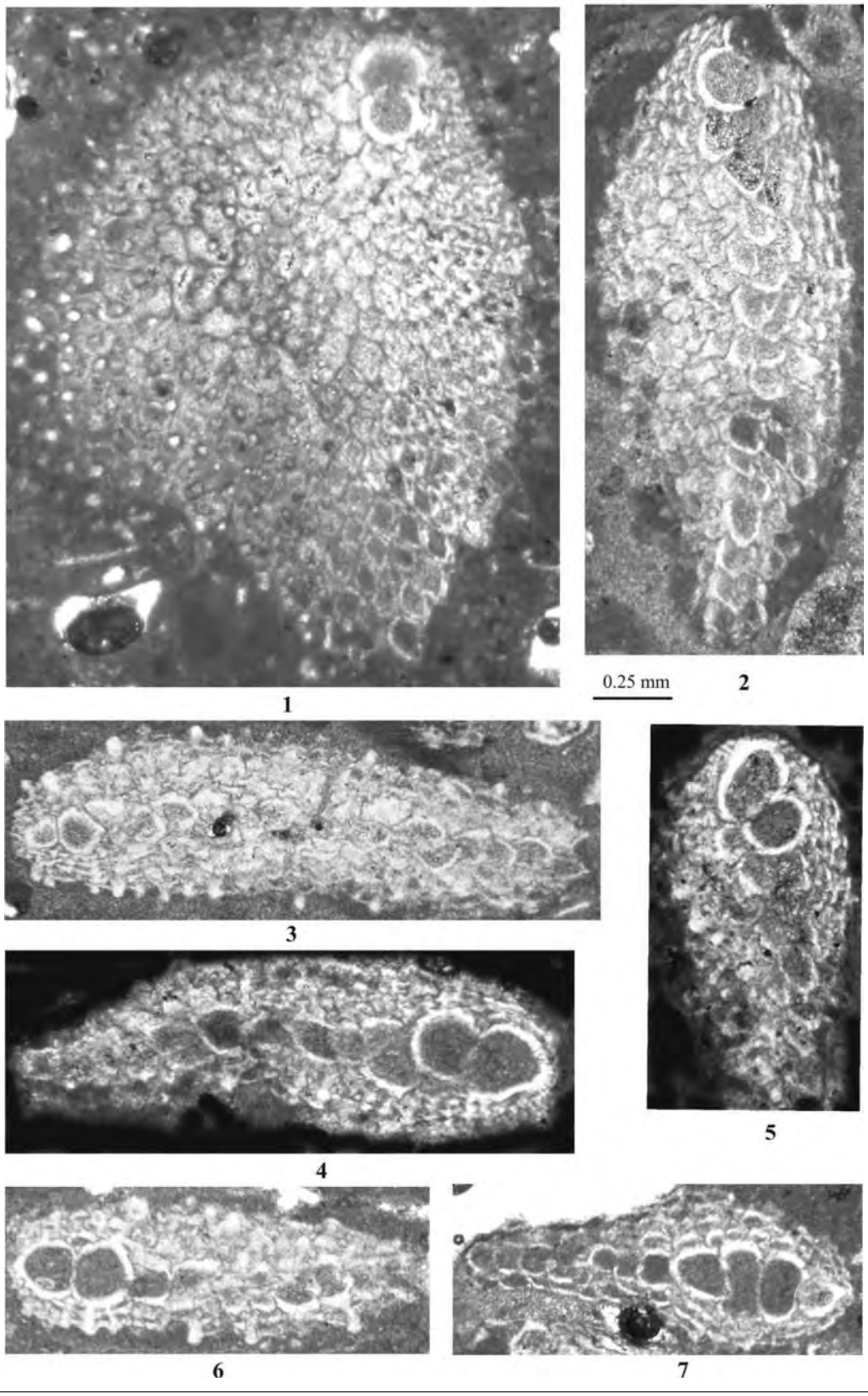

PLATE - 11

Burdigalian, Karamağara measured stratigraphical section, W Malatya, Eastern Turkey, X 60.

Figures 1-4: *Miogypsina polymorpha* (Rutten)

1: Centered transversal section, (HYM-45B/4/1),

2: Equatorial section, (HYM-45B/2/2),

3: Almost equatorial section, (HYM-48/1/1),

4: Transversal section tending to equatorial plane, (HYM-45B/5/1).

PLATE - 11

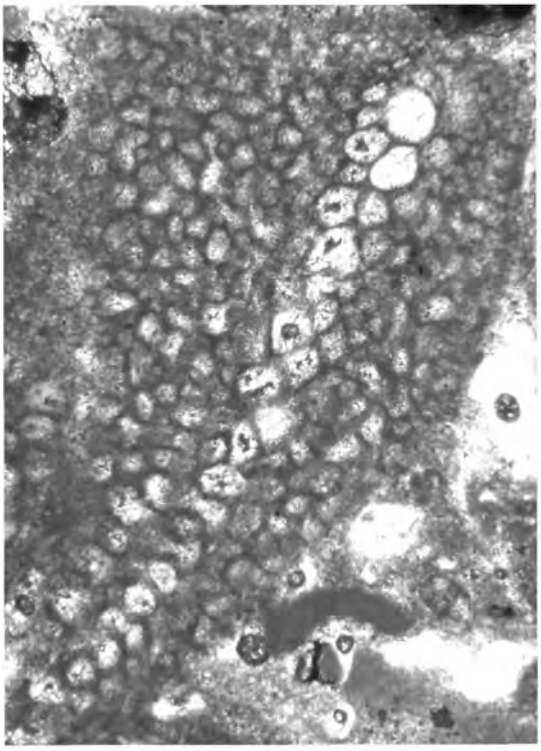

1

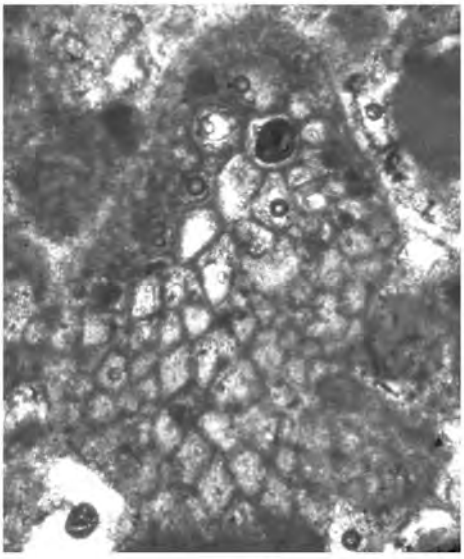

2

0.25 mm

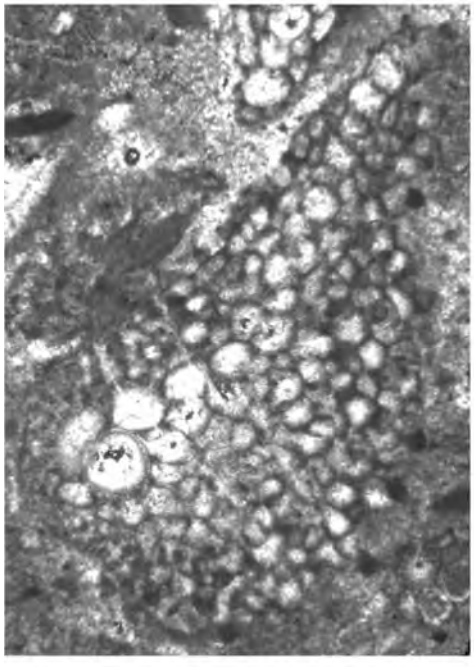

3

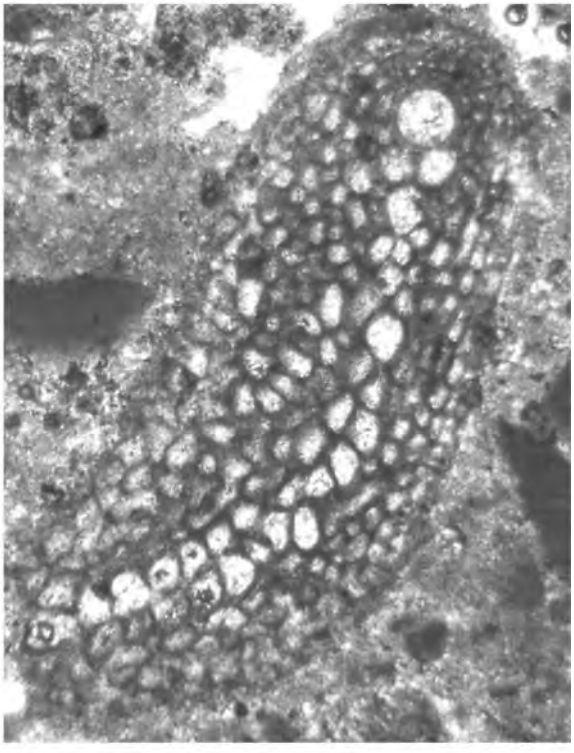

4

PLATE - 12

Rupelian-Early Chattian, Edilme and Develi measured stratigraphical sections, W Malatya, Eastern Turkey, X 50.

Figures 1-8: *Neorotalia lithothamnica* Uhlig, 1886

1: Transversal equatorial section, (FGM-19/29/2).

2: Equatorial section, (FGD-2B/13/2).

3: Transversal section, (FGM-19/22/1), dense ornaments in umbilical side are very clearly seen.

4: Noncentered equatorial section, (FGM-19/24/2), ornaments in umbilical side and short spines in last chambers are seen.

5: Almost equatorial section, (FGM-19/3/1).

6: Equatorial section, (FGM-19/3/1).

7: Axial section, (FGM-19/25/1).

8: Axial section, (FGM-19/28/1).

PLATE - 12

1

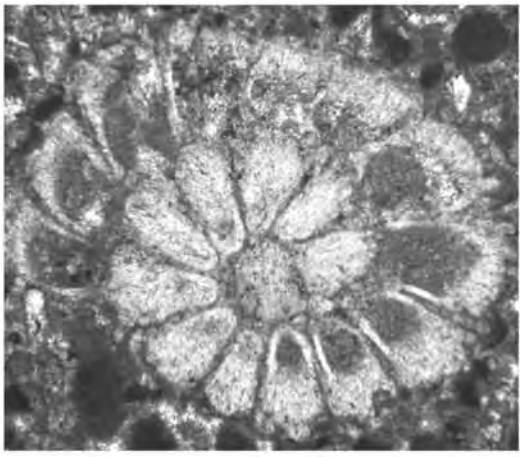

2

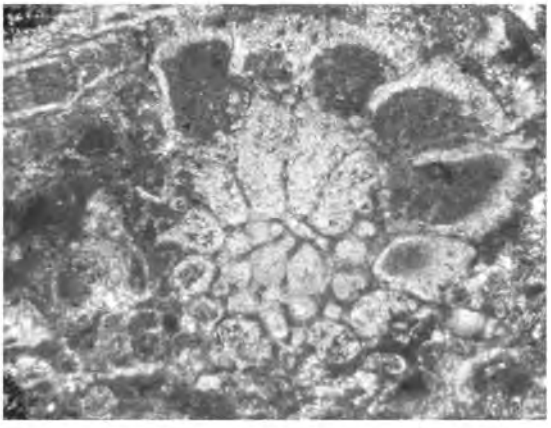

0.25 mm

3

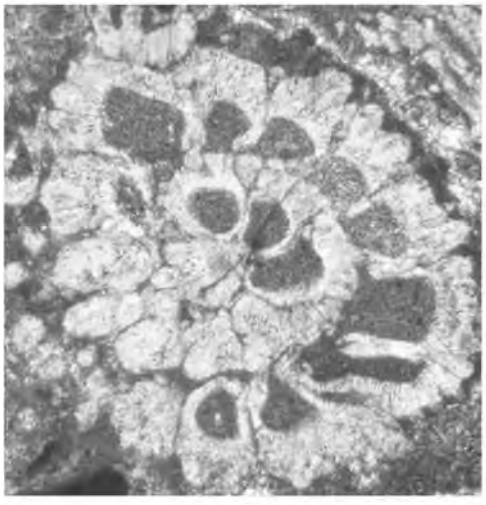

4

5

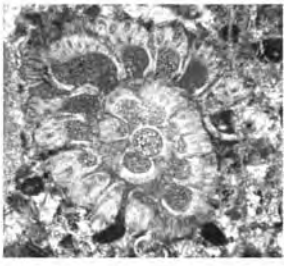

6

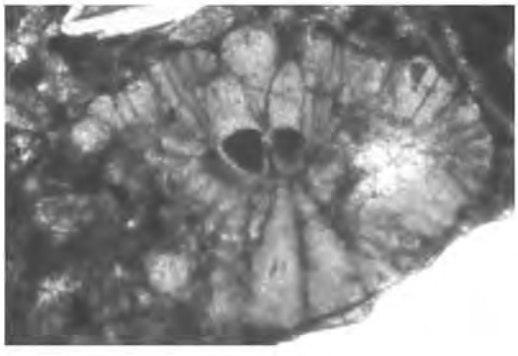

7

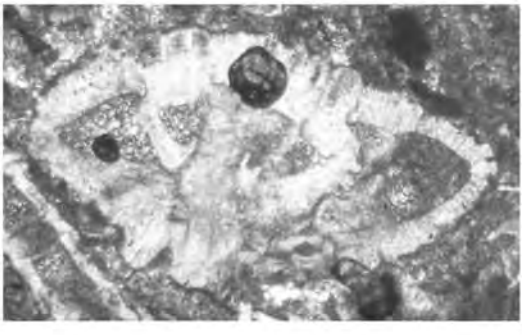

8

PLATE - 13

Figures 1, 2, 5: *Spiroclypeus vermicularis* Tan, 1937
Late Chattian, Develi measured stratigraphical section, W Malatya, Eastern Turkey, X 15.
1, 2: Equatorial section, A form, (FGD-7).
5: Axial section, A form, (FGD-7).
Figures 3, 4, 6, 7: *Spiroclypeus* sp.
Oligocene, Develi and Edilme measured stratigraphical sections, W Malatya, Eastern Turkey, X 15.
Equatorial section, (FGD-6, FGM-18, FGM-14).
Figures 8-10, 12-15: *Heterostegina assilinoides* Blanckenhorn, 1890 emend. Henson, 1937
Rupelian-Early Chattian, Edilme measured stratigraphical section, W Malatya, Eastern Turkey, X 20.
8, 9, 14, 15: Axial section, A form, (FGM-12B, FGM-5B, FGM-19, FGM-4A).
10: Uncompleted equatorial section, A form, (FGM-19/8).
12, 13: Equatorial section, A form, (FGM-19/1, FGM-19/2).
Figure 11: Nummulitidae (*Spiroclypeus* ?/ *Heterostegina* ? sp.)
Transversal equatorial section, (FGM-5B).
Figures 16-19: *Nummulites* cf. *vascus* Joly and Leymerie
Rupelian-Early Chattian, Edilme measured stratigraphical section, W Malatya, Eastern Turkey, X 20.
Axial sections, (FGM-5E/2/3, FGM-5E/3/1, FGM-5E/1/1, FGM-5E/5/5).
Figure 20: *Operculina* sp.
Equatorial section, (FGM-9B).
Figure 21: *Amphistegina* sp.
Equatorial section, (FGM-7A).

PLATE - 13

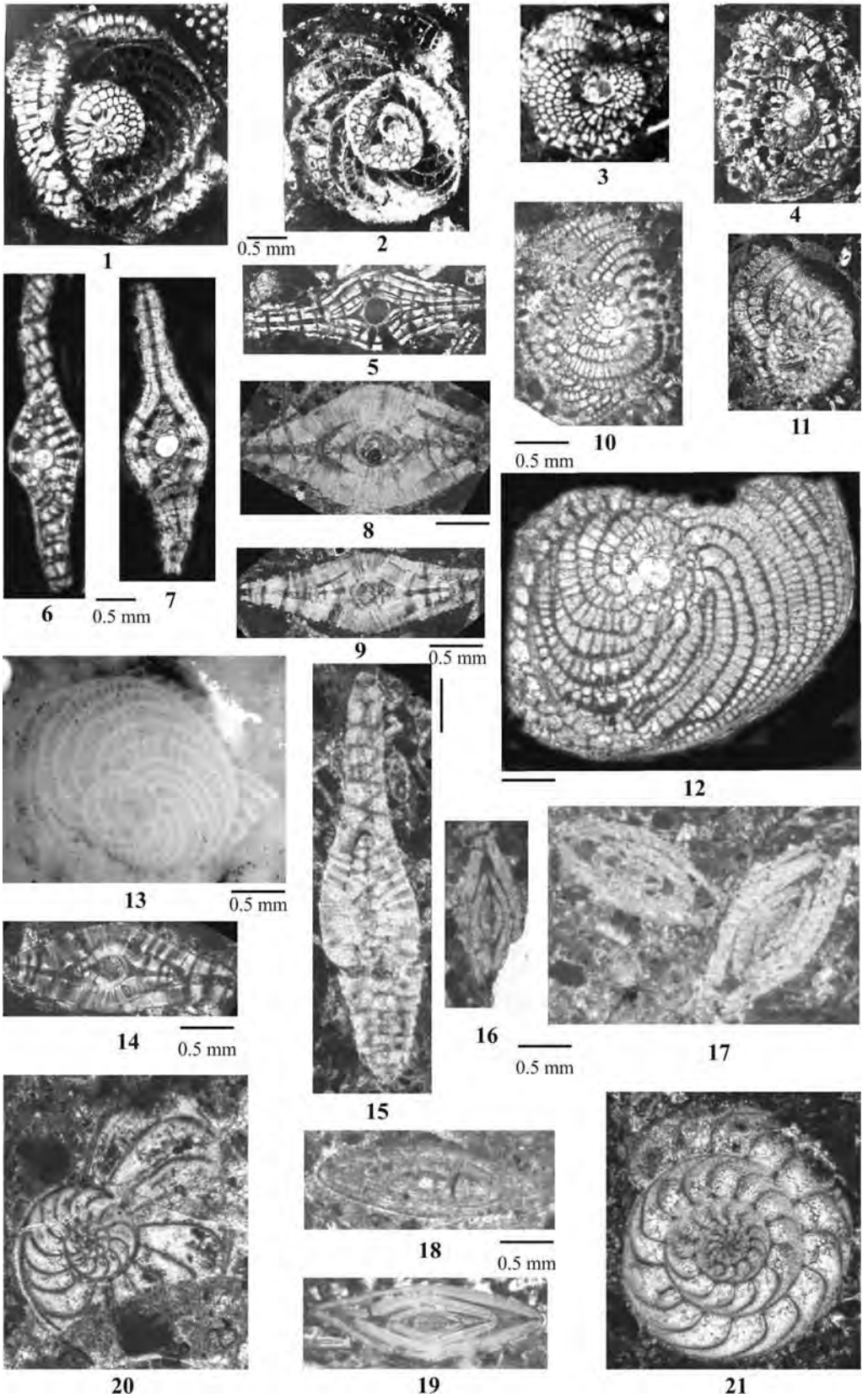
1
0.5 mm
2
3
4
5
6
0.5 mm
7
8
9
0.5 mm
10
0.5 mm
11
12
13
0.5 mm
14
0.5 mm
15
16
0.5 mm
17
18
0.5 mm
19
20
21

BULLETIN OF THE MINERAL RESEARCH AND EXPLORATION

Foreign Edition 2014 149

CONTENTS

Facies Characteristics And Control Mechanisms of Quaternary Deposits In The Lake Tuz Basin
.....Alper GÜRBÜZ and Nizamettin KAZANCI 1

Neotectonic-Period Characteristics, Seismicity, Geometry And Segmentation of The Tuz Gölü Fault Zone
.....Akın KÜRÇER and Y. Ergun GÖKTEN 19

Neogene Stratigraphy And Paleogeographic Evolution of The Karaburun Area, İzmir, Western Turkey
.....Fikret GÖKTAŞ 69

Benthic Foraminiferal Fauna of Malatya Oligo-Miocene Basin (Eastern Taurids, Eastern Turkey)
.....Fatma GEDİK 93

Protolith Nature And Tectonomagmatic Features of Amphibolites From The Qushchi Area, West Azerbaijan, NW Iran
.....Mohssen MOAZZEN 139

Glauberite-Halite Association In Bozkır Formation (Pliocene Çankırı-Çorum Basin, Central Anatolia, Turkey)
.....İlhan SÖNMEZ 153

Estimation of Swelling Pressure Using Simple Soil Indices
.....Kamil KAYABALI and Özgür YALDIZ 177

Two Examples For Imaging Buried Geological Boundaries: Sinkhole Structure And Seyit Hacı Fault, Karapınar, Konya
.....Ertan TOKER, Yahya ÇİFTÇİ, Aytekin AYVA and Akın KÜRÇER 189

The Assessment of Geothermal Potential of Turkey By Means Of Heat Flow Estimation
.....Uğur AKIN, Emin Uğur ULUGERGERLİ and Semih KUTLU 201

A Brief Note On Mineral Evolution And Biochemistry
.....José Mario AMİGO 211

Critisism on the paper "Possible Incision of The Large Valleys In Southern Marmara Region, Turkey (Nizamettin KAZANCI, Ömer EMRE, Korhan ERTURAÇ, Suzanne A.G. LEROY, Salim ÖNCEL, Özden İLERİ and Özlem TOPRAK)
.....Nizamettin KAZANCI 219

Acknowledgement 221

Notes to the authors 223

Bull. Min. Res. Exp. (2014) 149: 139-152

Bulletin of the
Mineral Research and Exploration

http://bulletin.mta.gov.tr

PROTOLITH NATURE AND TECTONOMAGMATIC FEATURES OF AMPHIBOLITES FROM THE QUSHCHI AREA, WEST AZERBAIJAN, NW IRAN

Mohssen MOAZZEN[a*]

[a] *Tebriz Üniversitesi, Yerbilimleri Bölümü, 5166, Tebriz, İran*

Keywords:
Amphibolite, sub-alkaline magma, relict clinopyroxene, volcanic arc, W Azerbaijan, NW Iran

ABSTRACT

Amphibolites from the Qushchi area in west Azerbaijan province, NW Iran are metabasites containing hornblende, plagioclase, epidote, garnet, relict igneous clinopyroxene and titanite, apatite and opaque minerals as accessory phases. They are spatially associated with an ophiolitic mélange but their relationship is not clear. Based on whole rock geochemistry of the amphibolites, they are formed from sub-alkaline andesite-basalt with a tholeiitic affinity. TiO_2 content of the analyzed amphibolite samples is mainly less than 1%, indicating an EMORB original character for the magma. Major and trace element geochemistry of the studied rocks indicate a volcanic arc setting for the rocks. Chemistry of relict igneous clinopyroxene shows that they are diopside in composition with Mg# of 86.75-88.78 and indicating tholeiitic magma type derived from volcanic arc setting, which is in agreement with the results from the whole rock chemistry. Low Ti content of the clinopyroxene points to a depleted mantle source for the magma of the protoliths of Qushchi amphibolites. There is no isotopic age constrains on the studied amphibolites, therefore their relation to the ophiolitic mélange of the area is uncertain especially that the mélange is allochthonous. Three possibilities can be proposed for the formation of the studied amphibolites. If these rocks are Late Cretaceous- Paleocene in age, they might have been formed as parts of a volcanic arc in the Neotethyan oceanic crust. In this case, the ophiolitic complex and the volcanic arc rocks all are metamorphosed at amphibolite facies following the Neotethys ocean closure and the continental collision. Based on field relations and comparing the studied amphibolites with similar amphibolites from the adjacent Khoy area, alternatively the amphibolite formation can be consider to predate the formation of Neotethys-related ophiolite mélange. Since the serpentinite in the ophiolitic mélange is not metamorphosed, the second explanations can be valid for the formation of the amphibolites. The third possibility is that the protolith of the amphibolites was contemporaneous with ophiolite formation, but this protolith is metamorphosed within the accretionary prism but the obducted ophiolitic rocks (including serpentinite) not subjected to metamorphism.

1. Introduction

The main suture of the Neotethys closure is along the Zagros orogen in Iran, which is continued to the northwest and is connected to the Izmir-Ankara-Erzincan and Bitlis sutures (Figure 1; Okay and Tüysüz, 1999; Göncüoglu et al., 2010; Moazzen et al., 2012; Topuz et al., 2013). Ophiolites in NW Iran appear in the Khoy, Chaldoran, Serow, Salmas and Piranshahr areas (Figure 2). Amphibolite and greenschist always accompany these ophiolites. Also amphibolites occur along with (or within) the ophiolitic rocks from the İzmir-Ankara-Erzincan and Bitlis sutures in Turkey. The main amphibolite

* *Corresponding author: Mohssen MOAZZEN, moazzen@tabrizu.ac.ir*

outcrops associated with Orhanlı, Tavşanlı Karaburhan (Eskişehir) and Dutluca ophiolites along the İzmir-Ankara-Erzincan suture are considered to be of Triassic-Cretaceous age (Sarıfakıoğlu et al., 2010). There are not much studies on amphibolites associated with ophiolitic complexes of NW İran. These amphibolites are considered as old (Precambrian) units or as rocks with unknown ages in most of the geological maps published by the geological survey of Iran.

Amphibolites can be found with considerable exposures along with Chaldoran, Khoy and Salmas ophiolites (Hassanipak and Ghazi, 2000; Khalatbari-Jafari et al., 2004; Juteau, 2004; Aftabi et al., 2006; Azizi et al., 2006; Moazzen and Oberhänsli, 2008; Monsef et al., 2010), (Figure 2). Amphibolites of the Qushchi area are adjacent to the Salmas ophiolitic complex (Figure 3). Two types of amphibolites are introduced on Salmas geological map (Khodabandeh, 2003). These are amphibolites associated with other metamorphic rocks (mainly pelitic schist and gneiss) with a probable Precambrian protolithic age and amphibolites and greenschists within the ophiolitic mélange of the Khoy area with Cretaceous age. Amphibolites with a probable Precambrian age are studied here. This age is proposed on the basis of stratigraphical relations and the fact that Permian limestone with distinctive fossils is not metamorphosed. Also Cambrian sedimentary rocks exhibit very low grade metamorphism. Therefore the reasonable age for the relatively high grade metamorphism is Precambrian. However tectonic contact between the rock units makes this conclusion on the age of the amphibolites uncertain. Exact isotopic age dating can resolve this problem.

The applicability of whole rock chemistry to metabasic rocks to determine the magmatic nature and tectonic setting of the parental magma has been debated. Different elements behave differently during metamorphism of mafic rocks. Some elements are mobile and some others act as relatively immobile elements in this regard. For instance K, Na, Si and Ca are mobile during metamorphism while P, Al and Ti are relatively immobile. Elements such as Zr, Sc and Y are practically immobile (Rollinson, 1993; Coish, 1997; Pearce and Cann, 1973; Floyd and Winchester, 1978). White (2001) considers alkali elements with high ionic potential such as K, Ba, Sr, Cs and Rb as mobile elements and Seewald and Seyfried (1990) believe that transitional elements Co, Cr, V, Ni, Nb, Ta and REE are immobile during metamorphism. In overall it is possible to use immobile elements such as P and Ti and rare elements such as Zr, Ta, Nb, V, Cr, Y and REE to distinguish the magmatic nature of the protolith of metamorphosed mafic rocks at greenschist to amphibolite facies. However at higher metamorphic grades, especially at the granulite facies and considering the possibility of partial melting of metabasic rocks at this P-T condition (Hartle and Pattison, 1996; Moazzen et al., 2013) any conclusion on magmatic nature of metabasic rocks protoliths should be treated with caution.

Results from whole rock chemistry of Qushchi amphibolites with emphasis on immobile elements and mineral chemistry of the relict igneous

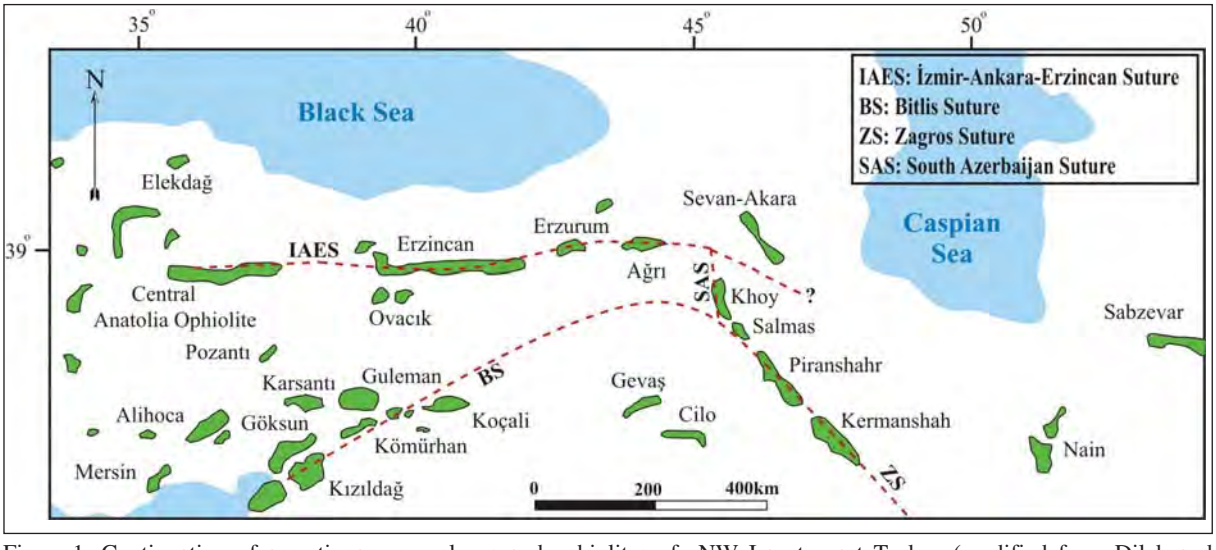

Figure 1- Continuation of accretionary complexes and ophiolites of NW Iran to east Turkey (modified from Dilek and Moores, 1990; Sarıfakıoğlu et al., 2010; Topuz et al., 2013).

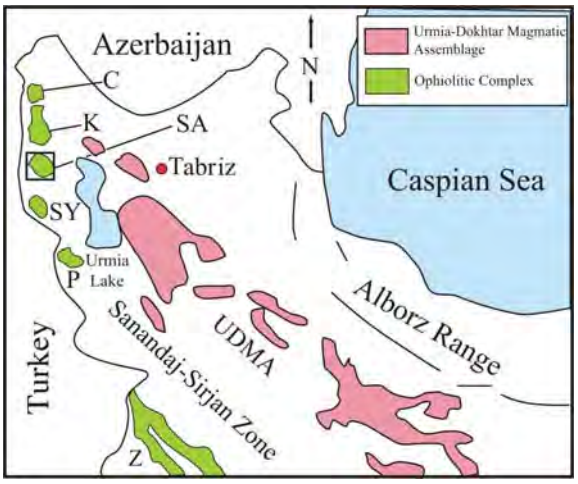

Figure 2- Schematic map of ophiolite outcrops in NW Iran. C; Chaldoran ophiolite complex. K: Khoy ophiolite complex. SY: Sylvana ophiolite complex. P: Piranshahr ophiolite complex. Z: Zagros ophiolites. SA: Study area.

clinopyroxenes in these rocks are used to put constrains on the petrological features and tectonomagmatic aspects of the parental magma forming the protolith of the studied amphibolites.

2. The Geological Background

The study area is located at NW of Iran and within the Sanandaj-Sirjan metamorphic belt according to the definition by Stöcklin (1968). Nabavi (1970) considers this area as a part of the Khoy-Mahabd sub-zone of the Alborz-Azerbaijan zone, based on structural and sedimentary facies relations. Stampfli (1978) suggested that NW Iran, including the study area, is a part of a volcano-molassic depression of central Iran. Stöcklin (1968) assumes that ophiolites of NW Iran have many similarities with ophiolites surrounding the central Iran micro-continent.

According to the field studies, the oldest rocks of the area are a complex of sedimentary, magmatic with granitic to dioritic composition, and greenschist to amphibolite facies metamorphic rocks (Figure 3). These rocks are exposed along the Salmas-Urmia road and are overlain by non-metamorphic Permian carbonates (Figure 4a). The metamorphic complex is always structurally below the Permian carbonates at all localities in NW Iran. Since the carbonate rocks are not metamorphosed, a possible Precambrian age is proposed for this complex. However radiometric

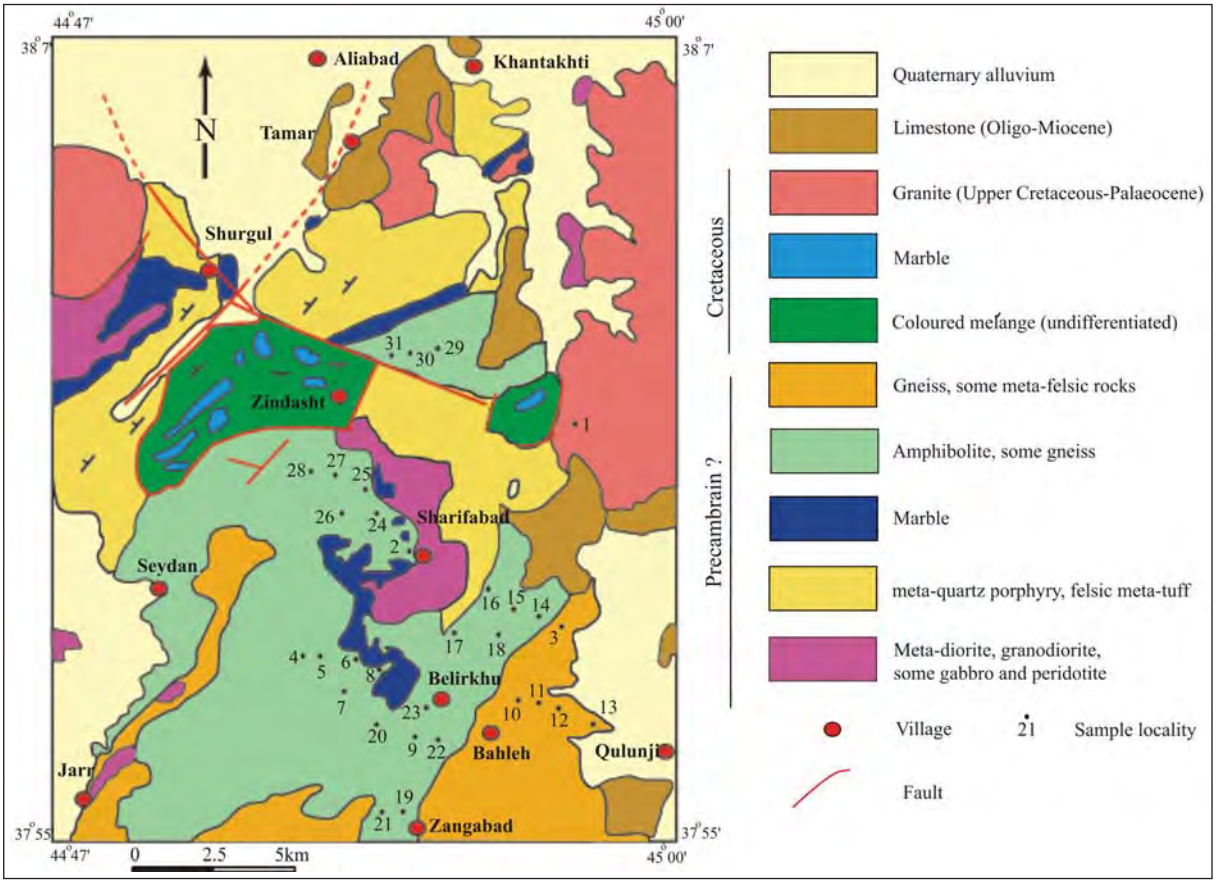

Figure 3- The geological map of the Qushchi area. The location of amphibolite samples are shown on the map.

age dating is necessary to prove this. The rock types of this complex in the studied area are voluminous amphibolites, both as coarse-grained foliated and fine-grained massif amphibolites, sometimes in lithological contact (Figure 4b) with lesser pelitic and psammitic schists, gneiss, meta-rhyolite, meta-rhyodacite, metabasalt, metadiorite and white crystalline marble. These rock types are mixed together due to severe tectonics and finding the original contacts is difficult, however the lithostratigraphic relations in some places show that amphibolites are covered by felsic metavolcanic rocks, which themselves are covered by marble. Granite of upper Cretaceous-Palaeocene age cut the metamorphic complex. Lower Cambrian Kahar formation with very low metamorphism is located at the top of the metamorphic rocks with a tectonic contact. The Cretaceous ophiolitic mélange of the area is composed of serpentinized peridotites, mafic rocks (gabbro, diabase and basalt), felsic rocks (diorite and andesite) and metamorphic rocks (greenschist and amphibolite with diorite and gabbro protolith (Khodabandeh, 2003) along with deep sea sediments such as radiolarian chert and pelagic limestone (Figure 3). Shale, sandstone and limestone of Cretaceous age show weak metamorphism. The Miocene rocks are represented by sandstone, conglomerate, shale and marl. Paleocene conglomerate covers these rocks discordantly.

Recent studies by Azizi et al. (2011) on metamorphic complex associated with the Khoy ophiolite (to the north of the study area, Figure 2) reveals that the protolith of metabasites of this complex have an Upper Proterozoic age which are metamorphosed at upper Jurassic to Lower Cretaceous at amphibolite facies. Amphibolites of the Qushchi area are spatially close to the Khoy amphibolites studied by Azizi et al. (2011). Also they show a similar structural position. Probably amphibolites from the Salmas area formed contemporaneously with the Khoy area amphibolites.

3. Petrography

Amphibolites from the Qushchi area can be divided into three main categories including amphibolites composed of plagioclase and hornblende, relict igneous clinopyroxene-bearing amphibolites and biotite-amphibolites. Plagioclase-hornblende amphibolites are dark green rocks with medium to coarse grain minerals composed of plagioclase, hornblende, titanite, with lesser amount of quartz and oxide minerals. Hornblende and plagioclase are the main mineral phases in the rocks. Titanite can be seen in two different forms, as primary and secondary titanite. Primary titanite is prismatic and is present among the other minerals with granoblastic texture, while the secondary titanite resulted from alteration of ilmenite is restricted to ilmenite rims. These type of amphibolites are mainly deformed and lineated. However some samples display relict doleritic texture inherited from the igneous rocks (Figure 5a). Hornblende alignment parallel to the rock lineation makes the rock orientation in some samples. Relict igneous clinopyroxene can be seen as core in some hornblende crystals (Figure 5b). Some samples are rich in hornblende (Figure 5c) and relatively large hornblende crystals give way to porphyroblastic

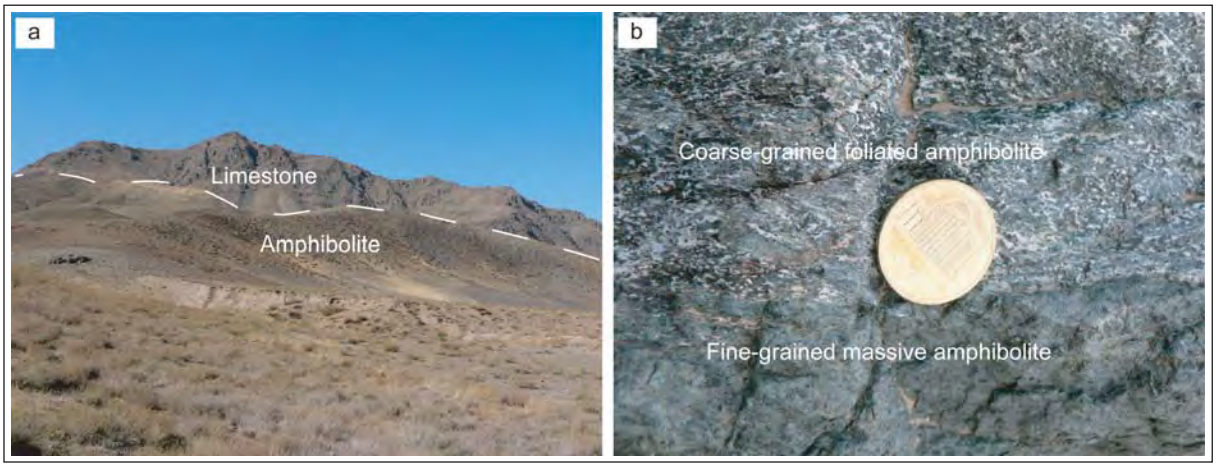

Figure 4- Field photos from the Qushchi amphibolite. a- amphibolites covered by non-metamorphosed Permian limestone. b- coarse-grained foliated amphibolite in contact with fine-grained massif (probably a former dyke) amphibolite.

texture in other samples (Figure 5d). In contrast, some samples have larger plagioclase crystals (Figure 5e). Fine-grain amphibolites are metamorphic products of basalts and fine-grained dolerites (Figure 5f). Some samples with relatively higher quartz contents are the results of metamorphism of quartz-diorite (Figure 6a). Small idioblastic hornblende crystals are formed on the larger hornblende in a few samples (Figure 6b). Existence of the apatite needles is a distinctive feature of many samples (Figure 6c).

Relict igneous clinopyroxene-bearing amphibolites are composed of hornblende, plagioclase, clinopyroxene, titanite and oxide minerals. Quartz is present in these rocks occasionally. Clinopyroxene always is surrounded by hornblende and is not in direct contact with other minerals in the rock (Figures 6e and 6d). This textural disequilibrium shows that the clinopyroxene crystals are relict igneous phases changed to amphibole from the rims during metamorphism. The studied amphibolites are similar to amphibolites from the Khoy area (Moazzen and Oberhänsli, 2008) in this regard.

Hornblende, plagioclase and biotite are the main phases in the biotite-amphibolites. Other minerals include quartz, apatite and oxide minerals. Biotite flakes contain inclusions of zircon. Oxide minerals are as both tiny xenoblastic and larger idioblastic crystals. The idioblastic ones are usually surrounded by an envelope of hornblende (Figure 6f). Biotite-amphibolites lack relict clinopyroxene and form a small part of the Qushchi amphibolites.

4. Methods

In order to determine the magmatic features of the protolith of Qushchi amphibolites, major and trace element analysis were carried out on whole rock samples. The samples were pulverized using a tungsten carbide mill at University of Potsdam, Germany. Then pressed pellets were made from the rock powders for trace elements analysis. About 2 gr of rock powder, 2% polyvinyle alcohol and borax were mixed to make the pressed pellets. Glass bids obtained from alkaline fusion of the sample powders were used for major elements analysis. A X-ray fluorescence at GeoForschungZentrum (GFZ) was employed for the analysis. The results are provided in table 1. Calibration was done using international and internal standards following the method described by Potts et al. (1992). The matrix corrections were done using the appropriate software. Repetition of analysis of standards, indicate relative errors of 1-3% for the major elements and ~5% for the trace elements.

Clinopyroxene in representative, optically well studied samples of the relict clinopyroxene-bearing amphibolites were analysed by a JEOL, JXA-8800 microprobe at Potsdam University. An accelerating voltage of 15 kv, a specimen current of 20 nA and current diameter of 1-3 μm were used. Counting time was 30 seconds on peaks and half-peak on background. Natural and synthetic standards (Fe_2O_3[Fe], rhodonite [Mn], rutile [Ti], MgO [Mg], wollastonite [Si, Ca], fluorite [F], orthoclase [Al, K] and albite [Na]) were used for calibration. Representative data are provided in table 2. Fe^{2+}/Fe^{3+} ratio is calculated based on stoichiometry (Droop, 1987). The analysed clinopyroxenes are diopside, based on the classification of Morimoto et al. (1988). The Mg# (Mg#=Mg/(Mg+Fe^{2+})) calculated for the clinopyroxenes is high and ranges from 86.75 to 88.78. The cationic values of Ti (0.003 atom per formula unit, apfu), Al (0.03-0.06 apfu), Fe^{3+}(0.03-0.05 apfu), Fe^{2+}(0.106-0.125 apfu), Mn (<0.005 apfu) and Na (0.015-0.028 apfu) are low and Si (1.96-1.98 apfu), Mg (0.815-0.856 apfu) and Ca (.958-0.975 apfu) values are relatively high in the studied clinopyroxenes. The Al^{VI}/Al^{IV} ratio is also low and ranges from 0.240 to 0.577.

5. The Nature Of The Amphibolite's Protolithic Magma And Its Tectonomagmatic Features

Major and trace elements composition of the Qushchi amphibolites indicate that they are products from metamorphism of the former igneous rocks (ortho-amphibolite). The evidence for this are the high Cr and low K_2O and Na_2O contents of the rocks pointing to an igneous source material. To identify the original rock type, Zr/TiO_2 versus Nb/Y diagram (Winchester and Floyd, 1977, immobile elements) is used (Figure 7a). As it is evident from this diagram, the parental rocks have andesite-basalt to basalt magmatic composition. This diagram also shows that the magma was of sub-alkaline type. Using major oxides also shows that the magma was sub-alkaline to K-poor sub-alkaline (Figure 7b). The chemistry of immobile and relatively immobile elements indicates that the magma had a tholeiitic affinity. All samples plot in the tholeiite field on diagram of Ti/Y versus Nb/Y (Figure 7c). Also TiO_2 versus Zr/P_2O_5 diagram shows tholeiitic basalt as the source material (Figure 7d). Therefore a tholeiitic magma can be considered for the parental igneous rocks of the Qushchi amphibolites. Only three samples out of 16 analyzed

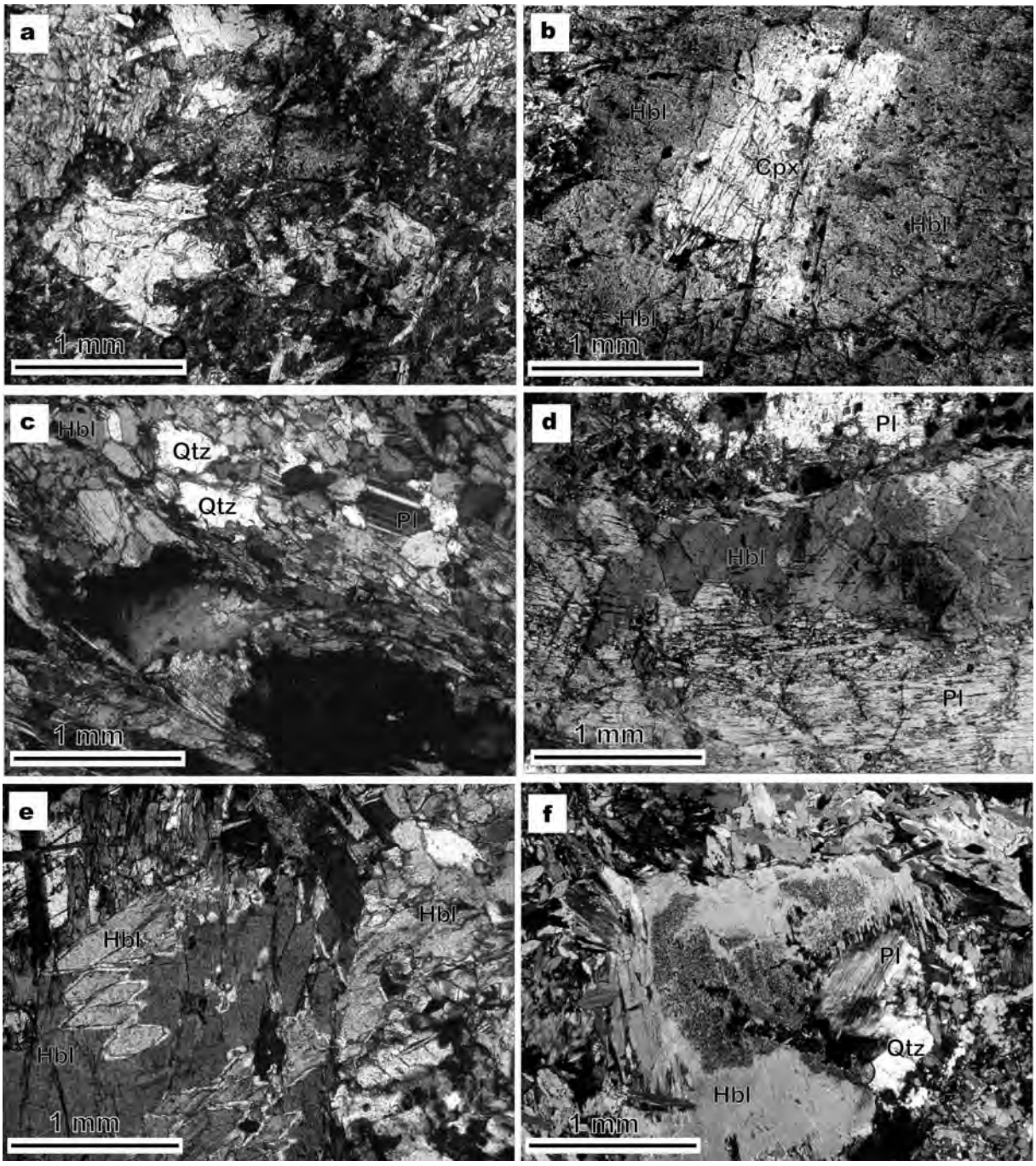

Figure 5- Photomicrographs of the studied amphibolites with their mineralogical and textural features. a: Relict doleritic texture in amphibolite. b: Relict clinopyroxene within hornblende. c: Amphibolite sample made mainly of hornblende with subordinate amount of plagioclase. d: Porphyroblastic amphibolite with relatively large hornblende. e: large plagioclase crystals in amphibolite. f: fine-grained amphibolite which is more likely formed by metamorphism of extrusive rocks. All photos in cross polarized light.

samples have TiO_2 contents more than 1 wt% (all less than 1.5 wt%). According to the TiO_2 contents and considering that TiO_2 is immobile during alteration and metamorphism up to amphibolite facies, an EMORB tholeiite can be proposed considering the chemical features, as the magma from which the mafic protolith of the Qushchi amphibolites were crystallized.

In order to find out the paleotectonic setting of the protoliths of the Qushchi amphibolites, discriminant diagrams for different tectonic settings of mafic rocks

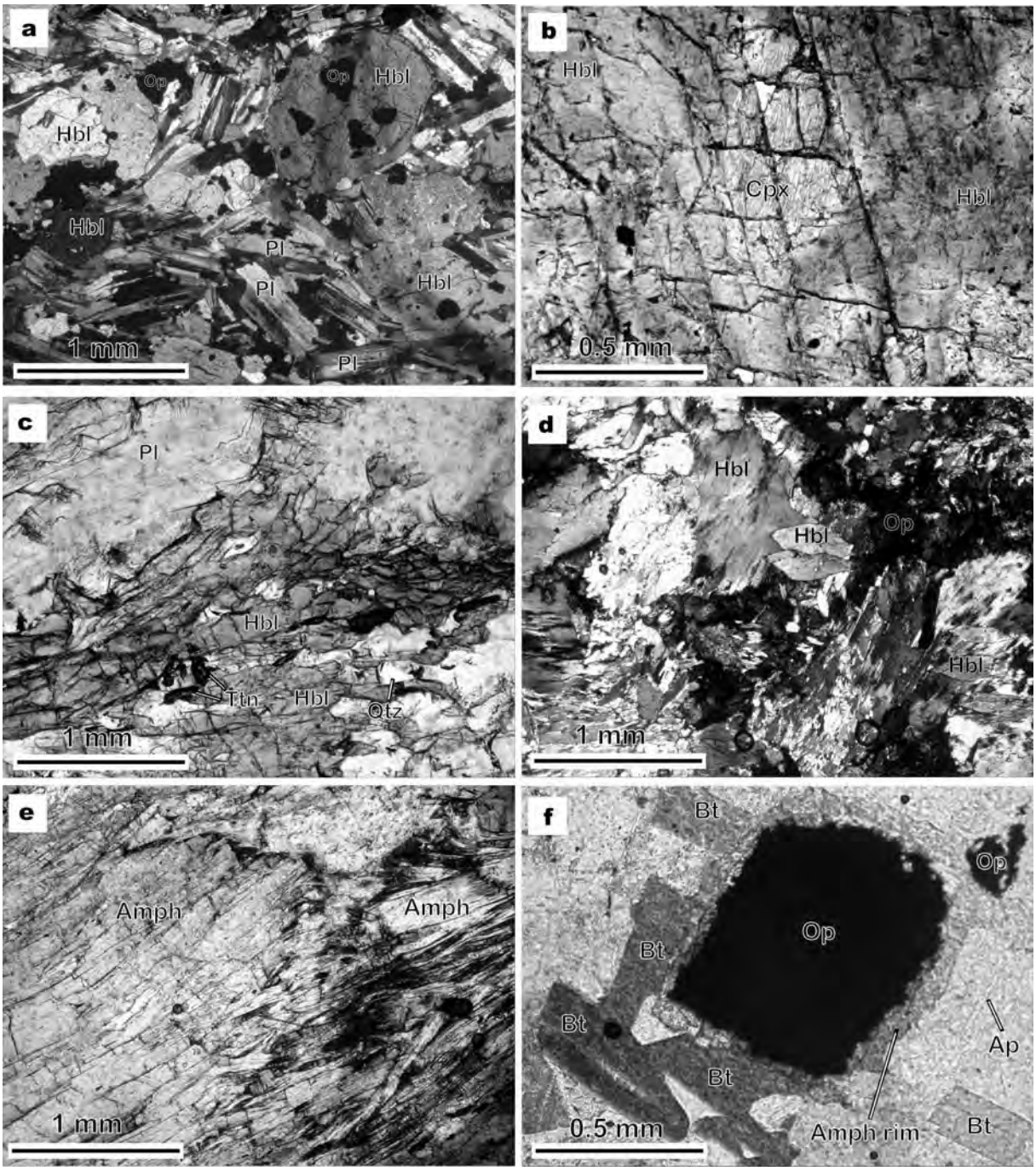

Figure 6- Photomicrographs of western Qushchi amphibolites (continued). a: amphibolite with relatively high quartz content with a quartz diorite protolith. b: idioblastic small hornblende grown on larger hornblende. c: numerous apatite needles in amphibolite. d and e: relict igneous clinopyroxene enveloped by amphibole and is not in direct contact with other minerals in the rock. f: opaque minerals surrounded by amphibole. a and d are in cross polarized light and all other images are in plain polarized light.

are used. In Cr versus Y diagram (Figure 8a) the studied samples plot in the mid-oceanic basalt (MORB), within plate basalt (WPB) and volcanic arc basalt (VAB) fields. Although most of the samples plot in the VAB field, it is not possible to make a clear decision on tectonic setting of the studied rocks. On TiO_2 versus Zr diagram (Figure 8b) most of the samples plot in the volcanic arc filed, although a few samples plot in the MORB and WPB fields. This is the case for the Nb/Y versus Ti/Y diagram as well (Figure 8c). Al_2O_3/TiO_2 versus CaO/TiO_2 diagram of figure 8d clearly indicates a volcanic arc setting for

Table 1- Whole rock composition of the amphibolite samples from the Qushchi area, NW Iran.

Sample	TSL10	TSL1B	TSL1E	TSL2B	TSL2G	TSL2L	TSL2M	TSL3B	TSL3A	TSL6A	TSL6B	TSL8B	TSL8A	TSL9A	TSL9B	TSL9E
Major oxides, wt%																
SiO_2	47.02	51.58	49.10	48.05	49.73	47.99	48.22	48.22	48.97	51.10	51.73	49.79	49.54	50.21	48.61	49.57
TiO_2	1.37	0.36	0.26	0.14	0.56	0.15	0.18	1.19	1.10	0.45	0.86	0.78	0.74	0.56	0.23	0.44
Al_2O_3	15.96	17.56	16.79	18.60	16.18	17.76	16.92	15.70	15.23	16.66	18.09	16.62	15.78	15.36	15.89	16.20
$Fe_2O^*_3$	10.60	6.26	5.77	4.11	8.13	4.17	4.47	10.19	9.83	7.45	7.66	7.41	8.33	8.40	5.63	5.90
MnO	0.18	0.13	0.10	0.08	0.12	0.08	0.09	0.17	0.16	0.14	0.13	0.14	0.15	0.14	0.11	0.12
MgO	8.18	6.78	10.35	10.53	8.11	10.92	11.61	8.04	8.00	7.09	5.47	10.09	9.77	9.51	11.69	9.17
CaO	9.69	11.60	13.89	14.67	13.01	15.43	15.54	10.67	10.39	10.67	9.38	8.99	10.52	10.52	11.87	13.89
Na_2O	2.45	3.42	1.84	1.34	2.39	0.97	0.90	2.28	2.38	2.84	3.28	3.78	3.20	3.58	2.85	2.14
K_2O	1.34	0.10	0.11	0.02	0.27	0.02	0.02	0.61	0.86	1.44	0.90	0.17	0.11	0.14	0.23	0.23
P_2O_5	0.15	0.04	0.03	0.01	0.05	0.01	0.02	0.12	0.11	0.03	0.18	0.09	0.07	0.08	0.04	0.03
LOI	2.67	2.01	1.54	2.13	1.18	2.14	1.71	2.53	2.66	1.84	2.12	1.80	1.46	1.29	2.47	1.92
Total	99.60	99.80	99.80	99.70	99.70	99.60	99.70	99.70	99.70	99.70	99.80	99.70	99.70	99.80	99.60	99.60
Trace elements, ppm																
Ba	205	43	201	21	23	20	21	181	170	172	147	25	40	78	141	105
Cr	296	28	275	1281	356	1142	1110	264	466	130	63	413	426	136	514	395
Ga	19	13	8	12	13	11	12	18	18	19	20	14	15	14	13	14
Nb	4	3	2	3	3	2	2	2	4	2	3	2	3	2	2	2
Ni	104	79	137	222	131	239	240	79	58	52	29	170	156	147	220	131
Rb	9	10	10	9	9	11	9	10	13	36	21	9	11	9	9	10
Sr	178	174	150	116	138	112	99	171	230	282	340	138	140	192	254	172
V	231	181	135	100	212	101	129	239	228	162	214	213	229	253	146	206
Y	28	12	8	5	16	3	8	26	25	19	14	19	19	15	8	13
Zn	120	39	32	20	60	21	19	84	77	63	65	49	49	42	30	34
Zr	71	22	23	11	38	10	10	93	92	40	46	54	46	33	18	23

Table 2- Representative analyses of relict igneous clinopyroxene in Qushchi amphibolites. Formula unit on the basis of 6 oxygen atoms.

SiO_2	54.80	54.71	54.29	54.52	54.36	54.43	54.16	54.29
TiO_2	0.04	0.03	0.03	0.02	0.11	0.07	0.05	0.09
Al_2O_3	1.06	0.71	1.13	0.94	1.30	1.42	1.16	1.25
Cr_2O_3	0.02	0.00	0.00	0.00	0.00	0.01	0.05	0.17
FeO	5.14	4.73	5.16	4.88	5.22	5.38	5.47	5.60
MnO	0.13	0.16	0.09	0.13	0.15	0.13	0.16	0.13
MgO	15.75	15.91	15.49	15.76	15.35	15.31	15.47	15.14
CaO	25.00	25.19	24.98	25.00	24.89	24.83	24.71	24.95
Na_2O	0.31	0.21	0.37	0.30	0.34	0.40	0.35	0.39
K_2O	0.00	0.00	0.00	0.00	0.00	0.00	0.00	0.00
Total	102.25	101.65	101.56	101.57	101.71	101.97	101.57	102.01
Si	1.97	1.98	1.96	1.97	1.96	1.96	1.96	1.96
Ti	0.00	0.00	0.00	0.00	0.00	0.00	0.00	0.00
Al	0.04	0.03	0.05	0.04	0.06	0.06	0.05	0.05
Cr	0.00	0.00	0.00	0.00	0.00	0.00	0.00	0.00
Fe^{+3}	0.04	0.03	0.05	0.04	0.03	0.04	0.05	0.04
Fe^{+2}	0.12	0.11	0.11	0.11	0.13	0.12	0.12	0.12
Mn	0.00	0.01	0.00	0.00	0.00	0.00	0.00	0.00
Mg	0.84	0.86	0.84	0.85	0.83	0.82	0.83	0.81
Ca	0.96	0.97	0.97	0.97	0.96	0.96	0.96	0.96
Na	0.02	0.01	0.03	0.02	0.02	0.03	0.02	0.03
K	0.00	0.00	0.00	0.00	0.00	0.00	0.00	0.00
Total	4.00	4.00	4.00	4.00	4.00	4.00	4.00	4.00
$Mg/(Mg+Fe^{2+})$	0.88	0.88	0.89	0.89	0.87	0.87	0.88	0.87
$Fe^{2+}/(Fe\text{-total})$	0.76	0.78	0.68	0.73	0.79	0.75	0.70	0.74
$Al/(Al+Fe^{3+}+Cr)$	0.54	0.49	0.49	0.50	0.63	0.60	0.49	0.52

the protolith of the amphibolites. To separate the rocks formed at volcanic arc setting and back arc basin, Ti/Zr versus Zr diagram is used (Figure 8e). Most of the samples are plotted in the volcanic arc setting. Therefore more likely the protolith of the Qushchi amphibolites were formed at a volcanic arc setting.

The mineral chemistry of the relict igneous clinopyroxenes in the studied rocks, is used to confirm the tectonic setting for the protolith. This is an accepted practice for igneous rocks (Nisbet and Pearce, 1977). Relict igneous clinopyroxenes from the Qushchi area, define a sub-alkaline magma type for the protoliths on Leterrier et al. (1982) diagrams (Figures 9). The low Na_2O content in the clinopyroxenes confirms the sub-alkaline nature for the magma and a relatively low pressure for clinopyroxene crystallization (Bonev and Stampfli, 2009). Also Ti content in Qushchi samples is low. This may reflect a depleted mantle nature for the source materials (Pearce and Norry, 1979).

Clinopyroxene composition is used to confirm volcanic arc setting for the magmas from which the protolith of the Qushchi amphibolites are crystallized. Considering Ti versus Ca diagram of Leterrier et al. (1982), the protolith of the amphibolites is formed at an orogenic environment (Figure 9a). In order to find the tectonic setting more precisely, F1 versus F2 diagram of Nisbet and Pearce (1977) and Ti+Cr versus Ca diagram of Leterrier et al. (1982) are used (Figure 9b and 9c). These diagrams indicate volcanic arc-oceanic floor basalt and volcanic arc setting.

6. Discussion and Conclusions

Amphibolites from the east of Qushchi in west Azerbaijan province of Iran mineralogically (high hornblende and plagioclase and low quartz content)

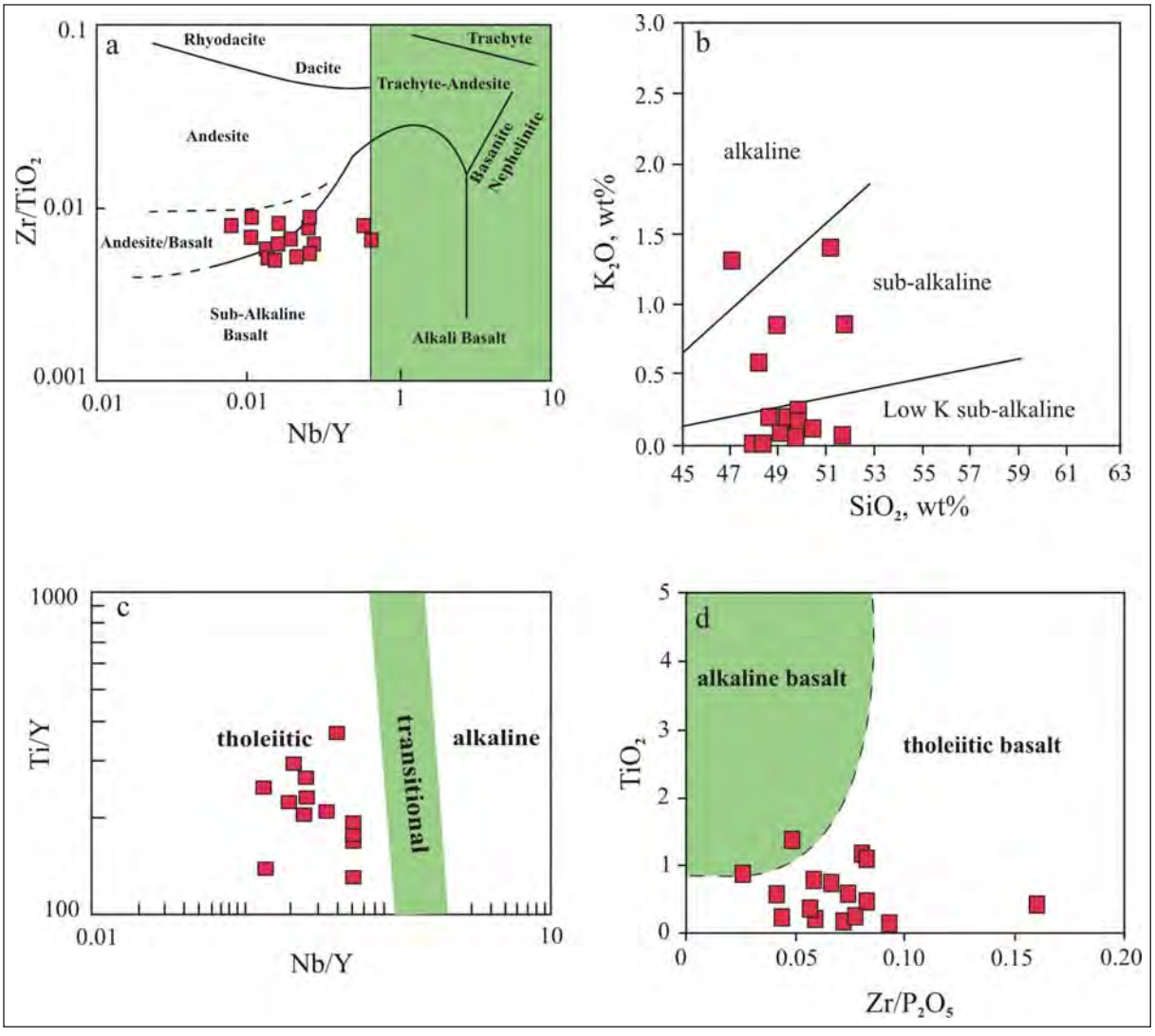

Figure 7- Diagrams used to identify the protolith nature of the Qushchi amphibolites. The protolith was andesite basalt and the original magma was sub alkaline tholeiite. Diagrams a and d from Winchester and Floyd (1977), diagram b from Middlemost (1975) and diagram c from Pearce (1982).

and chemically (low K_2O) are ortho-amphibolites resulted from metamorphism of mafic igneous rocks. The protolith was a sub alkaline andesite basalt to basalt. The magma forming the protolith was of tholeiitic nature. Tectonic setting discriminant diagrams show that this magma was formed at a volcanic arc setting. The exact age of the amphibolites is not known, but Haghipour and Aghanabati (1989) proposed a Precambrian-Paleozoic age for them based on the fact that the associated Permian limestone of the area (with tectonic contact) is not metamorphosed. Azizi et al. (2011) reported Upper Paleozoic age (U–Pb zircon) for protolith and Upper Cretaceous-Lower Triassic (Rb–Sr mineral isochron) for metamorphism of the Khoy amphibolites to the north of the study area. Since the non-metamorphosed Permian limestone is in tectonic contact with the studied amphibolites, it is not easy to conclude about the age of metamorphism in the Qushchi area. The ophiolitic mélange in the Salmas area is Upper Cretaceous-Paleocene in age. The studied amphibolite can be considered as tectonic slivers of this ophiolitic mélange.

If these rocks are Late Cretaceous- Paleocene in age, they might have been formed as parts of a volcanic arc in the Neotethyan oceanic crust. In this case, the ophiolitic complex and the volcanic arc rocks all are metamorphosed at amphibolite facies following the Neotethys ocean closure and the

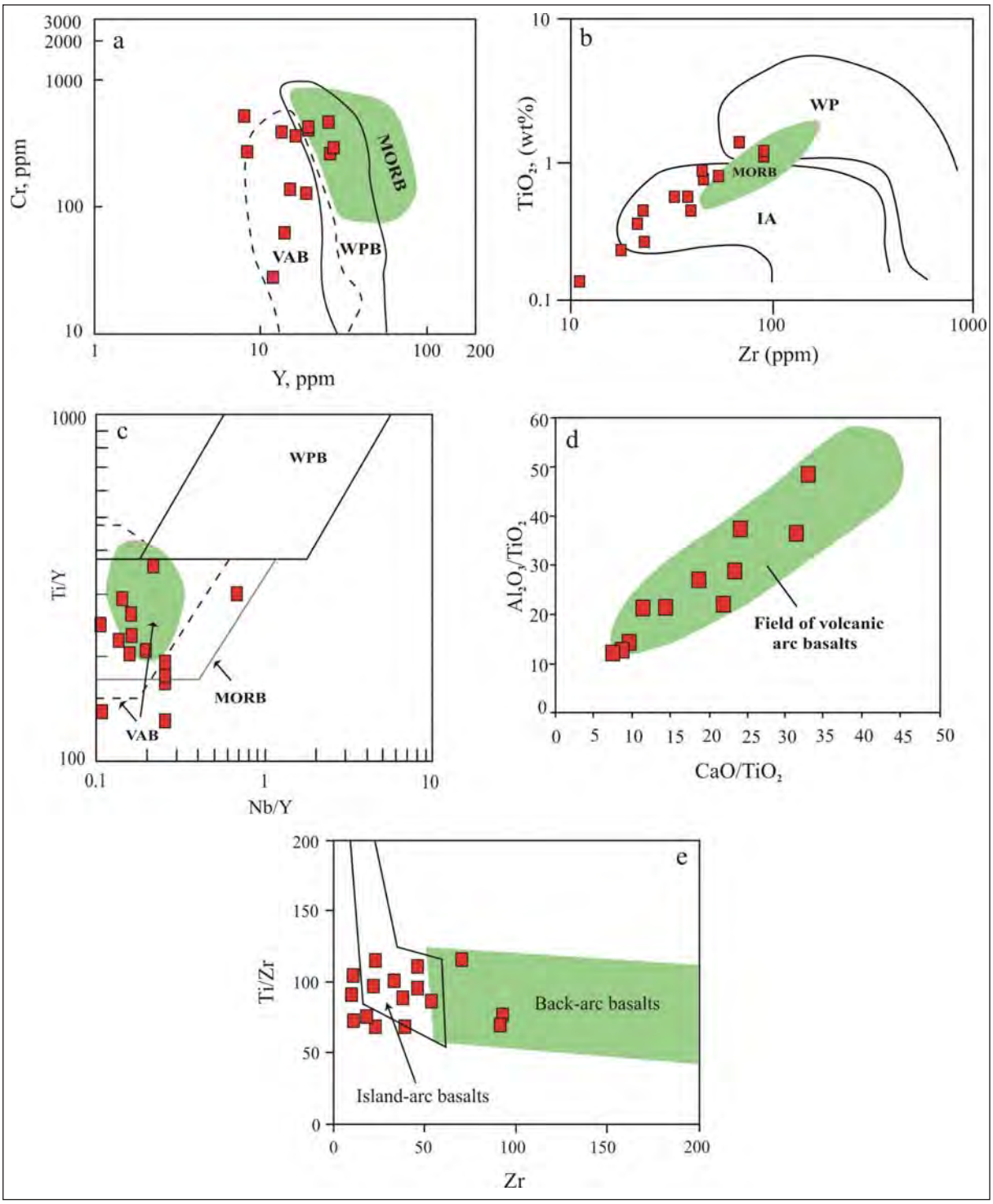

Figure 8- Tectonic discrimination diagrams to identify the tectonic environment of formation of the original magma of Qushchi amphibolites. See the text for explanations. Diagram a from Pearce et al. (1984), diagrams e, c, b from Pearce (1982) and diagram d from Sun and Nesbitt (1978).

continental collision. The alternative scenario is that the studied amphibolites are older than the ophiolitic mélange. In this case amphibolites from the Qushchi area are equivalents the similar amphibolites from the Khoy area, studied by Azizi et al. (2011) and they predate the closure of the Neotethys. However, considering that the serpentinites within the ophiolitic mélange lack the antigorite polymorph and are not

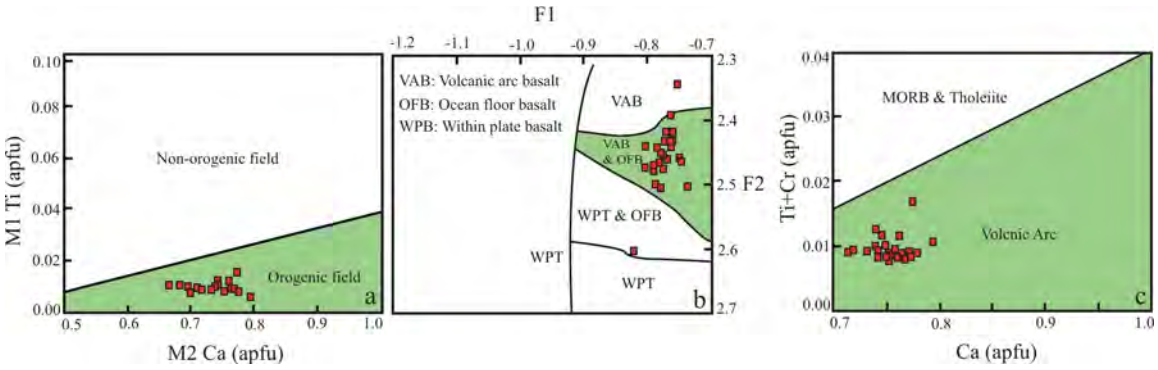

Figure 9- Relict igneous clinopyroxene composition in the amphibolites which indicate sub-alkaline type for the original magma. Diagram after Leterrier et al. (1982). a: The protolith of the amphibolites formed at an orogenic environment (diagram from Letterier et al., 1982). b: F1 versus F2 diagram of Nisbet and Pearce (1977) showing either volcanic arc basalt or ocean floor basalt for the protolith of the studied amphibolites. F1= -(0.012*SiO_2) - (0.0807*TiO_2) + (0.0026*Al_2O_3) - (0.0012*FeO) - (0.0026* MnO) + (0.0087 *MgO) - (0.0128*CaO) - (0.0419*Na_2O). F2= - (0.0469*SiO_2) - (0.0818*TiO_2) + (0.0212*Al_2O_3) - (0.0041*FeO) - (0.1435*MnO) + (0.0029*MgO) + (0.0085*CaO) + (0.016*Na_2O). c: Ti+Cr versus Ca diagram of Leterrier et al. (1982) clearly shows volcanic arc setting for the original magma of the Qushchi amphibolite protolith.

metamorphosed in amphibolite facies conditions, it is likely that the studied amphibolites are not part of the mélange. The third possibility is that the generation of protolith of the amphibolites was contemporaneous with ophiolite formation, but this protolith is metamorphosed within the accretionary prism but the obducted ophiolitic rocks (including serpentinite) are not metamorphosed. Radiometric age determinations from these amphibolites will help to solve this problem and to reconstruct their formation history.

Acknowledgements

This paper is supported financially by the Research Office of the University of Tabriz. I am grateful to C. Gunter and A. Musiol from Potsdam University for their help with analysis. Thoughtful reviews by Dr. M. C. Göncüoglu and Dr. O. Candan improved the manuscript. Generous helps by Dr. Taner Ünlü and Cahit Dönmez are highly appreciated.

Received: 14.04.2014
Accepted: 26.08.2014
Published: December 2014

References

Aftabi, A., Ghodrati, Z., MacLean, W. H. 2006. Metamorphic textures and geochemistry of the Cyprus-type massive sulfide lenses at Zurabad, Khoy, Iran. *Journal of Asian Earth Sciences* 27, 523–533.

Azizi, H., Moinvaziri, H., Mohajjel, M., Yagobpoor, A. 2006. PTt path in metamorphic rocks of the Khoy region (northwest Iran) and their tectonic significance for Cretaceous– Tertiary continental collision. *Journal of Asian Earth Sciences* 27, 1–9.

Azizi, H., Chung, S-L., Tanaka, T., Asahara, Y. 2011. Isotopic dating of the Khoy metamorphic complex (KMC), northwestern Iran: A significant revision of the formation age and magma source. *Precambrian Research* 185, 87–94

Bonev, N., Stampfli, G. 2009. Gabbro, plagiogranite and associated dykes in the supra-subduction zone, Evros Ophiolites, NE Greece. *Geological Magazine* 146, 72-91.

Coish, R.A. 1997. Rift and ocean floor volcanism from the late Proterozoic and Early Paleozoic of the Vermont Appalachians in Sinha, A.K., Whalen, J.B., Hogan, J.P. eds., The nature of magmatism in the Appalachian Orogen. *Geological Society of America Memoir* 191, 129-145.

Dilek, Y., Moores, E. M. 1990. Regional tectonics of Eastern Mediterranean ophiolites, in Malpas, I., Moores, E.M., Panagiotou, A., and Xenophontas, C., eds., Ophiolites- Oceanic Crustal Analogues. Proceedings of the Troodos Symposium: *Nicosia Geological Survey Department*, p. 295–309.

Droop, G. T. R. 1987. A general equation for estimating Fe^{3+}concentration in ferromagnesian silicates and oxides from microprobe analyses using stoichiometric criteria. *Mineralogical Magazine* 51, 431–435.

Floyd, P.A., Winchester, J.A. 1978. Identification and discrimination of altered and metamorphosed volcanics using immobile elements. *Chemical Geology* 21, 291-306.

Göncüoğlu, M. C., Sayit, K., Tekin, U.K. 2010. Oceanization of the northern Neotethys: geochemical evidence from ophiolitic mélange basalts within the Izmir-Ankara suture belt, NW Turkey. *Lithos* 116, 175–187.

Haghipour, A., Aghanabati, A. 1989. Geological map of Iran 1:2.500.000 scale. *Geological Survey of Iran*. Second edition.

Hartle, T. H. D., Pattison, D. R. M. 1996. Genesis of the Kapuskasing (Ontario) migmatitic mafic granulites by dehydration melting of amphibolite: the importance of quartz toreaction progress. *Journal of Metamorphic Geology* 14, 591–611

Hassanipak, A. A., Ghazi, A. M. 2000. Petrology, geochemistry and tectonic setting of the Khoy ophiolite, northwest Iran: implications for Tethyan tectonics. *Journal of Asian Earth Sciences* 18, 109-121.

Juteau, T. 2004. The ophiolites of Khoy (NW Iran): their significance in the Tethyan ophiolite belts of the Middle-East. *Comptes Rendus Geoscience* 336, 105–108

Khalatbari-Jafari, M., Juteau, J., Bellon, H., Whitechurch, H., Cotton, J., Emami, H. 2004. New geological, geochronological and geochemical investigations on the Khoy ophiolites and related formations, NW Iran. *Journal of Asian Earth Sciences* 23, 507–535

Khodabandeh, A. A., 2003. Geological map of Salmas. 1:100,000 map series, *Geological Survey of Iran*.

Leterrier, J., Maury, R. C., Thonon, P., Girad, D., Marchel, M. 1982. Clinopyroxene composition as a method of identification of the magmatic affinities of paleo-volcanic series. *Earth and Planetary Science Letters* 59, 139–154.

Middlemost, E. A. K. 1975. The basalt clan. *Earth Science Review* 11: 337-64.

Moazzen, M.; Oberhänsli, R. 2008. Whole rock and relict igneous clinopyroxene geochemistry of ophiolite-related amphibolites from NW Iran – Implications for protolith nature. *Neues Jahrbuch fur Mineralogie Abhandlungen* 185/1, 51–62.

Moazzen. M, Alchalan, S., Hajialioghli, R., Morishita, T., Rezaei, M. 2012. Ophiolitic peridotites from the Western Khoy ophiolitic complex, NW Iran; Petrological and geochemical characteristics and application for connecting the Baft-Khoy and Izmir-Ankara-Erzincan sutures. *In: Proceedings of International Earth Science Colloquium on the Aegean Region*, 1–5 October 2012, Izmir, Turkey, p 9.

Moazzen, M., Hajialioghli, R., Möller, A., Droop, G.T.R., Oberhänsli, R., Altenberger, U., Jahangiri, A. 2013. Oligocene partial melting in the Takab metamorphic complex, NW Iran: Evidence from in situ U-Pb geochronology. *Journal of Sciences, Islamic Republic of Iran* 24, 217-228.

Monsef, I., Rahgoshay, M., Mohajjel, M., Shafaii Moghaddam, H., 2010. Peridotites from the Khoy Ophiolitic Complex, NW Iran: Evidence of mantle dynamics in a supra-subduction-zone context. *Journal of Asian Earth Sciences* 38, 105–120.

Morimoto, N., Fabries, J., Ferguson, A. K., Ginzburg, I. V., Ross, M., Seifert, F., A., Zussman, J., Aoki, K., Gottardi, G. 1988. Nomenclature of pyroxenes. *Mineralogical Magazine* 52, 535–550.

Nabavi, M. H. 1976. An introduction to the geology of Iran. *Geological Survey of Iran*. (in Persian).

Nisbet, E. G., Pearce, J. A.1977. Clinopyroxene composition in mafic lavas from different tectonic settings. *Ibid*. 63, 149–160.

Okay, A.I., Tüysüz, O. 1999. Tethyan sutures of northern Turkey. In: Durand B, Jolivet L, Horvath E, Seranne M (eds) The Mediterranean Basins: tertiary extension within the Alpine Orogen. Geological Society London Special Publication, Volume. 156: 475–515.

Pearce, J.A. 1982. Trace element characteristics of lavas from destructive plate boundaries. In: Thorpe, R.S. (eds), andesites. *Wiley, Chichester*, 525-548.

Pearce, J.A., Cann, J.R. 1973. Tectonic setting of basic volcanic rocks determined using trace elements analysis. *Earth and Planetary Science Letters* 19, 290-300.

Pearce, J. A., Norry, M. J. 1979. Petrogenetic implications of Ti, Zr, Y and Nb variations in volcanic rocks. *Contributions to Mineralogy and Petrology* 69, 33-47.

Pearce J. A., Harris N. B. W., Tingle A. G. 1984. Trace element discrimination diagrams for the tectonic interpretation of granitic rocks. *Journal of Petrology* 25, 956–983.

Potts, P. J., Tindle, A. G., Webb, P. C. 1992. Geochemical Reference Material Compositions. *CRC Press, Boca Raton*, FL., USA.

Rollinson, H.R. 1993. Using geochemical data: evaluation, presentation, interpretation. *Longman Group*, UK, 1^{st} edition. 352p.

Sarifakioğlu, E., Özen, H., Çolakoğlu, A., Sayak, H. 2010. Petrology, mineral chemistry, and tectonomagmatic evolution of Late Cretaceous suprasubduction-zone ophiolites in the Izmir–Ankara–Erzincan Suture Zone, Turkey. *International Geology Review* 52(2-3) 187-222.

Seewald, J.C., Seyfried, W.E. 1990. The effect of temperature on metal mobility in Sub Sea floor hydrothermal systems: Constraints from basalts alteration experiments. *Earth and Planetary Science Letters*101, 388-403.

Stampfli, G.M. 1978. Etude géologique générale de l'Elburz oriental au S de Gonbad-e-Qabus, Iran N-E. Faculty of Science, University of Genève Thesis No. 1868, 329 pp.

Stöcklin, J. 1968. Structures history and tectonic of Iran: A review. *American Association of Petroleum Geologist Bulletin* 52(7)

Sun, S.-S., Nesbitt, R.W. 1978. Geochemical regularities and genetic significance of ophiolitic basalts. *Geology* 6, 689–693.

Topuz, G., Göçmengil, G., Rolland, Y., Çelik, F, Zack, T., Schmitt, A., K. 2013. Jurassic accretionary complex and ophiolite from northeast Turkey: No evidence for the Cimmerian continental ribbon. *Geology* 41, 255-258.

White, W.M. 2001. Geochemistry: An on-line text book, http://www.imwa.info/Geochmie, *John- Hopkins University press*. 700p.

Winchester, J.A., Floyd, P.A. 1977. Geochemical discrimination of different magmas series and their differentiation products using immobile elements. *Chemical Geology* 16, 325- 343.

BULLETIN OF THE MINERAL RESEARCH AND EXPLORATION

Foreign Edition 2014 149

CONTENTS

Facies Characteristics And Control Mechanisms of Quaternary Deposits In The Lake Tuz Basin
.....Alper GÜRBÜZ and Nizamettin KAZANCI 1

Neotectonic-Period Characteristics, Seismicity, Geometry And Segmentation of The Tuz Gölü Fault Zone
.....Akın KÜRÇER and Y. Ergun GÖKTEN 19

Neogene Stratigraphy And Paleogeographic Evolution of The Karaburun Area, İzmir, Western Turkey
.....Fikret GÖKTAŞ 69

Benthic Foraminiferal Fauna of Malatya Oligo-Miocene Basin (Eastern Taurids, Eastern Turkey)
.....Fatma GEDİK 93

Protolith Nature And Tectonomagmatic Features of Amphibolites From The Qushchi Area, West Azerbaijan, NW Iran
.....Mohssen MOAZZEN 139

Glauberite-Halite Association In Bozkır Formation (Pliocene Çankırı-Çorum Basin, Central Anatolia, Turkey)
.....İlhan SÖNMEZ 153

Estimation of Swelling Pressure Using Simple Soil Indices
.....Kamil KAYABALI and Özgür YALDIZ 177

Two Examples For Imaging Buried Geological Boundaries: Sinkhole Structure And Seyit Hacı Fault, Karapınar, Konya
.....Ertan TOKER, Yahya ÇİFTÇİ, Aytekin AYVA and Akın KÜRÇER 189

The Assessment of Geothermal Potential of Turkey By Means Of Heat Flow Estimation
.....Uğur AKIN, Emin Uğur ULUGERGERLİ and Semih KUTLU 201

A Brief Note On Mineral Evolution And Biochemistry
.....José Mario AMİGO 211

Critisism on the paper "Possible Incision of The Large Valleys In Southern Marmara Region, Turkey (Nizamettin KAZANCI, Ömer EMRE, Korhan ERTURAÇ, Suzanne A.G. LEROY, Salim ÖNCEL, Özden İLERİ and Özlem TOPRAK)
.....Nizamettin KAZANCI 219

Acknowledgement 221

Notes to the authors 223

Bull. Min. Res. Exp. (2014) 149: 153-175

Bulletin of the
Mineral Research and Exploration

http://bulletin.mta.gov.tr

GLAUBERITE-HALITE ASSOCIATION IN BOZKIR FORMATION (Pliocene, Çankırı-Çorum Basin, Central Anatolia, Turkey)

İlhan SÖNMEZ[a]*

[a] *Maden Tetkik ve Arama Genel Müdürlüğü, Maden Etüt ve Arama Dairesi, 06520 Ankara*

Keywords:
Çankırı-Çorum Basin, fossil evaporite, glauberite, halite, Pliocene, playa lake, sabhka.

ABSTRACT

Tertiary Çankırı – Çorum Basin is one of the biggest basin covering evaporitic formations in the Central Anatolia. During borehole drills carried out in Bozkır Formation which contain Pliocene aged evaporites in the basin, a thick rocksalt (halite, NaCl) deposit was detected that consisting of glauberite ($Na_2Ca(SO_4)_2$) interlayers (sabhka) synchronous with sedimentation. Rocksalt bearing layers in Bozkır formation which was deposited in playa-lake – sabhka environment, where seasonal changes are effective, were first defined as Tuz member in this study. Bozkır formation was divided into three zones in drillings carried out in sabhka – playa -lake transitional environment. From bottom to top, these are ordered as claystone-less anhydrite zone, rock salt-claystone-anhydrite-glauberite zone (Tuz member) and claystone-gypsum-less anhydrite zone. Rocksalt was cut in thicknesses reaching 115 meters within Tuz member. Rocksalt (playa-lake) which is mostly bedded and white, pale/dark gray colored is conformable with sedimentation and is low dipping. The level at which glauberite deposition within Tuz member is observed the thickest was defined as glauberite-mudstone zone. Glauberite mineral which is observed as disc and rosette shaped individual forms within mudstone dominant matrix was formed as a diagenetic mineral in saline mudflat environment (sabhka). In geochemical analyses carried out (XRD, XRF, SEM) it was detected that glauberite mineral had been crystallized following anhydrite mineral within matrix that includes complex crystal forms in sabhka environment, halite mineral had grown on glauberite mineral and it was sometimes observed in the form of fracture and crack infill. The glauberite mineral deposition which does not have an economical thickness is of great importance in terms of the existence of fossil Na-sulfate deposition scientifically in Çankırı-Çorum Basin.

1. Introduction

The study area is located in Çankırı-Çorum Basin which is one of the biggest Tertiary depositional basins of Turkey in the Central Anatolia, 25 km to the southeast of the Çankırı (Figure 1). New lithological findings were obtained during borehole drillings carried out in Bozkır formation which contains Pliocene evaporites in the basin.

Bozkır formation is generally represented by the alternation of claystone, gypsum/anhydrite and was deposited in playa-lake environment. During drillings in the formation thick rocksalt (halite, NaCl) deposition was detected which consists of glauberite ($Na_2Ca(SO_4)_2$) interlayers which were deposited in sabhka environments synchronous with sedimentation. These halite (NaCl) bearing layers were first defined as Tuz member in this study.

The purpose of this study is to reveal Na-sulfate (glauberite)-NaCl (halite) association which was first detected in Bozkır Formation in the basin, to establish evaporitic characteristics of the formation, to make

* *Corresponding author: İlhan SÖNMEZ, ilhan.sonmez@mta.gov.tr*

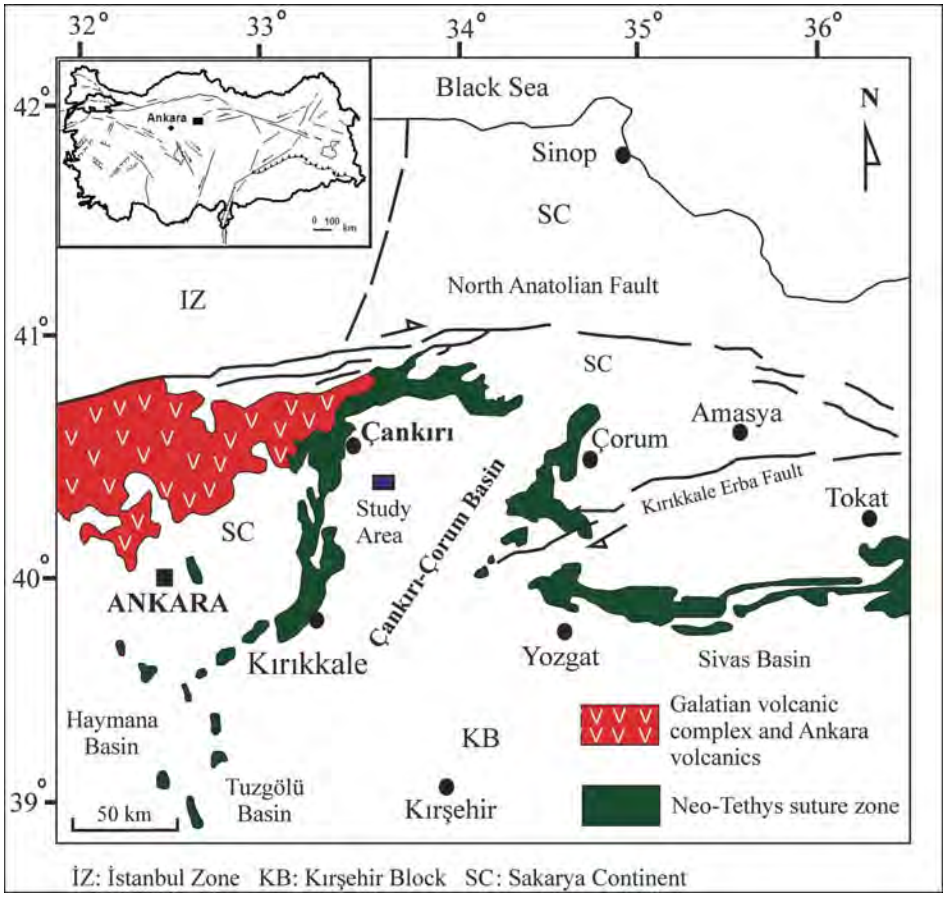

Figure 1- Location map of the study area (Karadeniz et al., 2004).

contribution for the interpretation of the basin and the production of new data in Na-sulfate explorations.

Na-sulfate form several minerals in nature but the most economical and mineable ones are; mirabilite (Na_2SO_4).$10H_2O$, thenardite (Na_2SO_4), glauberite ($Na_2Ca(SO_4)_2$) and bloedite ($Na_2Mg(SO_4)_2.4H_2O$). Na-sulfate minerals have hardness values in between 2-3, are colorless in pure state, transparent, easily dissoluble in water, bitterly and saline, with densities ranging between 1.49-2.8 gr/m^3. These occur in continental environments and cannot be well preserved in atmospheric conditions.

Rocksalt which is odorless, dissoluble in water, easily crumbled substance is formed by Na^+ and Cl^- ions, and is crystallized in the form of cubic crystallography. Although it is colorless in pure state it may appear in gray, yellow, red, and even green and blue colored in nature. The hardness of the halite mineral which shows plastic character under high pressure is 2.5 and the specific weight varies in between 2.10-2.55 gr/cm^3. The melting and boiling points of the mineral are 800°C and 1412°C, respectively.

Salt resources which have economic importance are divided into two categories as; solid and liquid. The salt exists in sea, lakes and in saline water resources as in liquid, but occurs as solid in the form of embedded rocksalt deposits. The seas form the biggest salt reservoirs of the world.

The presence of rocksalt in the basin has been known for many times and it was produced in solid form by room-pillar method (Çankırı Salt Cave, Potuk Salt). These operated halite mines are the salts which moved upward (i.e. salts that reached the surface by diapirism) before Pliocene. The rocksalt cut in Bozkır formation does not indicate any diapirism, compatible with sedimentation, as bedded and is in low dipping.

Operated rocksalt which emerged the surface as a result of diapirism is located in north of the study area. Quite steep slopes are observed in northern parts

of the study area, in Bozkır formation and in southern part of the operated salt mines (Figure 2). This slope increase occurs due to the deformation controlled by rocksalt tectonics which was generated by pre-Pliocene halite that had risen upward as a result of diapirism.

It was first determined both mineralogically and petrographically that Na-sulfate layers (glauberite) within Bozkır formation in Çankırı-Çorum Basin had turned into secondary gypsum minerals at or near the surface. Similarly; halite minerals which had also been substituted by the secondary gypsum mineral and textures that had formed with this special transformation was published (Gündoğan and Helvacı, 1999; Gündoğan and Helvacı, 2001; Helvacı and Gündoğan, 2008; Gündoğan and Helvacı, 2009). Gündoğan (2000) stated in his study that in geochemical analyses of these pseudomorphic secondary gypsums which were observed in some layers of the formation and formed as a result of glauberite alteration (Figure 3) contained Na_2O less than 1%. He also emphasized that special textures observed in petrographical studies were in the character of key data in Na-sulfate exploration.

Besides; the actual deposition of bloedite ($Na_2Mg(SO_4)_2.4H_2O$) was determined, which is another significant Na-sulfate mineral in the basin, in a seasonal lake environment and as a result of analyses carried out it was detected that this deposition was associated by thenardite and halite and gypsum in few amounts (Sönmez, 2010).

Çayırhan (Ankara) deposit in Beypazarı Basin located in the Central Anatolia is an example for sedimentary embedded Na-sulfate deposit which exists in small numbers in the world (Çelik et al., 1987). The deposit is located among layers of gypsum of the Kirmir Formation which deposited in Upper Miocene playa-lake environment. Na-sulfate exists as glauberite and thenardite in the deposit (Helvacı et al., 1989; Orti et al., 2002). It was observed that Na-sulfate occurrences in the formation mostly consisted of euhedral glauberite, and thenardite minerals which were observed among them bonded glauberite minerals by substitution and/or cementation (Gündoğan, 2000; Gündoğan and Helvacı, 2001; Helvacı and Gündoğan, 2008; Gündoğan and Helvacı, 2009).

In western Mediterranean region (Spain and France) evaporitic Na-sulfate bearing formations take place in different basins in Oligocene and Miocene ages. The association of glauberite-halite minerals was detected; especially, in Lower Miocene Lerin (Menduian et al., 1984) and Zaragoza Gypsum formations (Salvany et al., 2007) and in Oligocene Falce Gypsum formation in Ebro Basin (Spain), and in Lower Miocene saline unit in Madrid (Tajo) Basin (Ordonez and Garcia del Cura, 1994). In addition, this association was also encountered in Oligocene aged

Figure 2- Pre-Pliocene salt quarry in the north of the study area (image taken from Google Earth).

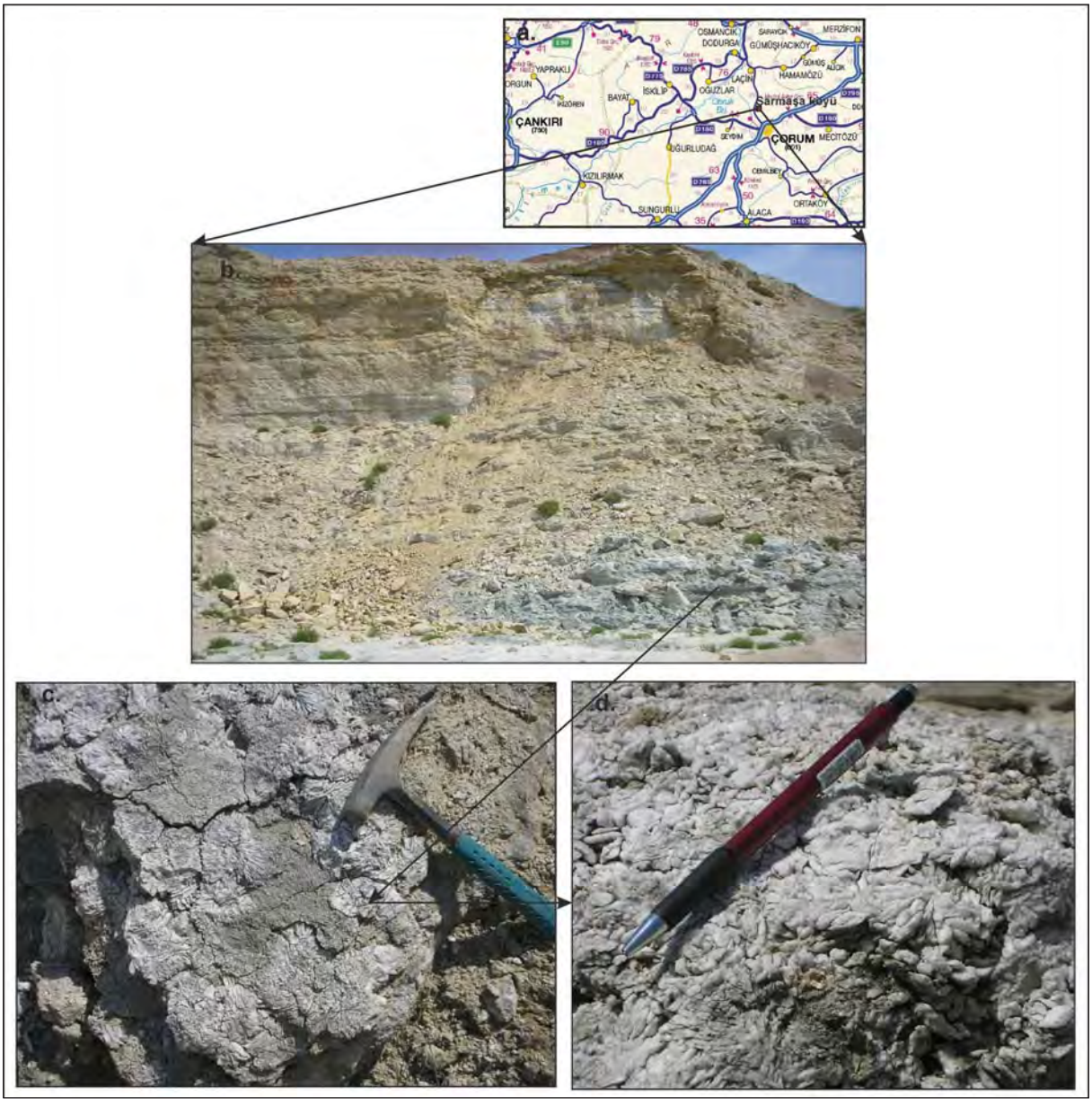

Figure 3- a-b) Gypsum quarry, Çorum Sarmaşa village; c) glauberite pseudomorphs which turned into gypsum; d) close up view.

Upper Evaporite formation in Valence Basin (France) (Dromart and Dumas, 1997).

1.1. Previous Studies

The study area is located in Çankırı-Çorum Basin which is one of the biggest sedimentary basins of Turkey. The basin is situated in the Central Anatolia between longitudes of 33.5°-35° and latitudes of 39.5°-41° (Figure 1).

When looking at previous studies it is seen that several investigations were carried out at different topics in the basin. Norman (1972) determined the recharge of Lower Tertiary sediments in addition to the stratigraphy of the basin in his study and stated that Çankırı basin was divided by faults in ENE-WSW directions, synchronous with the sedimentation. Şenalp (1974 *a, b*) in his study specified that the basin was characteristically in narrow and deep oceanic basin from Early Cretaceous to Middle Eocene, though most of the area was covered with terrigenous sediments. Studies related to Tertiary geology and stratigraphy have continued by Birgili et al. (1975), Akyürek et al. (1982), Yoldaş (1982) and Hakyemez et al. (1986). New findings

related to the tectonism and stratigraphy basin were obtained by Koçyiğit (1991). Tüysüz and Dellaloğlu (1994) in their study asserted that Early Tertiary paleogeographical evolution of the Çankırı Basin and its surround in the Central Anatolia had been controlled by a compressive regime which caused the closure of the Neotethys Ocean and continued even after that event. Kaymakçı (2000) discussed the tectonics and stratigraphy of the basin and presented new findings. Seyitoğlu et al. (1997, 2001) discussed fault systems which are effective in basin tectonics from a different point of view. Furthermore; evaporitic environments and its sedimentology in the basin starting from Middle Late Eocene were interpreted by Ergun (1977), Karadenizli (1999), Karadenizli and Kazancı (2000), Gündoğan (2000), Gündoğan and Helvacı (1999, 2001), Varol et al. (2002), Karadenizli et al. (2004). Moreover; exploratory studies of drilled industrial raw material were carried out between the years 2006-2010 by MTA and new data were extracted in the basin.

2. General Geology

Çankırı-Çorum basin is the biggest depositional area of the Central Anatolia in Tertiary time in terms of widespread area and bedding thickness. The basin like other Central Anatolian basins was formed by the convergence of Sakarya Continent and the Kırşehir Block located within Anatolide between Cretaceous-Eocene time intervals (Şengör and Yılmaz, 1981). It is the largest Tertiary basin in the Central Anatolia (Haymana, Tuz Lake, Sivas) (Figure 1). All these Central Anatolian Basins were defined as the collapse basins among rising plates (Görür et al., 1984).

Çankırı-Çorum Basin is located at a complex zone in which it was formed by Sakarya and Kırşehir continents with Ankara-Erzincan suture. Units belonging to Sakarya-Kırşehir continent and İzmir-Ankara-Erzincan Suture zone constitute the units at the bottom of basin. The basin is surrounded by the ophiolitic mélange at west and by the Kırşehir massive at south.

Mesozoic ophiolites located at the bottom of basin are unconformably overlain by Paleocene-Eocene flysch deposit consisting of sandstone-shale alternation. This flysch deposit is cut by basaltic Eocene volcanites (Bayat formation). All these units are then overlain by Oligo-Miocene deposits (Birgili et al., 1975).

A very thick sedimentary deposit takes place in the basin ranging from Cretaceous to Pliocene. Rocks until Oligocene were deposited in marine environment, however rocks which were deposited in and after Oligocene belong to continental environment.

Evaporitic units in Tertiary aged Çankırı-Çorum Basin occurred in four different geological times. In Late Eocene (Kocaçay formation) in which the first evaporitic deposition took place, shallow marine environment has become dominant. However, in evaporites of Oligocene (İncik formation), Miocene (Bayındır formation) and Pliocene (Bozkır formation) totally the lake environment has been dominant.

All rock units in the basin were deposited in fluvial and alluvial fan environments and is unconformably covered by Plio-Quaternary Değim formation.

The oldest unit located in the study area is Oligocene aged İncik formation (Figure 4). This formation consists of rock units which formed in fluvial and lake environments. Conglomerate, sandstone and mudstones of the formation take place within the study area. Bayındır formation which represents Miocene aged evaporites overlies İncik formation. Bayındır formation is then overlain by Upper Miocene Kızılırmak formation consisting of sediments of meandering and braided river environment and flood plain deposits associated with those environments. Then Bozkır formation which contains Pliocene evaporites covers Kızılırmak formation with regional unconformity.

Topuzsaray anticline which was developed by the effect of Upper Miocene compression in western part of the basin is an overturned anticline orienting in NE-SW directions and is located in NE part of the study area. Oil exploration drilling has also been carried out by TPAO on this anticline (Usta, 1992). Furthermore; in the study area, the Ovacık monocline (forced fold) is observed which was developed by the diapirism effect of pre Pliocene rocksalt (Figure 2 and 4).

3. Methodology

Within scope of the project of Central Anatolian Industrial Raw Material Explorations (2010-32-13-05.1) executed by MTA, the revision of 1/25.000 scale geological map, the measurement of the

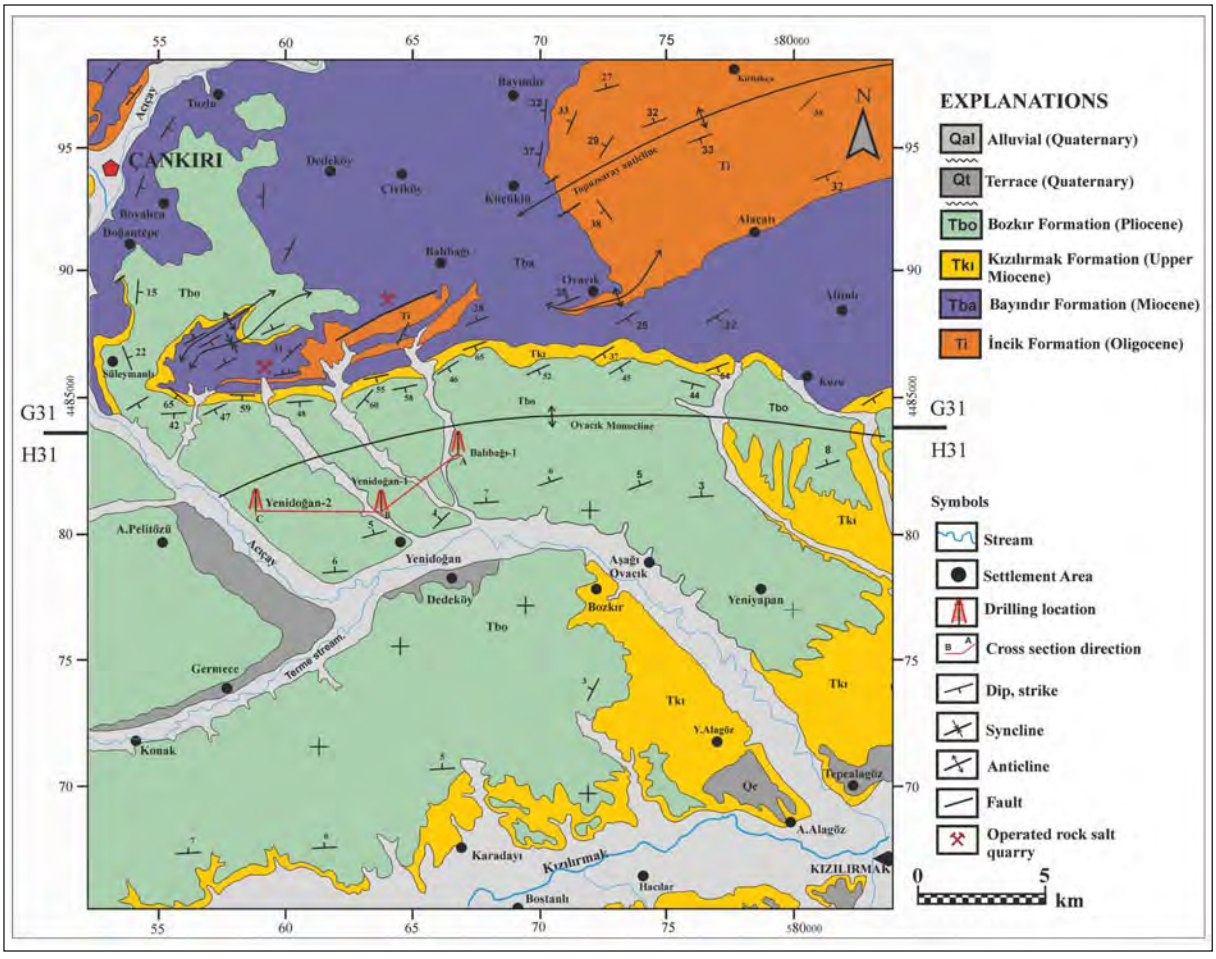

Figure 4- Geological map of the study area (from Birgili et al., 1975).

stratigraphic section and intense field observations were performed. Besides, total of 2068 m. exploratory borehole drillings were carried out at three locations in order to control embedded deposits (Table 1).

XRD samples were taken at certain intervals during borehole drilling studies performed in Bozkır formation. Chemical analyses were performed from rocksalt samples in halite-claystone-anhydrite-glauberite zone which is defined as the Tuz (halite) member. Interlayers of glauberite were used as for the XRD and XRF analyses. Representative samples were collected from glauberite interlayers and glauberite-mudstone zone where the glauberite mineralization is the thickest and observed the best within Tuz member. Then, SEM studies were done in order to understand the mineral associations and their crystal morphology. Besides, XRD and XRF analyses were carried out in samples taken from claystones within Tuz (halite) member.

Mineralogical analyses were performed by Philips PW XRD instrument in laboratories of the Dept. of Mineral Analyses and Technologies in MTA. Diffractograms were obtained using Cu-K radiation between 2.5°-70° and within 2θ interval. Samples were dried at 105°C during chemical analyses. Analyses were carried out in XRF instrument in IQ+ mode (unstandardized program) in the same laboratories.

Using four samples selected in SEM analyses, total of 40 secondary electron detector (SE) image and 15 EDS (Energy Dispersive X Ray Spectrometer) point analysis results were taken under FEI Quanta 400 MK2 model scanning electron microscope. EDS point analyses are the results of unstandardized, semi quantitative elementary and oxide analysis by EDAX Genesis XM4I model EDS detector. Elementary point analyses were made under kV:25.00 Tilt:0.00 Take-off:34.94 AmpT: 102.4 Det Type:SUTW, Sapphire Res:130.54 Lsec:10 detector conditions.

Table 1- Drilling studies carried out in Bozkır formation.

Drilling name	Elevation (m)	Drilling depth (m)	Tuz member entrance-exit (m)	Tuz member thickness (m)	Rocksalt thickness (m)	Glauberite-mudstone zone thickness (m).
Balıbağı-1	622	920	85-430	345	70	2,85
Yenidoğan-1	620	658	45-406	361	115,40	2,20
Yenidoğan-2	670	490	100-404	304	115,80	3,20

4. General Characteristics of Bozkır Formation

Bozkır formation which consists of evaporitic layers was first defined by Tanrıverdi (1973) and Birgili et al. (1975). The age of the formation is upper Miocene according to Tanrıverdi (1973) and Birgili et al. (1975). The age of the formation was determined as Upper Micene-Pliocene according to Kaymakçı (2000) and as Early Pliocene by Karadeniz et al. (2004).

Bozkır Formation was deposited in evaporitic lakes where palustrine conditions are observed in which seasonal changes are effective (Varol et al., 2002). Formation occurs by four main lithofacies groups as sulfates, carbonates, siliciclastics and chlorites (NaCl). Bozkır formation consists of massive bedded gypsum, halite, glauberite, anhydrite, gypsum arenite, individual gypsum crystals, thick claystone, dolomite and ooidic limestone. The thickness of the unit reaches 700 m. The basin has low dipping, widespread area in general (Figure 5).

Although there were carried out several studies in the formation, borehole drilling was first time performed within this project. Mainly, three lithological zones were observed in drillings (Figure 6). These are from bottom to top as; claystone-less anhydrite zone, halite-claystone-anhydrite-glauberite zone and claystone-gypsum-less anhydrite zone. Rocksalt bearing zone was named as Tuz (halite) member. As for the layers deposited in sabhka environment where the glauberite mineralization observed the thickest within this zone was named as glauberite-mudstone zone. In drillings lateral continuity was also detected in these zones (Figure 7).

The formation unconformably overlies Upper Miocene Kızılırmak formation and older units on margins of the basin, and is unconformably overlain by Plio-Quaternary Değim formation which was deposited in alluvial fan environment.

Bozkır formation was divided into three main depositional environments based on the measured section studies taken from different parts of the formation by Varol et al. (2002). These are alluvial, lake shore and lake center environments.

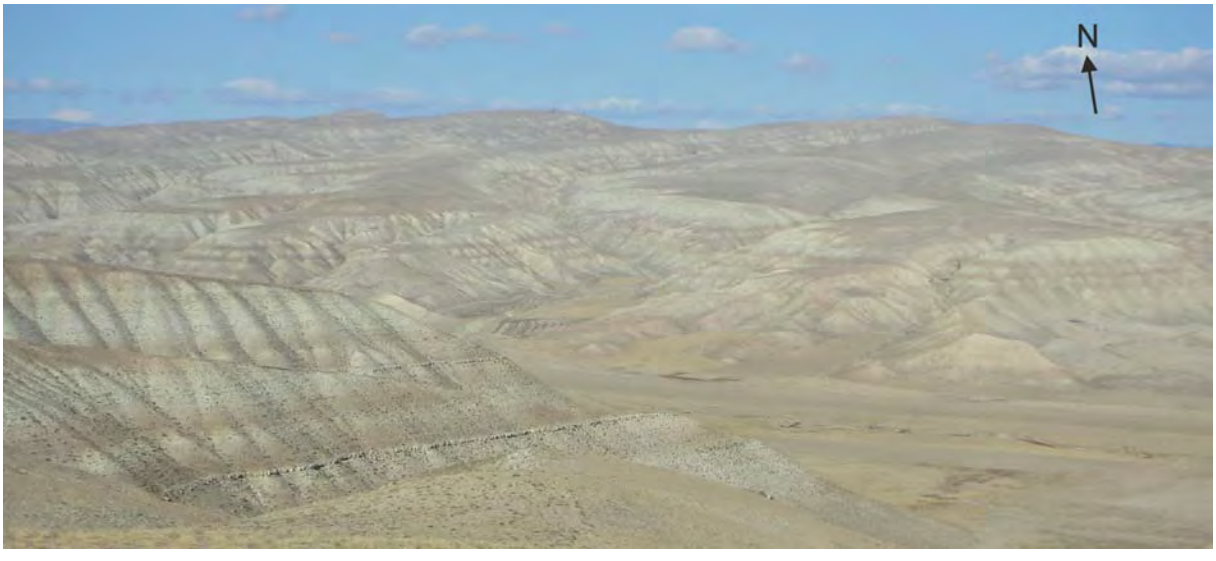

Figure 5- General view of the Bozkır formation (looking at N-NW from Çankırı-Çorum highway).

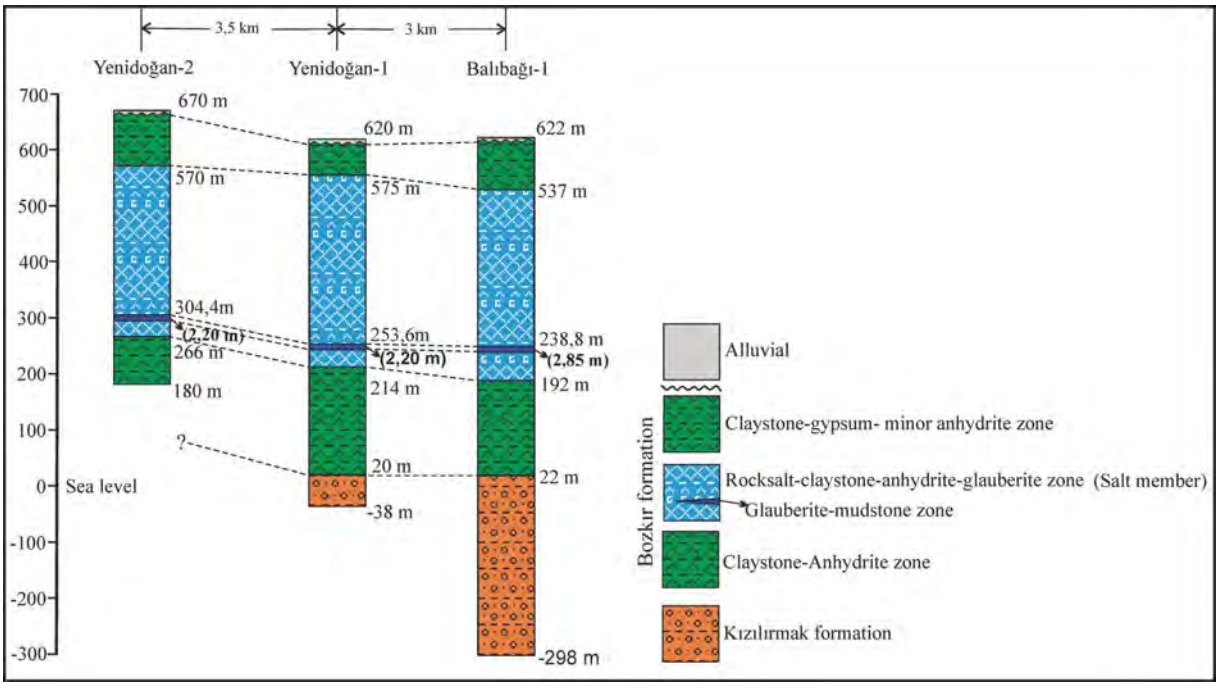

Figure 6- Drillings made in Bozkır formation.

Gündoğan (2000) in his study defined depositional environments of sulfate facies in Bozkır formation as wavy, transient, shallow, saline lake and sabhka. It was emphasized that nodular anhydrite and discoidal gypsums within claystones were formed as associated with variations in water level in sabhka environment and existed as intercalating within main lake deposits (selenitic gypsum and gypsum arenite).

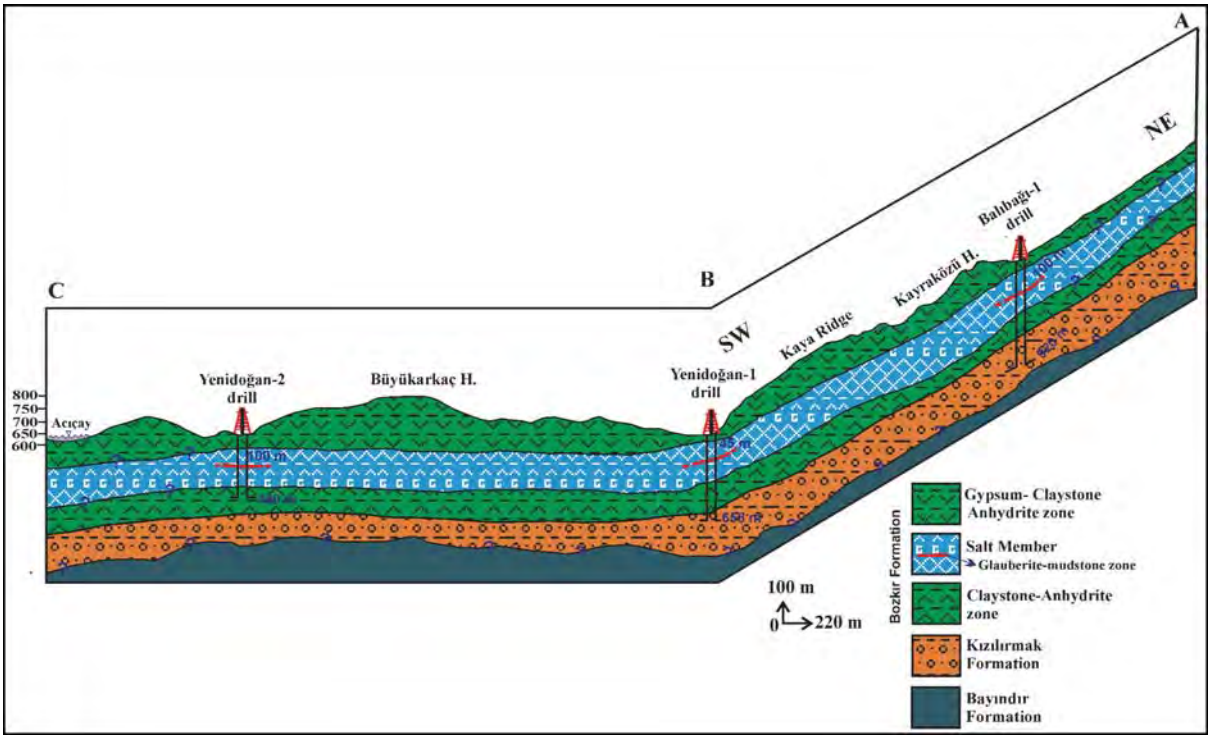

Figure 7- ABC cross section through drillings.

4.1. Tuz Member (Bozkır formation)

Tuz (halite) member which was detected in borehole drillings was performed in sabhka playa-lake transition in the Bozkır formation and is formed by rocksalt, claystone, anhydrite alternation consisting of glauberite interlayers (Figures 8 a, b, c, d). The member was deposited when the formation had been hydraulically isolated and in period when arid climate conditions had been prevalent.

In drillings, rocksalt was cut in thicknesses reaching 115 m within Tuz member which was observed the most in 362 m thickness. Rocksalt (playa-lake) which is mostly bedded and white, pale/dark gray colored is conformable with sedimentation and is low dipping (Figure 9).

The zone in which glauberite bearing layers, interlayering within playa-lake in Tuz member, is the thickest were defined as glauberite-mudstone zone and it was encountered at thicknesses of 3.2 m in drillings (Figure 10). Glauberite mineral which is observed as disc and rosette shaped individual crystals within mudstone dominant matrix was formed as a diagenetic mineral in saline mud plain environment (sabhka). In drillings carried out in sabhka- playa-lake transition zone, it was determined that sabhka deposits intercalated with playa-lake deposits (Figure 11). In addition to glauberite mineral which was formed within mudstone dominant matrix in saline mudflat environment, individual growths of halite mineral with nodular gypsum and anhydrite were also encountered (Figure 12).

Detritic minerals are observed as; various clay minerals, magnesite, quartz, feldspar group mineral and serpentine group mineral within the matrix from which it is formed by the mixture of several minerals.

Due to seasonal changes, Bozkır playa-lake has been recharged by both groundwater and surface waters. The bedded rocksalt has been deposited as a result of evaporation from lake water due to ionic enrichment in lake (Na^+, Cl^-) during arid periods

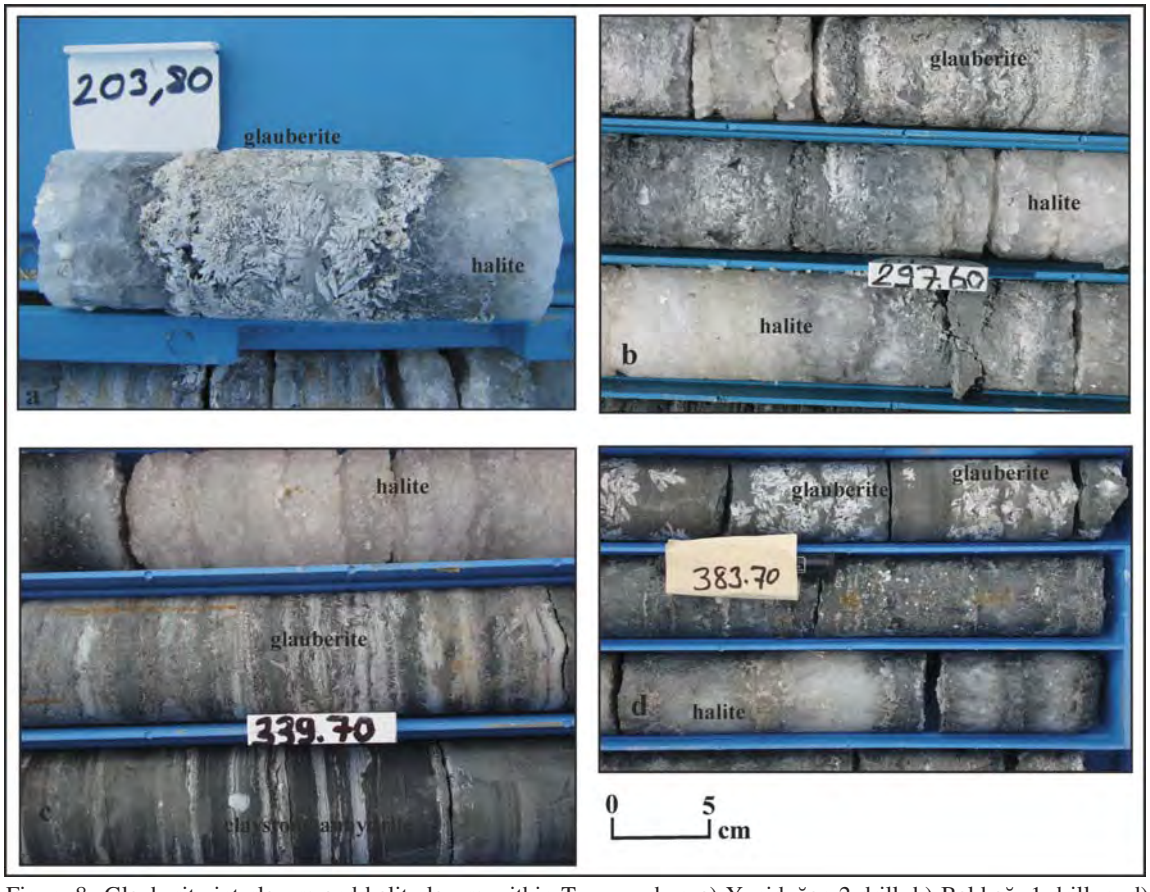

Figure 8- Glauberite interlayers and halite layers within Tuz member, a) Yenidoğan-2 drill, b) Balıbağı-1 drill, c, d) Yenidoğan-1 drill.

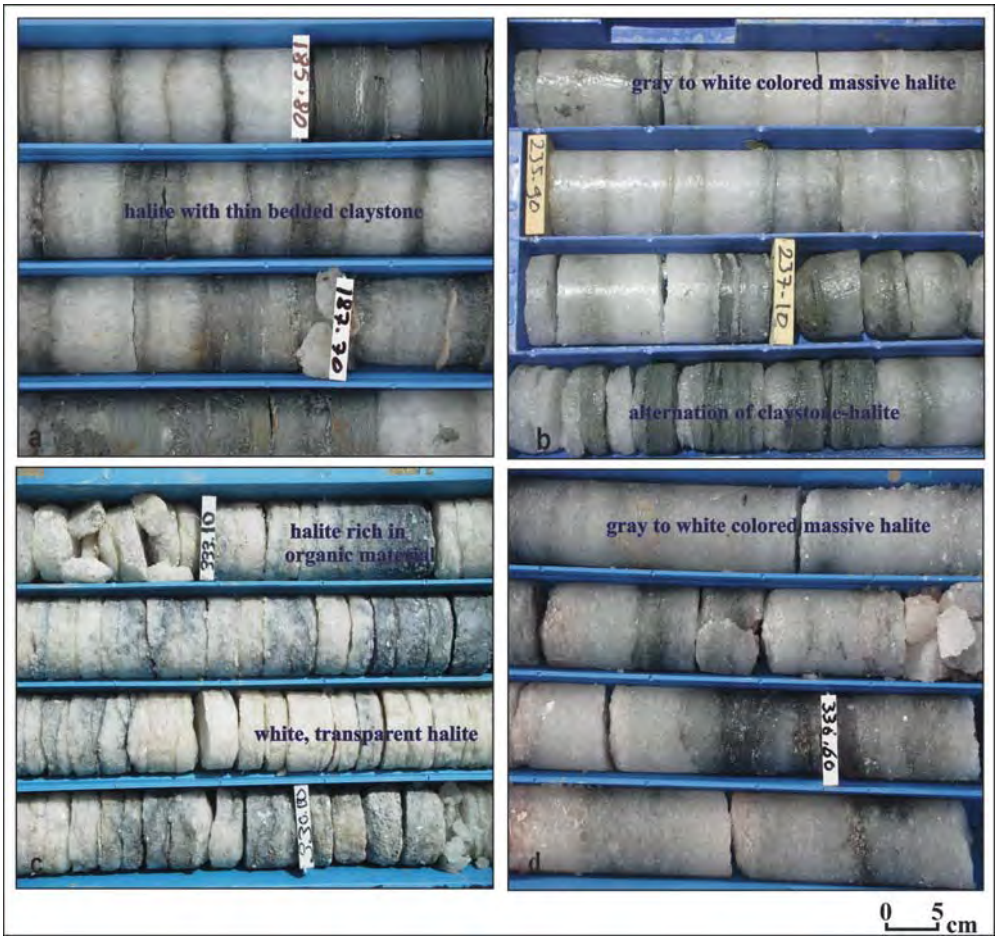

Figure 9- Rocksalt layers cut within Tuz member, a) Yenidoğan-1 drill, b) Balıbağı-1 drill, c) Yenidoğan-2 drill, d) Yenidoğan-1 drill.

where the playa lake has been hydraulically isolated (Figure 11).

When the lake passed into hydraulically open conditions in short and long terms, claystones have been mostly deposited. Varve lamination which occurs as a type of lamination due to seasonal changes is observed in claystones (Figure 13). The successive deposition of anhydrite, gypsum and halite on the other hand occurs due to chemical and temperature variations as a result of seasonal and/or climatic changes (Figure 14).

Moreover; rocksalt which was most probably deposited diagenetically between claystone and anhydrite in drillings was also detected as a different observation (Figure 15).

There are still discussions regarding the depositional source of the glauberite mineral whether it is primary or diagenetic in formation. Many studies related to actual and fossil Na-sulfate deposits indicate that glauberite was formed as a diagenetic mineral in saline mud-flat environment (Smooth and Lowenstein, 1991). In addition to that, it was suggested in some studies that some layers of the glauberite deposition were primarily deposited in subaqueous environment (Mees, 1999; Orti et al., 2002). Investigators who consider the primary origin for glauberite formation is less than the ones who consider that it had originated from an early diagenetic mineral (Salvany et al., 2007) as this mineral turns into gypsum at or near the surface.

4.2. Mineralogy

In geochemical analyses of the samples taken from rocksalt layers within Tuz member in Bozkır formation which is formed by the alternation of halite-claystone bearing interlayers of glauberite, Na^+ and Cl^- ratios were detected high and K_2O ratio was detected low (Table 2).

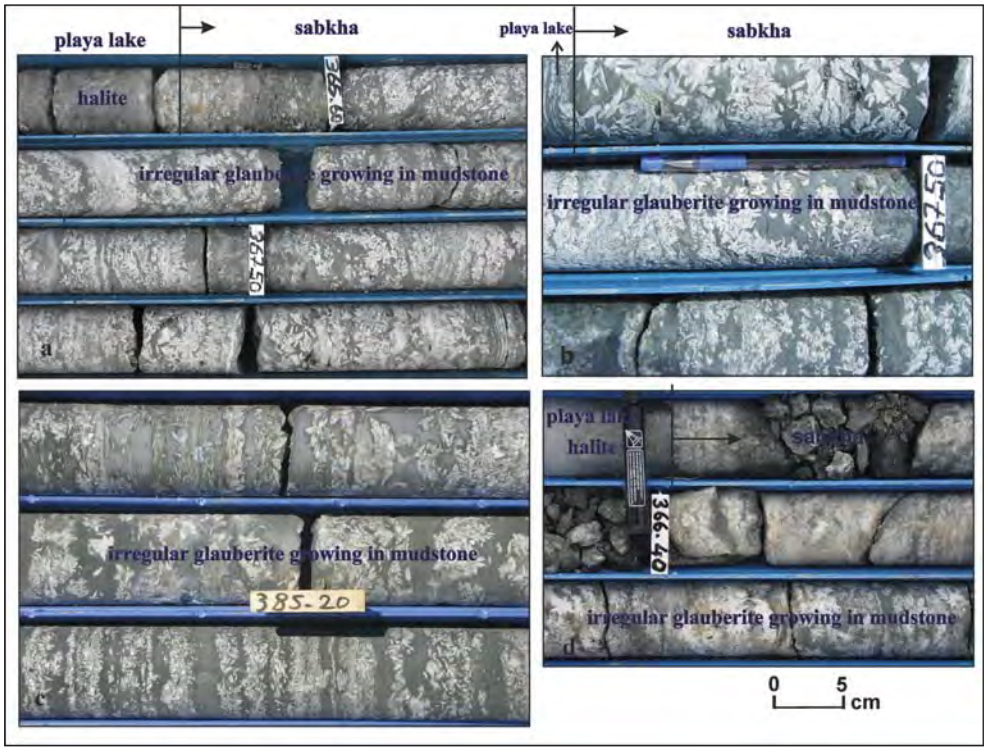

Figure 10- Glauberite-mudstone zone distinguished among playa-lake deposits in Tuz member; a, b) Yenidoğan-2 drill, c) Balıbağı-1 drill, d) Yenidoğan-1 drill.

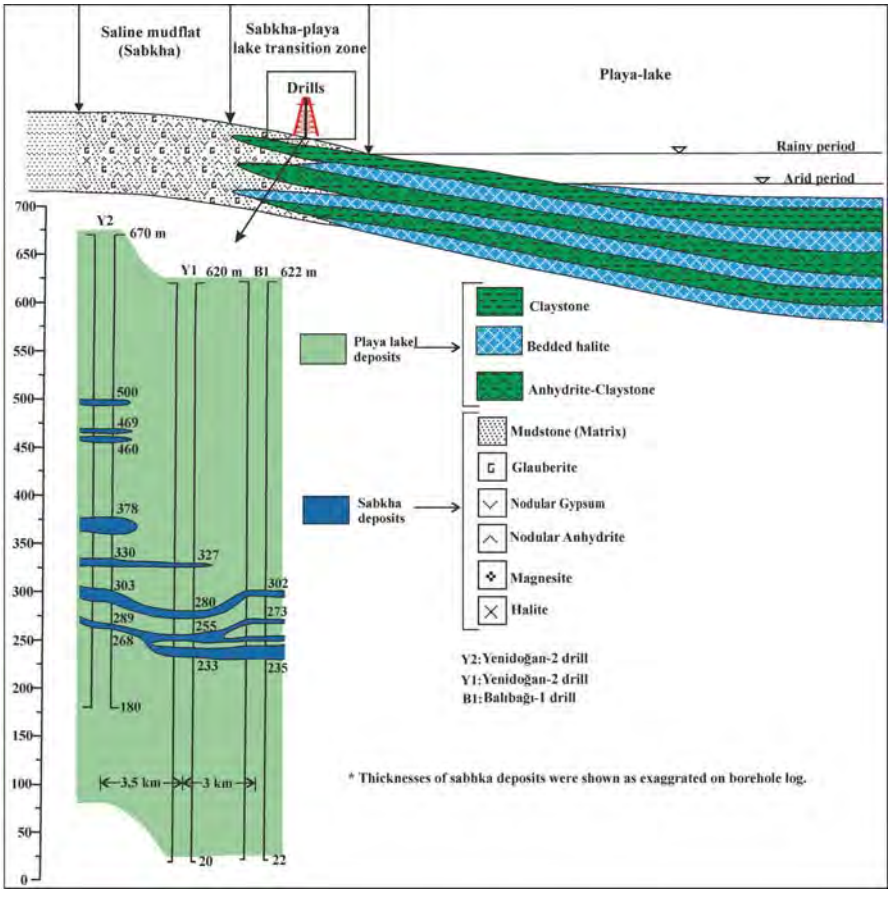

Figure 11- Schematic section showing the depositional environment of the Bozkır formation.

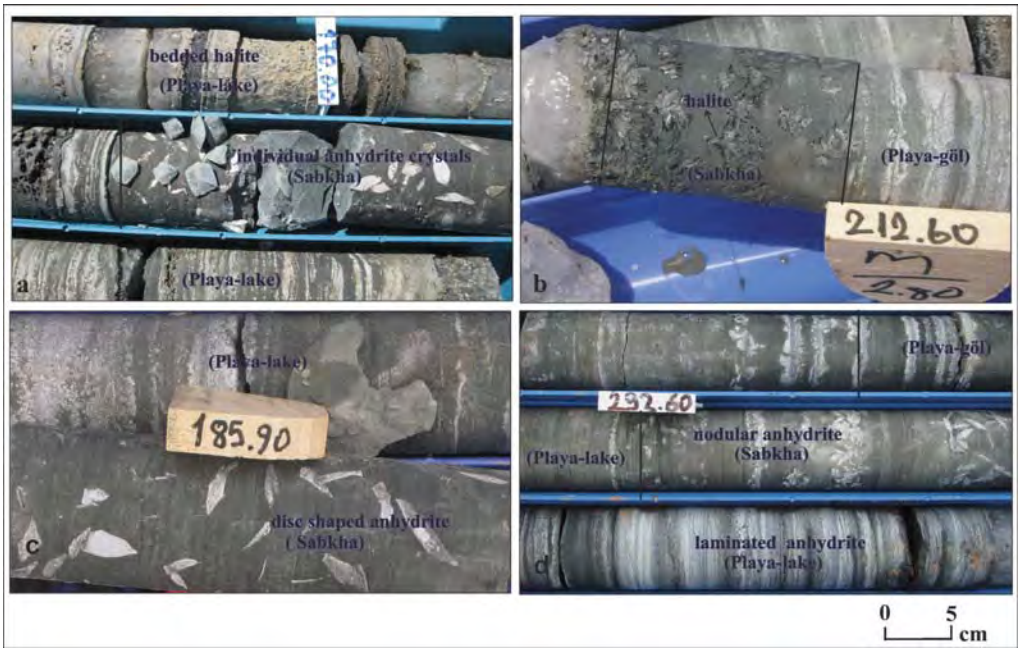

Figure 12- Individual growths of anhydrite and halite minerals in sabhka environment between playa lake; a, b) Yenidoğan-2 drill, c) Balıbağı-1 drill, d) Yenidoğan-1 drill.

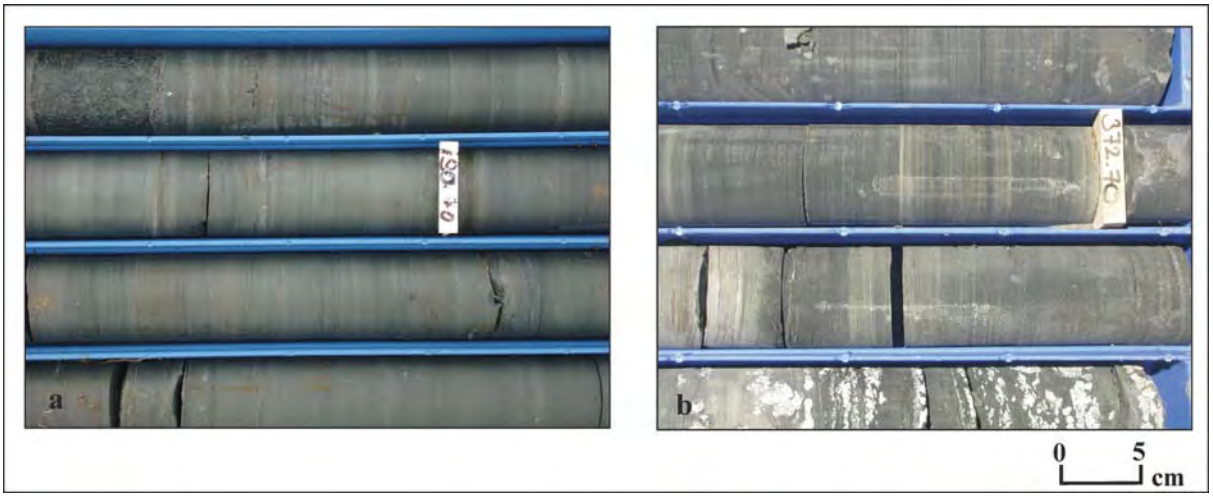

Figure 13- Varve lamination in claystones a) Yenidoğan-1 drill, b) Balıbağı-1 drill.

Glauberite mineral which was crystallized from an evaporitic surface water as a diagenetic mineral in the form of individual growths in saline lake mud-flat environment were detected in XRD analysis of the samples collected (Figure 16). Anhydrite and gypsum are other individual minerals crystallized in halite matrix (Figure 17). In analyses it was seen that magnesite ($MgCO_3$), dolomite ($CaMg(CO_3)_2$), halite (NaCl) and calcite ($CaCO_3$) minerals were observed within cryptocrystalline matrix which possessed a quite complex mineral assemblage and these are the other minerals observed in evaporitic environment (Figure 18).

Mg mineral which exists as a result of the alteration of ophiolitic rocks located at the bottom of the basin may be transported into the environment by surface and groundwaters and deposited from the lake water which its Mg^{+2}/Ca^{+2} ratio increases. Halite mineral both crystallizes individually in sabhka environment and exists in the matrix. Besides, it is deposited in aqueous environment by evaporation from lake water as bedded halite (Figure 9).

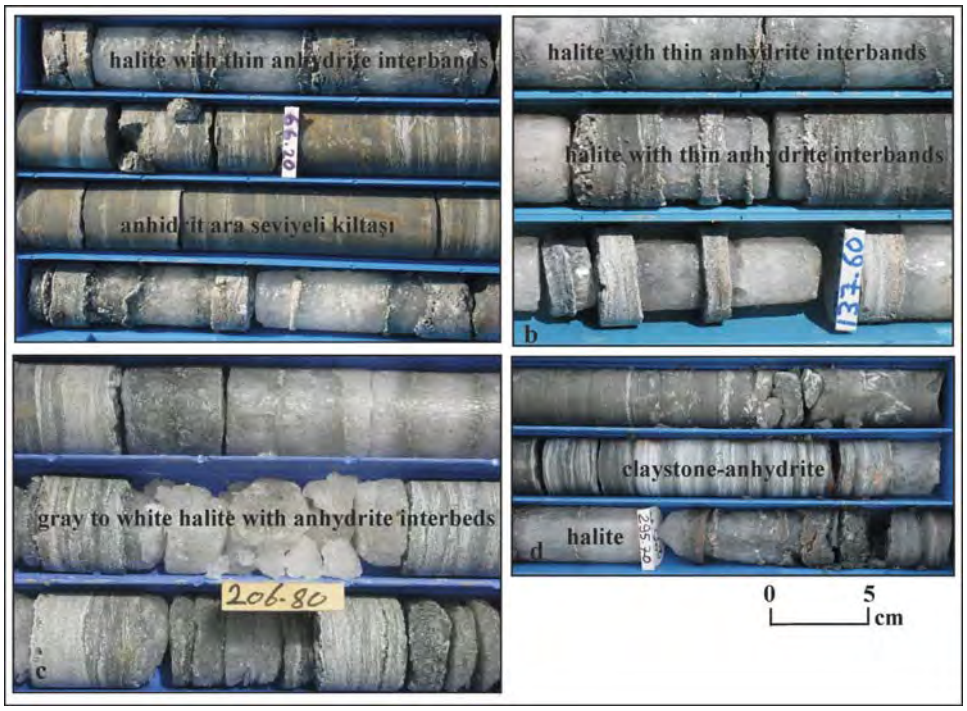

Figure 14- Alternation of rocksalt-anhydrite-claystone; a) Yenidoğan-1 drill, b) Yenidoğan-2 drill, c) Balıbağı-1 drill, d) Yenidoğan-1 drill.

Figure 15- Rocksalt which was deposited into sediment; a) Balıbağı-1 drill, b) Yenidoğan-1 drill.

Table 2- Chemical analysis of samples taken from drills (Oxide values were given in weight %)

Drilling name	Meter	Na	Cl	MgO	Al_2O_3	SiO_2	CaO	K_2O	Fe_2O_3	SrO	Br	Li	I	SO_3
Balıbağı-1	97.4	37.5	61.8	0.4	<0.1	0.3	0,1	<0.1	<0.1	<0.01	<0.01	<0.01	<0.01	<0.01
Balıbağı-1	264.6	37.5	60,2	<0.1,	<0.1,	0.2	1.0	<0.1	<0.1	0.03	<0.01	<0.01	<0.01	1.17
Balıbağı-1	319,1	38,1	61,4	0.2	<0.1	0.2	<0,1	<0.1	<0.1	0.02	<0.01	<0.01,	<0.01	0,07
Balıbağı-1	427.4	37.9	59,3	<0.1	<0.1	0.3	1.1	<0.1	<0.1	0.02	<0.01	<0.01,	<0.01	1.38
Yenidoğan-1	59.8	38,6	59,2	0.1	0.1	0.2	0,7	<0.1	0,2	<0.01	<0.01	<0.01	0.22	0,02
Yenidoğan-1	216,5	39,1	60,3	6 0,1	0.1	0.2	<0,1	<0.1	0,2	<0.01	<0.01	<0.01,	<0,01	0,01
Yenidoğan-1	339,4	39,1	59,8	0,1	0.1	0.2	0,2	<0.1	0,1	<0.01	<0.01	<0.01	<0,01	0,01
Yenidoğan-1	390,1	38,5	59,4	0,1	0,1	0,2	0,8	<0.1	0,1	0,06	<0.01	<0.01	<0,01	0,02
Yenidoğan-2	102,4	40,0	58,4	0,2	0,3	0,8	0,1	<0,1	0,3	0,11	<0.01	4 ppm	<0,01	0,01
Yenidoğan-2	211,4	33,6	45,9	1,9	2,9	9,2	2,4	0,4	3,2	0,01	<0.01	6 ppm	<0,01	0,01
Yenidoğan-2	310,4	40,4	58,8	<0,1	0,1	0,2	0,4	<0,1	0,1	0,01	<0.01	<1ppm	<0,01	0,01
Yenidoğan-2	399,0	40,0	59,0	0,1	0,2	0,4	0,2	<0,1	0,1	0,03	<0.01	<1ppm	<0,01	0,01

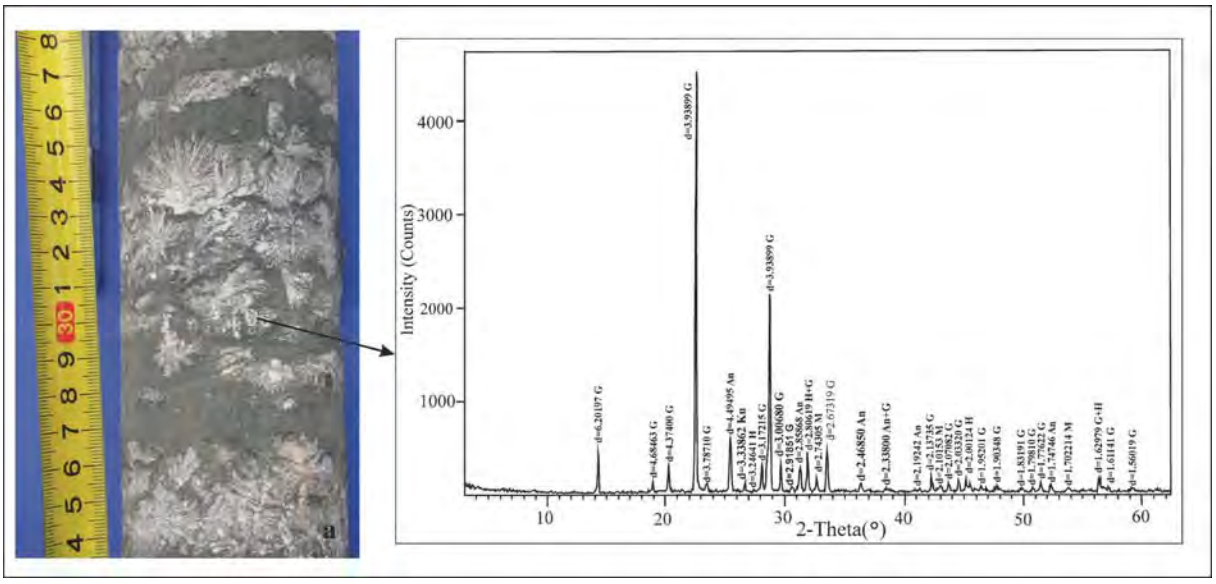

Figure 16- Interlayer of glauberite, a) Balıbağı-1 (340-340.15 m), b) XRD diffractogram of the sample taken from level which has disk like minerals, H: halite, G: glauberite, M: magnesite, An: anhydrite, Q: quartz.

Other minerals which were detected as a result of analyses in saline mudflat environment are palygorskite and zeolite group minerals (analcime, heulandite-clinopilolite) (Figures 18 and 19).

There is sodium enrichment due to evaporites (especially NaCl) in mudflat environment and this helps Na-rich clays to crystallize authigenically. Zeolites which are aqueous aluminum silicates (Na-K-Ca-Al aqueous silicates) occur as a result of the reaction between volcanic materials (tuff) with saline lake water. The source of the volcanic effect in Bozkır formation is considered as volcanic ash flows which occur due to Galatian massive on the western margin of the basin (Figure 1) and is transported into the environment by wind systems as the formation was deposited.

Palygorskite mineral $(Mg,Al)_2Si_4O_{10}(OH)\cdot 4(H_2O)$ which is aqueous magnesium-aluminum silicate composite clay mineral was detected within a matrix in XRD analyses (Figures 18, 19). Arid climates, saline alkaline lakes, environments in which pH is greater than 7 and where sources that supply Si and Mg into the basin are the most significant places of formation of this mineral (Weaver, 1989). In the study area where all these conditions are supplied, palygorskite formation in the environment indicates the increase of Al fetch in addition to Mg and Si enrichments.

Other minerals observed in samples collected from the matrix of glauberite bearing zone are detritic minerals which were transported into the basin such as; quartz, mix layered clay mineral, illite/mica group mineral, kaolinite group mineral, chlorite group mineral, talc group mineral, serpentine group mineral and feldspar group mineral.

Chemical analyses of samples which were taken from the differentiated zone as glauberite-mudstone in Tuz member are given in table 3. High Cl^-, MgO, Al_2O_3 and SiO_2 values in analysis originate from minerals in the matrix. Also, high Na_2O and low Cl^- ratios originate from higher glauberite content than halite content.

In claystones (Figure 14) which intercalate with bedded halite in subaqueous environment in Tuz member were detected evaporite minerals in low rate (anhydrite, halite), zeolite group mineral (analcime, heulandite-klinoplilolite), palygorskite and transported detritic minerals (quartz, illite/mica group minerals, chlorite group minerals, amorphous material, talc group mineral, serpentine group mineral, feldspar group mineral, amphibole group mineral, mix layered clay mineral) in analyses.

Although claystones have similar mineralogy with the matrix of the environment consisting of glauberite mineral in mudflat (subaerial), they have low Na_2O ratio and high MgO, Al_2O_3, SiO_2 ratios compared to glauberite bearing layers in chemical analyses (Table 4).

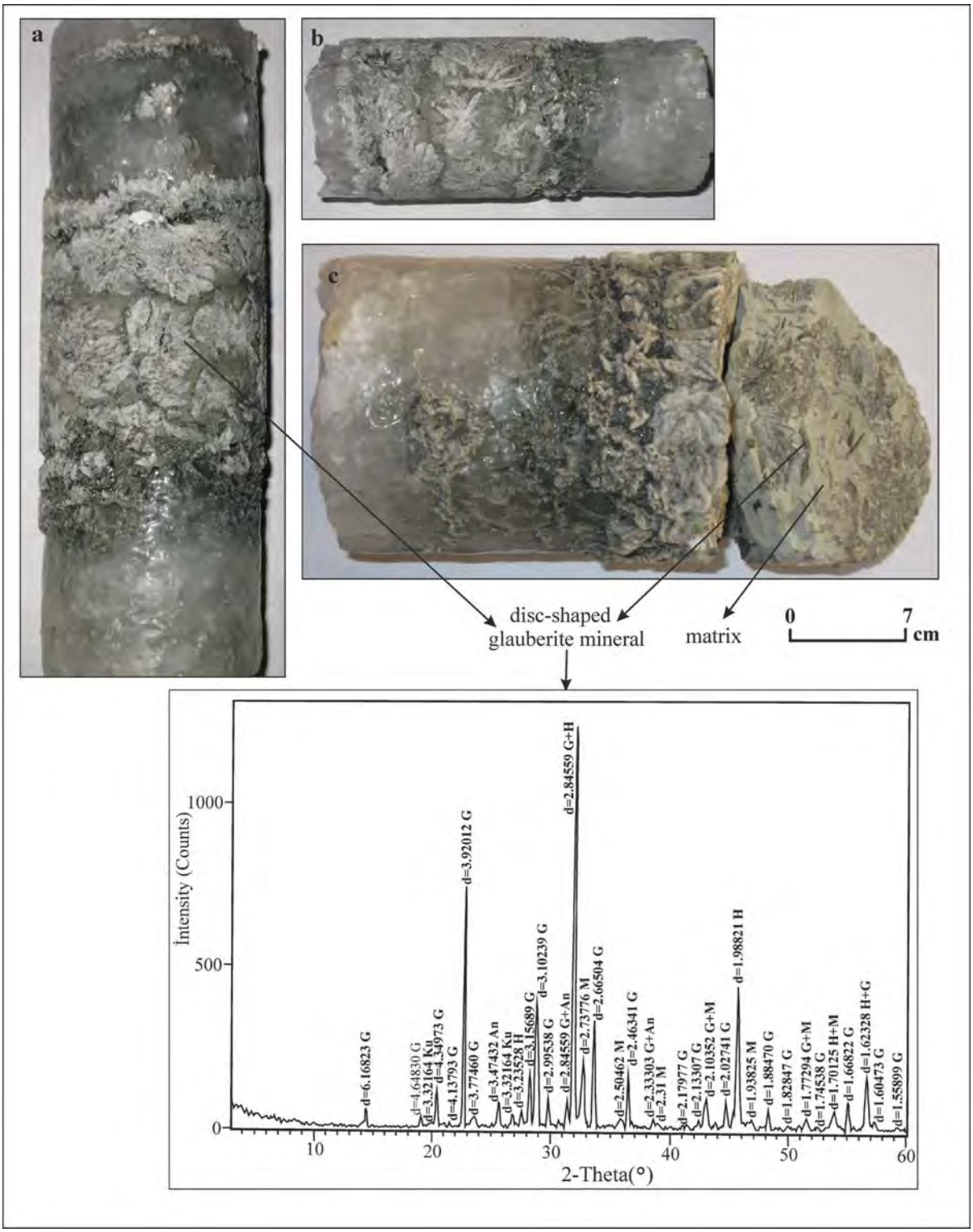

Figure 17- Interlayer of glauberite in rocksalt (Yenidoğan-2 drill, 158-158.35 m). a, b, c) photos of the same borehole, d) XRD diffractogram of the sample, H: halite, G: glauberite, M: magnesite, An: anhydrite, Q: quartz.

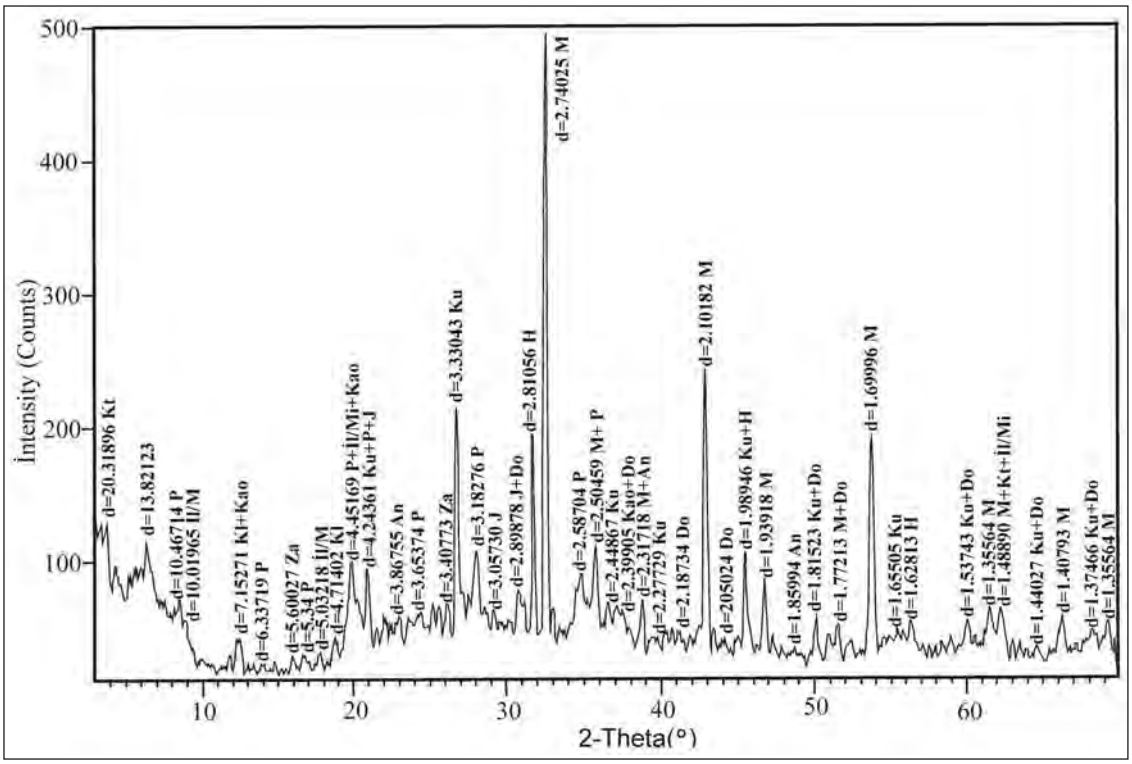

Figure 18- XRD diffractogram of the sample taken from the matrix of glauberite mudstone zone; Kt: mix layered clay mineral, P: palygorskite, İl/M: Illite mica group mineral, Kao: kaolinite group mineral, Za: zeolite (analcime), J: gypsum, An: anhydrite, Q: quartz, Do: dolomite, H: halite, M: magnesite, (Balıbağı-1 drill, 385.30 m).

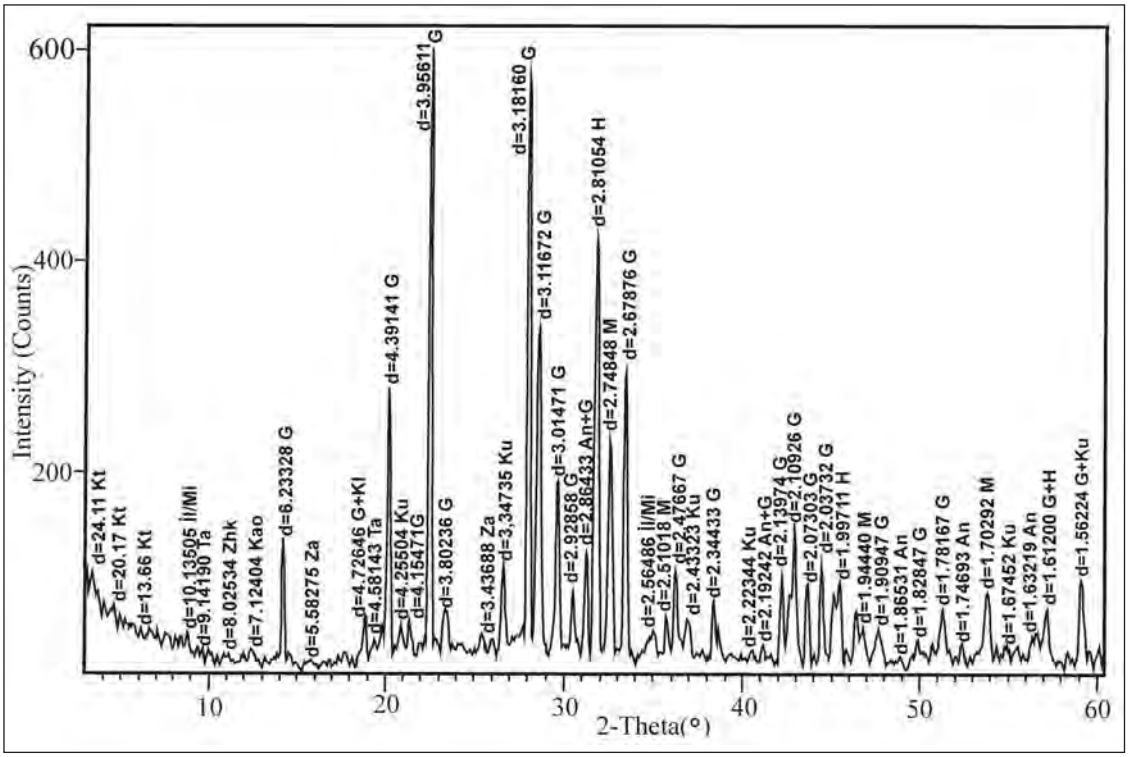

Figure 19- XRD diffractogram of the sample taken from glauberite mudstone zone; Kt: mix layered clay mineral, Ta: talc group mineral, Zhk: zeolite (Heulandite-Clinopilolite), G: Glauberite, P: palygorskite, İl/M: Illite mica group mineral, Kao: Kaolinite group mineral, Kl: chlorite group mineral, Za: Zeolite (analcime), J: Gypsum, An: Anhydrite, Q: Quartz, Do: Dolomite, H: Halite, M: Magnesite (Yenidoğan-2, 366.1 m).

Table 3- Chemical analysis of samples taken from glauberite mudstone zone (Oxide values were given in weight%).

Drilling name	Meter	Na_2O	Cl	MgO	Al_2O_3	SiO_2	CaO	K_2O	Fe_2O_3	A.Z	P_2O_5	TiO_2	MnO	SO_3
Balıbağı-1	385,3	10,8 1	,97	3,6	3,7	13,3	21,7	0,6	2,7	10,25	0,1	0,2	<0,1	30,2
Yenidoğan-1	340,0	16,0	1,82	6,4	3,5	12,1	13,8	0,5	2,1	8,0	0,1	0,2	<0,1	35,3
Yenidoğan-1	367,6	16,5	2,21	3,0	3,3	12,0	17,5	0,6	2,2	8,85	<0,1	0,2	<0,1	35,3
Yenidoğan-2	158,0	21,4	9,17	1,9	3,6	11,4	13,4	0,5	1,6	9,6	<0,1	0,2	<0,1	27,08
Yenidoğan-2	366,1	22,0	2,1	4,1	3,6	13,3	15,3	0,5	1,9	5,05	<0,1	0,2	<0,1	31,73

4.2.1. SEM Studies

SEM analyses were performed on glauberite bearing samples of which their mineralogical description had been carried out by XRD analysis. Secondary electron (SE) detector views of each detected mineral (morphological views) were taken and EDS point analyses were carried out in order to control their elemental contents.

In EDS point analyses carried out on morphological views of samples, euhedral and subhedral glauberite crystals were detected in the matrix (Figures 20 and 21).

Another mineral detected in SEM analyses is anhydrite mineral. These generally occur in euhedral form in cryptocrystalline or associates with glauberite mineral (Figure 23). It was determined that glauberite mineral had been crystallized following the anhydrite mineral (Figure 24).

During studies made in close up SE views of glauberite minerals, it was observed that halite mineral had grown on glauberite mineral and sometimes appeared in the form of fracture and crack infill (Figure 25). Besides, it was detected that halite mineral were developed on glauberite minerals in various crystal forms (Figures 26 and 27).

SEM-EDS analyses were performed in order to determine mineralogical characteristics of the cryptocrystalline matrix in which glauberite mineral is situated. In SE views and EDS point analyses, it was seen that the matrix had quite complex crystal

Table 4- Chemical analyses of samples taken from claystones deposited in playa lake within Tuz member (oxide values were given in weight %).

Drilling name	Meter	Na_2O	MgO	Al_2O_3	SiO_2	CaO	K_2O	Fe_2O_3	A.Z	P_2O_5	TiO_2	MnO
Balıbağı-1	269.4	2,1	11,4	5,6	20,7	418,8	0,9	4,9	30,75	0,1	0,4	0,2
Yenidoğan-1	273.0	2,7	5,9	8,4	33,4	220,7 1	,3	6,4	20,04	0,1	0,4	0,1
Yenidoğan-2	273.9	2,7	6,2	7,1	27,8	220,7	1,3	5,7	20,95	0,1	0,4	0,1
Balıbağı-1	280.3	3,3	6,0	10,1	37,2	113,3	1,5	7,4	16,7	0,1	0,6	0,2

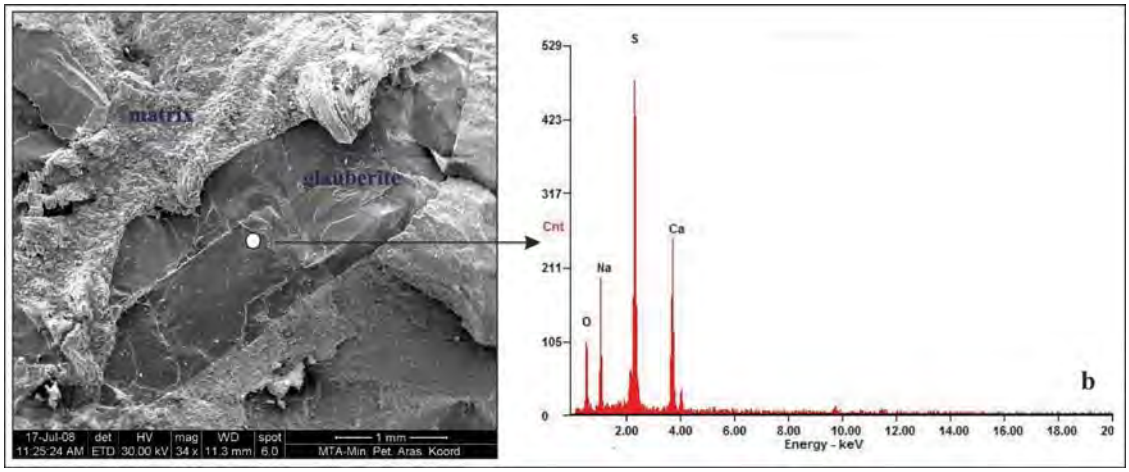

Figure 20- a) Euhedral glauberite crystal within matrix, b) EDS spectrum of the glauberite mineral (o: measurement point of EDS analysis taken on the crystal) (Balıbağı-1 drill, 385.30 m, XRD figure 18).

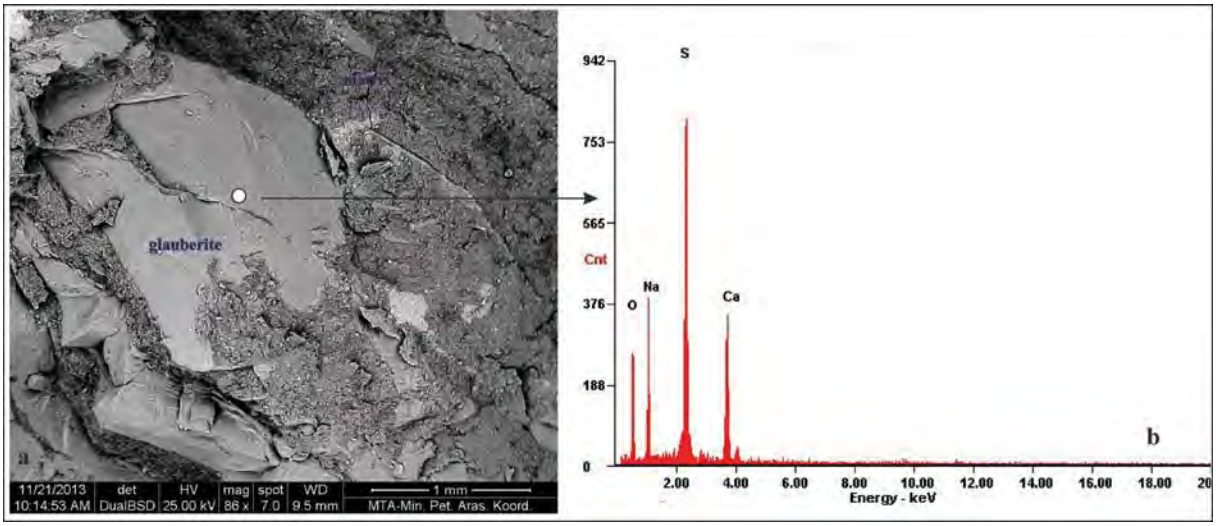

Figure 21- a) Subhedral glauberite mineral within matrix, b) EDS spectrum of the glauberite mineral, (o: measurement point of EDS analysis taken on the crystal). (Yenidoğan-1 drill, 340 m).

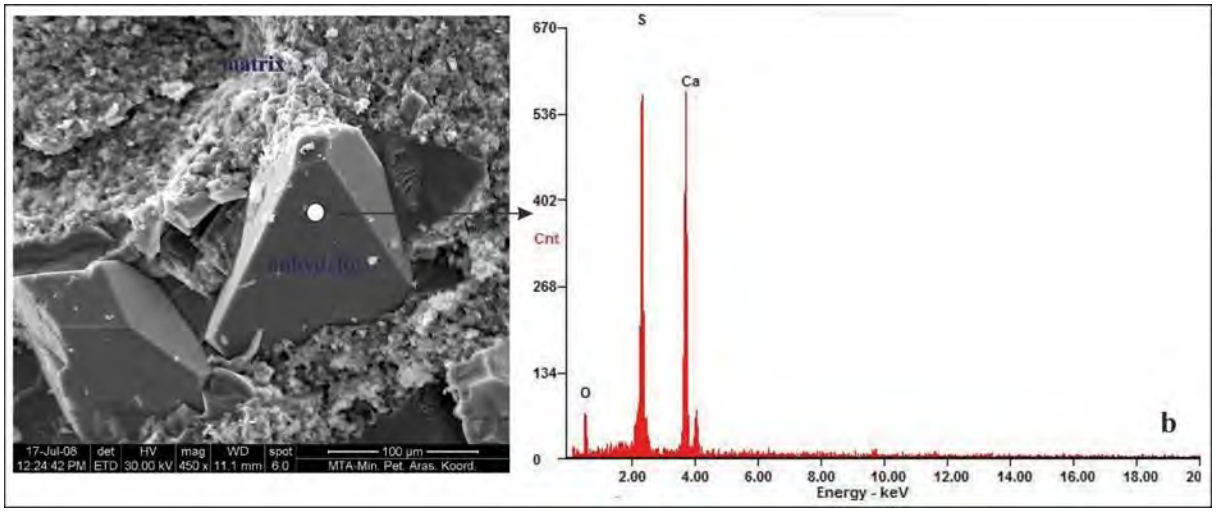

Figure 22- a) Euhedral anhydrite crystal within matrix, b) EDS spectrum of the anhydrite mineral, (o: measurement point of EDS analysis taken on the crystal), (Yenidoğan-2 drill, 366.1 m, XRD figure 19).

forms and elemental content (Figure 28). Quartz, calcite, zeolite group (analcime, heulandite-clinopilolite), palygorskite, illite/mica mineral group, feldspar mineral group were detected within magnesite and halite matrix.

As a result of SEM analyses based on the boundary relationships among minerals, the following occurrences were determined in sabhka environment (saline lake mud-flat). First gypsum and anhydrite minerals were crystallized within cryptocrystalline detritic matrix, then glauberite mineral was crystallized and grew on anhydrite minerals occasionally, and finally; halite mineral was crystallized. And this result is in accordance with evaporitic depositions in sabhka or saline environments in which the chain of formation starts with Ca compound minerals then passes into Na compound minerals.

5. Results

During borehole drillings carried out in Bozkır formation consisting of Pliocene aged evaporitic units in Çankırı-Çorum basin, thick rocksalt (halite) deposition which contain glauberite interlayer was determined.

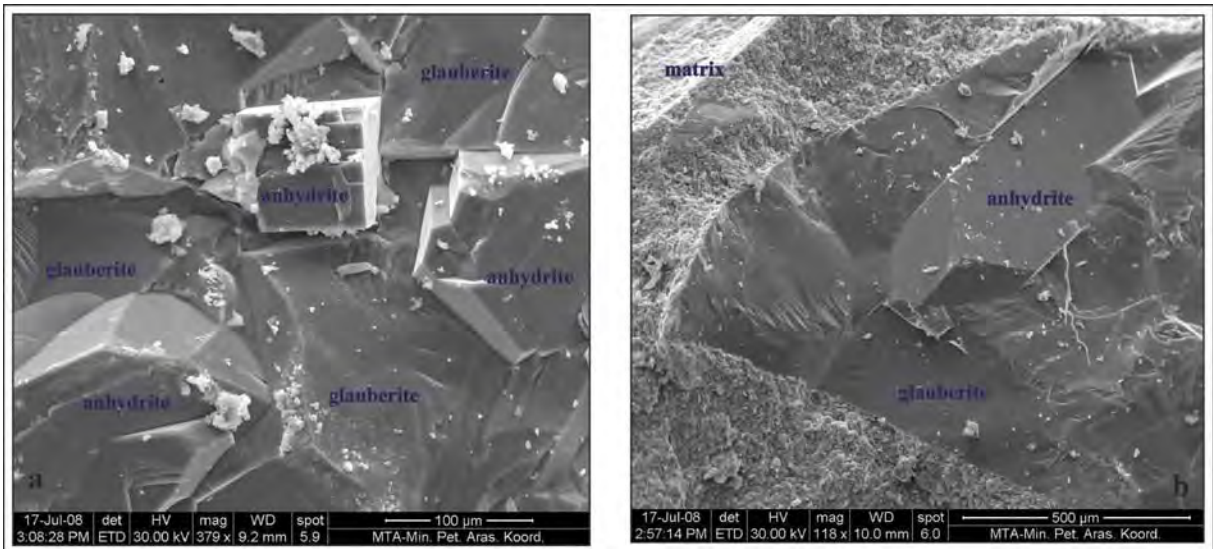

Figure 23- a) SE views of glauberite-anhydrite crystals, b) SE view of euhedral anhydrite mineral within glauberite mineral. (Balıbağı-1, 385.30 m, XRD figure 18).

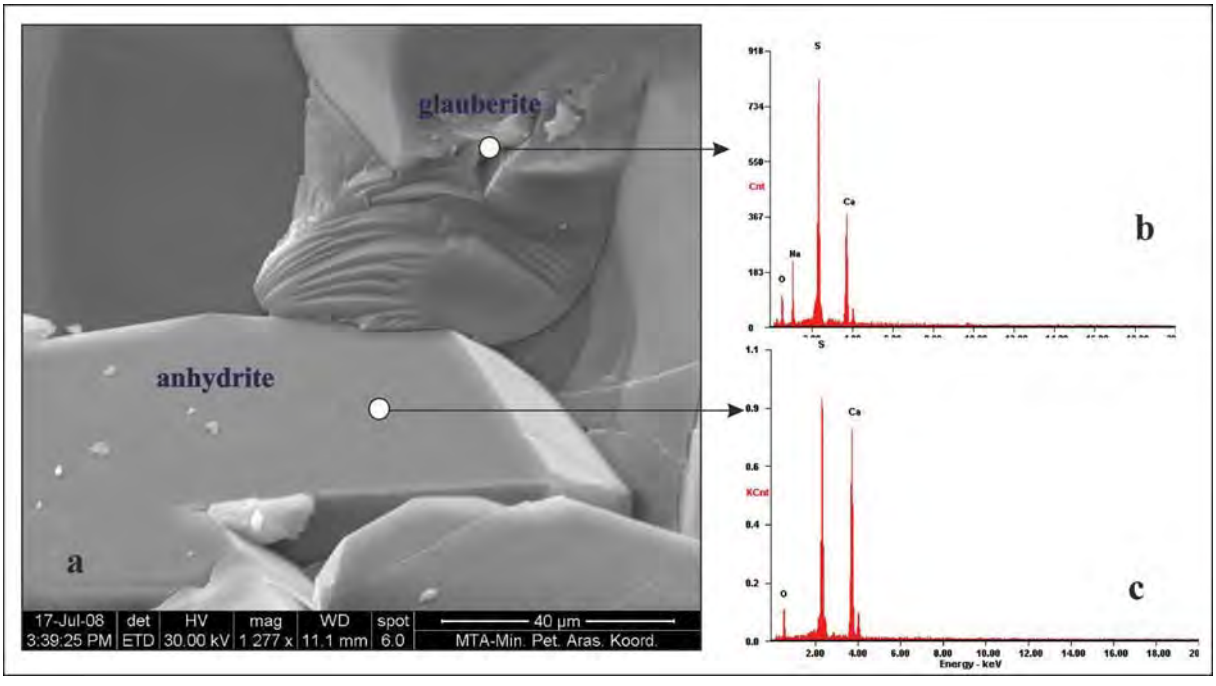

Figure 24- Concoidal fracture surfaces on glauberite mineral grown in anhydrite mineral, (o: measurement point of EDS analysis taken on the crystal) (Balıbağı-1 drill, 385.30 m XRD figure 18).

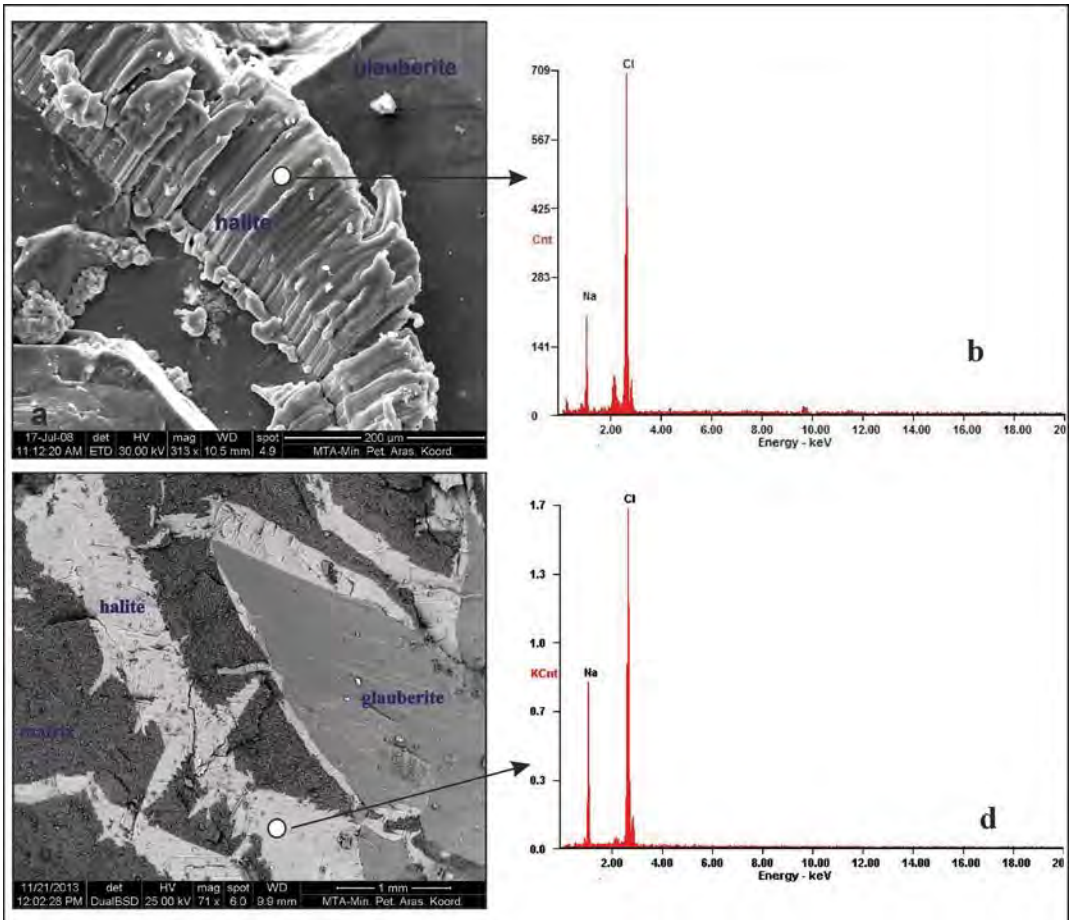

Figure 25- a) SE view of glauberite mineral on which halite mineral has grown (Yenidoğan-2 366,1 m, Figure 2), b) EDS spectrum of the halite mineral, c) SE view of the halite mineral which is observed in the form of fracture and crack infill, d) point of EDS analysis of halite mineral in the form of fracture and crack infill (Yenidoğan-2 drill, 158 m, XRD Figure 17) (o: measurement point of EDS analysis taken on the crystal).

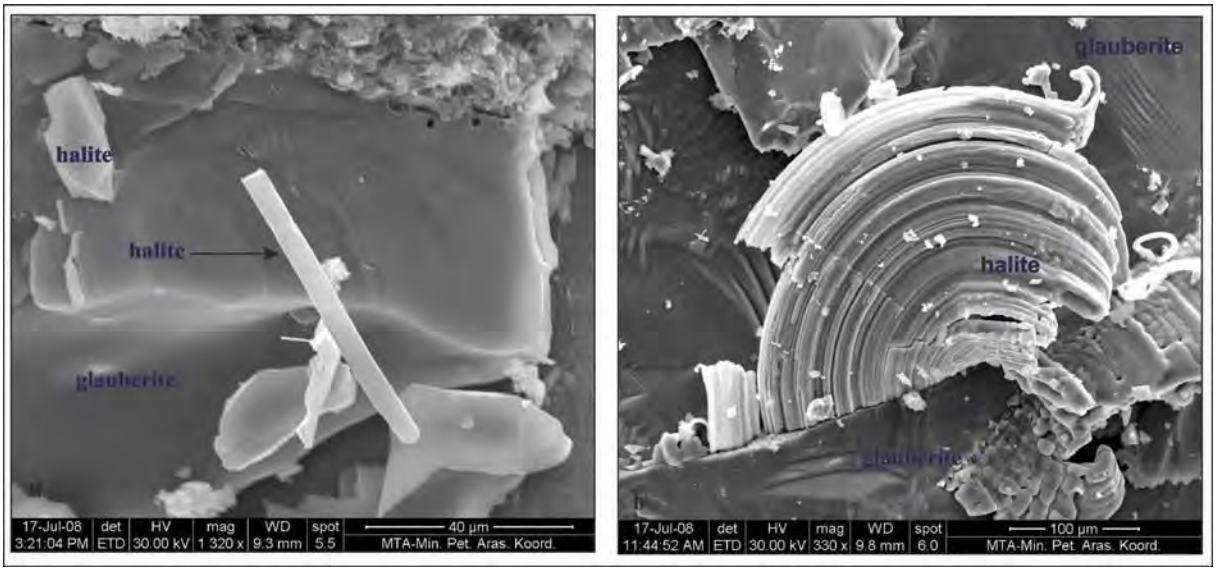

Figure 26- Crystallized halite forms on glauberite mineral, a) rod like halite crystal, b) concentric halite crystal (a, b: Balıbağı-1 drill, 385.30 m, XRD figure 18).

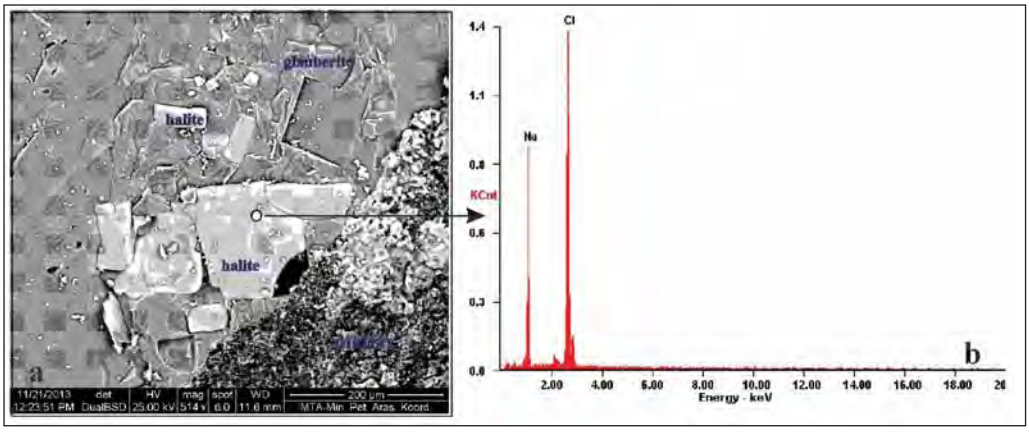

Şekil 27- Globerit minerali üzerinde gelişmiş prismatik özşekilli halit kristalleri, (O: kristal üzerinde alınan EDS analiz ölçüm noktası). (Yenidoğan-2 366,10 m XRD şekil 19).

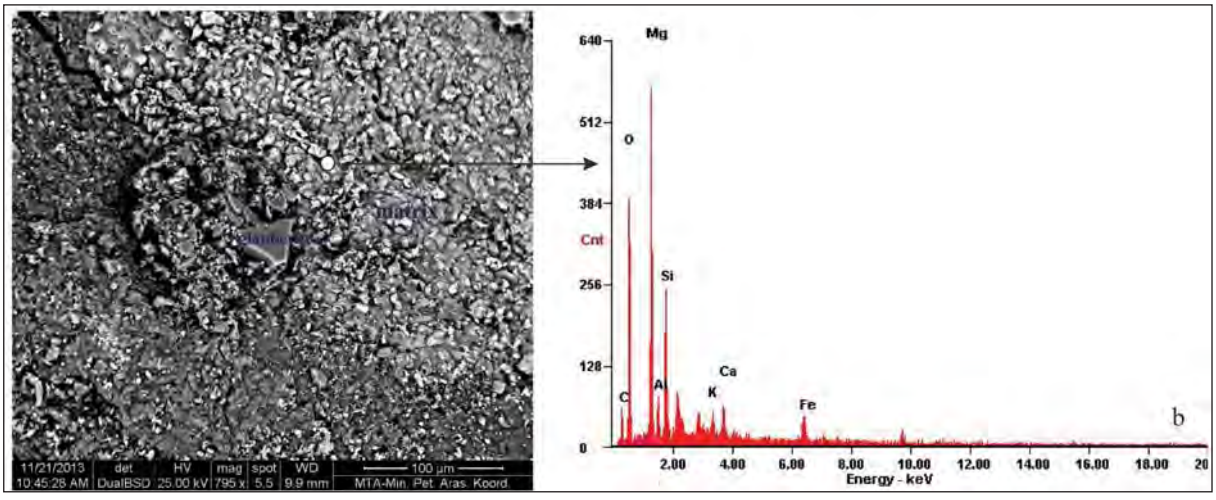

Figure 28- a) General view of the matrix which consists of glauberite layers, b) EDS spectrum of the matrix (o: measurement point of EDS analysis taken on crystal) (Yenidoğan-1 drill, 340 m).

Glauberite interlayers observed in Tuz member were deposited in sabhka environment and located as intercalating with playa lake sediments. Layers where the glauberite containing layers are the thickest were defined as glauberite-mudstone zone and were cut in thicknesses reaching 3.2 m.

In drillings which were performed in Tuz member in playa lake environment, 115 m thick rocksalt was cut which carries an economical potential. Glauberite mineral which does not have economical thickness is also important in revealing scientifically the existence of fossil Na-sulfate deposition in Çankırı-Çorum Basin.

In drilling studies performed at playa lake- sabhka transition zone in Bozkır formation, three lithological zones were detected in general. From bottom to top, these are claystone-less anhydrite zone, rocksalt-claystone-anhydrite-glauberite zone (zone consisting of sabhka interlayers) and claystone-gypsum-less anhydrite zone.

Glauberite mineral which is observed as disc and rosette shaped individual forms within mudstone dominant matrix was formed as a diagenetic mineral in saline mudflat environment (sabhka).

Glauberite mineral which was crystallized after anhydrite mineral in sabhka environment is observed as euhedral and subhedral within saline matrix. It was also detected that halite mineral had grown on glauberite mineral and was observed sometimes in the form of fracture and crack infill.

Acknowledgement

This study includes some of data obtained within the scope of "Central Anatolian Industrial Raw Material Explorations of Project" executed by the General Directorate of Mineral Research and Exploration (MTA). I thank to executives of the Dept. of Mineral Researches and Exploration for their contributions, to Prof. Baki Varol for his supports during field and office studies, to İnciser Girgin and Bilgin Çiftçi (MTA) for their helps during XRD and SEM analyses and to Aytaç Tulukçu (MTA) who helped in drawings.

Received: 10.03.2014
Accepted: 14.07.2014
Published: December 2014

References

Akyürek, B., Bilginer, E., Akbaş, B., Hepşen, N., Pehlivan, Ş., Sunu, O., Soysal, Y., Çatal, E.., Dağer, Z., Sözeri, B., Yıldırım, H. Hakyemez, Y. 1982. Ankara-Elmadağ-Kalecik dolayının temel jeolojisi. *Maden Tetkik ve Arama Genel Müdürlüğü Rapor No: 7298* Ankara (unpublished).

Birgili, S.,Yoldaş, R., Ünalan, G. 1975. Çankırı-Çorum havzasının jeolojisi ve petrol olanakları. *Maden Tetkik ve Arama Genel Müdürlüğü Rapor No: 5621* Ankara (unpublished).

Çelik, E., Kayakıran S., Kartalkanat, A.1987. Çayırhan doğal sodyum yatağı maden jeolojisi raporu ve dünyada sodyum sülfat. *Maden Tetkik ve Arama Genel Müdürlüğü Rapor No: 5621* Ankara (unpublished).

Dromart, G., Dumas, D. 1997. The Salt Basin of Valence (France): In: (Sedimentary deposition in Rift and Foreland Basins in France and Spain (Eds. G. Busson and B.Ch. Schreiber). *Columbia University Press,* New York, pp. 195-239.

Ergun, O.N., 1977. Sedimentology and Tertiary evaporites, Uğurludağ Area Çankırı - Çorum Basin, Turkey. Doktora Tezi, *Imperial College,* London, 260 s. (unpublished).

Görür, N., Oktay, F. Y., Seymen, İ., Şengör , A. M. C. 1984. Paleotectonic evolution of the Tuzgölü Basin complex, Central Turkey. Sedimentary record of a Neo-Tethyan closure, In: (Eds. Dixon, J. E. and Robertson, A. H. F.) The geological evolution of the eastern mediterranean*: Geological Society of London*, Special Paper, 17, 467-482.

Gündoğan, İ. 2000. Geology, mineralogy - petrography and economic potential of the Upper Miocene evaporites in the Beypazarı and Çankırı-Çorum Basins. Doktora Tezi, Dokuz Eylül Üniversitesi, 254 s. (unpublished).

Gündoğan, İ., Helvacı, C. 1999. Sodyum sülfat aramacılığında petrografik çalışmaların önemi. *1. Batı Anadolu Hammadde Kaynakları Sempozyumu,* 8-14 Mart 1999, İzmir, 370-377.

Gündoğan, İ., Helvacı, C. 2001. Sedimentological and petrographical aspects of Upper Miocene evaporites in Beypazarı and Çankırı- Çorum Basins, Turkey. *International Geology Reviews*, 43, 818–829.

Gündoğan, İ., Helvacı, C. 2009. Na-Ca Sülfat Mineral Dönüşümlerinin Petrografik Özellikleri ve Madencilik Araştırmalarındaki Önemi. *62. Türkiye Jeoloji Kurultayı Bildiri Özleri Kitabı-I,* 13-17 Nisan 2009, Ankara, s. 114-115.

Hakyemez, Y., Barkurt, M.Y., Bilginer, E., Pehlivan, Ş., Can, B.; Dağer, Z., Sözeri, B. 1986. Yapraklı-llgaz-Çankırı-Çandır dolayının jeolojisi. *Maden Tetkik ve Arama Genel Müdürlüğü Rapor No: 7966*, Ankara, (unpublished).

Helvacı, C., İnci, U., Yağmurlu, F., Yılmaz, H. 1989. Geologic framework of the Beypazarı district and Neogene trona deposits of the region, Turkey. *Doğa*, Vol. 13, No. 2, s.245-256.

Helvacı, C., Gündoğan, İ. 2008. Ülkemizdeki Na-Sülfat madenciliği ve Na-Sülfat aramacılığında petrografik dokuların önemi. *Prof. Dr. Servet Yaman Maden Yatakları-Jeokimya Çalıştayı. Ç.Ü. Jeoloji Mühendisliği Bölümü*, 23-25 Ekim 2008, Adana. Program kitabı, s.7-8.

Karadenizli, L. 1999. Çankırı-Çorum Havzası'ndaki Orta Eosen-Erken Miyosen Tortullarının Sedimantolojisi, Doktora Tezi Ankara Üniversitesi, 189 s. (unpublished).

Karadenizli, L., Kazancı, N. 2000. Çankırı-Çorum havzasındaki paleo-yükselti ve alt havzalar. *Cumhuriyetin 75. yıldönümü yerbilimleri ve madencilik kongresi,* Maden Tetkik ve Arama Genel Müdürlüğü, Ankara, Bildiriler s. 209-227.

Karadenizli, L., Saraç, G., Şen, Ş., Seyitoğlu, G., Antoine, P.O., Kazancı, N., Varol, B., Alçiçek, M.C., Gül, A., Erten, H., Esat, K., Özcan, F., Savaşçı, D., Antoine, A., Filoreau, X., Hervet, S., Bouvrain, G., De Bonis, L., Hakyemez, Y. 2004. Çankırı-Çorum Havzasının batı ve güney kesiminin memeli fosillere dayalı Oligo-Miyosen biyostratigrafisi ve dolgulama evrimi. *Maden Tetkik ve Arama Genel Müdürlüğü Rapor No: 10706*. Ankara, (unpublished).

Kaymakçı, N. 2000. Tectono-stratigraphical evolution of the Çankırı basin (Central Anatolia Turkey). PhD Thesis, Univ. Utrecht, Geologia Ultraiectina. 190, 247 p.

Koçyiğit, A. 1991. Changing stress orientation in progressive intracontinental deformation is indicated by the Neotectonics of the Ankara Region (NW Central Anatolia). *TPJD Bülteni*, 3 (1), 43-55.

Mees, F. 1999. Textural features of Holocene perennial saline lake deposits of the Taoudenni-Agorgott basin, northern Mali, *Sedimentary, Geology*, 127, 65-84.

Menduina, J.,Ordenez, S., Garcia del Cura M. A. 1984. Geology of the Cerezo del Rio Tiron Glauberite Deposits, *Burgos, Bol, Geol Minero* 95, 31-51.

Norman, T. 1972. Ankara doğusunda Yahşihan bölgesinde Üst Kretase-Alt Tersiyer yaşlı arazinin jeolojisi. Doktora Tezi, *ODTÜ Fen Bilimleri Enstitüsü*, Ankara (in Turkish).

Ordonez, S., Garcia del Cura, M.A. 1994. Deposition and diagenesis of sodium-calcium sulfate salts in the Tertiary saline lakes of the Madrid basin, Spain. Renault, R.W., Last, W.M. (Ed.). Sedimentology and Geochemistry of modern and ancient saline lakes. *SEPM* Special Publication, 50, 229-238.

Orti, F., Gündoğan, I., Helvacı, C. 2002. Sodium sulphate deposits of Neogene age: the Kirmir formation, Beypazarı Basin, Turkey. *Sedimentary.Geology*. vol. 146, p. 305-333.

Salvany, J.M., Veigas, J.G., Orti F. 2007. Glauberite-halite association of the Zaragoza Gypsum Formation (Lower Miocene,Ebro Basin, NE Spain), *Sedimentology*. 54, 443-467.

Salvany, J.M. 1997. Continental evaporitic sedimentation in Navarra during the Oligocene to Lower Miocene: Falces and Lerin Formations. In: Sedimentary deposition in rift and foreland basins İn France and Spain, Paleogene and Lower Neogene (Eds. G.Busson and B.Ch. Schreiber), *Columbia University Press*. New York, 397-419.

Seyitoğlu. G., Kazancı, N., Karakuş, K., Fodor, L., Araz. H., Karadenizli, L. 1997. Does continuous compressive tectonic regime exist during Late Palaeogene to Late Neogene in NW Central Anatolia, Turkey? Preliminary observations. *Turkish Journal of Earth Sciences*, 6, 77-83.

Seyitoğlu, G., Kazancı, N., Karadenizli, L., Şen, Ş., Varol, B., Karabıyıkoğlu, T. 2000. Rockfall avalanche deposits associated with normal faulting in the NW of Çankırı basin: İmplication fort he post – collisional tectonic evolution of the Neo-Tethyan suture zone. *Terra Nova*, 12/6, 245–251.

Smoot, J.P., Lowenstein, T.K. 1991. Depositional environments of non-marine evaporites. In: Evaporites, Petroleum and Mineral Resources (Ed. J.I., Melvin), Dev. *Sedimentology,* 50, 189-347.

Sönmez, İ., 2010. Çankırı-Çorum Havzasında Mevsimlik Göl Alanında Güncel Blödit Oluşumu. *Maden Tetkik ve Arama Dergisi*, 140, 37-55.

Şenalp M. 1974*a*. Tertiary sedimantation in part of Çankırı-Çorum basin, Central Anatolia. *Imperial.College London*, (unpublished).

Şenalp M 1974*b*. Çankırı-Çorum havzasının Sungurlu bölgesindeki karasal çökellerin sedimantolojisi. *Türkiye Jeoloji Kurumu Bülteni*, 24 (1) 65-74 (in Turkish).

Şengör, A. M. C., Yılmaz, Y. 1981. Tethyan evolution of Turkey: A plate tectonic approach. *Tectonophysics,* 75, 181–241.

Tüysüz, O., Dellaloğlu, A.A. 1992. Çankırı havzasının tektonik birlikleri ve havzanın Jeolojik evrimi. *Türkiye 9. Petrol Kongresi Bildirileri özeti*, 180 .

Usta, H. 1992. Topuzsaray-1 kuyusu , kuyu tamamlama raporu. *PIGEM* Arsivi.

Varol, B., Araz, H., Karadenizli, L., Kazancı, N., Seyitoğlu, G., Şen, Ş. 2002. Sedimentology of the Miocene evaporitıc succession in the North of Çankırı-Çorum Basin, central Anatolia, Turkey. *Carbonates and Evaporites*, 17/2, 197-209.

Yoldaş, R. 1982. Tosya (Kastamonu) ile Bayat (Çorum) arasındaki bölgenin jeolojisi. Doktora tezi, İst.Üniv., 311 s. (unpublished).

Weaver, C. E. 1989. Clays, Mud and Shales. Development in sedimentology, 44. Elsevier. *Amsterdam-Oxford*-New York-Tokyo, 819 s.

BULLETIN OF THE MINERAL RESEARCH AND EXPLORATION

Foreign Edition 2014 149

CONTENTS

Facies Characteristics And Control Mechanisms of Quaternary Deposits In The Lake Tuz Basin
.....Alper GÜRBÜZ and Nizamettin KAZANCI 1

Neotectonic-Period Characteristics, Seismicity, Geometry And Segmentation of The Tuz Gölü Fault Zone
.....Akın KÜRÇER and Y. Ergun GÖKTEN 19

Neogene Stratigraphy And Paleogeographic Evolution of The Karaburun Area, İzmir, Western Turkey
.....Fikret GÖKTAŞ 69

Benthic Foraminiferal Fauna of Malatya Oligo-Miocene Basin (Eastern Taurids, Eastern Turkey)
.....Fatma GEDİK 93

Protolith Nature And Tectonomagmatic Features of Amphibolites From The Qushchi Area, West Azerbaijan, NW Iran
.....Mohssen MOAZZEN 139

Glauberite-Halite Association In Bozkır Formation (Pliocene Çankırı-Çorum Basin, Central Anatolia, Turkey)
.....İlhan SÖNMEZ 153

Estimation of Swelling Pressure Using Simple Soil Indices
.....Kamil KAYABALI and Özgür YALDIZ 177

Two Examples For Imaging Buried Geological Boundaries: Sinkhole Structure And Seyit Hacı Fault, Karapınar, Konya
.....Ertan TOKER, Yahya ÇİFTÇİ, Aytekin AYVA and Akın KÜRÇER 189

The Assessment of Geothermal Potential of Turkey By Means Of Heat Flow Estimation
.....Uğur AKIN, Emin Uğur ULUGERGERLİ and Semih KUTLU 201

A Brief Note On Mineral Evolution And Biochemistry
.....José Mario AMİGO 211

Critisism on the paper "Possible Incision of The Large Valleys In Southern Marmara Region, Turkey (Nizamettin KAZANCI, Ömer EMRE, Korhan ERTURAÇ, Suzanne A.G. LEROY, Salim ÖNCEL, Özden İLERİ and Özlem TOPRAK)
.....Nizamettin KAZANCI 219

Acknowledgement 221

Notes to the authors 223

Bull. Min. Res. Exp. (2014) 149: 175-188

Bulletin of the
Mineral Research and Exploration

http://bulletin.mta.gov.tr

ESTIMATION OF SWELLING PRESSURE USING SIMPLE SOIL INDICES

Kamil KAYABALI[a*] and Özgür YALDIZ[a]

[a] *Ankara Üniversitesi Mühendislik Fakültesi Jeoloji Mühendisliği Bölümü, Tandoğan, Ankara 06100*

Keywords:
Expansive soils, swell pressure, free swell, Atterberg limits, water content, dry density

ABSTRACT

In arid to semiarid regions, damage from expansive soils to light structures in the long term may be as costly as damage by major natural hazards. Swell characteristics, including swell pressure, of expansive soils have been the subject of numerous studies. Studies examining this property employ almost exclusively the conventional oedometer apparatus, which indirectly measures swell pressure. The results of such studies are often speculative. This investigation covers 1000 swell tests on 124 soil samples, using constant swell and free swell tests. Identical specimens at different initial water contents and dry densities were constituted through static compaction for each soil sample. Atterberg limits were incorporated into regression analyses along with the water content and dry density data. The resulting empirical relationship reasonably predicts the swell pressure. The correlation between the data from constant volume and free swell tests was even more conclusive. Comparing the empirical form obtained from this investigation and the previously published two equations reveals that the other relationships dramatically underestimated the swell pressure, which was attributed to the use of indirect methods.

1. Introduction

Expansive soils may exhibit severe volume changes upon wetting and drying. Light structures such as pavement, canals, and utility lines are susceptible to damage because of the heave in underlying expansive soils. Large uplift forces from heave may even damage structural members of a building when the pressure exerted by the building on a soil foundation is smaller than the swelling pressure. Expansive soils exist in many parts of the world. As such, the cost of damage from heave alone accounts for more than any other foundation problem, reaching billions of dollars annually in some countries (Nelson and Miller, 1992; Siemens and Blatz, 2009).

Swelling potential is influenced by many factors such as clay mineral composition, amount of nonclay material present, density, size and orientation of clay particles, void ratio, cementation, size and thickness of the clay body, macrostructure, and depth below ground surface. Amongst those, the most significant factor appears to be the clay-mineral composition (Komornik and David, 1969).

The swelling pressure of expansive soils has been the subject of many investigations, and various methods have been proposed to assess the problem. The one-dimensional consolidation test is the most commonly used technique to quantitatively evaluate swelling pressure. Investigations to determine swelling pressure usually related the swelling behavior to certain physical properties such as initial moisture content, consistency limits, dry density, and clay content (Komornik and David, 1969; Nayak and Christiensen, 1971; Vijayvergiya and Ghazzaly, 1973; Attom and Barakat, 2000; Rao et al., 2004, to mention a few).

* *Corresponding author: Kamil KAYABALI, kayabali@ankara.edu.tr*

Basma et al. (1995) introduced two techniques termed the restrained swell test and the double oedometer swell test. They carried out a series of swell tests by employing four methods, including the most commonly used zero swell and swell consolidation tests. They concluded that the restrained swell test is best suited to determine swelling.

Shuai (1996) provided an excellent review of the testing procedures used to measure swelling pressure in expansive soils. Shuai gathered all available methods under two categories: the constant load oedometer test and the constant volume oedometer test. The first category listed the free swell, double oedometer, loaded swell oedometer tests, the direct model method, and the Chinese method, whereas the second category listed the constant volume oedometer, the Sullivan and McClelland, and strain controlled tests. Between the two methods, Shuai recommended the constant volume method because it does not involve volume change, while recognizing a key a limitation in the sampling disturbance is not accounted for.

Kayabalı and Demir (2011) utilized a simple and robust swell pressure measurement apparatus to conduct a series of swell tests on twelve statically compacted, high plasticity clay soils by employing the four methods cited by Basma et al. (1995), terming those as indirect tests, and their own constant volume test, which they termed as the direct method. They compared the results of indirect swell tests to those of the direct method, concluding that (1) the restrained test underestimates swelling pressure; (2) the swell-consolidation and zero swell tests significantly overestimate swelling pressure; (3) the results of the double oedometer test shows no correlation with the direct method; and (4) the correlation between the swell pressure from the direct method and the free swell test is considerably high and should be further investigated using a broader database. They also argued that the direct method may slightly underestimate the true swelling pressure, owing to the stiffness of the load cell of the measuring unit.

Many investigators proposed that the swelling pressure can be estimated using simple soil parameters. Nevertheless, the methods to determine the swelling pressure in almost all of those studies were the various versions of the one-dimensional consolidometer. Kayabalı and Demir (2011) pointed out that some of those indirect methods require more than one soil specimen for any soil sample and that all specimens be identical. In addition, those methods either significantly overestimate or underestimate the swelling pressure.

The scope of this investigation is to relate the swelling pressure to simple soil indices, specifically to the initial moisture content, dry density, and Atterberg limits, using the constant volume method. An empirical relationship between the free swell and swelling pressure is also developed by employing a much wider database.

2. Materials

This investigation uses 124 soil samples of different levels of plasticity, which were collected from different parts of Ankara, as bulk specimens. They were first oven-dried then pulverized to pass through a #40 sieve (some of the soil samples were sieved through both #40 and #200 meshes as part of another broader project). Their plasticity characteristics and USCS (Unified Soil Classification System; ASTM, 2000) classes are presented in table 1. The major tool employed for the investigation consists of a frame unit equipped with a load cell and a digital display (Figure 1).

3. Methods

Identical soil specimens were created from each of the 124 samples through static compaction. Swelling pressure testing was carried out in two phases. The first phase included only four soil samples (numbered 201–204 in table 1) subjected to extensive swelling pressure tests. During this part, two groups of specimens were considered. The first group consisted of soil specimens wetted at around 25% water content and was statically compressed in a cylindrical container of 50.5 mm in diameter until the applied load reached 1 kN, 2 kN, 3 kN, 4 kN, 5 kN, 6 kN, 7 kN, 8 kN, 9 kN, and 10 kN. This way, ten soil specimens of different initial dry densities were prepared. Each loading level included preparing three soil specimens of each kind of soil. The statically compacted soil specimens were then transferred into a consolidation ring of 20 mm in height and 50 mm in diameter, and the protruding part of the soil was carefully trimmed. The three soil specimens were placed in the constant volume swelling pressure test devices, as shown in figure 1. A slight seating load was applied to the statically compacted test specimen to eliminate the possible clearance between the rod attached to the digital load cell and the consolidation cell before initiating the inundation, and the seating

Figure 1- Constant volume swell test apparatus.

load (usually on the order of 10–20 N) was recorded. The specimen was then inundated, and the swelling pressure at the end of one day was recorded. The second group consisted of statically compacted specimens with water contents ranging from 20% to 30% with 1% increments. Those specimens were compressed until the load cell recorded a force of 10 kN, an arbitrarily determined value. Three specimens were prepared for each of four soil samples, as in the case of the first group. A similar procedure was followed to emplace the statically compacted specimens into the constant volume swelling pressure test devices (three of which were employed simultaneously). Likewise, a small seating load was applied prior to inundation, and after 24 hours the swelling pressure was recorded through the digital display of the testing unit. The initial load was deducted from the final reading, and the remaining amount was divided by the area of the test specimen, resulting in the swelling pressure.

The second phase of testing included measuring the swelling pressure and free swell of 120 samples. A sufficient amount of dry mass of each soil was mixed with a water content slightly higher than 25% (so that the yielding water content was nearly 25%) and was subjected to static compaction. Each mixture was loaded until the force display showed 10 kN. The transfer and trimming of the statically compacted soil were similar to those in the first phase. This time, however, six specimens from each of the 120 soil samples were prepared. Three were subjected to the swelling pressure test under constant volume conditions, and the remaining three specimens were reserved for the free swell test. One-dimensional consolidation test cells were employed for the free swell tests. The consolidation ring containing a specimen was emplaced into the consolidation cell. An initial seating pressure of 7 kPa was applied prior to inundation. The amount of free swell was recorded through the dial gauge at the end of one day, and the percent swell was computed by dividing the amount of free swell by the initial height of the specimen.

4. Experiments, Results and Discussion

Numerous investigations can be found in the literature that relate swell characteristics to initial water content and dry density. For example, the swell pressure versus water content shown in figure 2 (after Kayabalı and Demir, 2011) was based on tests on 40 artificially prepared specimens, which illustrates that there is almost a linear relationship between the initial water content and the swell pressure. Clearly, as the water content increases, the swell pressure decreases.

The relationship between dry density and swell pressure is such that as the dry density increases, the swell pressure increases. To demonstrate and emphasize the importance of this fact, a series of swell tests were executed on the samples numbered 201–204. The results are displayed in figure 3. Ten

Table 1- Plasticity and USCS classes of soils material used for is this investigation.

No.	LL	PL	USCS	No.	LL	PL	USCS	No.	LL	PL	USCS
1	66.3	29.3	CH	43	57.9	37.0	MH	85	62.2	27.8	CH
2	57.1	24.4	CH	44	55.3	25.0	CH	86	46.4	28.1	ML
3	62.0	30.0	CH	45	54.0	29.8	MH	87	78.4	29.1	CH
4	54.5	25.6	CH	46	49.8	26.1	CL	88	61.4	35.9	MH
5	69.8	32.9	CH	47	57.4	28.5	CH	89	62.8	29.9	CH
6	71.4	31.8	CH	48	54.6	30.1	MH	90	54.4	31.3	MH
7	79.0	33.9	CH	49	59.5	30.3	CH	91	70.2	43.8	MH
8	57.8	29.6	CH	50	55.9	24.2	CH	92	68.0	30.8	CH
9	73.9	33.3	CH	51	75.5	35.6	MH	93	64.1	36.6	MH
10	75.0	33.1	CH	52	66.7	31.6	CH	94	61.9	32.0	MH
11	49.3	29.8	ML	53	70.8	35.8	MH	95	65.1	30.7	CH
12	57.4	24.3	CH	54	63.7	31.5	CH	96	52.6	32.3	MH
13	69.2	26.6	CH	55	78.6	36.5	MH	97	60.7	30.5	CH
14	71.0	40.3	MH	56	78.1	38.6	MH	98	60.2	33.2	MH
15	66.3	39.1	MH	57	90.3	35.2	CH	99	62.2	35.3	MH
16	60.6	41.3	MH	58	71.1	35.7	MH	100	61.7	30.3	CH
17	57.0	29.9	CH	59	77.6	35.3	CH	101	52.6	33.9	MH
18	53.7	33.4	MH	60	83.9	35.0	CH	102	53.0	32.7	MH
19	52.6	30.5	MH	61	59.4	39.0	MH	103	56.7	32.5	MH
20	53.1	25.0	CH	62	81.0	26.5	CH	104	58.0	25.6	CH
21	50.3	24.8	CH	63	87.2	34.0	CH	105	54.7	30.4	MH
22	61.0	29.9	CH	64	84.5	41.4	MH	106	55.2	31.2	MH
23	56.3	28.8	CH	65	72.2	40.2	MH	107	57.0	29.9	CH
24	42.9	26.2	ML	66	64.3	40.5	MH	108	53.0	30.0	MH
25	65.2	27.2	CH	67	65.0	35.0	MH	109	56.3	31.0	MH
26	48.5	28.6	ML	68	55.1	36.3	MH	110	55.4	30.8	MH
27	74.4	29.6	CH	69	58.9	30.8	MH	111	66.2	39.6	MH
28	57.4	25.3	CH	70	64.3	27.3	CH	112	59.5	36.3	MH
29	65.2	33.8	MH	71	61.5	30.1	CH	113	65.1	30.8	CH
30	53.3	25.4	CH	72	64.9	30.2	CH	114	67.6	30.2	CH
31	54.6	30.9	MH	73	71.4	31.2	CH	115	63.8	31.8	CH
32	58.5	24.2	CH	74	55.6	33.7	MH	116	61.6	32.6	MH
33	69.0	29.2	CH	75	67.8	27.6	CH	117	67.7	31.4	CH
34	54.6	21.9	CH	76	53.8	33.3	MH	118	60.5	30.4	CH
35	57.4	29.2	CH	77	75.9	32.0	CH	119	64.6	32.9	MH
36	47.8	25.5	CL	78	65.0	30.5	CH	120	63.4	30.7	CH
37	77.1	26.5	CH	79	67.9	40.0	MH	201	90.3	35.2	CH
38	68.2	31.2	CH	80	55.9	27.8	CH	202	72.2	40.2	MH
39	62.7	24.0	CH	81	61.5	34.0	MH	203	88.0	29.7	CH
40	47.7	25.0	CL	82	70.2	29.4	CH	204	66.4	35.5	MH
41	67.3	37.1	MH	83	71.8	30.2	CH				
42	68.6	27.3	CH	84	51.9	25.2	CH				

experiments were conducted on each soil sample to evaluate the relationship between the swell pressure and dry density. Those experiments were conducted on artificially prepared soils with an approximate water content of 25%. It should be noted that an exact value of 25% cannot be achieved due to some evaporation during mixing of dry soil with a water content of more than 25%. Likewise, ten experiments were performed on the same samples to confirm the effect of the initial water content on swell pressure. This time the artificial specimens were prepared at nearly constant dry densities. Because it is difficult to set the dry density at the desired level, compaction was considered to be the controlling agent for the dry density. Accordingly, all specimens serving this purpose were compressed, up to 10 kN. Figure 3 shows that the swell pressure increases as the dry density increases. One of the graphs in figure 3 that shows swell pressure versus initial water content appears to violate our first interpretation of swell pressure linearly decreasing with the increasing initial water content (soil sample 202). A possible explanation for this would be that below a certain level of water content, the static compaction test for that specific soil sample may yield lower dry density values than tests illustrating the normal swell pressure versus initial water content behavior.

As the initial water content appears to be the most crucial parameter affecting the swell pressure, at what level of initial water content should experiments be conducted? Considering that the plastic limit would be an appropriate value, a series of swell pressure tests were performed. The results are displayed in figure 4 for 40 samples selected from the first 120 samples in table 1. figure 4 reveals two facts. First, there is not a meaningful relationship between plastic limit and swell pressure. Second, the yielding swell pressures are relatively low, suggesting that the water contents corresponding to plastic limits are high enough to be considered in swell pressure tests. Initial water contents therefore need to be somewhat lower than plastic limits. Considering that the majority of the plastic limits in the 120 samples were above 25, an initial water content of 25% was set as the key value for swell pressure tests. Using a single value would also help in comparing experiment results.

To establish an empirical relationship between easily defineable simple soil indices such as water content, dry density, Atterberg limits, and swell pressure, a series of swell pressure tests were carried out on 120 soil samples, whose consistency limits were well defined, using the apparatus shown in figure 1. Three swell pressure tests were executed on each soil sample. For these tests, three identical specimens, prepared with a 25% water content with the ultimate compression load of 10 kN, were set in three constant volume apparatus. The average swell pressures for 120 soil samples are given in table 2. It should be noted that all numbers in the table correspond to the average value obtained from the three tests.

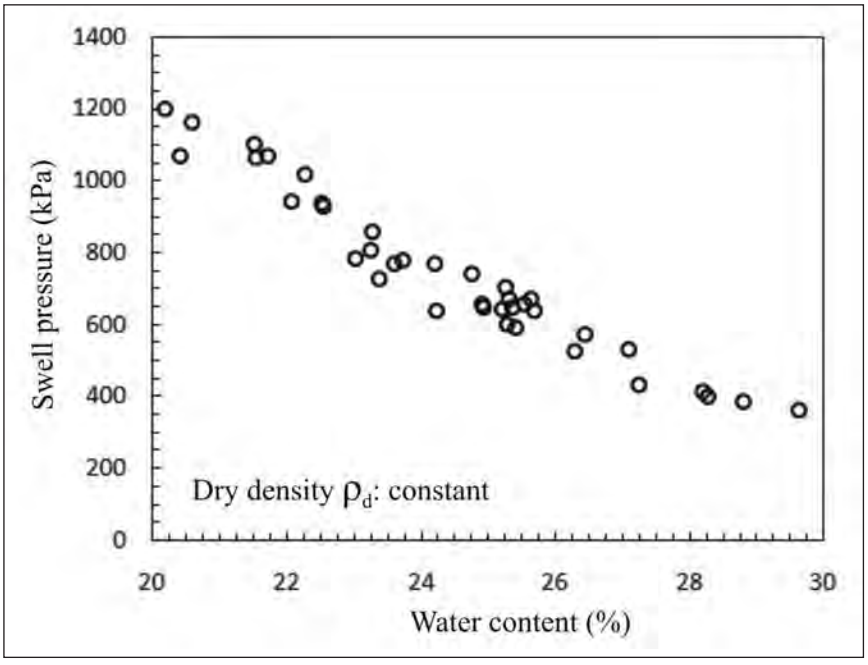

Figure 2- Relationship between the swell pressure and the initial water content (after Kayabalı and Demir, 2011).

A number of regression analyses were performed among the initial water content, dry density, liquid limit, plastic limit, and plasticity index using DATAFIT software (2008). The regression analyses were carried out interchangeably among those parameters to match the best coefficient for the correlation. Six hundred values were incorporated into the regression analyses. Of which, 360 constituted 120 soil samples, each having three specimens; the remaining 240 constituted the soils numbered 201 through 204 in table 1, each of which comprising 60 experiments (10 experiments for swell pressure versus water content with three repetitions for each soil sample, yielding 30 values and 10 experiments for swell pressure versus dry density, yielding another 30 values). The best relationship is obtained by including the initial water content, dry density, liquid limit, and plastic limit. The equation relating those four parameters to the swell pressure is as follows:

$$SP = -30.8w_i + 1025\rho_d + 6.35LL + 42.4PL - 2208 \quad (1)$$

where SP is the swell pressure in kPa. The regression coefficient (R^2) for this correlation is 0.724. Figure 5 compares the measured swell pressures for 600 experiments with the predicted swell pressures using Eqn. (1). The newly established empirical relationship appears to slightly underestimate swell pressures at ranges over 600 kPa, a reasonably meaningful threshold value below which a great majority of fine grained soils may be covered.

Including only initial water content and dry density in regression analyses to obtain swell pressure results in a poor correlation, with a regression coefficient of 0.08. This shows that, while the initial water content and dry density are two crucial factors affecting the swell pressure, they cannot be utilized without considering plasticity data. For this reason, the authors chose not to include such a figure in the text. It should be emphasized that, while figure 3 implies that the swelling pressure shows reasonably good relationships with water content and dry density, a regression analysis excluding plasticity characteristics does not yield a universally acceptable empirical relationship to predict the swelling pressure.

The literature review conducted prior to this investigation unveiled many previous studies that focused on the swell characteristics of expansive soils, including the empirical relationships. Few of such studies (Komornik and David, 1969; Vijayvergiya and Ghazzaly, 1973; Erzin and Erol, 2004) focused on relationships. For a comparison, studies by Komornik and David (1969) and Erzin and Erol (2004) were considered. Erzin and Erol (2004) related the initial water content (w_i in percent), dry density (ρ_d in g/cm^3), and plasticity index (PI) to swell pressure (SP in kgf/cm^2) in the following equation:

$$\log(SP) = -4.812 + 0.01405PI + 2.394\rho_d - 0.0163\, w_i. \quad (2)$$

Figure 6 shows a comparison between the measured swell pressures in this investigation and the predicted swell pressures using Eqns. (1) and (2). Astonishingly, the empirical relationship proposed by Erzin and Erol (2004) yields unusually low swell pressures. While the relationship by Erzin and Erol (2004) results in acceptable and consistent values when employing their own data, it dramatically underestimates the swell pressure using the data of this investigation. A possible reason for such a discrepancy is that their data is restricted to small number of tests and is dominated by high plasticity index values. The degree of underestimation by Eqn. (2) is about 50 times than that of Eqn. (1). The plasticity index of soil samples employed in this study ranges from 17 to 58. Thus, the similar setback may be of concern for the empirical relationship proposed in this investigation, particularly at higher ranges of the plasticity index, and such a situation requires further investigation.

Komornik and David (1969) related the swell pressure (SP in kgf/cm^2) to the initial water content (w_i in percent), dry density (ρ_d in kg/m^3), and liquid limit in the following form:

$$\log(SP) = -2.1 + 0.021LL + 0.00067\rho_d - 0.027\, w_i. \quad (3)$$

A comparison between the measured swell pressures in this investigation and the predicted swell pressures using Eqns. (1) and (3) is presented in figure 7. The empirical form by Komornik and David (1969) yields swell pressures with somewhat higher values than that by Erzin and Erol (2004); however, the degree of underprediction is still dramatic. That is, the degree of underprediction by Komornik and David's (1969) approach is about 10 times when compared to those obtained using Eqn. (1).

Swell pressures were also evaluated in correlation with free swell. Regarding free swell tests, three specimens were prepared for testing. The specimens were set in a conventional one-dimensional

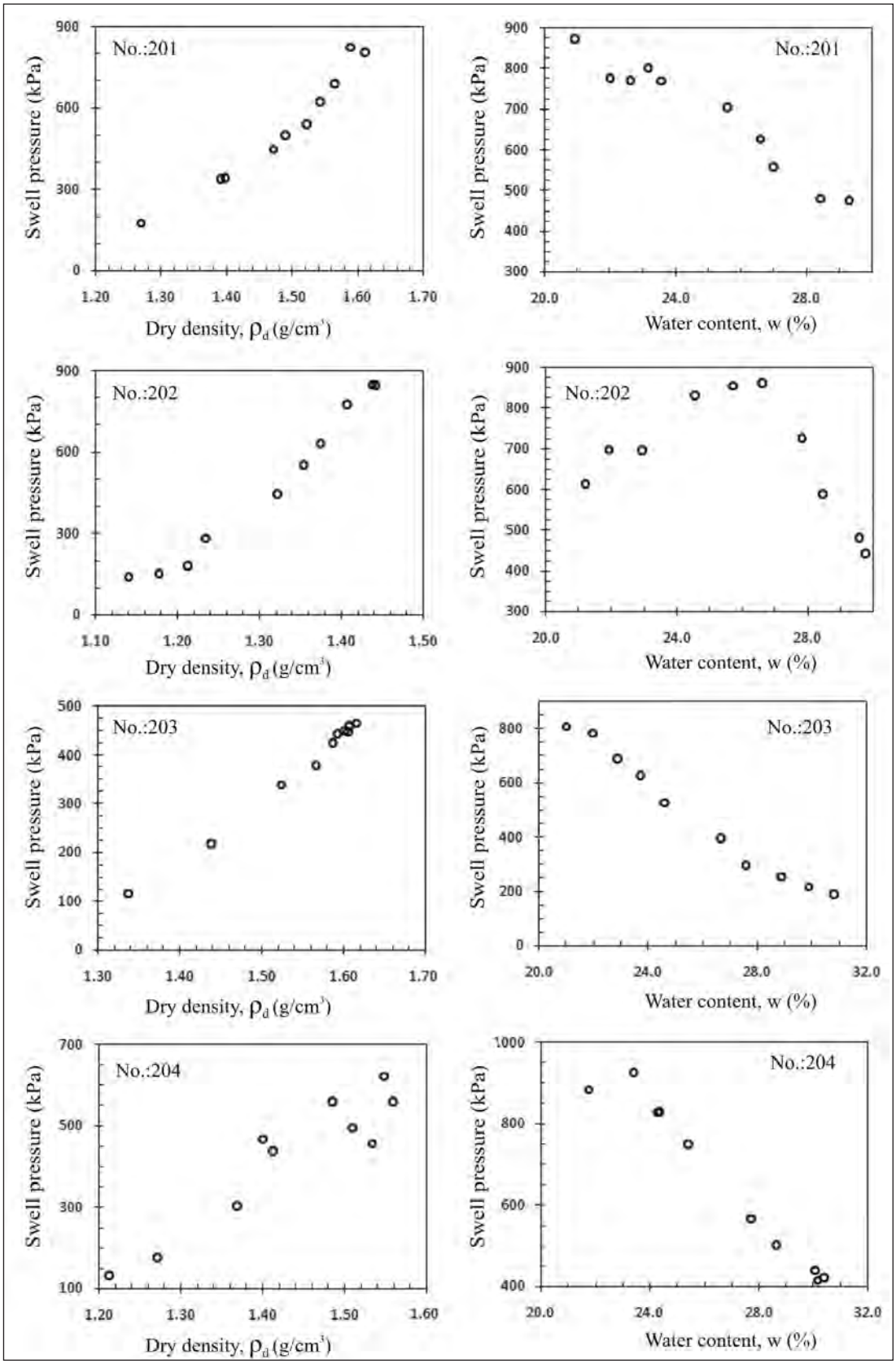

Figure 3- Swell pressure versus dry density (the left column), and swell pressure versus initial water content (the right column) graphs for soil samples 201–204.

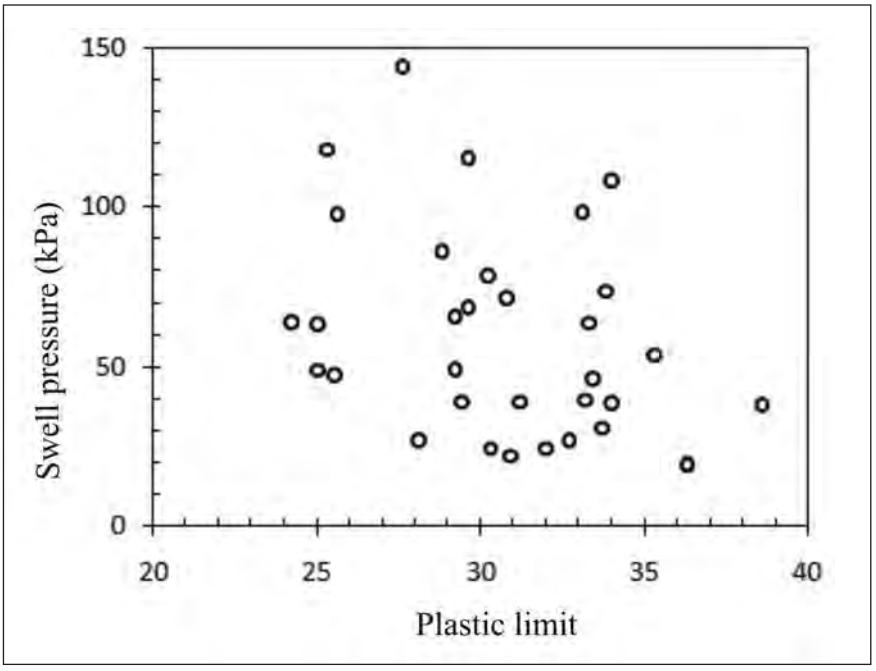

Figure 4- Relationship between swell pressure and plastic limit for 40 soil samples.

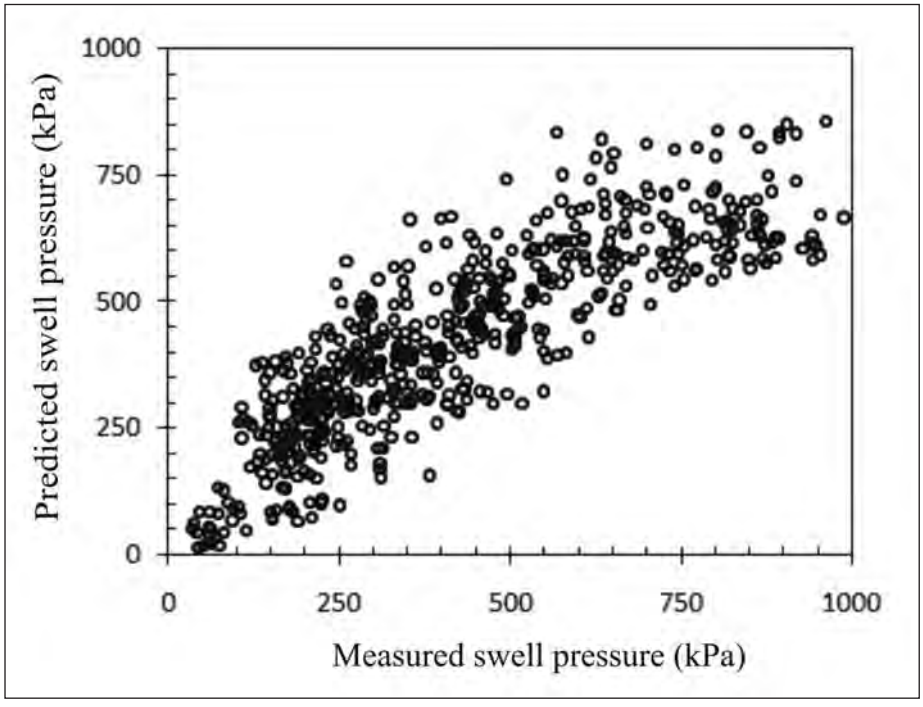

Figure 5- Predicted swell pressure versus measured swell pressure for 600 pairs of data.

Table 2- The initial water content (w_i), dry density (ρ_d), swell pressure (SP) and free swell (FS) values for 120 soil samples. Each number in the table represent the average of the results obtained from three specimens per soil sample.

No.	w_i (%)	ρ_d (g/cm^3)	SP (kPa)	FS (%)	No.	w_i (%)	ρ_d (g/cm^3)	SP (kPa)	FS (%)	No.	w_i (%)	ρ_d (g/cm^3)	SP (kPa)	FS (%)
1	25.2	1.61	351	9.1	41	26.3	1.47	507	12.8	81	24.9	1.57	405	6.3
2	25.4	1.61	184	5.5	42	26.3	1.57	246	8.1	82	24.8	1.59	341	8.9
3	25.5	1.59	344	8.4	43	26.4	1.53	290	6.4	83	24.9	1.60	477	9.6
4	25.4	1.60	160	4.2	44	26.1	1.57	46	2.6	84	25.8	1.60	83	3.1
5	24.8	1.59	673	13.3	45	26.1	1.55	170	5.2	85	25.9	1.59	326	9.6
6	25.2	1.60	551	10.8	46	25.4	1.58	60	2.7	86	26.0	1.58	227	7.5
7	25.3	1.60	682	15.4	47	25.7	1.59	125	5.5	87	25.8	1.61	335	11.1
8	25.5	1.59	261	7.8	48	26.1	1.59	162	5.4	88	25.5	1.49	256	7.4
9	25.7	1.60	569	12.3	49	25.4	1.59	200	6.8	89	25.7	1.60	230	7.9
10	25.3	1.62	497	10.8	50	25.7	1.56	76	2.9	90	25.6	1.56	206	6.0
11	25.5	1.55	245	7.3	51	25.3	1.59	604	13.8	91	27.1	1.41	676	14.8
12	25.4	1.61	74	4.3	52	25.3	1.60	332	8.8	92	25.7	1.59	330	9.3
13	26.0	1.58	158	7.3	53	24.6	1.58	598	9.8	93	25.0	1.56	448	8.3
14	26.3	1.45	853	19.1	54	25.2	1.60	325	6.8	94	25.7	1.59	175	6.8
15	26.1	1.47	711	15.8	55	26.2	1.56	744	15.6	95	25.6	1.58	383	7.1
16	25.7	1.42	626	15.2	56	25.9	1.57	607	11.9	96	25.6	1.59	204	5.8
17	25.6	1.60	155	6.0	57	25.7	1.54	931	22.6	97	25.6	1.59	221	5.8
18	25.7	1.52	316	6.6	58	27.3	1.54	405	9.2	98	25.6	1.58	313	7.9
19	25.5	1.55	224	3.6	59	26.6	1.59	529	12.6	99	25.6	1.57	425	7.9
20	25.6	1.60	258	4.0	60	27.1	1.58	635	13.4	100	26.0	1.59	196	7.9
21	25.6	1.55	58	2.5	61	25.0	1.58	389	8.5	101	25.8	1.55	232	5.6
22	26.4	1.58	317	9.2	62	26.7	1.59	219	10.0	102	26.2	1.55	168	4.6
23	25.8	1.59	295	9.3	63	27.2	1.56	454	12.0	103	26.0	1.57	264	7.6
24	25.4	1.56	47	1.8	64	25.3	1.39	841	20.4	104	24.7	1.58	160	5.8
25	25.0	1.62	218	8.1	65	26.6	1.44	849	18.1	105	26.1	1.58	171	5.9
26	25.4	1.56	80	2.5	66	25.5	1.45	799	18.9	106	26.1	1.57	215	7.0
27	25.4	1.63	249	9.1	67	25.8	1.62	293	7.6	107	26.2	1.59	165	5.6
28	25.7	1.60	133	5.1	68	25.5	1.48	411	9.1	108	25.8	1.58	154	5.3
29	26.1	1.58	319	10.0	69	25.1	1.58	520	10.0	109	25.6	1.57	227	5.9
30	25.7	1.62	51	3.3	70	25.2	1.55	454	9.4	110	25.7	1.59	205	6.2
31	25.6	1.56	116	4.7	71	25.6	1.57	220	7.2	111	26.2	1.49	613	12.8
32	25.9	1.61	39	2.3	72	26.0	1.60	359	9.1	112	26.0	1.56	291	7.6
33	25.9	1.60	243	9.4	73	26.0	1.59	407	10.8	113	26.2	1.57	314	8.2
34	25.8	1.62	64	4.0	74	25.4	1.58	285	6.0	114	25.8	1.58	298	9.6
35	25.6	1.60	220	8.5	75	28.3	1.53	205	7.4	115	25.2	1.60	306	8.6
36	25.8	1.61	64	3.1	76	25.6	1.57	246	5.6	116	25.4	1.59	294	7.6
37	25.8	1.61	314	6.5	77	25.6	1.63	249	7.7	117	25.7	1.60	275	8.3
38	25.6	1.58	137	4.9	78	25.4	1.60	244	7.9	118	24.9	1.60	212	6.2
39	25.6	1.60	131	5.6	79	25.3	1.60	544	9.6	119	25.4	1.60	318	8.8
40	25.2	1.59	52	2.3	80	25.1	1.61	176	6.1	120	25.1	1.61	275	8.7

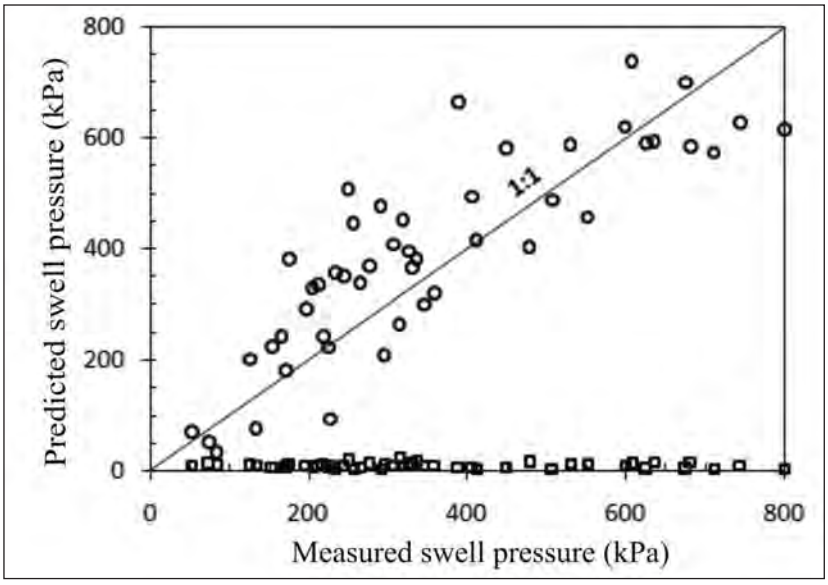

Figure 6- Comparison between the predicted swell pressures using the proposed relationship and the measured swell pressures (circles) and the swell pressures computed using the relationship by Erzin and Erol (2004) (squares).

consolidation testing apparatus (or oedometer). The amount of heave (the change in the height of a specimen, ΔL) measured at the end of 24 hours was recorded. The free swell (in percent) was determined as the heave divided by the original height of the specimen, L. The average values of three specimens per soil sample are presented in table 2. figure 8 shows two comparisons between the swell pressures obtained from the constant volume swell pressure test and the free swell test. First, 360 swell pressures were compared with 360 free swells for 120 samples. The regression coefficient for this correlation is 0.822, and the relationship obtained is as follows:

$$SP = 46.04FS - 63.43. \quad (4)$$

Second, the average swell pressure and the average free swell of three specimens per soil sample are compared for 120 soils. The quality of correlation with this comparison is slightly better than the previous one ($R^2 = 0.888$). The empirical relationship for this correlation is:

$$SP = 48.09FS - 76.01 \quad (5)$$

The constant volume swell pressure and free swell tests were all conducted over a 24-hour period. This length of time is selected only for the sake of convenience. At this point, one might raise a question regarding if this length of time is long enough for a soil specimen to undergo full swelling. To address such a likely criticism, a series of additional tests were executed. Three soil specimens representing the lowest, moderate, and highest swell pressures were subjected to swell pressure and free swell tests, and the amount of swell was monitored. Figure 9 illustrates the swell behavior with respect to elapsed time and reveals that, if not completely, almost all swelling takes place in a 24-hour period, which justifies our selection of time length for all swell tests.

5. Conclusions

Based on a comprehensive investigation comprising 1000 experiments that employ the constant volume and the free swell tests, the following conclusions were reached:

1. While the initial water content and dry density significantly affect the outcoming swell pressure, they cannot be used alone to predict swell pressure accurately.

2. Including Atterberg limits in regression analyses with the initial water content and dry density resulted in an empirical relationship with a reasonably good regression coefficient of 0.724. The empirical form of

$$SP = -30.8w_i + 1025\rho_d + 6.35LL + 42.4PL - 2208$$

is proposed to estimate the swell pressure for soils with the plasticity index up to about 60.

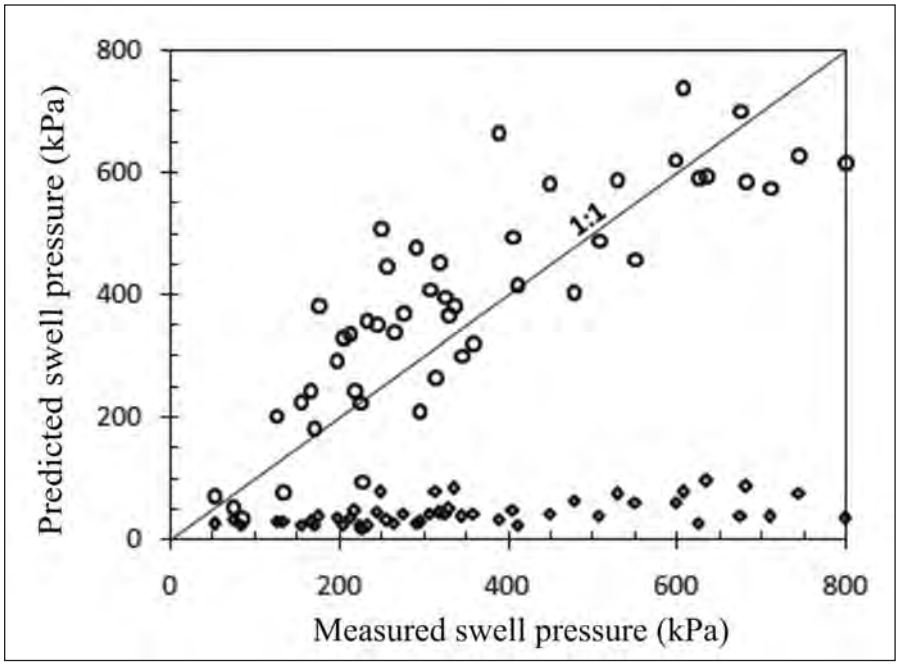

Figure 7- Comparison between the predicted swell pressures using the proposed relationship and the measured swell pressures (circles) and the swell pressures computed using the relationship by Komornik and David (1969) (squares).

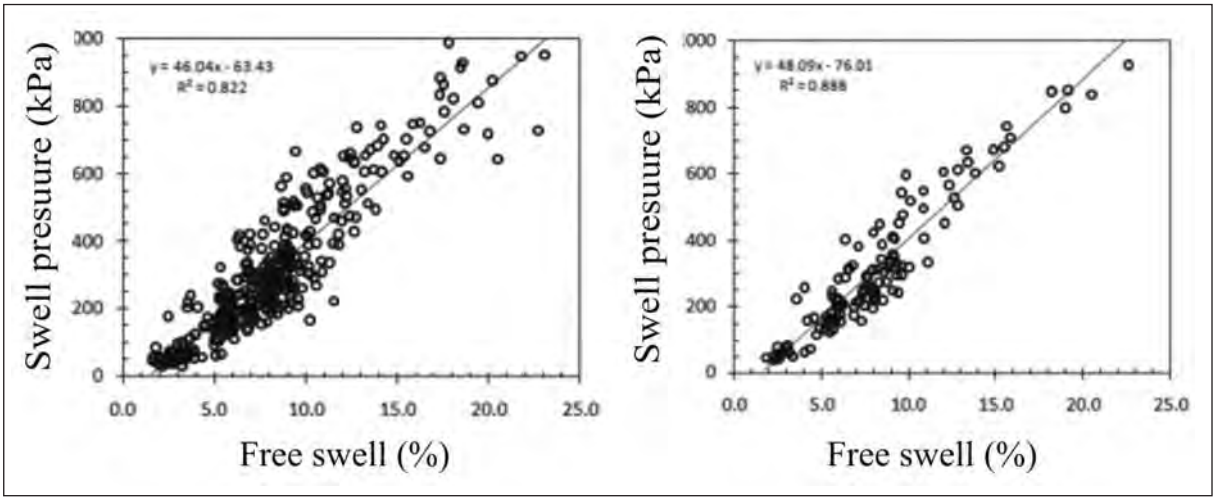

Figure 8- Comparisons between the swell pressures from the constant volume and free swell tests for 360 data pairs (left) and the average swell pressures and average free swells for 120 soil samples (right).

3. Comparing a large body of data from constant volume swell tests and free swell tests also unveils a remarkably good relationship in the following form ($R^2 = 0.888$):

$$SP = 48.1FS - 76.$$

4. Initial water content, dry density, and Atterberg limits are basic soil indices easily obtainable from all undisturbed samples. Swell pressure can be computed empirically by using those parameters without requiring further tests. Disturbed samples do not allow for determining the dry density. By making reasonable assumptions for dry density, index values obtained using disturbed soils may also provide an idea about the swell potential.

5. The free swell test is also a simple test that can be conducted almost in all laboratories. It can be used to confirm the accuracy of swell pressure obtained using the simple soil indices.

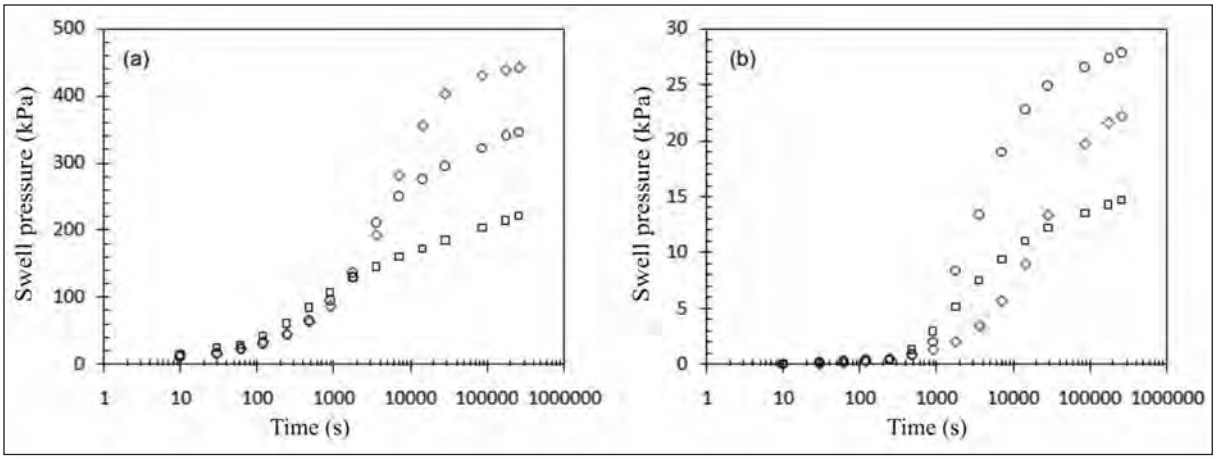

Figure 9- Swell pressure behavior (a) and free swell behavior (b) with respect to time for three selected soils.

6. The empirical relationships to determine swell pressure established in this investigation covers a plasticity index range of about 20–60. These relationships should be used cautiously for higher ranges, however. Further study is suggested to cover a higher range of the plasticity index.

7. Comparing the results of this investigation and those of two previous studies reveals that the other two relationships that also utilize the basic soil indices yield swell pressures up to 50 times smaller than those found using the empirical relationship proposed in the present study. Such a dramatic discrepancy can be attributed to several reasons. One reason is the use of the oedometer method. Kayabali and Demir (2011) showed that the swell pressures obtained from oedometer methods are highly speculative. Other reasons may include the limited amount of data, the specific range of soil plasticity, and the like.

Acknowledgments

The funding for this research came from the University of Ankara with the Grant No. 09B4343005.

Received: 17.12.2013
Accepted: 08.05.2014
Published: December 2014

References

American Society for Testing Materials. 2000. Standard practice for classification of soils for engineering purposes (Unified Soil Classification System): *ASTM D2487-00*, West Conshohocken, PA.

Attom M. F., Barakat, S. 2000. Investigation of three methods for evaluating swelling pressure of soils. *Environmental and Engineering Geoscience* 6, 3, 293-299.

Basma, A. A., Al-hamoud, A. S., Malkawi, A. H. 1995. Laboratory assessment of swelling pressure of expansive soils. *Applied Clay Science* 9, 355-368.

DATAFIT, 2008. Datafit Version 9.0.59, Oakdale Engineering, RC 101, 23 Tomey Road, Oakdale, PA, 15071 USA.

Erzin, Y., Erol, O. 2004. Correlations for quick prediction of swell pressures. *Electronic Journal of Geotechnical Engineering* 0476, 6 pp.

Kayabalı K., Demir, S. 2011, Measurement of swelling pressure: direct method versus indirect methods. *Canadian Geotechnical Journal* 48, 354-364.

Komornik, J., David, A. 1969. Prediction of swelling potential for compacted clays. *Journal of the Soil Mechanics and Foundation Engineering Division*, ASCE 95, 1, 209-225.

Nayak, N. V., Christiensen, R. W. 1971. Swelling characteristics of compacted expansive soils. *Clays and Clay Minerals* 19, 4, 251-261.

Nelson, D. J., Miller, D. J. 1992, *Expansive soils, problems and practice in foundation and pavement engineering*, Wiley, New York, 259 pp.

Rao, A. S., Phanikumar, B. R., Sharma, R. S. 2004. Prediction of swelling characteristics of remolded and compacted expansive soils using free swell index. *Quarterly Journal of Engineering Geology and Hydrogeology* 37, 217-226.

Shuai, F. 1996. Simulation of swelling pressure measurements on expansive soils. *PhD thesis*, University of Saskatchewan, Canada, 315 pp.

Siemens, G., Blatz, J. A. 2009, Evaluation of the influence of boundary confinement on the behaviour of unsaturated swelling clsy soils. *Canadian Geotechnical Journal* 46, 339-356.

Vijayvergiya, V. N., Ghazzaly, O. I. 1973. Prediction of swelling potential for natural clays. In: *Proceedings of the 3rd International Conference on Expansive Soils*, Haifa, Israel, 1, 227-236.

BULLETIN OF THE MINERAL RESEARCH AND EXPLORATION

Foreign Edition 2014 149

CONTENTS

Facies Characteristics And Control Mechanisms of Quaternary Deposits In The Lake Tuz Basin
.....Alper GÜRBÜZ and Nizamettin KAZANCI 1

Neotectonic-Period Characteristics, Seismicity, Geometry And Segmentation of The Tuz Gölü Fault Zone
.....Akın KÜRÇER and Y. Ergun GÖKTEN 19

Neogene Stratigraphy And Paleogeographic Evolution of The Karaburun Area, İzmir, Western Turkey
.....Fikret GÖKTAŞ 69

Benthic Foraminiferal Fauna of Malatya Oligo-Miocene Basin (Eastern Taurids, Eastern Turkey)
.....Fatma GEDİK 93

Protolith Nature And Tectonomagmatic Features of Amphibolites From The Qushchi Area, West Azerbaijan, NW Iran
.....Mohssen MOAZZEN 139

Glauberite-Halite Association In Bozkır Formation (Pliocene Çankırı-Çorum Basin, Central Anatolia, Turkey)
.....İlhan SÖNMEZ 153

Estimation of Swelling Pressure Using Simple Soil Indices
.....Kamil KAYABALI and Özgür YALDIZ 177

Two Examples For Imaging Buried Geological Boundaries: Sinkhole Structure And Seyit Hacı Fault, Karapınar, Konya
.....Ertan TOKER, Yahya ÇİFTÇİ, Aytekin AYVA and Akın KÜRÇER 189

The Assessment of Geothermal Potential of Turkey By Means Of Heat Flow Estimation
.....Uğur AKIN, Emin Uğur ULUGERGERLİ and Semih KUTLU 201

A Brief Note On Mineral Evolution And Biochemistry
.....José Mario AMİGO 211

Critisism on the paper "Possible Incision of The Large Valleys In Southern Marmara Region, Turkey (Nizamettin KAZANCI, Ömer EMRE, Korhan ERTURAÇ, Suzanne A.G. LEROY, Salim ÖNCEL, Özden İLERİ and Özlem TOPRAK)
.....Nizamettin KAZANCI 219

Acknowledgement 221

Notes to the authors 223

Bull. Min. Res. Exp. (2014) 149: 189-199

Bulletin of the
Mineral Research and Exploration

http://bulletin.mta.gov.tr


BULLETIN OF THE
MINERAL RESEARCH AND EXPLORATION

CONTENTS

TWO EXAMPLES FOR IMAGING BURIED GEOLOGICAL BOUNDARIES: SINKHOLE STRUCTURE AND SEYİT HACI FAULT, KARAPINAR, KONYA

Ertan TOKER[a*], Yahya ÇİFTÇİ[b], Aytekin AYVA[a] and Akın KÜRÇER[c]

[a] *Maden Tetkik ve Arama Genel Müdürlüğü Jeofizik Etütleri Dairesi Başkanlığı*
[b] *Maden Tetkik ve Arama Genel Müdürlüğü Maden Etüt ve Arama Dairesi Başkanlığı*
[c] *Maden Tetkik ve Arama Genel Müdürlüğü Jeoloji Etütleri Dairesi Başkanlığı*

Keywords:
Sinkhole, gravity, hyperbolic tilt angle, edge zone, derivative, tilt angle, anomaly, Seyit Hacı Fault, Karapınar, Konya.

ABSTRACT

Once anomalies with positive and negative circular closures are assessed together in potential field maps, the ones which have meaningful geometric structure appear as more distinguishable. When the edge detection is applied, the preliminary geological model about the geological structure may or may not be verified. When it is not verified then it is understood that the predicted geological model should be reconsidered and discussed again. In this study, the edge detection was introduced and the success of the method was tested in an artificial data. Following that, its effect on sinkholes was studied applying the method on detailed gravity data collected in Karapınar (Konya) region. At the same time, this method was applied on data related to active Seyit Hacı Fault zone. It was detected that the fault had shown continuity towards SW and these evidences were discussed.

1. Introduction

Edge detection methods in data processing stages of the potential field data can rapidly be applied rather than consuming time due to developments in computer technology. Derivative methods in edge detection processes (Euler deconvolution, tilt angle and their combinations) give good results in detecting boundary structures on data. The gravity anomaly occurs depending on the environment in which the target structure exists. It gives a negative value if the target structure exists in a denser geological environment than it. However; it exhibits a positive value if it is located in a less dense geological environment that it. The sensitivity of tilt angle in detecting especially the plutonic intrusions in gravity and magnetic methods and decoding buried ones have been studied by many investigators (Oruç, 2010; Akın et al., 2012; Toker, 2014; Toker and Çiftçi, 2014). In the method of hyperbolic tilt angle (HTA), as the ratios of variables in vertical and total horizontal derivatives are expressed hyperbolically different than the method of tilt angle, the result is not a vectorial but a scalar magnitude.

The detection of the edge boundaries of the horizontal derivative, the vertical derivative to localize the anomaly at a certain area and the analytical signal to give high values on edges of geological structures contribute a lot in terms of detectability. In previous studies, the 2nd order vertical derivative of the analytical signal (Hsu et al., 1996), total horizontal derivative of the tilt angle (Verdusco et al., 2004), hyperbolic tilt angle and 2nd order vertical derivatives of the tilt angle (Cooper and Cowan, 2004) were used in edge detection data processes.

In this article, the success of the edge detection method was examined in modelling the volumes of environments which show a clear edge relationship with the surrounding geological environment as it was in sinkhole boundaries. In this study, "shifting by a scalar" method was applied in order to make

* *Corresponding author: Ceyhan Ertan TOKER , toker.ertan@gmail.com*

boundary transitions to be more distinctive image using HTA method on a model. After the application, it was seen that more detectable images were obtained and the application was tested with actual field data.

2. Hyperbolic Tilt Angle (HTA) Method

Hyperbolic tangent function was expressed by Cooper and Cowan (2006) below as;

$$HTA = Tanh^{-1} = \frac{\frac{df}{dz}}{\left[\left(\frac{df}{dx}\right)^2 + \left(\frac{df}{dy}\right)^2\right]^{1/2}} \quad (1)$$

where; *f* is the potential field, *df/dz* is the first order vertical derivative of potential field (f), *df/dx* is the first order vertical derivative of the potential field (f) in x direction, *df/dy* is the first order vertical derivative of the potential field (f) in y direction. The operand in denominator is the amplitude of the horizontal derivative.

According to Zhou et al. (2013) who studied the consistency and limits of the method;

$$Z = \tanh x = \frac{\sinh x}{\cosh x} = \frac{e^x + e^x}{e^x - e^x} \quad (2)$$

The Equation 3 is obtained using the transformation in the formula (2) by means of single and double function characteristics of this function.

$$X = \tanh^{-1} Z = 0.5 * \ln\left(\frac{1+z}{1-z}\right) \quad (3)$$

and when the function is rearranged using Equations (1) and (3), the following equation is obtained (Zhou et al., 2013) as below;

$$HTA = 0.5 * \ln \frac{\left[\left(\frac{df}{dx}\right)^2 + \left(\frac{df}{dy}\right)^2\right]^{1/2} + \frac{df}{dz}}{\left[\left(\frac{df}{dx}\right)^2 + \left(\frac{df}{dy}\right)^2\right]^{1/2} - \frac{df}{dz}} \quad (4)$$

The "vertical derivative" in above equation can take positive and negative values. Local end values belonging to vertical derivative remove the equation from being stable (Zhou et al., 2013). Cooper (2103) suggests shifting negative contrast by a scalar. At the statement of the function given below, it is aimed at making the equation stable by adding a constant such as "k".

$$Tanh^{-1} = \frac{\frac{df}{dz}}{\left[\left(\frac{df}{dx}\right)^2 + \left(\frac{df}{dy}\right)^2\right]^{1/2} + k} \quad (5)$$

In the application, while the edge detection process of relatively negative circular closures is performed, the data process image can be made more accurate and understandable by shifting the residual negative contrast by a scalar such as "k".

When the hyperbolic tilt angle method is applied it is sufficient to make shifting as much as the amplitude of negative lines in the image. Within this respect, when selecting parameters of data process one should be careful about the advantages and disadvantages of this method as the wrong parameter might cause some details to get lost. Accordingly; if "k" parameter is selected greater than normal then data of the process may become poorer than normal. On the other hand, if "k" is selected smaller than normal, then the expected detection may not be achieved. Thus, it is very important to select the most suitable and confidential parameter that will remove negative oscillations originating from the density contrast of the environment.

In sample model study, the stable HTA image of the model was calculated by 0.3 mgal shifting oscillations in vertical derivative of the potential field data belonging to the gravity anomaly of the prism at 5 km depth which has 0.1 gr/cm^3 contrast (Figures 1a, b, c). The gravity effect of the model prism, the response of this gravity effect to HTA application and vertical derivative in 3D view were given in figures 2a, 2b and 1c, respectively.

In figure 2b, except the edge zone effects of the model prism it is seen that moirés observed in cross shapes are negative oscillations. As these oscillations are the effect of negatives of vertical derivative in 3D which is shown in Figure 1c, the anomaly which occurs by (k) 0.3 mgal shift of the vertical derivative is shown in figure 3b.

Figure 3 a) the gravity effect of the model prism in figure 1, b) HTA image shift in positive direction.

In model application given by Cooper (2013), ±0.1 gr/cm^3 gravity anomaly of prismatic structures

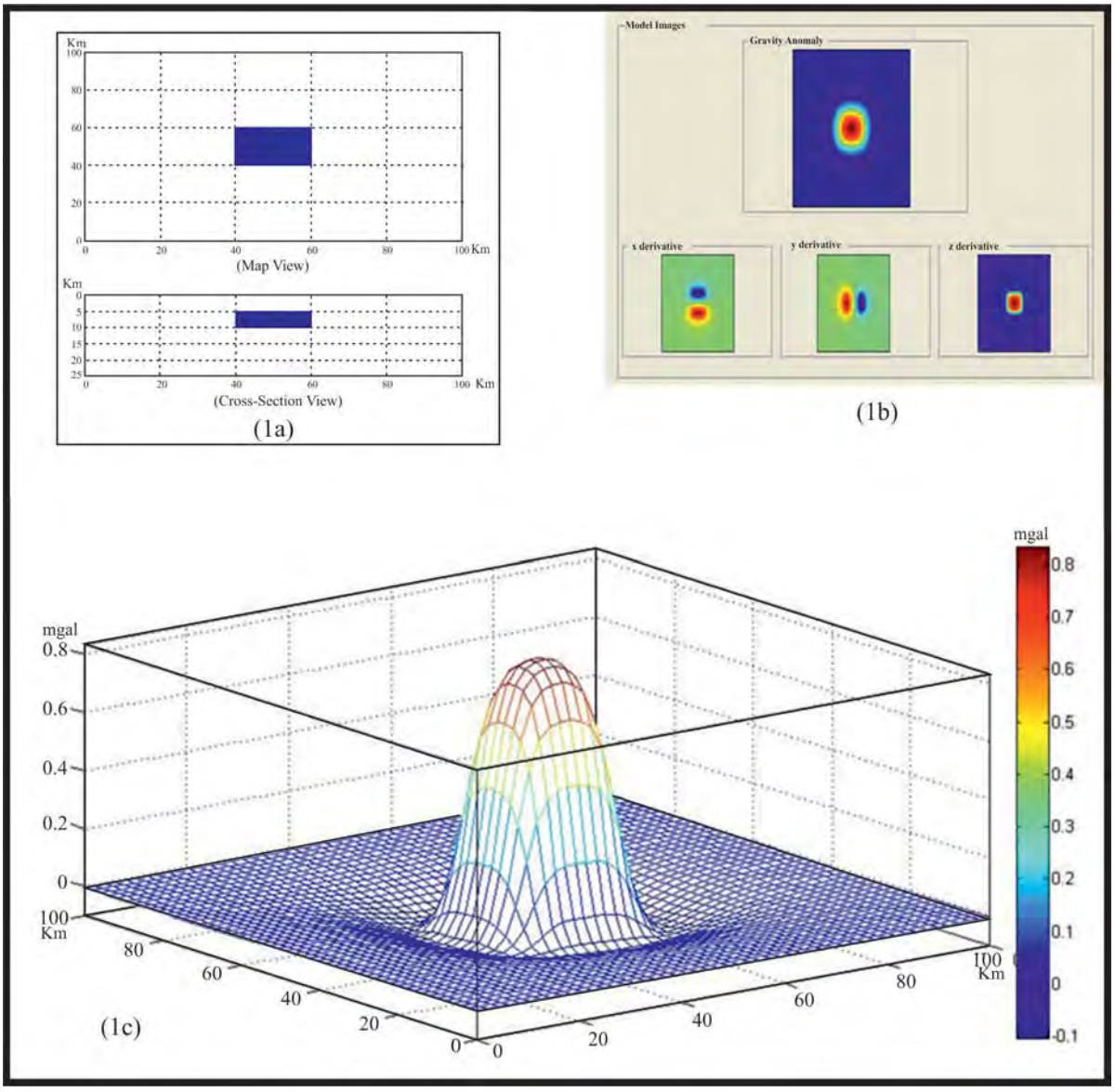

Figure 1- a) View of the model from top and side, b) The gravity effect of the model and its derivative components, c) Vertical derivative in 3D view.

at 5 km depth and negative-positive oscillated boundary imaging are given in figures 4a and 4b, respectively. Model structures which are seen on the lower left and on the upper right corners in Figure 4a and cause anomaly were remarked by black square line. The boundary imaging shift (k=0.3) according to Cooper (2013) was given in figure 5.

3. The Application of The Model On Field Data

The application defined above and examined on a model prism (Figure 5) was tested on actual field data and the results were compared. To do that, gravity data generated in Karapınar-Konya by Törk et al (2009) were used. The image obtained as a result of the hyperbolic tilt angle edge detection process applied on Bouguer gravity data was given in figure 6a.

Negative anomaly areas became apparent as independently or geometrically being associated with each other in some places on this image. Places which tend to form sinkhole structures became apparent in the form of negative circular closures on this map after performing HTA process. As this map was generated by applying only one data process on raw gravity data, many other processes which are applied during data simplification become unnecessary and

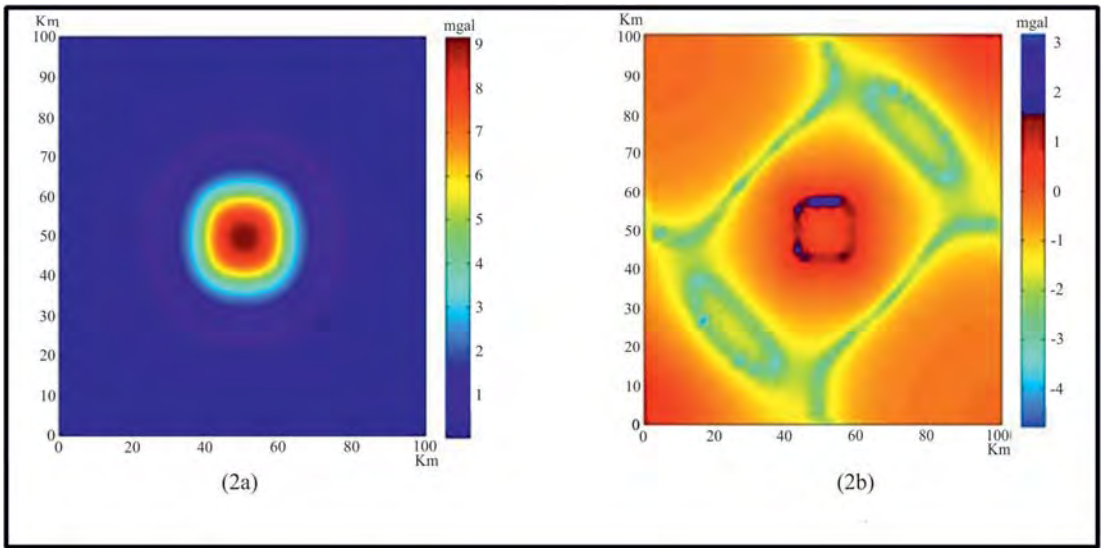

Figure 2- a) the gravity effect of the model prism in figure 1, b) hyperbolic tangent view.

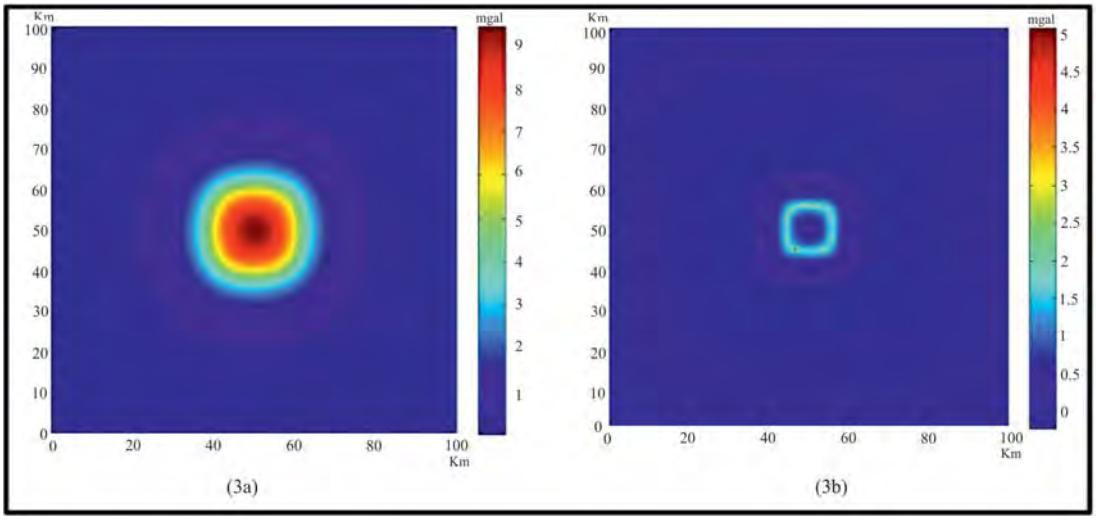

Figure 3- a) the gravity effect of the model prism in Figure 1, b) HTA image shift in positive direction.

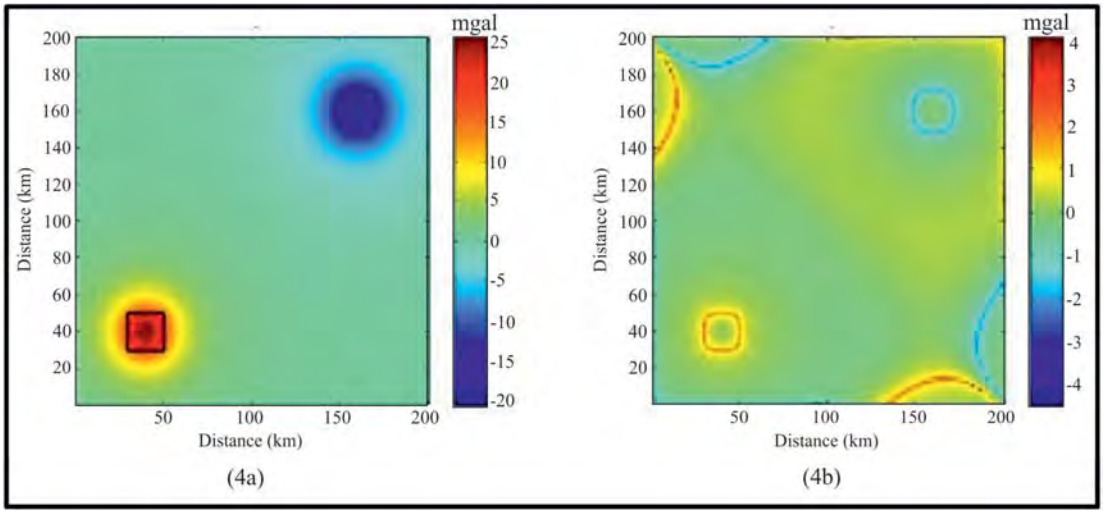

Figure 4- a) positive and negative anomalies of prismatic structures, b) negative-positive oscillations in boundary imaging.

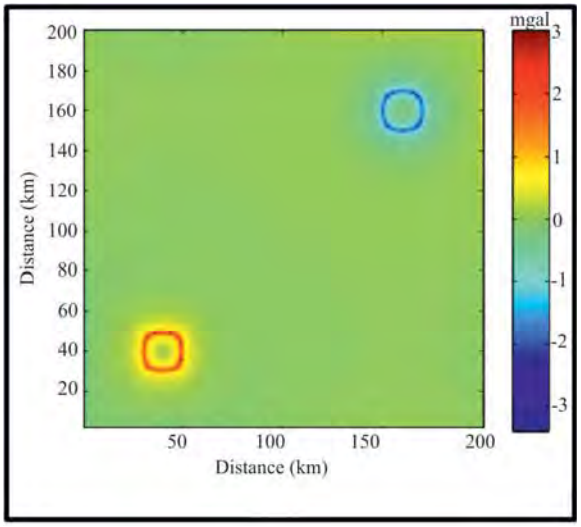

Figure 5- Boundary imaging shift by 0.3 k. (Cooper, 2013).

timesaving. The probability of error also decreases significantly as the process is simple. Thus, this map shows that this method can safely be used in edge detection processes of negative bodies. Suggestions asserted by Zhou et al. (2013) regarding the disadvantages of this process were responded by Cooper (2013) in the same volume of the journal and it was clearly shown that it is possible analytically and on model based (see Figure 5).

Figure 6b was obtained applying a series of processes in order to clearly reveal the sinkhole structures of the same field data.

3.1. Sinkhole Structure

Western and northwestern parts of Karapınar where the study area takes place is located in the main geomorphological region of the Central Anatolia namely the "Sinkhole Plateau" (Erol, 1990). Erol (1990) stated that sinkholes located in the sinkhole plateau developed in late Pleistocene, especially during the recent pluvial period (Würm) and there was a karstification in the region even earlier than this formation (middle-lower Pleistocene). When the Konya Lake was on pluvial level in Pleistocene, karstic underground erosion occurred along the detachment fault in SE-NW starting from high levels of Pleistocene Konya Lake (1030-1010 m) towards lower levels of Tuz Lake basin (1010 – 905 m). The groundwater flow has decreased during interpluvial period and the development of sinkhole has been interrupted until next phase. Findings in this study also support that block faulting played an important role on the development of sinkhole. Hence, all sinkhole structures in the region take place on the foot wall of Seyit Hacı Fault (Figures 7 and 8).

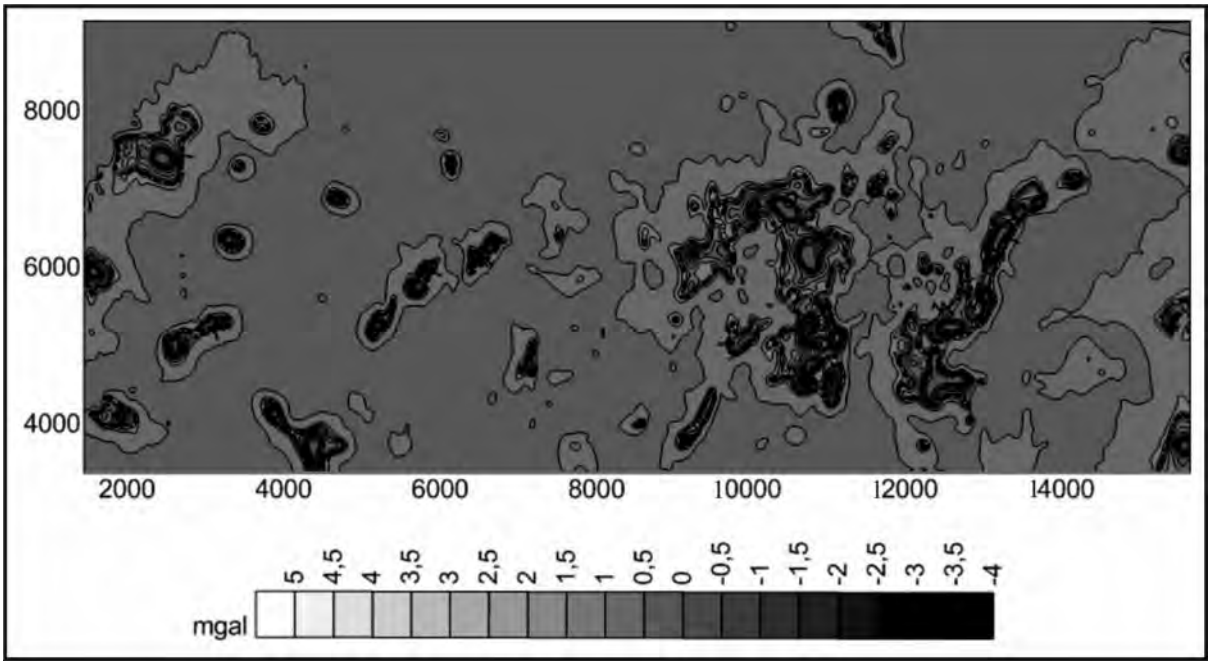

Figure 6- a) Image obtained as a result of the hyperbolic tilt angle edge detection process which was applied to Konya-Karapınar field data (field data were taken from Törk et al., 2009; see figure 8 for location, relative coordinate was used).

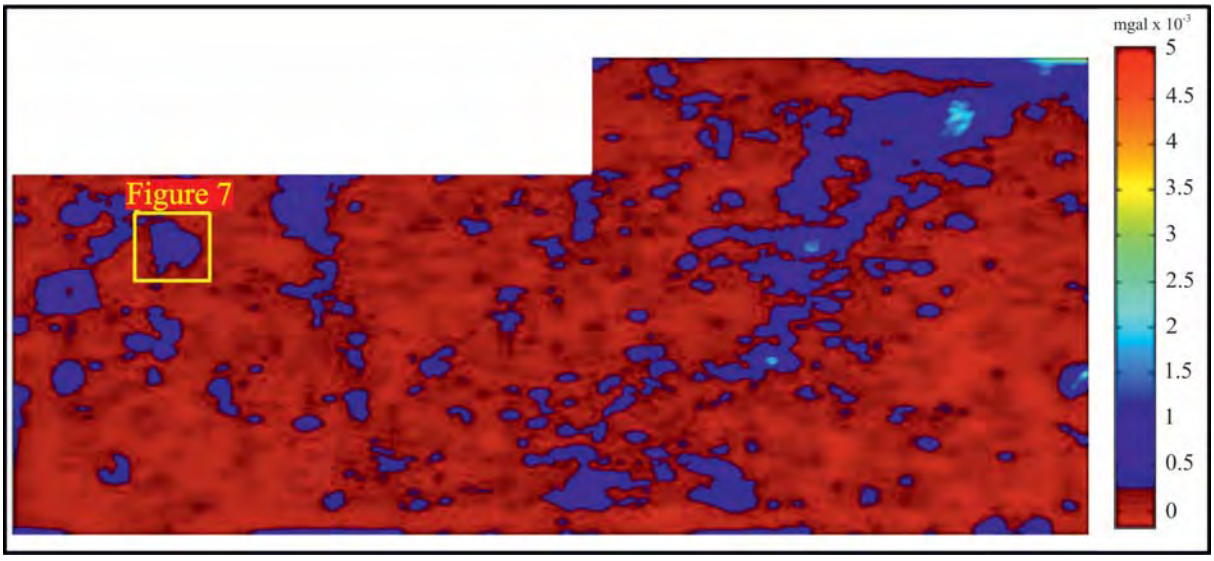

Figure 6- b) Field data with high pass filter, blue areas probably coincide with areas of sinkhole/karstic structures (relative coordinates are as in figure 6a, see figure 8 for location).

When these structures reach the surface following the advanced karstification/cave formation period, they are called as "sinkhole". Sinkholes which are geomorphologically formed in the form of smooth circular and cylindrical volumes in 3rd dimension often occur as in irregular geometry. Sinkholes due to the surrounding geological formations create a negative density difference.

Following the field application (as shown in Figure 6b) one sinkhole was selected on the field and shifting was applied in order to increase the distinguishability of boundary transitions of this structure. More detectable image was obtained as a result of the processes of which related results were shown in figures 7a, b and c.

The actual field data is seen in figure 7a. A collapsed structure in the field which is relatively low dense compared to surrounding environment and one of the zone at west in which dark blue colored negative values exist is observed. The source body of the data was foreseen as a shallow geological structure starting from a few meters at the surface and the edge detection technique was tested by HTA method (Figure 7b). However; it is seen in figure 7c that oscillations decrease and the collapse structure becomes localized in the application by selecting k as 0.3 (Figure 7c).

3.2. Seyit Hacı Fault

The study area is located in Konya-Eskişehir section of the Central Anatolia Neotectonic Region (Koçyiğit, 2000). This area is represented by structural elements (normal faults, horst and grabens) of the extensional tectonic regime products. The Karapınar graben which orients in NE-SW direction,

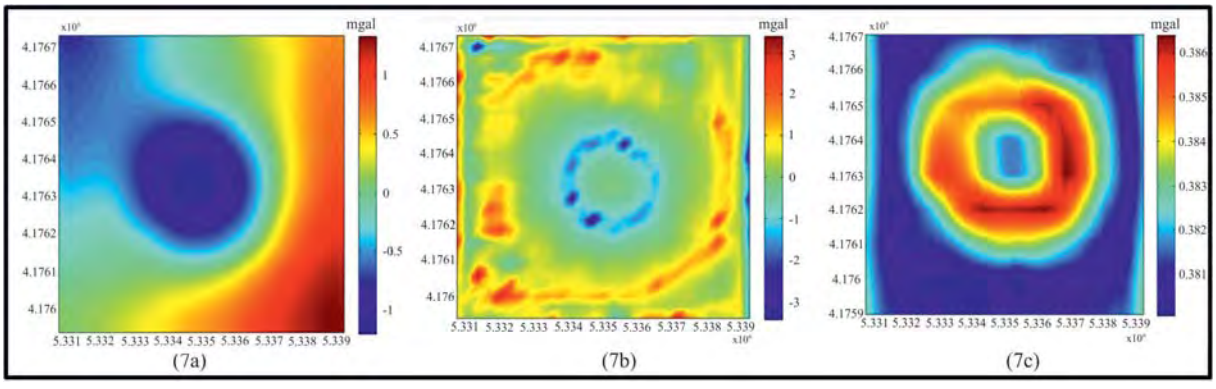

Figure 7- a) Negative anomaly, b) HTA view of the anomaly, c) shifted HTA image (see figure 6b for location).

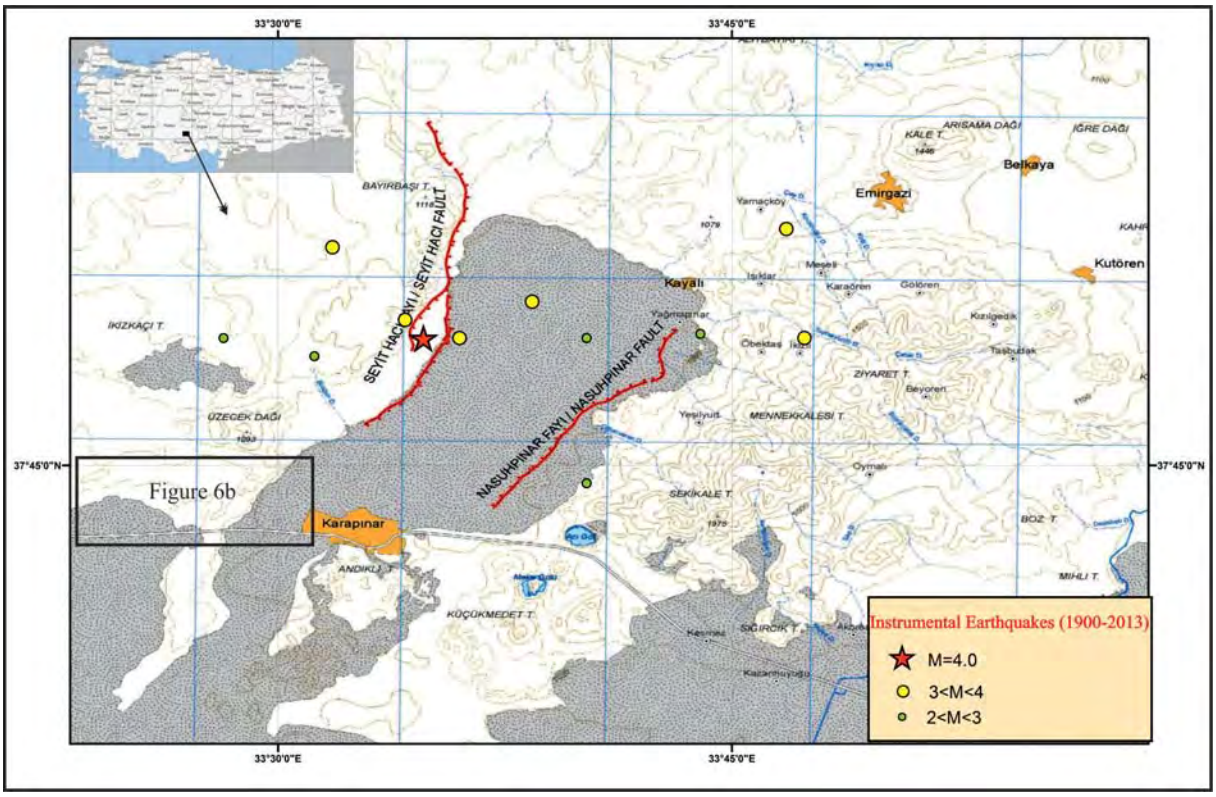

Figure 8- Location of the Karapınar Graben and Seyit Hacı Fault in 1/250 000 scaled Karaman sheet (NJ 36-11), series of Active Fault Map of Turkey (Emre et al., 2011).

24 km long and 8 km wide is one of these structural elements. The eastern and western borders of the Karapınar Graben are restricted by Nasuhpınarı and Seyit Hacı faults, respectively (Özalp et al., 2011). Emre et al. (2011) defined Seyit Hacı Fault as 18 km long, active normal fault which is formed by 2 segments (northern and southern segments) (Figure 8).

The northern segment is formed by two sub segments (fault section). The orientation of the northern segment is N15°E and 2.8 km long. The southern segment is totally 12 km long and has orientation in NNW, N-S and NNE directions.

In this study, the probable sinkhole structures which are considered to have occurred in western part of the Karapınar Graben were investigated by the Hyperbolic Tangent Method and subjected to the edge detection process. It was seen that there were many sinkhole structures which formed or probably to occur within different sizes in the region and these exhibited a linearity in NE-SW directions (Figures 6a, b). In order to discuss the relationship of this detected lineament with active faults in the region, high pass filtered field data (Figure 6b) of the investigated area was coordinated and plotted on 1/250 000 scaled Active Fault Map of Turkey, Karaman sheet (NJ36-11) (Emre et al., 2011) (Figure 9).

Anomaly which exhibits linearity in NE-SW directions corresponds to SW continuation of the Seyit Hacı Fault (Emre et al., 2011) (see Figure 8). It is considered that probable sinkhole structures seen in high pass filtered field data were developed on the hanging wall of another 3rd segment of the SE continuation of the Seyit Hacı Fault. The segment in question was named as "Seyit Hacı Fault, Segment 3". This segment is formed by 3 fault sections which are 8 km long, parallel to sub parallel in N40°E direction (Figure 10).

Tectonomorphological characteristics of the Seyit Hacı Fault segment 3 defined in this study can also be clearly observed in satellite images. Tectonomorphological elements (Figure 11) such as; linear fault scarps, alluvial fans arranged along the fault and hanging valleys indicate the activity of this segment of the fault.

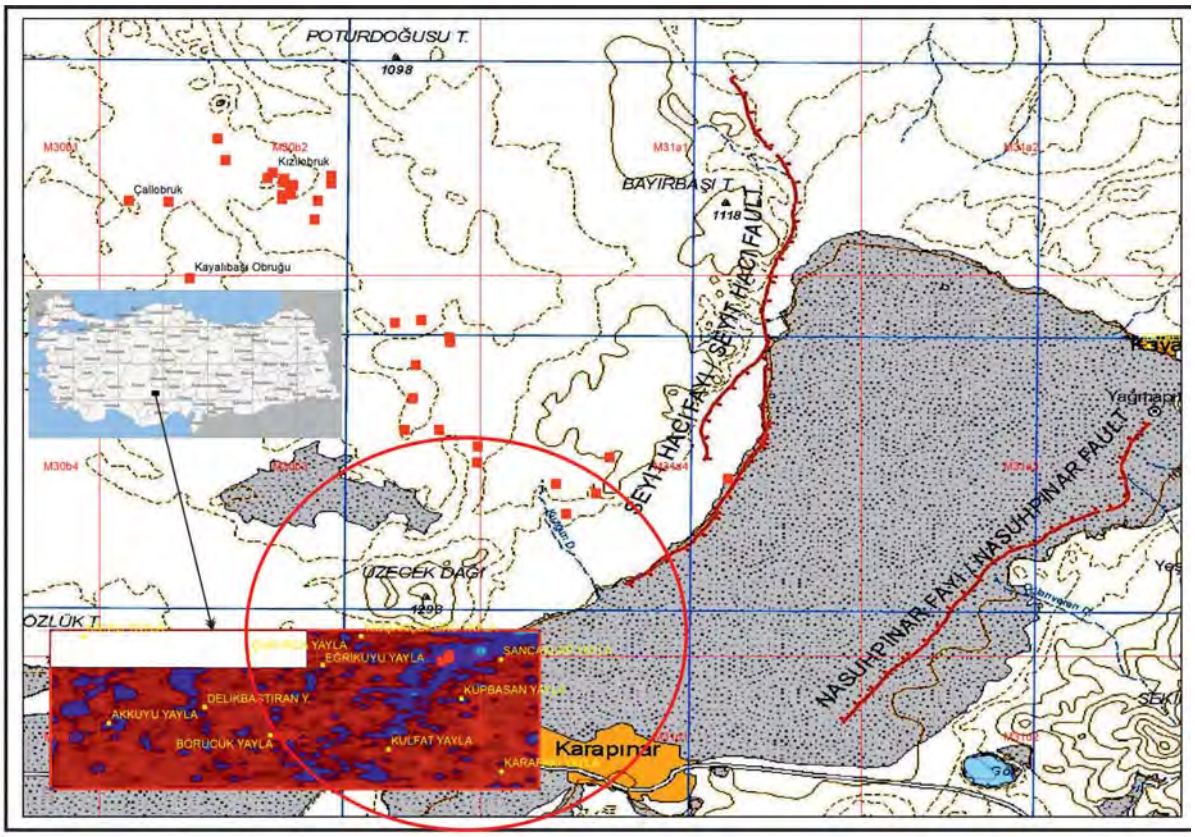

Figure 9- Location of high pass filtered field data of the study area on Active Fault Map of Turkey Series, 1/250.000 scaled (NJ 36-11) Karaman Sheet (Emre et al., 2011) (Red points represent recent sinkhole structures. All these structures were digitized using 1/250.000 scaled topography map and are located on the hanging wall).

Figure 10- Locations of Seyit Hacı Fault segments in Googleearth view. Seyit Haci fault segment 3 was mapped as a result of this study. Segments 1 and 2 were taken from Emre et al. (2011). (x3 vertical exaggeration, looking north with oblique angle).

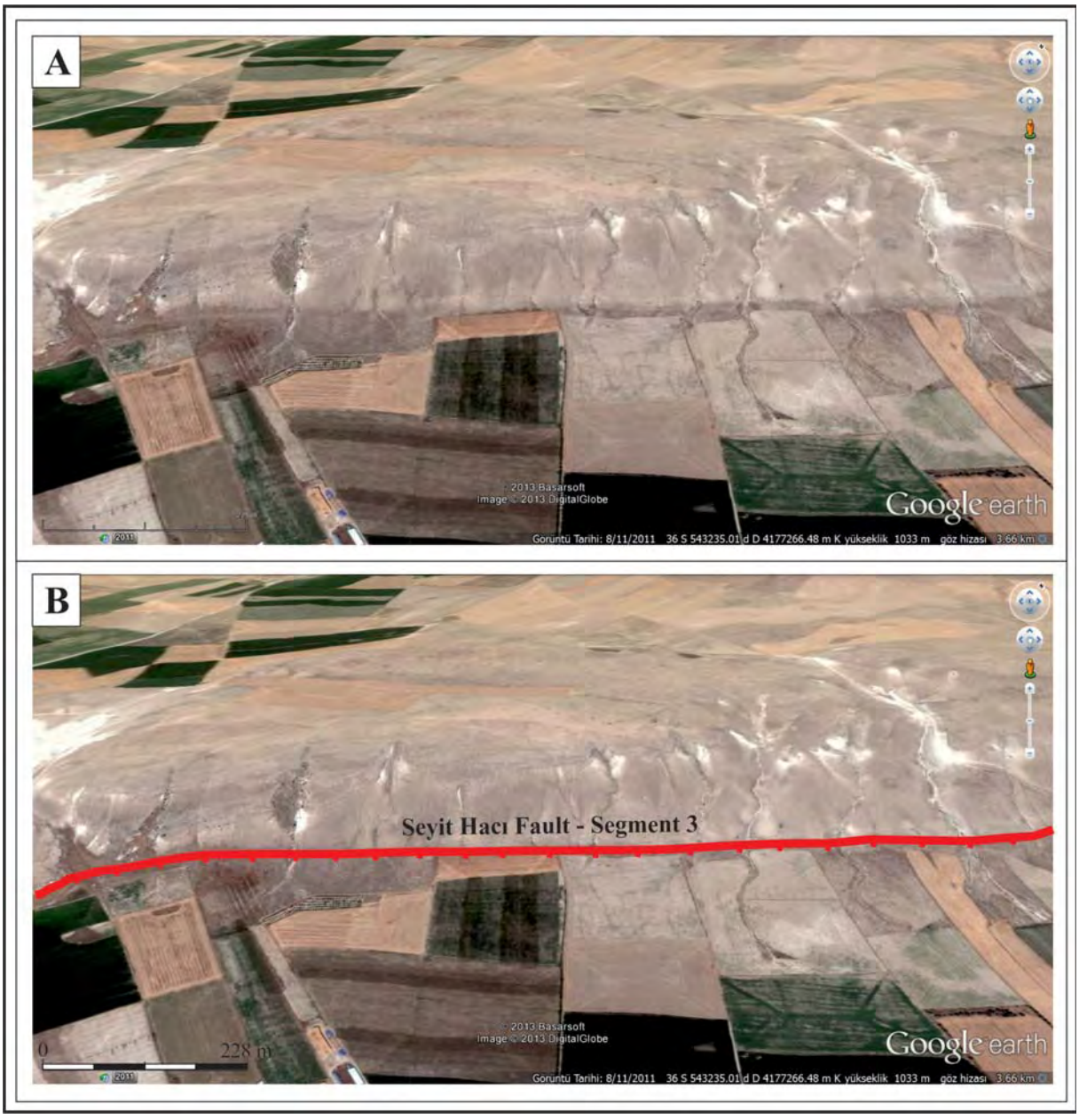

Figure 11- Googleearth view of Seyit Haci Fault, Segment 3. A: non-interpreted, B: interpreted (x3 vertical exaggeration, looking northwest with oblique angle).

4. Results and Discussion

In this article, Hyperbolic Tilt Angle (HTA), which is one the method applied in imaging buried geological structures by processing the potential data was introduced and tested on actual field data. First, the edge detection method of HTA was introduced. Then, in order to query the usage of this technique in detecting sinkhole or similar structures, model responses to edge detection processes which the buried prismatic model structures give were studied. And in the last stage, the application was tested by the actual field data and the edge detection of a sinkhole structure in Karapınar (Konya) region was realized. Besides, it was discussed that the neotectonic structure of the Seyit Hacı Fault which is located just at the NE section of the study area, orienting in NE-SW directions should continue towards SW as the 3rd segment by studying the anomaly type obtained in this investigation.

HTA method is one the methods used in this purpose and the image obtained is actually quite complicated compared to other derivative and phase

filters in terms of detectability. However, the weak point of the method was stated by Zhou et al. (2013). Nevertheless, Cooper (2013) said that it will be enough to shift by a scalar like "k" in order to stabilize this method and showed it on a model as well. Toker and Çiftçi (2014) discussed model responses belonging to all other edge detection techniques and this method in their articles called "Simav grabenin yapısal jeofiziği" (the Structural Geophysics of the Simav Graben). They established that the map (of which its vertical and horizontal amplitudes are proportioned) which is easily simplified in one step by being shifted with HTA method could produce quite useful results in detecting the boundary transitions of geological structures which cause negative anomaly for distinguishability. The same issue was discussed in more detail by Toker (2014). Consequently; it was shown in this article that shift process by a scalar makes HTA method more advantageous compared to the other derivative and phase filtering methods.

Vertical derivative to create negativity in total caused the stability of the method to be questioned (Zhou et al., 2013). In addition, it was understood that sinkhole structures which create 0.2 mgal relative difference within sediment (as it was in salt dome anomaly) and form 0.2 – 0.4 mgal negative differences with respect to its surround could be shifted by a scalar like "k" and their edge detection processes can safely be performed.

This article does not intend to show the comparison of skills of HTA method with respect to other edge detection methods but to show how the edge detection ability of HTA could easily be remediated. In addition, it was pointed out that most of the edge detection processes containing vertical derivative had a problem of depth. The environment of formation of sinkholes, which are indicated as the target structure in this study, to be in shallow depths has not created any problems in terms of the discrimination of process in vertical derivative in HTA method.

In this article, HTA method in edge detection techniques was also tested from the point of detectability of tectonic structures which associate a boundary relation with the surrounding geological structures as it was in sinkholes and quite successful result were obtained. Seyit Haci Fault is one the neotectonic structures of the Central Anatolia Region. The 3rd segment of this fault which has the characteristics of SW continuation has not been detected so far and has first been defined in this article. The anomaly lineament which is easily seen in figure 9 should represent the line in which deformations such as; fracturing/breaking developed on the 3rd segment of the fault and karstic/sinkhole type dissolution structures which developed as a result of the severe groundwater activity triggered by a sudden rise of block. Undoubtedly; this finding should be supported by paleoseismological studies in order to reinforce this information.

HTA method used in this study should be applied to geological bodies (dyke, layer, intrusive structure, mineral deposit, etc.) that have sufficient size, regular geometry, more definite density and susceptibility difference compared to surrounding geological environment. The model should be tested and the success of the method should be questioned in doing so. The success of the method will give way such a useful instrument to be used especially in the exploration of mineral deposits.

Acknowledgement

Model calculations in this study were made by modifying Potensoft Proses software developed by Arısoy and Dikmen (2011).

Gravity data mentioned in this study were generated within the project of "Konya havzasında karstik çöküntü alanlarının belirlenmesi ve tehlike değerlendirmesi projesi" and were used by the approve MTA (General Directorate of Mineral Research and Exploration).

Received: 27.11.2013
Accepted: 27.06.2014
Published: December 2014

References

Arısoy, M. Ö., Dikmen, Ü. 2011. Potensoft: MATLAB-based software for potential field data processing, modeling and mapping, *Computers and Geosciences*, 37, 7, pp. 935 – 942.

Akın, U., Şerifoğlu, B., Duru, M. 2012. Gravite ve manyetik yöntemlerde tilt açısı kullanılması, *Maden Tetkik ve Arama Dergisi* 143. s 1-12

Cooper, G. R. J., Cowan, D.R. 2004. Filtering using variable order vertical derivatives. *Computers and Geosciences,* vol. 30, 455-459

Cooper, G. R. J., Cowan, D. R. 2006. Enhanging potential field data using filters based on the local phase, *Computers and Geosciences,* 32 (10), 1585-1591.

Cooper, G. R. J. 2013. Reply to "A Discussion about the Hyperbolic Tilt Angle Method by Zhou et al.", *Computers and Geosciences*, 52, 496-497.

Emre, Ö., Duman, T.Y., Özalp, S. 2011. 1:250 000 Ölçekli Türkiye Diri Fay Haritası Serisi, Karaman (NJ 36-11) Paftası, Seri No: 27, *Maden Tetkik ve Arama Genel Müdürlüğü*, Ankara-Türkiye.

Erol, O. 1990. Konya-Karapınar Kuzeybatısındaki Obrukların Jeomorfolojik Gelişimi ile Konya ve Tuz Gölü Pleyistosen Plüviyal Gölleri Arasındaki İlişkiler. *İ. Ü. Deniz Bilimleri ve Coğrafya Ens. Bülteni*. Sayı. 7. İstanbul.

Hsu, S.K., Sibuet, J.C. & Shyu C.T. 1996. Depth to magnetic source using generalized analytic signal. *Geophysics*, vol. 61, 373-386

Koçyiğit, A. 2005. The Denizli graben-horst system and the eastern limit of western Anatolian continental extension: basin fill, structure, deformational mode, throw amount and episodic evolutionary history, SW Turkey, *Geodinamica Acta*, 18: 3-4.

Oruç, B. 2010. Edge Detection and Depth Estimation Using a Tilt Angle Map from Gravity Gradient Data of the Kozaklı - Central Anatolia Region, Turkey. *Pure and Applied Geophysics*, September 2011

Özalp, S., Emre, Ö., Duman, T.Y., Törk, K. 2011. Karapınar (Konya) Yöresindeki Çizgisel Uzanımlı Yer Çatlaklarının Kökeni Üzerine Paleosismolojik Bulgular. Aktif Tektonik Araştırma Grubu 15. Toplantısı, Bildiri Özleri Kitabı, s: 20-21. Çukurova Üniversitesi, Adana.

Toker, C. E., Çiftçi, Y. 2014. Simav Yarı Grabeninin Yapısal Jeofiziği. 67. Türkiye Jeoloji Kurultayı, Bildiri Özleri Kitabı, S. 126, Ankara.

Toker, C. E. 2014. Simav Havzasının Jeofizik Verilerle Analizi. *Maden Tetkik ve Arama Dergisi* 148, 119-139 Ankara.

Törk, K., Erduran, B., Güner, İ.N., Ateş, Ş., Avcı, K., Çınar, A., Keleş, S., Ayva, A., Demirbaş, Ş., Yılmaz, N.P. ve Sülükçü, S. 2009. Konya havzasında karstik çöküntü alanlarının belirlenmesi ve tehlike değerlendirmesi projesi, 2009 yılı ara raporu. Maden Tetkik ve Arama Report No: 11250, Ankara

Verdusco, B., Fairhead, J.D., Green, C.M. 2004. New insigth into magnetic derivatives for structural mapping Leading Edge, 23 (2), 116 – 119.

Zhou, W., Do, X., Li, J. 2013. A Discussion about hyperbolic tilt angle method, *Computer and Geoscience*, V. 52, p. 493-495.

BULLETIN OF THE MINERAL RESEARCH AND EXPLORATION

Foreign Edition 2014 149

CONTENTS

Facies Characteristics And Control Mechanisms of Quaternary Deposits In The Lake Tuz Basin
.....Alper GÜRBÜZ and Nizamettin KAZANCI 1

Neotectonic-Period Characteristics, Seismicity, Geometry And Segmentation of The Tuz Gölü Fault Zone
.....Akın KÜRÇER and Y. Ergun GÖKTEN 19

Neogene Stratigraphy And Paleogeographic Evolution of The Karaburun Area, İzmir, Western Turkey
.....Fikret GÖKTAŞ 69

Benthic Foraminiferal Fauna of Malatya Oligo-Miocene Basin (Eastern Taurids, Eastern Turkey)
.....Fatma GEDİK 93

Protolith Nature And Tectonomagmatic Features of Amphibolites From The Qushchi Area, West Azerbaijan, NW Iran
.....Mohssen MOAZZEN 139

Glauberite-Halite Association In Bozkır Formation (Pliocene Çankırı-Çorum Basin, Central Anatolia, Turkey)
.....İlhan SÖNMEZ 153

Estimation of Swelling Pressure Using Simple Soil Indices
.....Kamil KAYABALI and Özgür YALDIZ 177

Two Examples For Imaging Buried Geological Boundaries: Sinkhole Structure And Seyit Hacı Fault, Karapınar, Konya
.....Ertan TOKER, Yahya ÇİFTÇİ, Aytekin AYVA and Akın KÜRÇER 189

The Assessment of Geothermal Potential of Turkey By Means Of Heat Flow Estimation
.....Uğur AKIN, Emin Uğur ULUGERGERLİ and Semih KUTLU 201

A Brief Note On Mineral Evolution And Biochemistry
.....José Mario AMİGO 211

Critisism on the paper "Possible Incision of The Large Valleys In Southern Marmara Region, Turkey (Nizamettin KAZANCI, Ömer EMRE, Korhan ERTURAÇ, Suzanne A.G. LEROY, Salim ÖNCEL, Özden İLERİ and Özlem TOPRAK)
.....Nizamettin KAZANCI 219

Acknowledgement 221

Notes to the authors 223

Bull. Min. Res. Exp. (2014) 149: 201-210

Bulletin of the
Mineral Research and Exploration

http://bulletin.mta.gov.tr

THE ASSESSMENT OF GEOTHERMAL POTENTIAL OF TURKEY BY MEANS OF HEAT FLOW ESTIMATION

Uğur AKIN[a*], Emin U. ULUGERGERLİ[b] and Semih KUTLU[a]

[a] *Maden Tetkik ve Arama Genel Müdürlüğü, Jeofizik Etütleri Dairesi, ANKARA*
[b] *Çanakkale Onsekiz Mart Üniversitesi Mühendislik Fakültesi Jeofizik Mühendisliği Bölümü, ÇANAKKALE*

Keywords:
Heat flow, Curie temperature, Curie point depth, geothermal gradient

ABSTRACT

In this study, the heat flow distribution of Turkey was investigated in the interest of exploring new geothermal fields in addition to known ones. For this purposes, the geothermal gradient was estimated from the Curie point depth map obtained from airborne magnetic data by means of power spectrum method. By multiplying geothermal gradient with thermal conductivity values, the heat flow map of Turkey was obtained. The average value in the heat flow map of Turkey was determined as 74 mW/m^2. It points out existence of resources of geothermal energy larger than the average of the world resources. in terms of geothermal potential, the most significant region of Turkey is the Aydin and its surrounding with a value exceeding 200 mW/m^2. On the contrary, the value decreases below 30 mW/m^2 in the region bordered by Aksaray, Niğde, Karaman and Konya. The necessity of conducting a detailed additional studies for East Black sea, East and Southeast Anatolia is also revealed.

1. Introduction

Much of the heat on earth crust originates from the mantle and a very small amount from the decay of radioactive elements (radiogenic source heat). The heat from radiogenic origin is produced by short and long half-life isotopes on earth crust. While radiogenic isotopes with short half-life were effective during the first periods of the earth, the isotopes with long half-life (^{235}U, ^{238}U, ^{232}Th and ^{40}K), however have taken place in the production of radiogenic heat starting from the first period of the earth till today (Göktürkler, 2002). The relative ratios of sources of the heat energy at any point on the earth can be estimated as percentage (Akın and Çiftçi, 2011).

In Turkey, the most of the places with the high heat flow where both volcanic and/or tectonic activity occurred and geothermal sources exist (Figure 1).

Heat flow can be obtained via direct or indirect methods. Some of the direct methods are as follows.

The silica geothermometer calculates the heat flow using SiO_2 amount dissolved in spring waters (Fournier and Rowe, 1966, 1977). The calculation of heat flow by Bullard method is a preferred method for the wells drilled especially in sedimentary rocks (Bullard, 1939). The method is also useful when irregular heat gradient and conductivity are observed.

The modeling studies can take the different types of groundwater regime into calculation of subsurface heat distribution. In addition to these methods, the heat flow can also be calculated with the thermal gradient method. The thermal gradient is the rate of change of heat with respect to depth. The temperature change in vertical direction (dT/dz) is considered for the heat flow calculation. The unit of the coefficient

* *Corresponding author: Uğur AKIN, ugurakin11@gmail.com*

of thermal conductivity in SI system (International System of Units) is defined as W/m°C. If the heat in any medium, flows normal to surfaces within unit sections which are parallel to each other and reaches the steady state then the heat flow is equal to the multiplication of thermal conductivity by the thermal gradient.

There are studies which were carried out in the past using mentioned method and cover relatively narrow regions. The common point of previous studies is to discard the usage of the calculated rock thermal conductivities. Therefore; the researchers estimated the heat flow by using only one constant value for λ (the rock thermal conductivity coefficient) found in literature and considered to represent entire region.

Factors affecting the change in (λ) thermal conductivity coefficient during the formation of rock are as follows; temperature, pressure, porosity, density, grain size, degree of cementation, mineral and fluid content. In addition, porosity and ratio of water saturation are important. Depending on the water saturated or dry sample The differences can occur upto 30% for λ values estimated in the laboratory (Scharli and Raybach, 1984).

From 1969 to present, the heat flow studies, that uses different techniques and methods, have been subject to various geological and geophysical researches in many countries (İspir, 1972). Generally, heat flow values are higher than 83.8 mW/m^2 in tectonic zones and ocean ridges (Lee and Uyeda, 1965; Langseth and Taylor, 1967; McKenzie, 1967; Gorshkov, 1972; Zoneshin, 1975).

The heat flow is high in island arc formations, subduction zones, in deep fault zones and in the close vicinities of plate collision zones (Sclater, 1972). Over the mid ocean ridge, as moving away from the axis, a decline in the heat flow values is observed. This value becomes significantly low in oceanic trenches. Two out of three volcanoes are located in the Pacific Zone. The heat flow contribution varies depending on the geological age of tectonic unit; while Precambrian aged (>600 million years) geological formations possess low heat flow, Cenozoic aged (<70 million years) young folds possess a high heat flow.

Generally; the heat flows are usually high in volcanic regions but there are differences in heat flow values between old and young volcanic units, too. The heat flow has been a research topic in continental scale. EGT (European Geotraverse) project investigated the temperature variation along Europe. The temperature distribution along a line starting from the north of Scandinavia extending to the south of Crimea has been mapped upto depths of 60-70 km (Shen et al., 1991). The area has been divided into two regions in terms of its heat flow values, while the eastern part was represented with normal values (41.9 - 50.2 mW/m^2), the western part exceed to higher

Figure 1- Map of geothermal resources and volcanic areas (MTA, 2014).

values (83.8 mW/m^2). Areas with low heat flow are where Precambrian shields are present. Although the heat flow values observed in Baltic, Ukrainian and Indian Shields are 36 mW/m^2, 29.33 mW/m^2 and 38.5 mW/m^2, respectively, heat flow values becomes significantly low in Precambrian platforms of Eastern Europe and Siberia (Tables 1 and 2).

High heat flow values have been encountered in grabens. Heat flow values for Ren Graben as 83.8-167.6 mW/m^2, Baikal Graben as 83.8-209.5 mW/m^2, Cambay Graben as 83.8-104.7 mW/m^2 have been measured (Gupta et al., 1970; Gorshkov 1972; Tissot and Espitalie, 1975).

Fytikas (1980), with his study in the Aegean Sea, determined three high heat flow regions extending along tectonic structures. The first region possesses a high heat flow which occasionally exceeds 120 mW/m^2 and extends along Palegonian - Parnos zone (interior side of the Hellenic island arc) passes through Astipalia and Kavaros islands reaches Bodrum – Karaada. The second heat flow region is in the Central Aegean, takes place at western end of İzmir – Ankara zone and values exceed 100 mW/m^2. The last region forms a belt of high heat flow anomaly covering the shores of Macedonia, the northern Aegean islands, Biga and Gelibolu peninsulas.

Country-wide or local scale heat flow estimations of Turkey have been studied by many researchers. In these studies, it is found that high heat flow values for west Mediterranean while low values for east Mediterranean have been obtained. Besides, low heat flow values for Black Sea have been observed. In reality, due to rapid sedimentation, if a correction factor is applied, Black Sea appears to be a high heat flow zone (Ericson, 1970).

Tezcan and Turgay (1991) obtained the heat flow map and temperature distribution map at the depth of 1000 meters, selecting the average thermal conductivity coefficient as λ=2.1 W/m^{o}K^{-1} for Turkey. İlkışık (1995) conducted regional heat flow studies in western Anatolia using silica geothermometer on hot springs. Besides, he also estimated the average heat flow as 107±45 mW/m^2 and stated that it was 50-60% higher than the world average. Pfister (1995) did the detailed heat flow investigation in Marmara region. The heat flow distribution of the Aegean region was assessed with geothermal gradient measured in wells (Yemen, 1999).

Heat flow can be estimated from magnetic data indirectly (Akın and Duru, 2006; Akın et al. 2006). The aeromagnetic anomaly map of Turkey (Figure 2) defines the major tectonic and geological units of Anatolia, and reveals anomalies of many subsurface structures which cannot be observed on surface geology. Besides, it is also used to estimate the depth of magnetic basements and location of basins in present geography, even if they were formed at different geological times, it carries much information for the exploration of mineral deposits, geothermal resources, oil and gas bearing unit, etc.

Bhattacharyya (1965, 1966), Spector and Bhattacharyya (1966) used the power spectrum method, a statistical approach, in interpreting the potential field data. It is used to determine the depths of underground structures which cause a magnetic anomaly (Spector ve Grant, 1970). This method can

Table 1- Heat flow measurement values in various geological structures of continental crust (after Lee and Uyeda, 1965).

Geological Structure	**Average Heat Flow (mW/m^2)**
Precambrian Shields	38.5 ± 29.3
Paleozoic aged Orogenic areas	51.5 ± 16.76
Mesozoic-Cenozoic aged Orogenic areas	80.4 ± 20.5
Cenozoic aged volcanic areas (except for geothermal field)	90.5 ± 19.2

Table 2- Heat flow measurement values in various structures of oceanic crust (after Lee and Uyeda, 1965).

Heat flow in Oceans	**Average Heat Flow (mW/m^2)**
Oceanic Basins	53.6 ± 22.2
Mid-Ocean Ridges	76.2 ± 65.3
Oceanic depressions (trenches)	41.8 ± 25.5

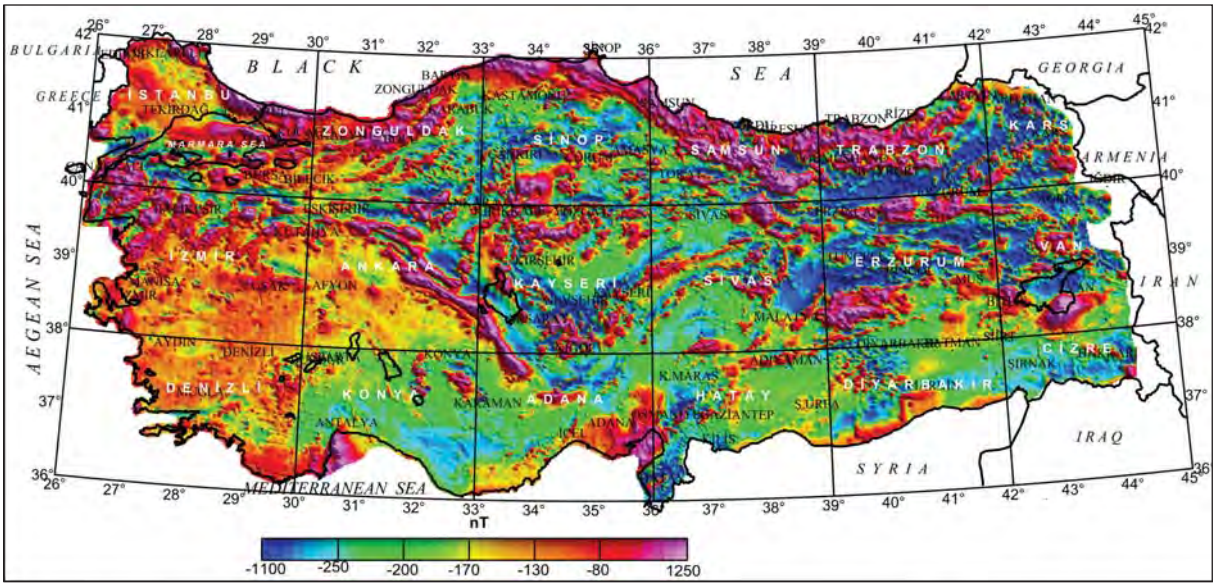

Figure 2- Aeromagnetic anomaly map of Turkey.

be applied both on profile and on map data (Figure 3). When the method is applied on gravity data, it estimates the lower depth of the main body on the other hand; when applied on magnetic data, it delineates the depth at which the Curie temperature is reached. Curie point temperature (CPT) is the critical temperature which is necessary for a ferromagnetic substance to lose its stable magnetism. Each substance has different Curie critical temperature. This temperature is named as the "Curie temperature" in the memory of Pierre Curie who studied in the area of paramagnetism.

The map of Curie point depth (CPD) of Turkey was produced by Karat and Aydın (2004) by means of the power spectrum. They showed that hot spring outflows are more dense in areas where the CPD is estimated shallow especially in Western and Central Anatolia regions (Figures 1 and 4).

It is know that hot spring outflows occurs along tectonic lines along the northern boundary of the shallower CPD zone covering western Anatolia and vicinity of Ankara, and earthquake epicenters are condensed especially on margins of shallow areas in West Anatolia. Additionally, shallow CPD at known oil fields in Southeast Anatolia presents structural

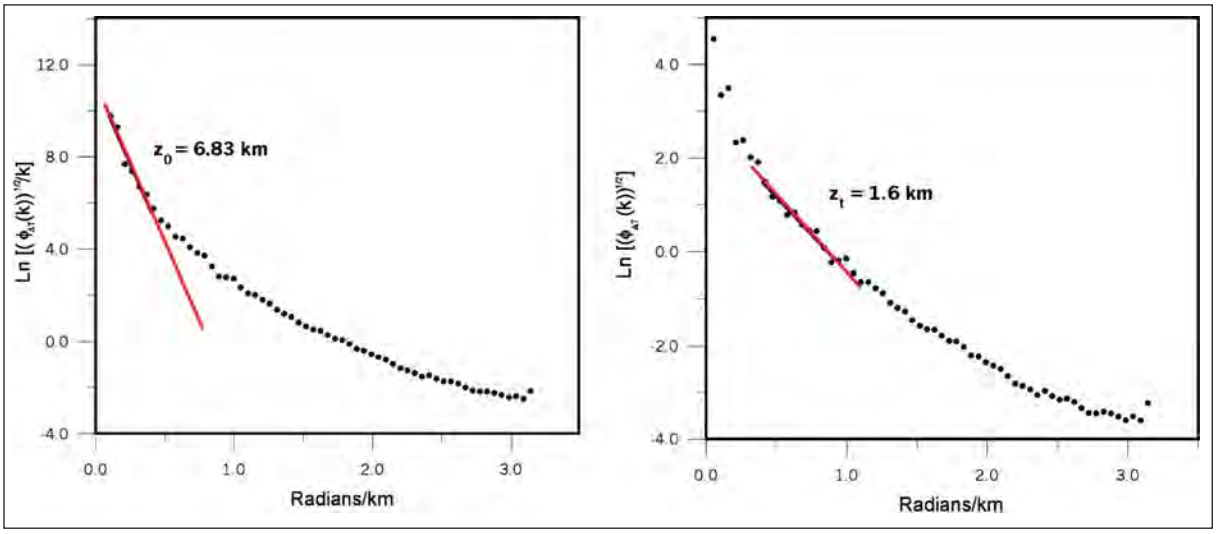

Figure 3- Sample curve for the Curie point depth of one block (north of Lake Van) (modified from Aydın et al., 2005).

similarities with Thrace region (Karat and Aydın, 2004) (Figure 4).

Şalk et al. (2005) estimated Curie point depths of the western Anatolia applying the power spectrum method to Magsat magnetic data with using the thermal conductivity value of 2 W/m°C. They showed that Curie point depths of young volcanic rocks and metamorphic units of the western Anatolia and heat flow values were coherent. They also revealed the relations between the source of heat in geothermal fields and deep magmatic bodies, young volcanic rocks which have not yet lost their heat and structural fault systems.

In this study, Curie point depths of Turkey are calculated by using aeromagnetic data of Turkey. Being a difference from previous research, instead of using fix thermal conductivity value, various in-situ conductivities, gathered in various projects, are used to produce an updated heat flow map. Obtained results are compared with previous result to check consistency and presented here for consideration of researchers

2. Geothermal Potential of Turkey

Geothermal fields are areas where the heat is transferred. Areas in which the heat flow is between 0-125.7 mW/m^2 are called as normal fields, whereas the areas in which the heat flow is higher than 125.7 mW/m^2 is called as geothermal fields.

Turkey has a large geothermal potential. There are more than 170 economically important geothermal fields and 1500 hot and mineralized water sources in the country. Spring outflows and reservoir temperatures of these waters are in between 20°-242°C (Figure 1). Geothermal spots usually appear around major grabens in western Anatolia, along the North Anatolian Fault Zone (NAFZ) and in the volcanic regions in Central and East Anatolian (Şimşek et al., 2005). The geothermal heat potential of Turkey is considered to be 31500 MWt at present conditions. General Directorate of Mineral Research and Exploration (MTA) has explored the presence of 190 geothermal fields within 50 years period. Geothermal fields through Turkey show a distribution as 79% in west Anatolia, 8,5% in Central Anatolia, 7,5% in Marmara Region and 0,5% in other areas. 94%, of the geothermal sources are in low to medium temperature and used for heating, thermal tourism and in mineral production. The remaining 6% however, is suitable for the production of electrical energy (MTA, 2014).

3. Geophysical Data and Technique

Aiming to provide a base information to explore the underground resources of Turkey, within the Department of Geophysical Researches of the MTA, aeromagnetic studies started in 1978 and completed in 1989. Total of 460.000 km aviation research was carried out over sea, lake and on land, covering an area of 813.639 km^2. However, due to border agreements between Turkey and its neighbor countries, these researches had to be stopped at 5 km

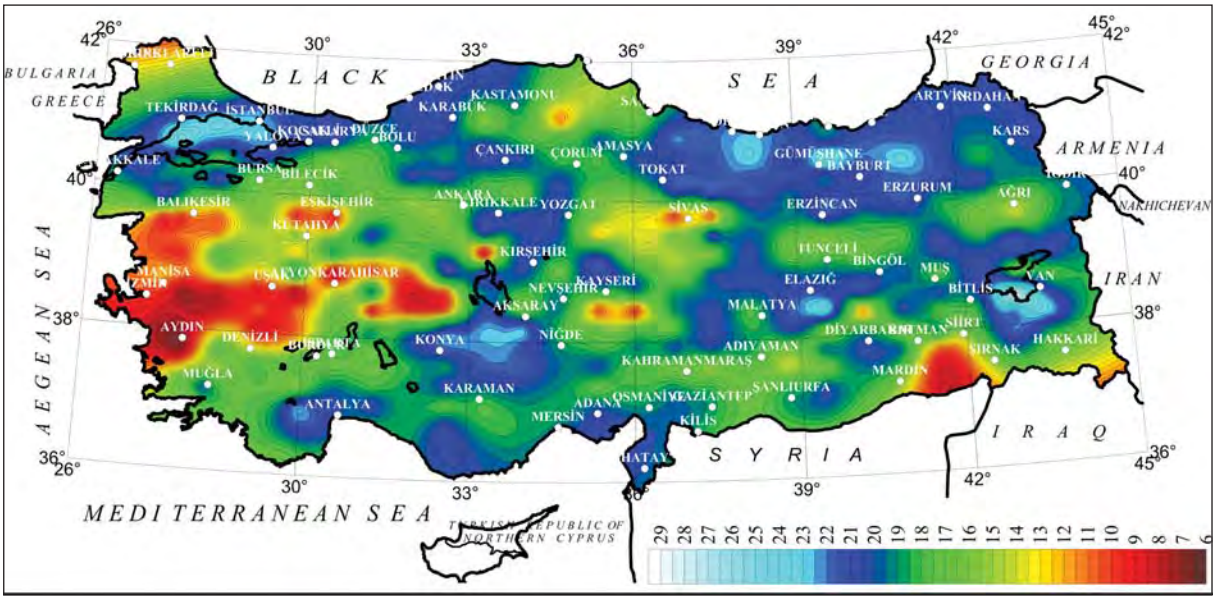

Figure 4- The map of Curie point depth (modified from Aydın et al., 2005).

to Syrian, Iranian and Iraqi borders and at 15 km to Former Soviet Union, Greek and Bulgarian borders. Flight lines were at a height of approximately 2000 feet (600m) and their directions were selected according to topographic obstacles and, mostly, the geological factors. Flight line intervals were kept around 1 to 5 km depending on existence of possible geothermal, mineral explorations and other potential resources. Measurements of diurnal change were recorded by magnetic base station in each flight sector and necessary corrections were completed by defining heading error. Different Data sets recorded on same sectors but at different times (considering annual changes of the geomagnetic field) were controlled and tied eachother by using the common lines which have same flight elevations (Karat and Aydın, 2004). IGRF 1985 (International Geomagnetic Reference Field) were applied to Aeromagnetic data for reduction.

Aydın et al. (2005) gridded the aeromagnetic data in size of 1x1 km and applied the spectral analysis technique over 380 blocks.

Using the technique suggested by Spector and grant (1970) and improved by Tanaka et al. (1999) and Okuba et al. (1985) Depth of Curie isotherm map was produced. The depth of source of magnetic anomaly was given in Equation 1 (Figure 3).

$$Z_b = 2Z_o - Z_t \qquad 1$$

where;

Z_b, lower depth of the magnetic source,

Z_o, depth of the center of the magnetic source,

Z_t, upper depth of the magnetic source.

Karat and Aydın (2004, 2005), with their estimation of Curie depth points, revealed that the western Anatolia was shallower than other regions. In the area covering Aydın-Denizli-Uşak and extends in west east directions, the depth was between 6 to 10 km. it is seen that Curie depth point is the shallowest in Aydın and its vicinity located in Menderes graben (Figure 4). In orogenic belts and high plateaus the calculated depths were between 20 to 29 km. The geothermal gradient was calculated from each grid cell of the map of Curie point depth and used for the map of heat flow.

As stated before, If the heat in any medium, flows normal to surfaces within unit sections which are parallel to each other and reaches the steady state then the heat flow, as given in Equation 2, is equal to the multiplication of thermal conductivity by the thermal gradient.

$$q=\lambda*(dT/dz) \qquad 2$$

where

q heat flow,

λ thermal conductivity coefficient of rock,

dT/dz geothermal gradient.

In this study, we used 579 the rock thermal conductivity values (λ), recorded through Turkey, by Karlı et al. (2006). In Table 3, λ values for Manisa–Çataloluk is given. In Equation 2, using in-situ thermal conductivity values instead of fixed λ coefficient, a new heat flow map was obtained (Figure 5).

Rock thermal conductivity data are not sufficient in eastern Black Sea, southeastern and eastern Anatolia regions. In future, when the number of samples is increased, much detailed maps in those regions will be possible to generate.

In western Anatolia horst graben systems of Menderes massif caused a crustal thinning. Due to this thinning, Curie point depths are shallow (between 7.3 – 15 km) in Aydın, Denizli and Uşak (Karat and Aydın 2004; Aydın et al., 2005). İzmir and its vicinity, with the average heat flow value of 101

Table 3- Measurement values of rock thermal conductivity coefficients taken by QTM (Quick Thermal Measurement) device (after Yemen, 1999).

Location	**Rock lithology and thickness (m)**		**QTM measurement λ (W/mºC)**
Manisa–Çataloluk	Marl	0-53	1.797
Manisa–Çataloluk	Pebble-tuff	53-85	1.375
Manisa–Çataloluk	Sandstone	85-122	3.228

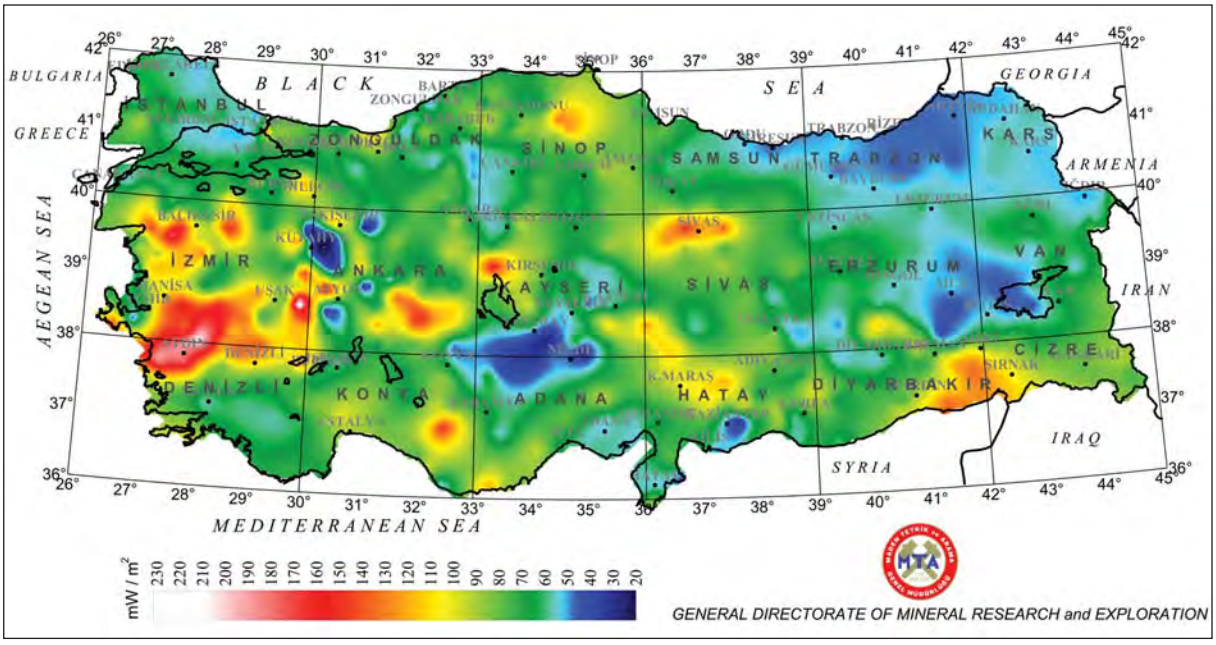

Figure 5- Updated heat flow map of Turkey.

mW/m^2, forms the most important region of Turkey in terms of geothermal potential.

At the north of Ankara-Erzincan Suture zone, in the Eastern Black Sea Region Heat flow values in Ordu, Artvin and Bayburt regions, are estimated as 57 mW/m^2 , 47 mW/m^2, 55 mW/m^2, respectively.

Heat flow values decrease, where the crust thickens, in areas of Bingöl, Bitlis, Muş, Batman and Van which are located as parallel to north of Bitlis Suture Zone. It was determined that lithological characteristics played an important role on the change of heat flow. Relative increases in the heat flow have become distinct in areas where granitoid, volcanite and gneisses are dense in the region.

Two areas are observed in the north and east of Lake Van, considered to be associated with each other with Curie point depths of 17-18 km, (Karat and Aydın, 2004).

Deep well drillings carried out by TPAO in Nemrut Mountain revealed that the temperature was less than expected. The heat flow map shows low heat flow values as 55 mW/m^2 in northeast of Lake Van (in the vicinity of Muradiye) and 46 mW/m^2 in Nemrut Mountain. The heat flow value is 71 mW/m^2 over the young volcanic rocks located in the anomaly region spreading at south of Ağrı and its surround.

In tectonically active areas of Anatolia and the regions of the young volcanism, the high heat flow indicates the enrichment of geothermal resources. The Curie point depth of the region between Sinop, Samsun and Çorum areas, which is the shallowest section of the Black Sea, is 11.6 km (Karat and Aydın, 2004). Hot springs located on margins of the anomaly support a crustal thinning in this place.

In the heat flow map, maximum values; 93 mW/m^2 at the southeast of Kastamonu and 128 mW/m^2 at the region between Sinop, Samsun and Çorum appear to be compatible with each other.

The Curie point depth of the most active faults in the shear zone between Erzincan–Tunceli in Turkey is 16 km. There are significant numbers of hot springs in the region. The values of 56 mW/m^2 were detected in Bingöl. This incompatibility, as mentioned in discussion, occurs due to lack of sufficient data cluster in eastern Anatolia region.

Along the narrow belt which starts from Hakkari to north of Urfa then to the north Adana and continue extending westward, shallow Curie point depths are observed. Curie point depth is getting shallow up to 11 km (Karat and Aydın, 2004). Estimated heat flow values in region between Şırnak, Siirt, Batman, Mardin region, in the north of Diyarbakır and Karacadağ are 132 mW/m^2, 116 mW/m^2 and 55 mW/m^2, respectively.

Although Erciyes is located in the area (Figure 1),There is not any distinctive hot springs in the south of Kayseri. In the heat flow map, along a narrow band extending from Kayseri to Gaziantep there is high heat flow maximum value of which increases up to 116 mW/m^2.

Trabzon and Kars and their vicinity are the lowest areas in terms of heat flow values and they are 52 mW/m^2 and 54 mW/m^2, respectively.

The maximum, minimum and average heat flow values together with Curie point depths for Turkey given in Table 4.

4. Discussion and Suggestions

The rock thermal conductivity of 579 samples collected throughout Turkey was assessed and the heat flow map of Turkey was produced. The number of rock thermal conductivity is not sufficient nor does it exhibit a homogenous distribution. These data display a sparse distribution in Eastern Black Sea, Southeastern and Eastern Anatolia regions. Through the additional researches, any increment in the number of samples will also enhance the value of maps that will be reproduced in future.

In the heat flow map of Turkey, the average heat flow value of the country was determined as 74 mW/m^2.

The resultant map of this study revealed that Turkey possesses a great geothermal potential. in terms of geothermal resources, the most significant region of Turkey is İzmir sheet in 1/500.000 scale with the average value of 101 mW/m^2. The Curie point depth within this region varies in between 6 to15 km.

The shallowest areas in the region are in Aydın and Denizli which are located in Menderes Graben (Karat and Aydın, 2004; Aydın et al., 2005). The minimum and maximum values in this region are also the highest and lowest values of Turkey as; below 30 mW/m^2 between Kütahya and Eskişehir, whereas as 229 mW/m^2 between Uşak and Afyon.

The average depth in Trabzon, Samsun and İstanbul sheets is 20 km. Their related average heat flow values were also detected as relatively low. Trabzon sheet especially in terms of heat flow were found to be the weakest region of Turkey in with the value of 52 mW/m^2 (Figure 1 and Table 4).

Table 4- The average heat flow and Curie values for Turkey on 1/500 000 scaled map.

1:500.000 scaled sheet	Maximum (mW/m^2)	Minimum (mW/m^2)	Average (mW/m^2)	Average Curie Depth (km)
İstanbul	123	51	66	20.3
Zonguldak	113	48	70	18.7
Sinop	129	52	78	17.9
Samsun	100	59	74	20.4
Trabzon	63	45	52	21.5
Kars	80	50	54	19.5
İzmir	229	29	101	12.2
Ankara	166	20	81	15.4
Kayseri	164	26	72	18.6
Sivas	152	50	81	17.5
Erzurum	116	41	61	19
Van	87	42	62	19.6
Denizli	191	56	86	16
Konya	148	48	80	18.9
Adana	118	34	67	19.6
Hatay	120	33	78	17.7
Diyarbakır	135	54	83	17.1
Cizre	126	64	87	19.3

In the light of the insufficient data Ankara, does not seem to be prosperous in terms of hot water sources and geothermal fields. Therefore; additional studies to be carried out on the Ankara sheet will probably define better the geothermal potential of the region.

Although Diyarbakır and Cizre have considerably high heat flow, the absence of hot water sources and geothermal fields are highly remarkable (Figure 1). Cizre has an approximate Curie point depth of 19.3 km and a low geothermal gradient with respect to Diyarbakır.

The Curie point depths of Adana, Van, Erzurum, Kars and Konya vary in between 18.9 to 19.6 km, nevertheless exhibit relatively weak characteristic in terms of heat flow.

Curie point depths on Sivas, Hatay and Sinop sheets show variation between 17.5 to 17.9 km. These values are shallower than the average Curie point depth of the country. Heat flow values of sheets are compatible with shallow Curie point depths and are above the country average. Sinop sheet which houses one part of the North Anatolian Fault system is as dense region in terms of hot water sources such as Zonguldak sheet and hot springs generally take place along the fault system.

Kayseri sheet which covers most of the Kırşehir massive remains below the country average with the Curie point depth of 18.6 km and heat flow value of 72 mW/m^2. Akın and Çiftçi (2011) presented that a some part of the heat flow of this sheet is originated from the radiogenic heat production. Volcanic rocks are dominant in the area. in terms of hot springs, geothermal fields and volcanic outcrops It is richer than many regions.

5. Results

Taking Curie point depth map of previous research as a base, using thermal conductivity values obtained in various projects a new heat flow map of Turkey was produced. The result obtained are in accord with the field observations. In addition to existing field, it is revealed that additional research needs to be conducted for the fields of east black sea, east Anatolia, south east Anatolia

Acknowledgement

The authors would like to present their deepest sincere and mercy to Dr. Mehmet Duru with whom we prepared MTA report of the heat flow map of Turkey (from magnetic data), the exemplary scientist in earth sciences who passed away soon before. We feel endless proud of working with him and getting to know such a person.

We would like to thank Dr. M. Özgü Arısoy (MTA) for his support and invaluable suggestions, Assoc. Prof. O. Pamukçu (DEU) and İ. Aydın (SDU) for their constructive criticism and contributions.

Received : 22.04.2014
Accepted: 15.09.2014
Published: December 2014

References

AFAD, 2014. T.C. Başbakanlık Afet ve Acil Durum Yönetimi Başkanlığı Deprem Araştırma Dairesi Başkanlığı. 17 Nisan 2014, http://www.deprem.gov.tr/sarbis/Shared/Default.aspx

Akın, U., Duru M. 2006. Türkiye Isı Akısı Haritası (manyetik verilerden) raporu. *Maden Tetkik ve Arama Genel Müdürlüğü*, Report No: 10840, Ankara (unpublished).

Akın, U., Duru, M., Kutlu, S., Ulugergerli, E.U. 2006. Heat flow map of Turkey (from magnetic data). *17.Geophysical Congress*, *Maden Tetkik ve Arama Genel Müdürlüğü*, Ankara (in Turkish). Extended Abstract CD.

Akın, U., Çiftçi, Y. 2011. Heat flow of the Kırşehir massif and geological sources of the radiogenic heat production. *Bull. Min. Exp. Res.,* 143, 53-73.

Aydın, İ., Karat, H.İ., Koçak, A. 2005. Curie-point depth map of Turkey. *Geophys. J. Int.* 162, 633-640.

Bal, A. 2004. Aydın İzmir civarının hava manyetik verilerinden ısı akısı değerlerinin belirlenmesi ve ısı akısı dağılımının İncelenmesi. Ankara Üniversitesi Fen Bilimleri Enstitüsü Jeofizik Mühendisliği Anabilim Dalı. 141s., Ankara (unpublished).

Bhattacharyya, B.K. 1965. Two dimensional harmonic analysis as a tool for magnetics interpretation. *Geophysics* 30, 829, 857.

Bhattacharya, B.K. 1966. Continous spectrum of the total magnetic field anomaly due to a rectangular prismatic body, *Geophysics*, 31, 97-121.

Bullard, E.C. 1939. Heat flow in South Africa. *Proc. Roy. Soc., London*, Ser. A., 173. 474-572.

Ericson, A.J. 1970. The measurement and interpretation of heat flow in the Mediterranean and Black Sea. Ph. D. Thesis, Cambridge, Mass., Massachusetts Institute of Technology, 272p.

Fytikas, M.D. 1980. Geothermal exploration in Greece. 2nd. Int. Sem on the Results of E.C. *Geothermal Energy Research, Strasbourgh*. (eds) A.S. Strub ve P. Ungemanch, 213 – 237, Reidel Publ., Dordrecht.

Fournier, R. O., Rowe, J. J. 1966. Estimation of underground temperatures from the silica content of water from hot springs and wet steam wells. *Am. J. Sci*., 264, 685-697.

Fournier, R. O., Rowe, J. J. 1977. The solubility of amorphous silica in water at high temperatures and high pressures. *American Mineralogist*. Volume 62, pages 1052-1056.

Gorshkov, G.S. 1972. Progress and problems in volcanology: *Tectonophysics*, 13, 1-4, 123-140.

Göktürkler, G. 2002. Yerbilimlerinde, Isı Transferi Modellemesi: Kararlı-Hal Kondüktif Isı İletimi. *Dokuz Eylül Üniversitesi Mühendislik Fakültesi Fen ve Mühendislik Dergisi*, 4, 3, 67-80.

Gupta, M.L., Verma, R.K., Hazma V.M., Venkateshwar, Rao.G., Rao, R.U.M. 1970. Terrestrial heat flow and tectonics of the Cambay basin (India). *Tectonophysics*, 10, 1-3, 147-163.

İlkışık, O.M. 1995. Regional heat flow in western Anatolia using silica temperature estimates from thermal springs. *Tectonophysics*, 244, 175-184.

İspir, Y. 1972. Arz içinde ısı akısı. *İ.Ü. Fen Fakültesi* Jeofizik Kürsüsü Öğretim yayınları 5. İstanbul.

Jongsma, D. 1974. Heat flow in the Agean Sea. *Geophys. J.R. Astr. Soc*., 37, 337-346.

Karat, H.İ., Aydın, İ. 2004. Türkiye Curie ısısı derinlik haritası raporu. *Maden Tetkik ve Arama Genel Müdürlüğü* Report No: 10638, Ankara (unpublished).

Karlı, R., Öztürk, S., Destur, M. 2006. Türkiye ısı akısı haritası projesi raporu. *Maden Tetkik ve Arama Genel Müdürlüğü* Report No: 10937, Ankara (unpublished).

Langseth, M.G., Taylor, P.T. 1967. Recent heat flow measuruments in the Indian ocean: *Journ. Geop. Research*., 72, 24 , 6249-6260.

Lee, W.H.K., Uyeda, S. 1965. Review of heat flow data: Terrestrial Heat Flow. *Geophysical Monograph Series Am. Geop. Union*. 8, 87-190.

Okubo, Y., Graf, R.J., Hansen, R.O., Ogawa, K., Tsu, H. 1985. Curie point depths of the island of Kyushu and surrounding areas, Japan. *Geophysics*, 50, 481–494.

McKenzie, D. P. 1967. Some remarks on heat flow and gravity anomalies; Journ. *Geop. Research* 72, 24. 6261-6273.

MTA, 2014. *Maden Tetkik ve Arama Genel Müdürlüğü,* 17.Nisan.2014, www.mta.gov.tr

Pfister, M. 1995. Geothermische Untersuchungen in der Region Marmara, NW-Turkei. Kartierung des Wärmeflusses und hydrothermale Modellrechnungen, (Geothermal investigations in the region of Marmara, NW-Turkey, terrestrial heat flow density and hydrothermal modelling), Diss. ETH, Nr. 11054, 231 p.

Scharli, U., Rybach, L. 1984. On the thermal conductivity of low porosity crystalline rocks. *Techtonophysics*, 103, 307-313.

Sclater, J.G. 1972. New perspectives in terrestrial heat flow: *Tectonophysics,* 13, 257-291.

Shen, P.Y., Wang, K., Back, A.E. 1991. Crustal thermal models along East European peotraverses: inverse solutions. *Tectonophysics*, 194, 363–385.

Spector, A., Bhattacharyya B.K. 1966, Energy Spectrum and autocorralation function of anomalies due to simple magnetic models. *Geophysical Prospecting*, 14, 242-272.

Spector, A., Grant, F.S. 1970. Statistical models for interpreting aeromagnetic data. *Geophysics*, 35, 293–302.

Şalk, M., Pamukçu, O., Kaftan, I. 2005. Determination of the Curie Point Depth and Heat Flow from Magsat Data of Western Turkey. *Journal of the Balkan Geophysical Society*, 8/4/149-160.

Şimşek, İ., Mertoğlu, O., Bakır, N., Akkuş, İ., Aydoğdu, Ö. 2005. Geothermal Energy Utilization Development and Projections - Country Update Report 2000 - 2004 of Turkey Proceedings World *Geothermal Congress*, Antalya, 24-29 April.

Tanaka, A., Okuba, Y., Matsubayashi, O. 1999. Curie point depth based on spectrum analysis of the magnetic anomaly data in East and Southeast Asia, *Tectonophysics*, 306, 461–470.

Tezcan, A. K., Turgay, M. I. 1991. Heat flow and temperature distribution in Turkey, in: *Geothermal Atlas of Europe*, edited by: Cermak, V., Haenal, R., and Zui, V., 84–85.

Tissot, B., Espitalie, J., 1975. L'evolution thermique de la matiere organique des sediments; applications d'une simulation mathematique; Potentiel petrolier des bassins sedimentaires et reconstitution de l'histoire thermique des sediments. *Revue de l'Institut Francais du Petrole et Annales des Combustibles Liquides* 30 (5): 743-777.

Vitorello, I., Pollack, H.N. 1980. On the variation of continental heat flow with age and the thermal evolution of continents. *J. Geophys. Res*. 85, 983-995.

Yemen, H. 1999. Ege bölgesi ısı akısı dağılımı. Yüksek lisans tezi. Süleyman Demirel Üniversitesi, Fen Bilimleri Enstitüsü. 101s., Isparta (unpublished).

Zonenshin, L.P. 1975. Problems of global tectonics; Bull. Am Assoc. Petrolum Geologist, 59, 1, 124-133.

BULLETIN OF THE MINERAL RESEARCH AND EXPLORATION

Foreign Edition 2014 149

CONTENTS

Facies Characteristics And Control Mechanisms of Quaternary Deposits In The Lake Tuz Basin
.....Alper GÜRBÜZ and Nizamettin KAZANCI 1

Neotectonic-Period Characteristics, Seismicity, Geometry And Segmentation of The Tuz Gölü Fault Zone
.....Akın KÜRÇER and Y. Ergun GÖKTEN 19

Neogene Stratigraphy And Paleogeographic Evolution of The Karaburun Area, İzmir, Western Turkey
.....Fikret GÖKTAŞ 69

Benthic Foraminiferal Fauna of Malatya Oligo-Miocene Basin (Eastern Taurids, Eastern Turkey)
.....Fatma GEDİK 93

Protolith Nature And Tectonomagmatic Features of Amphibolites From The Qushchi Area, West Azerbaijan, NW Iran
.....Mohssen MOAZZEN 139

Glauberite-Halite Association In Bozkır Formation (Pliocene Çankırı-Çorum Basin, Central Anatolia, Turkey)
.....İlhan SÖNMEZ 153

Estimation of Swelling Pressure Using Simple Soil Indices
.....Kamil KAYABALI and Özgür YALDIZ 177

Two Examples For Imaging Buried Geological Boundaries: Sinkhole Structure And Seyit Hacı Fault, Karapınar, Konya
.....Ertan TOKER, Yahya ÇİFTÇİ, Aytekin AYVA and Akın KÜRÇER 189

The Assessment of Geothermal Potential of Turkey By Means Of Heat Flow Estimation
.....Uğur AKIN, Emin Uğur ULUGERGERLİ and Semih KUTLU 201

A Brief Note On Mineral Evolution And Biochemistry
.....José Mario AMİGO 211

Critisism on the paper "Possible Incision of The Large Valleys In Southern Marmara Region, Turkey (Nizamettin KAZANCI, Ömer EMRE, Korhan ERTURAÇ, Suzanne A.G. LEROY, Salim ÖNCEL, Özden İLERİ and Özlem TOPRAK)
.....Nizamettin KAZANCI 219

Acknowledgement 221

Notes to the authors 223

Bull. Min. Res. Exp. (2014) 149: 211-218

Bulletin of the
Mineral Research and Exploration

http://bulletin.mta.gov.tr

A BRIEF NOTE ON MINERAL EVOLUTION AND BIOCHEMISTRY

José María AMIGÓ[a*]

[a] *Crystallography and Mineralogy Unit, Department of Geology, University of Valencia, 46100-Burjassot (Valencia), Spain*

Keywords:
geology, mineralogy, terrestrial and extraterrestrial mineral evolution, life existence, biochemistry.

ABSTRACT

The natural inorganic materials (minerals and rocks) exceed the limits of the Earth. Therefore, the geology, which is the study of the Earth, represents only a small part of the natural inorganic world. Certain questions about the genesis of the universe are related to the evolution of our solar system and the evolution of life on our planet. In this paper, recent contributions from experimental physical natural-sciences to the formation of the universe (about 15 billion BP) coupled with the occurrence of minerals (4 million years BP) and the biochemical appearance of life (not more than 3 million years) on the Earth are discussed. When Earth was formed, none of the more than 4,400 minerals we know today were existed. Cosmologists estimate that nearly ten billion years after the Big Bang the first elements produced by the melting process. The geological history of mineral evolution on the Earth is an interesting tool to study terrestrial and/or extraterrestrial mineralogy in regard to astronomy, biology, chemistry and other experimental natural sciences.

1. Introduction

The aim of this article is to relate the formation of minerals with the existence of life on the Earth as in the rest of the Universe. Earth and Universe are not independent things. The natural inorganic world extends beyond the limits of the Earth as indicated by several authors by the relationship between the geological evolution and the phenomenon of life (Banfield et al., 1998; Amigó and Ochando, 2001; Bleeker, 2002; Hazen and Ferry, 2010). Therefore, geology, that is the study of Earth, represents only a small part of the natural inorganic world. As a first approximation, we can establish a relationship between astronomy and geology; both are sciences that are based on knowledge obtained principally from observation. Scientific knowledge developed from these astronomical and geological observations obtained by experimental methods and techniques can make predictions connected to the past, present and future observable events. Accordingly, we can establish an evolutionary view of the Universe and Earth to integrate all biological, geological, physical and chemical viewpoints. In this sense, the genesis of the Universe is related to the formation of our solar system and the evolution of life on our planet. The age of universe is about 15 billion years while humans only arrived about 3 million years ago (Mann and Weiss, 1996), on a planet whose absolute geological age appears to be about 4.5 billion years. This age has been determined from precise geochronology using isotopic dating methods.

Then I will endeavour to summarise the geological history of the Earth from the point of view of the evolution of the biological, physical and chemical processes that have given rise to the approximately 4,400 minerals recognized on our planet (Hazen, 2010). A mineral is a homogeneous solid, in nature typically formed by inorganic processes, which has an ordered atomic arrangement in a three dimensional space, and having a defined chemical composition (but generally not fixed, varying within certain limits). However, we know

*Corresponding author: J.M. AMIGÓ, jose.m.amigo@uv.es

that the planet Earth is tectonically active, during which matter and energy interact with both outer space and with internal geological processes, resulting in plate tectonics (which interact to give rise the displacement and collision of continents causing earthquakes, volcanism and orogens), to the formation of natural resources (such as fossil fuels, rocks and minerals), and the origin and formation of life (arising from the interaction and evolution of the atmosphere and hydrosphere over the geological history of our planet as a result of complex biochemical reactions).

When the Earth formed, none of the more than 4400 minerals we know today existed (Hazen et al., 2008; Hazen, 2013). Cosmologists estimate that after 10 to -5, billion years following the Big Bang the first stars formed from the condensation of H and I (and probably some of Li), while the first elements were produced by melting processes (Schatz, 2010).

Only when giant stars transform into supernovas, nuclear reactions (nucleosynthesis) allow us to explain the observed abundances of chemical elements in the solar system and neighboring stars. These reactions (also called triple-?) take place over tens of millions of years and explain the formation of elements such as carbon and other with higher atomic number. Iron is the last stable element formed in this process. Therefore, diamond, graphite and SiC together with nitrides, oxides and silicates of magnesium should have been some of the mineral solid particles (nanometer-sized fan) being more abundant in planetesimals and interstellar matter condensation which gave rise to formation of first stars in the Universe (Clayton and Nittler, 2004). Perhaps for tens of millions of years were no more than a dozen of the unique mineral crystals in the Universe.

Starting from the formation of the solar system we can consider the following stages of biological, geological, physical and chemical differentiation affecting terrestrial minerals (Hazen et al., 2008):

- formed by accretion and differentiation of planetesimals in the presolar nebula;
- trained in primary geochemical differentiation of the Earth in an initial solid crust and a mantle-core cast undifferentiated;
- formed during the biogeochemistry evolution of Earth's atmosphere.

2. The First Terrestrial Minerals: Interstellar Dust Particles (> 4.5 Ga)

Mineral evolution (Figure 1) began within a large cloud of interstellar gas and dust, called the solar nebula, which was formed by accretion and differentiation of planetesimals (interstellar dust) that further collided and accreted to form the terrestrial planets in the solar system. During this stage, before 4.5 billion years ago, the accretionary reactions of planetesimals, gave rise to the asteroids, from which comets and meteorites originate. Asteroids have a mineral composition simpler than our planet. The first minerals [Stage 1. Chondritic mineral formation (> 4.5 Ga)] formed by accretion at this stage are for the most part refractory components of chondritic meteorites (stony). Chondritic meteorites contain carbonaceous chondrules, spherical in shape and nanometric size, and characterised by the presence of organic compounds (a variety of hydrocarbons and amino acids) of unclear origin (Wood, 1967; Masuda et al, 1973; Richardson, 1978). Probably these compounds are not of biological origin, but their presence would be related to the organic compounds formed in the outer part of the solar nebula and the nuclei from which the meteorites originated. At this stage prior to the consolidation of the crust, a few dozen minerals, probably in a number about 60, were formed; many of them were of nanometer sized.

The Hadean Eon (term not recognized by the International Commission on Stratigraphy), which is the first division of the Precambrian period, corresponds to the time of Earth formation, some 4.6 billion years ago, and ends about 3.8 billion B.P., when the first crust was formed (Goldblatt et al., 2010). During this early stage the Earth was subjected to an intense bombardment of meteorites [Stage 2. Alteration, differentiation and planetisimals metamorphism (4.5-4.4 Ga), A decrease in the Earth's temperature allowed the formation of mineral phases of low temperature (<100 °C) related to aqueous alteration of olivine and pyroxene to chlorite, serpentine, talc and other phyllosilicates as well as hydroxides, sulphates and carbonates. Also achondrite meteorites impacted as ferro-stone and siderite (composed of iron and nickel mainly) tending to modify the mineralogical composition of the Earth. The different types of stony achondrite meteorites represent the composition of the initial planetesimal crust of the Earth, with igneous mineralogical assemblage dominated by plagioclase and pyroxene. At this time, as a consequence of heavy meteorite bombardment that impacted on the Earth, some

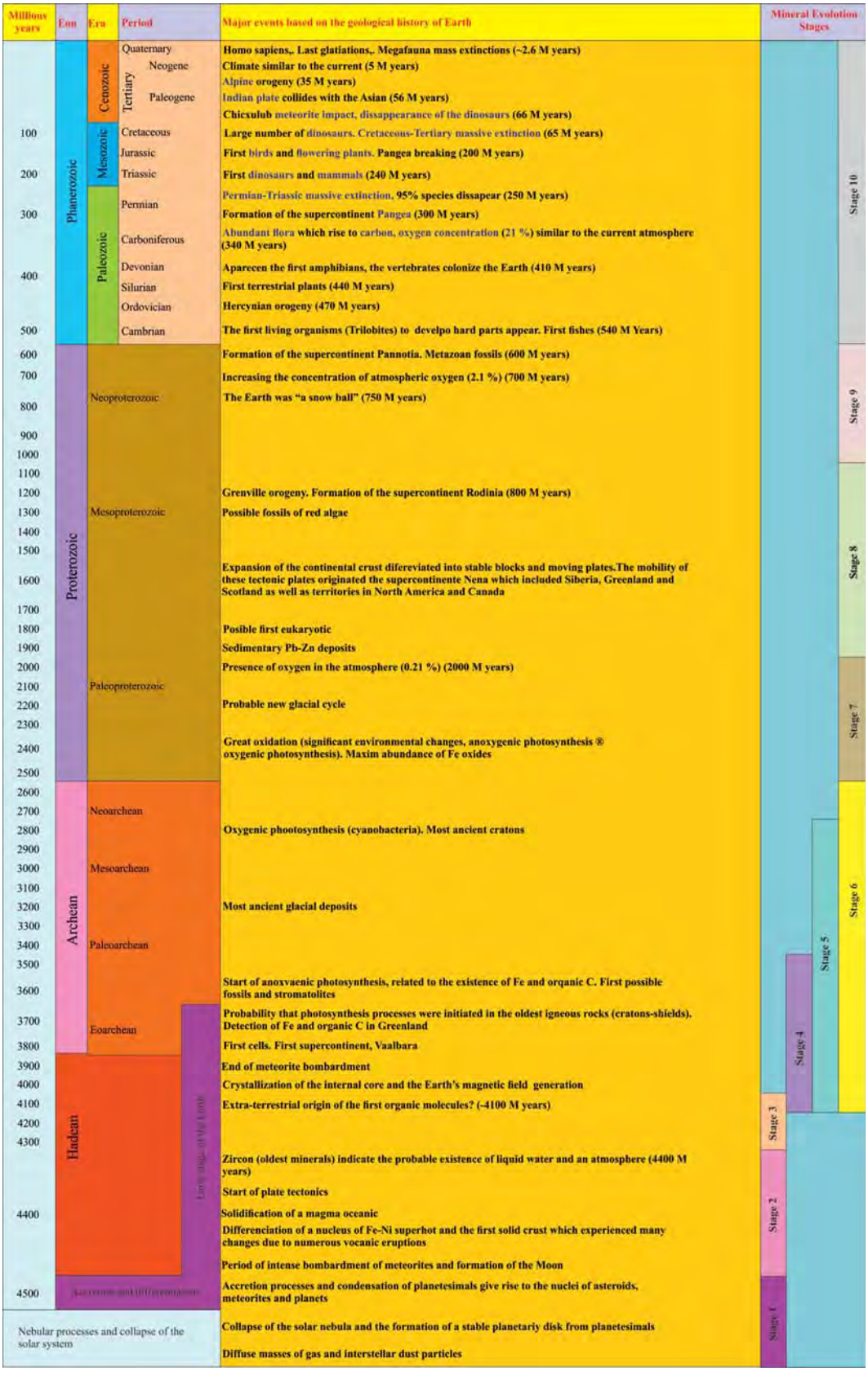

Figure 1- Geological time scale that summarises the main geological events and the different stages of mineral developments, that have taken place on Earth (based partly on a schema of Hazen et al., 2008).

important minerals were formed (Hartman and Davis, 1975; Nickel, 1995; Nickel and Grice, 1998; Aspaug et al., 2011), which have become the main components of terrestrial rocks, such as quartz SiO_2, feldspar $KAlSi_3O_8$, titanite $CaTiSiO_3$, zircon $ZrSiO_4$ and others, formed by processes of hydrothermal alteration and metamorphism. In contrast, the Fe-Ni meteorites originated the planetesimal core, with dominant Fe-Ni alloys (kamacite, taenite) and metal sulfide [troilite FeS_2], carbides, graphite and phosphides [barringerite $(Fe, Ni)_2P$, schreibersite $(Fe,Ni)_3P$], which were the initial source of prebiotic phosphorus. Other phosphates, high-pressure phases of SiO_2 (coesite) and diamond are also associated with Fe-Ni meteorites. About 250 minerals were generated at the end of this stage (Figure 1).

3. The Earth Cools: Formation Of The Current Crust And Mantle (4.5-2.5 Ga)

Before the discovery that the composition of the Moon is the same as that of the Earth's surface, it was believed that composition of the Moon resembles to that of entire Earth. The impact of a large asteroid or protoplanet caused a cataclysmic collision (~ 4.6 Ga ago) which melted the crust and part of the outer mantle. This large collision affected the Earth, Moon and possibly the other four terrestrial planets. The surfaces of these planets favored the crystallization of igneous rocks, affecting the mineralogy of these rocks after meteorite and comet impacts over a long period of time. However, it is apparent that the balanced terrestrial mineralogy experienced many changes to the current structure. One of the probable causes is the existence of petrological, geochemical and geodynamic processes related with the plate tectonics, which affected both the crust and the mantle. Geologists have identified Hadean rocks in Greenland, Canada and Australia. Some zircons in Australian quartzites have been dated at about 4.4 Ga (Wilde et al., 2001), estimated age of formation of the Earth (Figure 1) [Stage 3. Initiation of the evolution of rocks (4.5-4.0 Ga)]. At this stage the igneous activity (magmatic differentiation; Bowen, 1956), favored terrestrial-rich volatile elements and facilitated the formation of large variety of volcanic and plutonic rocks. All these processes of diversification and mineralogy led to the formation atmosphere and hydrosphere (Cloud, 1968).

The components of this early atmosphere had to be N_2, CO_2 and H_2O, and H_2S, with minor amounts of CO, H_2, and CH_4. An immediate mineralogical consequence of the interaction with this atmosphere would be the formation of hydrated silicates (initial formation of clay minerals) and hydroxides. Also at this stage, the terrestrial poles are cooled to below freezing point, leading to the appearance of crystalline H_2O by the first time. Along this stage about 350 minerals could be funned.

At the boundary between the Hadean and Archean Eons [Stage 4. Granite formation and initiation of formation of cratons (4.0-3.5 Ga)], first cratons appeared which are composed of geological formations of internal continental masses, stable rock fragments containing primitive crust of the Earth, as well as remnants of the mantle-lithosphere evolution (Hamilton, 1999). This step of mineral evolution involves that the planet has a sufficient internal heat to melt the initial basaltic crust leading to the formation of granitoids or granitic rocks (Leake, 1990). Although the exact time of occurrence of these rocks is still uncertain, the formation of a continental granitic crust required several hundreds of millions of years (Figure 1). The evolution of granitoids led to the formation of pegmatites, which accumulated rare elements and Li, Be, B, Nb, Ta, U, among others, resulting in formation of about 500 minerals or more.

The detection of continental masses and possible volcanic phenomena indicates the existence of geodynamic movements such as displacement of plates and subduction related to what we now know as the plate tectonics [Stage 5. Start of the plate tectonics (>>3.0 Ga)]. The initial moment of these geodynamic processes is still under scientific debate (Rogers, 1996; Stern, 2007). To some a little before 4 Ga, most of this activity seems to be clear towards to 3 Ga (Fig. 1). Continental masses with ages of 3800 and 3500 million of years are the oldest dated rocks on the Earth. Also in this stage are recognized the first Cu-Pb-Zn sulphide hydrothermal deposits located in Australian Craton (3.5 Ga), Au and U detrital deposits in the African shield (2.9-2.7 Ga) as well as U in Canada (2.4 Ga). But many of these deposits are associated with metamorphic processes that have led to the formation of a number of minority phases, such as selenides, tellurides, arsenides, antimonides and other sulfosalts. Another consequence of plate tectonics is the formation of intermediate pressure minerals such as kyanite Al_3SiO_5, lawsonite $CaAl_2Si_2O_82H_2O$, glaucophane $Na_2(Fe,Mg,Mn)_3AlSi_8O_{22}(OH)_2$, staurolite $(Fe,Mg)_2Al_9(Si,Al)_4O_{20}(O,OH)_4$, and jadeite $NaAlSi_2O_6$. Although it is difficult to quantify the minerals at this stage of the Earth evolution, perhaps 150 additional new minerals and sulfosalts were generated by these

geodynamic processes that took place in the crust and mantle.

In the Archean Eon which corresponds to beginning of biological life, the first bacteria appear to have been the origin of the formation of sedimentary Fe bands [hematite Fe_2O_3, magnetite $Fe^{2+}\ Fe^{3+}{}_2O_4$] and carbonate reefs. [siderite $FeCO_3$, dolomite $CaMg(CO_3)$, calcite $CaCO_3$,...] [Stage 6. Anoxygenic photosynthesis (3.9-2.5 Ga)] (Figure 1). Although the emerged land caused a pause in mineral evolution, weathering and the early life processes in these limited continental areas added 1500 new minerals. At this stage two groups of minerals, clays and transition metal sulfides, are normally considered.

4. Oxygen: The Molecule Of Life (2.5 Ga-Present)

Although there is no agreement (Lowenstam, 1981; Arrhenius, 2003; Parnell, 2004) on the origin of life, it requires a minimum of mineral evolution. There are different views on the origin of life on Earth. Some authors consider an exogenous or terrestrial origin, others consider that RNA first, then DNA and proteins at the end could have had an important role in the initial presence of life on Earth (Orgel, 1998).

The nature of the Earth's atmosphere changed in the Paleozoic Era when the concentration of oxygen in the Earth was increased (in the order of 0.1-0.2% of the actual concentration) [Stage 7. Great Oxidation (2.5-1.9 Ga)] (Fig. 1). This event begins with the increase of oxygen concentration by photosynthesis. This irreversible transformation of the Earth's atmosphere gradually changed the mineralogy of the Earth's surface (Bekker et al., 2004). At the beginning of this stage (~2.5-1.8 Ga), a great abundance (~ 90%) of Fe-Mn deposits of economic interest and other sedimentary minerals were formed [kutnohorite $Ca(Mn,Mg,Fe)\ (CO_3)_2$, pyrolusite MnO_2, rhodochrosite $MnCO_3$, rhodonite $(Mn,Fe,Ca)SiO_3$, riebeckite $Na_2Fe_5Si_8O_{22}(OH)_2$, chamosite $(Fe,Mg)_5\ (Al_2Si_3O_{10}(OH,O)_8$, chrysocolla $(Cu,Al)_2H_2SiO_5\ (OH)_4nH_2O$, turquoise $CuAl_6(PO_4)_4(OH)_84H_2O$, chalcan-thite $CuSO_45H_2O$, malachite $Cu_2(CO_3)(OH)_2$, azurite $Cu_3(CO_3)_2\ (OH)_2$, brochantite $Cu_4(SO_4)(OH)_6$]. Most of these minerals are associated with oxygenation by photosynthesis and oxidative weathering. More than 2500 minerals are hydrated, resulting from oxidative weathering of other minerals, although some were initially formed in anoxic environment (low in oxygen). The biochemical processes associated with the "Great Oxidation" event would be responsible, directly and indirectly, for the formation of the majority of currently existing 4400 minerals. For almost one million years there was no or limited mineral evolution (Holland, 2006). During this period, there was a clear separation between water layers in the ocean; more oxygenic surface layers and anoxygenic deeper layers [Stage 8. Ocean intermediate (1.9-1.0 Ga)]. At this period, sedimentary iron bands, which are characteristic of the Precambrian, abruptly cease indicating that the chemistry of oceans is greatly influenced by microbial activity and solar radiation. The transition from Paleoproterozoic to Mesoproterozoic indicates that mineralogical processes are very similar. There are no major mineralogical changes. We distinguish Pb-Zn sedimentary deposits in cratonic borders (~ 1.8 Ga), U deposits formed by weathering of granitic rocks in Canada and Australia (1.8-1.1 Ga) and sedimentary deposits of Cu in the center-southern Africa and Central Europe (1.4-0.2 Ga) (Figure 2) (Evans, 2013; Marschall et al., 2013).

The ninth stage of mineral evolution is characterized by major changes in climate and atmospheric composition. [Stage 9. Neoproterozoic glaciations (1.0-0.542 Ga)]. Some geologists have verified that towards the end of Proterozoic Eon, in rocks dated between 0.75 and 0.85 Ga, there are significant signs of glaciation. It seems that these glaciations affected all continents, in a way that the icy regions extended into tropical latitudes. What is still a geological debate is whether the surface of the seas and oceans froze completely, or almost completely (Figure 1). Volcanic activity continued at this stage, increasing CO_2 concentrations in the atmosphere, favoring the formation of aragonite. Also towards the end of this stage, the atmospheric oxygen concentration changes from <2% to ~ 15% of the current values which increases the formation of clay minerals on the surface of the continents (Kennedy et al., 2006) and the P concentration in seawater.

At the beginning of the Phanerozoic Eon biology dominates mineral evolution [Stage 10. Phanerozoic biomineralization (<0.542 Ga)]. The formation of nearly 60 minerals has been influenced by microbes, plants, invertebrates and vertebrates (humans included) (Figure 1). Accordingly, So in the Cambrian the first organisms are developed with hard parts. The mineral composition of these Cambrian skeletons are calcite and/or aragonite $CaCO_3$,

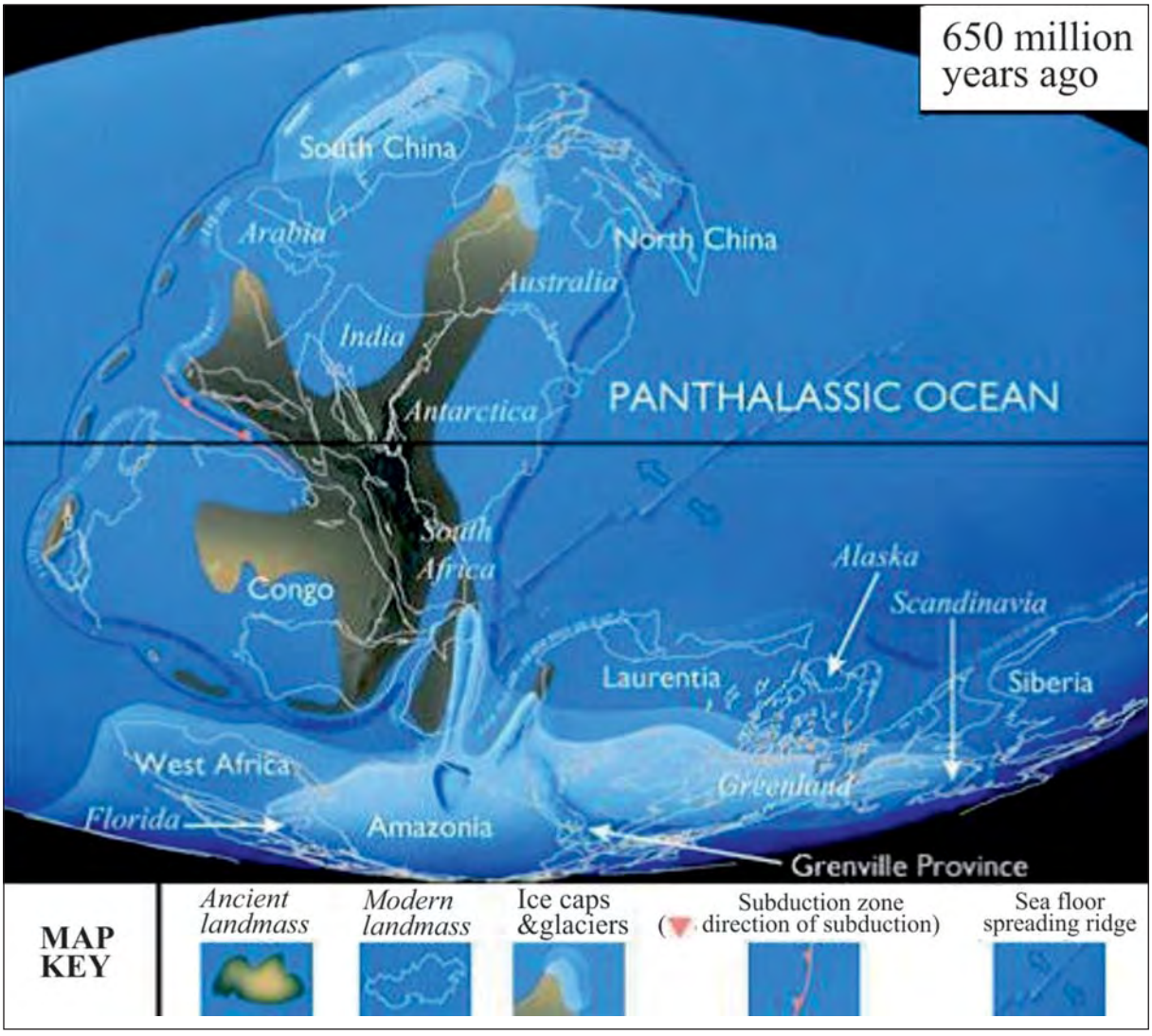

Figure 2- Rodinia, formed during the middle Proterozoic (~ 1100 million years), is the oldest supercontinent for which no record is available. (Evans, 2013; Marschall et al., 2013). Digitized by Principe Felipe Science Museum of Valencia.

magnesium calcite $(Mg_XCa_{1-X})CO_3$, apatite $Ca_5(PO4)_3$ (Cl,F,OH) and opal $SiO_2{\cdot}nH_2O$. Calcium carbonates are, by volume, the most important biominerals as part of the hard parts of corals, molluscs and invertebrates (Stolarski et al., 2007). The calcite seems to dominate from the Cambrian to the beginning of the Carboniferous, but a sudden change to aragonite is observed towards the end of the Paleozoic to mid-Jurassic. These changes could be due to variations in the chemistry of the oceans, which could have facilitated the formation of skeletons with a mineral composition of magnesium calcite and aragonite. Phosphates are found in the skeletons of vertebrates (major minerals of teeth and bones) and invertebrates (e.g., in the shells of brachiopods). The precipitation of phosphates [hydroxyapatite $Ca_5(PO_4)_3$ $(OH)Ca_5$ and fluorapatite $Ca_5(PO_4)_3(F)$ principally] was facilitated by microorganisms present in the sea water, giving rise to formation of phosphor deposits currently exploited. During the Carboniferous large areas of forests were successively entombed giving rise to coal strata. Some scientists suggest that atmospheric oxygen concentrations in this period could be reached at ~35% (the current is 21%). The expansion of terrestrial vegetation, although did not alter the appearance of the land surface, has favored the formation of soils as well as clay mineral deposits that are exploited for ceramics and construction.

5. Conclusions

Minerals are commonly classified based on their chemistry (silicates, carbonates, halides, ..., according to the Dana's classification) or their crystallochemical character [Nesosilicates, cyclosilicates, inosilicates, phyllosilicates, tectosilicates, according to structural criteria established for silicates by Bragg (son)]. That is not normally related with terrestrial minerals within geodynamic history of the Earth. The geological history of mineral evolution is an interesting alternative to relate terrestrial mineralogy, as the extraterrestrial, with biology. It should be kept in mind that biology and geology are a part of the physical and natural sciences (Reventós et al., 2012), including biochemistry.

Received: 20.01.2014
Accepted: 14.07.2014
Published: December 2014

References

Amigó, J.M., Ochando, L.E. 2001. Geologia i química del cosmos i de la Terra. *Publicacions de la Universitat de València*, 568 p.

Aspaug, E., Jutzi, M., Movshovitz, M. 2011. Chondrula formation during planetesimal accretion. *Earth and Planetary Science Letters*, 308 (3-4) 369-379.

Arrhenius, G.O. 2003. Crystals and Life. *Helvetica Chimica Acta*, 86, 1569-1586.

Banfield, J.F., Welch, S.A., Edwards, K.J. 1998. Microbes as geochemical agents. *The Geochemical Society News*, 96, 11–17.

Bekker, A., Holland, H.D., Wang, P.-L., Rumble III, D., Stein, H.J., Hannah, J.L., Coetzee, L.L., Beukes, N.J. 2004. Dating the rise of atmospheric oxygen. *Nature*, 427 (8), 117-120.

Bleeker, W. 2002. Archaean tectonics: A review, with illustrations from the Slave craton. In C.M.R. Fowler, C.J. Ebinger, and C.J. Hawkesworth, Eds., The Early Earth: Physical, Chemical, and Biological Development. *Geological Society of London*, *Special Publication No*. 99, 151–181.

Bowen, N.L. 1956. The evolution of the igneous rocks. *Dover Publications*, 332 p.

Clayton, D.D., Nittler, L.R. 2004. Astrophysics with presolar stardust. *Annual Review of Astronomy and Astrophysics*, 42, 39-78.

Cloud, P.E. 1968. Atmospheric and Hydrospheric Evolution on the Primitive Earth. *Science*, 160, 729-736.

Evans, D.A.D. 2013. Reconstructing pre-Pangean supercontinents. *Geological Society of America Bulletin*, 125(11-12), 1735-1751.

Goldblatt, C., Zahnle, K.J., Sleep, N.H., Nisbet, E.G. 2010. The Eons of Chaos and Hades. *Solid Earth*, 1,1-3.

Hamilton, W.B. 1999. Archean magmatism and deformation were not products of plate tectonics. *Precambrian Research*, 91 (1-2), 143-179.

Hartman, W.K, Davis, R.D. 1975. Satellite-Sized Planetesimals and Lunar Origin. *Icarus*, 24, 504-515.

Hazen R.M., Papineau D., Bleeker W., Downs R.T., Ferry J.M., McCoy T.J., Sverjensky D.A., Yang, H. 2008. Mineral evolution. *American Mineralogist*, 93, 1693-1720.

Hazen, R.M. 2010. Evolution of Minerals. *Scientific American*, 302, 58-65.

Hazen R. M. 2013. Paleomineralogy of the Hadean eon: a preliminary special list. *American Journal of Science*, 313, 807-843.

Hazen, R.M., Ferry, J.M. 2010. Mineral evolution: Mineralogy in the Fourth Dimension. *Elements*, 6, 9-12.

Holland, H.D. 2006. The oxygenation of the atmosphere and oceans. *Philosophical Transactions of The Royal Society*, B361, 903-915.

Kennedy, M.J., Droser, M., Mayer, L.M., Pevear, D. and Mrofka, D. 2006. Late Precambrian oxygenation: Inception of the clay mineral factory. *Science*, 311, 1446-1449,

Leake, B.G. 1990. Granite magmas: their sources, initiation and consequences of emplacement. *Journal of the Geological Society*, 147, 579-589.

Lowenstam, H.A. 1981. Minerals formed by organisms. *Science*, 211, 1126-1131.

Mann, A., Weiss, M. 1996. Hominoid Phylogeny and Taxononmy: a consideration of the molecular and Fossil Evidence in a Historical Perspective. *Molecular Phylogenetics and Evolution*, 5(1), 169-181.

Marschall, H.R., Hawkesworth, C.J., Leat, P.T. 2013. Mesoproterozoic subduction under the eastern edge of the Kalahari-Grunehogne Craton preceding Rodinia assembly: The Ritscherflya detrital zircon, Ahlmann- ryggen (Dronning Maud Land, Antarctica). *Precambrian Research*, 236, 31-45.

Masuda, A., Nakumara N., Tanaka, T. 1973. Fine Structures of normalized rare earth patterns of chondrites. *Geochimica et Cosmochimica Acta*, 37, 2, 239- 248.

Nickel, E.H. 1995. The definition of mineral. *Canadian Mineralogist*, 33, 689-690.

Nickel, E.H., Grice, J.D. 1998. The IMA commission on news minerals and mineral names: Procedures and guidelines on mineral nomenclature. *Canadian Mineralogist*, 36, 913-926.

Orgel, L.O. 1998. The origin of life – a review of facts and speculations. *Trends in Biochemical Sciences*, 23 (12), 491-495.

Parnell, J. 2004. Plate tectonics, surface mineralogy, and early evolution of life. *International Journal of Astrobiology*, 3, 131-137.

Reventós, M.M., Rius, J., Amigó, J.M. 2012. Mineralogy and geology: The role of crystallography since the discovery of X-ray diffraction in 1912. *Revista de la Sociedad Geológica de España*, 25 (3-4), 133-143.

Richardson, S.M. 1978. Vein formation in the C1 carbonaceous chondrites. *Meteoritics*, 13, 141-159.

Rogers, J.J.W. 1996. A history of continents in the past three billions years. *Journal of Geology*, 104(1), 91-107.

Schatz, H. 2010. The evolution of elements and isotopes. *Elements*, 6, 13-17.

Stern, R.J. 2007. When and how did plate tectonics begin? Theoretical and empirical considerations. *Chinese Science Bulletin*, 52 (5), 578-591.

Stolarski, J., Meiborn, A., Prsenioslo, R., Mazur, M. 2007. A Cretaceous scleractinian coral with calcitic skeleton. *Science*, 318, 92-94.

Wilde, S.A., Valley, J.W., Peck, W.H., Graham C.M. 2001. Evidence from detrital zircons for the existence of continental crust and oceans on the Earth 4.4 Gyr ago. *Nature*, 409, 175-178.

Wood, J.A. 1967. Chrondrites: Their metallic minerals, thermal histories, and parent planets. *Icarus*, 6 (1-3) 1-49.

BULLETIN OF THE MINERAL RESEARCH AND EXPLORATION

Foreign Edition 2014 149

CONTENTS

Facies Characteristics And Control Mechanisms of Quaternary Deposits In The Lake Tuz Basin
.....Alper GÜRBÜZ and Nizamettin KAZANCI 1

Neotectonic-Period Characteristics, Seismicity, Geometry And Segmentation of The Tuz Gölü Fault Zone
.....Akın KÜRÇER and Y. Ergun GÖKTEN 19

Neogene Stratigraphy And Paleogeographic Evolution of The Karaburun Area, İzmir, Western Turkey
.....Fikret GÖKTAŞ 69

Benthic Foraminiferal Fauna of Malatya Oligo-Miocene Basin (Eastern Taurids, Eastern Turkey)
.....Fatma GEDİK 93

Protolith Nature And Tectonomagmatic Features of Amphibolites From The Qushchi Area, West Azerbaijan, NW Iran
.....Mohssen MOAZZEN 139

Glauberite-Halite Association In Bozkır Formation (Pliocene Çankırı-Çorum Basin, Central Anatolia, Turkey)
.....İlhan SÖNMEZ 153

Estimation of Swelling Pressure Using Simple Soil Indices
.....Kamil KAYABALI and Özgür YALDIZ 177

Two Examples For Imaging Buried Geological Boundaries: Sinkhole Structure And Seyit Hacı Fault, Karapınar, Konya
.....Ertan TOKER, Yahya ÇİFTÇİ, Aytekin AYVA and Akın KÜRÇER 189

The Assessment of Geothermal Potential of Turkey By Means Of Heat Flow Estimation
.....Uğur AKIN, Emin Uğur ULUGERGERLİ and Semih KUTLU 201

A Brief Note On Mineral Evolution And Biochemistry
.....José Mario AMİGO 211

Critisism on the paper "Possible Incision of The Large Valleys In Southern Marmara Region, Turkey (Nizamettin KAZANCI, Ömer EMRE, Korhan ERTURAÇ, Suzanne A.G. LEROY, Salim ÖNCEL, Özden İLERİ and Özlem TOPRAK)
.....Nizamettin KAZANCI 219

Acknowledgement 221

Notes to the authors 223

Bulletin of the
Mineral Research and Exploration

http://bulletin.mta.gov.tr

CRITISISM on the paper " Possible incision time of the large valleys in southern Marmara region, Turkey (N. Kazancı, Ö. Emre, K. Erturaç, S. A.G. Leroy, S. Öncel, Ö. İleri, Ö. Toprak)" appeared in Bulletin of the Mineral Research and Exploration 148, 1-17.

Nizamettin KAZANCI[a*]

[a] *Ankara Üniversitesi Mühendislik Fakültesi, Jeoloji Müh. Bölümü, 06100 Tandoğan/Ankara*

Keywords:
Landforms of the Marmara region, Criticism

ABSTRACT

The letter aims to inform and correct some lack in the Kazancı et al. (2014) published in the previous issue of this journal for respect to readers and to Journal.

Introduction

The paper to be criticized here (Kazancı et al., 2014) aims to give a date on the formation time about large-scale landforms of the Marmara region, as stated its title clearly. Landforms are significant formations, not only geography but also for geology as earth processes can be seen and/or described directly on them. Therefore, ages of landforms of a region must be known for further interpretations. Previously, it has been accepted that geographic framework of Turkey was appeared by Alpine orogenesis and consequently large-scale non-volcanic landforms took place in Miocene (Erinç, 1955, 1973; Erol, 1981; Darkot and Tuncel, 1981). However, these ideas had been hypothetical assumptions of the general geology and they were not based on any dating. These common opinions were started to discuss after development of "Plate Tectonic" and "Neotectonic" concepts (Şengör, 1980; Şengör and Yılmaz, 1981), soon after they have been modified significantly by working of active faults which gave rise to hazardous earthquakes (Şaroğlu et al., 1987; Emre et al., 2012). In respect to known situation, the description of Marmara landforms based on analytical data as "300 ka" by Kazancı et al (2014) is an important discovery. The obtained age has been also compared with sediment succession and its controlling tectonism in the Sea of Marmara. The criticism to the mentioned paper are due to some missing lines and references in figures 2 and 4 where active faults were shown. They have been also noticed by some other readers.

Figure 2 and figure 4 which are important supplements of the paper show general geology and topography of the region, respectively. In both figures, inner parts of the Sea of Marmara are giving as empty places, except for a limited area where active faults and bathymetry have been drawn colorfully based on a reference. It is right ethically not to include the unobserved places into the study areas, however, they are uncertainities in the maps. The active faults were not discussed in detail as well. The only reference about the faults is Emre et al (2012). Tectonism and active faults were not the main scope of the study and it is acceptable not to include them in the discussion, but the lack of any other reference may bring to mind that it is the only study about the Sea of Marmara. However, the mentioned reference is the main source for the active faults in continental areas. In addition, Emre et al. (2012) gave relevant citations (i.e. İmren et al., 2001; Rangin et al., 2001; Kuşçu et al., 2002; Le Pichon et al., 2001;

* *Corresponding author:* Nizamettin KAZANCI, Nizamettin.Kazanci@ankara.edu.tr

2003; Armijo et al., 2002, 2005; Cormier et al., 2006) for active faults of the sea, and Rangin et al (2001) for colorful bathymetry. All these references and their results could have been used in the paper.

Another mistake in the paper is the address of one of the authors (S.Ö). He is still working for GYTE, but his address pointed as if he is a personnel of Ankara University.

References

Armijo, R., Meyer, B., Navarro, S., King, G., Barka, A. 2002. Asymmetric slip partitioning in the Sea of Marmara pull-apart: A clue to propagation processes of the North Anatolian fault? *Terra Nova*, 14, 2, 80–86.

Armijo, R., Pondard, N., Meyer, B., Uçarkuş, G., Mercier de Lepinay, B., Malavieille, J., Dominguez, S., Gustcher, M.-A., Schmidt, S., Beck, C., Çağatay, N., Çakır, Z., Imren, C., Eris, K., Natalin, B., Özalaybey, S., Tolun, L., Lefevre, I., Seeber, L., Gasperini, L., Rangin, C., Emre, O., Sarıkavak, K. 2005. Submarine fault scarps in the Sea of Marmara pull-apart (North Anatolian Fault): implications for seismic hazard in Istanbul. *Geochemistry Geophysics Geosystems*, 6, 6, 1-29.

Cormier, M.H., Seeber, L., McHugh, C.M.G., Polonia, A., Çağatay, N., Emre, Ö., Gasperini, L., Görür, N., Bortoluzzi, G., Bonatti, E., Ryan, W.B.F., Newman, K.R. 2006. North Anatolian Fault in the Gulf of İzmit (Turkey): Rapid vertical motion in response to minor bends of a nonvertical continental transform. *Journal of Geophysical Research*, 111, B04102.

Darkot, B., Tuncel, M. 1981. Marmara bölgesi coğrafyası. İstanbul Üniversitesi *Coğrafya Enstitüsü Yayını*, No 118, İstanbul.

Emre, Ö., Duman, T.Y., Özalp, S., Elmacı, H., Olgun Ş., Şaroğlu, F. 2012. Açıklamalı Türkiye Diri Fay Haritası, Ölçek 1:1.250.000. *Maden Tetkik ve Arama Genel Müdürlüğü Özel Yayın Serisi*-30, 33s.

Erinç, S. 1955. Orta Ege bölgesinin jeomorfolojisi. *Maden Tetkik ve Arama Genel Müdürlüğü Report No*: 2217, Ankara, (unpublished).

Erinç, S. 1973. Türkiye'nin şekillenmesinde neotektoniğin rolü ve jeomorfoloji-jeodinamik ilişkileri. *Jeomorfoloji Dergisi* 5, 11-26.

Erol, O. 1981. Neotectonic and geomorphological evolution of Turkey. *Z. Geomorph. N.F. Suppl. Bd*, 40, 193-211.

İmren, C., Le Pichon, X., Rangin, C., Demirbağ, E., Ecevitoğlu, B., Görür, N. 2001. The North Anatolian Fault within Sea of Maramara: a new interpretation based on multi-channel seismic and multi- beam bathymetry data. *EPSL*, 186

Kazancı, N., Emre, Ö., Erturaç, K., Leroy, S. A. G., Öncel, S., İleri, Ö., Toprak, Ö. 2014. Güney Marmara bölgesindeki büyük vadilerin olası deşilme zamanı. *Maden Tetkik ve Arama Dergisi* 148, 1-17.

Kuşçu, İ., Okamura, M., Matsuoka, H., Awata, Y. 2002. Active faults in the Gulf of İzmit on the North Anatolian Fault, NW Turkey: a high-resolution shallow seismic study. *Marine Geologys*, 190, 1–2, 421–443.

Le Pichon, X., Şengör, A.M.C., Demirbağ, E., Rangin, C., İmren, C., Armijo, R., Görür, N., Çağatay, N., Mercier de Lepinay, B., Meyer, B., Saatçılar, R., Tok, B. 2001. The Active Main Marmara Fault. *Earth and Planetary Science Letters*, 192, 595-616.

Le Pichon, X., Chamot-Rooke, N., Rangin, C., Şengör, A.M.C. 2003, The North Anatolian Fault in the Sea of Marmara. *Journal of Geophysical Research*, 108, B4, 2179.

Rangin, C., Demirbağ, E., İmren, C., Crusson, A., Normand, A., Le Drezen, E., Le Bot, A. 2001. Marine Atlas of the Sea of Marmara (Turkey). *IFREMER, Paris*, ISBN 2-84433-068-1

Şaroğlu, F. Emre, Ö. ve Boray, A. 1987. Türkiye'nin diri fayları ve depremselliği. *Maden Tetkik ve Arama Genel Müdürlüğü Report No*: 8174, Ankara, (unpublished).

Şengör, A.M.C. 1980. Türkiyenin neotektoniğinin esasları: *Türkiye Jeoloji Kurumu Konferanslar dizisi*, 2, 40 s.

Şengör, A.M.C. ve Yılmaz, Y. 1981. Tethyan evolution of Turkey; a plate tectonic approach: *Tectonophysics*, 75, 181-241.